

4.1 WINGS AT ANGLE OF ATTACK

A great deal of theoretical and experimental work has been done toward the development of airfoil sections. Theoretical airfoil design is hampered by the existence of viscous effects in the form of a "boundary layer" of low-energy air between the airfoil surface and the free stream. This boundary layer affects chiefly the section drag and maximum lift characteristics but also has minor effects on lift-curve slope, angle of attack for zero lift, and section pitching-moment coefficient.

Since the boundary layer is influenced by surface roughness, surface curvature, pressure gradient, heat transfer between the surface and the boundary layer, and viscous interaction with the free stream, it is apparent that no simple theoretical considerations can accurately predict all the airfoil characteristics. For these reasons, experimental data are always preferable to theoretical calculations.

Airfoils have been optimized for many specific characteristics, including: high maximum lift, low drag at low lift coefficients, low drag at high lift coefficients, low pitching moments, low drag in the transonic region, and favorable lift characteristics beyond the critical Mach number. Optimization of an airfoil in one direction usually compromises it in another. Thus, low-drag airfoils have poor high-lift characteristics, and high-lift airfoils have low critical Mach numbers.

It is apparent from the above that any generalized charts for airfoil section characteristics, including the ones in this handbook, must be used with caution.

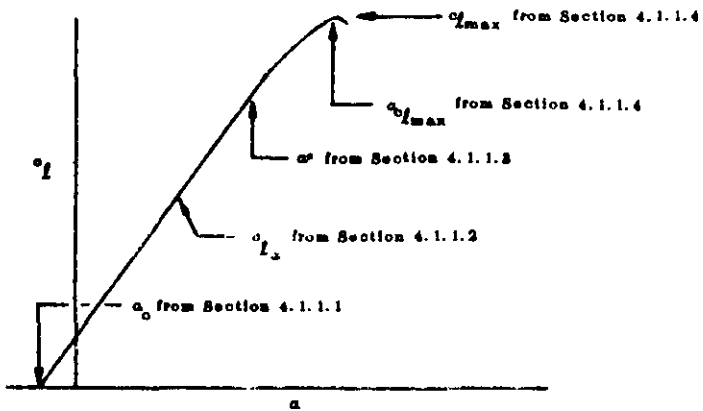
Included in this Section are tabulated NACA experimental and theoretical data that are used and discussed in detail in Sections 4.1.1.1, 4.1.1.2, 4.1.1.3, 4.1.1.4, 4.1.2.1, and 4.1.2.2.

Table 4.1.1-A summarizes experimental data for the NACA four- and five-digit airfoils. Table 4.1.1-B gives corresponding data for the NACA 6-series airfoils. The data, from reference 1, are for smooth-leading-edge conditions and 9×10^6 Reynolds number.

Information is presented on the following airfoil characteristics:

1. angle of attack at zero lift, α_0
2. lift-curve slope, $c_{l\alpha}$
3. angle of attack at which the lift curve deviates from linear variation, α^*
4. maximum lift coefficient, $c_{l_{max}}$
5. angle of attack for maximum lift coefficient, $\alpha_{c_{l_{max}}}$
6. design lift coefficient c_{l_i}
7. angle of attack at design lift coefficient, α_i

From these first five quantities the approximate section lift-curve shape can be synthesized, as illustrated in the following figure:



Experimental data for a large number of additional airfoils are available in the literature. These airfoils may be located with the aid of table 4.1.1-C.

Table 4.1.1-D presents theoretical aerodynamic characteristics of various airfoil mean lines. This theoretical information is used to approximate characteristics of NACA-type airfoils for which experimental data are not available.

REFERENCES

1. Abbott, I. H., von Doenhoff, A. E., and Stivers, L. S., Jr.: Summary of Airfoil Data. NACA TR 824, 1945. (U)
2. Pinkerton, R. M., and Greenberg, H.: Aerodynamic Characteristics of a Large Number of Airfoils Tested in the Variable-Density Wind Tunnel. NACA TR 626, 1938. (U)
3. Jacobs, E. N., and Abbott, I. H.: Airfoil Section Data Obtained in the N.A.C.A. Variable-Density Wind Tunnel as Affected by Support Interference and Other Corrections. NACA TR 669, 1939. (U)
4. Jacobs, E. N., Pinkerton, R. M., and Greenberg, H.: Tests of Related Forward-Camber Airfoils in the Variable-Density Wind Tunnel. NACA TR 610, 1937. (U)
5. Jacobs, E. N., Ward, K. E., and Pinkerton, R. M.: The Characteristics of 75 Related Airfoil Sections from Tests in the Variable-Density Wind Tunnel. NACA TR 460, 1938. (U)
6. Loftin, L. K., Jr.: Theoretical and Experimental Data for a Number of NACA 6A-Series Airfoil Sections. NACA TR 808, 1948. (U)
7. Daley, B. N., and Dick, E. S.: Effect of Thickness, Camber, and Thickness Distribution on Airfoil Characteristics at Mach Numbers up to 1.0. NACA TN 2607, 1958. (U)
8. Lindsay, W. F., Stevenson, D. B., and Daley, B. N.: Aerodynamic Characteristics of 24 NACA 16-Series Airfoils at Mach Numbers between 0.8 and 0.8. NACA TN 1548, 1948. (U)
9. Biegels, F. W.: Aerodynamische Profile. Oldenbourg, Munich, 1958. (U)

TABLE 4.1.1-A
EXPERIMENTAL LOW SPEED AIRFOIL SECTION AERODYNAMIC CHARACTERISTICS*
 $R = 9 \times 10^6$, Smooth Leading Edge
4- and 5-Digit Airfoils

Airfoil	α_0 (deg)	c_{m_0}	$\frac{c_L}{\alpha}$ (per deg)	a.c.	$\alpha_{L_{max}}$ (deg)	$\alpha_{L_{max}}$	α^* (deg)
0006	0	0	.108	.280	9.0	.82	9.0
0009	0	0	.108	.280	18.4	1.82	11.4
1408	0.8	-.028	.108	.280	14.0	1.88	10.0
1410	-1.0	-.020	.108	.247	14.8	1.80	11.0
1412	-1.1	-.028	.108	.262	18.2	1.88	12.0
2412	-2.0	-.047	.108	.247	16.8	1.88	9.8
2415	-2.0	-.049	.108	.246	16.4	1.88	10.0
2418	-2.3	-.050	.108	.241	14.0	1.47	10.0
2421	-1.8	-.040	.108	.241	16.0	1.47	8.0
2424	-1.8	-.040	.098	.281	16.0	1.38	8.4
4412	-8.8	-.088	.108	.247	14.0	1.87	7.8
4415	-8.8	-.088	.108	.248	18.0	1.84	8.0
4418	-8.8	-.088	.108	.242	14.0	1.88	7.2
4421	-8.8	-.088	.108	.288	16.0	1.47	8.0
4424	-8.8	-.082	.100	.288	16.0	1.38	6.8
28012	-1.4	-.014	.107	.247	16.0	1.78	12.0
28015	-1.0	-.007	.107	.248	18.0	1.73	10.0
28018	-1.2	-.008	.104	.248	16.0	1.80	11.8
28021	-1.2	0	.108	.288	16.0	1.80	10.8
28024	-0.6	0	.087	.281	16.0	1.40	8.7

α^* = angle of attack at which lift curve ceases to be linear.

TABLE 4.1.1-B
EXPERIMENTAL LOW SPEED AIRFOIL SECTION AERODYNAMIC CHARACTERISTICS **
 $R = 9 \times 10^6$, Smooth Leading Edge
6-Series Airfoils

Airfoil	α_0 (deg)	c_{m_0}	$\frac{c_L}{\alpha}$ (per deg)	a.c.	$\alpha_{L_{max}}$ (deg)	$\alpha_{L_{max}}$	α^* (deg)
68-006	0	.008	.112	.288	10.0	.87	7.7
-009	0	0	.111	.288	11.0	1.18	10.7
68-206	-1.8	-.087	.112	.284	10.8	1.06	8.0
-209	-1.4	-.082	.110	.282	12.0	1.4	10.8
-210	-1.2	-.088	.118	.281	14.8	1.86	8.6
68-012	0	0	.116	.288	14.0	1.48	12.8
-212	-2.0	-.088	.114	.288	14.8	1.88	11.4
-412	-2.8	-.076	.117	.271	18.0	1.77	9.8

(Contd.)

*LIFT COEFFICIENTS USED IN THESE CHARTS IS BASED ON CHORD

TABLE 4.1.1-B (Contd)

Airfoil	α_0 (deg)	c_{m_0}	γ_α (per deg)	s.o.	$\alpha_{\alpha_{\text{max}}}$ (deg)	α_{max}	α^* (deg)
63-015	0	0	.117	.271	16.0	1.47	11.0
-215	-1.0	-.080	.116	.267	16.0	1.60	8.8
-415	-2.0	-.068	.116	.262	16.0	1.68	10.0
-615	-3.0	-.106	.117	.266	16.0	1.67	8.6
63-016	0	0	.118	.271	16.0	1.54	11.2
-216	-1.4	-.088	.118	.271	16.0	1.85	8.0
-416	-2.7	-.064	.118	.272	16.0	1.57	7.0
-616	-3.8	-.097	.118	.267	16.0	1.59	4.2
63-021	0	0	.118	.273	17.0	1.88	9.0
-221	-1.5	-.088	.118	.269	16.0	1.44	9.2
-421	-2.8	-.062	.120	.275	16.0	1.48	6.7
63-4-420	-2.2	-.058	.108	.265	14.0	1.42	7.0
63-4-420 $a = .8$	-2.4	-.087	.111	.265	16.0	1.85	6.0
63(420)-422	-3.2	-.068	.112	.271	14.0	1.86	6.0
63(420)-517	-8.0	-.084	.108	.264	16.0	1.60	8.0
64-006	0	0	.108	.266	9.0	.8	7.2
-009	0	0	.110	.262	11.0	1.17	10.0
64-108	0	-.018	.110	.265	10.0	1.1	10.0
-110	-1.0	-.020	.110	.261	18.0	1.4	10.0
64-206	-1.0	-.040	.110	.268	12.0	1.08	8.0
-208	-1.2	-.088	.113	.267	10.6	1.28	8.8
-209	-1.5	-.040	.107	.261	18.0	1.40	8.0
-210	-1.6	-.040	.110	.268	14.0	1.48	10.8
64-012	0	0	.111	.263	14.0	1.45	11.0
-112	-0.8	-.017	.118	.267	14.0	1.80	12.2
-212	-1.3	-.027	.118	.262	16.0	1.85	11.0
-412	-3.6	-.065	.112	.267	16.0	1.67	8.0
64-015	0	0	.112	.267	18.0	1.48	18.0
-215	-1.6	-.080	.112	.265	16.0	1.87	10.0
-415	-2.8	-.070	.115	.264	16.0	1.66	8.0
64-018	0	-.004	.111	.266	17.0	1.80	12.0
-218	-1.3	-.027	.118	.271	16.0	1.88	10.0
-418	-2.0	-.065	.116	.273	14.0	1.57	8.0
-618	-3.8	-.085	.116	.273	16.0	1.88	5.6
64-021	0	+.005	.110	.274	14.0	1.80	10.8
-221	-1.2	-.029	.117	.271	18.0	1.82	6.8
-421	-2.8	-.068	.120	.276	18.0	1.42	6.4
65-006	0	0	.108	.268	12.0	.92	7.6
-008	0	0	.107	.264	11.0	1.08	9.8
65-206	-1.6	-.081	.106	.267	12.0	1.08	8.0
-209	-1.2	-.081	.106	.269	12.0	1.80	10.0
-210	-1.6	-.084	.108	.262	18.0	1.40	9.6
65-410	-3.6	-.087	.113	.263	16.0	1.82	8.0

(Contd.)

TABLE 4.1.1-B (Cont'd.)

Airfoil	α_0 (deg)	α_m	α_{L} (per deg)	a.o.	α_{Lmax} (deg)	α_{Lmax}	α^* (deg)
65-012	0	0	.110	.261	14.0	1.86	10.0
-212	-1.0	-.082	.108	.261	14.0	1.47	9.4
-212 $\alpha = .6$	-1.4	-.088	.108	.269	14.0	1.80	9.6
-412	-3.0	-.070	.111	.265	18.0	1.86	10.6
65-018	0	0	.111	.287	18.0	1.42	11.2
-218	-1.2	-.082	.112	.269	18.5	1.58	10.0
-418	-2.6	-.060	.111	.268	16.0	1.81	8.7
-418 $\alpha = .8$	-2.6	-.061	.111	.264	20.0	1.60	7.0
65(218)-114	-0.7	-.019	.112	.268	18.0	1.44	10.8
65(218)-418 $\alpha = .6$	-3.0	-.087	.106	.267	18.0	1.80	6.0
65-018	0	0	.100	.262	17.0	1.44	10.0
-418 $\alpha = .8$	-3.0	-.081	.112	.266	20.0	1.58	4.4
-618	-4.0	-.100	.110	.278	20.0	1.80	4.9
65-018	0	0	.100	.287	18.0	1.87	10.0
-218	-1.2	-.080	.100	.268	18.0	1.48	8.8
-418	-2.4	-.059	.110	.265	18.0	1.84	4.9
-418 $\alpha = .6$	-2.4	-.055	.115	.267	18.0	1.80	6.0
-618	-4.0	-.102	.112	.276	18.0	1.84	5.2
-618 $\alpha = .8$	-4.2	-.078	.104	.265	20.0	1.51	5.8
65-021	0	0	.112	.267	18.5	1.40	7.4
-221	-1.3	-.020	.115	.274	20.5	1.46	6.0
-421	-2.4	-.066	.116	.272	22.0	1.56	5.0
-421 $\alpha = .6$	-2.6	-.082	.116	.272	20.0	1.48	5.6
65(421)-420	-2.4	-.081	.118	.275	20.0	1.52	4.7
65-006	0	0	.100	.262	9.0	1.80	6.5
-009	0	0	.108	.269	10.0	1.05	10.0
65-206	-1.4	-.086	.108	.267	10.0	1.00	7.0
-209	-1.0	-.084	.107	.267	11.0	1.17	8.0
-210	-1.8	-.088	.110	.261	11.0	1.27	10.0
65-012	0	0	.106	.265	14.0	1.28	11.2
-212	-1.2	-.082	.102	.269	14.0	1.46	11.6
65-018	0	.006	.108	.265	18.0	1.85	12.0
-218	-1.8	-.081	.108	.260	16.0	1.80	11.4
-418	-2.6	-.068	.108	.260	17.0	1.80	10.0
65(218)-018	0	0	.108	.260	14.0	1.88	10.0
-218	-2.0	-.044	.114	.262	18.0	1.58	8.8
-218 $\alpha = .6$	-1.2	-.080	.100	.267	16.0	1.48	7.0
-418	-2.6	-.068	.100	.265	18.0	1.80	4.0
65A010	0	.008	.108	.264	18.0	1.90	10.0
65A210	-1.5	-.040	.108	.267	14.0	1.48	10.0
64A010	0	0	.110	.268	12.0	1.28	10.0
64A210	-1.5	-.040	.106	.261	8.0	1.44	10.0
64A410	-3.0	-.060	.100	.264	16.0	1.61	10.0
64A212	-2.0	-.040	.100	.262	14.0	1.84	11.0
64A216	-2.0	-.040	.098	.262	18.0	1.80	12.0

* = angle of attack at which lift curve ceases to be linear.

TABLE 4.1.1-C
BIBLIOGRAPHY OF SUBSONIC AIRFOIL DATA

NOTES: 1. For airfoil designations see Section 2.1.1
 2. For a comprehensive coverage of additional airfoil sections see Reference 9.
 3. Single asterisk denotes data at positive and negative angles of attack.

Reference 1	CLARK	Y*	Reference 2	Reference 3	N.A.C.A.	Reference 4	Reference 5	Reference 6	Reference 7	Reference 8
N.A.C.A. 67, 1-215 ↓ 747A815 747A415		Y-B		N.A.C.A. 0012	2512				N.A.C.A. 68A009	
		YM-15*		0018	2515				64A004	
		YM-18*		0018	2521				64A006	
		Y-6		0018	2612				64A206	
		Y-8		0021	2712				64A506	
		Y-10		0025	N.A.C.A. 4212				64A009	
		Y-14		0030	4806				64A012	
		Y-18*		2212	4809				65A009	
		Y-22		2409	4812					
				4406	4815					
				4409	4818					
					4821					
					4806					
					4809					
					4812					
					4815					
					4818					
					4821					
					4806					
					4809					
					4812					
					4815					
					4818					
					4821					
					4806					
					4809					
					4812					
					4815					
					4818					
					4821					
					4806					
					4809					
					4812					
					4815					
					4818					
					4821					
					4806					
					4809					
					4812					
					4815					
					4818					
					4821					
					4806					
					4809					
					4812					
					4815					
					4818					
					4821					
					4806					
					4809					
					4812					
					4815					
					4818					
					4821					
					4806					
					4809					
					4812					
					4815					
					4818					
					4821					
					4806					
					4809					
					4812					
					4815					
					4818					
					4821					
					4806					
					4809					
					4812					
					4815					
					4818					
					4821					
					4806					
					4809					
					4812					
					4815					
					4818					
					4821					
					4806					
					4809					
					4812					
					4815					
					4818					
					4821					
					4806					
					4809					
					4812					
					4815					
					4818					
					4821					
					4806					
					4809					
					4812					
					4815					
					4818					
					4821					
					4806					
					4809					
					4812					
					4815					
					4818					
					4821					
					4806					
					4809					
					4812					
					4815					
					4818					
					4821					
					4806					
					4809					
					4812					
					4815					
					4818					
					4821					
					4806					
					4809					
					4812					
					4815					
					4818					
					4821					
					4806					
					4809					
					4812					
					4815					
					4818					
					4821					
					4806					
					4809					
					4812					
					4815					
					4818					
					4821					
					4806					
					4809					
					4812					
					4815					
					4818					
					4821					
					4806					
					4809					
					4812					
					4815					
					4818					
					4821					
					4806					
					4809					
					4812					
					4815					
					4818					
					4821					
					4806					
					4809					
					4812					
					4815					
					4818					
					4821					
					4806					
					4809					
					4812					
					4815					
					4818					
					4821					
					4806					
					4809					
					4812					
					4815					
					4818					
					4821					
					4806					
					4809					
					4812					
					4815					
					4818					
					4821					
					4806					
					4809					
					4812					
					4815					
					4818					
					4821					
					4806					
					4809					
					4812					
					4815					
					4818					
					4821					
					4806					
					4809					
					4812					
					4815					
					4818					
					4821					
					4806					
					4809					
					4812					
					4815					
					4818					
					4821					
					4806					

TABLE 4.1, I-D
THEORETICAL LOW SPEED AERODYNAMIC CHARACTERISTICS OF VARIOUS AIRFOIL MEAN LINES**

Mean Line	α_1	α_1 (deg)	$c_{m0/4}$ at α_1	
Four-Digit Series				
62	0.9	2.81	-0.118	
63	0.8	1.80	-0.184	
64	0.76	0.74	-0.187	
65	0.75	0	-0.187	
66	0.76	-0.74	-0.223	
67	0.80	-1.60	-0.266	
Five-Digit Series				
210	0.80	2.09	-0.006	
220	0.80	1.86	-0.010	
230	0.80	1.65	-0.014	
240	0.80	1.45	-0.019	
250	0.80	1.26	-0.026	
6-Series				
$a = 0$	1.0	4.56	-0.088	
0.1	1.0	4.48	-0.080	
0.2	1.0	4.17	-0.084	
0.3	1.0	3.84	-0.106	
0.4	1.0	3.46	-0.121	
0.5	1.0	3.04	-0.189	
0.6	1.0	2.58	-0.168	
0.7	1.0	2.09	-0.179	
0.8	1.0	1.54	-0.202	
0.9	1.0	0.90	-0.228	
1.0	1.0	0	-0.260	

* "Corresponding" cambers are those for which the chordwise position of maximum camber is the same.

** Lift coefficient is based on airfoil chord.

4.1.1.1 SECTION ZERO-LIFT ANGLE OF ATTACK

Reynolds number and roughness have a small effect on section zero-lift angle of attack. Reference 1 shows that variations due to these causes are usually restricted to less than 1°.

Up to the critical Mach number the effect of compressibility on the zero-lift angle of attack is negligible. Above the critical Mach number, however, compressibility effects can cause large changes in this parameter. Reference 2 presents Mach number effects on some cambered sections.

For supersonic Mach numbers it is advisable to use the method of characteristics or the generalized shock-expansion method (reference 3). The charts and tables of this Section, however, are restricted to low speeds.

HANDBOOK METHOD

Experimental data from reference 4 on the zero-lift angle of attack for NACA four- and five-digit and 6-series airfoils are presented in tables 4.1.1-A and 4.1.1-B, respectively. Data on many additional airfoils may be located in the literature with the help of table 4.1.1-C.

For airfoil series not included in this summary, the theoretical characteristics tabulated in table 4.1.1-D may be used in conjunction with the aforementioned experimental data to derive the zero-lift angle of attack according to the following method. The zero-lift angle of attack is given by the equation (assuming a lift-curve slope of 2π)

$$\alpha_0 = k(\alpha_i - \frac{57.3}{2\pi} c_{L_i}) \quad 4.1.1.1-a$$

$$= k(\alpha_i - 9.12 c_{L_i})$$

where c_{L_i} and α_i are the design lift coefficient and angle of attack for the design lift coefficient, respectively. The factor K is empirical (reference 4) and depends upon the airfoil series. For NACA airfoil sections the values are:

$$\begin{aligned} K &= 0.93 \text{ NACA Four-Digit Series} \\ &= 1.08 \text{ NACA Five-Digit Series} \\ &= 0.74 \text{ NACA 6-Series} \end{aligned}$$

Theoretical section design lift coefficients and corresponding angles of attack for NACA four- and five-digit and 6-series airfoils are given in table 4.1.1-D. For airfoils other than those included in table 4.1.1-D, the tabulated values of α_i and c_{L_i} may be linearly scaled, as indicated in the sample problems below and in table 4.1.1-D. The zero-lift angle of attack so obtained may be adjusted by judicious use and comparison with the experimental data of related airfoils. Wherever possible, however, experimental data should be used. The accuracy of this method as compared to experimental data is shown in table 4.1.1.1-A.

SAMPLE PROBLEM

Example 1: Find the theoretical α_0 for the NACA 2415 section. The calculation of the theoretical α_0 for this section should be based on the NACA 64 mean line, for which

$\alpha_i = 0.74^\circ$ and $c_{L_i} = .76$ (Table 4.1.1-D)

$$\alpha_i = (.74) 2/6$$

$$= 0.25^\circ$$

$$c_{L_i} = (.76) 2/6$$

$$= 0.25$$

From equation 4.1.1.1-a

$$\alpha_o = .93 \left(.25 - \frac{57.3 \times .25}{2\pi} \right)$$

$$= -1.91^\circ$$

This result compares to $\alpha_o = -2.0^\circ$ experimentally.

Example 2: Find the theoretical α_o for the NACA 65₂-415, $a = 0.5$ airfoil. ($c_{L_i} = .4$)

The NACA $a = 0.5$ mean line serves as a base in this case, for which the tabulated data of table 4.1.1-D indicate that $\alpha_i = 3.04^\circ$ when $c_{L_i} = 1.0$. The desired value of α_i for the given airfoil is then

$$\alpha_i = 3.04 \times \frac{.4}{1.0}$$

$$= 1.22^\circ$$

Substitution into equation 4.1.1.1-a yields

$$\alpha_o = .74 \left(1.22 - \frac{57.3 \times .4}{2\pi} \right)$$

$$= -1.80^\circ$$

TABLE 4.1.1.1-A
SUBSONIC ZERO-LIFT ANGLE OF ATTACK
SUBSTANTIATION DATA

Airfoil	α_o , deg Calculated (Equation 4.1.1-a)	α_o , deg Test*	$\Delta\alpha_o$, deg (Calc. - Test)
14xx	-1.0	-1.0 to -0.8	-0.2 to 0
24xx	-1.8	-2.8 to -1.8	-0.1 to +0.4
44xx	-3.8	-4.8 to -3.8	0 to +0.5
280xx	-1.2	-1.4 to -0.8	-0.4 to +0.2
6x - 1xx	-0.7	-1.0 to -0.7	0 to +0.3
6x - 2xx	-1.8	-2.0 to -1.0	-0.2 to +0.7
6x - 4xx	-2.7	-3.2 to -2.2	-0.5 to +0.5
6x - 6xx	-4.0	-4.0 to -3.8	-0.4 to 0
6xx - 6xx $a = .5$	-2.7	-4.2	+1.5
6xx - 2xx $a = .6$	-1.0	-1.4	+0.4
6xx - 4xx $a = .8$	-2.2	-3.0	+0.8
6x - 8xx	-3.4	-3.0	-0.4

*The maximum and minimum values for the experimental values are due primarily to thickness-ratio variations.

$$\text{Average Error} = \frac{\sum |\Delta\alpha_o|}{n} = 0.4^\circ$$

REFERENCES

1. Loftin, L. K., Jr., and Smith, H. A.: Aerodynamic Characteristics of 15 NACA Airfoil Sections at Seven Reynolds Numbers From 0.7×10^6 to 9.0×10^6 . NACA TN 1945, 1949. (U)
2. Stack, J., and von Doenhoff, A. E.: Tests of 16 Related Airfoils at High Speeds. NACA TR 492, 1934. (U)
3. Eggers, A. J., Jr., Savin, R. C., and Syvertson, C. A.: The Generalized Shock-Expansion Method and Its Application to Bodies Travelling at High Supersonic Airspeeds. Jour. Aero. Sci., April 1955.
4. Abbott, I. H., von Doenhoff, A. E., and Stivers, L. S., Jr.: Summary of Airfoil Data. NACA TR 824, 1946. (U)
5. Pinkerton, R. M., and Greenberg, H.: Aerodynamic Characteristics of a Large Number of Airfoils Tested in the Variable-Density Wind Tunnel. NACA TR 628, 1938. (U)

4.1.1.2 SECTION LIFT-CURVE SLOPE

The theoretical incompressible lift-curve slope (based on the Kutta-Joukowski hypothesis of finite velocity at the trailing edge) may be approximated by the equation (for angles of attack below α^* as given in Section 4.1.1).

$$c_{\ell_\alpha} = 6.28 + 4.7 t/c \left[1 + .00375 \phi_{TE} \right] \text{ (per rad)}$$

where ϕ_{TE} is the total trailing-edge angle in degrees. However, boundary-layer effects cause the actual lift-curve slopes to fall considerably below the theoretical values.

On thin wings the loss in lift-curve slope due to Reynolds-number effects is approximately 15 percent at $R_\ell = 10^6$. For thicker wings the losses are further aggravated by the adverse pressure gradient over the rear section due to thickness distribution. To a certain extent this can be correlated with trailing-edge angle. Very thin wings with leading-edge bubble-type separation also suffer additional lift-curve-slope losses. Reference 1 discusses viscous effects on the aerodynamic characteristics of wing sections.

The effects of leading-edge roughness on lift-curve slope can be very severe in some cases. Losses as large as 30 percent, due to the effects of the standard NACA leading-edge roughness, are shown in reference 7.

Up to the critical Mach number of the airfoil section, lift-curve slope follows the Prandtl-Glauert compressibility rule. Beyond the critical Mach number, thick conventional sections suffer large lift-slope changes due to local shock formation on first the upper and then the lower airfoil surfaces. References 2, 3, and 4 show these effects for a series of thick airfoils. An example of Mach-number effects on the lift-curve slope of a thin airfoil is contained in reference 5. Certain airfoils, notably the NACA 8-series (reference 6), are specifically designed to avoid these transonic effects.

Two methods are presented in this section for estimating the airfoil section lift-curve slope at speeds up to the critical Mach number. One uses the large body of available experimental section data, while the other is based on the semiempirical method of reference 8.

No specific methods are presented in the transonic and supersonic speed regimes. Transonic airfoil section characteristics are highly variable with airfoil section, and it is suggested that reference be made to experimental data on the particular airfoil in question. At supersonic speeds theoretical pressure distribution about an arbitrary section can be calculated by generalized shock-expansion theory, second-order theory, or the method of characteristics (see reference 3 of Section 4.1.1.1).

A. SUBSONIC

DATCOM METHODS

1. Method 1

Experimental lift-curve-slope data from reference 7 are presented in table 4.1.1-A for the NACA four- and five-digit airfoils and in table 4.1.1-B for the NACA 6-series airfoils. The effect of the NACA standard roughness on these data is indicated in figure 4.1.1.2-7. The NACA standard roughness is obtained by the use of 0.011-inch carborundum grains applied over the first 8 percent of the 24-inch-chord test models. Experimental lift-curve slopes for many other airfoils may be found in the literature with the aid of table 4.1.1-C.

Low-speed values of c_{ℓ_α} obtained from Section 4.1.1 may be corrected for compressibility effects up to the critical Mach number by application of the Prandtl-Glauert compressibility correction; i.e., $(c_{\ell_\alpha})_M = c_{\ell_\alpha}/\beta$.

2. Method 2

This method is basically the semiempirical method of reference 8. The method accounts for the development of the boundary layer for airfoils with transition fixed at the leading edge and with maximum thickness less than approximately 20 percent. The airfoil section lift-curve slope at Mach numbers up to the critical Mach number is given by

$$c_{\ell_\alpha} = \frac{1.05}{\beta} \left[\frac{c_{\ell_\alpha}}{(c_{\ell_\alpha})_{\text{theory}}} \right] (c_{\ell_\alpha})_{\text{theory}} \quad 4.1.1.2-a$$

where

$$\left[\frac{(c_{\ell_\alpha})}{(c_{\ell_\alpha})_{\text{theory}}} \right]$$

is an empirical correction factor obtained from figure 4.1.1.2-8a. This factor accounts for the development of the boundary layer towards the airfoil trailing edge. It is related to the Reynolds number with transition fixed at the airfoil leading edge, and the trailing-edge angle defined as the angle between straight lines passing through points at 90 and 99 percent of the chord on the upper and lower airfoil surfaces.

$$(c_{\ell_\alpha})_{\text{theory}}$$

is the theoretical airfoil section lift-curve slope obtained from figure 4.1.1.2-8b. The values of $(c_{\ell_\alpha})_{\text{theory}}$ have been determined using the Kutta-Joukowski hypothesis. Since $(c_{\ell_\alpha})_{\text{theory}}$ is relatively insensitive to the exact value of the trailing-edge angle, a value of $\phi_{TE} = 20^\circ$, representing the upper limit of the method, has been chosen as a constant in evaluating this parameter. Consequently, $(c_{\ell_\alpha})_{\text{theory}}$ is presented as a function only of airfoil thickness ratio.

$$\beta$$

is the Prandtl-Glauert compressibility correction factor $\sqrt{1 - M^2}$.

The constant 1.05 of equation 4.1.1.2-a is an empirical correlation factor based on a large body of test data.

The method is limited to attached flow conditions and must therefore be applied with caution to airfoils with maximum thickness exceeding approximately $0.20c$, airfoils with trailing-edge angles greater than approximately 20° , and airfoils at high angles of attack.

Although the position of transition is important in determining the boundary-layer thickness at the trailing edge, no attempt has been made to estimate the effect of variation of transition position. The available experimental data do not clearly define the behavior of the transition-position movement; consequently, development of general design charts to predict the variation in section lift-curve slope with transition-position movement does not appear feasible. The transition will occur at or near the leading edge on both the upper and lower surfaces of the airfoil for most full-scale practical cases.

A comparison of test data with c_{ℓ_α} calculated by this method is presented as table 4.1.1.2-A.

Sample Problem

Method 2

Given: Airfoil tested in reference 9.

NACA 0006 airfoil

$M = 0.15; \beta = 0.99$

$R_\ell = 4.5 \times 10^6$

$t/c = 0.06$

$$\frac{Y_{90}}{2} = 0.720$$

$$\frac{Y_{99}}{2} = 0.130$$

(Y in percent chord)

Compute:

$$\tan \frac{1}{2} \phi'_{TE} = \frac{\frac{Y_{90}}{2} - \frac{Y_{99}}{2}}{9} = 0.066$$

$$\frac{c_{\ell_\alpha}}{(c_{\ell_\alpha})_{\text{theory}}} = 0.880 \text{ (figure 4.1.1.2-8a)}$$

$$(c_{\ell_\alpha})_{\text{theory}} = 6.58 \text{ per rad (figure 4.1.1.2-8b)}$$

Solution:

$$c_{\ell_\alpha} = \frac{1.05}{\beta} \left[\frac{c_{\ell_\alpha}}{(c_{\ell_\alpha})_{\text{theory}}} \right] (c_{\ell_\alpha})_{\text{theory}} \quad (\text{equation 4.1.1.2-a})$$

$$= \frac{1.05}{0.99} (0.880) (6.58)$$

$$= 6.14 \text{ per rad}$$

$$= 0.107 \text{ per deg}$$

This compares with a test value of 0.103 per degree obtained from reference 9.

REFERENCES

1. Nonweller, T.R.: The Design of Wing Sections. Aircraft Engineering, Volume XXVIII, Number 329, July 1956. (U)
2. Ladson, C.L.: Two-Dimensional Airfoil Characteristics of Four NACA 6A-Series Airfoils at Transonic Mach Numbers up to 1.26. NACA RM L57F06, 1957. (U)
3. Lindsey, W.F., and Humphreys, M.D.: Effects of Aspect Ratio on Airflow at High Subsonic Mach Numbers. NACA TN 2720, 1962. (U)
4. Gullstrand, T.R.: The Flow Over Two-Dimensional Aerofoils at Incidence in the Transonic Speed Range. KTH Aero TN 27, (Sweden), 1952. (U)
5. Holder, D.W., and Cash, R.F.: Experiments with a Two-Dimensional Aerofoil Designed to be Free from Turbulent Boundary-Layer Separation at Small Angles of Incidence for all Mach Numbers. ARC R&M 3100, 1969. (U)
6. Graham, D.J.: The Development of Cambered Airfoil Sections Having Favorable Lift Characteristics at Supercritical Mach Numbers. NACA TR 947, 1949. (U)
7. Abbott, I.H., von Doenhoff, A.E., and Stivers, L.S., Jr: Summary of Airfoil Data. NACA TR 824, 1945. (U)
8. Anon: Royal Aeronautical Society Data Sheets - Aerodynamics, Vol. II (Wings 01.01.06), 1955. (U)
9. Gambucci, J.B.: Section Characteristics of the 0006 Airfoil with Leading-Edge and Trailing-Edge Flaps. NACA TN 3797, 1956. (U)

10. Sears, R.I.: Wind-Tunnel Data on the Aerodynamic Characteristics of Airplane Control Surfaces. NACA WR L-663, 1943. (U)
11. Loftin, L.K., Jr., and Smith, H.A.: Aerodynamic Characteristics of 15 NACA Airfoil Sections at Seven Reynolds Numbers from 0.7×10^6 to 9.0×10^6 . NACA TN 1945, 1949. (U)
12. Berggren, R.E., and Graham, D.J.: Effects of Leading-Edge Radius and Maximum Thickness-Chord Ratio on the Variation with Mach Number of the Aerodynamic Characteristics of Several Thin NACA Airfoil Sections. NACA TN 3172, 1954. (U)
13. Cahill, J.F., and Racisz, S.F.: Wind-Tunnel Investigation of Seven Thin NACA Airfoil Sections to Determine Optimum Double-Slotted-Flap Configurations. NACA TN 1545, 1948. (U)
14. Loftin, L.K., Jr., and Cohen, K.S.: Aerodynamic Characteristics of a Number of Modified NACA Four-Digit-Series Airfoil Sections. NACA TN 1591, 1948. (U)
15. Wenzinger, C.J., and Harris, T.A.: Wind-Tunnel Investigation of N.A.C.A. 23012, 23021, and 23030 Airfoils with Various Sizes of Split Flap. NACA TR 668, 1939. (U)
16. Wenzinger, C.J., and Gauvin, W.E.: Wind-Tunnel Investigation of an N.A.C.A. 23012 Airfoil with a Slotted Flap and Three Types of Auxiliary Flap. NACA TR 879, 1939. (U)
17. Wenzinger, C.J., and Harris, T.A.: Wind-Tunnel Investigation of an N.A.C.A. 23012 Airfoil with Various Arrangements of Slotted Flaps. NACA TR 664, 1939. (U)
18. Ilk, R.J.: High-Speed Aerodynamic Characteristics of Four Thin NACA 63-Series Airfoils. NACA RM A7J23, 1947. (U)
19. Van Dyke, M.D.: High-Speed Subsonic Characteristics of 16 NACA 6-Series Airfoil Sections. NACA TN 2670, 1952. (U)
20. Loftin, L.K., Jr., and Burnsall, W.J.: Theoretical Effects of Variations in Reynolds Number Between 3.0×10^6 and 25.0×10^6 Upon the Aerodynamic Characteristics of a Number of NACA 6-Series Airfoil Sections. NACA TN 1773, 1948. (U)
21. Loftin, L.K. Jr.: Aerodynamic Characteristics of the NACA 64-010 and 0010-1.10 40/1.061 Airfoil Sections at Mach Numbers From 0.30 to 0.85 and Reynolds Numbers From 4.0×10^6 to 8.0×10^6 . NACA TN 3244, 1954. (U)
22. Gottlieb, S.M.: Two-Dimensional Wind-Tunnel Investigation of Two NACA 6-Series Airfoils with Leading-Edge Slats. NACA RM L8K22, 1949. (U)
23. Loftin, L.K., Jr., and Burnsall, W.J.: The Effects of Variations in Reynolds Number Between 3.0×10^6 and 25.0×10^6 Upon the Aerodynamic Characteristics of a Number of NACA 6-Series Airfoil Sections. NACA TR 964, 1950. (U)
24. Loftin, L.K., Jr., and Smith, H.A.: Two-Dimensional Aerodynamic Characteristics of 34 Miscellaneous Airfoil Sections. NACA RM L8L08, 1949. (U)
25. Bogdonoff, S.M.: Wind-Tunnel Investigation of a Low-Drag Airfoil Section with a Double Slotted Flap. NACA WR L-679, 1943. (U)
26. Quinn, J.H., Jr.: Wind-Tunnel Investigation of Boundary-Layer Control by Suction on the NACA 653-418, $a=1.0$ Airfoil Section with a 0.29-Airfoil-Chord Double Slotted Flap. NACA TN 1071, 1946. (U)
27. Quinn, J.H., Jr.: Wind-Tunnel Investigation of the NACA 654-421 Airfoil Section with a Double Slotted Flap and Boundary-Layer Control by Suction. NACA TN 1395, 1947. (U)
28. Braslow, A.L.: Two-Dimensional Wind-Tunnel Investigation of Sealed 0.22 Airfoil-Chord Internally Balanced Ailerons of Different Contour on an NACA 65(112)-213 Airfoil. NACA TN 1099, 1946. (U)
29. Braslow, A.L., and Loftin, L.K., Jr.: Two-Dimensional Wind-Tunnel Investigation of an Approximately 4-Percent-Thick NACA 66-Series-Type Airfoil Section with a Double Slotted Flap. NACA TN 1110, 1946. (U)
30. Loftin, L.K., Jr.: Theoretical and Experimental Data for a Number of NACA 6A-Series Airfoil Sections. NACA TN 1368, 1947. (U)
31. Kelly, J.A., and Hayter, N.L.F.: Lift and Pitching Moment at Low Speeds of the NACA 64A010 Airfoil Sections Equipped with Various Combinations of a Leading-Edge Slat, Leading-Edge Flap, Split Flap, and Double-Slotted Flap. NACA TN 3007, 1953. (U)
32. Summers, J.L., and Trean, S.L.: The Effects of Amount and Type of Camber on the Variation with Mach Number of the Aerodynamic Characteristics of an 10-Percent-Thick NACA 64A-Series Airfoil Section. NACA TN 2096, 1960. (U)
33. Racisz, S.F.: Investigation of NACA 65(112)A111 (Approx.) Airfoil with 0.35-Chord Slotted Flap at Reynolds Numbers up to 25 Million. NACA TN 1463, 1947. (U)

TABLE 4.1.1.2-A
SUBSONIC AIRFOIL SECTION LIFT-CURVE SLOPE
DATA SUMMARY AND SUBSTANTIATION
METHOD 2

Ref.	NACA Airfoil Section	M	β	$R_l \times 10^{-6}$	$\frac{Y_{90}}{2}$ % c	$\frac{Y_{99}}{2}$ % c	$c_l \alpha$ Calc. (per deg)	$c_l \alpha$ Test (per deg)	e Percent Error
9	0006	0.15	0.99	4.5	0.720	0.130	0.107	0.103	3.9
7	↓	—	1.00	9.0	↓	↓	0.108	0.108	0
↓	0009	—	—	↓	1.090	0.200	0.108	0.109	-0.9
10	↓	—	—	2.76	↓	↓	0.101	0.097	4.1
11	0012	<0.15	0.99	3.0	1.448	0.260	0.101	0.103	-1.9
10	0015	—	1.00	2.76	1.810	0.330	0.097	0.097	0
12	0004-1.1	0.30	0.955	1.0	0.622	0.110	0.104	0.106	-1.9
↓	0010-1.1	↓	↓	↓	1.556	0.260	0.097	0.095	2.1
7	1408	—	1.00	9.0	0.965	0.175	0.108	0.109	-0.9
—	1410	—	—	—	1.207	0.220	0.107	0.108	-0.9
↓	1412	—	—	↓	1.447	0.270	0.106	0.108	-1.9
13	1410	<0.18	0.98	6.0	1.207	0.225	0.107	0.106	0.9
14	2408	—	1.00	↓	0.955	0.355	0.107	0.106	0.9
7	2412	—	—	9.0	1.450	0.260	0.106	0.106	1.0
—	2415	—	—	—	1.810	0.340	0.105	0.106	-0.9
↓	2418	—	—	↓	2.170	0.400	0.102	0.103	-1.0
11	4412	<0.15	0.99	9.0	1.465	0.270	0.107	0.108	-0.9
↓	4415	↓	↓	6.0	1.825	0.335	0.102	0.105	-2.9
15	23012	0.105	0.99	3.5	1.455	0.265	0.102	0.107	-4.7
16	—	—	—	—	—	—	0.102	0.105	-2.9
17	—	—	—	—	—	—	0.102	0.107	-4.7
11	—	<0.15	—	—	—	—	0.096	0.096	0
—	—	—	—	—	—	—	0.101	0.102	-1.0
↓	—	—	—	—	—	—	0.107	0.107	0
7	—	—	1.00	—	—	—	0.106	0.107	-0.9
↓	23015	—	—	↓	—	—	0.105	0.107	-1.9
11	—	<0.15	0.99	8.9	—	—	0.106	0.104	1.9
—	—	↓	—	6.0	—	—	0.103	0.105	-1.9
15	23021	0.105	—	3.5	2.760	0.500	0.097	0.097	0
7	63-006	—	1.00	9.0	0.383	0.050	0.111	0.112	-0.9
↓	63-009	—	1.00	↓	0.550	0.080	0.112	0.111	0.9
18	63-208	0.30	0.955	1.0	0.496	0.020	0.108	0.106	1.9
↓	63-206	↓	↓	↓	0.383	0.025	0.108	0.110	-1.8
7	—	—	1.00	9.0	—	—	0.111	0.112	-0.9
↓	63-209	—	—	—	0.550	0.035	0.112	0.110	1.8
↓	63-210	—	—	—	0.604	0.030	0.112	0.113	-0.9
13	—	<0.18	0.98	—	—	—	0.114	0.110	3.6
19	63-212	0.30	0.955	1.0	0.707	0.030	0.108	0.108	0
18	↓	—	—	—	—	—	0.108	0.107	0.9
↑	63-210	—	—	—	0.604	0.030	0.108	0.105	2.9
7	63-012	—	1.00	9.0	0.707	0.020	0.112	0.116	-3.4
—	63-212	—	—	—	0.707	0.030	0.112	0.114	-1.8
↓	63-412	—	—	—	0.700	0.015	0.112	0.117	-4.3
11	63-215	<0.15	0.99	3.0	0.855	0.037	0.108	0.116	-6.9
—	—	↓	—	6.0	—	—	0.112	0.114	1.8
↓	—	—	—	9.0	—	—	0.114	0.114	0
20	63-018	—	1.00	1.50	0.985	0.025	0.115	0.116	-0.9
7	64-006	—	—	9.0	0.423	0.030	0.110	0.109	0.9
↓	64-009	—	—	↓	0.611	0.040	0.111	0.110	0.9
21	64-010	0.3	0.955	3.85	0.671	0.030	0.112	0.120	-6.7
13	64-208	<0.18	0.98	6.0	0.550	0.030	0.111	0.114	-2.6
7	64-206	—	1.00	9.0	0.423	0.020	0.110	0.110	0
↓	64-210	—	—	↓	0.671	0.035	0.111	0.110	0.9
11	64-409	<0.15	0.99	6.0	0.610	0.025	0.109	0.106	2.8
19	64-212	0.30	0.955	1.0	0.786	0.035	0.107	0.105	1.9

TABLE 4.1.1.2-A (CONT'D)

Ref.	NACA Airfoil Section	M	β	$R_L \times 10^{-6}$	$\frac{Y_{90}}{2}$ % c	$\frac{Y_{99}}{2}$ % c	$\frac{c_L}{c_D}$ Calc. (per deg)	$\frac{c_L}{c_D}$ Test (per deg)	% Percent Error
13	64-212	<0.18	0.98	6.0	0.786	0.036	0.111	0.115	-3.5
7	64-012	-	1.00	9.0	0.786	0.050	0.112	0.111	0.9
↓	64-412	-	↓	↓	0.784	0.035	0.112	0.112	0
11	64-612	<0.16	0.99	6.0	0.782	0.030	0.111	0.112	-0.9
22	64-212	-	1.00	↓	0.786	0.036	0.108	0.108	0.9
11	64-215	<0.15	0.99	↓	0.948	0.036	0.110	0.111	-0.9
↓	64-318	↓	↓	↓	1.110	0.045	0.110	0.109	0.9
7	65-008	-	1.00	9.0	0.738	0.040	0.109	0.107	1.9
↓	65-008	-	↓	↓	0.610	0.040	0.110	0.106	4.8
23	↓	↓	↓	3.0	↓	↓	0.106	0.110	-4.5
↓	↓	↓	↓	9.0	↓	↓	0.110	0.111	-0.9
7	65-206	-	↓	25.0	↓	↓	0.111	0.112	-0.9
↓	65-208	-	↓	9.0	0.510	0.030	0.110	0.106	4.8
↓	65-210	-	↓	↓	0.738	0.035	0.110	0.108	3.8
13	↓	<0.18	0.98	3.0	↓	↓	0.106	0.106	0
18	65-208	0.30	0.955	1.0	0.664	0.030	0.108	0.105	1.0
↓	65-212	↓	↑	↓	0.946	0.060	0.106	0.102	2.9
7	65-012	-	1.00	9.0	0.947	0.060	0.110	0.110	0
↓	65-212	-	↓	↓	0.946	0.045	0.110	0.108	1.9
↓	65-212	-	↓	↓	0.946	0.050	0.110	0.108	1.9
↓	a = .6	↓	↓	↓	↓	↓	↓	↓	↓
11	65-215	<0.15	0.99	1.0	1.141	0.060	0.101	0.108	-4.7
↓	↓	↓	↓	6.0	↓	↓	0.108	0.108	1.9
24	65-3-316	-	1.00	8.9	1.240	0.150	0.110	0.109	0.9
↓	a = .8	↓	↓	↓	↓	↓	↓	↓	↓
26	65-3-118	-	1.00	6.0	1.324	0.060	0.107	0.117	-8.5
26	65-3-418	-	↓	1.9	1.316	0.065	0.101	0.104	-2.9
↓	↓	↓	↓	6.0	↓	↓	0.107	0.111	-3.6
7	65-3-618	-	↓	9.0	1.325	0.060	0.110	0.110	0
27	65-421	-	↓	1.0	1.500	0.060	0.098	0.107	-8.4
↓	↓	↓	↓	2.2	↓	↓	0.102	0.104	-1.9
28	65(112)-213	0.15	0.99	8.0	1.026	0.060	0.110	0.102	7.8
7	65-008	-	1.0	9.0	0.665	0.060	0.109	0.100	9.0
↓	65-008	-	↓	↓	0.961	0.060	0.108	0.103	4.9
10	↓	0.10	0.99	2.76	↓	↓	0.103	0.100	3.0
7	65-208	-	1.00	9.0	0.665	0.040	0.108	0.108	0
↓	65-209	-	↓	↓	0.960	0.065	0.107	0.107	0
↓	65-210	-	↓	↓	1.063	0.060	0.107	0.110	-2.7
19	65-208	0.30	0.955	1.0	0.863	0.060	0.103	0.100	3.0
↓	65-212	↓	↓	↓	1.233	0.060	0.101	0.097	4.1
13	65-210	<0.18	0.98	3.0	1.063	0.050	0.103	0.097	6.2
7	65(215)-016	-	1.00	9.0	1.587	0.100	0.105	0.105	0
↓	65(215)-216	-	↓	↓	1.588	0.080	0.105	0.114	-7.9
24	65(215)-114	-	↓	6.2	1.400	0.030	0.103	0.108	-4.6
11	65-215	<0.15	0.99	3.0	1.490	0.075	0.098	0.099	-1.0
↓	↓	↓	↓	9.0	↓	↓	0.108	0.105	1.0
29	65(215)-214	-	1.00	↓	1.580	0.190	0.105	0.106	-0.9
30	63A010	-	↓	6.0	1.030	0.130	0.106	0.106	0
↓	63A210	-	↓	9.0	1.030	0.120	0.108	0.103	4.9
7	64A010	-	↓	↓	1.062	0.130	0.108	0.110	-1.8
31	↓	0.2	0.98	7.0	↓	↓	0.101	0.098	3.1
↓	↓	↓	↓	2.0	↓	↓	0.108	0.107	0.9
30	↓	64A210	-	1.00	3.0	↓	0.102	0.108	-5.6
↓	↓	64A410	-	↓	6.0	1.060	0.120	0.106	0.107
↓	↓	64A410	-	↓	9.0	1.062	0.125	0.108	0.105

TABLE 4.1.1.2-A (CONTD)

Ref.	NACA Airfoil Section	M	β	$R_L \times 10^{-6}$	$\frac{Y_{90}}{2} \% c$	$\frac{Y_{99}}{2} \% c$	$c_L \alpha$ Calc. (per deg)	$c_L \alpha$ Test (per deg)	% Percent Error
32	64A310	0.30	0.955	1.0	1.065	0.110	0.103	0.102	1.0
	64A610				1.070	0.125	0.103	0.107	-3.7
	64A910				1.036	0.110	0.103	0.103	0
30	64 ₁ A212	—	1.00	6.0	1.280	0.150	0.104	0.104	0
	64 ₂ A215	—		9.0	1.550	0.170	0.106	0.101	5.0
33	65(112)-A111	—		5.9	1.125	0.165	0.105	0.106	-0.9
7	63A010	—		9.0	1.030	0.130	0.108	0.105	2.9
	63A210	—			1.030	0.120	0.108	0.103	4.9
	64A210	—			1.060	0.120	0.108	0.105	2.9
	64A410	—			1.062	0.125	0.108	0.100	8.0
	64 ₁ A212	—			1.280	0.150	0.107	0.100	7.0
	64 ₂ A215	—			1.550	0.170	0.106	0.095	11.6
$\text{Average Error} = \frac{\sum e }{n} = 2.4\%$									

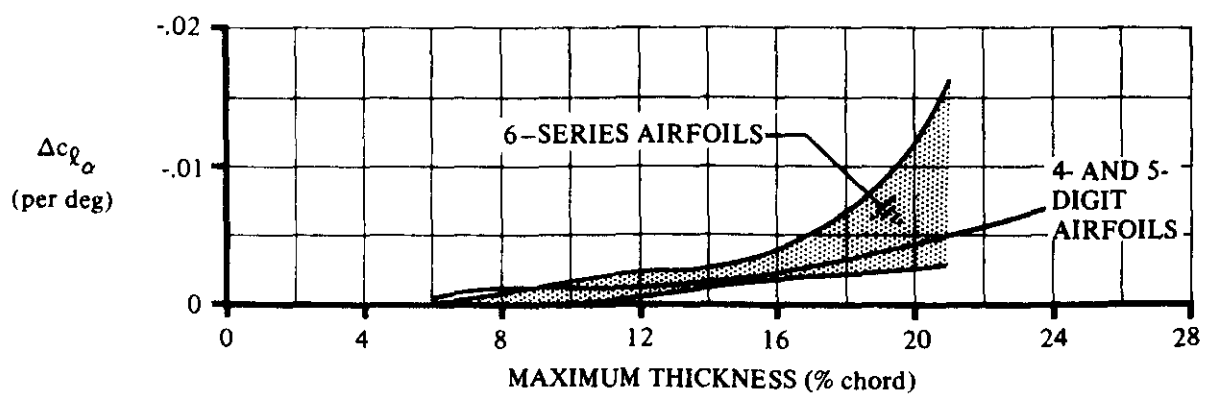


FIGURE 4.1.1.2-7 EFFECT OF NACA ROUGHNESS ON SECTION LIFT-CURVE SLOPE

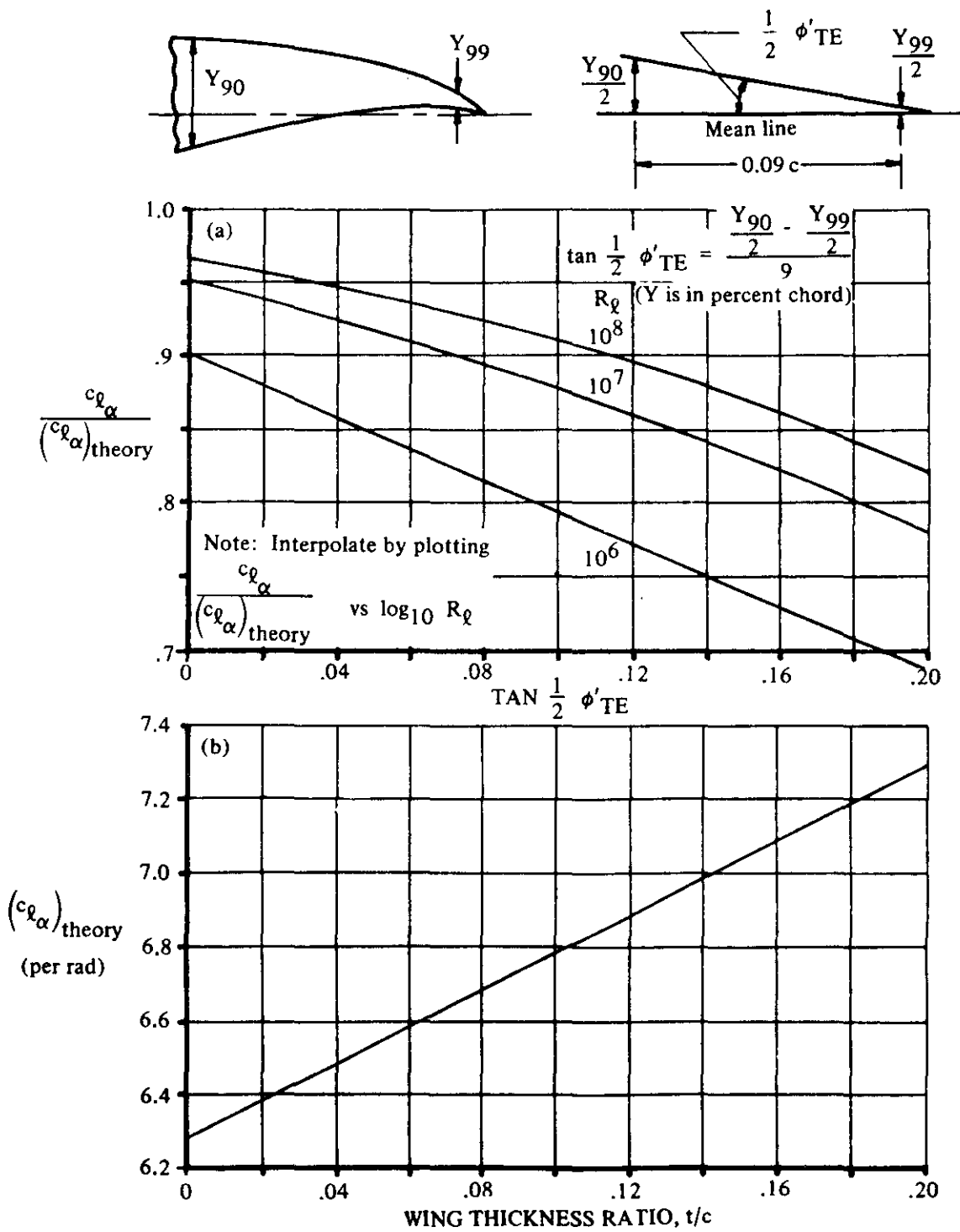


FIGURE 4.1.1.2-8 TWO-DIMENSIONAL LIFT-CURVE SLOPE
METHOD 2

4.1.1.3 SECTION LIFT VARIATION WITH ANGLE OF ATTACK NEAR MAXIMUM LIFT

Flow-separation patterns, which determine the stall characteristics of airfoil sections, are due to the effects of viscosity. These flow separation patterns can be classified into three types:

1. Separation near the trailing edge.
2. Separation of the short-bubble type near the leading edge.
3. Separation of the long-bubble type near the leading edge.

A complete discussion of these types of flow separation, as they affect airfoil stall characteristics, is contained in reference 1. They are also discussed in Section 4.1.1.4 with respect to their effect on section maximum lift. Some of the more pertinent factors affecting these stall types are discussed below.

Trailing-Edge Stall

Trailing-edge stall occurs on wings of thickness-to-chord ratios of approximately 12 percent and greater. It is characterized by a gradual separation starting at the section trailing edge and progressing forward with increasing angle of attack. When the separation has moved forward to about the section midchord, maximum lift is reached. The stall for these sections is mild, with a gradual rounding of the lift and moment curves near c_{lmax} .

Leading-Edge Stall

As the thickness ratio of airfoils decreases, the nose shape becomes progressively sharper. At some point the increasingly severe adverse pressure gradients behind the nose pressure peak cause the lift of the airfoil to be limited by separation starting at the airfoil nose.

Local leading-edge separation on the airfoil upper surface may occur at angles of attack well below those for maximum lift. At these lower angles, the separated laminar boundary layer changes to turbulent and reattaches to the airfoil, leaving a bubble of trapped low-energy air between the separated boundary layer and the airfoil surface. The mechanism of the reattachment is discussed in references 2 and 3. Transition of the boundary layer must precede reattachment, and for this reason the relative stability of the boundary layer at separation is very important. If the boundary-layer Reynolds number based on the displacement thickness is greater than about 450, then transition and reattachment take place in a very short distance, giving rise to a "short bubble". If, on the other hand, the boundary-layer Reynolds number is less than 450, transition and reattachment are considerably delayed, with a resulting "long bubble". The different characteristics of these two bubbles and their effects on stall are discussed below.

. . . Short-Bubble Leading-Edge Stall

The short bubble is characteristically one percent of the airfoil chord in length and decreases in size with increasing angle of attack. Because of its small size, the bubble has little effect on the section pressure distribution until at some angle of attack the flow abruptly ceases to reattach, thereby separating the flow over the entire upper surface of the airfoil. For this airfoil the lift and pitching-moment curves are quite linear right up to stall. The stall itself is violent, with large changes in lift and pitching moment.

. . . Long-Bubble Leading-Edge Stall

The long bubble, like the short bubble, consists of a laminar separation followed by a turbulent reattachment. However, as the angle of attack increases, the size of the long bubble also increases until, at maximum lift, the bubble covers the entire upper surface of the airfoil.

For the long-bubble type of separation, the maximum lift achieved is, in general, lower than that for either the short-bubble type or the trailing-edge type. The stall for the long bubble is mild, with gradual rounding of the lift and moment curves.

Reynolds Number Effects

Since the type of bubble formed depends on the Reynolds number of the boundary layer at the point of separation, it is apparent that changes in free-stream Reynolds number can cause the stall of an airfoil to change from one type to another. If the Reynolds number is high enough, boundary-layer transition may take place before the point where laminar separation would occur, and no bubble will be formed at all. The tables and charts pertaining to this section are based primarily on a Reynolds number of 9×10^6 . For other Reynolds numbers, reference 4 may be used, which contains a summary of the types of stall to be expected as a function of Reynolds number.

HANDBOOK METHOD

The shape of the section lift curve just below the stall angle of attack can be approximated from a knowledge of the angle of attack at which the lift curve begins to deviate from the linear slope, the maximum lift, angle of attack for maximum lift, and the lift-curve slope. The lift curve just before the stall can then be constructed with acceptable accuracy, as illustrated schematically in Section 4.1.1.

The parameters $c_{l_{\max}}$, $\alpha_{c_{l_{\max}}}$, and α_0 are discussed in Sections 4.1.1.4 and 4.1.1.1. The angle of attack α^* at which the lift curve deviates from the linear is tabulated for the NACA four-and five-digit and 6-series airfoils in tables 4.1.1-A and 4.1.1-B, respectively. The data, from reference 5, are for smooth surfaces, 9×10^6 Reynolds number, and low speeds.

REFERENCES

1. McCullough, G. B., and Gault, D. E.: Examples of Three Representative Types of Airfoil-Section Stall at Low Speed. NACA TN 2802, 1951. (U)
2. Crabtree, L. F., and Weber, J.: Some Effects of Flow Separation on Thin Wings With Unswept Leading Edges. R.A.E. Gt. Brit. TN Aero 2403. (U)
3. Crabtree, L. F.: Effects of Leading-Edge Separations on Thin Wings in Two-Dimensional Incompressible Flow. IAS Preprint No. 689, 1957.
4. Gault, D. E.: A Correlation of Low-Speed, Airfoil-Section Stalling Characteristics With Reynolds Number and Airfoil Geometry. NACA TN 8963, 1957. (U)
5. Abbott, I. H., von Doenhoff, A. E., and Stivers, L. S., Jr.: Summary of Airfoil Data. NACA TR 824, 1946. (U)

4.1.1.4 SECTION MAXIMUM LIFT

Subsonic section maximum lift is sensitive to many parameters, including airfoil thickness, location of maximum thickness, camber, position of maximum camber, Mach number, Reynolds number, free-stream turbulence, and airfoil surface condition (roughness). These parameters influence section maximum lift by determining the type of flow separation that limits the lift. Broadly speaking, the separation patterns may be classified into three types:

1. Trailing-edge separation.
2. Leading-edge separation of the short-bubble type.
3. Leading-edge separation of the long-bubble type.

The distinctive features of each of these types of separation are discussed in section 4.1.1.3.

For airfoils that stall as a result of flow separation from the leading edge (thin airfoils), the section maximum lift may be correlated with airfoil-leading-edge geometry. The leading-edge parameter that best correlates the section maximum lift is the Δy -parameter, the difference between the upper-surface ordinates at the 6-percent-chord and 0.15-percent-chord stations, respectively. This parameter is presented as a function of airfoil thickness for several standard airfoils in Section 2.2.1.

For thicker symmetrical airfoils, i.e., those that stall as a result of separation from the trailing edge, a relatively local leading-edge parameter is no longer sufficient. The maximum lift of these sections is correlated by using the position of maximum thickness in addition to the Δy -parameter.

Reference 1 indicates that for thin airfoils there is a maximum lift increment due to camber when the pressure distribution near the nose is identical to that of the corresponding uncambered airfoil. The procedure used in the Handbook is to add an increment of lift, accounting for the effect of camber, to the symmetrical-airfoil maximum lift. Empirically, the increment is a function of maximum-thickness position as well as position and magnitude of maximum camber.

Reynolds number and free-stream turbulence are analogous in their effects on section maximum lift. For thin airfoils an increase in Reynolds number or turbulence causes boundary-layer transition earlier, changing a long-bubble to a short-bubble separation. This increases lift. Roughness, if it causes transition early enough, has the same effect. For thicker airfoils roughness merely decreases the energy of the boundary layer, thus lowering maximum lift.

Mach number effects are very severe on thick airfoils. Maximum lift coefficient begins to drop, starting at $M \approx 0.2$, as illustrated typically in figure 4.1.1.4-8b.

For supersonic speeds, maximum lift can be calculated by the method of reference 2, which makes the assumptions that the upper-surface limit pressure is 70 percent of vacuum and the lower-surface pressure is a function of the total pressure behind a normal shock wave at the free-stream Mach number and the projected area of the lower surface perpendicular to the free-stream direction. Section maximum-lift values obtained by this procedure appear to be slightly low.

HANDBOOK METHOD

In this Section two-dimensional-airfoil maximum-lift information is presented in two forms: tabulated data for specific NACA airfoils and generalized design charts from which the maximum lift of nonstandard airfoils may be approximated. Actual test data should be used whenever possible, however.

Section data for maximum lift and angle of attack for maximum lift for the NACA four- and five-digit airfoils are presented in table 4.1.1-A for smooth-leading-edge conditions, a Reynolds number of 9×10^6 , and low speeds. Corresponding information for the NACA 6-series airfoils is presented in table 4.1.1-B. Additional airfoils may be located in the literature with the aid of table 4.1.1-C.

The generalized design charts of this Section are empirically derived from experimental data of references 3, 4, 5, and 6. The section maximum lift coefficient is determined by the equation

$$c_{l_{\max}} = (c_{l_{\max}})_{\text{base}} + \Delta_1 c_{l_{\max}} + \Delta_2 c_{l_{\max}} \\ + \Delta_3 c_{l_{\max}} + \Delta_4 c_{l_{\max}} + \Delta_5 c_{l_{\max}}$$
4.1.1.4-a

where the various contributions are obtained as follows:

1. $(c_{l_{\max}})_{\text{base}}$ is obtained from figure 4.1.1.4-5 as a function of Δ_y and position of maximum thickness. The Δ_y -parameter for a cambered airfoil is the same as that of the corresponding uncambered airfoil, that is, the uncambered airfoil having the same thickness distribution. This reference value is for uncambered airfoils with smooth leading edges, at 9×10^6 Reynolds number and low speed.
2. $\Delta_1 c_{l_{\max}}$ accounts for the effect of camber for airfoils having the maximum thickness at 30-percent chord. Figure 4.1.1.4-6 gives $\Delta_1 c_{l_{\max}}$ as a function of percent camber and maximum-camber location. The percent camber and position of maximum camber for standard NACA airfoils are discussed in Section 2.2.1.
3. $\Delta_2 c_{l_{\max}}$ amounts to an increment by which $\Delta_1 c_{l_{\max}}$, the "camber" term for airfoils having their maximum thickness at 30-percent chord, must be modified for airfoils having their maximum thickness at some other position. This increment is obtained from figure 4.1.1.4-7a. (If the maximum thickness is at 30-percent chord, $\Delta_2 c_{l_{\max}}$ is zero).
4. $\Delta_3 c_{l_{\max}}$, presented in figure 4.1.1.4-7b, gives the lift increment due to Reynolds number for Reynolds numbers other than 9×10^6 .
5. $\Delta_4 c_{l_{\max}}$, shown in figure 4.1.1.4-8a, gives the lift increment due to roughness. The roughness in this case is the standard NACA roughness and is represented by 0.011-inch grit applied over the first 8-percent chord. This curve is given only as an indication of roughness effects. Actual airplane roughnesses vary considerably and their effects may be quite different from those shown in figure 4.1.1.4-8a.
6. $\Delta_5 c_{l_{\max}}$ is a correction for Mach numbers greater than approximately 0.2. No generalized charts are presented for Mach number effects. The lift increment due to Mach number should be obtained from test data of similar airfoils when available. Figure 4.1.1.4-8b shows representative effects on particular airfoils.

Table 4.1.1.4-A compares experimental data with results obtained by the use of this method.

SAMPLE PROBLEM

Given:

66₂-415 Airfoil section

R = 6 x 10⁶

M = .10

Airfoil surface in smooth condition

Compute:

t/c = 15-percent chord*

Position of maximum thickness: 45-percent chord*

Position of maximum camber: 50-percent chord*

Amount of camber: 2.2-percent chord*

$\Delta_y = 2.75$ (from Section 2.2.1)

$(c_{l_{max}})_{base} = 1.34$ (from figure 4.1.1.4-5)

$\Delta_1 c_{l_{max}} = .16$ (from figure 4.1.1.4-6)

$\Delta_2 c_{l_{max}} = .08$ (from figure 4.1.1.4-7a)

$\Delta_3 c_{l_{max}} = -.02$ (from figure 4.1.1.4-7b)

$\Delta_4 c_{l_{max}} = 0$

$\Delta_5 c_{l_{max}} = 0$

*See Section 2.2.1 for airfoil description

Solution:

$$c_{l_{max}} = (c_{l_{max}})_{base} + \Delta_1 c_{l_{max}} + \Delta_2 c_{l_{max}} + \Delta_3 c_{l_{max}} + \Delta_4 c_{l_{max}} + \Delta_5 c_{l_{max}}$$
$$= 1.56$$

$c_{l_{max}} = 1.60$ from test data of reference 4.

TABLE 4.1.1.4-A
AIRFOIL SECTION MAXIMUM LIFT
DATA SUMMARY AND SUBSTANTIATION

Ref.	Airfoil	Position of max. thickness (% chord)	Camber	Position of max. camber (% chord)	Δ_y	$B \times 10^{-6}$	$(\alpha_l)_{max}$ base	$\Delta_1 \alpha_l_{max}$	$\Delta_2 \alpha_l_{max}$	$\Delta_3 \alpha_l_{max}$	α_l_{max} Calc.	α_l_{max} Test	Percent Error, %
4	0009	80	0	----	2.88	9.0	1.38	----	----	----	1.38	1.32	3.0
	1410	80	1.0	40	2.60	9.0	1.48	.11	----	----	1.59	1.50	6.0
	2418	80	2.0	40	3.80	9.0	1.87	.06	----	-.23	1.40	1.40	0
	4412	80	4.0	40	3.08	9.0	1.88	.17	----	-.18	1.62	1.52	6.0
7	4815	80	4.0	80	3.60	8.0	1.87	.06	----	-.08	1.60	1.67	-4.2
	4821	80	4.0	80	3.24	8.0	1.41	-.08	----	-.05	1.55	1.55	-8.0
	6808	80	6.0	80	1.80	9.0	1.02	.64	----	-.08	1.63	1.65	-1.2
	8808	80	6.0	80	2.88	8.0	1.86	.48	----	-.01	1.78	1.78	0
4	28012	80	1.8	18	3.08	9.0	1.58	.09	----	----	1.67	1.70	-5.0
	28021	80	1.8	18	3.24	9.0	1.41	0	----	----	1.41	1.50	-6.0
8	48012	80	3.7	18	3.08	8.0	1.88	.14	----	0	1.72	1.84	-6.0
	68012	80	6.8	18	3.08	8.0	1.88	.14	----	0	1.72	1.84	-6.0
8	68-009	88	0	----	2.00	25.0	1.30	----	----	.08	1.26	1.28	3.4
	68-209	88	1.1	50	2.00	25.0	1.20	.03	.18	.06	1.49	1.55	9.6
	68-112	88	0	----	2.68	25.0	1.48	----	----	.02	1.48	1.41	8.0
	68-212	88	1.1	50	2.88	25.0	1.48	.08	.08	.02	1.65	1.64	7.1
4	68-412	88	2.2	50	2.68	9.0	1.48	.17	.08	----	1.72	1.77	-2.8
	68-018	88	0	----	3.88	9.0	1.48	----	----	----	1.48	1.54	-8.0
	68-018	88	3.3	50	3.98	9.0	1.48	.11	-.02	----	1.67	1.59	-1.8
	68-108	40	.88	50	1.70	9.0	1.08	.02	.20	----	1.28	1.10	16.4
	68-112	40	.88	50	2.52	9.0	1.40	.04	.11	----	1.55	1.60	8.8
	68-018	40	0	----	3.78	9.0	1.44	----	----	----	1.44	1.50	-4.0
	68-218	40	1.1	50	3.75	9.0	1.44	.08	.04	----	1.51	1.53	-1.8
	68-418	40	2.2	50	3.75	9.0	1.44	.07	.04	----	1.55	1.57	-1.8
	68-018	40	3.3	50	3.75	9.0	1.44	.11	.04	----	1.59	1.58	0.6
	68-018	40	0	----	2.00	9.0	1.44	----	----	-.10	1.84	1.85	-0.7
	68-418	40	2.2	50	2.90	9.0	1.44	.16	.08	-.10	1.86	1.45	7.6
	68-009	48	0	----	1.88	9.0	1.04	----	----	----	1.04	1.05	-1.0
	68-309	48	1.1	50	1.88	9.0	1.04	.08	.20	----	1.27	1.17	8.8
	68-018	48	0	----	3.80	9.0	1.36	----	----	----	1.85	1.84	0.7
	68-418	48	2.2	50	3.80	9.0	1.38	.12	.08	----	1.86	1.86	0
Average Error in α_l_{max} = $\frac{\sum e }{n} = 6.0\%$													

REFERENCES

1. Reshko, A.: Computation of the Increment of Maximum Lift due to Flaps. Douglas Aircraft Company Report RM 28826, 1959. (U)
2. Mayer, J. P.: A Limit Pressure Coefficient and an Estimation of Limit Forces on Airfoils at Supersonic Speeds. NACA RM L8F28, 1948. (U)
3. Pinkerton, R. M., and Greenberg, H.: Aerodynamic Characteristics of a Large Number of Airfoils Tested in the Variable-Density Wind Tunnel. NACA TR 628, 1938 (U)
4. Abbott, I. H., and von Doenhoff, A. E., and Stivers, L. S., Jr.: Summary of Airfoil Data. NACA TR 824, 1948. (U)
5. Jacobs, E. N., and Abbott, I. H.: Airfoil Section Data Obtained in the NACA Variable-Density Tunnel as Affected by Support Interference and Other Corrections. NACA TR 669, 1939. (U)
6. Jacobs, E. N., Pinkerton, R. M., and Greenberg, H.: Tests of Related Forward-Camber Airfoils in the Variable-Density Wind Tunnel. NACA TR 610, 1937. (U)
7. Jacobs, E. N., Ward, K. E., and Pinkerton, R. M.: The Characteristics of 78 Related Airfoil Sections from Tests in the Variable-Density Wind Tunnel. NACA TR 460, 1938. (U)
8. Loftin, L. K., Jr., and Burnsall, W. J.: The Effects of Variations in Reynolds Number between 3.0×10^6 and 26.0×10^6 upon the Aerodynamic Characteristics of a Number of NACA 6-Series Airfoil Sections. NACA TN 1778, 1948. (U)

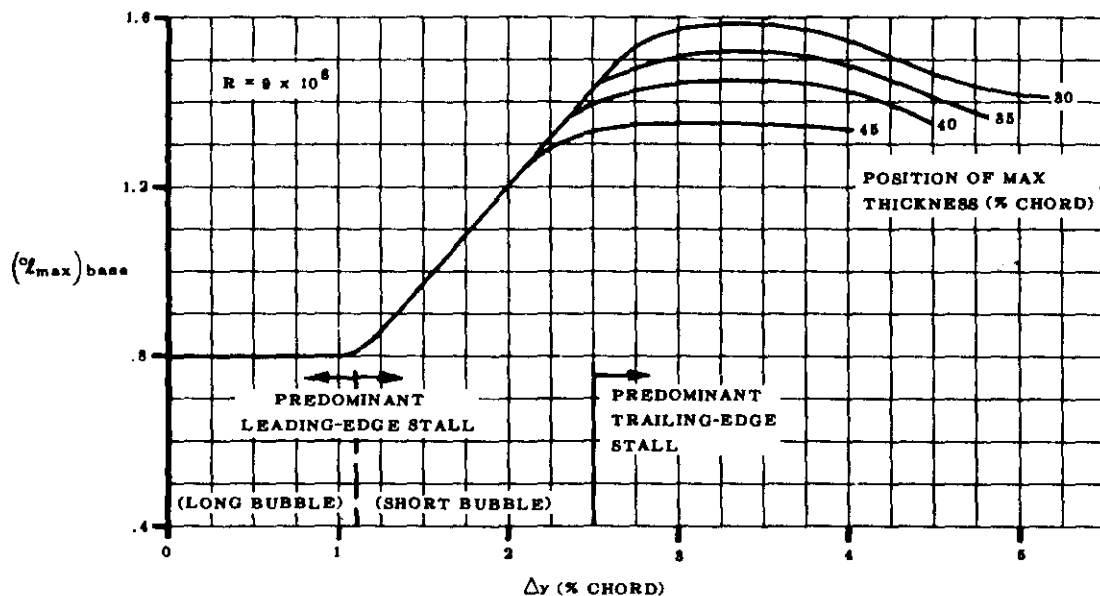


FIGURE 4.1.1.4-5 AIRFOIL SECTION MAXIMUM LIFT COEFFICIENT OF UNCAMBERED AIRFOILS

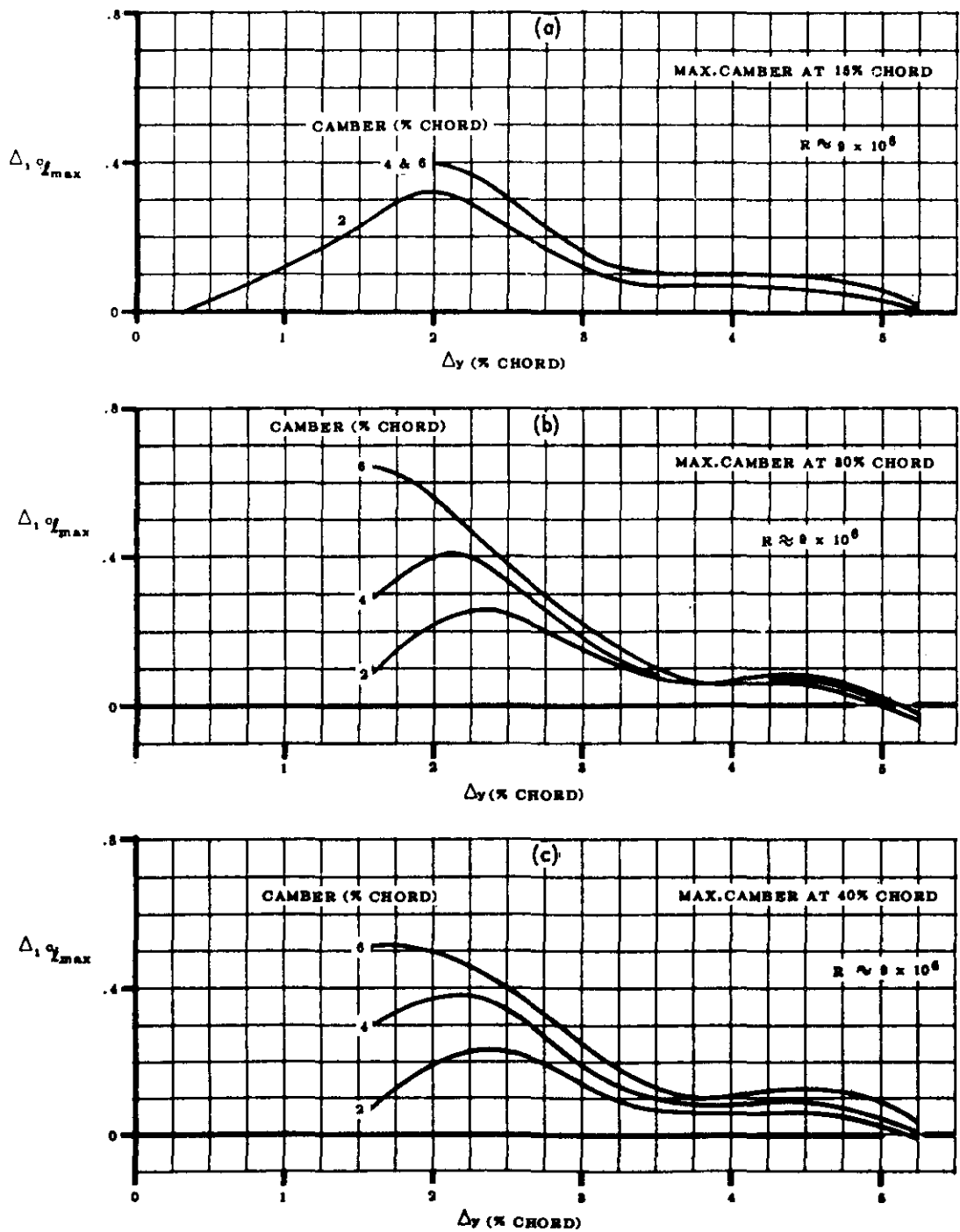


FIGURE 4.1.1.4-6 EFFECT OF AIRFOIL CAMBER LOCATION AND AMOUNT ON SECTION MAXIMUM LIFT

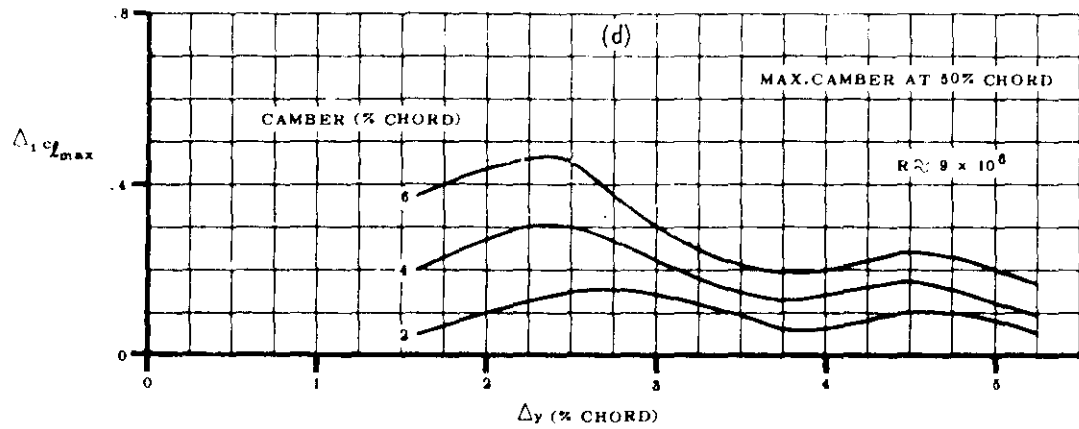


FIGURE 4.1.1.4-6 (Cont'd) EFFECT OF AIRFOIL CAMBER LOCATION AND AMOUNT ON SECTION MAXIMUM LIFT

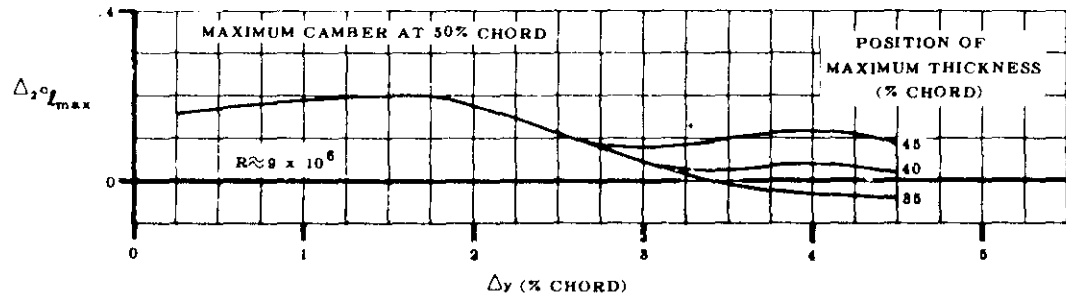


FIGURE 4.1.1.4-7a EFFECT OF POSITION OF MAXIMUM THICKNESS ON SECTION MAXIMUM LIFT

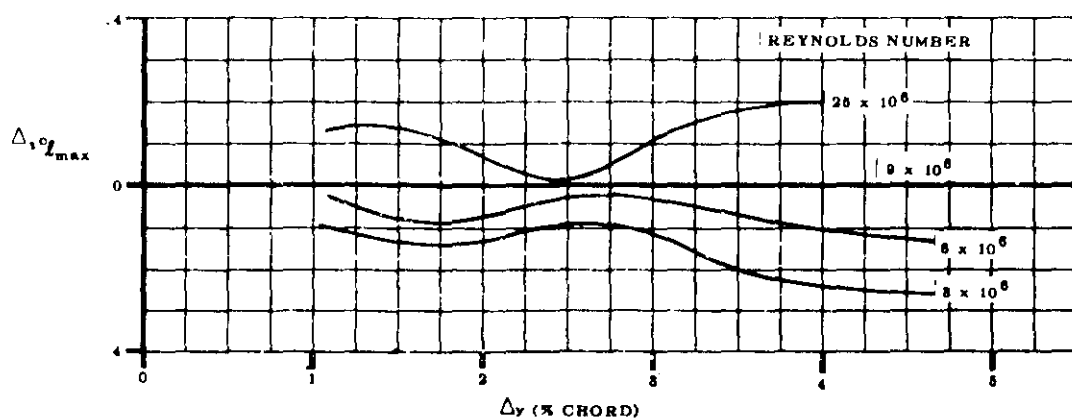


FIGURE 4.1.1.4-7b EFFECT OF REYNOLDS NUMBER ON SECTION MAXIMUM LIFT

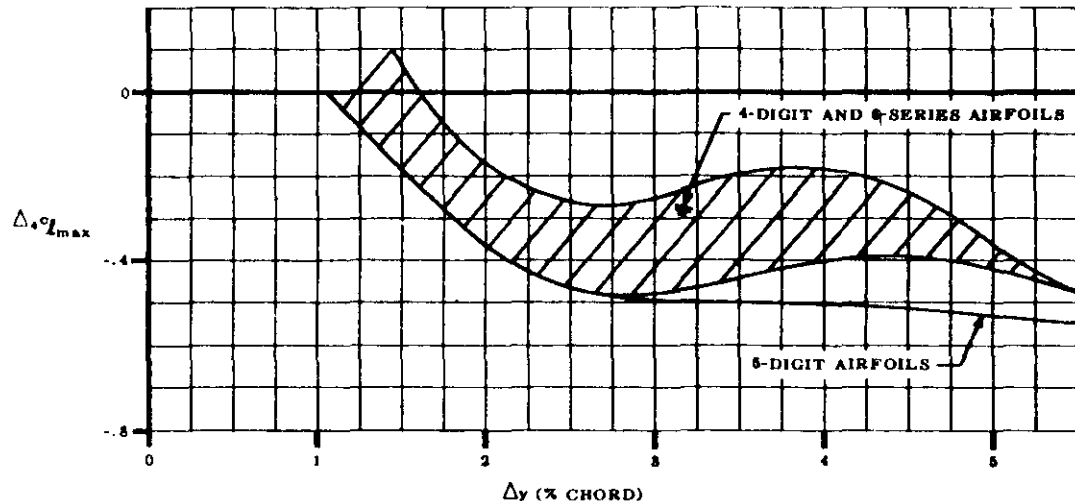


FIGURE 4.1.1.4-8a EFFECT OF NACA STANDARD ROUGHNESS ON SECTION MAXIMUM LIFT

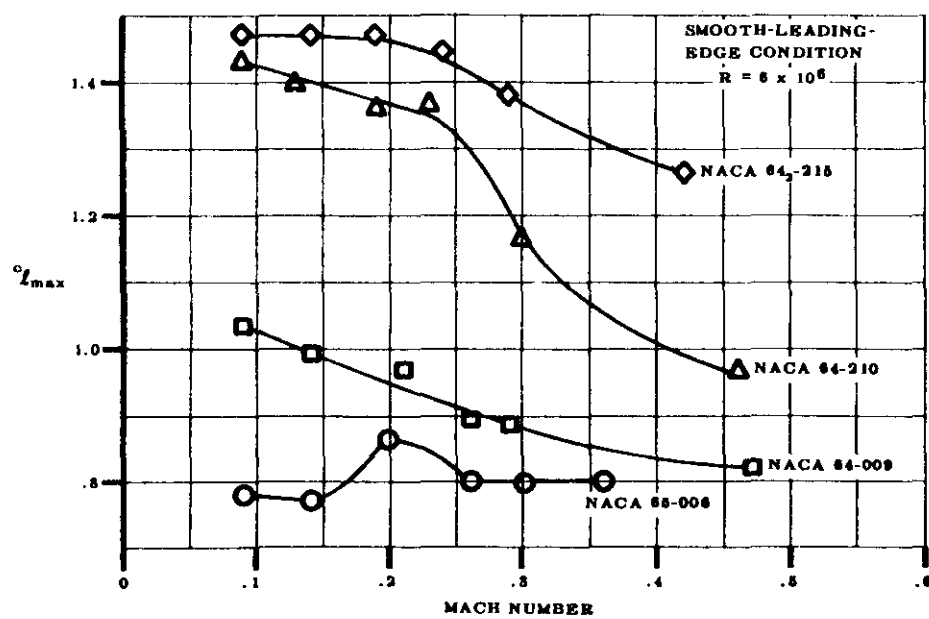


FIGURE 4.1.1.4-8b TYPICAL VARIATION OF SECTION MAXIMUM LIFT WITH FREE-STREAM MACH NUMBER

4.1.2 SECTION PITCHING MOMENT

4.1.2.1 SECTION ZERO-LIFT PITCHING MOMENT

The zero-lift pitching-moment coefficient is included for various NACA four- and five-digit and NACA 6-series airfoil sections in tables 4.1.1-A and 4.1.1-B. These data should be used wherever possible in preference to theoretical data in stability and control calculations.

These tables are applicable to Mach numbers below the critical. Above the critical Mach number, appreciable changes in zero-lift pitching moment may be present because of compressibility effects.

Additional section data may be located in the literature with the aid of table 4.1.1-C.

The theoretical pitching-moment coefficients of the various airfoil mean lines at the design lift coefficients are proportional to the section design lift coefficient or mean-line ordinate (camber) and may be scaled up or down as shown in the sample problems below or in table 4.1.1-D. Since the theoretical thin-airfoil aerodynamic center is at the quarter-chord point, the theoretical zero-lift pitching moment is identical to the theoretical pitching moment about the quarter-chord point at the design lift coefficient, shown in table 4.1.1-D.

Sample Problems

Example 1: Find the theoretical c_{m_0} about the quarter-chord point for the 2415 airfoil. Using the 64 mean line as a base, for which $c_{m_0} = -0.157$ (table 4.1.1-D), the required pitching-moment coefficient is

$$\begin{aligned} c_{m_0} &= -0.157 \times 2/6 \\ &= -0.052 \end{aligned}$$

The experimental value for this section is -.049 (table 4.1.1-A).

Example 2: Find the c_{m_0} about the quarter-chord point for the NACA 65₂-215, $a = 0.5$ airfoil. The design lift coefficient for this airfoil is 0.2. Using the 6-series mean line for $a = 0.5$, for which $c_{m_0} = -.139$ (table 4.1.1-D), gives the desired pitching-moment coefficient:

$$\begin{aligned} c_{m_0} &= -.139 \times .2 \\ &= -.028 \end{aligned}$$

4.1.2.2 SECTION PITCHING-MOMENT VARIATION WITH LIFT

A. SUBSONIC

The aerodynamic center of thin airfoil sections is theoretically located at the quarter-chord point. Experimentally, the aerodynamic-center location is a function of section thickness ratio and trailing-edge angle. Experimental data should always be used in preference to the theory.

The summary of experimental aerodynamic characteristics of various NACA four- and five-digit and 6-series airfoil sections given in tables 4.1.1-A and 4.1.1-B includes aerodynamic-center location.

Figure 4.1.2.2-3 presents the generalized aerodynamic center for the useful range of airfoil thickness ratios and trailing-edge angles. Trailing-edge angles, as defined on figure 4.1.2.2-3 are given for standard NACA airfoils in Section 2.2.1. A comparison of experimental data with results based on these charts is shown in table 4.1.2.2-A.

B. SUPERSONIC

Section pitching-moment variation with lift at supersonic speeds is primarily a function of section thickness, thickness distribution, and camber. For conditions where there is no flow separation, shock-expansion theory gives results that are in good agreement with experimental data.

At the higher angles of attack, especially for the thicker sections, flow separation takes place on the upper rear portion of the airfoil. Under these circumstances the experimental center of pressure is farther forward than that predicted by theory.

At very high angles of attack, the shock detaches from the section leading edge. The center of pressure then tends toward the 50-percent-chord point as the angle of attack increases toward 90°.

Figure 4.1.2.2-4 gives the position of the center of pressure for three airfoil sections as a function of Mach number, angle of attack, and thickness ratio. These results are calculated from shock-expansion theory (reference 1) and are strictly applicable only when the flow is everywhere attached.

REFERENCE

1. Handbook of Supersonic Aerodynamics, NAVORD Report 1488, Vol 8, Section 6, 1957. (U)

TABLE 4.1.2.2-A
AIRFOIL-SECTION AERODYNAMIC-CENTER POSITION
DATA SUMMARY AND SUBSTANTIATION

Airfoil Section	ϕ_{TR} (deg)	$X_{a.c.}$ Test	$X_{a.c.}$ Calc.	$\Delta X_{a.c.}$ (Calc.-Test)
2421	27.5	.261	.237	-.004
2424	31.4	.231	.232	+.001
4415	19.6	.245	.245	0
4418	23.6	.242	.242	0
4421	27.5	.238	.237	-.001
4424	31.4	.239	.232	-.007
63-615	4.8	.266	.268	+.002
63-018	5.7	.271	.271	0
63-418	5.7	.272	.271	-.001
63-021	6.6	.273	.274	+.001
63-221	6.6	.269	.274	+.005
64A010	10.5	.253	.253	0
64A215	15.8	.252	.252	0
64A212	13.6	.252	.251	-.001
64-006	2.3	.258	.257	-.001
64-009	3.5	.260	.262	+.002
64-012	4.6	.259	.265	+.006
64-015	5.8	.268	.267	-.001
64-018	6.9	.268	.269	+.001
64-021	8.1	.273	.272	-.001
65-006	2.9	.256	.256	0
65-015	7.2	.259	.265	+.006
65-021	10.1	.270	.269	-.001
66-006	5.6	.258	.253	-.005
66-015	9.3	.265	.262	-.003
66-021	13.0	.275	.265	-.010
23024	31.4	.231	.232	+.001
0006	7.9	.250	.249	-.001
1412	15.7	.250	.248	-.002
23012	15.7	.241	.248	+.007
23018	23.6	.241	.242	+.001
23021	27.5	.234	.237	+.003
23024	31.5	.223	.231	+.008
Average Error = $\frac{\sum \Delta X_{a.c.} }{n} = 0.003$				

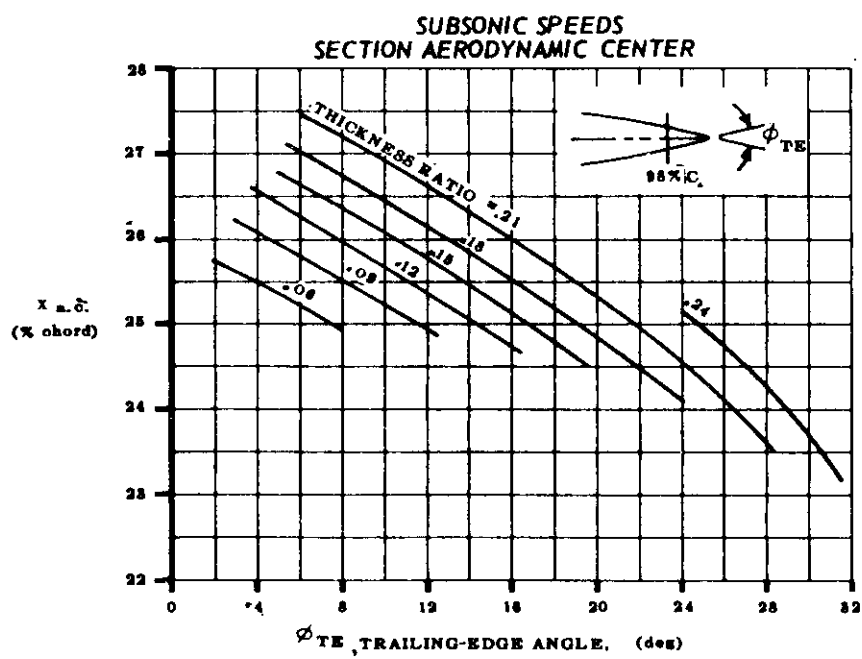


FIGURE 4.1.2.2-3 EFFECT OF TRAILING-EDGE ANGLE ON SECTION AERODYNAMIC-CENTER LOCATION

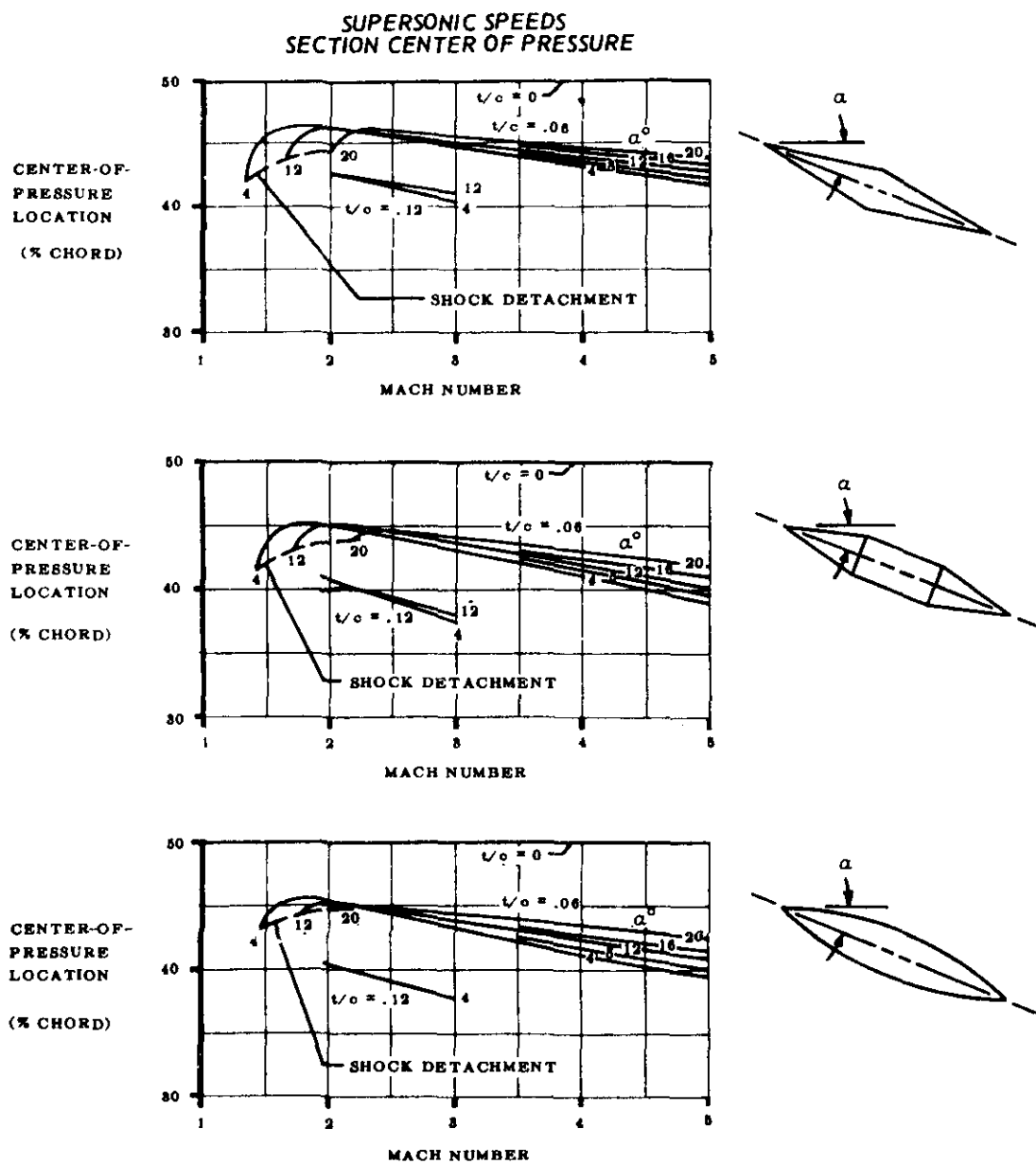


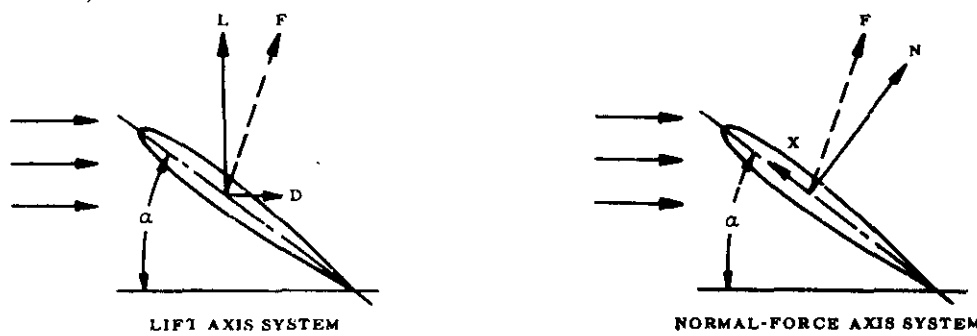
FIGURE 4.1.2.2-4 EFFECT OF THICKNESS AND ANGLE OF ATTACK ON CENTER OF PRESSURE LOCATION

4.1.3 WING LIFT

In the following group of Sections, (4.1.3.1 through 4.1.3.4), methods are presented for calculating the lift and normal force on wings at any angle of attack and any speed. An accurate determination of wing lift characteristics is important, since many other calculations are based on the wing-alone properties, e.g., all wing-body lift estimates and wing and wing-body rolling-moment calculations.

For this reason the approximations that are made in calculating wing lift in certain of the following Sections must be clearly understood in terms of their effect on the accuracy of the resulting numerical values.

The aerodynamic forces acting on a wing may be represented by a single force vector. This vector is conventionally resolved into two orthogonal components. The directions of the components are defined by the axis system selected. The two axis systems used most often are illustrated in the sketch below.



In the lift axis system, the force vector F is resolved into components perpendicular and parallel to the free stream. These components are called lift and drag, respectively. In the normal-force axis system, the force vector is resolved into components perpendicular to and parallel to the wing chord, called the normal force and the chord force, respectively.

The equations relating the lift, drag, normal-force, and chord-force coefficients are

$$C_N = C_L \cos \alpha + C_D \sin \alpha \quad 4.1.3-a$$

$$C_X = -C_D \cos \alpha + C_L \sin \alpha \quad 4.1.3-b$$

$$C_L = C_N \cos \alpha + C_X \sin \alpha \quad 4.1.3-c$$

$$C_D = C_N \sin \alpha - C_X \cos \alpha \quad 4.1.3-d$$

If the resultant force vector is nearly normal to the wing surface, the chordwise force component can be neglected and

$$F \approx N \quad X \approx 0 \quad 4.1.3-e$$

$$C_L \approx C_N \cos \alpha \quad 4.1.3-f$$

$$C_D \approx C_N \sin \alpha \quad 4.1.3-f$$

The resultant force vector is nearly normal to the wing surface for all low-aspect-ratio wings and for high-aspect-ratio wings at angles of attack beyond the stall at subsonic speeds. It is also nearly normal to the wing surface for all wings at supersonic speeds. However, for high-aspect-ratio wings at angles of attack below the stall, the resultant force vector is more nearly perpendicular to the free-stream direction than normal to the wing surface.

For purposes of continuity through the complete speed and angle-of-attack envelope it is convenient to introduce a pseudonormal force $C_{N'}$, defined by the equation

$$C_N' = \frac{C_L}{\cos \alpha} \quad 4.1.3\cdot g$$

As indicated by the discussion above, this C_N' is essentially the true normal force for all situations except that of high-aspect-ratio wings at angles of attack below the stall.

In the following Sections C_N' is used for C_N throughout. Sample problems in Section 4.1.3.3 show comparisons between experimental C_N values and calculated C_N' values, and between experimental and calculated C_L values for several configurations.

4.1.3.1 WING ZERO-LIFT ANGLE OF ATTACK

The method presented in this section is restricted to subsonic speeds. In the transonic and supersonic speed regimes it is suggested that reference be made to experimental data.

A. SUBSONIC

The effect of planform geometry on the zero-lift angle of attack of untwisted, constant-section wings is relatively small. Therefore, the method applied to such planforms is based on airfoil section properties.

For untwisted, constant-section wings the zero-lift angle of attack, taken from reference 1, is

$$(\alpha_0)_{\theta=0} = \alpha_i - \frac{c_{L_i}}{c_{L_\alpha}} \quad (\text{degrees}) \quad 4.1.3.1-a$$

where c_{L_i} , α_i , and c_{L_α} are the section design lift coefficient, angle of attack for design lift coefficient, and section lift-curve slope, respectively. These data may be obtained from Section 4.1.1.

Equation 4.1.3.1-a is applicable to swept wings if the airfoils are defined parallel to the free stream.

If definition of the airfoil section parallel to the free stream is not available for a particular swept wing, then α_0 may be approximated by

$$(\alpha_0)_{\theta=0} = \tan^{-1} \left[\frac{\tan (\alpha_0)_{\theta=0}}{\cos \Lambda} \right] \quad (\text{degrees}) \quad 4.1.3.1-b$$

where

Λ is the sweepback of some constant-percent chord line.

$(\alpha_0)_{\theta=0, \Lambda=0}$ is the zero-lift angle of attack of an untwisted, constant-section wing of zero-degree sweepback obtained by using equation 4.1.3.1-a. Values of c_{L_i} , α_i , and c_{L_α} used in equation 4.1.3.1-a are based on the airfoil section in a plane normal to the particular constant-percent chord line.

For wings with constant airfoil sections and linear twist, lifting-line theory may be used as in reference 2 to obtain α_0 as a function of planform geometry. This method uses the equation

$$\alpha_0 = (\alpha_0)_{\theta=0} + \left(\frac{\Delta \alpha_0}{\theta} \right) \theta \quad (\text{degrees}) \quad 4.1.3.1-c$$

where

$(\alpha_0)_{\theta=0}$ is the zero-lift angle of attack of the untwisted, constant-section wing, given by equation 4.1.3.1-a.

$\frac{\Delta\alpha_0}{\theta}$ is the change in wing zero-lift angle of attack due to a unit change in linear wing twist. This parameter is obtained from figure 4.1.3.1-4.

θ is the twist of the wing tip with respect to the root section, in degrees (negative for washout). A linear spanwise twist distribution is assumed (all constant-percent points of the local chords lie in straight lines along the span).

Test data have indicated that if the airfoil is cambered the zero-lift angle of attack varies with Mach number, particularly above the critical Mach number. A Mach number correction to be applied to cambered airfoils is presented as figure 4.1.3.1-5. This chart gives the ratio of the zero-lift angle of attack at any subsonic Mach number to the corresponding value at $M = 0.3$. This chart is based on the data of references 3, 4, and 5 and is to be considered as a first-order approximation only.

Unfortunately, there are not enough data to substantiate the theoretical results as applied to either untwisted or twisted wings. Consequently, experimental data should be used whenever possible.

Sample Problem

Given: An untwisted, constant-section wing.

$$A = 6.0 \quad \Lambda_{c/4} = 6.34^\circ \quad \lambda = 0.50 \quad \theta = 0$$

$$\text{NACA 23012 airfoil (streamwise)} \quad \frac{Y_{90}}{2} = 1.455 \quad \frac{Y_{99}}{2} = 0.265$$

$$\text{Low speed; } \beta = 1.0 \quad R_L = 1 \times 10^6 \text{ (based on MAC)}$$

Compute:

$$\left. \begin{array}{l} \alpha_i = 1.65^\circ \\ c_{l_i} = 0.30 \end{array} \right\} \quad (\text{table 4.1.1-D})$$

Determine c_{l_α} (Section 4.1.1.2)

$$\tan \frac{1}{2} \phi'_{TE} = \frac{\frac{Y_{90}}{2} - \frac{Y_{99}}{2}}{9} = \frac{1.455 - 0.265}{9} = 0.132$$

$$\frac{c_{l\alpha}}{(c_{l\alpha})_{\text{theory}}} = 0.760 \quad (\text{figure 4.1.1.2-8a})$$

$$(c_{l\alpha})_{\text{theory}} = 6.89 \text{ per rad} \quad (\text{figure 4.1.1.2-8b})$$

$$c_{l\alpha} = \frac{1.05}{\beta} \left[\frac{c_{l\alpha}}{(c_{l\alpha})_{\text{theory}}} \right] (c_{l\alpha})_{\text{theory}} \quad (\text{equation 4.1.1.2-a})$$

$$= \frac{1.05}{1.0} [0.760] (6.89) = 5.50 \text{ per rad}$$

$$= 0.096 \text{ per deg}$$

Solution:

$$(\alpha_0)_{\theta=0} = \alpha_i - \frac{c_{l_i}}{c_{l\alpha}} \quad (\text{equation 4.1.3.1-a})$$

$$= 1.65 - \frac{0.30}{0.096}$$

$$= -1.48 \text{ deg}$$

REFERENCES

1. Abbott, I. H., von Doenhoff, A. E., and Stivers, L. S., Jr.: Summary of Airfoil Data. NACA TR 824, 1946. (U)
2. DeYoung, J., and Harper, C. W.: Theoretical Symmetric Span Loading at Subsonic Speeds for Wings Having Arbitrary Plan Form. NACA TR 921, 1948. (U)
3. Graham, D. J.: The Development of Cambered Airfoil Sections Having Favorable Lift Characteristics at Supercritical Mach Numbers. NACA TR 947, 1949. (U)
4. Stack, J., and von Doenhoff, A. E.: Tests of 16 Related Airfoils at High Speeds. NACA TR 492, 1934. (U)
5. Johnson, B. H., Jr., and Shibata, H. H.: Characteristics Throughout the Subsonic Speed Range of a Plane Wing and of a Cambered and Twisted Wing, Both Having 45° of Sweepback. NACA RM A51D27, 1951. (U)

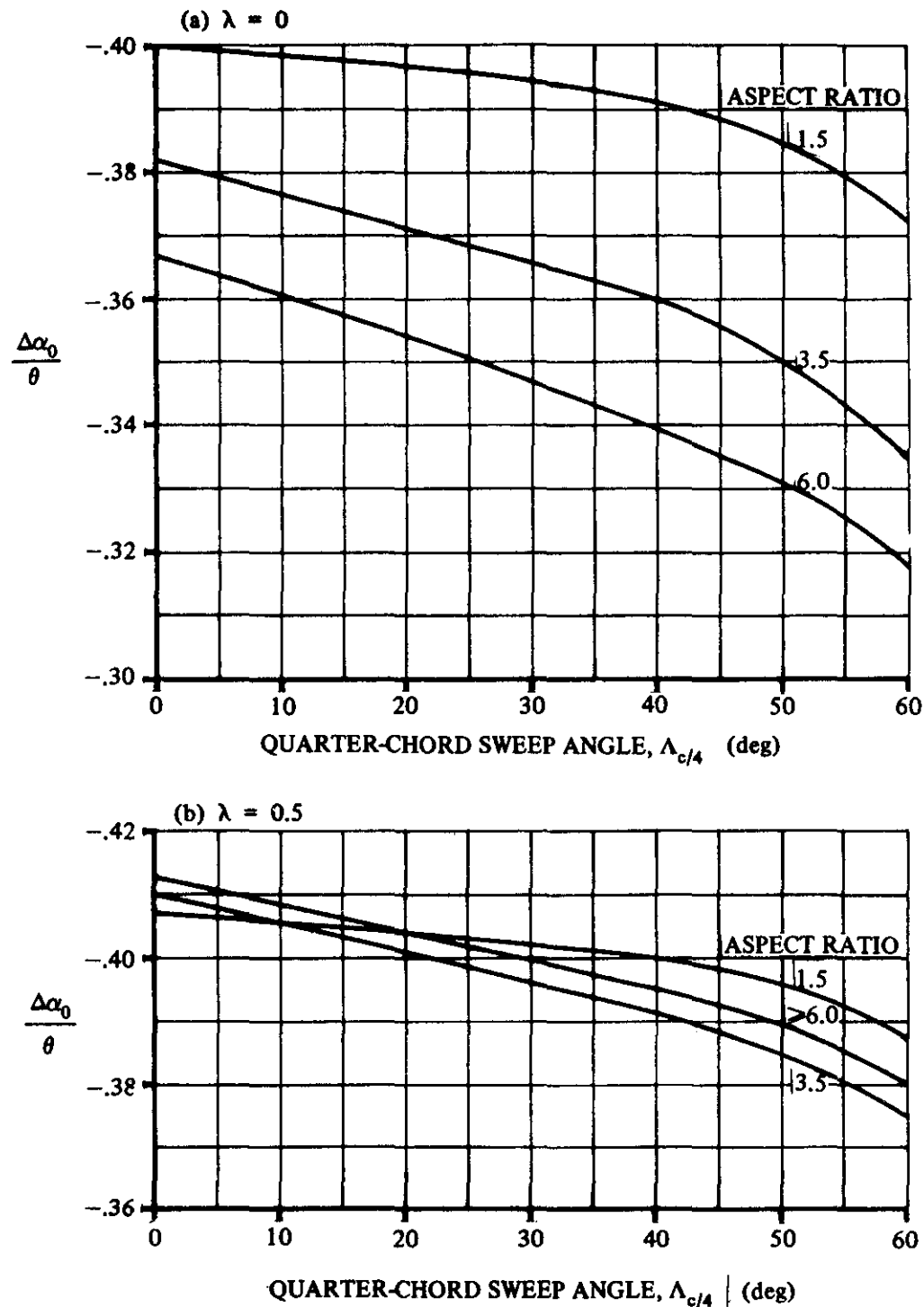


FIGURE 4.1.3.1-4 EFFECT OF LINEAR TWIST ON WING ANGLE OF ATTACK FOR ZERO LIFT

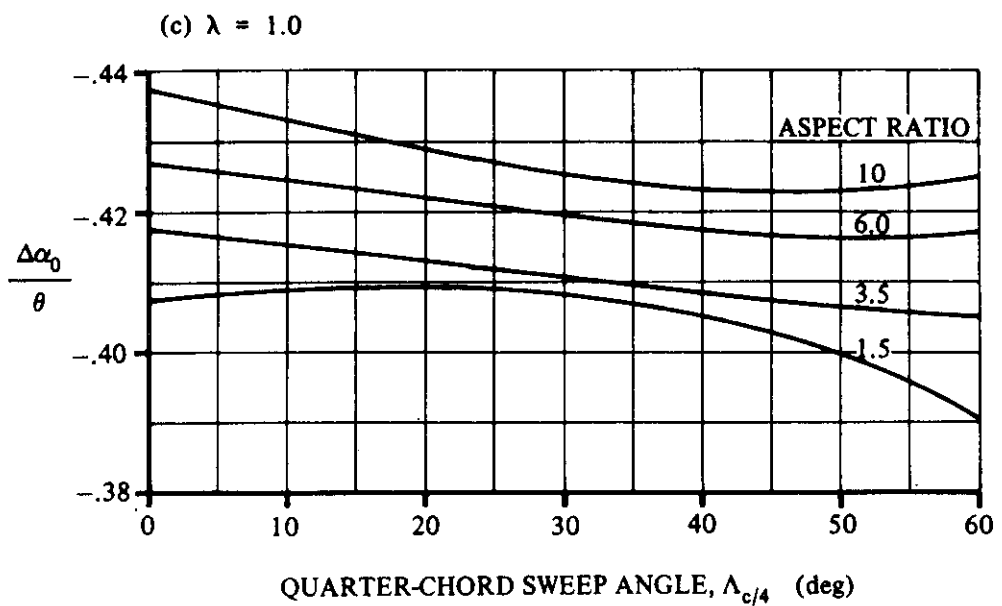


FIGURE 4.1.3.1-4 (CONTD)

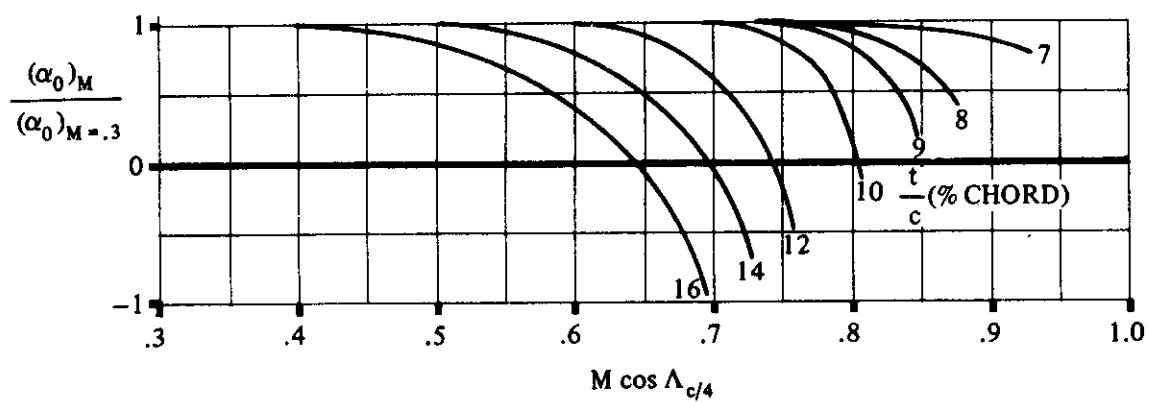


FIGURE 4.1.3.1-5 MACH NUMBER CORRECTION FOR ZERO-LIFT ANGLE OF ATTACK OF CAMBERED AIRFOILS

4.1.3.2 WING LIFT-CURVE SLOPE

The lift on a wing at angle of attack results from the distributed pressures over the surface of the wing. At subsonic speeds, most of the lift on a wing is derived from a region of low pressure on the upper surface near the leading edge. The magnitude and distribution of this pressure field is such that its integrated value over the wing surface results in a force vector that is very nearly perpendicular to the free-stream direction. This is the well-known lift-force vector. The rate of change of this vector with angle of attack is the lift-curve slope $dC_L/d\alpha$, usually written as $C_{L\alpha}$.

At supersonic speeds the pressure distribution over the wing is quite different. The pressure integration results in a force vector that is more nearly perpendicular to the wing-chord plane rather than to the free-stream direction. This is called the normal force and its variation with angle of attack in coefficient form is $dC_N/d\alpha$, or $C_{N\alpha}$.

For small angles of attack, $C_{L\alpha}$ is interchangeable with $C_{N\alpha}$. At higher angles of attack the distinction is important.

For finite, three-dimensional wings, the free-stream direction with reference to the wing local-airfoil sections is determined by the free-stream angle of attack decreased by the local induced angle of attack. The lift vector is tilted back by an angle equal to the local induced angle. This force vector can be resolved into two components – one perpendicular to and one parallel to the free-stream direction.

For high-aspect-ratio wings there is a certain justification in using $C_{L\alpha}$ as $C_{N\alpha}$ below stall angles, since the induced angle is small. For angles of attack beyond the stall, the total-force vector is essentially normal to the wing chord. For very low-aspect-ratio wings at high angles of attack, the induced effects are large and the local-force vector is tilted back through a large angle.

A. SUBSONIC

Theories for calculating the subsonic lift on three-dimensional wings fall into two general classes, lifting-surface theories and lifting-line theories. Lifting-surface theories, such as those of References 1 and 2, give highly accurate results for both wing lift and pitching moment. Since they are rather difficult to apply, however, they are usually reserved for detailed analyses of specific wings, particularly low-aspect-ratio wings, where the induced-camber and induced-angle-of-attack effects are important.

Lifting-line theories are widely used for calculating the lift-curve slopes of high-aspect-ratio wings, where chord-loading effects are less important. Certain modified lifting-line theories (References 3 and 4) give lift-curve slopes (but not pitching moments) that are quite accurate, even for very low aspect ratios. The explanation for this unexpected accuracy is given in Reference 5.

At subsonic speeds methods are presented for determining the lift-curve slope of the following two classes of wing planforms:

Straight-Tapered Wings (conventional, fixed trapezoidal wings)

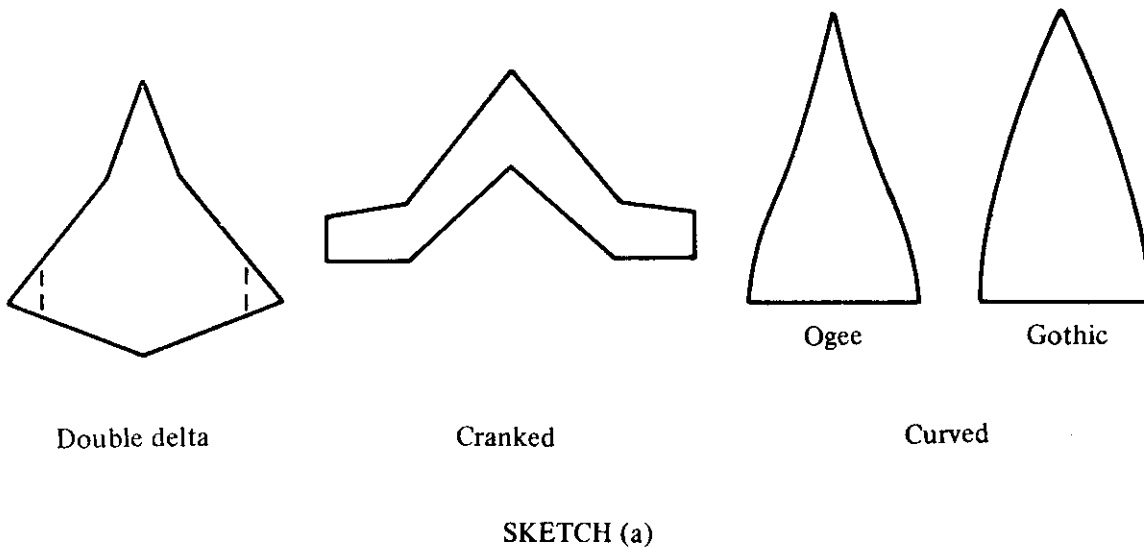
Non-Straight-Tapered Wings

Double-delta wings (composite wings with $A \approx 3$ or less)

Cranked wings (composite wings with $A \approx 3$ or greater)

Curved (Gothic and ogee) wings

These three general categories of non-straight-tapered wings are illustrated in Sketch (a), and their wing-geometry parameters are presented in Section 2.2.2.



Two separate methods are presented for straight-tapered wings. Method 1, taken from Reference 3, is applicable to the majority of configurations. In this method, the wing taper ratio has been eliminated as a parameter by the use of the midchord sweep angle rather than the conventional quarter-chord or leading-edge sweep angle. This permits a considerable simplification in the presentation of wing-lift-curve-slope information. Because of this simplification, the method of Reference 3 has been chosen for presentation in this section for estimating the lift-curve slope of straight-tapered wings. It gives results that agree with slender-wing theory (Reference 6) at very low aspect ratios and with two-dimensional section data at infinite aspect ratios.

Method 2, taken from Reference 7, is applicable only at $M = 0.2$ for highly swept, constant-section, low-aspect-ratio, delta or clipped-delta configurations with large thickness ratios; i.e., $0.10 \leq t/c \leq 0.30$. The unique feature of this method is its consideration of the vortex-induced lift. In contrast to the conventional constant lift-curve slope, this method allows for one or two breaks in the lift-curve slope to account more accurately for the vortex-induced lift contribution.

The lift-curve slopes of non-straight-tapered wings are treated in Reference 8. The planforms investigated include double delta, cranked, and curved (Gothic and ogee). Methods for predicting the lift-curve slope near zero lift for these planforms are based on the work of Spencer in Reference 9. This work consists of an extension of the results presented for conventional wings in Reference 3 to include wings having variation in sweep along the span. Since lift curves of double-delta and curved wings are considered nonlinear throughout the lift range, the lift-curve slope near zero lift is of little significance by itself. On the other hand, experimental results show

that the lift curves for cranked wings (defined as composite wings with aspect ratios approximately three or greater) exhibit a linear range up to approximately eight degrees angle of attack. Consequently, the method of Reference 9, as modified by an empirical correlation factor, is used for the prediction of $C_{L\alpha}$ for cranked wings with round-nosed airfoils.

DATCOM METHODS

Straight-Tapered Wings

Method 1

The three-dimensional lift-curve slope of conventional wings is presented in Figure 4.1.3.2-49 as a function of wing aspect ratio, midchord sweep angle, Mach number, and section (defined parallel to the free stream) lift-curve slope. The factor κ of Figure 4.1.3.2-49 is the ratio of the two-dimensional lift-curve slope (per radian) at the appropriate Mach number to $2\pi/\beta$; i.e., $(c_{L\alpha})_M / (2\pi/\beta)$. Section lift-curve slope (per degree) is obtained from Section 4.1.1.2.

A sweep-conversion formula is given in Section 2.2.2, from which the midchord sweep for any straight-tapered wing may be determined.

Application of the method is illustrated in the sample problem following the non-straight-tapered-wing methods of this paragraph, and in the sample problems following the straight-tapered-wing methods for transonic speeds in Paragraph B.

Method 2

This semiempirical method is taken from Reference 7, ignoring the small wing-planform nose-radius effects. The semiempirical method was developed by using the test results of Reference 7, correlated with the theoretical predictions based on lifting-surface theory. Because of its semiempirical nature, the method should be restricted to $M = 0.2$ conditions for highly swept, constant-section, low-aspect-ratio, delta or clipped-delta configurations with the following geometric characteristics:

$$0.58 \leq A \leq 2.55$$

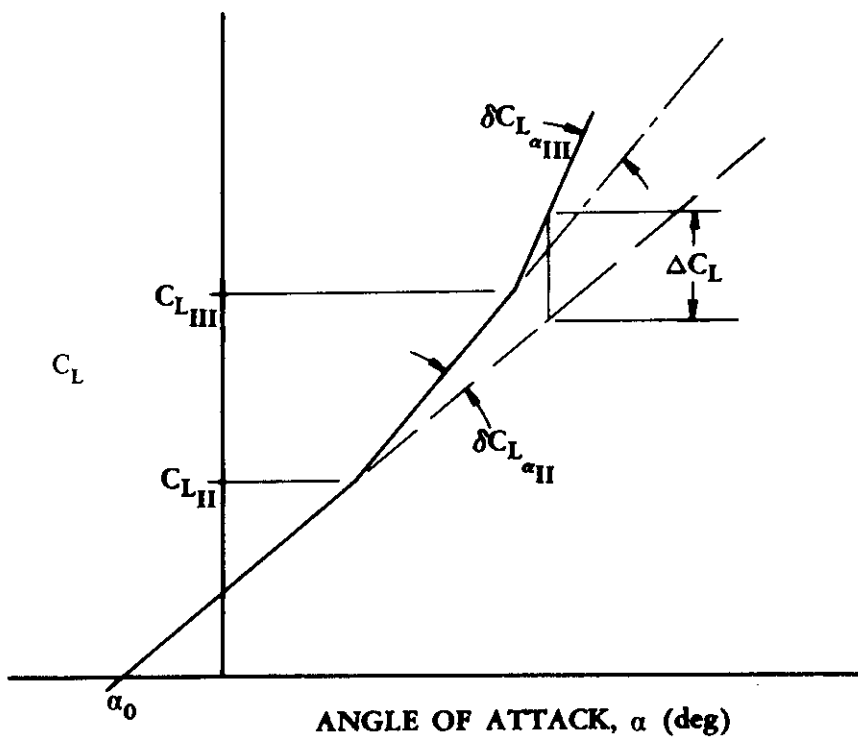
$$0 \leq \lambda \leq 0.3$$

$$63^\circ \leq \Lambda_{LE} \leq 80^\circ$$

$$0.10 \leq t/c \leq 0.30$$

$$\Lambda_{TE} = 0$$

The determination of the breaks in the lift-curve slope (C_{LII} and C_{LIII} in Sketch (b)), is contingent upon the availability of section upper-surface pressure data for the particular airfoil section being considered. In the method formulation of Reference 7, the pressure data were derived by means of a computer-program solution for the potential flow equations for two-dimensional incompressible flow, by the method of conformal transformation according to Imai (Reference 10). However, test data from Reference 11 or any other source of valid experimental data will satisfy the requirement.



SKETCH (b)

For round-nosed-planform configurations, the reader is referred to Reference 7, where three different planform nose-radius models were tested. Although a procedure was developed to account for the incremental nose-radius effects, it requires a computer-program lifting-surface theory as a basis.

The lift-curve slope for a low-aspect-ratio, delta or clipped-delta wing may be approximated by the following procedure:

Step 1. Determine the low-lift-region lift-curve slope uncorrected for thickness effects by

$$(C_{L\alpha})_{\text{theory}} = 8 \tan^{-1} \frac{\pi A}{16 + \pi A / (1 + 2 \lambda \tan \Lambda_{LE})} \quad 4.1.3.2-a$$

where

A is the wing aspect ratio.

λ is the wing taper ratio.

Λ_{LE} is the wing leading-edge sweep.

- Step 2.** Determine the low-lift-region lift-curve slope, based on the wing planform area, by correcting the theoretical value in Step 1 for thickness effects.

$$(C_{L\alpha})_{\text{basic}} = (C_{L\alpha})_{\text{theory}} \left[\frac{C_{L\alpha}}{(C_{L\alpha})_{\text{theory}}} \right] \quad 4.1.3.2-b$$

where

$(C_{L\alpha})_{\text{theory}}$ is from Step 1 above.

$\frac{C_{L\alpha}}{(C_{L\alpha})_{\text{theory}}}$ is from Figure 4.1.3.2-50a as a function of aspect ratio, taper ratio, and thickness ratio.

- Step 3.** Plot the maximum negative upper-surface section pressure coefficient C_{p_u} and its corresponding section lift coefficient c_l on Figure 4.1.3.2-50b for three or four different section lift coefficients. These pressure data are supplied by the user and may be theoretical or taken from a source of experimental data such as Reference 11. When a sufficient number of points have been plotted, fair a smooth line through the points. Now determine where the faired line intersects the value of $(C_{L\alpha})_{\text{theory}}$ as determined above in Step 1. The point of intersection determines the value of $C_{L_{II}}$, read on the abscissa scale of the figure. The value for $C_{L_{II}}$ is the lift coefficient where the vortex lift component necessitates the first change in the lift-curve slope (see Sketch (b)). The point of intersection also defines the maximum negative upper-surface section pressure coefficient C_{p_u} used in the next step.
- Step 4.** Plot the maximum negative upper-surface section pressure coefficient C_{p_u} versus its corresponding nondimensional chordwise location x/c . (These pressure data are supplied by the user as above in Step 3.) Read the chordwise location x/c corresponding to the value of C_{p_u} determined in Step 3.
- Step 5.** Determine the value of $C_{L_{III}}$ from Figure 4.1.3.2-51 as a function of taper ratio, sweep, thickness ratio, and the chordwise location of C_{p_u} . The value for $C_{L_{III}}$ is the lift coefficient where the vortex lift component necessitates a second change in the lift-curve slope (see Sketch (b)).
- Step 6.** Determine the value of $(C_{L\alpha})_{\text{limit}}$ from the following:

$$(C_{L\alpha})_{\text{limit}} = 0.0467 (\sin \Lambda_c)^{1/4} \text{ (per deg)} \quad 4.1.3.2-c$$

where

Λ_c is the complement of the leading-edge sweep angle Λ_{LE} ; i.e., $\Lambda_c = 90^\circ - \Lambda_{LE}$.

Step 7. Determine the incremental increase in lift-curve slope $\delta C_{L_{\alpha II}}$ starting at $C_{L_{II}}$ according to the following criteria:

If	Then
$(C_{L\alpha})_{\text{limit}} - (C_{L\alpha})_{\text{basic}} \geq 0.0067$	$\delta C_{L\alpha II} = 0.0067 \text{ per deg}$
$(C_{L\alpha})_{\text{limit}} - (C_{L\alpha})_{\text{basic}} < 0.0067$	$\delta C_{L\alpha II} = (C_{L\alpha})_{\text{limit}} - (C_{L\alpha})_{\text{basic}}$
$(C_{L\alpha})_{\text{limit}} \leq (C_{L\alpha})_{\text{basic}}$	$\delta C_{L\alpha II} = 0$

Step 8. Determine the total lift-curve slope in the region between $C_{L_{II}}$ and $C_{L_{III}}$ using

$$\left(C_{L_\alpha}\right)_{II} = \left(C_{L_\alpha}\right)_{basic} + \left(\delta C_{L_\alpha}\right)_{II} \quad 4.1.3.2-d$$

where

$(C_{L\alpha})_{\text{basic}}$ is from Step 2.

$(\delta C_{L_\alpha})_{II}$ is from Step 7.

Step 9. Determine the incremental increase in lift-curve slope δC_{L_aIII} starting at C_{LIII} according to the following criteria:

If	Then
$(C_{L\alpha})_{\text{limit}} - (C_{L\alpha})_{\text{basic}} > 0.012;$	$(\delta C_{L\alpha})_{\text{III}} = 0.012 \text{ per deg}$
$(C_{L\alpha})_{\text{limit}} - (C_{L\alpha})_{\text{basic}} < 0.012;$	$(\delta C_{L\alpha})_{\text{III}} = (C_{L\alpha})_{\text{limit}} - (C_{L\alpha})_{\text{basic}}$
$(C_{L\alpha})_{\text{limit}} \leq (C_{L\alpha})_{\text{basic}};$	$(\delta C_{L\alpha})_{\text{III}} = 0$

Step 10. Determine the total lift-curve slope in the region beyond $C_{L_{\infty}}$ using

$$\left(C_{L_a} \right)_{III} = \left(C_{L_a} \right)_{basic} + \left(\delta C_{L_a} \right)_{III} \quad 4.1.3.2-e$$

where

$(C_{L_\alpha})_{\text{basic}}$ is from Step 2.

$(\delta C_{L_\alpha})_{III}$ is from Step 9.

The entire lift-curve slope may now be constructed as shown in Sketch (b). (Note that the wing zero-lift angle of attack α_0 is determined by using Section 4.1.3.1.)

No substantiation of this method is possible because of the lack of low-aspect-ratio test data having wing thickness ratios of $0.10 \leq t/c \leq 0.30$. Application of this method is illustrated in the sample problem on Page 4.1.3.2-8.

Non-Straight-Tapered Wings

Double-Delta Wings

Although the lift-curve slope near zero lift of double-delta wings is of little significance by itself, this $C_{L\alpha}$ is used in the correlation of nonlinear lift of double-delta wings at subsonic speeds in Section 4.1.3.3.

This method, taken from Reference 9, consists of an extension of the method of Reference 3 by use of an effective value of $\cos \Lambda_{c/2}$, which is defined as the area-weighted average of the local value of $\cos \Lambda_{c/2}$.

The subsonic lift-curve slope of double-delta wings is obtained from the procedure outlined in the following steps:

Step 1. Divide the wing into n sections, each section being assumed to have constant sweep angles within its boundary. (See Section 2.2.2 for wing-geometry parameters.)

Step 2. Using the wing geometry determined in Step 1, obtain $(\cos \Lambda_{c/2})_{\text{eff}}$ by

$$(\cos \Lambda_{c/2})_{\text{eff}} = \frac{1}{S_W} \sum_{j=1}^{j=n} (\cos \Lambda_{c/2})_j S_j \quad 4.1.3.2-f$$

where

S_W is the total wing area.

j denotes one section of n sections having constant sweep angles within its boundary.

S_j is the total area of one section of n sections.

$(\cos \Lambda_{c/2})_j$ is the cosine of the sweep angle of the half-chord line of one section of n sections.

Step 3. Obtain the lift-curve slope by application of the method used to determine $C_{L\alpha}$ of straight-tapered wings, but with $(\Lambda_{c/2})_{\text{eff}}$ used in place of $\Lambda_{c/2}$ in the design chart (Figure 4.1.3.2-49).

Application of this technique is illustrated in the sample problem on Page 4.1.3.2-10.

Cranked Wings

The subsonic lift-curve slope of cranked wings with round-nosed airfoils is obtained by applying an empirical correlation to the method of Reference 9.

The equation for $C_{L\alpha}$ of cranked wings, taken from Reference 8, is

$$C_{L\alpha} = \left(C_{L\alpha} \right)_{\text{pred}} \frac{\left(C_{L\alpha} \right)_{\text{test}}}{\left(C_{L\alpha} \right)_{\text{pred}}} \quad 4.1.3.2-g$$

where

$\left(C_{L\alpha} \right)_{\text{pred}}$ is the lift-curve slope of the cranked wing, predicted by the method outlined above for the double-delta planform.

$\frac{\left(C_{L\alpha} \right)_{\text{test}}}{\left(C_{L\alpha} \right)_{\text{pred}}}$ is the empirical correlation factor of subsonic lift-curve slope for cranked wings. It is presented as a function of wing aspect ratio and Mach number in Figure 4.1.3.2-52. (All cranked wings analyzed in Reference 8 had round leading edges, and the use of Figure 4.1.3.2-52 is restricted accordingly.)

A comparison of test data for 12 configurations with $C_{L\alpha}$ of cranked wings having round-nosed airfoils calculated by this method is presented as Table 4.1.3.2-A (taken from Reference 8). The test data are for four wing-alone and eight wing-body configurations. Three of the wing-alone configurations have two breaks in the leading edge. Although no attempt has been made to define the effects of wing thickness ratio, poor accuracy generally results for $t/c > 0.09$. It should also be noted that the calculated accuracy deteriorates as Mach number exceeds 0.80. No configuration had a body-diameter-to-wing-span ratio greater than 0.147 and, consequently, the wing-body interference is considered to be negligible. It is suggested that this method be restricted to values of $M \leq 0.80$ and $t/c \leq 0.10$.

It is suggested that the subsonic lift-curve slope of cranked wings with sharp-nosed airfoils be obtained by direct application of the method outlined for double-delta planforms.

Curved Wings

No method is presented for estimating the subsonic lift-curve slope of curved wings because of their nonlinear lift characteristics.

Sample Problems

1. Method 2

Given: The following straight-tapered, constant-section, low-aspect-ratio, clipped-delta configuration.

$$A = 0.823$$

$$\lambda = 0.18$$

$$\Lambda_{LE} = 73.5^\circ$$

NACA 2412 airfoil

$$M = 0.2$$

Compute:

$$(C_{L\alpha})_{\text{theory}} = 8 \tan^{-1} \frac{\pi A}{16 + \pi A / (1 + 2\lambda \tan \Lambda_{LE})} \quad (\text{Equation 4.1.3.2-a})$$

$$= 8 \tan^{-1} \frac{0.823\pi}{16 + 0.823\pi / [1 + 2(0.18)(3.376)]}$$

$$= 1.195 \text{ per rad} = 0.0209 \text{ per deg}$$

$$\frac{1}{3+A} \left(\frac{1-\lambda}{1+2\lambda} \right)^2 = \frac{1}{3+0.823} \left[\frac{1-0.18}{1+2(0.18)} \right]^2 = 0.0951$$

$$\frac{C_{L\alpha}}{(C_{L\alpha})_{\text{theory}}} = 0.98 \quad (\text{Figure 4.1.3.2-50a})$$

$$(C_{L\alpha})_{\text{basic}} = (C_{L\alpha})_{\text{theory}} \frac{C_{L\alpha}}{(C_{L\alpha})_{\text{theory}}} \quad (\text{Equation 4.1.3.2-b})$$

$$= (0.0209)(0.98)$$

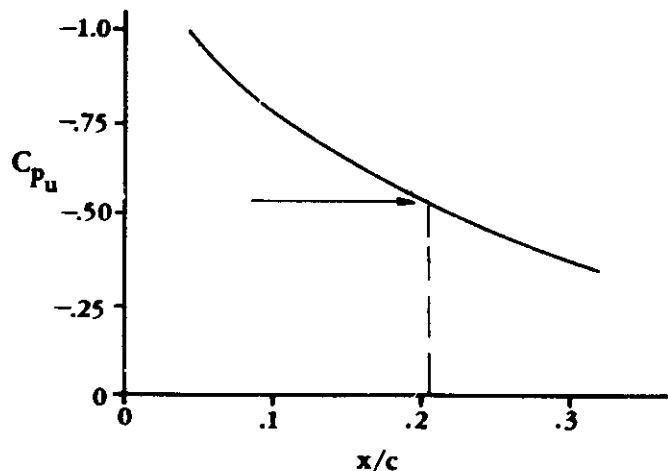
$$= 0.0205 \text{ per deg} \quad (\text{valid for } C_L < C_{LII})$$

The following pressure data for a NACA 2412 airfoil are (Reference 11):

c_x	C_{p_u}	x/c
0	-0.37	0.30
0.253	-0.56	0.19
0.5	-0.95	0.05

The above data are now plotted on Figure 4.1.3.2-50b. From Figure 4.1.3.2-50b we now obtain a value of 0.222 for C_{LII} at a value of -0.53 for C_{p_u} .

Plot C_{p_u} versus x/c



From the above plot $x/c = 0.204$ for $C_{p_u} = -0.53$.

$$\frac{x/c}{(1+\lambda)(1-x/c) \tan \Lambda_{LE}} = \frac{0.204}{(1+0.18)(1-0.204)(3.376)} = 0.0643$$

$C_{L_{III}} = 0.467$ (Figure 4.1.3.2-51)

$$\Lambda_c = 90^\circ - \Lambda_{LE} = 90^\circ - 73.5^\circ = 16.5^\circ$$

$$\begin{aligned} (C_{L\alpha})_{\text{limit}} &= 0.0467 (\sin \Lambda_c)^{1/4} \quad (\text{Equation 4.1.3.2-c}) \\ &= 0.0467 (\sin 16.5^\circ)^{1/4} \\ &= 0.0342 \text{ per deg} \end{aligned}$$

$$(C_{L\alpha})_{\text{limit}} - (C_{L\alpha})_{\text{basic}} = 0.0342 - 0.0205 = 0.0137$$

Since $0.0137 > 0.0067$, $(\delta C_{L\alpha})_{II} = 0.0067$ (Step 7)

$$\begin{aligned} (C_{L\alpha})_{II} &= (C_{L\alpha})_{\text{basic}} + (\delta C_{L\alpha})_{II} \quad (\text{Equation 4.1.3.2-d}) \\ &= 0.0205 + 0.0067 \\ &= 0.0272 \text{ per deg} \quad (\text{valid for } 0.222 \leq C_L \leq 0.467) \end{aligned}$$

Since $0.0137 > 0.012$, $\delta C_{L\alpha_{III}} = 0.012 \text{ per deg}$ (Step 9)

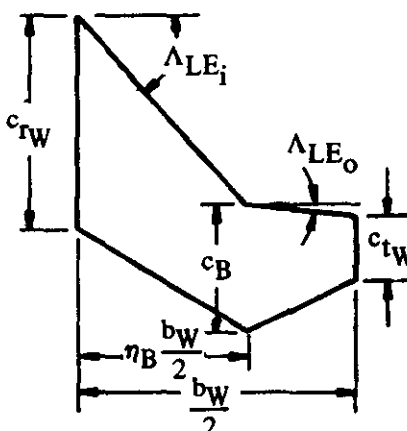
$$\begin{aligned} (C_{L\alpha})_{III} &= (C_{L\alpha})_{\text{basic}} + (\delta C_{L\alpha})_{III} \quad (\text{Equation 4.1.3.2-e}) \\ &= 0.0205 + 0.012 \\ &= 0.0325 \text{ per deg} \quad (\text{valid for } C_L > 0.467) \end{aligned}$$

Solution:

The entire lift curve can now be constructed assuming the wing zero-lift angle of attack α_0 has been determined using Section 4.1.3.1.

2. Non-Straight-Tapered Wings

Given: The cranked-wing planform of Reference 29. (See Section 2.2.2 for wing-planform geometry.)



$$\begin{aligned} A_W &= 4.0 & S_W &= 2.25 \text{ sq ft} & b_w/2 &= 18.0 \text{ in.} \\ \eta_B &= 0.6 & S_i &= 1.641 \text{ sq ft} & S_o &= 0.609 \text{ sq ft} \\ c_TW &= 13.85 \text{ in.} & c_B &= 8.03 \text{ in.} & c_TW &= 4.15 \text{ in.} \\ \lambda_W &= 0.30 & \lambda_i &= 0.58 & \lambda_o &= 0.517 \\ \Lambda_{LE_i} &= 48.6^\circ & \Lambda_{LE_o} &= 7.7^\circ & & \\ \Lambda_{c/2_i} &= 40.9^\circ & \Lambda_{c/2_o} &= -7.7^\circ & & \end{aligned}$$

Compute:

$$\begin{aligned}
 (\cos \Lambda_c/2)_{\text{eff}} &= \frac{1}{S_W} \sum_{j=1}^{j=n} (\cos \Lambda_c/2)_j S_j = \frac{1}{S_W} [(\cos \Lambda_c/2)_i S_i + (\cos \Lambda_c/2)_o S_o] \\
 &= \frac{1}{2.25} [(0.756)(1.641) + (0.991)(0.609)] = 0.820
 \end{aligned} \quad (\text{Equation 4.1.3.2-f})$$

$$(\Lambda_c/2)_{\text{eff}} = 34.9^\circ ; \tan(\Lambda_c/2)_{\text{eff}} = 0.6976$$

$$c_{L_\alpha} = 6.00 \text{ per rad (Section 4.1.1)}$$

$$c_{L_{\alpha_M}} = \frac{c_{L_\alpha}}{\beta} = \frac{6.00}{0.6} = 10.0 \text{ per rad}$$

$$\kappa = \frac{c_{L_{\alpha_M}}}{(2\pi/\beta)} = \frac{10.0(0.6)}{2\pi} = 0.955$$

$$\frac{A}{\kappa} [\beta^2 + \tan^2(\Lambda_c/2)_{\text{eff}}]^{\frac{1}{2}} = \frac{4.0}{0.955} [0.36 + 0.4866]^{\frac{1}{2}} = 3.85$$

$$\frac{(C_{L_\alpha})_{\text{pred}}}{A} = 1.00 \text{ per rad (Figure 4.1.3.2-49)}$$

$$(C_{L_\alpha})_{\text{pred}} = 4.00 \text{ per rad}$$

$$\beta A = (0.6)(4.0) = 2.40$$

$$\frac{(C_{L_\alpha})_{\text{test}}}{(C_{L_\alpha})_{\text{pred}}} = 1.081 \text{ (Figure 4.1.3.2-52)}$$

Solution:

$$\begin{aligned}
 C_{L_\alpha} &= (C_{L_\alpha})_{\text{pred}} \frac{(C_{L_\alpha})_{\text{test}}}{(C_{L_\alpha})_{\text{pred}}} \quad (\text{Equation 4.1.3.2-g}) \\
 &= (4.00)(1.081) \\
 &= 4.324 \text{ per rad} \\
 &= 0.0755 \text{ per deg}
 \end{aligned}$$

This compares with a test value of 0.075 per degree from Reference 29.

B. TRANSONIC

The transonic characteristics of wings are very difficult to predict. The current status of the problem is summarized in Reference 12. It is pointed out in this reference that although transonic theory gives results of surprisingly good accuracy in many cases, the mathematical difficulties in solving nonlinear partial differential equations of the mixed elliptic-hyperbolic type have limited its application to a few simple configurations.

On the other hand, wind-tunnel tests cover a wide variety of configurations but are of questionable accuracy because of wall-interference effects. These interference effects are both difficult to determine analytically and difficult to eliminate. Simply testing smaller models is not always sufficient, even in slotted-wall tunnels (Reference 12).

In spite of the uncertainties in test data, the straight-tapered-wing design charts of this section are based largely on experimental data from wind-tunnel tests. This is done because of certain important flow-separation effects not accounted for by theory and because of the limited scope of existing solutions for transonic theory. The limited experimental data for non-straight-tapered wings preclude development of design methods for those planforms at transonic speeds. However, a chart is presented that indicates the trend of transonic data for double-delta wings and for cranked wings with an aspect ratio of approximately three.

Thick, unswept, straight-tapered wings show increases in lift-curve slope with Mach number up to Mach numbers slightly beyond the critical. The slope then drops abruptly to a low value followed by a rise near Mach=1.0 to a value almost as high as the value at the critical Mach number (see Sketch (c), for type "A" wings). This behavior for two-dimensional sections is illustrated in References 13, 14, and 15. Reducing either the aspect ratio or the wing-thickness ratio or both reduces the magnitude of these effects. For very thin wings and for wings of very low aspect ratio these transonic nonlinearities do not exist (see Sketch (c) for type "B" wings). Increasing the sweep angle raises the wing critical Mach number. However, the increase is never as large as that predicted by simple sweep theory. Reference 16 shows that three-dimensional effects in the regions of the wing root and tip prevent the full benefits of sweep from being realized.

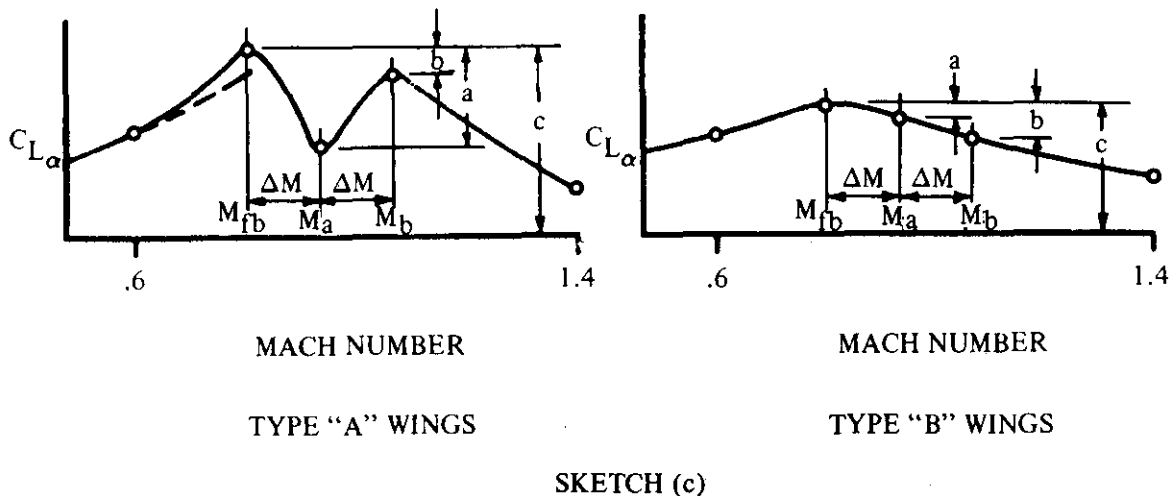
The transonic nonlinearities in lift-curve slope are related to the appearance of local shocks located asymmetrically on the upper and lower surfaces of the wing. Prediction of the exact shock-wave location is somewhat involved, since there is an interaction between the shocks on the upper and lower surfaces (Reference 17). Camber, thickness ratio, and thickness distribution all have pronounced effects on section transonic lift characteristics. Proper combination of the above geometric parameters can prevent transonic lift losses even for quite thick sections (Reference 18). Wings that do have large transonic lift losses at zero angle of attack show marked recovery at higher angles of attack (Reference 19).

DATCOM METHODS

Straight-Tapered Wings

The procedure for constructing the transonic lift-curve slope of conventional planforms is outlined in the following steps. In following this procedure, reference should be made to the schematic sketch below. The method is based on data for the untwisted and uncambered wings of References 19 and 47 through 51. These data are compared in Table 4.1.3.2-B with the values calculated from the charts.

The charts are limited to wings having symmetrical airfoils of conventional thickness distribution and are for zero angle of attack only.



- Step 1. Calculate the force-break Mach number M_{fb} . This is obtained from Figure 4.1.3.2-53a for zero wing sweep. A correction for sweep effects is provided by Figure 4.1.3.2-53b.
- Step 2. Compute the theoretical lift-curve slope at the force-break Mach number by the method of paragraph A.
- Step 3. The actual lift-curve slope at the force-break Mach number is found by means of the ratio $(C_{L\alpha})_{fb} / (C_{L\alpha})_{theory}$ obtained from Figure 4.1.3.2-54a.
- Step 4. The abrupt decrease in lift-curve slope above the force-break Mach number is described by the ratio a/c (see Sketch (c)). This ratio is given in Figure 4.1.3.2-54b. The Mach number M_a at which the lift-curve slope reaches its minimum value is

$$M_a = M_{fb} + 0.07$$

The lift-curve slope at M_a is

$$(C_{L\alpha})_a = \left(1 - \frac{a}{c}\right)(C_{L\alpha})_{fb}$$

For wings that do not exhibit large transonic lift losses (Sketch (c)), the lift-curve slope at M_a may still be obtained from the ratio a/c as given in Figure 4.1.3.2-54b. In all cases, c is the lift-curve slope at the force-break Mach number as obtained in Step 3.

- Step 5. The subsequent rise in $C_{L\alpha}$ (Sketch (b)) is given by the ratio b/c as presented in Figure 4.1.3.2-54c. The Mach number at this point is

$$M_b = M_{fb} + 0.14$$

The lift-curve slope is

$$(C_{L\alpha})_b = \left(1 - \frac{b}{c}\right) (C_{L\alpha})_{fb}$$

An identical procedure is used for wings of type "B."

- Step 6. The lift-curve slope at $M = 0.6$ is calculated by the straight-tapered-wing method of Paragraph A of this section.
- Step 7. The lift-curve slope at $M = 1.4$ is calculated by the straight-tapered-wing method of Paragraph C of this section.
- Step 8. The complete transonic lift-curve slope between Mach numbers 0.6 and 1.4 can now be constructed by fairing a curve through the points obtained by means of Steps 1 through 7.

Non-Straight-Tapered Wings

During the course of the program reported in Reference 8 an empirical correlation of the lift-curve slope of double-delta and cranked wings at $M = 1.0$ was achieved. This correlation is presented herein as Figure 4.1.3.2-55. It is suggested that it be used as a guide for fairing between subsonic and supersonic values of $C_{L\alpha}$ of composite wings with an aspect ratio of three or less.

The configurations used in the correlation vary in aspect ratio from 1.33 to 3.0. The inboard-panel sweepback is 78° for the lower correlation points and 60° for the upper correlation points. Spanwise positions of the leading-edge break η_B vary from approximately 0.30 to 0.70.

Sample Problems

1. Straight-Tapered Wing of Type "A."

Given: Wing tested in Reference 48.

$$A = 4.0 \quad \lambda = 1.0 \quad \Lambda_{LE} = 0 \quad \text{NACA } 63A010 \text{ airfoil}$$

Compute:

$$M_{fb} = 0.842 \text{ (Figure 4.1.3.2-53a)}$$

$$(C_{L\alpha})_{\text{theory}} \quad \text{at } M_{fb}$$

$$c_{\varrho_\alpha} = 6.02 \text{ per rad (Section 4.1.1)}$$

$$c_{\varrho_{\alpha_M}} = \frac{c_{\varrho_\alpha}}{\beta}$$

$$\kappa = \frac{c_{\varrho_{\alpha_M}}}{(2\pi/\beta)} = \frac{(c_{\varrho_\alpha}/\beta)}{(2\pi/\beta)} = \frac{c_{\varrho_\alpha}}{2\pi} = 0.958$$

$$\frac{A}{\kappa} \left[\beta_{fb}^2 + \tan^2 \Lambda_{c/2} \right]^{1/2} = \frac{4.0}{0.958} (0.291)^{1/2} = 2.25$$

$$\frac{(C_{L\alpha})_{\text{theory}}}{A} = 1.25 \text{ per rad (Figure 4.1.3.2-49)}$$

$$(C_{L\alpha})_{\text{theory}} = 5.0 \text{ per rad}$$

$$\frac{(C_{L\alpha})_{fb}}{(C_{L\alpha})_{\text{theory}}} = 0.96 \text{ (Figure 4.1.3.2-54a)}$$

$$(C_{L\alpha})_{fb} = 4.80 \text{ per rad}$$

$$\frac{a}{c} = 0.35 \text{ (Figure 4.1.3.2-54b)}$$

$$M_a = M_{fb} + 0.07 = 0.912$$

$$(C_{L\alpha})_a = \left(1 - \frac{a}{c}\right) (C_{L\alpha})_{fb} = 3.12 \text{ per rad}$$

$$\frac{b}{c} = 0.15 \text{ (Figure 4.1.3.2-54c)}$$

$$M_b = M_{fb} + 0.14 = 0.982$$

$$(C_{L\alpha})_b = \left(1 - \frac{b}{c}\right) (C_{L\alpha})_{fb} = 4.08 \text{ per rad}$$

$$(C_{L\alpha})_{M=0.6} \quad (\text{Paragraph A})$$

$$\frac{A}{\kappa} \left[\beta^2 + \tan^2 \Lambda_{c/2} \right]^{1/2} = \frac{4.0}{0.958} (0.64)^{1/2} = 3.34$$

$$\frac{(C_{L\alpha})_{M=0.6}}{A} = 1.065 \text{ per rad (Figure 4.1.3.2-49)}$$

$$(C_{L\alpha})_{M=0.6} = 4.26 \text{ per rad}$$

$$(C_{L\alpha})_{M=1.40} \quad (\text{Paragraph C})$$

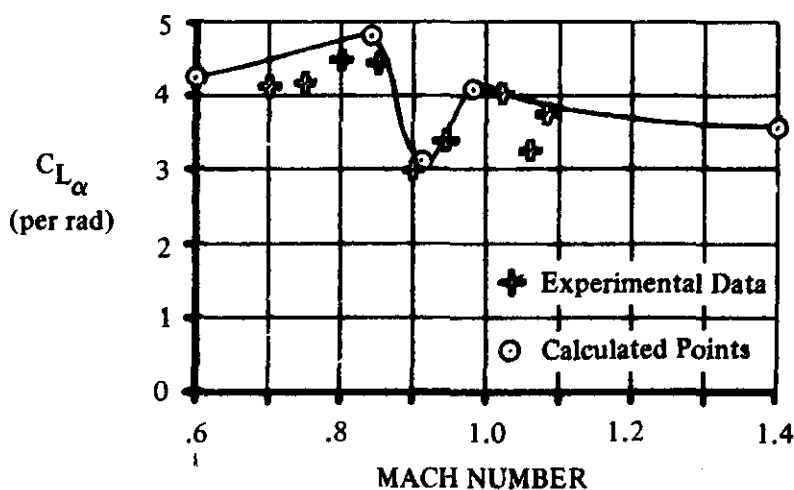
$$1/(\beta A) = 0.255$$

$$\beta C_{N\alpha} = 3.50 \text{ per rad (Figure 4.1.3.2-56g)}$$

$$(C_{N\alpha})_{M=1.4} = 3.57 \text{ per rad}$$

Solution:

The complete lift-curve slope as a function of Mach number may now be constructed as shown in the following diagram.



2. Straight-Tapered Wing of Type "B"

Given: Wing tested in Reference 47.

$$A = 2.67 \quad \lambda = 0.2 \quad \Lambda_{LE} = 45^\circ \quad \text{NACA 63A004 airfoil}$$

Compute:

$$(M_{fb})_{\Lambda=0} = 1.00 \text{ (Figure 4.1.3.2-53a)}$$

$$\Lambda_c/2 = 26.6^\circ$$

$$(M_{fb})_{\Lambda} = 1.00 \text{ (Figure 4.1.3.2-53b)}$$

$$(C_{L\alpha})_{\text{theory}} \text{ at } (M_{fb})_{\Lambda}$$

$$c_{q\alpha} = 6.47 \text{ per rad (Section 4.1.1.2)}$$

$$c_{q\alpha_M} = \frac{c_{q\alpha}}{\beta}$$

$$\kappa = \frac{c_{L\alpha_M}}{(2\pi/\beta)} = \frac{(c_{L\alpha}/\beta)}{(2\pi/\beta)} = \frac{c_{L\alpha}}{2\pi} = 1.03$$

$$\frac{A}{\kappa} \left[(\beta_{fb})^2 + \tan^2 \Lambda_{c/2} \right]^{1/2} = \frac{2.67}{1.03} (0.251)^{1/2} = 1.30$$

$$\frac{(C_{L\alpha})_{\text{theory}}}{A} = 1.435 \text{ per rad (Figure 4.1.3.2-49)}$$

$$(C_{L\alpha})_{\text{theory}} = 3.83 \text{ per rad}$$

$$\frac{(C_{L\alpha})_{fb}}{(C_{L\alpha})_{\text{theory}}} = 1.085 \text{ (Figure 4.1.3.2-54a)}$$

$$(C_{L\alpha})_{fb} = 4.16 \text{ per rad}$$

$$\frac{a}{c} = 0.005 \text{ (Figure 4.1.3.2-54b)}$$

$$M_a = M_{fb} + 0.07 = 1.07$$

$$(C_{L\alpha})_a = \left(1 - \frac{a}{c}\right) (C_{L\alpha})_{fb} = 4.14 \text{ per rad}$$

$$\frac{b}{c} = 0.075 \text{ (Figure 4.1.3.2-54c)}$$

$$M_b = M_{fb} + 0.14 = 1.14$$

$$(C_{L\alpha})_b = \left(1 - \frac{b}{c}\right) (C_{L\alpha})_{fb} = 3.85$$

$$(C_{L\alpha})_{M=0.6} \quad (\text{Paragraph A})$$

$$\frac{A}{\kappa} \left[\beta^2 + \tan^2 \Lambda_{c/2} \right]^{1/2} = \frac{2.67}{1.03} [0.64 + 0.251]^{1/2} = 2.45$$

$$\frac{(C_{L\alpha})_{M=0.6}}{A} = 1.22 \text{ per rad (Figure 4.1.3.2-49)}$$

$$(C_{L\alpha})_{M=0.6} = 3.26 \text{ per rad}$$

$$(C_{L\alpha})_{M=1.4} \quad (\text{Paragraph C})$$

$$\beta/\tan \Lambda_{LE} = 0.98; \quad A \tan \Lambda_{LE} = 2.67$$

$$\tan \Lambda_{LE} (C_{N\alpha})_{\text{theory}} = 3.55 \text{ per rad (Figure 4.1.3.2-56b)}$$

$$(C_{N\alpha})_{\text{theory}} = 3.55 \text{ per rad}$$

$$\Delta y = 0.88 \text{ (Figure 2.2.1-8)}$$

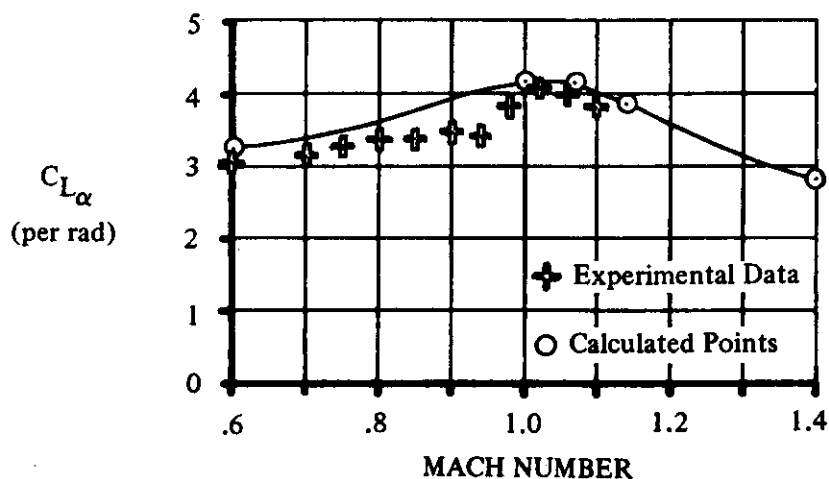
$$\Delta y_L = \frac{\Delta y}{\cos \Lambda_{LE}} = 1.245$$

$$\frac{C_{N\alpha}}{(C_{N\alpha})_{\text{theory}}} = 0.795 \text{ (Figure 4.1.3.2-60)}$$

$$(C_{N\alpha})_{M=1.4} = 2.82 \text{ per rad}$$

Solution:

The complete lift-curve slope as a function of Mach number may now be constructed as shown in the following diagram.



C. SUPERSONIC

Methods are presented for determining the wing normal-force-curve slope of the following two classes of wing planforms:

Straight-Tapered Wings (conventional, fixed trapezoidal wings)

Non-Straight-Tapered Wings

Double-delta wings

Cranked wings

Curved (Gothic and ogee) wings

These three general categories of non-straight-tapered wings are illustrated in Sketch (a) (paragraph A). Their wing-geometry parameters are presented in Section 2.2.2.

At supersonic speeds, the normal-force-curve slope C_{N_α} of conventional, double-delta, and cranked wings is adequately predicted by theoretical calculations except where the effects of thickness become important.

The design charts pertaining to these wing planforms are based on the following references:

Reference 20 – in the region of supersonic leading and trailing edges

Reference 21 – in the region of subsonic leading edges and supersonic trailing edges

Reference 22 – in the regions of tip-root interaction and tip-tip interaction

Reference 23 – in the region of subsonic leading and trailing edges

Reference 6 – for values of $A\beta \leq 1/4$ and $\sigma \leq 1.0$ where $\sigma = 1/4[A(1 + \lambda) \tan \Lambda_{LE}]$

References 24 and 25 – for values of $A\beta \leq 1/4$ and $\sigma \geq 1.0$

In addition, an empirically determined “lift-interference factor” from Reference 8 is applied to correlate the results for double-delta and cranked wings. The theoretical results are based on linear theory with the exception of the region where $A\beta \leq 1/4$, which is based on slender-wing theory. Thin airfoils have been assumed in these theories. Thickness effects are not important except for conditions where the Mach lines lie on or near the wing leading edge. Under these conditions the wing-leading-edge shock position is displaced forward from its theoretical position by the finite thickness effects of the leading edge. This displacement results in substantial losses in normal-force-curve slope.

For straight-tapered wings with sharp leading edges, the airfoil nose semiwedge angle (measured perpendicular to the wing leading edge) determines the shock position relative to the wing and hence the normal-force-curve slope. Experimental data indicate that the parameter corresponding to the nose semiwedge angle of the supersonic airfoil is $\Delta y / \cos \Lambda_{LE}$, where Δy is the difference between the upper-surface ordinates expressed in percent chord at the 6-percent- and 0.15-percent-chord stations (Figure 2.2.1-8). This is the same Δy discussed in Section 4.1.3.4 with regard to

airfoil maximum lift. It can be shown that for double-wedge and biconvex airfoils there is a linear relationship between Δy and the leading-edge semiwedge angle, given by

$$\Delta y_{\perp} = 5.85 \tan \delta_{\perp}$$

where

$$\Delta y_{\perp} = \frac{\Delta y}{\cos \Lambda_{LE}}$$

and δ_{\perp} is the semiwedge angle normal to the leading edge. Either δ_{\perp} or Δy_{\perp} , whichever is more convenient, may be used to calculate thickness effects for straight-tapered wings with sharp-nosed airfoils.

Figure 4.1.3.2-60 presents the leading-edge-thickness effect on the normal-force-curve slope of straight-tapered wings in the form of a ratio of actual normal-force-curve slope to theoretical normal-force-curve slope. This chart is empirically derived from the experimental data of Reference 26 of this section and References 11 through 17, 26, and 45, of Section 4.1.3.3.

For double-delta and cranked wings empirical correlation factors for round-nosed and sharp-nosed airfoils (from Reference 8) are applied, which account for leading-edge effects.

The method presented for determining the normal-force-curve slope of curved (Gothic and ogee) wings consists of a semiempirical correlation based on the theoretical results of Squire in Reference 27.

Because of the nonlinear nature of the normal-force curve at high angles of attack, the methods presented for estimating $C_{N\alpha}$ are limited to low angles of attack.

Wings with inverse taper ($\lambda > 1$) have not been considered. Wings with swept-forward leading edges are included through the use of the reversibility theorem (Reference 28). The reversibility theorem states that the normal-force-curve slope of the wing in forward flight equals the normal-force-curve slope of the same wing in reverse flight at the same Mach number.

DATCOM METHODS

Straight-Tapered Wings

The supersonic normal-force-curve slope of conventional wings is obtained as outlined in the following steps:

- Step 1. Obtain the theoretical normal-force-curve slope from Figures 4.1.3.2-56a through 4.1.3.2-56f, except for rectangular wings. The theoretical normal-force-curve slope for rectangular wings must be obtained from Figure 4.1.3.2-56g. These charts should be used for $M \geq 1.4$. For Mach numbers less than 1.4 the transonic method of Paragraph B should be used.
- Step 2. For wings approaching the sonic-leading-edge condition, the theoretical $C_{N\alpha}$ value obtained from Step 1 should be multiplied by the empirical thickness correction factor from Figure 4.1.3.2-60.

Non-Straight-Tapered Wings

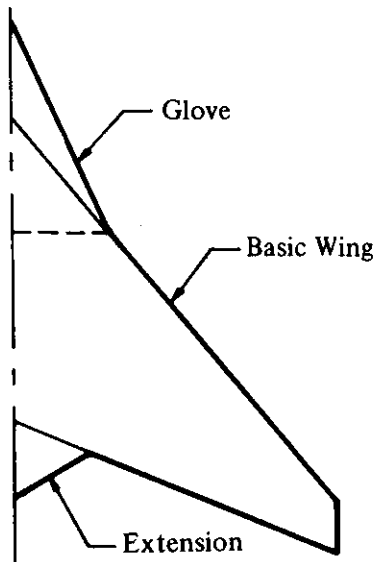
Double-Delta Wings

This method, taken from Reference 8, uses the linear-theory design charts of the straight-tapered-wing method with appropriate empirical correction factors. Application of the method requires that the wing planform be broken down as follows (see Sketch (d)):

Basic Wing — the outboard leading and trailing edges extended to the center line.

Glove — a delta wing superimposed over the basic wing. The glove leading edge is that of the inboard panel.

Extension — that portion of the wing behind the trailing edge of the basic wing for wings with broken trailing edges.



SKETCH (d)

The method is applicable to double-delta wings having breaks in the leading- and/or trailing-edge sweep at only one spanwise station.

The normal-force-curve slope of the total wing is

$$C_{N\alpha} = K_L \left[\left(C_{N\alpha} \right)_{bw} \frac{S_{bw}}{S_w} \left(C_{LE} \right)_{bw} + \left(C_{N\alpha} \right)_g \frac{S_g}{S_w} \left(C_{LE} \right)_g + \left(C_{N\alpha} \right)_E \frac{S_E}{S_w} \right] \quad 4.1.3.2-h$$

where

K_L is an empirically derived "lift-interference factor" obtained from Figure 4.1.3.2-61.

$$\frac{S_{bw}}{S_w}, \frac{S_g}{S_w}, \frac{S_E}{S_w}$$

are the ratios of the areas of the basic wing, glove, and trailing-edge extension, respectively, to the total wing area. (See Section 2.2.2 for wing-geometry parameters.)

$$(C_{N\alpha})_{bw}, (C_{N\alpha})_g$$

are the normal-force-curve slopes of the basic wing and glove, respectively.

$(C_{N\alpha})_{bw}$ is obtained from Figures 4.1.3.2-56a through 4.1.3.2-56f.
 $(C_{N\alpha})_g$ is obtained from either Figure 4.1.3.2-56a or Figure 4.1.3.2-63.

$$(C_{LE})_{bw}, (C_{LE})_g$$

are empirically derived “leading-edge-effect factors” obtained from Figure 4.1.3.2-62 as functions of Mach number and the respective planform leading-edge sweepback.

$$(C_{N\alpha})_E$$

is the normal-force-curve slope of the trailing-edge extension, shown schematically in Sketch (e), and is given by

$$(C_{N\alpha})_E = \frac{(C_{N\alpha})_1 \frac{S_1}{S_w} - (C_{N\alpha})_2 \frac{S_2}{S_w}}{S_E/S_w} \quad 4.1.3.2-i$$

where

$$(C_{N\alpha})_1$$

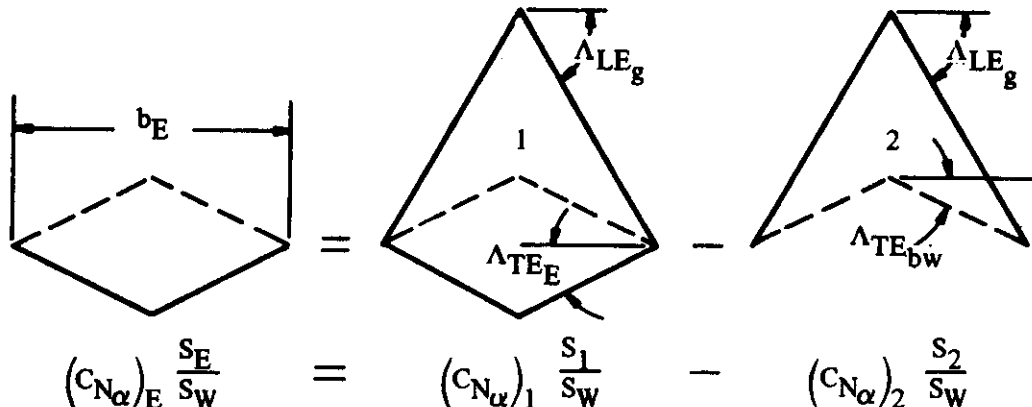
is the normal-force-curve slope of a zero-taper-ratio wing with $\Lambda_{LE} = \Lambda_{LEg}$ and $\Lambda_{TE} = \Lambda_{TE_E}$, obtained from Figure 4.1.3.2-56a or Figure 4.1.3.2-63.

$$(C_{N\alpha})_2$$

is the normal-force-curve slope of a zero-taper-ratio wing with $\Lambda_{LE} = \Lambda_{LEg}$ and $\Lambda_{TE} = \Lambda_{TE_{bw}}$, obtained from Figure 4.1.3.2-56a or Figure 4.1.3.2-63.

$$\frac{S_1}{S_w}, \frac{S_2}{S_w}$$

are the ratios of the areas of the two zero-taper planforms to the total wing area.



SKETCH (e)

It is recommended that Figure 4.1.3.2-63 be used to obtain the normal-force-curve slopes of the zero-taper-ratio wings rather than Figure 4.1.3.2-56a because of the upper limit of the parameter $A \tan \Lambda_{LE}$ of Figure 4.1.3.2-56a. The use of Figure 4.1.3.2-63 is very convenient since the normal-force-curve slope is presented in the form $C_{N\alpha}/A$, which eliminates the necessity of calculating the area of each individual panel.* All that is required to solve Equation 4.1.3.2-i is the total wing planform area S_w and the span b_E of the trailing-edge extension. Using values of $C_{N\alpha}/A$ from Figure 4.1.3.2-63, Equation 4.1.3.2-i becomes

$$\left(C_{N\alpha}\right)_E \frac{S_E}{S_w} = \left[\left(\frac{C_{N\alpha}}{A}\right)_1 - \left(\frac{C_{N\alpha}}{A}\right)_2 \right] \frac{b_E^2}{S_w} \quad 4.1.3.2-j$$

Application of this method is illustrated in Sample Problem 1 on Page 4.1.3.2-29.

A comparison of test data for 26 configurations with $C_{N\alpha}$ of double-delta wings calculated by this method is presented as Table 4.1.3.2-C (taken from Reference 8). All but two of the configurations listed in the table are wing-body combinations. All predictions were made by using the theoretical planform (leading and trailing edges extended to the center line) for the total planform area and neglecting body effects. No configuration had a ratio of body diameter to wing span greater than 0.15; consequently, the wing-body interference is considered to be negligible. The wing-thickness-ratio range covered (0.02 to 0.07) is consistent with current practice and no significant effects of wing thickness ratio are evident.

It should be noted that the maximum error generally occurs on wing-body configurations with large inboard sweep angles ($\Lambda_{LE_i} > 78^\circ$). This can conceivably result from two sources. Configurations with large inboard sweep have a large portion of the theoretical glove planform submerged in the body, making the assumption of negligible wing-body interference effects less valid; and the "leading-edge-effect factors" presented in Figure 4.1.3.2-62 are not well defined for sharp-nosed airfoils at low values of $\beta/\tan \Lambda_{LE}$.

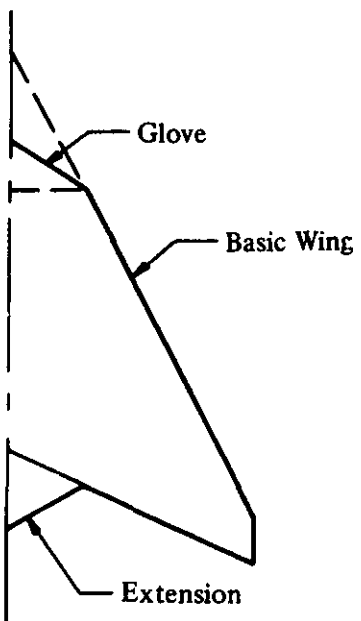
It is recommended that this method be restricted to the Mach-number range, $1.2 \leq M \leq 3.0$. For $M = 1.0$ the empirical correlation presented in Paragraph B should be used.

Another class of double-delta wings of practical interest are those with the outboard wing sweep greater than the inboard wing sweep. No configuration with $\Lambda_{LE_o} > \Lambda_{LE_i}$ was analyzed during the investigation reported in Reference 8; however, a method of approach for treating such configurations is suggested.

Defining the basic-wing breakdown as before results in some additional basic-wing area created forward of the wing sweep break as illustrated in Sketch (f).

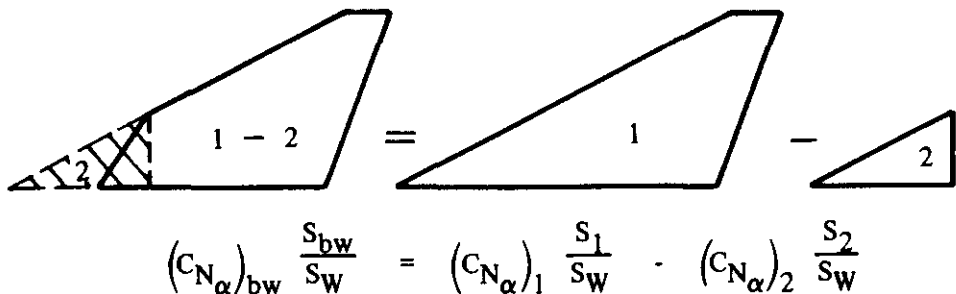
*Figure 4.1.3.2-63 may also be applied with equal facility to obtain normal-force-curve slope of the glove. Using $(C_{N\alpha}/A)_g$ from Figure 4.1.3.2-63

$$(C_{N\alpha})_g \frac{S_g}{S_w} = \left(\frac{C_{N\alpha}}{A}\right)_g \frac{b_g^2}{S_w}$$



SKETCH (f)

For this class of double-delta wings the normal-force-curve slope of the basic wing is determined by extending the basic-wing leading edge to the configuration center line, calculating the normal-force-curve slope of the extended basic-wing panel, and calculating and subtracting the normal-force-curve slope of the section of the basic-wing panel forward of the wing sweep break. This is shown schematically in Sketch (g).



SKETCH (g)

Based on this definition of the normal-force-curve slope of the basic wing, the total wing normal-force-curve slope is given by Equation 4.1.3.2-h with the "lift-interference factor" K_L replaced by K .

$$C_{N\alpha} = K \left[(C_{N\alpha})_{bw} \frac{S_{bw}}{S_w} (C_{LE})_{bw} + (C_{N\alpha})_g \frac{S_g}{S_w} (C_{LE})_g + (C_{N\alpha})_E \frac{S_E}{S_w} \right] \quad 4.1.3.2-k$$

where

K is an empirical correlation factor which corresponds to the "lift-interference factor" K_L . Not enough force data are available to allow correlation of this parameter; however, based on a limited amount of experimental rolling-moment data, K appears to be approximately one.

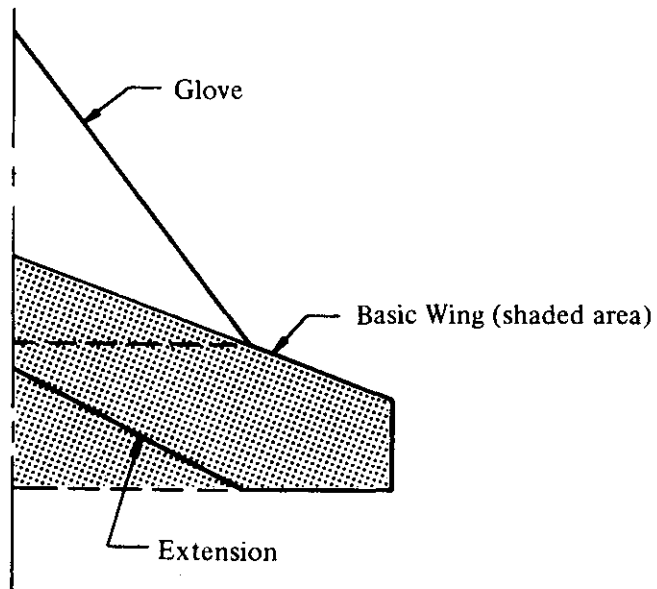
The remaining parameters are defined as before.

Although not enough data are available to substantiate application of the foregoing analysis to double-delta planforms with $\Lambda_{LE_o} > \Lambda_{LE_i}$, it can be concluded that the method will become less valid for wings employing sharp-nosed airfoils and large outboard sweep angles, since the "leading-edge-effect factors" are not well defined for wings with sharp-nosed airfoils at low values of $\beta/\tan \Lambda_{LE}$.

Application of this method is illustrated in Sample Problem 2 on Page 4.1.3.2-32.

Cranked Wings

The method used to predict the normal-force-curve slope of double-delta wings is also applicable to cranked wings. However, for cranked wings with broken trailing edges the inboard trailing-edge sweep angle may be greater than the outboard trailing-edge sweep angle. Since the basic wing is defined as in the double-delta wing breakdown, this results in some additional area being created behind the inboard trailing edge as illustrated in Sketch (h).



Cranked wing with $\Lambda_{TE_i} > \Lambda_{TE_o}$

SKETCH (h)

This additional area is considered to be the trailing-edge extension. Defining $(C_{N\alpha})_1$ and $(C_{N\alpha})_2$ exactly as for the double-delta wing results in a negative normal-force-curve increment for the trailing-edge extension.

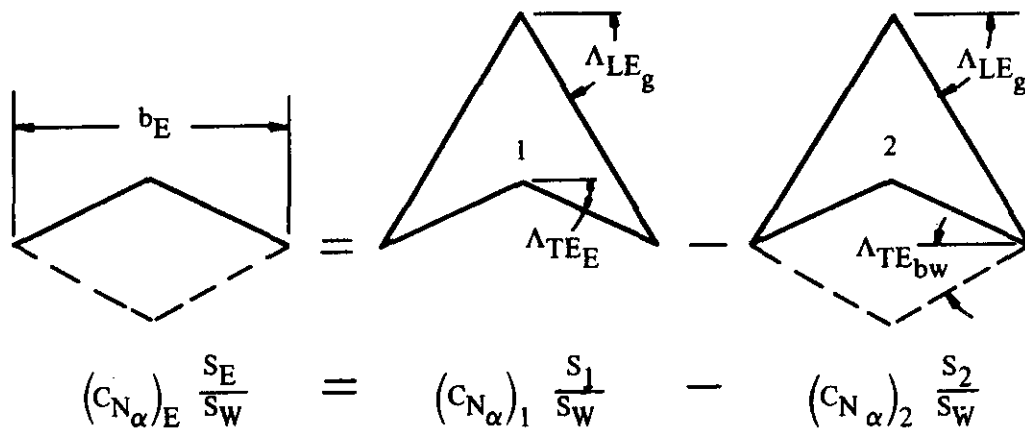
This method is applicable to cranked wings having breaks in the leading- and/or trailing-edge sweep at only one spanwise station.

The normal-force-curve slope of the total wing is given by Equation 4.1.3.2-h; i.e.,

$$C_{N\alpha} = K_L \left[(C_{N\alpha})_{bw} \frac{S_{bw}}{S_w} (C_{LE})_{bw} + (C_{N\alpha})_g \frac{S_g}{S_w} (C_{LE})_g + (C_{N\alpha})_E \frac{S_E}{S_w} \right]$$

where all the parameters are defined under Equation 4.1.3.2-h of the double-delta-wing method.

The normal-force-curve slope of the trailing-edge extension for the case where the inboard trailing-edge sweep angle is greater than the outboard trailing-edge sweep angle is shown schematically in Sketch (i).



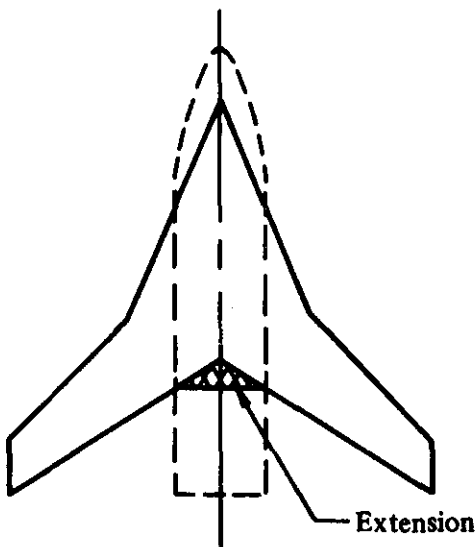
SKETCH (i)

Application of this technique is illustrated in Sample Problem 3 on Page 4.1.3.2-34.

A comparison of test data for seven configurations with $C_{N\alpha}$ of cranked wings calculated by this method is presented as Table 4.1.3.2-D (taken from Reference 8). The configurations listed in the table are either wing-body combinations or wing-body combinations with nacelles included in the body. The inboard leading-edge sweep angles are generally lower than those on the double-delta wings, which would tend to alleviate the body effects on the glove discussed under the

double-delta-wing method. The wing thickness-ratio range covered (0.02 to 0.08) is consistent with current practice and no significant effects of wing thickness ratio are evident.

Five of the configurations had small ratios of body diameter to wing span and the predictions for those configurations were based on the theoretical planform extended to the body center line. The configurations of References 65 and 66 had nacelles included in the body, and an effective extension was included as part of the planform as shown in Sketch (j). Since the definition of the extension was somewhat arbitrary, this technique should not be considered as a general wing-body prediction technique.



SKETCH (j)

Although all the configurations investigated had round-nosed airfoils, the application of the method to cranked wings with sharp-nosed airfoils should give equally good results except in the low supersonic Mach-number range. The "leading-edge-effect factors" are not well defined for sharp-nosed airfoils at low values of $\beta/\tan \Lambda_{LE}$ and must be considered as a possible source of error at low supersonic Mach numbers.

It is recommended that this method be restricted to the Mach number range, $1.2 < M < 3.0$. For $M = 1.0$ the empirical correlation presented in Paragraph B can be used for cranked wings with aspect ratios of approximately three.

Curved Wings

This method, taken from Reference 8, is based on the theoretical results of Squire in Reference 27.

The supersonic normal-force-curve slope of curved (Gothic and ogee) planforms is obtained from the procedure outlined in the following steps:

Step 1. Using the given wing geometry calculate the aspect ratio A , the planform shape parameter p , and the wing slenderness parameter $b_w/(2\ell)$. (See Section 2.2.2 for wing-geometry parameters.)

Step 2. At the desired value of $\frac{\beta b_w}{2\ell}$ obtain $\left(\frac{C_{N_\alpha}}{A}\right) \left(\frac{1+p}{p}\right)$ from Figure 4.1.3.2-64.

Step 3. Calculate the supersonic normal-force-curve slope by

$$C_{N_\alpha} = \left[\left(\frac{C_{N_\alpha}}{A} \right) \left(\frac{1+p}{p} \right) \right] A \left(\frac{p}{1+p} \right) \quad 4.1.3.2-t$$

Application of this method is illustrated in Sample Problem 4 on Page 4.1.3.2-36.

A comparison of test data for 18 configurations with C_{N_α} of curved wings calculated by this method is presented as Table 4.1.3.2-E (taken from Reference 8). Four of the configurations listed in the table are wing-body combinations with small ratios of body diameter to wing span. The calculations for these configurations were made by using the theoretical planform extended to the body center line and neglecting body effects. All models employed thin wings ($0.008 \leq t/c \leq 0.06$) with sharp leading edges.

The method provides satisfactory results for low supersonic Mach numbers and may be applied over the Mach number range, $1.0 \leq M \leq 3.0$.

On some ogee-wing-body configurations the leading-edge sweep becomes very large near the wing-body juncture. For such configurations, unrealistic values of p will be obtained if "good engineering judgment" is not exercised in extending the planform to the center line. The error that could result is illustrated by the somewhat analogous cases of wings W_1 , W_4 , and W_7 of Reference 79 (see Table 4.1.3.2-E). These configurations are ogee wings with very slender apexes and, consequently, low values of p . It is believed that the slender apex behaves more as a body than as part of the lifting surface. For these wings the method underestimates the normal-force-curve slope from 6.5 to 21.7 percent.

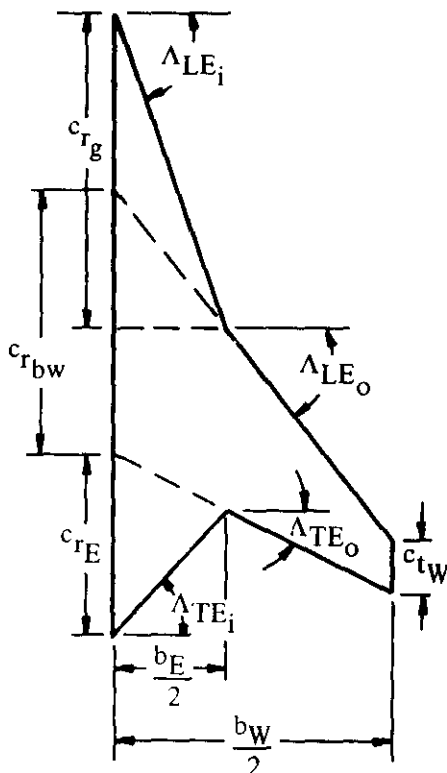
The calculated results for the configuration of Reference 81 are as much as 22 percent in error. However, the model is a sonic-design, blended wing-body configuration with unusual bumps in the wing surface near the wing-body juncture, and it is suspected that the bumps significantly affect the pressure distribution at supersonic speeds. It is significant that at subsonic speeds, test data for this configuration correlate quite well with the predicted lift at angle of attack (see results for Reference 43 in Table 4.1.3.3-D).

The authors of Reference 8 note that moderately low-aspect-ratio wings ($1.5 \leq A \leq 3.0$) have linear lift-curve slopes up to approximately eight degrees angle of attack at supersonic speeds. However, the low-aspect-ratio-wing ($A \leq 1.3$) data of Reference 79 show a break in the lift curve at approximately two degrees angle of attack. Unfortunately, the program reported in Reference 8 did not include an investigation of the supersonic wing-lift variation with angle of attack for irregular-shaped wings.

Sample Problems

1. Double-Delta Wing

Given: Double-delta wing of Reference 58.



Total Wing

$$A_W = 2.42 \quad \lambda_W = 0.086 \quad b_W = 24.0 \text{ in.}$$

$$\Lambda_{LE_i} = 70.67^\circ \quad \Lambda_{LE_o} = 51.63^\circ$$

$$S_W = 238 \text{ sq in.} \quad \eta_B = 0.40$$

$$\Lambda_{TE_i} = -47.37^\circ \quad \Lambda_{TE_o} = 26.62^\circ$$

Basic Wing

$$A_{bw} = 3.50 \quad \lambda_{bw} = 0.20 \quad S_{bw} = 164.6 \text{ sq in.}$$

$$\Lambda_{LE_{bw}} = \Lambda_{LE_o} = 51.63^\circ \quad \Lambda_{TE_{bw}} = \Lambda_{TE_o} = 26.62^\circ$$

Glove

$$A_g = 1.402 \quad \lambda_g = 0 \quad \Lambda_{LEg} = \Lambda_{LEi} = 70.67^\circ \quad S_g = 65.7 \text{ sq in.}$$

Extension

$$\frac{b_E}{2} = \eta_B \frac{b_W}{2} = 4.8 \text{ in.} \quad \Lambda_{TE_E} = \Lambda_{TE_i} = -47.37^\circ$$

Additional Characteristics:

$$\text{Sharp-nosed airfoil} \quad M = 2.01; \beta = 1.744$$

Compute:

$$(C_{N\alpha})_{bw}$$

$$\tan \Lambda_{LE_{bw}}/\beta = 0.724; (A \tan \Lambda_{LE})_{bw} = 4.421$$

$$\beta(C_{N\alpha})_{bw} = 4.24 \text{ per rad (Figure 4.1.3.2-56b)}$$

$$(C_{N\alpha})_{bw} = 2.43 \text{ per rad}$$

$$\beta/\tan \Lambda_{LE_{bw}} = 1.38$$

$$(C_{LE})_{bw} = 0.993 \text{ (Figure 4.1.3.2-62)}$$

$(C_{N\alpha})_g$ (Since $\lambda = 0$, either Figure 4.1.3.2-56a or 4.1.3.2-63 can be used.) (See footnote on Page 4.1.3.2-23.)

$$\beta/\tan \Lambda_{LE_g} = 0.612; (A \tan \Lambda_{LE})_g = 3.99$$

$$\tan \Lambda_{LE_g} (C_{N\alpha})_g = 4.90 \text{ per rad (Figure 4.1.3.2-56a)}$$

$$(C_{N\alpha})_g = 1.72 \text{ per rad}$$

$$(C_{LE})_g = 0.995 \text{ (Figure 4.1.3.2-62)}$$

$$(C_{N\alpha})_E \frac{S_E}{S_W} \text{ (use Figure 4.1.3.2-63)}$$

$$\beta/\tan \Lambda_{LE_1} = \beta/\tan \Lambda_{LE_g} = 0.612$$

$$\frac{\tan \Lambda_{TE_1}}{\tan \Lambda_{LE_1}} = \frac{\tan \Lambda_{TE_E}}{\tan \Lambda_{LE_g}} = -0.381$$

$$\left(\frac{C_{N\alpha}}{A}\right)_1 = 1.58 \text{ (Figure 4.1.3.2-63)}$$

$$\beta/\tan \Lambda_{LE_2} = \beta/\tan \Lambda_{LE_g} = 0.612$$

$$\frac{\tan \Lambda_{TE_2}}{\tan \Lambda_{LE_2}} = \frac{\tan \Lambda_{TE_{bw}}}{\tan \Lambda_{LE_g}} = 0.176$$

$$\left(\frac{C_{N\alpha}}{A}\right)_2 = 1.07 \text{ per rad (Figure 4.1.3.2-63)}$$

$$(C_{N\alpha})_E \frac{s_E}{s_W} = \left[\left(\frac{C_{N\alpha}}{A}\right)_1 \cdot \left(\frac{C_{N\alpha}}{A}\right)_2 \right] \frac{b_E^2}{s_W} \text{ (Equation 4.1.3.2-j)}$$

$$= (1.58 - 1.07) \frac{(9.6)^2}{238}$$

$$= 0.197 \text{ per rad}$$

$$\frac{1}{\beta} (C_{N\alpha})_g \frac{s_g}{s_W} = \frac{1}{1.744} (1.72) \left(\frac{65.7}{238}\right) = 0.272$$

$$K_L = 0.830 \text{ (Figure 4.1.3.2-61)}$$

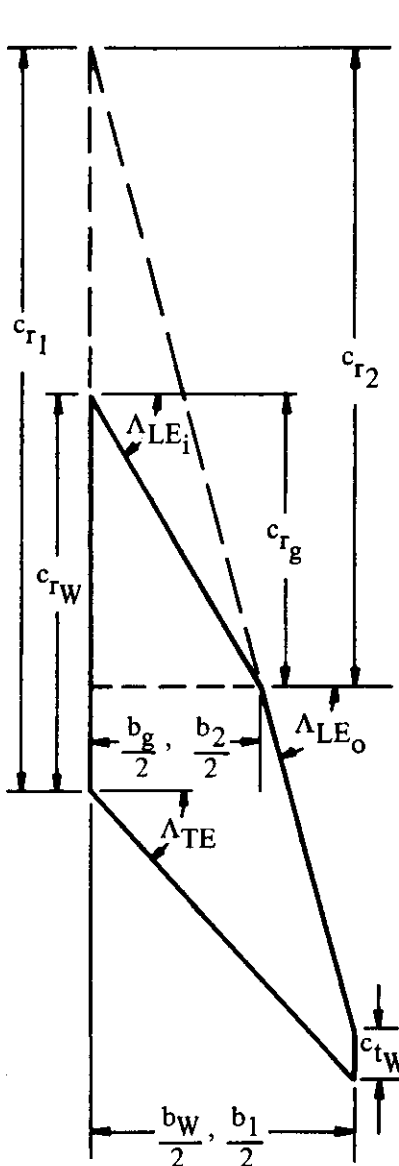
Solution:

$$\begin{aligned} C_{N\alpha} &= K_L \left[(C_{N\alpha})_{bw} \frac{s_{bw}}{s_W} (C_{LE})_{bw} + (C_{N\alpha})_g \frac{s_g}{s_W} (C_{LE})_g + (C_{N\alpha})_E \frac{s_E}{s_W} \right] \text{ (Equation 4.1.3.2-h)} \\ &= 0.830 \left[(2.43) \left(\frac{164.6}{238}\right) (0.993) + (1.72) \left(\frac{65.7}{238}\right) (0.995) + 0.197 \right] \\ &= 0.830 [1.670 + 0.472 + 0.197] \\ &= 1.941 \text{ per rad} \\ &= 0.0339 \text{ per deg} \end{aligned}$$

This compares with a test value of 0.0351 per degree from Reference 58.

2. Double-Delta Wing ($\Lambda_{LE_o} > \Lambda_{LE_i}$)

Given: The double-delta wing of Reference 75. Configuration has no trailing-edge extension.



Total Wing

$$A_w = 1.86 \quad \lambda_w = 0.130$$

$$\Lambda_{LE_i} = 60^\circ \quad \Lambda_{LE_o} = 75^\circ$$

$$S_w = 275.9 \text{ sq in.} \quad \eta_B = 0.654$$

$$\Lambda_{TE} = 47.5^\circ$$

Glove

$$\frac{S_g}{S_w} = 0.346 \quad \lambda_g = 0 \quad \Lambda_{LE_g} = \Lambda_{LE_i} = 60^\circ$$

$$A_g = 2.31$$

Extended Planforms

$$\frac{S_1}{S_w} = 1.405 \quad \lambda_1 = 0.0698$$

$$\Lambda_{LE_1} = \Lambda_{LE_o} = 75^\circ$$

$$A_1 = 1.327$$

$$\frac{S_2}{S_w} = 0.745 \quad \lambda_2 = 0$$

$$\Lambda_{LE_2} = \Lambda_{LE_o} = 75^\circ$$

$$A_2 = 1.072$$

Additional Characteristics

Sharp-nosed airfoil $M = 3.71; \beta = 3.573$

Compute:

$$(C_{N\alpha})_g$$

$$\tan \Lambda_{LE_g} / \beta = 0.485; (A \tan \Lambda_{LE})_g = 4.0$$

$$\beta(C_{N\alpha})_g = 4.0 \text{ (Figure 4.1.3.2-56a)}$$

$$(C_{N\alpha})_g = 1.12 \text{ per rad}$$

$$\beta/\tan \Lambda_{LE_g} = 2.06$$

$$(C_{LE})_g = 1.03 \text{ (Figure 4.1.3.2-62)}$$

$$(C_{N\alpha})_{bw} \frac{S_{bw}}{S_W}$$

$$(C_{N\alpha})_l$$

$$\beta/\tan \Lambda_{LE_1} = 0.957; (A \tan \Lambda_{LE})_1 = 4.94$$

$$\tan \Lambda_{LE_1} (C_{N\alpha})_l = 4.40 \text{ per rad (Figures 4.1.3.2-56a through -56c, interpolated)}$$

$$(C_{N\alpha})_l = 1.179 \text{ per rad}$$

$$(C_{N\alpha})_2$$

$$\beta/\tan \Lambda_{LE_2} = 0.957; (A \tan \Lambda_{LE})_2 = 4.0$$

$$\tan \Lambda_{LE_2} (C_{N\alpha})_2 = 4.08 \text{ (Figure 4.1.3.2-56a)}$$

$$(C_{N\alpha})_2 = 1.093 \text{ per rad}$$

$$(C_{N\alpha})_{bw} \frac{S_{bw}}{S_W} = (C_{N\alpha})_1 \frac{S_1}{S_W} \cdot (C_{N\alpha})_2 \frac{S_2}{S_W}$$

$$= (1.179) (1.405) \cdot (1.093) (0.745)$$

$$= 0.842 \text{ per rad}$$

$$\beta/\tan \Lambda_{LE_{bw}} = 0.957$$

$$(C_{LE})_{bw} = 0.94 \text{ (Figure 4.1.3.2-62)}$$

Solution:

$$C_{N\alpha} = K \left[(C_{N\alpha})_{bw} \frac{S_{bw}}{S_W} (C_{LE})_{bw} + (C_{N\alpha})_g \frac{S_g}{S_W} (C_{LE})_g \right] \text{ (Equation 4.1.3.2-k)}$$

$$= 1.0 [(0.842)(0.94) + (1.12)(0.346)(1.03)]$$

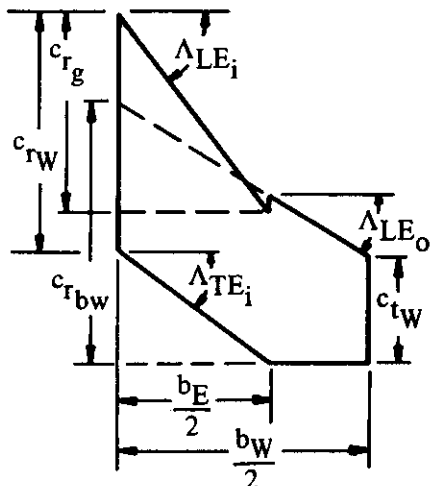
$$= 1.190 \text{ per rad}$$

$$= 0.0208 \text{ per deg}$$

This compares with a test value of 0.024 per degree from Reference 75.

3. Cranked Wing ($\Lambda_{TE_i} > \Lambda_{TE_o}$)

Given: Cranked wing of Reference 32. The inboard trailing-edge sweep angle is greater than the outboard trailing-edge sweep angle. (See Sketches (h) and (i).)



Total Wing

$A_W = 2.91$	$\lambda_W = 0.44$
$\Lambda_{LE_i} = 53.13^\circ$	$\Lambda_{LE_o} = 32.16^\circ$
$S_W = 40.04 \text{ sq in.}$	$\eta_B = 0.60$
$\Lambda_{TE_i} = 37.3^\circ$	$\Lambda_{TE_o} = 0$

Basic Wing

$A_{bw} = 2.73$	$\lambda_{bw} = 0.40$	$\Lambda_{LE_{bw}} = \Lambda_{LE_o} = 32.16^\circ$
$S_{bw} = 42.77 \text{ sq in.}$	$b_{bw} = 10.8 \text{ in.}$	$\Lambda_{TE_{bw}} = \Lambda_{TE_o} = 0$

Glove

$A_g = 3.0$	$\Lambda_{LE_g} = \Lambda_{LE_i} = 53.13^\circ$	$S_g = 14.00 \text{ sq in.}$	$\lambda_g = 0$
-------------	---	------------------------------	-----------------

Extension

$$\frac{b_E}{2} = \eta_B \frac{b_W}{2} = 3.24 \text{ in.} \quad \Lambda_{TE_E} = \Lambda_{TE_i} = 37.3^\circ$$

Additional Characteristics

Round-nosed airfoil $M = 1.40; \beta = 0.98$

Compute:

$$(C_{N\alpha})_{bw}$$

$$\tan \Lambda_{LE_{bw}} / \beta = 0.642; (A \tan \Lambda_{LE})_{bw} = 1.715$$

$$\beta (C_{N\alpha})_{bw} = 3.42 \text{ per rad (Figures 4.1.3.2-56c through -56f, interpolated)}$$

$$(C_{N\alpha})_{bw} = 3.49 \text{ per rad}$$

$$\beta / \tan \Lambda_{LE_{bw}} = 1.560$$

$$(C_{LE})_{bw} = 0.99 \text{ (Figure 4.1.3.2-62)}$$

$$(C_{N\alpha})_g \text{ (Since } \lambda = 0, \text{ either Figure 4.1.3.2-56a or 4.1.3.2-63 can be used.)}$$

(See footnote on Page 4.1.3.2-23.)

$$\beta / \tan \Lambda_{LE_g} = 0.735; (A \tan \Lambda_{LE})_g = 4.0$$

$$\tan \Lambda_{LE_g} (C_{N\alpha})_g = 4.575 \text{ per rad (Figure 4.1.3.2-56a)}$$

$$(C_{N\alpha})_g = 3.43 \text{ per rad}$$

$$(C_{LE})_g = 0.93 \text{ (Figure 4.1.3.2-62)}$$

$$(C_{N\alpha})_E \frac{S_E}{S_W} \text{ (use Figure 4.1.3.2-63)}$$

$$\beta / \tan \Lambda_{LE_1} = \beta / \tan \Lambda_{LE_g} = 0.735$$

$$\frac{\tan \Lambda_{TE_1}}{\tan \Lambda_{LE_1}} = \frac{\tan \Lambda_{TE_E}}{\tan \Lambda_{LE_g}} = 0.571$$

$$\left(\frac{C_{N\alpha}}{A} \right)_1 = 0.650 \text{ per rad (Figure 4.1.3.2-63)}$$

$$\beta / \tan \Lambda_{LE_2} = \beta / \tan \Lambda_{LE_g} = 0.735$$

$$\frac{\tan \Lambda_{TE_2}}{\tan \Lambda_{LE_2}} = \frac{\tan \Lambda_{TE_{bw}}}{\tan \Lambda_{LE_g}} = 0$$

$$\left(\frac{C_{N\alpha}}{A} \right)_2 = 1.16 \text{ per rad (Figure 4.1.3.2-63)}$$

$$\left(C_{N\alpha}\right)_E \frac{S_E}{S_W} = \left[\left(\frac{C_{N\alpha}}{A} \right)_1 - \left(\frac{C_{N\alpha}}{A} \right)_2 \right] \frac{b_E^2}{S_W} \quad (\text{Equation 4.1.3.2-j})$$

$$= (0.650 - 1.16) \frac{(6.48)^2}{40.04}$$

$$= -0.535 \text{ per rad}$$

$$\frac{1}{\beta} \left(C_{N\alpha}\right)_g \frac{S_g}{S_W} = \frac{1}{0.98} (3.43) \frac{(14.00)}{(40.04)} = 1.224$$

$$K_L = 0.74 \text{ (Figure 4.1.3.2-61)}$$

Solution:

$$C_{N\alpha} = K_L \left[\left(C_{N\alpha}\right)_{bw} \frac{S_{bw}}{S_W} (C_{LE})_{bw} + \left(C_{N\alpha}\right)_g \frac{S_g}{S_W} (C_{LE})_g + \left(C_{N\alpha}\right)_E \frac{S_E}{S_W} \right] \quad (\text{Equation 4.1.3.2-h})$$

$$= 0.74 \left[(3.49) \frac{(42.77)}{(40.04)} (0.99) + (3.43) \frac{(14.00)}{(40.04)} (0.93) - 0.535 \right]$$

$$= 0.74 [3.691 + 1.115 - 0.535]$$

$$= 3.160 \text{ per rad}$$

$$= 0.0552 \text{ per deg}$$

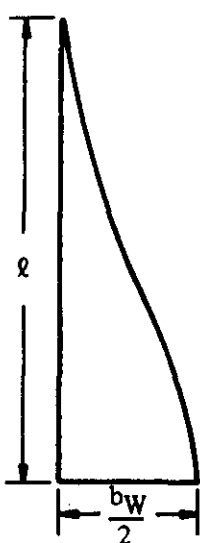
This compares with a test value of 0.0563 per degree from Reference 32.

4. Curved Wing

Given: Ogee wing of Reference 80.

$$A_W = 1.20 \quad b_W = 12.0 \text{ in.} \quad l = 20.0 \text{ in.} \quad S_W = 120 \text{ sq in.}$$

$$M = 1.82; \beta = 1.52$$



Compute:

Planform shape parameter

$$p = S_W/(b_W \ell) = (120)/[(12)(20)] = 0.50$$

Wing slenderness parameter

$$b_W/(2\ell) = (12.0)/[(2)(20)] = 0.30$$

$$\frac{\beta b_W}{2\ell} = \frac{(1.52)(12.0)}{(2)(20.0)} = 0.456$$

$$\left(\frac{C_{N_\alpha}}{A} \right) \left(\frac{1+p}{p} \right) = 4.18 \text{ per rad} (\text{Figure 4.1.3.2-64})$$

Solution:

$$\begin{aligned} C_{N_\alpha} &= \left(\frac{C_{N_\alpha}}{A} \right) \left(\frac{1+p}{p} \right) A \left(\frac{p}{1+p} \right) \text{ (Equation 4.1.3.2-8)} \\ &= (4.18)(1.20) \left(\frac{0.50}{1+0.50} \right) \\ &= 1.672 \text{ per rad} \\ &= 0.0292 \text{ per deg} \end{aligned}$$

This compares with a test value of 0.0285 per degree from Reference 80.

D. HYPERSONIC

The theoretical normal-force-curve slope of a flat plate at zero angle of attack approaches zero as the Mach number becomes large. The interrelated effects of viscosity, heat transfer, and detached shock waves due to blunt leading edges cause considerable deviations of the normal-force-curve slope from the theoretical values. These effects are discussed more fully in Paragraph D of Section 4.1.3.3. The magnitude of these effects on surface pressures, although large enough to be important under certain conditions, has not been determined. The method presented herein is based on linear theory and is intended only as a first-order approximation of the normal-force-curve slope of straight-tapered planforms at hypersonic speeds.

DATCOM METHOD

The hypersonic portions of Figures 4.1.3.2-56a through 4.1.3.2-56g may be used to obtain a first-order approximation of the normal-force-curve slope at zero angle of attack for conventional wings of zero thickness. For planforms with wedge airfoils an approximation of the normal-force-curve slope at zero angle of attack may be obtained by applying the results of Figure 4.1.3.2-65. This figure, based on two-dimensional supersonic slender-airfoil theory, presents the ratio of C_{N_α} of wedge airfoils to C_{N_α} of flat-plate airfoils.

REFERENCES

1. Multhopp, H.: Methods for Calculating the Lift Distribution of Wings (Subsonic Lifting-Surface Theory). ARC R&M 2884, 1950. (U)
2. Falkner, V.M.: The Calculation of the Aerodynamic Loading on Surfaces of Any Shape. ARC R&M 1910, 1943. (U)
3. Lowry, J.G., and Polhamus, E.: A Method for Predicting Lift Increments Due to Flap Deflection at Low Angles of Attack in Incompressible Flow. NACA TR 3911, 1957. (U)
4. DeYoung, J., and Harper, C.W.: Theoretical Symmetric Span Loading at Subsonic Speeds for Wings Having Arbitrary Plan Form. NACA TR 921, 1948. (U)
5. Lawrence H.R.: Lift Distribution on Low Aspect Ratio Wings at Subsonic Speeds. Jour. Aero. Sci., October 1951. (U)
6. Jones, R.T.: Properties of Low-Aspect-Ratio Pointed Wings at Speeds Below and Above the Speed of Sound. NACA TR 835, 1946. (U)
7. Crosthwait, E.L., and Seath, D.D.: Subsonic Characteristics of Low Aspect Ratios. FDL-TDR-64-103, 1965. (U)
8. Benepe, D. B., Kouri, B. G., Webb, J. B., et al: Aerodynamic Characteristics of Non-Straight-Taper Wings. AFFDL-TR-66-73, 1966. (U)
9. Spencer, B.J., Jr.: A Simplified Method for Estimating Subsonic Lift-Curve Slope at Low Angles of Attack for Irregular Planform Wings. NASA TM X-525, 1961. (U)
10. Imai, I., Kaji, I., and Umeda, K.: Mapping Functions of the N.A.C.A. Airfoils into the Unit Circle. Jour. of the Faculty of Science, Hokkaido Univ., Japan, Ser. II, Vol. III, No. 8, 1950. (U)
11. Riegels, F.W.: Aerofoil Sections. Butterworths, London, 1961. (U)
12. Spreiter, J.R.: Aerodynamics of Wings and Bodies at Transonic Speeds. Jour. Aero. Sci., August 1959.
13. Ledson, C.L.: Two-Dimensional Airfoil Characteristics of Four NACA 6A-Series Airfoils at Transonic Mach Numbers up to 1.25. NACA RM L57F05, 1957. (C) Title Unclassified
14. Lindsey, W.F., and Humphreys, M.D.: Effects of Aspect Ratio on Airflow at High Subsonic Mach Numbers. NACA TN 2720, 1952. (U)
15. Gullstrand, T.R.: The Flow Over Two-Dimensional Aerofoils at Incidence in the Transonic Speed Range. KTH (Sweden) Aero TN 27, 1952. (U)
16. Neumark, S.: Critical Mach Numbers for Thin Untapered Swept Wings at Zero Incidence. ARC R&M 2821, 1954. (U)
17. Pearcey, H.H., and Stuart, C.M.: Methods of Boundary-Layer Control for Postponing and Alleviating Buffeting and Other Effects of Shock-Induced Separation. I.A.S. Preprint Paper FF-22, IAS National Summer Meeting, Los Angeles, California, June 16-19, 1959. (U)
18. Graham, D.J.: The Development of Cambered Airfoil Sections Having Favorable Lift Characteristics at Supercritical Mach Numbers. NACA TR 947, 1949. (U)
19. Polhamus, E.C., and King, T.J., Jr.: Aerodynamic Characteristics of Tapered Wings Having Aspect Ratios of 4, 6, and 8, Quarter-Chord Lines Swept Back 45°, and NACA 631A012 Airfoil Sections. NACA RM L51C26, 1951. (U)
20. Harmon, S.M., and Jeffreys, I.: Theoretical Lift and Damping in Roll of Thin Wings With Arbitrary Sweep and Taper at Supersonic Speeds. Supersonic Leading and Trailing Edges. NACA TN 2114, 1950. (U)
21. Malvestuto, F.S., Margolis, K., and Ribner, H.S.: Theoretical Lift and Damping in Roll at Supersonic Speeds of Thin Sweptback Tapered Wings With Streamwise Tips, Subsonic Leading Edges, and Supersonic Trailing Edges. NACA TR 970, 1950. (U)
22. Lapin, E.: Charts for the Computation of Lift and Drag of Finite Wings at Supersonic Speeds. Douglas Aircraft Company Report SM 13480, 1949. (U)
23. Cohen, D.: Formulas for the Supersonic Loading, Lift, and Drag of Flat Sweptback Wings With Leading Edges Behind the Mach Lines. NACA TR 1050, 1951. (U)
24. Mangler, K.W.: Calculation of the Pressure Distribution Over a Wing at Sonic Speeds. ARC R&M 2888, 1955. (U)
25. Mirels, H.: Aerodynamics of Slender Wings and Wing-Body Combinations Having Swept Trailing Edges. NACA TN 3105, 1954. (U)
26. Lampert, S.: Normal-Force Characteristics of Delta Wings at Supersonic Speed. Jour. Aero. Sci., September 1957. (U)

27. Squire, L.C.: Some Applications of 'Not-So-Slender' Wing Theory to Wings With Curved Leading Edges. ARC R&M 3278, 1962. (U)
28. Heaslet, M.A., and Spreiter, J.R.: Reciprocity Relations in Aerodynamics. NACA TR 1119, 1953. (U)
29. Goodson, K.W., and Becht, R.E.: Wind-Tunnel Investigation at High Subsonic Speeds of the Stability Characteristics of a Complete Model Having Sweptback-, M-, W-, and Cranked-Wing Plan Forms and Several Horizontal-Tail Locations. NACA RM L54C29, 1954. (U)
30. Grant, F.C., and Sevier, J.R., Jr.: Transonic and Supersonic Wind-Tunnel Tests of Wing-Body Combinations Designed for High Efficiency at a Mach Number of 1.41. NASA TN D-435, 1960. (U)
31. Mansell, C.J.: Low-Speed Wind-Tunnel Tests on Two Thin Cranked Wings With 60-Degree Sweepback Inboard. ARC R&M 2995, 1957. (U)
32. Wakefield, R.M.: Effects of Wing-Crank, Leading-Edge Chord Extensions and Horizontal-Tail Height on the Longitudinal Stability of Swept-Wing Models at Mach Numbers from 0.6 to 1.4. NASA TM X-92, 1959. (U)
33. Henderson, W.P., and Hammond, A.D.: Low-Speed Investigation of High-Lift and Lateral Control Devices on a Semispan Variable-Sweep Wing Having an Outboard Pivot Location. NASA TM X-542, 1961. (U)
34. Lange, R.H.: Maximum Lift Characteristics of a Wing With the Leading Edge Sweepback Decreasing From 45° at the Root to 20° at the Tip at Reynolds Numbers From 2.4×10^6 to 6.0×10^6 . NACA RM L50A04a, 1950. (U)
35. Kruger, W.: Six Component Measurements on a Cranked Swept-Back Wing. Great Britain Ministry of Supply Translation 816, 1947. (U)
36. Luckert, H.J.: High-Speed Investigations on Various Wing Forms and Wing Sections for the Development of the ARAQO 234 Wings. Great Britain Ministry of Supply Translation 279, 1947. (U)
37. Lockwood, V.E., McKinney, L.W., and Lamar, J.E.: Low-Speed Aerodynamic Characteristics of a Supersonic Transport Model With a High Aspect Ratio Variable-Sweep Warped Wing. NASA TM X-979, 1964. (C) Title Unclassified
38. Jernell, L.S.: The Effects of Conical Camber on the Longitudinal Aerodynamic Characteristics of a Variable-Sweep Wing-Fuselage Configuration at Mach Numbers From 0.50 to 3.50. NASA TM X-804, 1964. (C) Title Unclassified
39. Trescot, C.D., Jr., and Spencer, B.J., Jr.: Effect of Reynolds Number on the Low-Speed Longitudinal Aerodynamic Characteristics of Two Variable-Wing-Sweep Airplane Configurations. NASA TM X-434. (C) Title Unclassified
40. Becht, R.E., and Byrnes, A.L., Jr.: Investigation of Low-Speed Aerodynamic Characteristics of a Variable-Sweep Airplane Model With a Wing Having Partial-Span Cambered-Leading-Edge Modifications. NACA RM L52G08a, 1952. (U)
41. Cook, A.M., Greif, R.K., and Aoyagi, K.: Large-Scale Wind-Tunnel Investigation of Low-Speed Aerodynamic Characteristics of Supersonic Transport Model Having Variable-Sweep Wings. NASA TN D-2824, 1965. (U)
42. Spearman, M.L.: Longitudinal and Lateral Aerodynamic Characteristics at Mach Numbers From 0.60 to 2.20 of a Variable-Sweep Fighter Model With Wing Sweep Angles from 25° to 75°. NASA TM X-710, 1962. (C) Title Unclassified
43. Henderson, W.P.: Low-Speed Aerodynamic Characteristics of a Double-Pivot Variable-Wing-Sweep Airplane Configuration Having Conventional and Outboard Horizontal Tail Surfaces. NASA TM X-773, 1963. (C) Title Unclassified
44. Spencer, B.J., Jr.: Low-Speed Longitudinal Aerodynamic Characteristics Associated With Variations in the Geometry of the Fixed Portion of a Variable-Wing-Sweep Airplane Configuration Having an Outboard Pivot. NASA TM X-625, 1962. (C) Title Unclassified
45. Donlan, C.J., and Sleeman, W.C., Jr.: Low-Speed Wind-Tunnel Investigation of the Longitudinal Stability Characteristics of a Model Equipped With a Variable-Sweep Wing. NACA RM L9B18, 1949. (U)
46. Spencer, B.J., Jr.: Stability and Control Characteristics at Low Subsonic Speeds of an Airplane Configuration Having Two Types of Variable-Sweep Wings. NASA TM X-303, 1960. (U)
47. Emerson, H.: Wind-Tunnel Investigation of the Effect of Clipping the Tips of Triangular Wings of Different Thickness, Camber, and Aspect Ratio—Transonic Bump Method. NASA TN 3671, 1956. (U)
48. Nelson, W., and McDevitt, J.: The Transonic Characteristics of 17 Rectangular, Symmetrical Wing Models of Varying Aspect Ratio and Thickness. NACA RM A51A12, 1951. (U)
49. Turner, T.: Effects of Sweep on the Maximum Lift Characteristics of Four Aspect-Ratio 4 Wings at Transonic Speeds. NACA RM L50H11, 1950. (U)
50. Stanbrook, A.: The Lift-Curve Slope and Aerodynamic-Centre Position of Wings at Subsonic and Supersonic Speeds. RAE TN Aero 2328, 1954. (C) Title Unclassified

51. Harris, W.: A Wind-Tunnel Investigation at High Subsonic and Low Supersonic Mach Numbers on a Series of Wings With Various Sweepback, Taper, Aspect Ratio, and Thickness. Part 2. Comparison of Lift and Stability Data. AFTR 6669, 1952. (C) Title Unclassified
52. Luoma, A.V.: Stability and Control Characteristics at Transonic Speeds of a Variable-Wing-Sweep Airplane Configuration With Outboard Panels Swept 113.24° and 75°. NASA TM X-342, 1960. (C) Title Unclassified
53. Bielat, R.P., Robins, A.W., and Alford, W.J., Jr.: The Transonic Aerodynamic Characteristics of Two Variable-Sweep Airplane Configurations Capable of Low-Level Supersonic Attack. NASA TM X-304, 1960. (C) Title Unclassified
54. Ayers, T.G.: Transonic Aerodynamic Characteristics of a Variable-Wing-Sweep Tactical Fighter Model. Phase 1. NASA TM X-1039, 1964. (C) Title Unclassified
55. Ayers, T.G.: Transonic Aerodynamic Characteristics of a Variable-Wing-Sweep Tactical Fighter Model. Phase 2. NASA TM X-1040, 1964. (C) Title Unclassified
56. Re, R.J., and Simonson, A.J.: Transonic Longitudinal Aerodynamic Characteristics of a Variable-Sweep Tactical-Fighter Model With Wing Sweeps of 25°, 65°, 85°, and 106°. NASA TM X-731, 1962. (C) Title Unclassified
57. Alford, W.J., Jr., Luoma, A.V., and Henderson, W.P.: Wind-Tunnel Studies at Subsonic and Transonic Speeds of a Multiple-Mission Variable-Wing-Sweep Airplane Configuration. NASA TM X-206, 1959. (U)
58. Cooper, M., and Sevier, J.R., Jr.: Effect of a Series of Inboard Plan-Form Modifications on the Longitudinal Characteristics of Two 47° Sweptback Wings of Aspect Ratio 3.5, Taper Ratio 0.2, and Different Thickness Distributions at Mach Numbers of 1.61 and 2.01. NACA RM L53E07a, 1953. (U)
59. Anon: Small-Scale Wing-Body Planform Investigation at Mach Numbers from 0.40 to 2.94. Unpublished Data. (U)
60. Durgin, F.A.: A Study of Twist and Camber on Wings in Supersonic Flow. FDL-TDR-64-109, 1964. (U)
61. Kuhns, R.M.: HSWT-083-0 Analysis Report, Supersonic Transport Lifting Fuselage Investigation. Convair San Diego Report AD-SST-012, 1961. (U)
62. Sevier, J.R., Jr.: Aerodynamic Characteristics at Mach Numbers of 1.41 and 2.01 of a Series of Cranked Wings Ranging in Aspect Ratio From 4.00 to 1.74 in Combination With a Body. NASA TM X-172, 1960. (U)
63. Sevier, J.R., Jr.: Effects of Series of Inboard Plan-Form Modifications on the Longitudinal Characteristics of Two Unswept Wings of Aspect Ratio 3.5, Taper Ratio 0.2, and Different Thickness Distributions at Mach Numbers of 1.61 and 2.01. NACA RM L53K11, 1954. (U)
64. Anon: Wind-Tunnel Tests of a Series of Wing-Body Configurations for Investigation of Supersonic Lift/Drag Ratios. Unpublished Data. (U)
65. Anon: Unpublished Wind-Tunnel Test Data. (U)
66. Spearman, M.L., and Robinson, R.B.: Effects of Wing Sweep and Horizontal-Tail Position on the Aerodynamic Characteristics at a Mach Number of 2.2 of a Variable-Sweep Airplane Configuration Having an Inboard Wing Pivot. NASA TM X-585, 1961. (U)
67. Landrum, E.J., and Babb, C.D.: Effect of Skewed Wing-Tip Controls on a Variable-Sweep Wing-Fuselage Configuration at Mach Numbers From 2.60 to 4.62. NASA TM X-1031, 1964. (C) Title Unclassified
68. Driver, C., and Spearman, M.L.: Aerodynamic Characteristics at a Mach Number of 2.20 of a Variable-Sweep Fighter Model With Wing Sweeps of 50°, 60°, and 75°. NASA TM X-1041, 1964. (C) Title Unclassified
69. Jernell, L.S.: Aerodynamic Characteristics at Mach Numbers From 2.50 to 4.63 of a Variable-Sweep Model at Sweep Angles from 55° to 75°. NASA TM X-959, 1964. (C) Title Unclassified
70. Landrum, E.J.: Effect of Skewed Wing-Tip Controls on a Variable-Sweep Wing-Fuselage Configuration at Mach Numbers of 1.41 and 2.20. NASA TM X-951, 1964. (C) Title Unclassified
71. Spearman, M.L., and Harris, R.V., Jr.: The Longitudinal and Lateral Aerodynamic Characteristics at Mach Numbers of 1.41 and 2.20 of a Variable-Sweep Fighter Model With Wing Sweeps Varying From 25° to 75°. NASA TM X-759, 1963. (C) Title Unclassified
72. Spearman, M.L., and Robinson, R.B.: Stability and Control Characteristics at a Mach Number of 2.01 of a Variable-Sweep Airplane Configuration Capable of Low-Level Supersonic Attack—Outer Wing Swept 75°. NASA TM X-310, 1960. (C) Title Unclassified
73. Robinson, R.B., and Howard, P.W.: Stability and Control Characteristics at a Mach Number of 2.2 of a Variable-Sweep Airplane Configuration Having a 12-Percent-Thick Wing Swept 75° and an Inboard Pivot Location. NASA TM X-435, 1960. (C) Title Unclassified

74. Foster, G.V., and Morris, O.A.: Stability and Control Characteristics at a Mach Number of 1.97 of an Airplane Configuration Having Two Types of Variable-Sweep Wings. NASA TM X-323, 1960. (U)
75. Foster, G.V.: Stability and Control Characteristics at Mach Numbers of 2.50, 3.00, and 3.71 of a Variable-Wing-Sweep Configuration With Outboard Wing Panels Swept Back 75°. NASA TM X-267, 1960. (U)
76. Spearman, M.L.: Static Longitudinal and Lateral Aerodynamic Characteristics at Mach Numbers of 1.41 and 2.20 of a Model of a Low-Aspect-Ratio 83.5° Delta-Wing Airplane Having Auxiliary Variable-Sweep Wing Panels. NASA TM X-708, 1963. (C) Title Unclassified
77. Shaw, D.S.: Supersonic Investigation of the Static Stability, Performance, and Control of a Variable-Sweep Tactical Fighter Model. Phase 1. NASA TM X-1045, 1965. (C) Title Unclassified
78. Shaw, D.S., and Wassum, D.L.: Supersonic Investigation of the Static Stability, Performance, and Control of a Variable-Sweep Tactical Fighter Model. Phase 2. NASA TM X-1046, 1965. (C) Title Unclassified
79. Iggleston, M.S.: Tabulated Lift, Drag, and Pitching Moment From Wind-Tunnel Tests on 30 Slender Wings of Ogee and Other Planforms, With Various Thickness Distributions, at $M = 1.4, 1.61$, and 1.91 . RAE TN Aero 2694, 1960. (U)
80. Squire, L.C., and Capps, D.S.: An Experimental Investigation of the Characteristics of an Ogee Wing From $M = 0.4$ to $M = 1.8$. ARC CP 585, 1962. (U)
81. Holdaway, G.H., and Mellenthin, J.A.: Evaluation of Blended Wing-Body Combinations With Curved Plan Forms at Mach Numbers Up to 3.5. NASA TM X-379, 1960. (U)
82. Hicks, R.M., and Hopkins, E.J.: Effects of Spanwise Variation of Leading-Edge Sweep on the Lift, Drag, and Pitching Moment of a Wing-Body Combination at Mach Numbers From 0.7 to 2.94. NASA TN D-2236, 1964. (U)
83. Corlett, W.A., and Foster, G.V.: Aerodynamic Characteristics of a Tailless Fixed-Wing Supersonic Transport Model at Mach Numbers From 1.80 to 2.86. NASA TM X-992, 1964. (C) Title Unclassified
84. Foster, G.V., and Corlett, W.A.: Aerodynamic Characteristics of a Tailless Fixed-Wing Supersonic Transport Configuration at Mach Number 2.20. NASA TM X-960, 1964. (C) Title Unclassified
85. Cook, T.A.: Wind-Tunnel Measurements at Mach Numbers Up to 2.80 of the Effects of Gulling on the Longitudinal and Lateral Stability and Drag of a Cambered, Slender Ogee Wing. ARC CP 803, 1965. (U)
86. Rolls, L.S., Koenig, D.G., and Drinkwater, F.J., III: Flight Investigation of the Aerodynamic Properties of an Ogee Wing. NASA TN D-3071, 1965. (U)
87. Earnshaw, P.B.: Low-Speed Wind-Tunnel Tests on a Series of Cambered Ogee Wings. ARC CP 775, 1963. (U)
88. Keating, R.F.A.: Low-Speed Wind-Tunnel Tests on Sharp-Edged Gothic Wing of Aspect-Ratio 3/4. ARC CP 576, 1960. (U)
89. Squire, L.C.: Measurement of Lift and Pitching Moment on 4 Ogee Wings at Supersonic Speeds. ARC CP 673, 1962. (U)
90. Taylor, C.R.: Measurements at Mach Numbers Up to 2.8 of the Longitudinal Characteristics of One Plane and Three Cambered Slender 'Ogee' Wings. ARC R&M 3328, 1961. (U)
91. Isaacs, D.: Measurement at Subsonic and Supersonic Speeds of Longitudinal and Lateral Stability of a Slender Cambered Ogee Wing Including Effects of a Fin, Canopy Nose, and Trailing-Edge Controls. ARC R&M 3390, 1965. (U)
92. Dobson, M.D., and King-Underwood, R.: Wind-Tunnel Tests Between $M = .4$ and 2.0 on Cambered Wing of Slender Ogee Planform. ARC CP 778, 1965. (U)
93. Eggers, A.J., Jr., Syvertson, C.A., and Kraus, S.: A Study of Inviscid Flow About Airfoils at High Supersonic Speeds. NACA TR 1123, 1953. (U)
94. Creager, M.O.: Surface Pressure Distribution at Hypersonic Speeds For Blunt Delta Wings at Angle of Attack. NASA Memo 5-12-59A, 1959. (U)
95. Messiter, A.F.: Lift of Slender Delta Wings According to Newtonian Theory. AIAA, Vol. I, No. 4, 1963. (U)
96. Olstad, W.B.: Theoretical Evaluation of Hypersonic Forces, Moments and Stability Derivatives For Combinations of Flat Plates, Including Effects of Blunt Leading Edges, by Newtonian Impact Theory. NASA TN D-1015, 1962. (U)

TABLE 4.1.3.2-A
SUBSONIC LIFT-CURVE SLOPE OF CRANKED WINGS
DATA SUMMARY AND SUBSTANTIATION

Ref.	Config.	A	λ_i	λ_o	η_B	Λ_{LE_i}	Λ_{LE_o}	$\frac{d}{b}$	$\frac{t}{c}$	LER	M	$R_L \max \times 10^{-6}$	$C_{L\alpha}$ Calc.	$C_{L\alpha}$ Test	% Percent Error
29	WB	4.00	.580	.517	.600	48.6	7.7	.139	.06	Round	.8	2.5 to 3.0	.0755	.0750	0.7
30	WB	2.91	.333	.500	.500	67.01	61.7	.139	.04-.03	Round	.9	2.2 to 3.5	.073	.0830	-6.9
31	WB	3.00	1.0	.075	.549	60	60	.109	.06	Round	.8	2.24	.0536	.0490	9.4
32 ^(a)	WB	2.98	.455	.654	.583	59	48.5	.097	.06	Round	.18	2.56	.0587	.0520	12.9
32 ^(a)	WB	2.91	.641	.625	.600	53.13	32.16	.147	.06-.03	Round	.6	1.5	.0454	.0455	-0.2
	WB	2.91	.641	.625	.600	53.13	43.22	.147	.06-.03	Round	.8	1.5	.0464	.0460	0.9
	WB	2.91	.641	.625	.600	53.13	43.22	.147	.06-.03	Round	.9	1.5	.0582	.0590	-1.4
	WB	2.91	.641	.625	.600	53.13	43.22	.147	.06-.03	Round	.6	1.5	.0657	.0670	-1.9
	WB	2.91	.641	.625	.600	53.13	43.22	.147	.06-.03	Round	.8	1.5	.0728	.0740	-1.6
	WB	2.91	.641	.625	.600	53.13	43.22	.147	.06-.03	Round	.9	1.5	.0565	.0580	-2.6
33	W	5.20	.339	.268	.379	60.0	25		.045-.06	Round	.13	2.65	.0600	.0610	-1.6
34 ^(b)	W	4.18	.531	.686	-	45.30	20		.09	Round	.13	6.0	.0642	.0629	2.1
35 ^(b)	W	5.02	.530	.198	-	45.30	25		.15	Round	.13	1.9	.0665	.0614	8.3
36 ^(b)	W	6.1	.585	.480	-	37.03, 28.27	22.63		.105-.09	Round	.550	.6 to 1.0	.0800	.0770	3.9
	W	6.1	.585	.480	-	37.03, 28.27	22.63		.105-.09	Round	.602		.0816	.0800	2.0
	W	6.1	.585	.480	-	37.03, 28.27	22.63		.105-.09	Round	.649		.0843	.0860	-2.0
	W	6.1	.585	.480	-	37.03, 28.27	22.63		.105-.09	Round	.705		.0873	.0910	-4.1
	W	6.1	.585	.480	-	37.03, 28.27	22.63		.105-.09	Round	.748		.0907	.0930	-2.5
	W	6.1	.585	.480	-	37.03, 28.27	22.63		.105-.09	Round	.777		.0932	.1020	-8.6
	W	6.1	.585	.480	-	37.03, 28.27	22.63		.105-.09	Round	.803		.0960	.0945	1.6
	W	6.1	.585	.480	-	37.03, 28.27	22.63		.105-.09	Round	.835		.1007	.0960	4.9
37	WBV	8.47	.197	.386	.212	76	16	.062	-	Round	.2	3.6	.0634		
38	WB	6.18	.294	.463	.308	65	12	.066	.06-.02	Round	.5	.73	.0691		
															(c)

(a) Notched L.E.

(b) Two breaks in L.E.

(c) This information is classified CONFIDENTIAL.

$$\text{Average Error} = \frac{\sum |e|}{n} = 3.9\%$$

TABLE 4.1.3.2-B
TRANSONIC LIFT-CURVE SLOPES OF STRAIGHT-TAPERED WINGS
DATA SUMMARY AND SUBSTANTIATION

Ref.	Airfoil Section	A	λ	$\Lambda_{c/2}$ (deg)	$R_f \times 10^{-6}$	M_{fb}	$(C_L)_a$ _{fb}	M_a	$(C_L)_a$ _a	M_b	$(C_L)_a$ _b	Theoretical (T) Experimental (E)
48	63A010	6	1	0	2.0	.82	6.1	.89	3.2	.96	6.2	T
		6	1	0	2.0	.82	6.3	.89	4.1	.95	4.6	E
		6	1	0	2.0	.84	7.0	.91	5.0	.98	5.9	T
		6	1	0	2.0	.84	6.5	.90	5.1	.95	5.5	E
		4	1	0	2.0	.84	4.8	.91	3.12	.98	4.08	T
		4	1	0	2.0	.84	4.7	.90	3.0	.98	4.2	E
		4	1	0	2.0	.87	5.4	.94	4.5	1.01	4.5	T
		4	1	0	2.0	.86	4.7	.94	4.1	.98	4.7	E
		4	1	0	2.0	.91	5.9	.98	5.5	1.05	5.1	T
		4	1	0	2.0	.94	5.9	.98	5.4	1.05	4.9	E
		2	1	0	2.0	.98	2.9	1.05	2.9	1.12	2.5	T
		2	1	0	2.0	1.0	3.1	1.07	3.3	1.17	2.7	E
49	65A006	2	1	0	2.0	1.0	3.4	1.07	3.5			
		2	1	0	2.0	1.0	3.3	1.07	3.5			
		1	1	0	2.0	1.0	3.3	1.07	3.5	1.14	2.9	T
		1	1	0	2.0	1.0	3.2	1.07	3.1			E
		1	1	0	2.0	1.0	1.4	1.07	1.6*	1.14	1.2	T
		1	1	0	2.0	1.0	1.4	1.07	1.5	1.14	1.3*	E
		1	1	0	2.0	1.0	1.5	1.07	1.7	1.14	1.3	T
		1	1	0	2.0	1.0	1.3	1.07	1.5	1.14	1.4	E
		1	1	0	2.0	1.0	1.6	1.07	1.8	1.14	1.4	T
		1	1	0	2.0	1.0	1.3	1.07	1.6	1.14	1.0*	E
		4	.6	43.2	.46	.94	4.0	1.01	3.8	1.08	3.5	T
		4	.6	32.5	.46	.93	4.8	1.0	4.4	1.07	4.2	E
19	63A012	4	.68	43.6	.57	.92	3.6	.99	1.5	1.06	3.0	T
		6	.56	43.6	.57	.875	4.1	.945	1.4	1.015	3.5	E
		8	.45	43.6	.57	.875	4.6	.945	1.3	1.015	3.9	T
		8	.45	43.6	.57	.875	4.1	1.0	1.6	1.125	2.9	E
47	63A006	4	0	26.6	2.4	.92	5.2	.99	4.8	1.06	4.5	T
		1	.5	33.4	2.9	1.0	1.6	1.07	1.9	1.14	1.5	E
		1.08	.3	44.0	2.6	1.0	1.7	1.07	1.9	1.14	1.6	T
		1.67	.2	38.7	2.5	1.0	1.9	1.07	1.9	1.14	1.9*	E
		1.71	.4	26.5	2.7	1.0	2.6	1.07	2.9	1.14	2.4	T
		1.71	.4	26.5	2.7	1.0	2.8	1.07	2.9	1.14	2.7*	E
		2.46	.1	33.6	2.5	1.0	3.7	1.07	3.8	1.14	3.4	T
		2.67	.2	26.6	2.5	1.0	3.7	1.07	3.6	1.14	3.2*	E
		2.67	.2	26.6	2.5	1.0	4.2	1.07	4.1	1.14	3.9	T
		2.67	.2	26.6	2.5	1.0	4.0	1.07	3.9	1.14	3.7*	E

*EXTRAPOLATED VALUES

TABLE 4.1.3.2-C
SUPersonic NORMAL-FORCE-CURVE SLOPE OF DOUBLE-DELTA WINGS
DATA SUMMARY AND SUBSTANTIATION

Ref.	Config.	A	λ_i	λ_o	η_B	Λ_{LE_i}	Λ_{LE_o}	$\frac{d}{b}$	$\frac{t}{c}$	LER	M	C_{Na} Calc.	C_{Na} Test	% Percent Error
58	WB	3.15	.510	.295	.400	64.07	51.63	.125	.06	Sharp	1.61	.0477	.0462	3.2
		2.86	.407			70.67					1.61	.0442	.0437	1.1
											2.01	.0366	.0355	3.1
		2.86	.407			64.07					1.61	.0458	.0450	1.8
		2.62	.339			70.67					1.61	.0421	.0416	1.2
		2.62	.339			64.07					1.61	.0443	.0431	2.8
		2.42	.292			70.67					1.61	.0411	.0402	2.2
											2.01	.0339	.0351	- 3.4
59	WB	2.01	.416	.302	.313	78	53.3	.127	.03	Sharp ^(a)	1.10	.0523	.0540	- 3.1
											1.40	.0431	.0440	- 2.0
											2.00	.0332	.0320	3.8
											2.94	.0242	.0230	5.2
		1.96	.295	.344	.405	78	48.5	.127	.03		1.10	.0487	.0500	- 2.6
											1.40	.0405	.0410	- 1.2
											1.98	.0313	.0270	15.9
											2.94	.0227	.0221	2.7
		1.93	.180	.454	.498	78	38.1	.127	.03		1.10	.0476	.0469	1.5
											1.40	.0380	.0363	4.7
60	W										1.98	.0276	.0259	6.6
		1.30	.196	0	.414	82	60	.147	.03		2.94	.0205	.0199	3.0
											1.10	.0322	.0320	0.6
											1.40	.0299	.0280	6.8
											1.98	.0249	.0230	8.3
											2.94	.0194	.0170	14.1
		1.33	.302	.163	.403	82	60	.147	.03	Sharp	1.10	.0350	.0390	- 10.3
											1.40	.0323	.0330	- 2.1
											1.98	.0282	.0270	4.4
											2.94	.0207	.0200	3.5
61	W	1.55	.301	0	.400	82	59	.144	.03		1.10	.0382	.0410	- 6.8
											1.40	.0336	.0350	- 4.0
											1.98	.0280	.0280	0
											2.94	.0207	.0210	- 1.4
		1.72	.358	0	.414	77.4	59	.127	.03		1.10	.0421	.0460	- 8.5
60	W										1.39	.0359	.0390	- 7.9
											3.0	.0221	.0200	10.5
		2.25	.29	0	.415	78	60	--	.04	Round	1.2	.0614	.0506	1.6
											2.0	.0315	.0310	1.6
61	W	2.39	.376	0	.128	82.9	50	--	.07-.03	Round	3.0	.0216	.0228	- 5.3
											4.0	.0166	.0173	- 4.0

TABLE 4.1.3.2-C (CONT'D)

Ref.	Config.	A	λ_i	λ_o	η_B	Λ_{LE_i}	Λ_{LE_o}	$\frac{d}{b}$	$\frac{t}{c}$	LER	M	c_{Na} Calc.	c_{Na} Test	* Percent Error
62	WB	2.35	.229	.625	.700	61.7	30	.150	.06	Round ^(b)	1.41	.0520	.0515	1.0
											2.01	.0366	.0365	0.3
63	WB	3.15	.508	.295	.400	49.59	20.85	.125	.06	Sharp	2.01	.0363	.0382	- 5.0
		2.86	.407			63.07					2.01	.0346	.0360	- 3.9
		2.62	.339			70.10					2.01	.0328	.0332	- 1.2
		2.86	.407			49.59					1.61	.0428	.0440	- 2.7
		2.62	.339			63.07					2.01	.0355	.0369	- 3.8
		2.42	.292			70.10					2.01	.0337	.0348	- 3.2
		2.43	.448	0	.259	78	60	.077	.018-.040	Sharp	2.98	.0232	.0224	3.6
											2.59	.0262	.0254	3.1
											2.20	.0315	.0304	3.6
											1.53	.0402	.0382	5.2
											1.17	.0451	.0459	- 1.7
		1.52	.479	.102	.216	83.35	62	.095	.018-.029		2.98	.0220	.0210	4.8
											2.81	.0231	.0231	0
											2.20	.0280	.0289	- 3.1
											2.59	.0242	.0238	1.7
											1.59	.0344	.0346	- 0.6
		1.26	.627	0	.181	83.0	70	.100	.02		2.98	.0219	.0216	1.4
											2.98	.0219	.0208	5.3
		1.06	.627	.102	.197	83.0	70	.092	.02		2.98	.0201	.0209	- 3.8
											2.98	.0201	.0207	- 2.9
											2.59	.0220	.0228	- 3.5
											2.59	.0220	.0226	- 2.7

(a) These models had theoretically round L.E.'s inboard but were analyzed as sharp due to small size of model and small t/c.

(b) This model had a flat plate wing with a blunt T.E.

Average Error = $\frac{\sum |e|}{n} = 3.7\%$

TABLE 4.1.3.2-D
SUPersonic NORMAL-FORCE-CURVE SLOPE OF CRANKED WINGS
DATA SUMMARY AND SUBSTANTIATION

Ref.	Config.	A	λ_i	λ_o	η_B	Λ_{LE_i}	Λ_{LE_o}	$\frac{d}{b}$	$\frac{t}{c}$	LER	M	C_{Na} Calc.	C_{Na} Test	% Percent Error
30	WB	2.91	.353	.500	.500	67.01	61.7	.139	.04-.03	Round	1.41	.0456	.0433	5.3
32	WB	2.91	.641	.625	.600	53.13	32.16	.147	.06-.03	Round	2.01	.0401	.0355	13.0
66	WBVN	3.59	.409	.650	.421	70	50	.186	?	Round	1.4	.0562	.0563	- 2.0
67	WB	4.43	.389	.464	.404	65	45	.079	.06-.02	Round	2.2	.0375	.0568	0.9
											2.60	.0299	.0390	- 3.8
											2.96	.0260		
											3.95	.0201		
38	WB	4.43	.389	.464	.404	65	45	.079	.06-.02	Round	1.20	.0660		
											2.30	.0343		
											2.60	.0317		
											3.00	.0267		
											3.50	.0212		
65	WBVN	3.80	.374	.289	.297	74.17	50	.211	.08	Round	1.70	.0407	.0390	4.4
											2.00	.0345	.0334	3.3
											2.20	.0310	.0324	-4.3
											2.50	.0274	.0289	-5.2
(a) This information is classified CONFIDENTIAL.													$\text{Average Error} = \frac{\sum e }{n} = 4.7\%$	

TABLE 4.1.3.2-E
SUPersonic NORMAL-FORCE-CURVE SLOPE OF CURVED (GOTHIC AND OGEE) WINGS
DATA SUMMARY AND SUBSTANTIATION

Ref.	Config.	Planform	A	$\frac{b_W}{2\ell}$	p	$\frac{d}{b}$	$\frac{t}{c}$ (root)	M	C_{Na} Calc.	C_{Na} Test	ϵ Percent Error
79	W ₁	Ogee	.75	.141	.375	—	.008 ^(a)	1.41	.0180	.0230	-21.7
	W ₄		1.00	.188	.375	—	.010 ^(a)	1.61	.0178	.0211	-15.6
	W ₇		1.33	.25	.375	—	.012 ^(a)	1.41	.0237	.0283	-14.2
	W ₁₂		1.00	.25	.500	—	.014 ^(a)	1.41	.0283	.0286	-1.0
	W ₃₂		1.11	.25	.450	—	.013 ^(a)	1.41	.0293	.0288	1.7
	W ₁₀		.75	.188	.500	—	.012 ^(a)	1.61	.0282	.0270	4.4
	W ₁₁		.75	.25	.667	—	.016 ^(a)	1.41	.0218	.0219	0
	W ₁₃		1.00	.25	.500	—	.014 ^(a)	1.61	.0205	.0204	0.5
	W ₃	Gothic	.75	.25	.667	—	.016 ^(a)	1.41	.0255	.0265	-3.8
	W ₆		1.00	.333	.667	—	.018 ^(a)	1.61	.0245	.0253	-3.2
	W ₉		1.33	.444	.667	—	.021 ^(a)	1.41	.0392	.0388	1.0
	W ₁₄		.857	.25	.583	—	.015 ^(a)	1.61	.0349	.0373	-6.4
	W ₂₀		.938	.25	.533	—	.015 ^(a)	1.41	.0307	.0335	-8.4
	W ₂₁		1.00	.25	.500	—	.015 ^(a)	1.61	.0268	.0258	3.9
	WB	Ogee	1.2	.300	.600	.133	.05	1.00	.0277	.0259	6.9
								1.25	.0247	.0251	-1.6
								1.32	.0283	.0289	-2.1
								1.42	.0272	.0263	3.4
								1.61	.0253	.0261	-3.1
								1.91	.0243	.0351	-2.3
								1.32	.0338	.0332	1.8
								1.42	.0329	.0327	0.6
								1.61	.0310	.0309	0.3
								1.82	.0292	.0285	1.5
80											

TABLE 4.1.3.2-E (CONTD)

Ref.	Config.	Planform	A	$\frac{b_w}{2L}$	p	$\frac{d}{b}$	$\frac{t}{c}$ (root)	M	C_{Na} Calc.	C_{Na} Test	* Percent Error
81	WB	Ogee	2.0	.540	.540	.08	.03	1.00	.0612	.0570	7.4
								1.05	.0614	.0595	3.2
								1.10	.0694	.0610	- 2.6
								1.20	.0553	.0622	-11.1
								1.60	.0418	.0635	-21.9
								1.80	.0378	.0475	-20.4
								2.00	.0347	.0445	-22.0
								2.20	.0318	.0360	-11.7
								2.35	.0304	.0350	-13.1
82	WB	Ogee	1.98	.35	.353	.127	.02	1.40	.0413	.0466	-11.4
								1.98	.0328	.0358	- 8.4
								2.94	.0260	.0238	5.0
								1.4	.0248	.0255	- 2.7
								1.8	.0234	.0227	3.1
								2.2	.0215	.0210	2.4
85	WB	Ogee	.924	.208	.45	.112	.059	2.4	.0207	.0197	5.1
								2.8	.0191	.0182	4.9
(a) Flat Plate Models								$\text{Average Error} = \frac{\sum e }{n} = 6.2\%$			

SUBSONIC SPEEDS

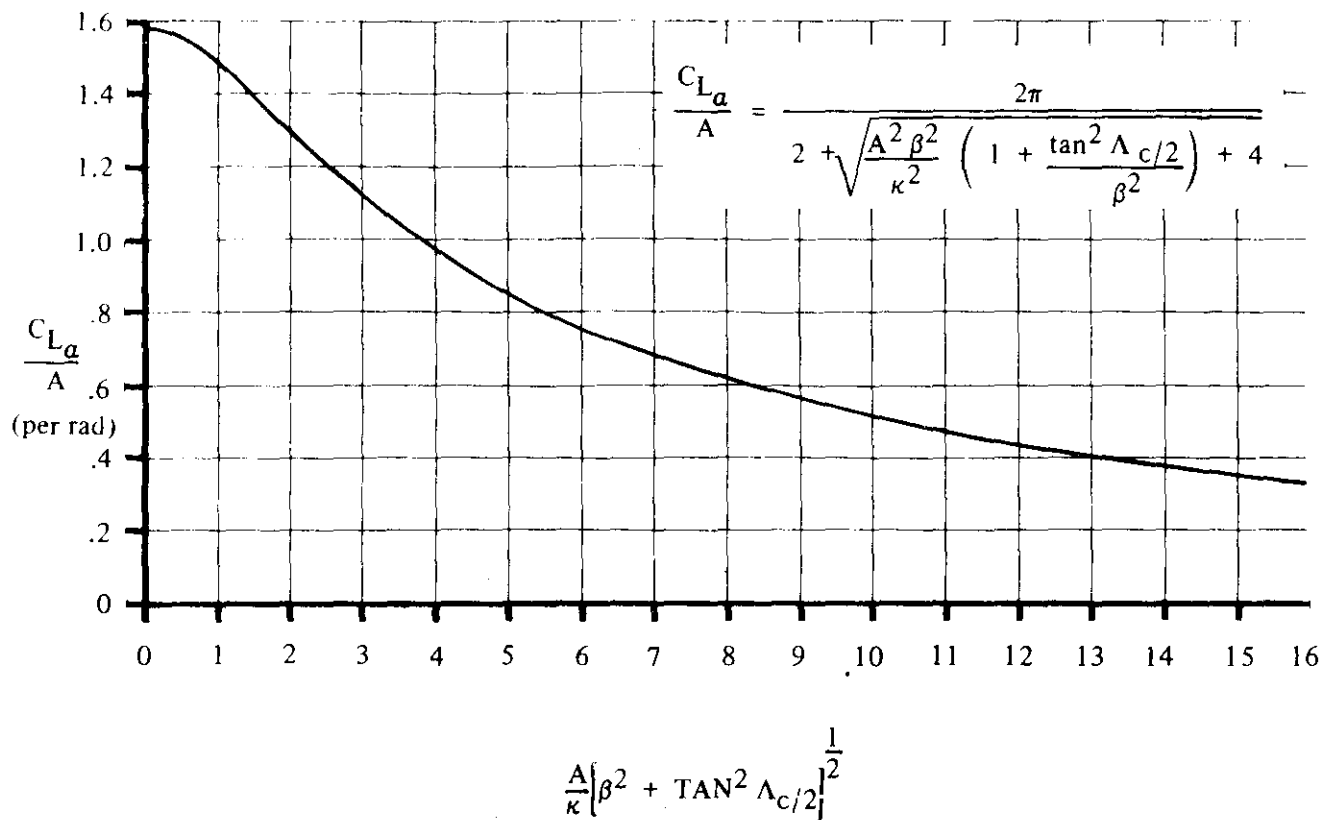


FIGURE 4.1.3.2-49 SUBSONIC WING LIFT-CURVE SLOPE

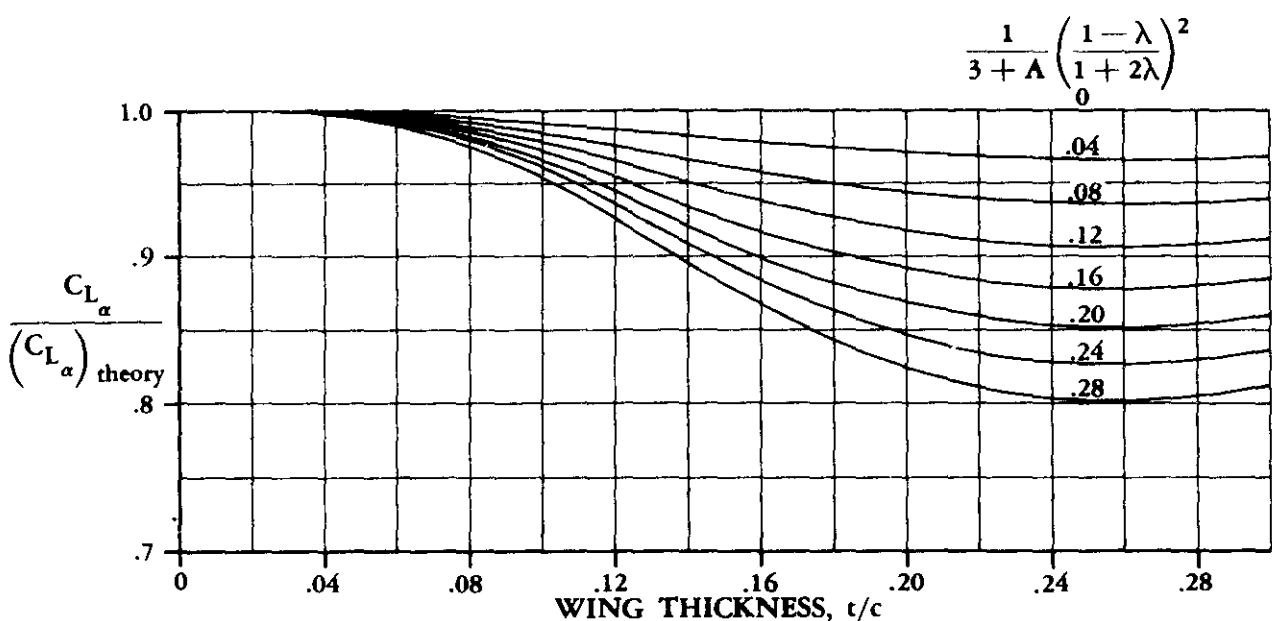


FIGURE 4.1.3.2-50a WING LIFT-CURVE-SLOPE THICKNESS CORRECTION FACTOR

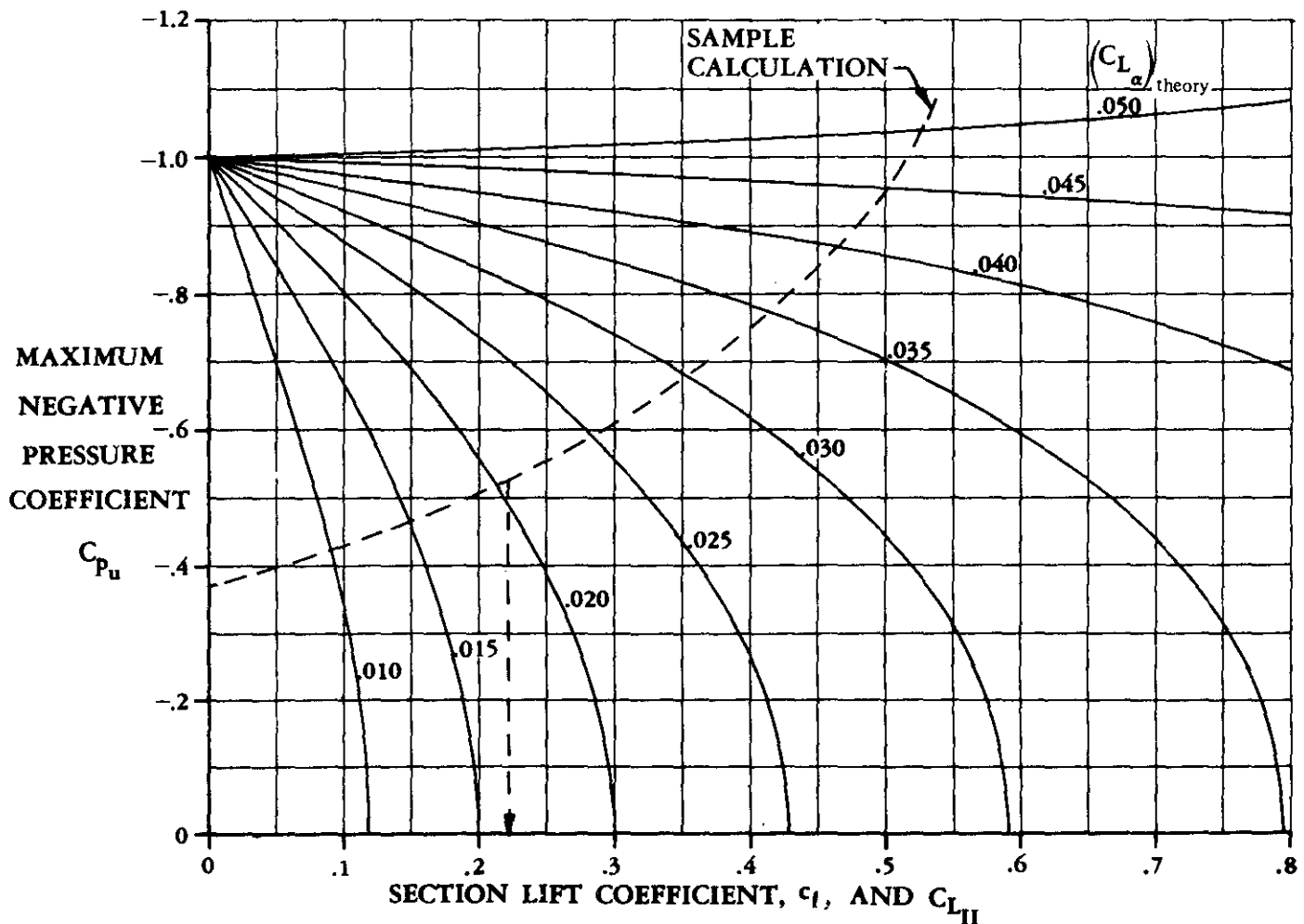


FIGURE 4.1.3.2-50b ESTIMATION OF $C_{L_{II}}$

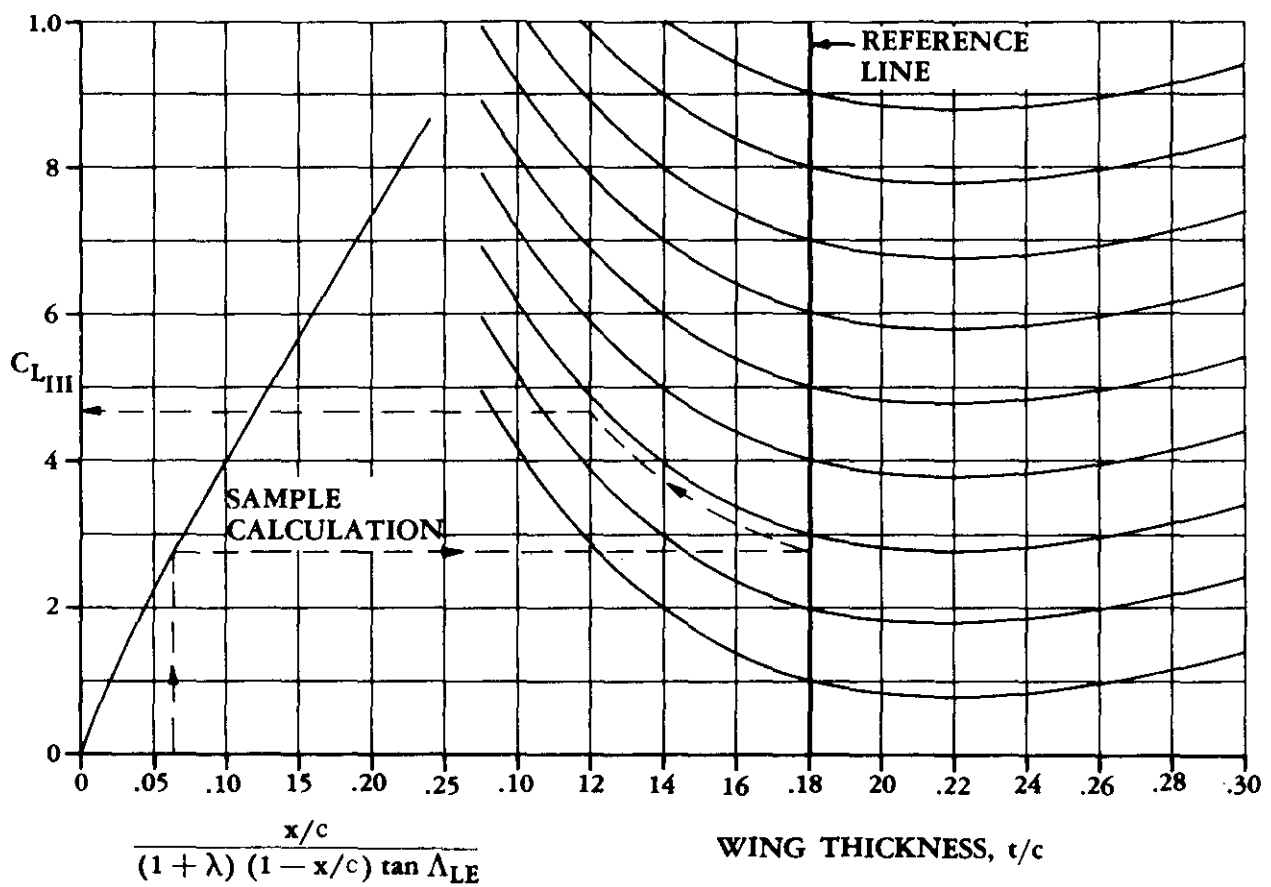


FIGURE 4.1.3.2-51 ESTIMATION OF $C_{L_{III}}$

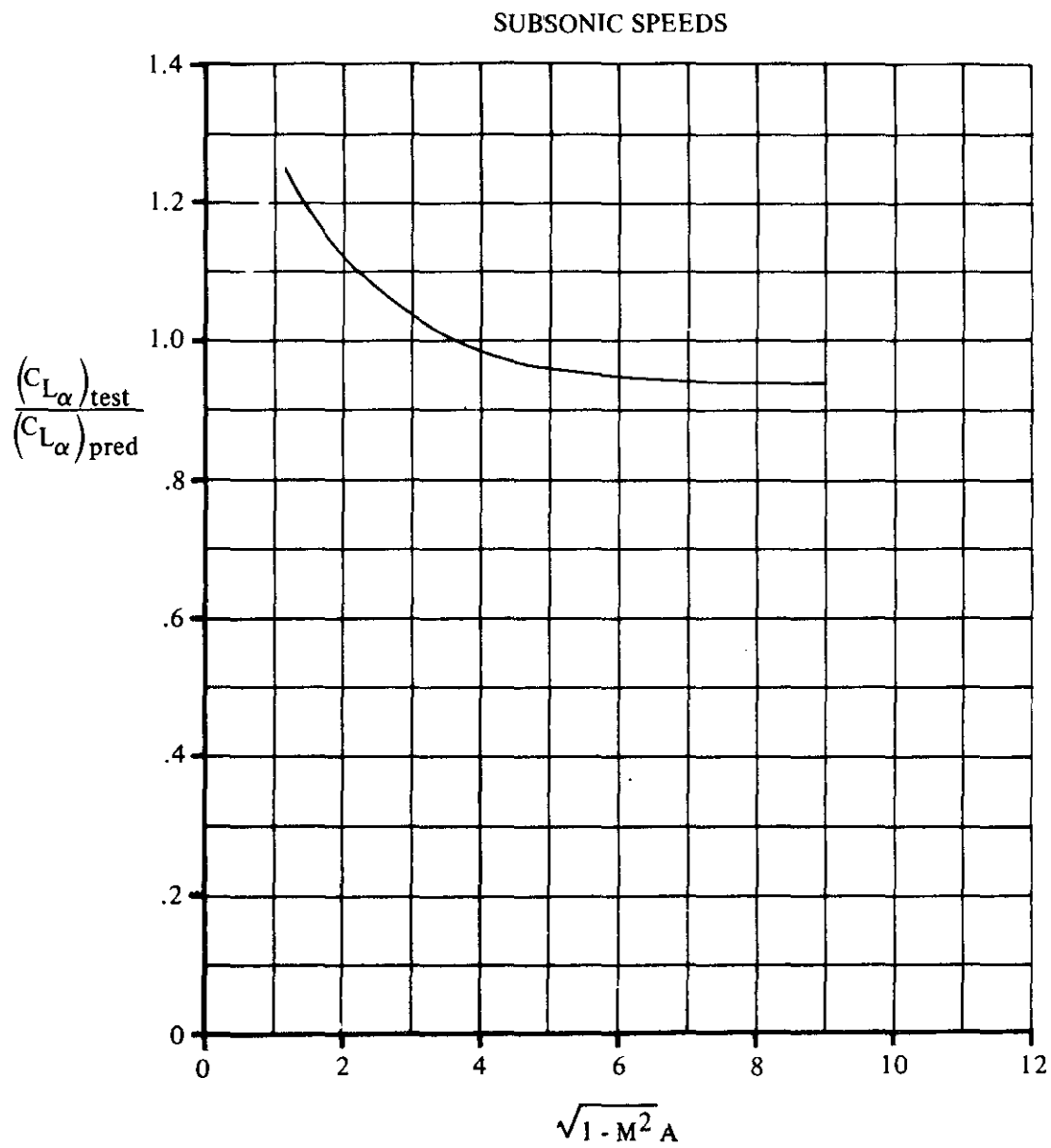


FIGURE 4.1.3.2-52 CORRELATION OF SUBSONIC LIFT-CURVE SLOPE FOR CRANKED PLANFORMS HAVING ROUND-NOSED AIRFOILS

TRANSONIC SPEEDS

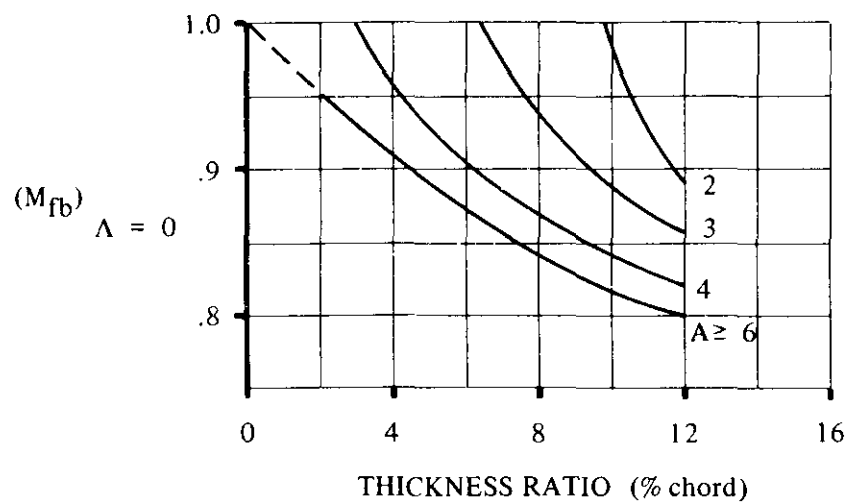


FIGURE 4.1.3.2-53a TRANSONIC FORCE-BREAK MACH NUMBER FOR ZERO SWEEP

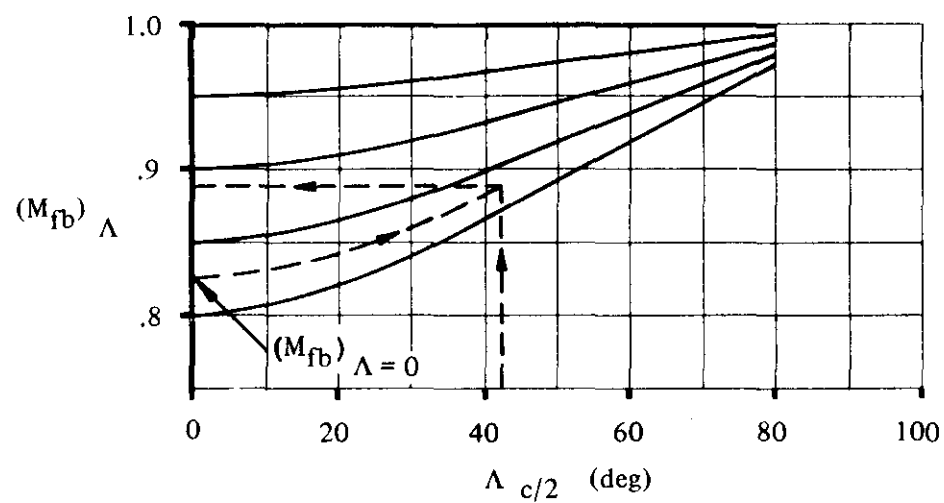


FIGURE 4.1.3.2-53b TRANSONIC SWEEP CORRECTION FOR FORCE-BREAK MACH NUMBER

TRANSONIC SPEEDS

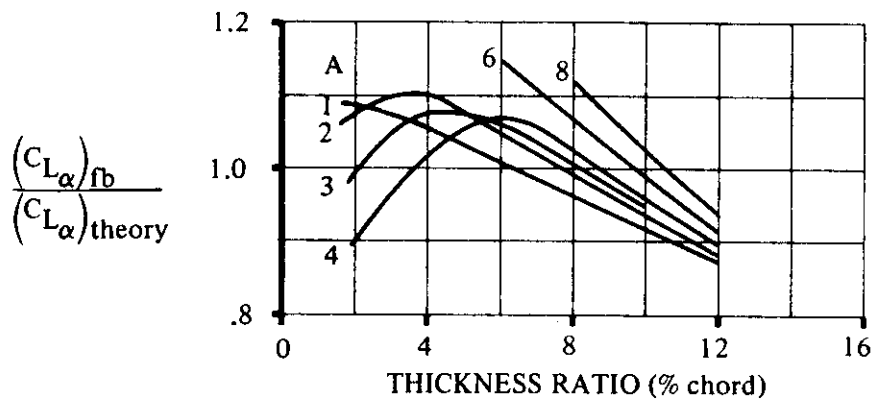


FIGURE 4.1.3.2-54a CORRECTION TO LIFT-CURVE SLOPE AT FORCE-BREAK MACH NUMBER

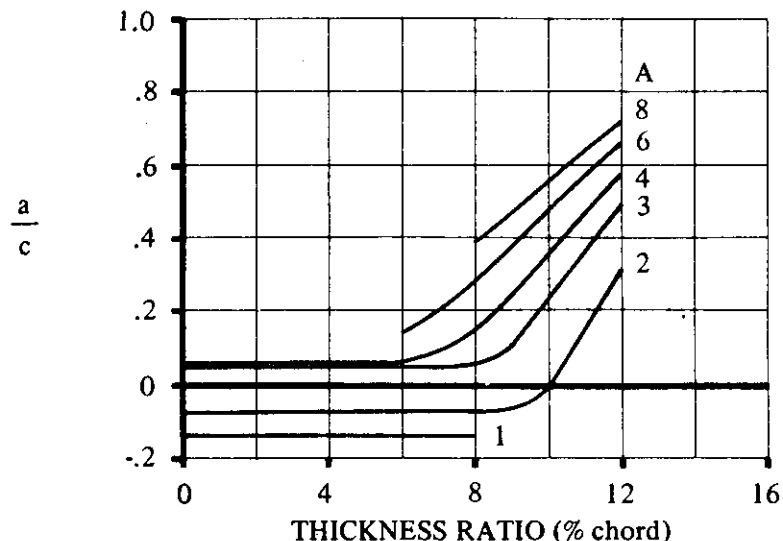


FIGURE 4.1.3.2-54b CHART FOR DETERMINING LIFT-CURVE SLOPE AT M_a

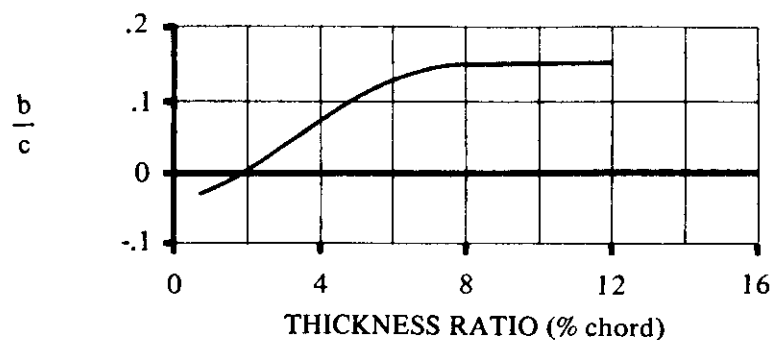


FIGURE 4.1.3.2-54c CHART FOR DETERMINING LIFT-CURVE SLOPE AT M_b

TRANSONIC SPEEDS

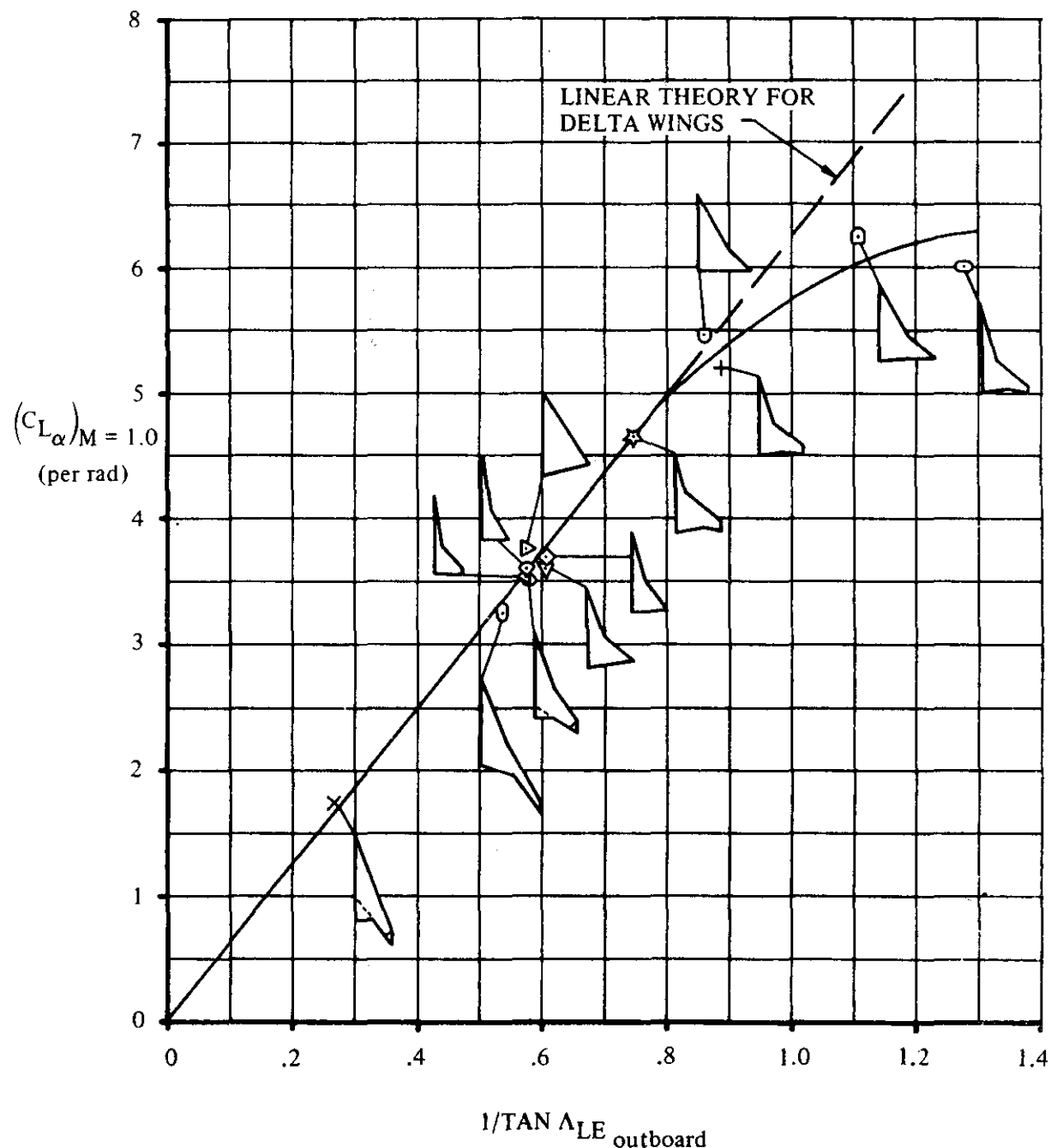


FIGURE 4.1.3.2-55 EMPIRICAL CORRELATION OF LIFT-CURVE SLOPE OF COMPOSITE PLANFORMS AT MACH 1

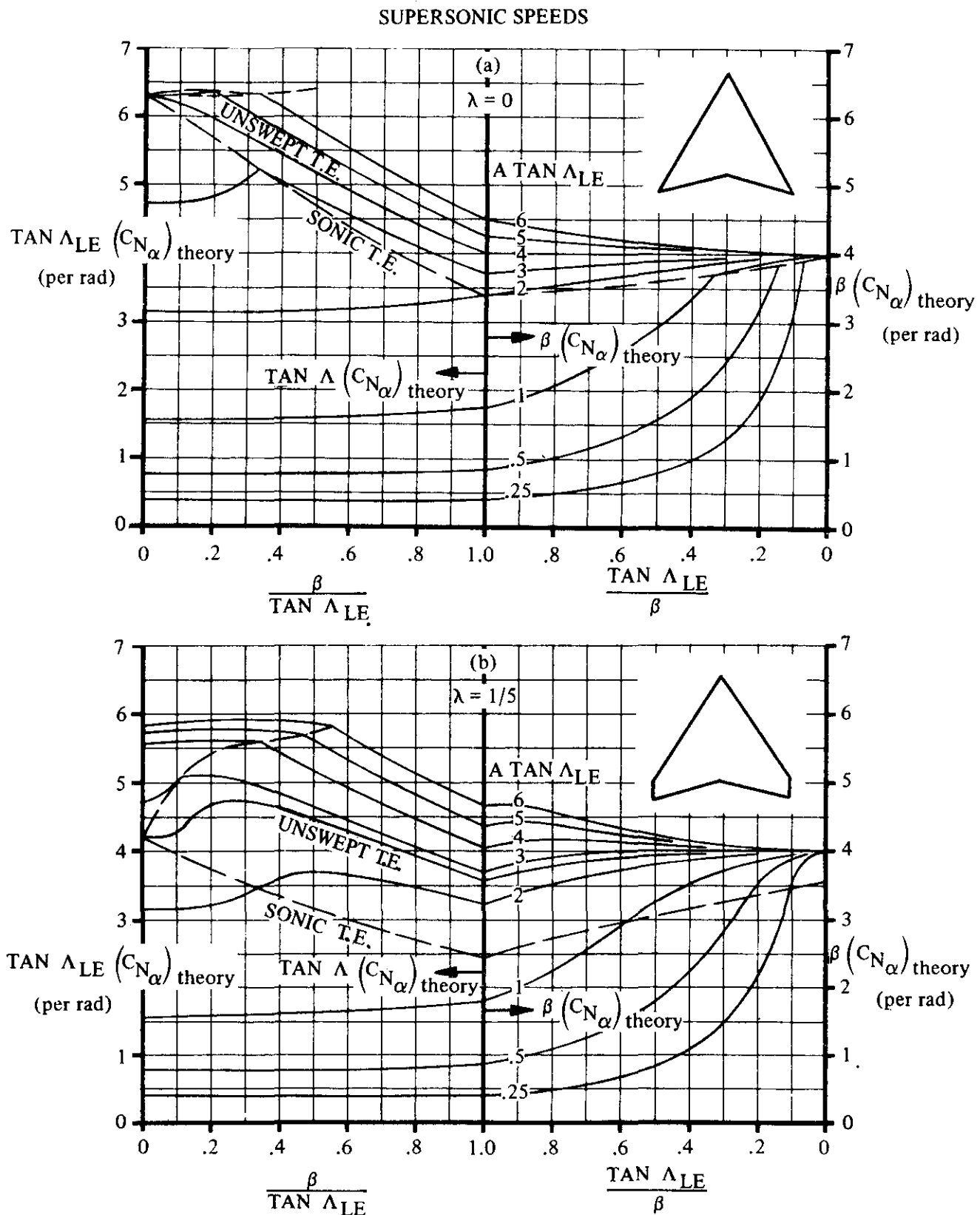


FIGURE 4.1.3.2-56 WING SUPersonic NORMAL-FORCE-CURVE SLOPE

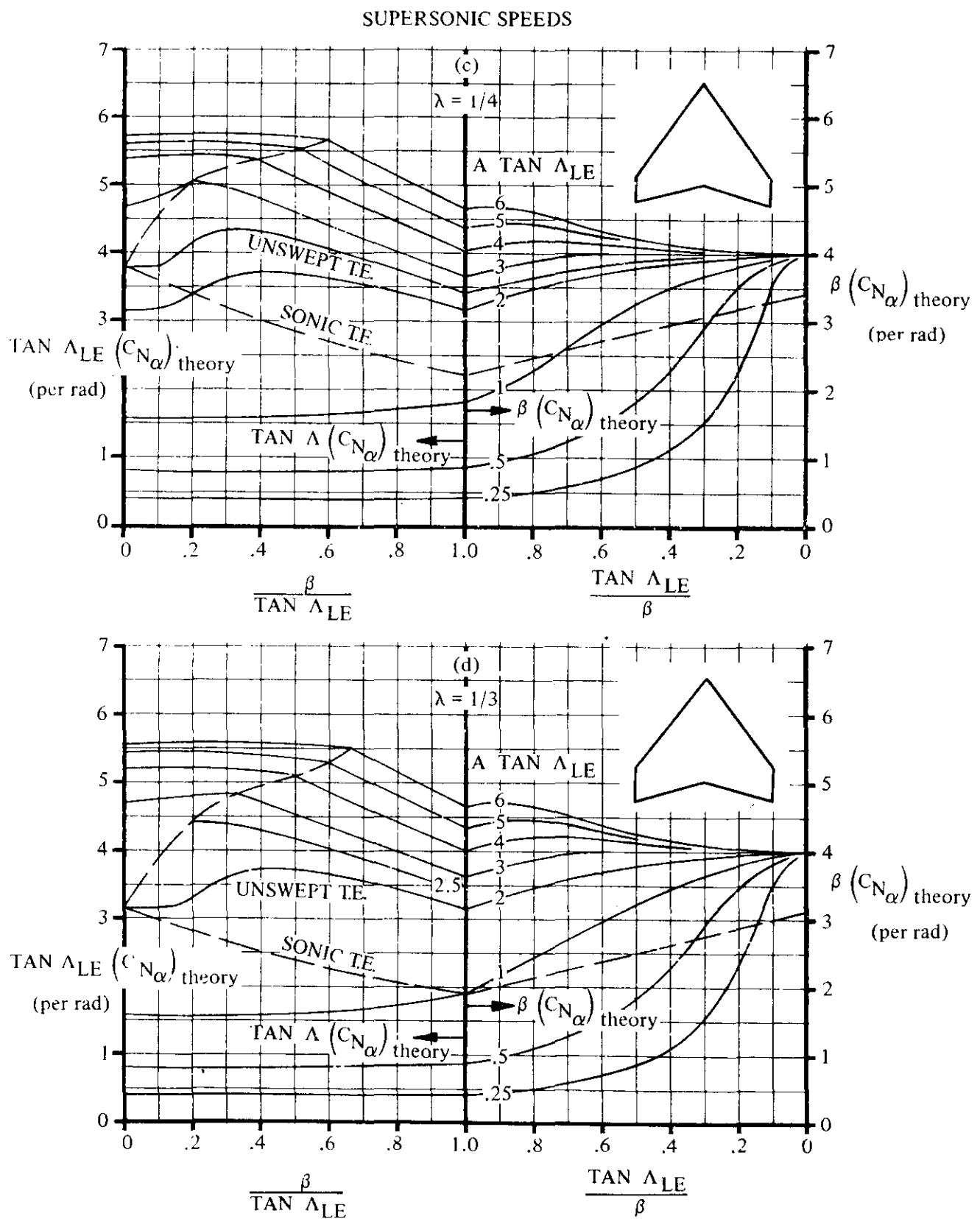


FIGURE 4.1.3.2-56 (CONTD)

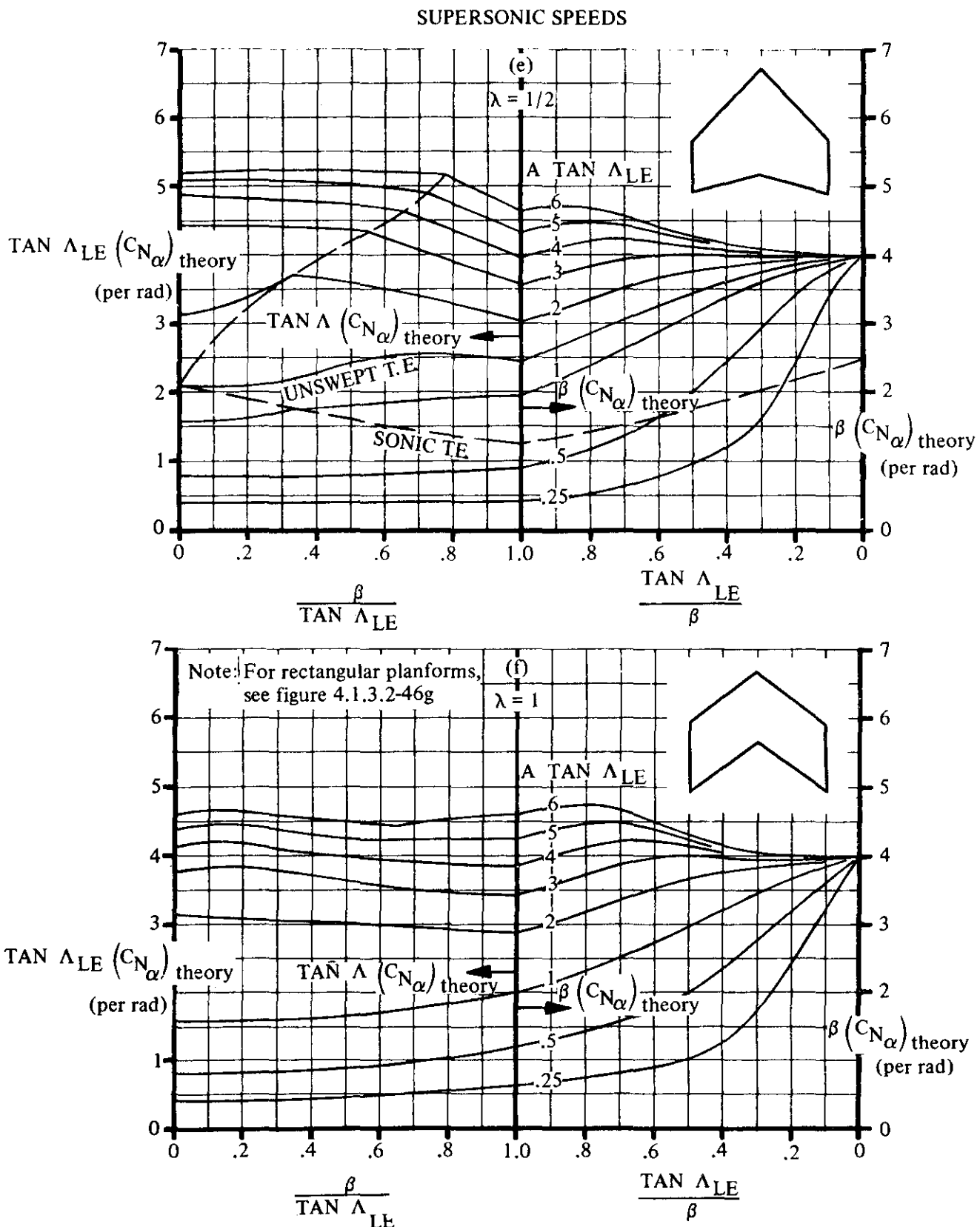


FIGURE 4.1.3.2-56 (CONT'D)

SUPersonic SPEEDS

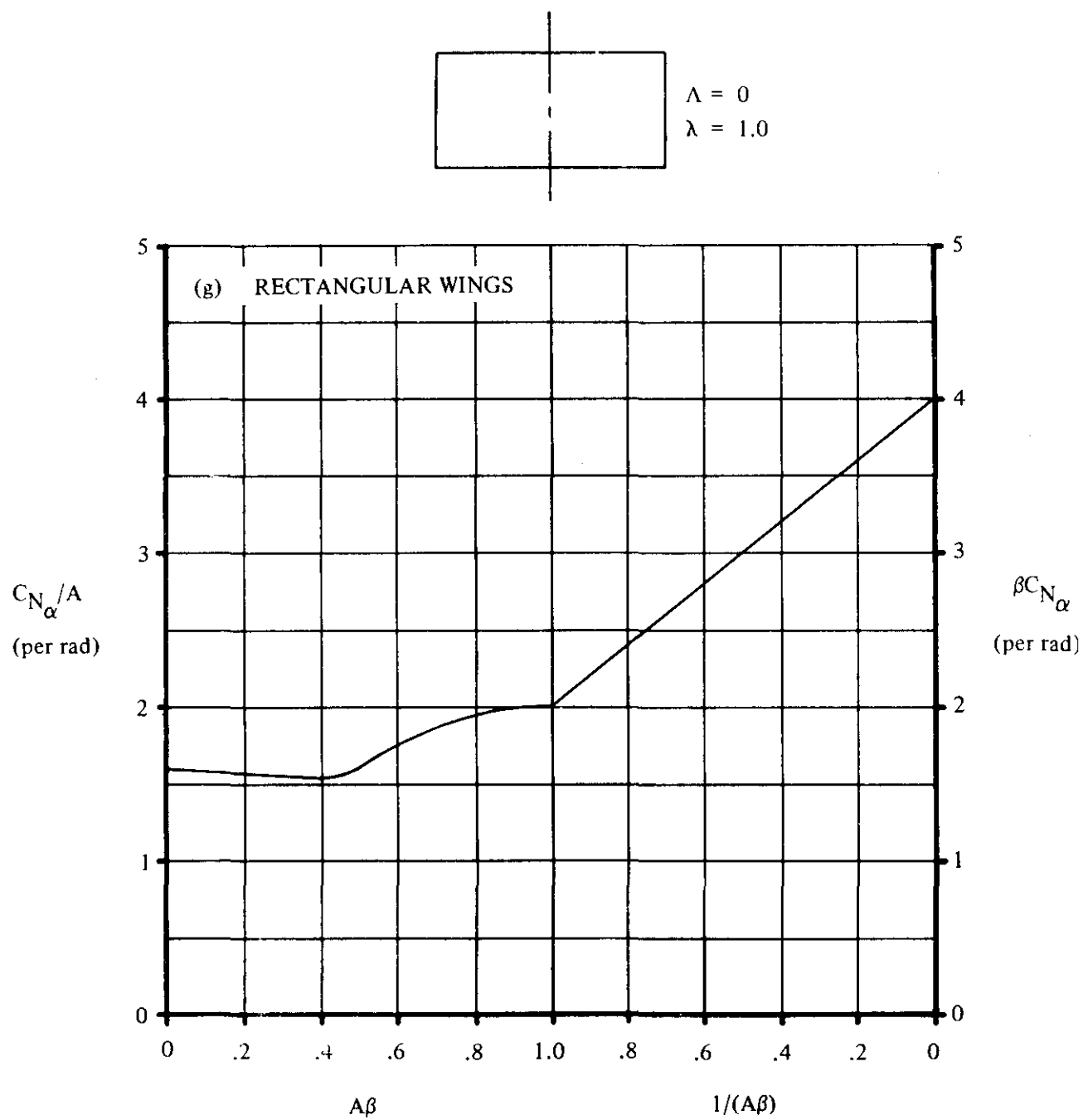


FIGURE 4.1.3.2-56 (CONTD)

SUPersonic SPEEDS

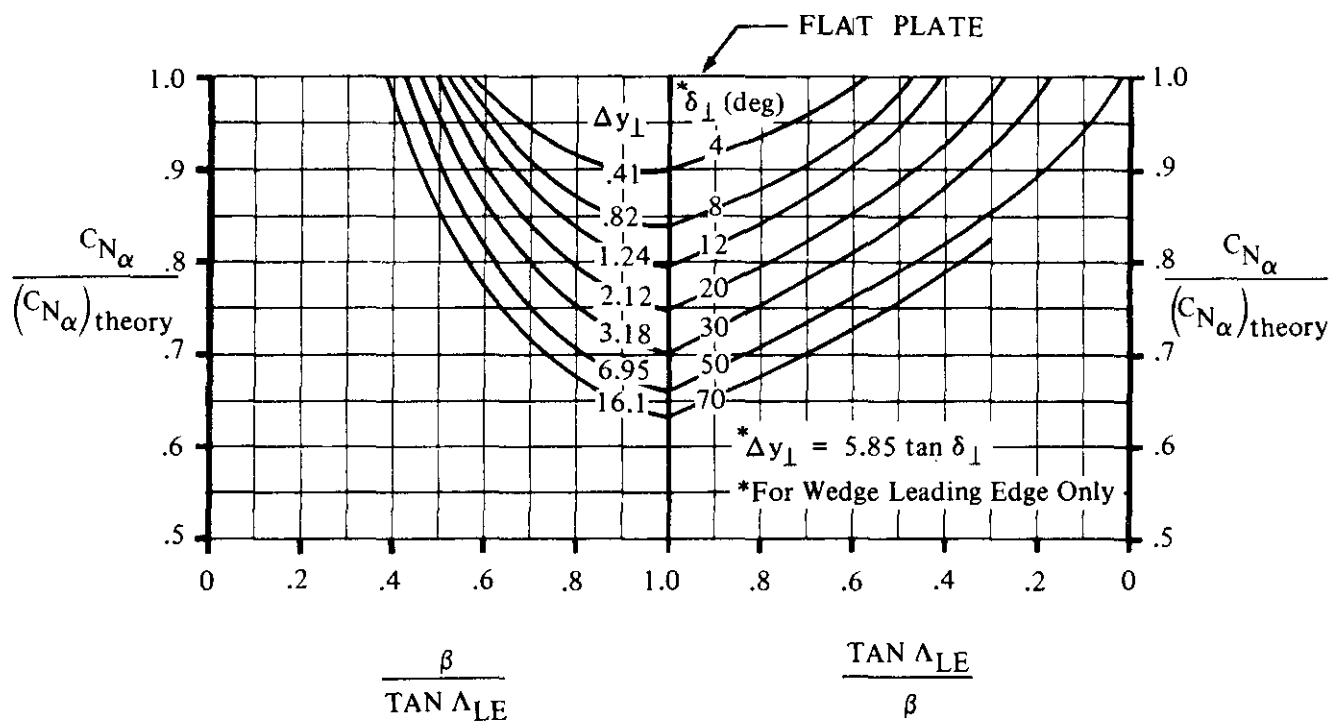


FIGURE 4.1.3.2-60 SUPersonic WING LIFT-CURVE-SLOPE CORRECTION FACTOR FOR SONIC-LEADING-EDGE REGION

SUPersonic SPEEDS

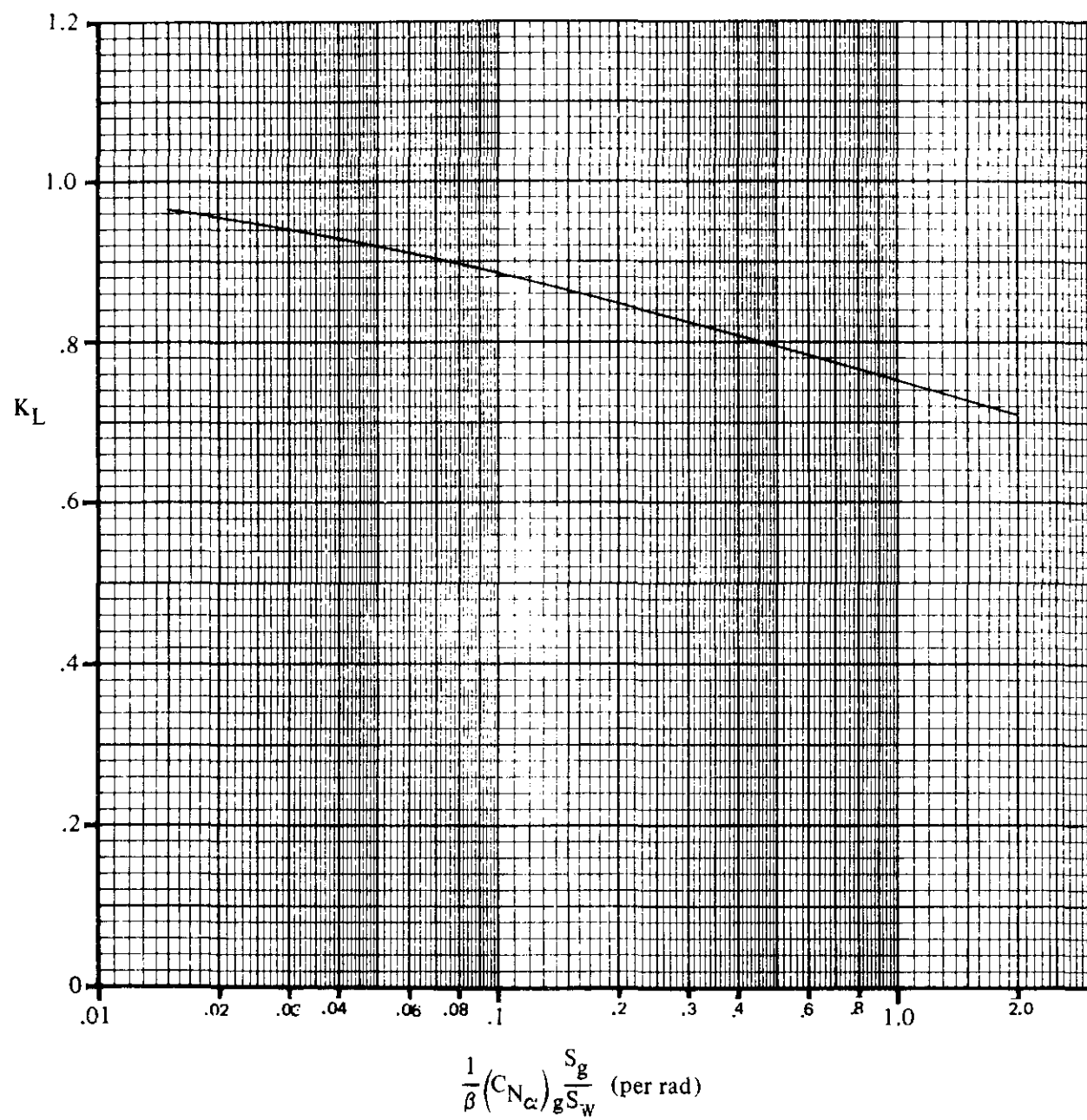


FIGURE 4.1.3.2-61 LIFT-INTERFERENCE FACTOR FOR NORMAL-FORCE-CURVE SLOPE AT SUPersonic SPEEDS

SUPersonic SPEEDS

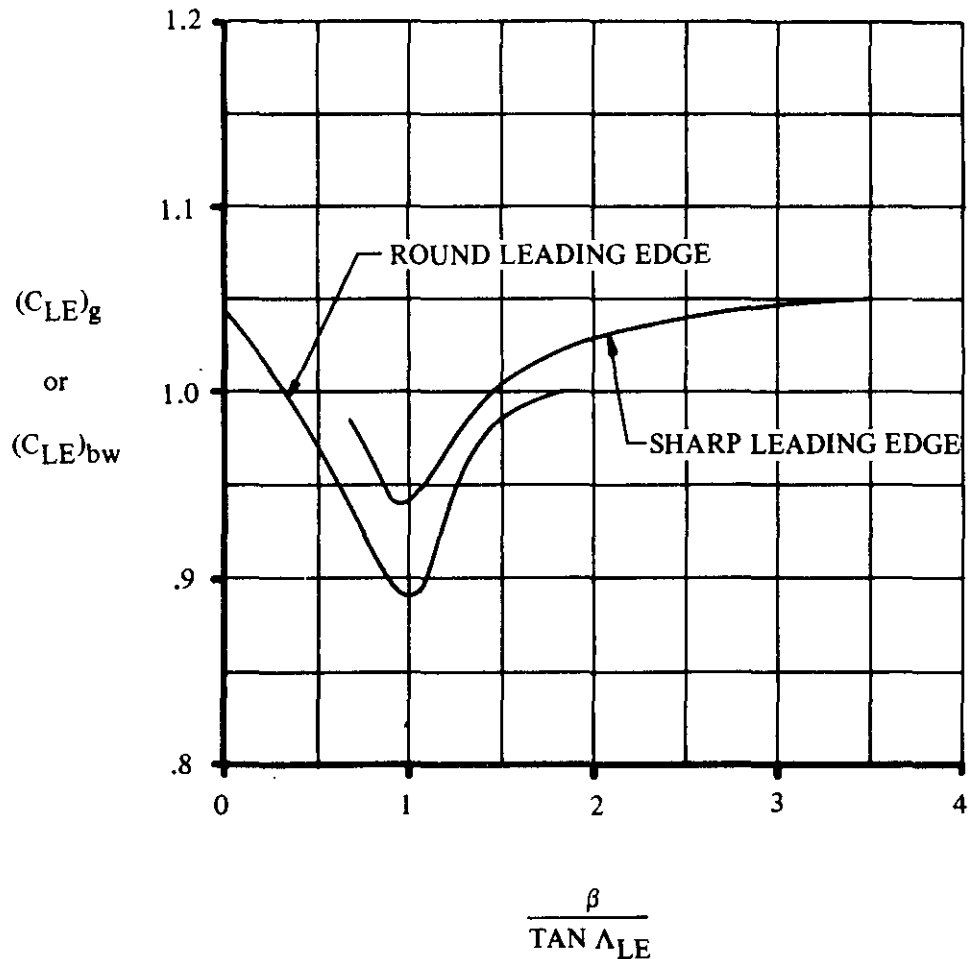


FIGURE 4.1.3.2-62 LEADING-EDGE-EFFECT FACTORS $(C_{LE})_g$ AND $(C_{LE})_{bw}$ FOR NORMAL-FORCE-CURVE SLOPE AT SUPersonic SPEEDS

SUPersonic SPEEDS

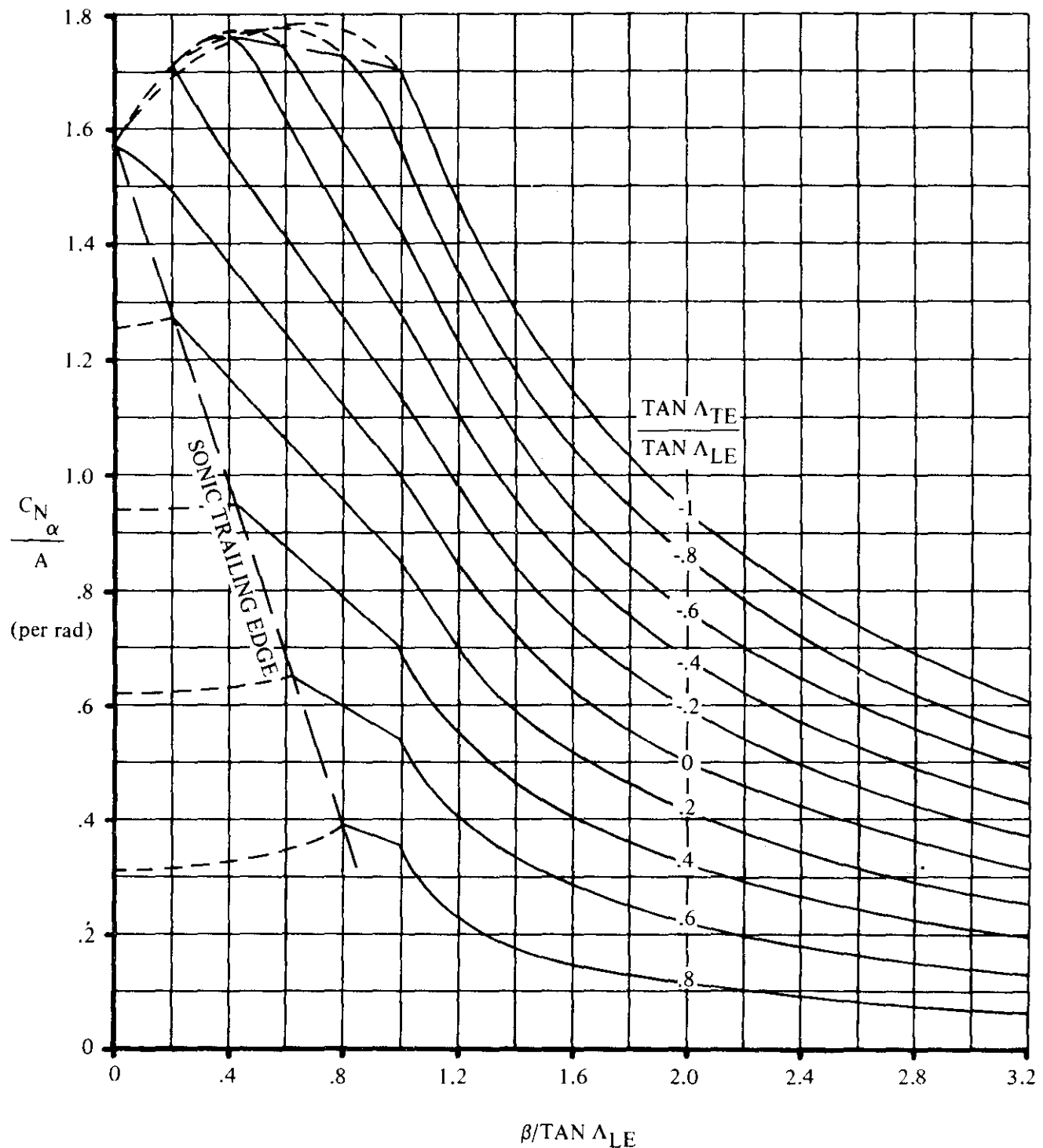


FIGURE 4.1.3.2-63 WING SUPersonic NORMAL-FORCE-CURVE SLOPE, $\lambda = 0$

SUPersonic SPEEDS

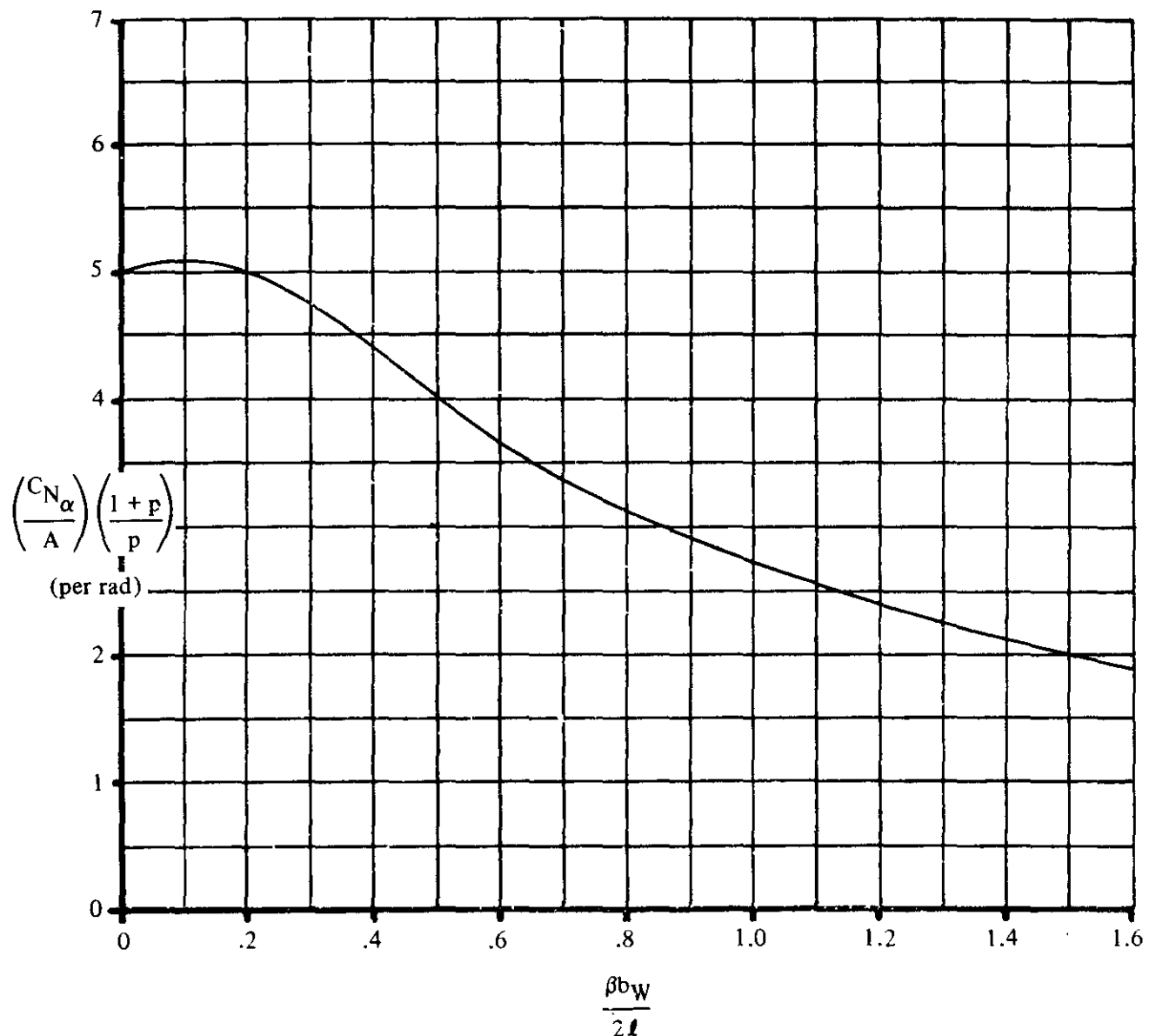


FIGURE 4.1.3.2-64 CORRELATION OF NORMAL-FORCE-CURVE SLOPE AT SUPersonic SPEEDS FOR GOTHIC AND OGEe PLANFORMS HAVING SHARP-NOSED AIRFOILS

HYPERSONIC SPEEDS

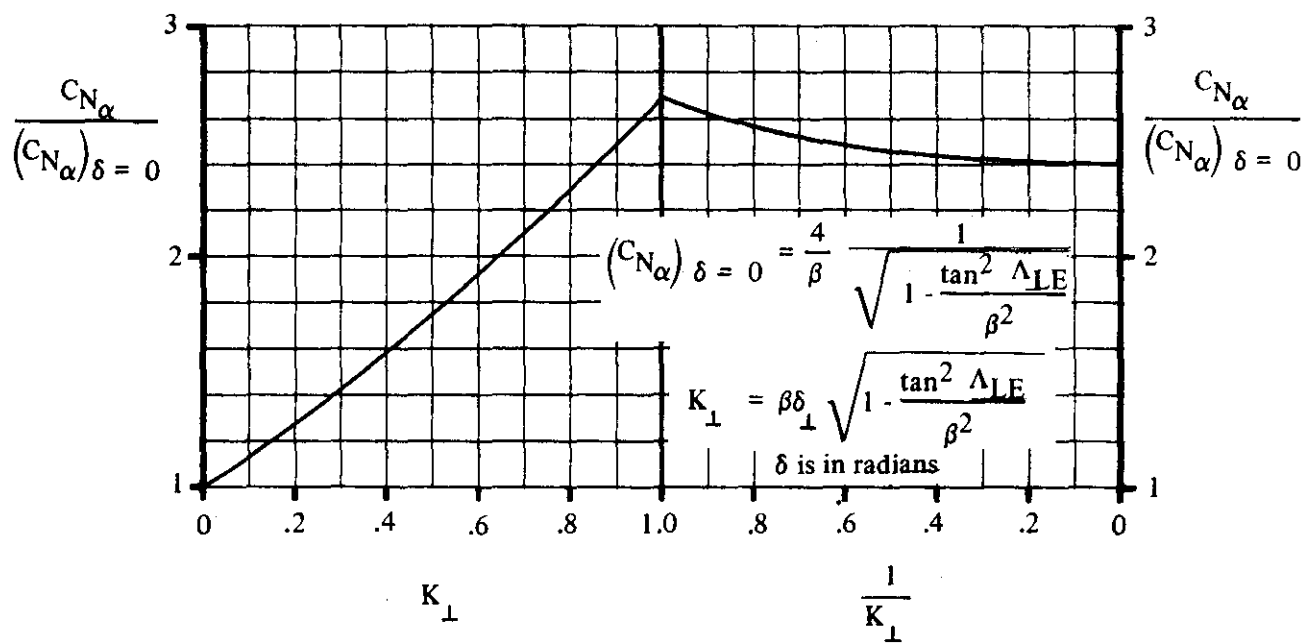


FIGURE 4.1.3.2-65 NORMAL-FORCE-CURVE SLOPE FOR THIN-WEDGE PROFILES FROM TWO-DIMENSIONAL SUPERSONIC-HYPersonic SLENDER-AIRFOIL THEORY

4.1.3.3 WING LIFT IN THE NONLINEAR ANGLE-OF-ATTACK RANGE

Methods are presented for determining the lift at subsonic speeds of the following two classes of wing planforms:

Straight-Tapered Wings (conventional, fixed, trapezoidal wings)

Non-Straight-Tapered Wings

Double-delta wings (composite wings with $A \approx 3$ or less)

Cranked wings (composite wings with $A \approx 3$ or greater)

Curved (Gothic and ogee) wings

These three general categories of non-straight-tapered wings are illustrated in sketch (a) of Section 4.1.3.2. Their wing-geometry parameters are presented in Section 2.2.2.

The lift at subsonic speeds of non-straight-tapered wings is treated in reference 1. Semiempirical methods are presented for double-delta and cranked wings; whereas the method presented for curved wings is strictly empirical. These methods are restricted to angles of attack of 20° or less.

The methods presented at transonic, supersonic, and hypersonic speeds are restricted to estimation of the lift of conventional straight-tapered wings.

A general procedure is presented for calculating the lift on conventional, straight-tapered wings at angles of attack from 0 to 90° at all speeds, based on the following equation:

$$\frac{C_L}{\cos \alpha} = C'_N = C_{N_a} \frac{\sin 2\alpha}{2} + C_{N_{aa}} |\sin \alpha| \sin \alpha$$

The quantity C_{N_a} is the linear-theory normal-force-curve slope for the appropriate speed regime

(approximated by C_{L_a} at subsonic and transonic speeds). The nonlinear coefficient $C_{N_{aa}}$ is presented in a series of charts based on empirical correlations in most cases. The absolute-value notation in the second term of the above equation insures the correct sign sense for the nonlinear term at negative angles of attack.

The above form of the normal-force equation gives results equivalent to those of linear theory at low angles of attack and equivalent to those of cross-flow theory at 90° angle of attack.

For the subsonic speed range, the linear nature of the lift curve for unswept, high-aspect-ratio wings suggests that the general method outlined above may be unnecessarily complicated. Therefore, an alternate procedure for these wings is presented in paragraph A of this section. Besides being considerably simpler than the general method, the alternate method is, in certain cases, more accurate. However, this simplified method is limited to unswept, high-aspect-ratio wings at subsonic speeds and at angles of attack below the stall.

Although nominally applicable to all untwisted, straight-tapered wings, the general method works best for thin, symmetrical, low-aspect-ratio wings. The reason for this is that certain two-dimensional section properties influence the three-dimensional lift on thick, high-aspect-ratio wings. These effects are not directly accounted for by the general method.

A. SUBSONIC

Straight-Tapered Wings

Simplified Method for High-Aspect-Ratio Wings

The subsonic lift characteristics of unswept, high-aspect-ratio wings are determined by planform geometry, as well as by the integrated airfoil section characteristics. The lift curve is essentially linear up to the angle of attack near the stall at which flow separation causes the lift curve to become nonlinear. The shape of the curve just prior to and at the stall is determined by the stalling characteristics of the airfoil and the stall pattern of the three-dimensional wing. In general, the radius of curvature of the lift curve near and at the stall is greater for the wing than for the individual airfoil sections, since all span stations of a wing do not stall at the same free-stream angle of attack. The three-dimensional effects of the wing thus cause a softening of the stall.

DATCOM METHOD

The lift curve for unswept, high-aspect-ratio wings up to the stall angle of attack may be approximated by the following procedure:

1. Determine the zero-lift angle of attack of the wing by the method given in Section 4.1.3.1.
2. Determine the lift-curve slope of the wing by the method of Section 4.1.3.2.
3. Determine the maximum lift and angle of attack for maximum lift of the wing by the method of Section 4.1.3.4.
4. Determine the quantity α^* from Section 4.1.1.
5. With the above information construct the complete lift curve.

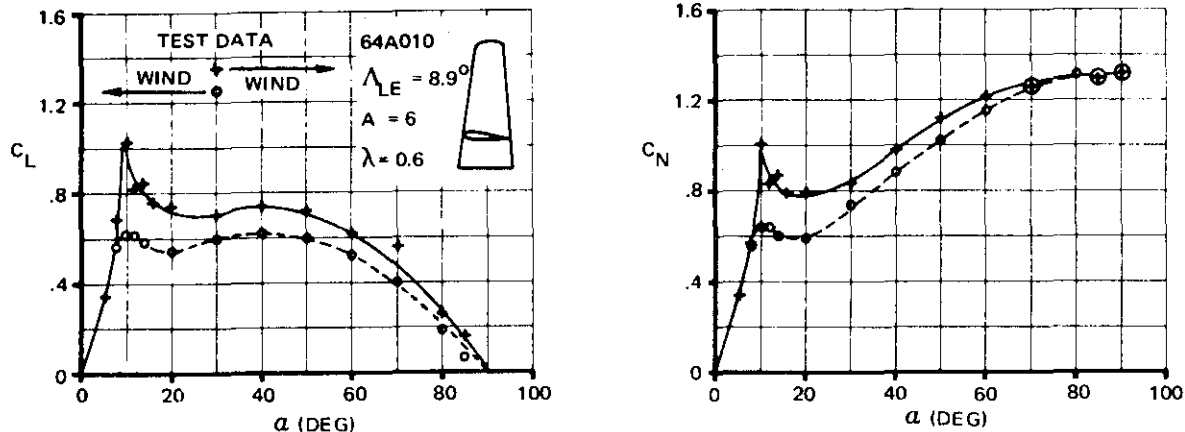
General Method for Wings of Any Aspect Ratio

Charts are presented for calculating the normal force on wings at subsonic speeds for angles of attack from 0 to 90° . The method is based on the experimental data of references 2 through 7 and is valid for the Mach number range $0 < M < 0.6$. A comparison of experimental data with results based on these charts is shown in table 4.1.3.3-A.

At angles of attack below the stall the lift on wings is a function of the parameters discussed in the sections dealing with wing lift-curve slope and maximum lift (Sections 4.1.3.2 and 4.1.3.4, respectively).

Beyond the stall, the normal-force coefficients for all wings vary in a highly nonlinear manner. The precise nature of the variation depends upon the individual wing. However, for all wings the normal-force coefficient approaches the value predicted for a flat plate as the wing angle of attack approaches 90° .

Sketch (a) shows some typical lift curves and corresponding normal-force curves.



The aspect-ratio-6 wing with the 64A010 airfoil reaches a maximum lift coefficient at a relatively low angle of attack. Following this, the lift drops abruptly and then stabilizes at nearly constant level for approximately the next 30° of angle of attack.

For the same wing with a sharp leading edge (represented by the wing in reverse flow) the maximum lift coefficient is not nearly as large as in the previous case, but the drop subsequent to the maximum lift is also much less. The result is that for angles of attack beyond stall, the lift on the blunt wing is not greatly different from the lift on the sharp wing.

This effect is accounted for in this section by making the drop in lift following maximum lift reflect the difference between the actual maximum lift and the maximum lift determined by the low-aspect-ratio method of Section 4.1.3.4. (This latter method gives results corresponding to those for a thin airfoil.)

For very low-aspect-ratio rectangular wings experimental data (reference 2) occasionally show a hysteresis in the normal-force curve near maximum lift, with different lift-curve shapes, depending on whether the angle of attack is increasing or decreasing. For these wings the results of this section must be applied with caution, since they do not reflect this hysteresis.

Reynolds number was not accounted for in the analysis of this method. There is a Reynolds-number effect on the lift-curve shape for the thicker wings, but within the Reynolds-number limitations listed on the charts the values predicted are of sufficient accuracy for most purposes.

DATCOM METHOD

The general method for estimating the subsonic normal force on conventional, straight-tapered uncambered wings for angles of attack from 0 to 90° is outlined in the following steps:

Step 1. Subsonic Normal Force at Angles of Attack Below the Stall.

The basic equation is

$$\frac{C_L}{\cos \alpha} = C'_N = C_{N_a} \frac{\sin 2\alpha}{2} + C_{N_a} \sin \alpha |\sin \alpha| \quad 4.1.3.3-a$$

The normal-force-curve slope C_{N_a} is obtained from Section 4.1.3.2.* For high-aspect-ratio

* C_{L_a} is used for C_{N_a}

wings, the lift curve is based on the appropriate section lift-curve slope. For low-aspect ratios and borderline aspect ratios (defined in Section 4.1.3.4), the section lift-curve slope is assumed to be 2π ($\kappa = 1$ in figure 4.1.3.2-49).

The nonlinear coefficient C_{Naa} is calculated as the sum of two terms:

$$C_{Naa} = (C_{Naa})_{ref} + \Delta C_{Naa} \quad 4.1.3.3-b$$

The reference nonlinear coefficient $(C_{Naa})_{ref}$ is based on C'_N at $C_{L_{max}}$ (the normal force at maximum lift), given by

$$C'_N @ C_{L_{max}} = \frac{C_{L_{max}}}{\cos \alpha_{C_{L_{max}}}} \quad 4.1.3.3-c$$

where $C_{L_{max}}$ and $\alpha_{C_{L_{max}}}$ are obtained as outlined in Section 4.1.3.4 for the wing in question. Finally, $(C_{Naa})_{ref}$ is given by

$$(C_{Naa})_{ref} = \frac{C'_N @ C_{L_{max}} - C_{Na} \left(\frac{1}{2}\right) \sin 2\alpha_{C_{L_{max}}}}{\sin \alpha_{C_{L_{max}}} |\sin \alpha_{C_{L_{max}}}|} \quad 4.1.3.3-d$$

The incremental nonlinear lift coefficient ΔC_{Naa} is now read from figure 4.1.3.3-55a as a function of the parameter J and the ratio of the tangent of the angle of attack in question to the tangent of the angle of attack at $C_{L_{max}}$. The wing-shape parameter J is defined by the equation

$$J = 0.3 (C_1 + 1) \frac{A}{\beta} \cos \Lambda_{LE} \left\{ (C_1 + 1) (C_2 + 1) - \left[\frac{(C_2 + 1) A \tan \Lambda_{LE}}{7} \right]^3 \right\} \quad 4.1.3.3-e$$

The constants C_1 and C_2 are the empirical taper-ratio constants of Section 4.1.3.4.

The wing lift coefficient may now be calculated for any angle of attack up to and including the stall by substituting the appropriate values of C_{Na} and C_{Naa} in equation 4.1.3.3-a.

Step 2. Subsonic Normal Force at Angles of Attack Beyond the Stall.

The equation for the nonlinear coefficient at angles of attack beyond the stall is

$$C_{Naa} = (C_{Naa})_{ref} + \left[(C_{Naa})_{90^\circ} - (C_{Naa})_{ref} \right] \left[1 - \frac{\tan \alpha_{C_{L_{max}}}}{\tan \alpha} \right] + \beta^2 D \frac{C_{Na}}{2.3} \left(\frac{C_{L_{max}}}{C_{L_{max}}^*} \right)^2 \quad 4.1.3.3-f$$

where

$$(C_{Naa})_{ref}$$

is the reference nonlinear coefficient based on C'_N at $C_{L_{max}}$, calculated as outlined in step 1.

$$(C_{Naa})_{90^\circ}$$

is the normal-force coefficient at $\alpha = 90^\circ$. At 90° , $C_{Naa} = C'_N$ since $\sin^2 \alpha = 1$ and $\frac{\sin 2\alpha}{2} = 0$. The quantity C'_N is obtained from figure 4.1.3.3-55b as a function of aspect ratio (references 3 and 4).

$$\beta$$

is the Mach number parameter, $\sqrt{1 - M^2}$.

$$D$$

is an empirical nonlinear term read from the right-hand side of figure 4.1.3.3-55a.

$$C_{L_{max}}$$

is the maximum lift coefficient obtained as outlined in Section 4.1.3.4 for the wing in question.

$$C_{L_{max}}^*$$

is the maximum lift coefficient of the wing, calculated by using the low-aspect-ratio method of paragraph B of Section 4.1.3.4. If the wing in question has a low aspect ratio by the definition of Section 4.1.3.4, then $C_{L_{max}}^* = C_{L_{max}}$ and the last term in equation 4.1.3.3-f is

$\beta D^2 \frac{C_{Naa}}{2.3}$. If the wing in question has a high aspect ratio by the definition of Section 4.1.3.4, the value of $(C_{L_{max}})_{base}$ is obtained from figure 4.1.3.4-23 at $(C_1 + 1) \frac{A}{\beta} \cos \Lambda_{LE} = \frac{4}{\beta}$.

Substituting values of C_{Naa} determined by equation 4.1.3.3-f, together with the value of C_{Naa} from figure 4.1.3.2-49, into equation 4.1.3.3-a gives the wing normal-force coefficient for angles of attack between the stall angle and 90° .

For cambered wings the procedure outlined in steps 1 and 2 must be altered slightly. Potential theory states that the lift-curve slope of a wing is unaltered by camber. Thus the lift is defined by

$$C_L = C_{L_a} (\alpha - \alpha_0)$$

where α_0 is the angle of attack for zero lift. For angles of attack below the stall an equivalent angle of attack for the cambered wing is defined as $\alpha_e = \alpha - \alpha_0$. Then, the equations for lift are

$$C_L = C_N' \cos \alpha$$

$$C_N' = C_{N_a} \frac{\sin 2\alpha_e}{2} + C_{Naa} \sin \alpha_e |\sin \alpha_e| \quad (\text{equation 4.1.3.3-a})$$

where C_{Naa} is given by equation 4.1.3.3-b, but with $\alpha_{C_{L_{max}}}$ replaced by $(\alpha_e)_{C_{L_{max}}}$ in determining

$(C_{Naa})_{ref}$ and ΔC_{Naa} ; i.e.,

$$(C_{Naa})_{ref} = \frac{C'_N @ C_{L_{max}} - C_{Na} \left(\frac{1}{2}\right) \sin 2(a_e)_{C_{L_{max}}}}{\sin(a_e)_{C_{L_{max}}} \left| \sin(a_e)_{C_{L_{max}}} \right|} \quad (\text{equation 4.1.3.3-d})$$

ΔC_{Naa} is read from figure 4.1.3.3-55a as a function of J , and the ratio $\frac{\tan a_e}{\tan(a_e)_{C_{L_{max}}}}$.

For angles of attack beyond the stall, the linear term vanishes as a approaches 90° , and the equivalent angle of attack for the cambered wing is defined as

$$a_e = a \left[1 + \frac{a_0}{90^\circ - a_{C_{L_{max}}}} \right] - \frac{90^\circ a_0}{90^\circ - a_{C_{L_{max}}}} \quad 4.1.3.3-g$$

where a , a_0 , and $a_{C_{L_{max}}}$ are measured in degrees. Then, as before,

$$C_L = C'_N \cos a$$

$$C'_N = C_{Na} \frac{\sin 2a_e}{2} + C_{Naa} \sin a_e |\sin a_e| \quad (\text{equation 4.1.3.3-a})$$

where C_{Naa} is given by equation 4.1.3.3-f with $(C_{Naa})_{ref}$ calculated as outlined above for the cambered wing at angles of attack below the stall, and $a = a_e$.

In applying the above methods to a wing which is on the borderline between a high aspect ratio and a low aspect ratio as defined in Section 4.1.3.4, i.e., $\frac{3}{(C_1 + 1) \cos \Lambda_{LE}} \leq A \leq \frac{4}{(C_1 + 1) \cos \Lambda_{LE}}$, either the high- or the low-aspect-ratio procedure of Section 4.1.3.4 may be applied to determine the wing maximum-lift characteristics. It is suggested that the low-aspect-ratio procedure be applied as this facilitates application of equation 4.1.3.3-f, since $C_{L_{max}}^* = C_{L_{max}}$.

Three sample problems are included on pages 4.1.3.3-11 through 4.1.3.3-23 to illustrate the calculation procedure for estimating wing lift in the nonlinear angle-of-attack range of conventional, straight-tapered wings. Comparison with experimental data is presented in each case.

Sample problems 1 and 2 emphasize the high-angle-of-attack characteristics of a low-aspect-ratio and a high-aspect-ratio wing, respectively. Comparison is made between the calculated and experimental values for both lift and normal force. Agreement between the calculated and experimental values near stall is not particularly good for the high-aspect-ratio wing. However, the experimental data in this case should be viewed with caution, since it indicates a highly nonlinear lift curve prior to stall for a high-aspect-ratio wing.

Sample problem 3 illustrates the special case of a cambered wing, as well as a more representative comparison of lift at the lower angles of attack.

Non-Straight-Tapered Wings

Semiempirical methods, taken from reference 1, are presented for estimating the nonlinear lift of double-delta and cranked wings at subsonic speeds. The nonlinear lift of double-delta wings is based on the hypothesis that an expression similar to that developed by Külchermann (reference 8) for the nonlinear lift of small-aspect-ratio wings with leading-edge separation may be applied to double-delta planforms. By using such an approach, a correlation proportional to the linear lift-curve slope was developed that is strongly dependent on the inboard-panel geometry. The characteristic behavior exhibited by the experimental data of cranked wings led the authors of reference 1 to conclude that the flow field about these wings is similar to that about a low-aspect-ratio delta wing with leading-edge separation. On the basis of these observations, the nonlinear lift of cranked wings has been related to the correlation for the nonlinear lift of double-delta wings.

The nonlinear lift of curved (Gothic and ogee) wings has been correlated in reference 1 by the empirical method developed by Peckham in reference 9.

The following methods for estimating the nonlinear lift of non-straight-tapered wings are limited to angles of attack of 20° or less.

DATCOM METHODS

Double-Delta Wings

The nonlinear lift of double-delta wings at subsonic speeds is obtained from the procedure outlined in the following steps:

Step 1. Calculate the subsonic wing lift-curve slope C_{L_a} by the method presented for double-delta wings in paragraph A of Section 4.1.3.2.

Step 2. Obtain values of the parameter $\frac{C_L}{C_{L_a}} \frac{A_i}{\eta_B}$ at angles of attack of $4^{\circ}, 8^{\circ}, 12^{\circ}, 16^{\circ}$, and 20°

from figure 4.1.3.3-56. This parameter is correlated as a function of wing aspect ratio A , the leading-edge sweepback of the inboard panel Λ_{LE_i} , and the Mach number parameter

$\beta = \sqrt{1 - M^2}$. It should be noted that for angles of attack up to 8° , an aspect-ratio dependence exists at Mach numbers above 0.7. Not enough data are available at high subsonic Mach numbers to allow investigation of the aspect-ratio dependence above 8° angle of attack.

Step 3. Calculate C_L by

$$C_L = \left(\frac{C_L}{C_{L_a}} \frac{A_i}{\eta_B} \right) \frac{C_{L_a}}{A_i/\eta_B} \quad 4.1.3.3-h$$

where

η_B is the spanwise location of the break in the leading edge expressed in percent of wing semispan.

A_i is the aspect ratio of the planform formed by the two inboard panels

Step 4. Plot calculated values of C_L versus α and fair a curve through the points tangent to C_{L_a} near zero lift.

Application of this technique is illustrated by sample problem 4 at the conclusion of paragraph A (page 4.1.3.3-23).

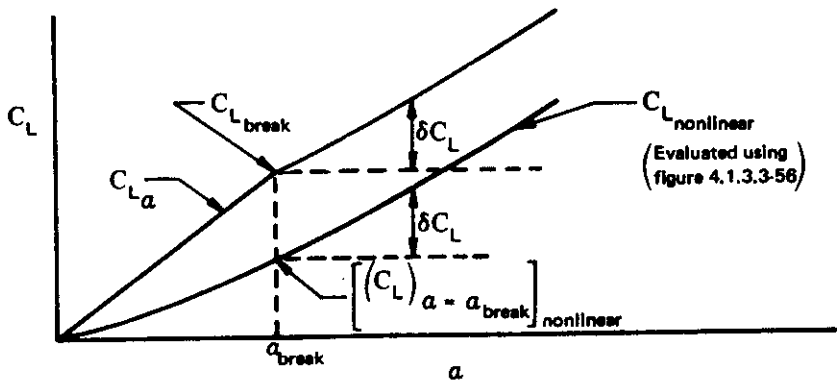
A comparison of test data for 21 configurations with the nonlinear lift of double-delta wings calculated by this method is presented as table 4.1.3.3-B (taken from reference 1). The largest errors generally occur at $\alpha = 4^\circ$ with the accuracy improving as the angle of attack increases. The ratio of body diameter to wing span of the models investigated varied from 0.077 to 0.149, and no apparent effects of relative body size are evident. No significant effects of thickness ratio on lift are evident over the limited thickness-ratio range covered (0.02 to 0.04). The Reynolds numbers of the test data fall into two ranges, 1.04×10^6 to 3.6×10^6 and 17.1×10^6 to 20.3×10^6 . Although there are not enough data to allow a quantitative prediction of Reynolds-number effect, it is reasonable to expect that Reynolds number will influence the lift.

Although no attempt was made to define the effect of leading-edge shape on lift, even with round leading edges a highly-swept wing should be expected to have leading-edge separation at the higher angles of attack. With separated flow over the entire leading edge, the resulting vortex pattern should be equivalent to that for a wing with a sharp leading edge. Since the vortex pattern exerts a strong influence on the flow field, at the higher angles of attack the aerodynamic characteristics of wings with round and sharp leading edges should be similar.

It is difficult to assess quantitatively the validity of the aspect-ratio dependence, shown in figure 4.1.3.3-56, at Mach numbers above 0.7. This dependence is based on only nine configurations, and no data are available above 8° angle of attack.

Cranked Wings

The nonlinear lift of cranked wings at subsonic speeds is related to the correlation for the nonlinear lift of double-delta wings presented as figure 4.1.3.3-56. The prediction method consists of a construction procedure for the buildup of lift above the angle of attack at which the lift curve breaks. The break in the lift curve is defined as that point where the lift drops off from the linear value, and the curve itself also becomes nonlinear. The cranked wings examined during the analysis reported in reference 1 showed a break in the lift curve at angles of attack between 6° and 7° . The prediction method is illustrated schematically in sketch (b).



SKETCH (b)

By referring to sketch (b), the nonlinear lift of cranked wings at subsonic speeds is obtained from the procedure outlined in the following steps:

- Step 1. Calculate the subsonic wing lift-curve slope C_{L_a} by the method presented for cranked wings in paragraph A of Section 4.1.3.2.

Step 2. Obtain a_{break} as a function of the leading-edge sweepback of the inboard panel from figure 4.1.3.3-57.

Step 3. Calculate $C_{L_{break}}$ by

$$C_{L_{break}} = C_{L_a} a_{break} \quad 4.1.3.3-i$$

Step 4. Obtain values of the parameter $\frac{C_L}{C_{L_a}} \frac{A_i}{\eta_B}$ at angles of attack of $4^\circ, 8^\circ, 12^\circ, 16^\circ$, and 20° from figure 4.1.3.3-56, and calculate $C_{L_{nonlinear}}$ using equation 4.1.3.3-h. (See double-delta-wing method of this paragraph.)

Step 5. Obtain $[C_L]_{a=a_{break}}$ by plotting $C_{L_{nonlinear}}$ versus a from step 4, and then calculate δC_L by

$$\delta C_L = [C_L - (C_L)_{a=a_{break}}]_{nonlinear} \quad 4.1.3.3-j$$

Step 6. Add the δC_L values obtained in step 5 to the $C_{L_{break}}$ value obtained in step 3 to obtain the total C_L for each a above a_{break} ; i.e.,

$$C_L = C_{L_{break}} + \delta C_L \quad 4.1.3.3-k$$

Application of this technique is illustrated by sample problem 5 on page 4.1.3.3-25.

A comparison of test data for seven configurations with the nonlinear lift of cranked wings calculated by this method is presented as table 4.1.3.3-C (taken from reference 1). The ratio of body diameter to wing span of the models investigated varied from 0.062 to 0.147, and no apparent effects of relative body size are evident. No significant effects of thickness ratio on lift are evident over the limited thickness-ratio range covered (0.02 to 0.06).

Before attempting to assess the validity of the method some salient features should be pointed out. The accuracy of the method is strongly dependent on knowing a_{break} . Since the break in the lift curve is essentially a type of stall phenomenon, Reynolds number may have a significant effect on a_{break} . Unfortunately, a lack of data prevented a detailed study of Reynolds number effects during the correlation reported in reference 1. The method also assumes a sharp discontinuity at a_{break} ; however, test data show that as aspect ratio is reduced the break in the lift curve becomes less apparent, and for the lower-aspect-ratio wings the lift curve exhibits a gradual transition from the linear to the nonlinear region. Furthermore, the shape of the nonlinear lift curve is based on the correlation derived for double-delta wings, which is restricted to wings with small or zero trailing-edge sweep angles.

From the foregoing discussion it might be expected that the method would give acceptable results when applied to wings with moderate to high aspect ratios and small or zero trailing-edge sweep angles. Of the seven configurations listed in table 4.1.3.3-C, these conditions are met only by the configurations of references 37, 38, and 39. The average error for the nine calculated points of those references is 4.9 percent.

It is difficult to assess quantitatively the effect of Mach number on the accuracy of the method. However, it should be pointed out that the curves of figure 4.1.3.3-56 have been extrapolated to account for low values

of $\beta \tan \Lambda_{LE_1}$ for the configuration of reference 28 at $M = 0.80, 0.85$, and 0.90 and for the configurations of reference 36 at $M = 0.90$.

Since the configurations of references 38 and 39 had twisted and cambered wings, their lift curves were significantly displaced from the origin. In analyzing the test data for these configurations the lift curves were shifted so that $C_{L,a=0} = 0$. The calculated results for these configurations compared well with the adjusted test values, indicating that twist and camber have a negligible effect on the shape of the lift curve in the nonlinear region.

Test data show that the lift curve tends to fall off at approximately 16° angle of attack at $M = 0.80$ and 0.85 for the configuration of reference 28, and at approximately 12° angle of attack throughout the Mach range tested for both configurations of reference 36. This trend indicates that the inboard panel is beginning to stall; consequently, the method should not be expected to give reliable results for these configurations at higher angles of attack.

Curved Wings

The nonlinear lift of curved (Gothic and ogee) wings at subsonic speeds was correlated in reference 1 by Peckham's method (reference 9) where the ratio of lift to the square root of the wing slenderness parameter plotted versus angle of attack converges on a single curve.

The nonlinear lift is obtained from the procedure outlined in the following steps:

Step 1. Using the given wing geometry calculate the wing slenderness parameter $\frac{b_w}{2l}$. (See Section 2.2.2 for wing-geometry parameters.)

Step 2. At the desired values of angle of attack obtain $C_L \sqrt{\frac{b_w}{2l}}$ from figure 4.1.3.3-58.

Step 3. Calculate C_L at each a by

$$C_L = \frac{C_L}{\sqrt{\frac{b_w}{2l}}} \sqrt{\frac{b_w}{2l}} \quad 4.1.3.3-l$$

Application of this technique is illustrated by the sample problem on page 4.1.3.3-28.

A comparison of test data for 11 configurations with the nonlinear lift of curved wings calculated by this method is presented as table 4.1.3.3-D (taken from reference 1). The results indicate that the best accuracy is obtained at the lower Mach numbers and for configurations with aspect ratios near 1.0. Three of the configurations analyzed were wing-bodies, and for these configurations no significant wing-body interference effects were evident. However, it should be noted that no blended wing-body configurations are included in the correlation. Such configurations have a very thick cross section near the apex that should be expected to cause a loss in lift. The two blended wing-body configurations of references 43 and 44 were analyzed during the investigation reported in reference 1, and it was found that the lift predicted using figure 4.1.3.3-58 was about 10 percent higher than test data throughout the angle-of-attack range of both configurations.

Since there is no theoretical basis for this method, it should be used with caution outside the planform parameter ranges covered in the correlation. The correlation of figure 4.1.3.3-58 is based on data from sharp-edged, thin, Gothic and ogee wings with moderate trailing-edge sweep angles ($\pm 15^\circ$). The planform param-

eter ranges of the data are

$$0.75 \leq A \leq 2.00$$

$$0.45 \leq \frac{S_w}{b_w l} \leq 0.667$$

$$0.25 \leq \frac{b_w}{2l} \leq 0.54$$

Sample Problems

Conventional, Straight-Tapered Wings

1. High-Angle-of-Attack Characteristics of a Low-Aspect-Ratio Wing.

Given: Delta wing of reference 25.

$$A = 2.0 \quad \lambda = 0 \quad \Lambda_{LE} = 63.5^\circ \quad \text{NACA 0005 airfoil (free-stream direction)}$$

$$M = 0.2; \beta = 0.98 \quad R_\infty = 1.2 \text{ to } 2.2 \times 10^6 \text{ (based on MAC)}$$

$$\kappa = 1.0 \text{ (assumed)} \quad \Lambda_{c/2} = 45.2^\circ$$

Compute: Angles of attack below the stall

Find $C_{L_{max}}$ and $\alpha_{C_{L_{max}}}$ as outlined in Section 4.1.3.4 and C_{Na} from Section 4.1.3.2.

$$A < \frac{3}{(C_1 + 1) \cos \Lambda_{LE}}; \text{ therefore, use low-aspect-ratio method.}$$

$$\Delta y = 1.38 \text{ (figure 2.2.1-8)}$$

$$C_1 = 0, C_2 = 0 \text{ (figure 4.1.3.4-24b)}$$

$$(C_1 + 1) \frac{A}{\beta} \cos \Lambda_{LE} = \frac{2}{0.98} (0.4462) = 0.91$$

$$(C_{L_{max}})_{base} = 1.29 \text{ (figure 4.1.3.4-23a)}$$

$$(C_2 + 1) A \tan \Lambda_{LE} = 2(2.006) = 4.01$$

$$\Delta C_{L_{max}} = 0 \text{ (figure 4.1.3.4-24a)}$$

$$C_{L_{max}} = (C_{L_{max}})_{base} + \Delta C_{L_{max}} \text{ (equation 4.1.3.4-g)}$$

$$= 1.29$$

$$(a_{C_L \max})_{\text{base}} = 34.6^\circ \text{ (figure 4.1.3.4-25a)}$$

$$A \cos \Lambda_{LE} [1 + (2\lambda)^2] = 2(0.4462) [1 + 0] = 0.8924$$

$$\Delta a_{C_L \max} = -0.1^\circ \text{ (figure 4.1.3.4-25b)}$$

$$\begin{aligned} a_{C_L \max} &= (a_{C_L \max})_{\text{base}} + \Delta a_{C_L \max} \quad (\text{equation 4.1.3.4-h}) \\ &= 34.5^\circ \end{aligned}$$

Find $C_{L a}$

$$\frac{A}{K} \left[\beta^2 + \tan^2 \Lambda_{c/2} \right]^{\frac{1}{2}} = 2.81$$

$$C_{L a}/A = 1.15 \text{ per rad (figure 4.1.3.2-49)}$$

$$C_{L a} = C_{N a} = \left(\frac{C_{L a}}{A} \right) A = (1.15)(2.0) = 2.30 \text{ per rad}$$

Find $(C_{N aa})_{\text{ref}}$

$$C'_N @ C_{L \max} = \frac{C_{L \max}}{\cos a_{C_{L \max}}} \quad (\text{equation 4.1.3.3-c})$$

$$= \frac{1.29}{0.8241} = 1.565$$

$$(C_{N aa})_{\text{ref}} = \frac{C'_N @ C_{L \max} - C_{N a} \left(\frac{1}{2} \right) \sin 2a_{C_{L \max}}}{\sin a_{C_{L \max}} \left| \sin a_{C_{L \max}} \right|} \quad (\text{equation 4.1.3.3-d})$$

$$= \frac{1.565 - 2.30 \left(\frac{0.9336}{2} \right)}{(0.5664)^2} = 1.53$$

Find J

$$J = 0.3(C_1 + 1) \frac{A}{\beta} \cos \Lambda_{LE} \left\{ (C_1 + 1)(C_2 + 1) - \left[\frac{(C_2 + 1) A \tan \Lambda_{LE}}{7} \right]^3 \right\} \quad (\text{equation 4.1.3.3-e})$$

$$= 0.3(1) \left(\frac{2}{0.98} \right) (0.4462) \left\{ 1 - \left[\frac{2(2.006)}{7} \right]^3 \right\}$$

$$= 0.222$$

Solution: Angles of Attack Below the Stall

$$\frac{C_L}{\cos \alpha} = C'_N = C_{N_a} \frac{\sin 2\alpha}{2} + C_{N_{aa}} \sin \alpha |\sin \alpha| \quad (\text{equation 4.1.3.3-a})$$

$$C_{N_{aa}} = (C_{N_{aa, ref}}) + \Delta C_{N_{aa}} \quad (\text{equation 4.1.3.3-b})$$

$$= 1.53 + \Delta C_{N_{aa}}$$

① α (deg)	② $\frac{\tan \alpha}{\tan \alpha / C_{L_{max}}}$	③ $\Delta C_{N_{aa}}$ fig. 4.1.3.3-55a	④ $C_{N_{aa}}$ eq. 4.1.3.3-b 1.53 + ③	⑤ $C_{N_{aa}} \sin^2 \alpha$	⑥ $C_{N_a} \frac{\sin 2\alpha}{2}$	⑦ C'_N eq. 4.1.3.3-a ⑤ + ⑥	⑧ C_L = $(C'_N \cos \alpha)$
5	0.126	0.80	2.33	0.018	0.200	0.218	0.22
10	0.268	0.80	2.33	0.070	0.393	0.463	0.46
15	0.390	0.73	2.26	0.151	0.575	0.726	0.70
20	0.530	0.65	2.18	0.266	0.739	0.994	0.93
25	0.680	0.45	1.98	0.364	0.881	1.236	1.12
30	0.840	0.25	1.78	0.445	0.996	1.441	1.25
34.5	1.000	0	1.63	0.491	1.070	1.561	1.29

Compute: Angles of Attack Above the Stall

$$C_{L_{max}}^* = C_{L_{max}} \quad (\text{low-aspect-ratio wing})$$

$$(C_{N_{aa}})_{90^\circ} = 1.20 \quad (\text{figure 4.1.3.3-55b})$$

$$(C_{N_{aa}})_{ref} = 1.53 \quad (\text{calculated on page 4.1.3.3-12})$$

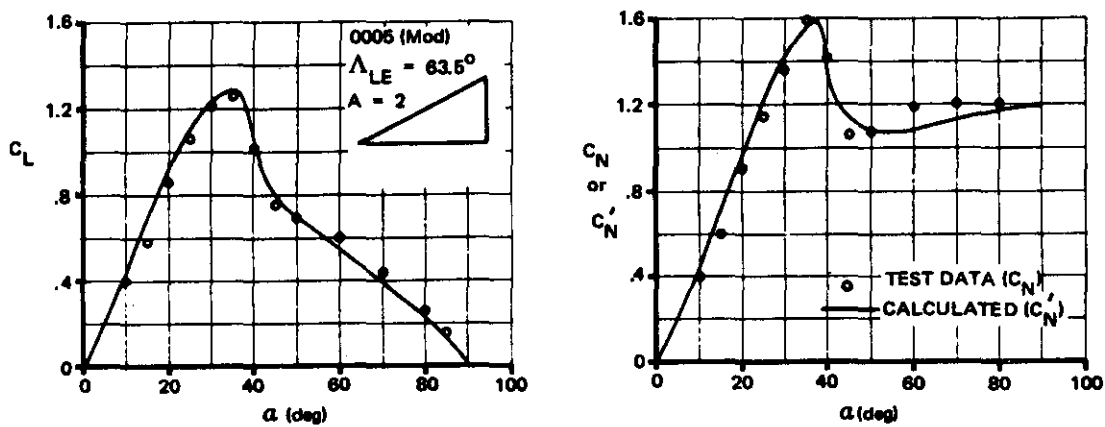
Solution: Angles of Attack Above the Stall

$$\frac{C_L}{\cos \alpha} = C'_N = C_{N_a} \frac{\sin 2\alpha}{2} + C_{N_{aa}} \sin \alpha |\sin \alpha| \quad (\text{equation 4.1.3.3-a})$$

$$\begin{aligned}
 C_{Naa} &= (C_{Naa})_{ref} + [(C_{Naa})_{90^\circ} - (C_{Naa})_{ref}] \left[1 - \frac{\tan \alpha_{C_L \max}}{\tan \alpha} \right] + \beta^2 D \frac{C_{Na}}{2.3} \left(\frac{C_L \max}{C_L^* \max} \right)^2 \\
 &= 1.53 + (1.20 - 1.53) \left[1 - \frac{\tan \alpha_{C_L \max}}{\tan \alpha} \right] + 0.96 D \frac{2.30}{2.3} (1) \\
 &= 1.20 + 0.33 \frac{\tan \alpha_{C_L \max}}{\tan \alpha} + 0.96 D
 \end{aligned}
 \quad (\text{equation 4.1.3.3-f})$$

① α (deg)	② $\frac{\tan \alpha_{C_L \max}}{\tan \alpha}$	③ D fig. 4.1.3.3-55e	④ $C_{N\alpha\alpha}$ eq. 4.1.3.3-f 1.2 + .33(2) + .96(3)	⑤ $C_{N\alpha\alpha} \sin^2 \alpha$	⑥ $C_N \frac{\sin 2\alpha}{2}$	⑦ C'_N eq. 4.1.3.3-e ⑤ + ⑥	⑧ C_L = $(C'_N \cos \alpha)$
37	0.912	-0.20	1.309	0.474	1.11	1.584	1.26
40	0.819	-0.85	0.654	0.270	1.13	1.400	1.07
45	0.687	-1.43	0.054	0.027	1.15	1.177	0.83
50	0.577	-1.54	-0.088	-0.062	1.13	1.078	0.69
60	0.397	-1.27	0.112	0.084	0.996	1.080	0.54
70	0.250	-0.88	0.438	0.387	0.74	1.127	0.38
90	0	0	1.200	1.200	0	1.200	0

A comparison of the calculated values and the experimental data of reference 25 is presented as sketch (c).



SKETCH (c)

2. High-Angle-of-Attack Characteristics of a High-Aspect-Ratio Wing.

Given: Wing 7 of reference 25.

$$A = 6.0 \quad \lambda = 0.5 \quad \Lambda_{LE} = 8.9^\circ \quad \text{NACA 64A010 airfoil (free-stream direction)}$$

$$M = 0.2; \quad \beta = 0.98 \quad R_f = 1.5 \text{ to } 2.2 \times 10^6 \quad (\text{based on MAC})$$

$$\kappa = 1.0 \text{ (assumed)} \quad \Lambda_{c/2} = 2.6^\circ$$

Compute: Angles of Attack Below the Stall

Find $C_{L_{max}}$ and $a_{C_{L_{max}}}$ as outlined in Section 4.1.3.4 and C_{N_a} from Section 4.1.3.2.

$$A > \frac{4}{(C_1 + 1) \cos \Lambda_{LE}}; \text{ therefore, use high-aspect-ratio method}$$

$$\Delta y = 2.10 \quad (\text{figure 2.2.1-8})$$

$$c_{L_{max}} = 1.23 \text{ at } R_f = 9 \times 10^6 \quad (\text{table 4.1.1-B})$$

$$\Delta_3 c_{L_{max}} = -0.14 \text{ for } R_f = 2.0 \times 10^6 \quad (\text{figure 4.1.1.4-7b, extrapolated})$$

$$c_{L_{max}} = 1.23 - 0.14 = 1.09 \quad (\text{adjusted for test } R_f)$$

$$\frac{C_{L_{max}}}{c_{L_{max}}} = 0.895 \quad (\text{figure 4.1.3.4-21a})$$

$$\Delta C_{L_{max}} = 0 \quad (\text{figure 4.1.3.4-22})$$

$$C_{L_{max}} = \left(\frac{C_{L_{max}}}{c_{L_{max}}} \right) c_{L_{max}} + \Delta C_{L_{max}} \quad (\text{equation 4.1.3.4-d})$$

$$= (0.895)(1.09) = 0.975$$

Find C_{L_a}

$$\frac{A}{\kappa} \left[\beta^2 + \tan^2 \Lambda_{c/2} \right]^{1/2} = 5.89$$

$$C_{L_a}/A = 0.76 \text{ per rad} \quad (\text{figure 4.1.3.2-49})$$

$$C_{L_a} = C_{N_a} = \left(\frac{C_L a}{A} \right) A = (0.76)(6) = 4.56 \text{ per rad}$$

$$\Delta a_{C_{L_{\max}}} = 1.0^\circ \text{ (figure 4.1.3.4-21b)}$$

$$a_0 = a_i - \frac{c_{L_i}}{c_{L_a}} = 0 - \frac{0}{0.110} = 0 \text{ (equation 4.1.3.1-a)}$$

$$a_{C_{L_{\max}}} = \frac{C_{L_{\max}}}{C_{L_a}} + a_0 + \Delta a_{C_{L_{\max}}} \text{ (equation 4.1.3.4-e)}$$

$$= \frac{0.975}{4.56/(57.3)} + 0 + 1.0 = 13.3^\circ$$

Find $(C_{N_{aa}})_{ref}$

$$C'_N @ C_{L_{\max}} = \frac{C_{L_{\max}}}{\cos a_{C_{L_{\max}}}} = \frac{0.975}{0.9732} = 1.002 \text{ (equation 4.1.3.3-c)}$$

$$(C_{N_{aa}})_{ref} = \frac{C'_N @ C_{L_{\max}} - C_{N_a} \left(\frac{1}{2} \right) \sin 2a_{C_{L_{\max}}}}{\sin a_{C_{L_{\max}}} |\sin a_{C_{L_{\max}}}|} \text{ (equation 4.1.3.3-d)}$$

$$= \frac{1.002 - 4.56 \frac{0.4478}{2}}{(0.2300)^2} = -0.359$$

Find J

$$C_1 = 0.3, C_2 = 1.06 \text{ (figure 4.1.3.4-24b)}$$

$$J = 0.3 (C_1 + 1) \frac{A}{\beta} \cos \Lambda_{LE} \left\{ (C_1 + 1)(C_2 + 1) - \left[\frac{(C_2 + 1) A \tan \Lambda_{LE}}{7} \right]^3 \right\} \text{ (equation 4.1.3.3-e)}$$

$$= 0.3 (1.31) \frac{6}{0.98} (0.988) \left\{ (1.31)(2.06) - \left[\frac{(2.06)(6)(0.1566)}{7} \right]^3 \right\}$$

$$= 6.36$$

Solution: Angles of Attack Below the Stall

$$\frac{C_L}{\cos \alpha} = C'_N = C_{N_a} \frac{\sin 2\alpha}{2} + C_{N_{aa}} \sin \alpha |\sin \alpha| \text{ (equation 4.1.3.3-a)}$$

$$C_{N_{aa}} = (C_{N_{aa}})_{ref} + \Delta C_{N_{aa}} \text{ (equation 4.1.3.3-b)}$$

$$C_{N_{aa}} = -0.359 + \Delta C_{N_{aa}}$$

① α (deg)	② $\frac{\tan \alpha}{\tan \alpha C_{L_{max}}}$	③ $\Delta C_{N_{aa}}$ fig. 4.1.3.3-55a	④ $C_{N_{aa}}$ eq. 4.1.3.3-b -0.359 + ③	⑤ $C_{N_{aa}} \sin^2 \alpha$	⑥ $C_{N_a} \frac{\sin 2\alpha}{2}$	⑦ C'_N eq. 4.1.3.3-a ⑤ + ⑥	⑧ $= (C'_N \cos \alpha)$
5	0.370	2.84	2.48	0.019	0.396	0.415	0.41
10	0.746	1.80	1.44	0.043	0.780	0.823	0.81
13.3	1.000	0	-0.36	-0.019	1.021	1.002	0.98

Compute: Angles of Attack Above the Stall

$C_{L_{max}}^*$ (calculated using the low-aspect-ratio method of Section 4.1.3.4)

$$(C_{L_{max}})_{base} = 0.79 \text{ (figure 4.1.3.4-23b at } (C_1 + 1) \frac{A}{\beta} \cos \Lambda_{LE} = \frac{4}{\beta}, \Delta y = 2.10)$$

$$(C_2 + 1) A \tan \Lambda_{LE} = (2.06)(6)(0.1566) = 1.94$$

$$\Delta C_{L_{max}} = -0.08 \text{ (figure 4.1.3.4-24a)}$$

$$C_{L_{max}}^* = (C_{L_{max}})_{base} + \Delta C_{L_{max}} \text{ (equation 4.1.3.4-g)}$$

$$= 0.79 + (-0.08) = 0.71$$

$$(C_{N_{aa}})_{90^\circ} = 1.30 \text{ (figure 4.1.3.3-55b)}$$

$$(C_{N_{aa}})_{ref} = -0.359 \text{ (calculated on page 4.1.3.3-16)}$$

Solution: Angles of Attack Above the Stall

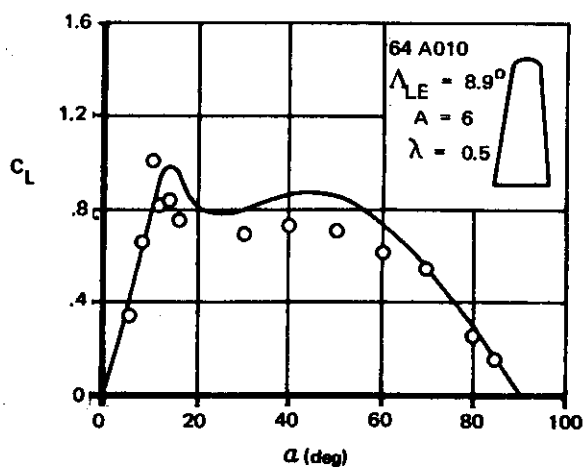
$$\frac{C_L}{\cos \alpha} = C'_N = C_{N_a} \frac{\sin 2\alpha}{2} + C_{N_{aa}} \sin \alpha |\sin \alpha| \text{ (equation 4.1.3.3-a)}$$

$$\begin{aligned}
 C_{Naa} &= (C_{Naa})_{ref} + \left[(C_{Naa})_{90^\circ} - (C_{Naa})_{ref} \right] \left[1 - \frac{\tan \alpha_{C_L_{max}}}{\tan \alpha} \right] + \beta^2 D \frac{C_{Na}}{2.3} \left(\frac{C_{L_{max}}}{C_{L_{max}}^*} \right)^2 \\
 &= -0.359 + (1.3 + 0.359) \left[1 - \frac{\tan \alpha_{C_L_{max}}}{\tan \alpha} \right] + 0.96D \left(\frac{4.56}{2.3} \right) \left(\frac{0.975}{0.71} \right)^2 \\
 &= 1.3 - 1.659 \left(\frac{\tan \alpha_{C_L_{max}}}{\tan \alpha} \right) + 3.588D
 \end{aligned}
 \quad (\text{equation 4.1.3.3-f})$$

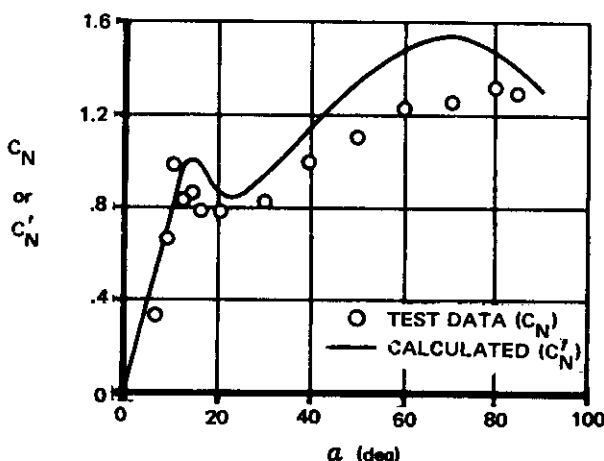
① ② ③ ④ ⑤ ⑥ ⑦ ⑧

α (deg)	$\frac{\tan \alpha_{C_L_{max}}}{\tan \alpha}$	D fig. 4.1.3.3-55a	$C_{N\alpha\alpha}$ eq. 4.1.3.3-f 1.3 - 1.66 ② + 3.58 ③	$C_{N\alpha\alpha} \sin^2 \alpha$	$C_{N\alpha} \frac{\sin 2\alpha}{2}$	C'_N eq. 4.1.3.3-a ⑤ + ⑥	$= C'_N \cos \alpha$
16	0.825	-0.80	-2.94	-0.22	1.21	0.99	0.95
18	0.728	-1.32	-4.64	-0.44	1.34	0.90	0.86
20	0.649	-1.50	-5.16	-0.60	1.47	0.87	0.82
22	0.585	-1.54	-5.20	-0.73	1.58	0.85	0.79
30	0.409	-1.32	-4.11	-1.03	1.97	0.94	0.81
50	0.198	-0.70	-1.54	-0.90	2.25	1.35	0.87
70	0.086	-0.30	0.08	0.07	1.47	1.54	0.53
90	0	0	1.30	1.30	0	1.30	0

A comparison of the calculated values and the experimental data of reference 25 is presented as sketch (d).



SKETCH (d)



3. Angle-of-Attack Characteristics of a Cambered Wing

Given: The wing of reference 26.

$$A = 9.0 \quad \lambda = 0.4 \quad \Lambda_{LE} = 2.2^\circ \quad \text{NACA } 63_1 - 210 \text{ airfoil (free-stream direction)}$$

$$\begin{aligned} \text{Position of maximum t/c} &= 0.45c \\ \text{Position of maximum camber} &= 0.50c \\ \text{Amount of camber} &= 0.011c \end{aligned}$$

$$M = 0.30; \beta = 0.954 \quad R_L = 2.5 \times 10^6 \quad (\text{based on MAC})$$

$$\kappa = 1.0 \text{ (assumed)} \quad \Lambda_{c/2} = 3.25^\circ$$

Compute: Angles of Attack Below the Stall

Find $C_{L_{max}}$ and $a_{C_{L_{max}}}$ as outlined in Section 4.1.3.4 and C_{N_a} from Section 4.1.3.2.

$$A > \frac{4}{(C_1 + 1) \cos \Lambda_{LE}}; \text{ therefore, use high-aspect-ratio method}$$

$$\Delta y = 2.20 \quad (\text{figure 2.2.1-8})$$

$$(c_{L_{max}})_{\text{base}} = 1.28 \quad (\text{uncambered wing at } R_L = 9 \times 10^6) \quad (\text{figure 4.1.1.4-5})$$

$$\Delta_1 c_{L_{max}} = 0.07 \quad (\text{figure 4.1.1.4-6d})$$

$$\Delta_2 c_{L_{max}} = 0.15 \quad (\text{figure 4.1.1.4-7a})$$

$$\Delta_3 c_{L_{max}} = -0.13 \quad (\text{figure 4.1.1.4-7b})$$

$$\begin{aligned} c_{L_{max}} &= (c_{L_{max}})_{\text{base}} + \Delta_1 c_{L_{max}} + \Delta_2 c_{L_{max}} + \Delta_3 c_{L_{max}} \quad (\text{equation 4.1.1.4-a}) \\ &= 1.30 + 0.07 + 0.15 - 0.13 = 1.39 \end{aligned}$$

$$\frac{C_{L_{max}}}{c_{L_{max}}} = 0.90 \quad (\text{figure 4.1.3.4-21a})$$

$$\Delta C_{L_{max}} = -0.105 \quad (\text{figure 4.1.3.4-22})$$

$$\begin{aligned} C_{L_{max}} &= \left(\frac{C_{L_{max}}}{c_{L_{max}}} \right) c_{L_{max}} + \Delta C_{L_{max}} \quad (\text{equation 4.1.3.4-d}) \\ &= (0.90)(1.39) - 0.105 = 1.15 \end{aligned}$$

$$\Delta a_{C_{L_{\max}}} = 0.5^{\circ} \text{ (figure 4.1.3.4-21b)}$$

Find C_{L_a}

$$\frac{A}{\kappa} \left[\beta^2 + \tan^2 \Lambda_{c/2} \right]^{1/2} = 8.60$$

$$C_{L_a}/A = 0.59 \text{ per rad (figure 4.1.3.2-49)}$$

$$C_{L_a} = C_{N_a} = \left(\frac{C_{L_a}}{A} \right) A = (0.59)(9) = 5.31$$

$$a_0 = a_i - \frac{c_{L_i}}{c_{L_a}} = 0 - \frac{0.2}{0.113} = -1.77^{\circ} \text{ (equation 4.1.3.1-a)}$$

$$a_{C_{L_{\max}}} = \frac{C_{L_{\max}}}{C_{L_a}} + a_0 + \Delta a_{C_{L_{\max}}} \text{ (equation 4.1.3.4-e)}$$

$$= \frac{1.15}{5.31/(57.3)} + (-1.77) + 0.5 = 11.14^{\circ}$$

Find $(C_{N_{aa}})_{ref}$

$$C'_N @ C_{L_{\max}} = \frac{C_{L_{\max}}}{\cos a_{C_{L_{\max}}}} = \frac{1.15}{0.9815} = 1.17 \text{ (equation 4.1.3.3-c)}$$

$$(a_e)_{C_{L_{\max}}} = a_{C_{L_{\max}}} - a_0 = 12.91^{\circ}$$

$$(C_{N_{aa}})_{ref} = \frac{C'_N @ C_{L_{\max}} - C_{N_a} \left(\frac{1}{2} \right) \sin 2(a_e)_{C_{L_{\max}}}}{\sin (a_e)_{C_{L_{\max}}} \left| \sin (a_e)_{C_{L_{\max}}} \right|} \text{ (equation 4.1.3.3-d with } a_{C_{L_{\max}}} = (a_e)_{C_{L_{\max}}})$$

$$= \frac{1.17 - (5.31) \left(\frac{0.4355}{2} \right)}{(0.2235)^2} = \frac{0.0137}{0.0500} = 0.274$$

Find J

$$C_1 = 0.43, C_2 = 1.09 \text{ (figure 4.1.3.4-24b)}$$

$$J = 0.3 (C_1 + 1) \frac{A}{\beta} \cos \Lambda_{LE} \left\{ (C_1 + 1)(C_2 + 1) - \left[\frac{(C_2 + 1) A \tan \Lambda_{LE}}{7} \right]^3 \right\} \text{ (equation 4.1.3.3-e)}$$

$$= 0.3 (1.43) \frac{9}{0.954} (0.9993) \left\{ (1.43)(2.09) - \left[\frac{(2.09)(9)(0.0384)}{7} \right]^3 \right\}$$

$$= 12.10$$

ution: Angles of Attack Below the Stall

$$\frac{C_L}{\cos \alpha} = C'_N = C_{N_a} \frac{\sin 2a_e}{2} + C_{N_{aa}} \sin a_e |\sin a_e| \text{ (equation 4.1.3.3-a with } a = a_e)$$

$$C_{N_{aa}} = (C_{N_{aa}})_{ref} + \Delta C_{N_{aa}} \text{ (equation 4.1.3.3-b)}$$

$$C_{N_{aa}} = 0.274 + \Delta C_{N_{aa}}$$

① α (deg)	② a_e (deg)	③ $\frac{\tan a_e}{\tan (a_e) C_{L_{max}}}$	④ $\Delta C_{N_{aa}}$ fig. 4.1.3.3-55a	⑤ $C_{N_{aa}}$ eq. 4.1.3.3-b .274 + ④	⑥ $C_{N_{aa}} \sin^2 a_e$	⑦ $C_N \frac{\sin 2a_e}{2}$	⑧ C'_N eq. 4.1.3.3-a ⑥ + ⑦	⑨ $= (C'_N \cos \alpha)$
0	1.77	0.1349	2.83	3.10	0.0030	0.1639	0.1669	0.167
4	5.77	0.4409	2.83	3.10	0.0313	0.5313	0.5626	0.561
8	9.77	0.7513	1.75	2.02	0.0582	0.8881	0.9463	0.937
10	11.77	0.9092	0.65	0.92	0.0383	1.0601	1.0984	1.082
11.14	12.91	1.00	0	0.27	0.0130	1.1563	1.1693	1.147

Compute: Angles of Attack Above the Stall

$C_{L_{max}}^*$ (Calculated using the low-aspect-ratio method of Section 4.1.3.4)

$$(C_{L_{max}})_{base} = 0.79 \text{ (figure 4.1.3.4-23a at } (C_1 + 1) \frac{A}{\beta} \cos \Lambda_{LE} = \frac{4}{\beta}, \Delta y = 2.20)$$

$$(C_2 + 1) A \tan \Lambda_{LE} = (2.09)(9)(0.0384) = 0.723$$

$$\Delta C_{L_{max}} = -0.105 \text{ (figure 4.1.3.4-24a)}$$

$$C_{L_{max}}^* = (C_{L_{max}})_{base} + \Delta C_{L_{max}} \text{ (equation 4.1.3.4-g)}$$

$$= 0.79 + (-0.105) = 0.685$$

$$(C_{N_{aa}})_{90^\circ} = 1.37 \text{ (figure 4.1.3.3-55b)}$$

$$(C_{Naa})_{ref} = 0.274 \text{ (calculated on page 4.1.3.3-20)}$$

Solution: Angles of Attack Above the Stall

$$\frac{C_L}{\cos \alpha} = C'_N = C_{Na} \frac{\sin 2a_e}{2} + C_{Naa} \sin a_e |\sin a_e| \quad (\text{equation 4.1.3.3-a with } \alpha = a_e)$$

$$C_{Naa} = (C_{Naa})_{ref} + \left[(C_{Naa})_{90^\circ} - (C_{Naa})_{ref} \right] \left[1 - \frac{\tan(a_e) C_{L_{max}}}{\tan a_e} \right] + \beta^2 D \frac{C_{Na}}{2.3} \left(\frac{C_{L_{max}}}{C_{L_{max}}^*} \right)^2$$

(equation 4.1.3.3-f with $\alpha = a_e$)

$$= 0.274 + (1.37 - 0.274) \left[1 - \frac{\tan(a_e) C_{L_{max}}}{\tan a_e} \right] + 0.91 D \frac{5.31}{2.3} \left(\frac{1.15}{0.685} \right)^2$$

$$= 1.37 - 1.096 \frac{\tan(a_e) C_{L_{max}}}{\tan a_e} + 5.92 D$$

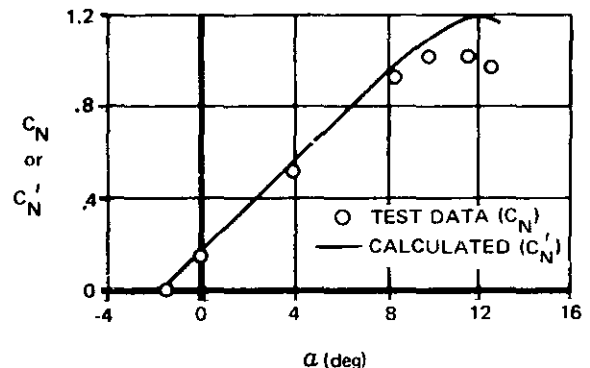
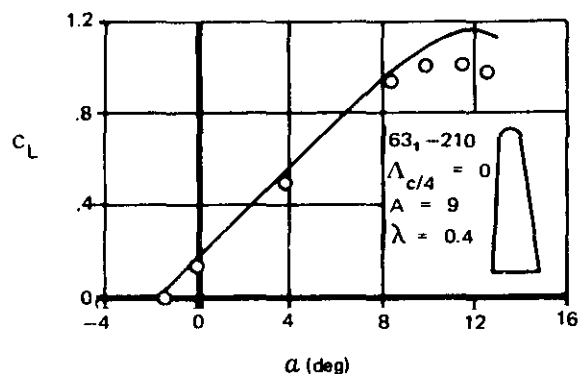
$$a_e = a \left[1 - \frac{a_0}{90^\circ - a_{C_{L_{max}}}} \right] - \frac{90 a_0}{90^\circ - a_{C_{L_{max}}}} \quad (\text{equation 4.1.3.3-g})$$

$$= a \left[1 - \frac{(-1.77)}{90 - 11.14} \right] - \frac{90 (-1.77)}{90 - 11.14}$$

$$= 1.022 a + 2.020$$

①	②	③	④	⑤	⑥	⑦	⑧	⑨
α deg	α_e deg	$\frac{\tan(\alpha_e) C_{L_{max}}}{\tan a_e}$	D fig. 4.1.3.3-55e	C_{Naa} eq. 4.1.3.3-f $1.37 + 1.096 \frac{③}{④} + 5.92 \frac{④}{④}$	$C_{Naa} \sin^2 \alpha_e$	$C_{Na} \frac{\sin 2\alpha_e}{2}$	C'_N eq. 4.1.3.3-a $(⑥ + ⑦)$	C_L $= (C'_N \cos \alpha)$
11.2	13.47	0.9570	-0.05	0.0251	0.0014	1.203	1.204	1.181
12	14.28	0.9006	-0.25	-1.0970	-0.0668	1.269	1.202	1.176
13	15.31	0.8371	-0.70	-3.691	-0.2574	1.328	1.071	1.044

A comparison of the calculated values and the experimental data of reference 26 is presented as sketch (e).

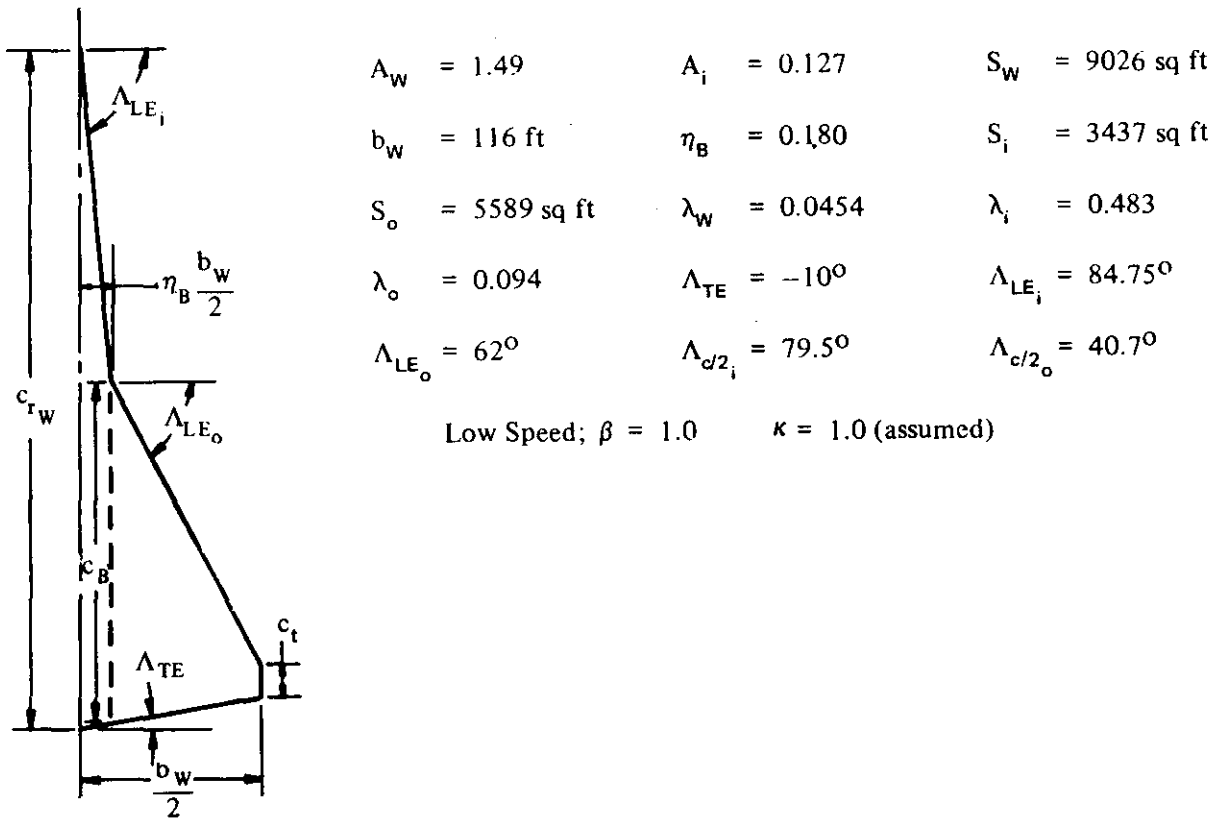


SKETCH (e)

Non-Straight-Tapered Wings

4. Double-Delta Wing

Given: The double-delta wing of reference 27.



Compute:

$$C_{L_a} \text{ (Section 4.1.3.2)}$$

$$(\cos \Lambda_{c/2})_{\text{eff}} = \frac{1}{S_W} \sum_{j=1}^{j=n} (\cos \Lambda_{c/2})_j S_j \quad (\text{equation 4.1.3.2-f})$$

$$= \frac{1}{S_W} (\cos \Lambda_{c/2})_i S_i + (\cos \Lambda_{c/2})_o S_o$$

$$= \frac{1}{9026} [(0.1822)(3437) + (0.7581)(5589)]$$

$$= 0.5388$$

$$(\Lambda_{c/2})_{\text{eff}} = 57.4^\circ; \tan (\Lambda_{c/2})_{\text{eff}} = 1.5637$$

$$\frac{A}{\kappa} \left[\beta^2 + \tan^2 (\Lambda_{c/2})_{\text{eff}} \right]^{\frac{1}{2}} = 1.49 [1.0 + (1.5637)^2]^{\frac{1}{2}} = 2.77$$

$$C_{L_a}/A = 1.16 \text{ per rad (figure 4.1.3.2-49)}$$

$$C_{L_a} = 1.728 \text{ per rad}$$

$$\beta \tan \Lambda_{LE_i} = (1.0)(10.884) = 10.884$$

$$\frac{A_i}{\eta_B} = \frac{0.127}{0.180} = 0.706$$

Solution:

$$C_L = \left(\frac{C_{L_a}}{C_{L_a}} \frac{A_i}{\eta_B} \right) \frac{C_{L_a}}{A_i/\eta_B} \quad (\text{equation 4.1.3.3-h})$$

①

②

③

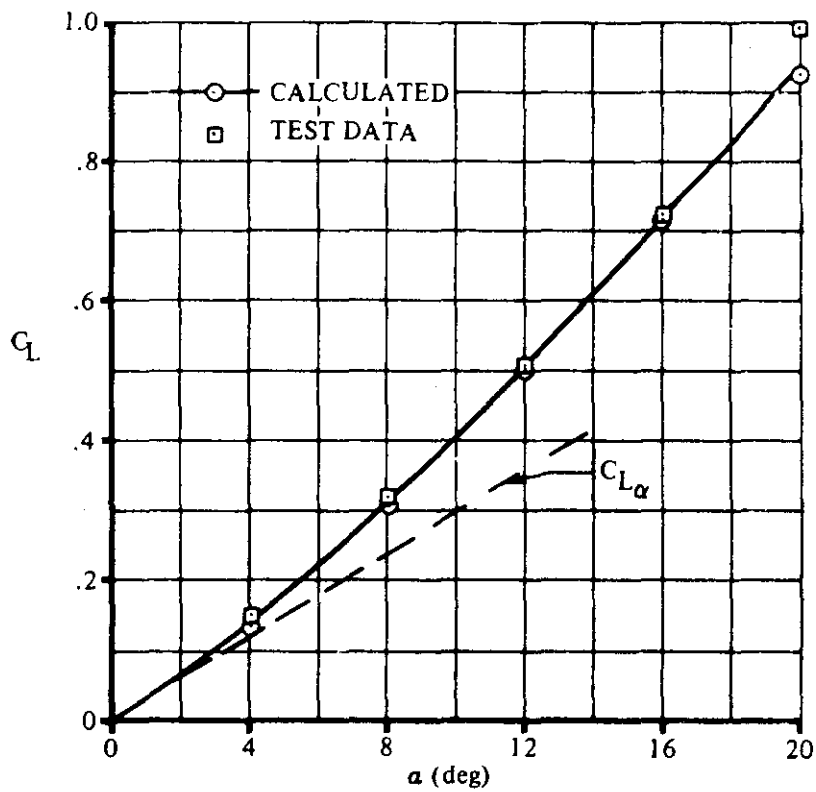
④

⑤

⑥

α (deg)	$\beta \tan \Lambda_{LE_i}$	$\left(\frac{C_{L_a}}{C_{L_a}} \frac{A_i}{\eta_B} \right)$ fig. 4.1.3.3-56	C_{L_a} (per rad)	$\frac{A_i}{\eta_B}$	$\frac{C_L}{C_{L_a}}$ eq. 4.1.3.3-h ③④/⑤
4	10.884	0.055	1.728	0.706	0.1346
8		0.127			0.3110
12		0.208			0.5079
16		0.294			0.7196
20		0.380			0.9301

The calculated values of C_L are plotted versus α and a curve faired through the calculated points tangent to C_L near zero lift. (see sketch (f)).



SKETCH (f)

5. Cranked Wing

Given: The cranked wing of reference 28. This is the configuration of the sample problem of paragraph A of Section 4.1.3.2. Some of the characteristics are repeated.

$$A_w = 4.0 \quad S_w = 2.25 \text{ sq ft} \quad S_i = 1.641 \text{ sq ft} \quad b_w = 3.0 \text{ ft}$$

$$\eta_B = 0.60 \quad \Lambda_{LE_i} = 48.6^\circ \quad A_i = 1.97 \quad M = 0.80; \beta = 0.60$$

Compute:

$$C_{L\alpha} = 4.324 \text{ per rad} = 0.0755 \text{ per deg (sample problem, paragraph A, Section 4.1.3.2)}$$

$$\frac{1}{\tan \Lambda_{LE_i}} = \frac{1}{1.1343} = 0.882$$

$$\alpha_{break} = 5.9^\circ \text{ (figure 4.1.3.3-57)}$$

$$C_{L_{break}} = C_{L_a} a_{break} \quad (\text{equation 4.1.3.3-i})$$

$$= (0.0755)(5.9) = 0.445$$

$$\beta \tan \Lambda_{LE_i} = (0.6)(1.1343) = 0.681$$

$$\frac{A_i}{\eta_B} = \frac{1.97}{0.60} = 3.283$$

$$C_{L_{nonlinear}} = \left(\frac{C_L}{C_{L_a}} \frac{A_i}{\eta_B} \right) \frac{C_{L_a}}{A_i/\eta_B} \quad (\text{equation 4.1.3.3-h})$$

① α (deg)	② $\beta \tan \Lambda_{LE_i}$	③ $\left(\frac{C_L}{C_{L_a}} \frac{A_i}{\eta_B} \right)$ fig. 4.1.3.3-56	④ C_{L_a} (per rad)	⑤ $\frac{A_i}{\eta_B}$	⑥ $C_{L_{nonlinear}}$ eq. 4.1.3.3-h ③④ / ⑤
4	0.681	0.158	4.324	3.283	0.208
8		0.283			0.373
12		0.415			0.547
16		0.555			0.731
20		0.686			0.902

Plot $C_{L_{nonlinear}}$ versus α and read $\left[(C_L)_a = a_{break} \right]_{\text{nonlinear}}$ at a_{break} .

$\left[(C_L)_a = a_{break} \right]_{\text{nonlinear}} = 0.285$ (constructed, see sketch (g))

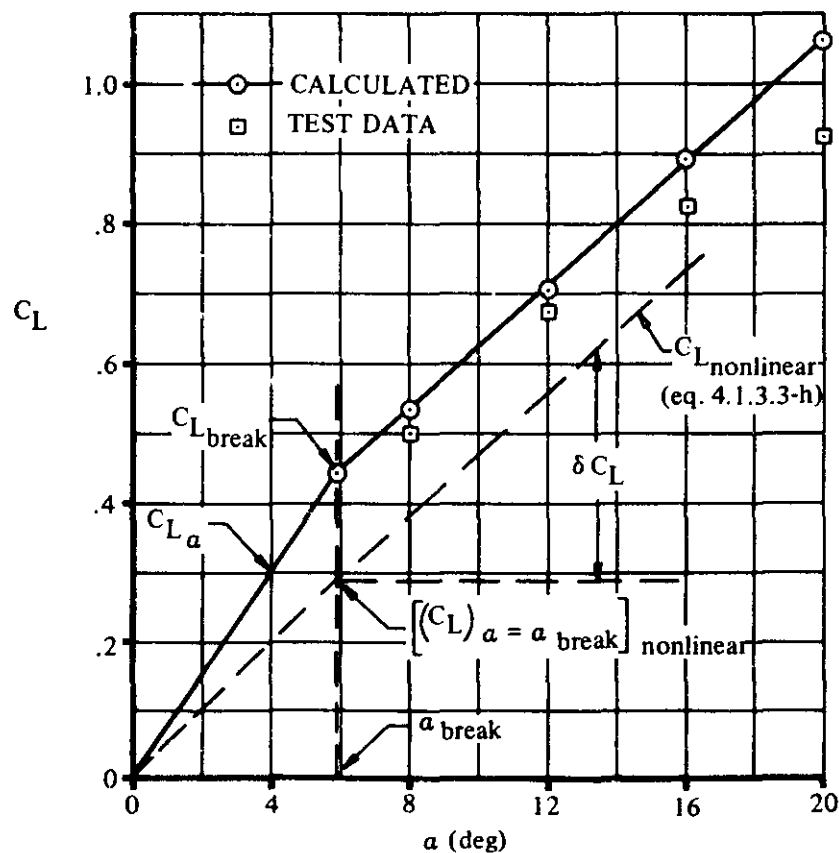
Solution: $a > a_{break}$

$$C_L = C_{L_{break}} + \delta C_L \quad (\text{equation 4.1.3.3-k})$$

$$\delta C_L = \left[C_L - (C_L)_a = a_{break} \right]_{\text{nonlinear}} \quad (\text{equation 4.1.3.3-j})$$

①	②	③	④	⑤	⑥
α (deg)	C_L (nonlinear)	$(C_L)_{\alpha=\alpha_{break}}$ (nonlinear)	δC_L eq. 4.1.3.3-j ② - ③	$C_{L_{break}}$	C_L eq. 4.1.3.3-k ④ + ⑤
5.9	0.285	0.285	0	0.445	0.445
8	0.373		0.088		0.533
12	0.547		0.262		0.707
16	0.731		0.446		0.891
20	0.902		0.617		1.062

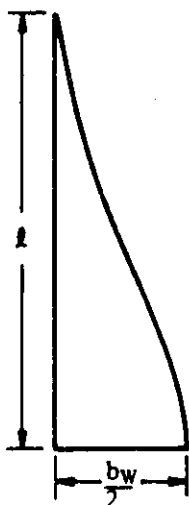
These calculated values of C_L are plotted versus α on sketch (g).



SKETCH (g)

6. Curved Wing

Given: The ogee wing of reference 29.



$$A = 1.20 \quad b_w = 12.0 \text{ in.} \quad l = 20.0 \text{ in.}$$

$$M = 0.4$$

Compute:

Wing slenderness parameter

$$\frac{b_w}{2l} = \frac{12.0}{2(20.0)} = 0.30$$

$$\sqrt{\frac{b_w}{2l}} = 0.548$$

Solution:

$$C_L = \frac{C_L}{\sqrt{\frac{b_w}{2l}}} \sqrt{\frac{b_w}{2l}} \quad (\text{equation 4.1.3.3-1})$$

①

②

③

④

α (deg)	$C_L / \sqrt{\frac{b_w}{2l}}$ fig. 4.1.3.3-58	$\sqrt{\frac{b_w}{2l}}$	C_L eq. 4.1.3.3-1 ② ③
4	0.249	0.548	0.136
8	0.625		0.268
12	0.850		0.465
16	1.210		0.864
20	1.580		0.865

These calculated results are compared with test data in table 4.1.3.3-D at angles of attack of 4°, 8°, and 12°.

B. TRANSONIC

No specific charts are presented for determining the transonic lift characteristics of wings at high angles of attack. The best source of information of this type is experimental data on similar configurations, e.g., reference 10. If such information is not immediately available, the method of the following paragraphs may be used as a guide to obtain trends.

For thin, low-aspect-ratio, conventional wings, an indication of the lift characteristics at high angles of attack at transonic speeds may be obtained by the following procedure:

1. Calculate the complete lift curves for $M = 0.6$ and $M = 1.4$ by the methods of paragraphs A and C, respectively, of this section.
2. Obtain the wing lift-curve slope at low angles of attack, as outlined in Section 4.1.3.2, for intermediate Mach numbers.
3. Obtain the wing maximum-lift variation with Mach number and angle of attack for maximum lift as outlined in Section 4.1.3.4.
4. Using as a guide the information determined in the first three steps, construct the approximate lift curves for the range of Mach numbers between 0.6 and 1.4.

For thick, high-aspect-ratio, conventional wings the same procedure may be used except that the transonic lift-curve slopes obtained from Section 4.1.3.2 apply only to the first few degrees of angle of attack and may be misleading if extrapolated to higher angles. Section 4.1.3.2 gives a more detailed discussion of this problem. For any wing, local nonlinearities at high angles of attack are likely to exist at Mach numbers between 0.8 and 0.95. Again, it is best to use experimental data.

C. SUPERSONIC

Conventional, swept wings at supersonic speeds may be conveniently divided into two major categories:

Wings with subsonic leading edges, that is, wings for which $\beta/\tan \Lambda_{LE} < 1$

Wings with supersonic leading edges, that is, wings for which $\beta/\tan \Lambda_{LE} > 1$

The supersonic-leading-edge category may be further subdivided according to whether or not the leading-edge shock is attached or detached.

In order to provide continuity between these various supersonic regimes, as well as with the subsonic regime, the normal-force equation, 4.1.3.3-a, has again been used. As before, the first term is based on linear theory and the second accounts for nonlinear effects. The linear term is taken from Section 4.1.3.2 and the nonlinear coefficient C_{Naa} is given in the charts of this section. The charts of this section are based on references 11 through 19. Table 4.1.3.3-E presents substantiation data and compares the results obtained with this method to experimental data for the subsonic-leading-edge case. Tables 4.1.3.3-F and 4.1.3.3-G present corresponding information for the supersonic-leading-edge cases. Table 4.1.3.3-F is for wings having attached shocks at low angles and detached shocks at high angles. Table 4.1.3.3-G is for wings having detached shocks throughout the angle-of-attack range.

Supersonic Normal-Force Coefficient of Wings with Subsonic Leading Edges

For conventional, swept wings with subsonic leading edges at supersonic free-stream Mach numbers, the nonlinear character of the normal-force curve is primarily a function of $\beta/\tan \Lambda_{LE}$ and to a lesser degree of C_{N_a} . The lift characteristics are similar to the subsonic maximum-lift characteristics of low-aspect-ratio wings, in that the maximum-lift coefficient first increases, then decreases with increasing aspect ratio (see Section 4.1.3.4). As with the subsonic wings, the critical leading-edge sweep angle at which reversal occurs seems to lie between 60° and 65° . Therefore, the influence of C_{N_a} has been separated into two regimes.

In the first regime, for sweep angles less than 62.5° , C_{N_a} is used directly as derived from linear theory. In the second regime, for sweep angles greater than 62.5° , the lift-curve slope is modified by an empirical correction factor.

DATCOM METHOD

The procedure for finding the supersonic pseudo normal-force coefficient C'_N of a straight-tapered wing with subsonic leading edges at high angles of attack is as follows:

Step 1. The normal-force-curve slope C_{N_a} for the conventional wing is found from Section 4.1.3.2.

This includes the modifying effect of thickness on normal-force-curve slope as given in figure 4.1.3.2-60. In this figure, thickness is represented by δ_\perp , the semiwedge angle normal to the leading edge of wings having sharp leading edges, and by Δy_\perp , the leading-edge parameter normal to the leading edge of wings having rounded leading edges.

Step 2. An empirical parameter E is found from one of the two following equations:

$$E = C_{N_a} \text{ for } \frac{\tan \Lambda_{LE}}{1.92} \leq 1$$

$$E = C_{N_a} \left[\frac{\tan \Lambda_{LE}}{1.92} + C \left(\frac{\tan \Lambda_{LE}}{1.92} - 1 \right) \right] \text{ for } \frac{\tan \Lambda_{LE}}{1.92} > 1$$

where C is a thickness term from figure 4.1.3.3-59a and δ_\perp in this figure is the leading-edge parameter normal to the leading edge; for wings having rounded leading edges, $\delta_\perp = \tan^{-1} \frac{\Delta y_\perp}{5.85}$

Step 3. The nonlinear coefficient $C_{N_{aa}}$ is found from figure 4.1.3.3-59b as a function of

$E \left(\frac{\beta}{\tan \Lambda_{LE}} \right)$ and the angle-of-attack parameter $\left[\frac{(C_{N_a})_{theory}}{C_{N_a}} \right] \beta \tan \alpha$ or its reciprocal.

Step 4. The total lift and approximate normal-force coefficients are obtained using equation 4.1.3.3-a; i.e.,

$$\frac{C_L}{\cos \alpha} = C'_N = C_{N_a} \frac{\sin 2\alpha}{2} + C_{N_{aa}} \sin \alpha |\sin \alpha|$$

Application of this technique is illustrated by the sample problem on pages 4.1.3.3-34 through 4.1.3.3-36.

Supersonic Normal-Force Coefficient of Wings With Supersonic Leading Edges

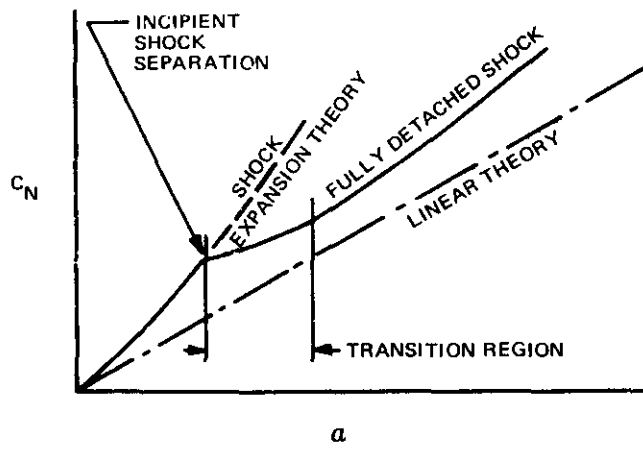
For conventional wings with supersonic leading edges, the wing leading-edge shock may or may not be attached, depending on the angle of attack and the wing thickness.

When the shock is attached, shock-expansion theory (summarized in reference 20) gives accurate results. Shock-expansion theory states that the pressures acting on a wing are a direct function of the airfoil thickness and profile shape. For the total integrated normal forces, however, little accuracy is lost if the wing is assumed to be a flat plate.

Thickness effects may not be neglected, even approximately, in determining the conditions under which an attached shock will detach. A shock will start to detach whenever the sum of the angle of attack and the semiwedge angle, both measured normal to the leading edge, exceeds the value of an expression given in reference 20; in other words,

$$\alpha_1 + \delta_1 > \frac{4}{3\sqrt{3}(\gamma+1)} \frac{(M_1^2 - 1)^{3/2}}{M_1^2}$$

where M_1 is the Mach number normal to the leading edge and $\gamma = 1.4$. This function is plotted in figure 4.1.3.3-61b. As the angle of attack is increased beyond this value for incipient shock detachment, an angle-of-attack transition region occurs (see sketch (h)), wherein the normal-force characteristics of a given wing gradually come to resemble those of a similar wing of somewhat greater thickness at a lower angle of attack. When the angle of attack reaches the upper limit of the transition region, the shock may be considered to be fully detached.



SKETCH (h)

For wings where the leading-edge shock is detached, no theory exists for the prediction of normal forces. However, examination of experimental data shows that a nonlinear force coefficient may be defined and presented in much the same way as was done for supersonic wings with subsonic leading edges. This is to be expected, since a local subsonic region exists near the leading edge when the shock is detached. For these wings, the nonlinear coefficient C_{Naa} is a function of C_{Na} only.

DATCOM METHOD

The first step is to determine whether the leading-edge shock is attached or detached at zero angle of attack. This is determined by using figure 4.1.3.3-61b. Set $\delta_{\text{eff},\perp}$ (see figure 4.1.3.3-61b) equal to the semiwedge angle of the wing perpendicular to the wing leading edge δ_{\perp} , and calculate the upstream Mach number perpendicular to the wing leading edge at zero angle of attack by

$$(M_{\perp})_{a=0} = M_{\infty} \sqrt{1 - \sin^2 \Lambda_{LE}}$$

The leading-edge shock condition is then determined by the boundary of figure 4.1.3.3-61b. If the shock is detached, follow procedure (1) below; if the shock is attached, follow procedure (2).

1. Supersonic Wings With Detached Shock at Zero Angle of Attack

The procedure for finding the supersonic pseudo normal-force coefficient C'_N at high angles of attack of a straight-tapered wing with supersonic leading edges and with a detached shock is as follows:

Step 1.a. The derivative C_{N_a} is calculated from Section 4.1.3.2. C_{N_a} is the theoretical normal-force-curve slope of figures 4.1.3.2-56a through 4.1.3.2-56g multiplied by the empirical thickness correction of figure 4.1.3.2-60.

Step 1.b. The equivalent lift-curve slope E is calculated from the appropriate one of the two following equations:

$$E = C_{N_a} \text{ for } \frac{\tan \Lambda_{LE}}{1.92} \leq 1.0$$

$$E = C_{N_a} \left[\frac{\tan \Lambda_{LE}}{1.92} + C \left(\frac{\tan \Lambda_{LE}}{1.92} - 1 \right) \right] \text{ for } \frac{\tan \Lambda_{LE}}{1.92} > 1$$

where C is determined from figure 4.1.3.3-59a as a function of the semiwedge angle normal to the leading edge.

The nonlinear coefficient $C_{N_{aa}}$ is determined from figure 4.1.3.3-60a as a function of E and the angle-of-attack parameter used as the abscissa.

Step 1.c. The total lift and approximate normal-force coefficients are obtained using equation 4.1.3.3-a; i.e.,

$$\frac{C_L}{\cos a} = C'_N = C_{N_a} \frac{\sin 2a}{2} + C_{N_{aa}} \sin a |\sin a|$$

2. Supersonic Wings With Attached Shock at Zero Angle of Attack

The procedure for finding the supersonic pseudo normal-force coefficient C'_N at high angles of attack of a straight-tapered wing with supersonic leading edges and with an attached shock is as follows:

Step 2.a. The derivative C_{N_a} is calculated from Section 4.1.3.2. C_{N_a} is the theoretical normal-force slope of figures 4.1.3.2-56a through 4.1.3.2-56g multiplied by the empirical thickness correction of figure 4.1.3.2-60.

Step 2.b. Determine the angle of attack a^* at which the shock will start to detach. This is obtained by using figure 4.1.3.3-61b. For unswept wings, the value of $\delta_{eff\perp}$ at the start of shock detachment is obtained from figure 4.1.3.3-61b at $M_\perp = M_\infty$. Then the angle of attack at which the shock will start to detach is determined by

$$a^* = \delta_{eff\perp} - \delta_\perp$$

For swept wings $\delta_{eff\perp}$ must be determined by graphical interpolation, since there is an interdependence between the Mach number and the angle of attack normal to the leading edge. These relations for swept wings are

$$M_\perp = M_\infty \sqrt{1 - \sin^2 \Lambda_{LE} \cos^2 a}$$

$$a_\perp = \tan^{-1} \left(\frac{\tan a}{\cos \Lambda_{LE}} \right)$$

where M_∞ is the free-stream Mach number, M_\perp is the Mach number perpendicular to the leading edge, a is the wing angle of attack, and a_\perp is the angle of attack normal to the leading edge.

For a selected range of a 's, calculate $\delta_{eff\perp}$ and M_\perp using the above equations and the relationship

$$\delta_{eff\perp} = a_\perp + \delta_\perp$$

Then plot M_\perp versus $\delta_{eff\perp}$ on figure 4.1.3.3-61b. The intersection of this curve and the boundary curve of figure 4.1.3.3-61b determines the value of $\delta_{eff\perp}$ at which the shock will start to detach. Then the angle of attack at which the shock will start to detach is determined by

$$a^* = \tan^{-1} \left[\tan(\delta_{eff\perp} - \delta_\perp) \cos \Lambda_{LE} \right]$$

Step 2.c. The angle-of-attack-transition increment between incipient shock detachment and full detachment is now determined from figure 4.1.3.3-61a. To enter this figure, the nonlinear normal-force coefficient at incipient shock separation C_{Naa}^* must be known. This is read

from figure 4.1.3.3-60b by entering on the abscissa $\left(\beta \tan a \text{ or } \frac{1}{\beta \tan a}\right)$ at the angle of attack corresponding to incipient shock separation as already calculated in step 2.b.

$C_{Naa}^* = C_{Naa}$ is then read from the appropriate β -curve.

Step 2.d. The total lift and approximate normal-force coefficients may now be calculated for the three different angle-of-attack ranges using equation 4.1.3.3-a; i.e.,

$$\frac{C_L}{\cos a} = C'_N = C_{Na} \frac{\sin 2a}{2} + C_{Naa} \sin a |\sin a|$$

where

C_{Na} is from step 2.a.

C_{Naa} for the attached-shock range is read from figure 4.1.3.3-60b.

C_{Naa}^* for the fully-detached-shock range is read from figure 4.1.3.3-60a in the manner outlined in step 1.b. of the section on detached shocks.

C_{Naa} in the transition range is interpolated graphically or calculated analytically from the linear-interpolation formula

$$C_{Naa} = C_{Naa}^* - \left(\frac{a - a^*}{a' - a^*} \right) \left(C_{Naa}^* - C'_{Naa} \right)$$

In the above formula the starred quantities are measured at incipient-shock-separation conditions, and primed quantities are measured at the end of the transition region, where the shock is fully detached.

Application of this technique is illustrated by sample problem 2 on pages 4.1.3.3-36 through 4.1.3.3-39.

Sample Problems

1. Supersonic Pseudo-Normal-Force Coefficient of Wing With Subsonic Leading Edge.

Given: Wing 4a of reference 15.

$$A = 0.562 \quad \lambda = 0 \quad \Lambda_{LE} = 82^\circ \quad M = 6.9; \quad \beta = 6.83$$

Airfoil: 5-percent-thick (free-stream direction) double wedge with maximum thickness at 50-percent chord

Compute:

$$C_{N_a} \text{ (Section 4.1.3.2)}$$

δ_L , semiwedge angle normal to wing leading edge

$$\delta_L = \frac{\text{semiwedge angle}}{\cos \Lambda_{LE}} = \frac{1}{2} \left(\frac{0.05}{0.5} \right) \frac{1}{0.1392} (57.3) = 20.55^\circ$$

$$\frac{\beta}{\tan \Lambda_{LE}} = 0.960 \text{ (subsonic leading edge)}$$

$$A \tan \Lambda_{LE} = 4.00$$

$$(C_{N_a})_{\text{theory}} = 0.573 \text{ per rad (figure 4.1.3.2-56a)}$$

$$\frac{C_{N_a}}{(C_{N_a})_{\text{theory}}} = 0.750 \text{ (figure 4.1.3.2-60)}$$

$$C_{N_a} = (0.750)(0.573) = 0.430 \text{ per rad}$$

Empirical Parameter E

$$\frac{\tan \Lambda_{LE}}{1.92} = 3.71; \text{ therefore, use second equation listed under step 1.b. of Datcom method.}$$

$$C_{N_a} \frac{\tan \Lambda_{LE}}{1.92} = 1.595$$

$$C = 1.30 \text{ (figure 4.1.3.3-59a)}$$

$$\begin{aligned} E &= C_{N_a} \left[\frac{\tan \Lambda_{LE}}{1.92} + C \left(\frac{\tan \Lambda_{LE}}{1.92} - 1 \right) \right] \\ &= 0.43 [3.71 + (1.30)(3.71 - 1)] \\ &= 3.11 \end{aligned}$$

$$E \frac{\beta}{\tan \Lambda_{LE}} = 3.00$$

Solution:

$$C'_N = C_{N_a} \frac{\sin 2a}{2} + C_{N_a a} \sin a |\sin a| \text{ (equation 4.1.3.3-a)}$$

C_{Naa} is obtained from figure 4.1.3.3-59b.

(1) α (deg)	(2) $\frac{C_N \alpha}{(C_N \alpha)_{\text{theory}}} \frac{1}{\beta \tan \alpha}$	(3) $C_N \alpha \alpha$ fig. 4.1.3.3-59b	(4) $C_N \alpha \alpha \sin^2 \alpha$	(5) $C_N \frac{\sin 2\alpha}{2}$	(6) C'_N eq. 4.1.3.3-a (4) + (5)	(7) $(C'_N C_L \cos \alpha)$
8	0.783	0.12	0.002	0.059	0.06	0.06
12	0.517	0.44	0.019	0.087	0.11	0.11
16	0.384	0.64	0.048	0.114	0.16	0.15
20	0.302	0.78	0.091	0.138	0.23	0.22
24	0.247	0.90	0.149	0.160	0.31	0.28
28	0.207	1.00	0.220	0.178	0.40	0.35
32	0.176	1.09	0.306	0.193	0.50	0.42
36	0.151	1.15	0.397	0.204	0.60	0.49
40	0.131	1.22	0.504	0.212	0.72	0.55

2. Supersonic Pseudo-Normal-Force Coefficient of Wing with Supersonic Leading Edge

Given: Wings 1A and 1B of reference 15

$$A = 2.31 \quad \lambda = 0 \quad \Lambda_{LE} = 60^\circ \quad M = 6.91; \beta = 6.83$$

Airfoil: 5-percent-thick double wedge with maximum thickness at 50-percent chord

Compute:

Determine whether the leading-edge shock is attached or detached at zero angle of attack.

δ_{\perp} = semiwedge angle normal to wing leading edge

$$\delta_{\perp} = \frac{\text{semiwedge angle}}{\cos \Lambda_{LE}} = \frac{\frac{1}{2} \left(\frac{0.05}{0.5} \right)}{0.500} (57.3) = 5.7^\circ$$

$$(M_{\perp})_{\alpha=0} = M_{\infty} \sqrt{1 - \sin^2 \Lambda_{LE}} = 3.45$$

For the conditions $(M_{\perp})_{\alpha=0} = 3.45$ and $\delta_{\text{eff}\perp} = 5.7^\circ$, the leading-edge shock is attached (see figure 4.1.3.3-61b); therefore, follow procedure (2) of the Datcom method.

C_{N_a} (Section 4.1.3.2)

$$\frac{\tan \Lambda_{LE}}{\beta} = 0.254$$

$$A \tan \Lambda_{LE} = 4.00$$

$$(C_{N_a})_{\text{theory}} = 0.586 \text{ per rad (figure 4.1.3.2-56a)}$$

$$\frac{C_{N_a}}{(C_{N_a})_{\text{theory}}} = 1.0 \text{ (figure 4.1.3.2-60)}$$

$$C_{N_a} = 0.586 \text{ per rad}$$

Determine the angle of attack for which the shock will start to detach (α^*).

① α (deg)	② $\tan \alpha$	③ $\frac{\tan \alpha}{\cos \Lambda_{LE}}$	④ α_{\perp} ($\tan^{-1} \frac{③}{④}$) (deg)	⑤ $\delta_{eff\perp}$ ($\alpha_{\perp} + \delta_{\perp}$) (deg)	⑥ $\cos \alpha$	⑦ M_{\perp} $= M_{\infty} \sqrt{1 + \sin^2 \Lambda_{LE} \cos^2 \alpha}$
4	0.0699	0.1399	7.96	13.7	0.9976	3.48
8	0.1450	0.2901	16.18	21.9	0.9903	3.56
12	0.2121	0.4252	23.04	28.7	0.9781	3.67
16	0.2867	0.5734	29.83	35.6	0.9613	3.82
20	0.3640	0.7280	36.06	41.8	0.9397	4.01
24	0.4452	0.8904	41.68	47.4	0.9135	4.22

Plot $\delta_{eff\perp}$ versus M_{\perp} on figure 4.1.3.3-61b. At the intersection of this curve and the boundary curve of figure 4.1.3.3-61b, read $\delta_{eff\perp}$ at the start of shock detachment.

$$\delta_{eff\perp} = 38.5^{\circ}$$

$$\begin{aligned} \alpha^* &= \tan^{-1} \left[\tan (\delta_{eff\perp} - \delta_{\perp}) \cos \Lambda_{LE} \right] \\ &= \tan^{-1} \left[\tan (38.5 - 5.7) \cos 60^{\circ} \right] \\ &= \tan^{-1} (0.3223) = 17.9^{\circ} \end{aligned}$$

Solution: Angles of Attack for Fully Attached Shock

$$C'_N = C_{Na} \frac{\sin 2\alpha}{2} + C_{Naa} \sin \alpha |\sin \alpha| \quad (\text{equation 4.1.3.3-a})$$

C_{Naa} is obtained from figure 4.1.3.3-60b.

① α (deg)	② $\beta \tan \alpha$	③ C_{Naa} fig. 4.1.3.3-60b	④ $C_{Naa} \sin^2 \alpha$	⑤ $C_N \frac{\sin 2\alpha}{2}$	⑥ C'_N eq. 4.1.3.3-a ④ + ⑤	⑦ C_L ($C'_N \cos \alpha$)
4	0.478	0.32	0.002	0.041	0.043	0.043
8	0.960	0.62	0.012	0.081	0.093	0.092
	$\frac{1}{\beta \tan \alpha}$					
12	0.689	0.93	0.040	0.119	0.159	0.156
16	0.510	1.17	0.089	0.155	0.244	0.235
17.9	0.453	1.27	0.120	0.171	0.291	0.277

Solution: Angles of Attack in the Transition Range

$$\Delta\alpha = 8.2^\circ \text{ (figure 4.1.3.3-61a at } C_{Naa}^* = 1.27)$$

$$a' = \text{angle of attack for fully detached shock} = a^* + \Delta\alpha = 26.1^\circ$$

$$\left[\frac{C_{Na}}{(C_{Na})_{\text{theory}}} \right] \frac{1}{\beta \tan a} = 0.301 \text{ (at } a' = 26.1^\circ)$$

Empirical Parameter E

$\frac{\tan A_{LE}}{1.92} = 0.902$; therefore, $E = C_{Na} = 0.586$ (first equation listed under step 1.b. of Datcom method for wings with detached shock)

$$C'_{Naa} = 1.23 \text{ (figure 4.1.3.3-60a at } a' = 26.1^\circ)$$

$$C_{Naa} = C_{Naa}^* - \left(\frac{a - a^*}{a' - a^*} \right) (C_{Naa}^* - C'_{Naa})$$

$$= 1.27 - \left(\frac{a - 17.9}{26.1 - 17.9} \right) (1.27 - 1.23)$$

$$= 1.27 - (a - 17.9)(0.005)$$

$$C'_N = C_{N_a} \frac{\sin 2a}{2} + C_{N_{aa}} \sin a |\sin a| \quad (\text{equation 4.1.3.3-a})$$

① α (deg)	② $C_{N_{\alpha\alpha}}$	③ $C_{N_{\alpha\alpha}} \sin^2 \alpha$	④ $C_{N_\alpha} \frac{\sin 2\alpha}{2}$	⑤ C'_N eq. 4.1.3.3-a (③+④)	⑥ $-(C'_N \cos \alpha)$
20	1.26	0.147	0.188	0.336	0.315
24	1.24	0.206	0.218	0.423	0.386

Solution: Angles of Attack for Fully Detached Shock

$$C'_N = C_{N_a} \frac{\sin 2a}{2} + C_{N_{aa}} \sin a |\sin a| \quad (\text{equation 4.1.3.3-a})$$

$C_{N_{aa}}$ is obtained from figure 4.1.3.3-60a.

① α (deg)	② $\frac{C_{N_\alpha}}{(C_{N_\alpha})_{\text{theory}}} \frac{1}{\beta \tan \alpha}$	③ $C_{N_{\alpha\alpha}}$ fig. 4.1.3.3-60a	④ $C_{N_{\alpha\alpha}} \sin^2 \alpha$	⑤ $C_{N_\alpha} \frac{\sin 2\alpha}{2}$	⑥ C'_N eq. 4.1.3.3-a (④+⑤)	⑦ $(C'_N \cos \alpha)$
28	0.275	1.31	0.289	0.243	0.532	0.470
32	0.234	1.43	0.402	0.263	0.865	0.864
36	0.202	1.46	0.504	0.279	0.783	0.633

D. HYPERSONIC

At hypersonic speeds, the calculation of surface pressures on wings is complicated by several interrelated phenomena. These include the boundary layer, the shock wave, heat transfer between the wing and the gas, dissociation, and ionization. The relative importance of each of these phenomena as they affect the aerodynamic characteristics of wings traveling at hypersonic speeds has not been fully assessed.

Boundary layers affect the surface pressures by the displacement of the inviscid flow. This displacement of the flow also affects the shock-wave pattern and hence the surface pressures. At very low Reynolds numbers the inviscid flow between the boundary layer and the shock wave is entirely absorbed by the boundary layer, and the boundary layer interacts directly with the shock wave. In general, the Reynolds number decreases with increasing Mach number along the flight corridor because of the low densities at the altitudes associated with flight at high hypersonic speeds. Thus boundary-layer effects become important at the higher hypersonic speeds.

Because of aerodynamic heating at hypersonic speeds, lifting surfaces usually use blunt leading edges. Detached shocks are thus present ahead of the wing leading edge. Pressures on the surface near the leading edge behind the detached shock are large compared to oblique-shock, inviscid, flat-plate values at the same angle of attack. This "overpressure" decays with distance from the leading edge in a manner that depends on the free-stream Mach number, leading-edge radius, Reynolds number, and heat-transfer characteristics.

An empirical method presented in references 21 and 22 attempts to account for these Reynolds-number and detached-shock effects. This method combines inviscid-flow theory, blast-wave theory, and a viscous-interaction parameter. The examples presented in references 21 and 22 give some idea of the magnitude of these effects on the surface pressures. Because of the scarcity of test data, however, the range of applicability of this method is undetermined. The accuracy claimed in the references is ± 15 percent.

Heat transfer between the gas and the wing surface affects the boundary-layer thickness and hence the surface pressures. The hotter the boundary layer, the thicker it becomes, and vice versa. Gas properties, notably the viscosity and ratio of specific heats, change with temperature. Increasing temperature increases the viscosity and decreases the specific-heat ratio. An indication of the effect of surface temperature on pressure distribution is shown in reference 22.

At high speed and/or low altitudes the extreme temperatures behind the detached shock wave cause dissociation of the atmospheric molecules into their atomic constituents. Under conditions of still higher temperature the atoms ionize and the gas becomes a conducting medium. These phenomena are generally restricted to the leading-edge region. Chapter VIII of reference 23 treats these problems.

Small-disturbance theory has yielded many useful hypersonic similarity forms both for two-dimensional sections and for axisymmetric bodies (chapter II of reference 23). Hypersonic similarity is basically limited to low angles of attack and slender bodies, although successful applications have been made that do not meet these conditions. The hypersonic-similarity concept is discussed and used in Section 4.2.1.2.

The only simple closed-form solution available for the estimation of the normal-force curve of blunt wings at hypersonic speeds is obtained from Newtonian or impact theory (reference 23). Newtonian theory assumes that the component of momentum normal to the surface is canceled (flow remains parallel to the surface after impact), giving rise to a normal force. Several modifications of Newtonian theory that have been developed are discussed in paragraph D of Section 4.2.1.1.

Newtonian theory does not account for many of the real gas interaction effects previously discussed. At high angles of attack or at high Mach numbers the surface pressures attributable to these interactions are small compared to the impact pressures. At low angles of attack or low Mach numbers they are no longer small compared to the impact pressures.

Newtonian theory also assumes that the pressures on the leeward surfaces (those not "seen" from the free-stream direction) are equal to the ambient pressure. Again, this is a good approximation at high angles of attack or high Mach numbers, because the actual pressures on the leeward surfaces compared to those on the forward-facing areas are small. At low Mach numbers or angles of attack the leeward pressures are no longer small compared to the positive pressures, and Newtonian theory gives less accurate results.

The general field of hypersonic flow is treated in references 23 and 24.

DATCOM METHOD

The curves of figures 4.1.3.3-59b through 4.1.3.3-60b are based on test data for the high supersonic Mach numbers and converge to Newtonian-theory flat-plate values for high hypersonic Mach numbers. It is recommended that these charts be used in conjunction with the normal-force-curve-slope information from paragraph C of Section 4.1.3.2 to obtain the total normal-force curve of wings in hypersonic flow.

REFERENCES

1. Benepe, D. B., Kouri, B. G., Webb, J. B., et al: Aerodynamic Characteristics of Non-Straight-Taper Wings. AFFDL-TR-66-73, 1966. (U)
2. Winter, H.: Flow Phenomena on Plates and Airfoils of Short Span. NACA TM 798, 1936. (U)
3. Michael, W. H., Jr.: Flow Studies in the Vicinity of a Modified Flat-Plate Rectangular Wing of Aspect Ratio 0.25. NACA TN 2790, 1952. (U)
4. Bartlett, G. E., and Vidal, R. J.: Experimental Investigation of Influence of Edge Shape on the Aerodynamic Characteristics of Low Aspect Ratio Wings at Low Speeds. Jour. Aero. Sci., Vol. 22, No. 8, August 1955. (U)
5. Anderson, A. E.: An Investigation at Low Speed of a Large-Scale Triangular Wing of Aspect Ratio Two. II – The Effect of Airfoil Section Modifications and the Determination of the Wake Downwash. NACA RM A7H28, 1947. (U)
6. Cahill, J. F., and Gottlieb, S. M.: Low-Speed Aerodynamic Characteristics of a Series of Swept Wings Having NACA 65A006 Airfoil Sections. (Revised) NACA RM L50F16, 1950. (U)
7. Letko, W.: Experimental Determination at Subsonic Speeds of the Oscillatory and Static Lateral Stability Derivatives of a Series of Delta Wings with Leading-Edge Sweep from 30° to 86.5° . NACA RM L57A30, 1957. (U)
8. Küchemann, D.: A Non-Linear Lifting-Surface Theory for Wings of Small Aspect Ratio with Edge Separations. RAE Aero 2540, 1955. (U)
9. Peckham, D. H.: Low-Speed Wind-Tunnel Tests on a Series of Uncambered Slender Pointed Wings with Sharp Edges. RAE Aero 2613, 1958. (U)
10. Emerson, H. F.: Wind-Tunnel Investigation of the Effect of Clipping the Tips of Triangular Wings of Different Thickness, Camber, and Aspect Ratio – Transonic Bump Method. NACA TN 3671, 1956. (U)
11. Gallagher, J. J., and Mueller, J. N.: An Investigation of the Maximum Lift of Wings at Supersonic Speeds. NACA TR 1227, 1955. (U)
12. Kaattari, G. E.: Pressure Distributions on Triangular and Rectangular Wings to High Angles of Attack – Mach Numbers 1.45 and 1.97. NACA RM A54D19, 1954 (U)
13. Bertram, M. H., and McCauley, W. D.: Investigation of the Aerodynamic Characteristics at High Supersonic Mach Numbers of a Family of Delta Wings Having Double-Wedge Sections With the Maximum Thickness at 0.18 Chord. NACA RM L54G28, 1954. (U)
14. Bertram, M. H., and McCauley, W. D.: An Investigation of the Aerodynamic Characteristics of Thin Delta Wings With a Symmetrical Double-Wedge Section at a Mach Number of 6.9. NACA RM L56B14, 1955. (U)
15. Kaattari, G. E.: Pressure Distributions on Triangular and Rectangular Wings to High Angles of Attack – Mach Numbers 2.46 and 3.36. NACA RM A54J12, 1955. (U)
16. Boatright, W. B.: Experimental Study and Analysis of Loading and Pressure Distributions on Delta Wings Due to Thickness and to Angle of Attack at Supersonic Speeds. NACA RM L56I14, 1956. (U)
17. Pitts, W. C.: Force, Moment, and Pressure-Distribution Characteristics of Rectangular Wings at High Angles of Attack and Supersonic Speeds. NACA RM A55K09, 1956. (U)
18. Smith, F. M.: Experimental and Theoretical Aerodynamic Characteristics of Two Low-Aspect-Ratio Delta Wings at Angles of Attack to 50° at a Mach Number of 4.07. NACA RM L57E02, 1957. (U)
19. Hill, W. A.: Experimental Lift of Low-Aspect-Ratio Triangular Wings at Large Angles of Attack and Supersonic Speeds. NACA RM A57I17, 1957. (U)
20. Ames Research Staff: Equations, Tables, and Charts for Compressible Flow. NACA TR 1135, 1953. (U)
21. Creager, M. O.: Surface Pressure Distribution at Hypersonic Speeds for Blunt Delta Wings at Angle of Attack. NASA Memo 5-12-59A, 1959. (U)
22. Creager, M. O.: An Approximate Method for Calculating Surface Pressures on Curved-Profile Blunt Plates in Hypersonic Flow. NASA TN D-71, 1959. (U)

23. Hayes, W. D., and Probstein, R. F.: Hypersonic Flow Theory. Academic Press, New York and London, 1959. (U)
24. Truitt, R. W.: Hypersonic Aerodynamics. The Ronald Press Company, New York, 1959. (U)
25. Koenig, D. G.: Low-Speed Tests of Semispan Wing Models at Angles of Attack from 0° to 180° . NASA Memo 2-27-59A, 1959. (U)
26. Boddy, L. E., and Sutton F. B.: Effects of Wing-Tip Turrets on the Aerodynamic Characteristics of a Typical Bomber-Wing Model. NACA RM A9B09, 1949. (U)
27. Magruder, W. M., et al: Low Speed Characteristics of the Double-Delta SST. Lockheed Horizons, Issue 1, Spring 1965, pp. 28-47. (U)
28. Goodson, K. W., and Becht, R. E.: Wind-Tunnel Investigation at High Subsonic Speeds of the Stability Characteristics of a Complete Model Having Sweepback-, M-, W-, and Cranked-Wing Planforms and Several Horizontal-Tail Locations. NACA RM L54C29, 1954. (U)
29. Squire, L. C., and Capps, D. S.: An Experimental Investigation of the Characteristics of an Ogee Wing from $M = 0.4$ to $M = 1.8$. ARC CP 585, 1962. (U)
30. Anon: Small-Scale Wing-Body Planform Investigation at Mach Numbers from 0.40 to 2.94. Unpublished Data. (U)
31. Anon: Large-Scale Double-Delta Wing-Body Planform Investigation at Low Speed. Unpublished Data. (U)
32. Cayot, J. E., and Kuchar, C. E.: System 125A Summary Data Report, Transonic Tests of a 1/30-Scale Model of the WS-125A Airplane (WADC 168). Convair, General Dynamics, F/W Rpt. FZT-25-013, 1957. (C) Title Unclassified
33. Anon: System 125A, Convair Model 25, Summary Data Report, Subsonic Tests of a Preliminary 1/27-Scale Force Model (CVAL 201). Convair, General Dynamics, F/W Rpt. FZT-25-004, 1956. (C) Title Unclassified
34. Grant, F. C., and Sevier, J. R., Jr: Transonic and Supersonic Wind-Tunnel Tests of Wing-Body Combinations Designed for High Efficiency at a Mach Number of 1.41. NASA TN D-435, 1960. (U)
35. Mansell, C. J.: Low-Speed Wind-Tunnel Tests on Two Thin Cranked Wings With 60-Degree Sweepback Inboard. ARC R&M 2995, 1957. (U)
36. Wakefield, R. M.: Effects of Wing-Crank, Leading-Edge Chord Extensions and Horizontal-Tail Height on the Longitudinal Stability of Swept-Wing Models at Mach Numbers from 0.60 to 1.4. NASA TM X-92, 1959. (U)
37. Henderson, W. P., and Hammond, A. D.: Low-Speed Investigation of High-Lift and Lateral Control Devices on a Semispan Variable-Sweep Wing Having an Outboard Pivot Location. NASA TM X-542, 1961. (U)
38. Lockwood, V. E., McKinney, L. W., and Lamar, J. E.: Low-Speed Aerodynamic Characteristics of a Supersonic Transport Model with a High Aspect Ratio Variable Sweep Warped Wing. NASA TM X-979, 1964. (C) Title Unclassified
39. Jernell, L. S.: The Effects of Conical Camber on the Longitudinal Aerodynamic Characteristics of a Variable-Sweep Wing-Fuselage Configuration at Mach Numbers from 0.50 to 3.50. NASA TM X-804, 1963. (C) Title Unclassified
40. Holdaway, G. H., and Mellenthin, J. A.: Evaluation of Blended Wing-Body Combinations with Curved Plan Forms at Mach Numbers up to 3.50. NASA TM X-379, 1960. (U)
41. Hicks, R. M., and Hopkins, E. J.: Effects of Spanwise Variation of Leading-Edge Sweep on the Lift, Drag, and Pitching Moment of a Wing-Body Combination at Mach Numbers from 0.7 to 2.94. NASA TN D-2236, 1964. (U)
42. Eernshaw, P. B.: Low-Speed Wind-Tunnel Tests on a Series of Cambered Ogee Wings. ARC CP 775, 1964. (U)
43. Squire, L. C.: Further Experimental Investigations of the Characteristics of Cambered Gothic Wings at Mach Numbers From 0.4 to 2.0. ARC R&M 3310, 1963. (U)
44. Dobson, M. D., and King-Underwood, R.: Wind-Tunnel Tests Between $M = 0.4$ and 2.0 on a Cambered Wing of Slender Ogee Planform. ARC CP 778, 1965. (U)
45. Ergebnisse der aerodynamische Versuchsanstalt Goettingen, 1932. (U)

TABLE 4.1.3.3-A
SUBSONIC WING-LIFT VARIATION WITH ANGLE OF ATTACK
DATA SUMMARY AND SUBSTANTIATION

Ref.	A	Λ_{LE}	λ	Δy	M	$R_L \times 10^{-6}$	$C_{L_{max}}$	$\alpha_{C_{L_{max}}} \text{ (deg)}$	J	$\alpha \text{ (deg)}$	$C_L \text{ Calc.}$	$C_L \text{ Test}$	% Percent Error
3	.26	0	1.0	.745	-0.1	2.1	1.06	45	.139	10	.16	.16	6.6
										20	.45	.417	7.9
										30	.77	.715	7.7
										40	1.02	.986	3.4
										45	1.06	1.06	0
4	1.6	0	1.0	.726	-0.1	2.0	.985	26	.836	5	.21	.190	10.5
										10	.38	.40	- 5.0
										15	.60	.65	- 7.7
										20	.82	.85	- 3.5
										26	.985	*	-
4	1.23	30	.698	.63	-0.1	2.9	1.06	35	.815	5	.17	.175	- 2.8
										10	.375	.38	- 1.3
										15	.6	.66	- 9.1
										20	.815	.85	- 4.1
										25	.98	.98	0
										30	1.05	*	-
										35	1.05	*	-
4	1.6	69.5	0	.26	-0.1	3.0	1.34	35	1.28	5	.185	.175	6.7
										10	.395	.375	5.3
										15	.63	.60	5.0
										20	.875	.86	1.7
										25	1.08	1.11	- 2.7
										30	1.24	1.285	- 3.5
										35	1.34	1.37	- 2.2
5	2	63.4	0	.749	-0.15	14.6	1.37	34.5	.218	5	.22	.22	0
										10	.465	.465	0
										15	.73	.695	5.0
										20	.98	.935	2.7
										25	1.165	1.165	0
										30	1.32	1.345	- 1.8
										34.5	1.37	1.34	2.2

TABLE 4.1.3.3-A (Contd)

Ref	A	Λ_{LE}	λ	$\Delta\gamma$	M	$R_f \times 10^{-6}$	$C_L \text{ max}$	$\alpha_{C_L \text{ max}}$ (deg)	J	α (deg)	C_L Calc.	C_L Test	* Percent Error									
6	2	48.4	.6	1.2	-0.2	6.0	1.034	27.2	1.08	8	.407	.356	14.6									
										12	.575	.575	0									
										16	.755	.78	-3.2									
										20	.905	.955	-5.2									
										24	.99	1.033	-4.2									
										27.2	1.02	*	-									
6	6	48.2	.6	1.2	-0.2	6.0	1.14	31.7	-4.6	8	.447	.424	5.4									
										12	.640	.625	2.4									
										16	.80	.78	2.5									
										20	.938	.88	6.6									
										24	1.045	.972	7.5									
										28	1.120	1.025	9.2									
										31.7	1.150	*	-									
6	4	48.6	.3	1.2	-0.2	6.0	1.06	25.8	1.2	4	.23	.24	-4.2									
										8	.47	.50	-6.0									
										12	.70	.70	0									
										16	.88	.90	-2.2									
										20	1.01	1.01	0									
										24	1.06	1.07	.9									
										25.9	1.08	1.04	1.9									
6	4	1.0	1.0	1.2	0.2	6.0	1.026	25.2	.56	8	.442	.40	10.5									
										12	.648	.67	-3.3									
										16	.826	.83	-0.5									
										20	.965	.935	2.1									
										24	1.032	1.01	2.2									
										25.2	1.028	1.015	1.3									
										28	.91	.965	-5.7									
$\text{Average Error} = \frac{\sum e }{n} = 3.7\%$																						
*Experimental Data Not Available.																						

TABLE 4.1.3.3-B
 SUBSONIC WING-LIFT VARIATION WITH ANGLE OF ATTACK
 DOUBLE-DELTA WINGS
 DATA SUMMARY AND SUBSTANTIATION

Ref.	Config.	A	λ_i	λ_o	η_B	Λ_{LE_i} (deg)	Λ_{LE_o} (deg)	$\frac{d}{b}$	$\frac{l}{c}$	LER	M	$R_{MAC} \times 10^{-6}$	α (deg)	C_L Calc.	C_L Test	ϵ Percent Error
30	WB	2.01	.416	.302	.313	78	53.3	.127	.03	Sharp ^(a)	.4	1.04	4	.165	.167	-1.2
													8	.348	.352	-1.1
													12	.559	.555	.7
													16	.774	.786	-1.5
													20	.991	.981	1.0
													4	.186	.194	-4.1
													8	.370	.389	-4.9
													4	.233	.213	9.4
													8	.442	.444	-.5
	WB	1.96	.295	.344	.405	78	48.5	.127	.03	Sharp ^(a)	.4	1.14	4	.144	.162	-11.1
													8	.305	.324	-5.9
													12	.490	.501	-2.2
													16	.679	.698	-2.7
													20	.869	.892	-2.6
													4	.166	.171	-3.5
													8	.334	.351	-4.8
													4	.208	.189	10.1
	WB	1.93	.180	.454	.498	78	38.1	.127	.03	Sharp ^(a)	.4	1.15	4	.130	.137	-5.1
													8	.274	.284	-3.5
													12	.440	.443	-.7
													16	.609	.611	-.3
	WB	1.93	.180	.454	.498	78	38.1	.127	.03	Sharp ^(a)	.7	1.15	4	.148	.159	-6.9
													8	.308	.319	-3.4
													4	.183	.177	3.4
													8	.357	.345	3.5
	WB	1.30	.196	0	.414	82	60	.147	.03	Sharp ^(a)	.4	1.70	4	.118	.095	24.2
													8	.239	.222	7.7
													12	.393	.357	10.1
													16	.543	.500	8.6
													20	.701	.642	9.2
													4	.128	.111	15.3
													8	.259	.246	5.3
													4	.134	.127	5.5
	WB	1.33	.302	.163	.403	82	60	.147	.03	Sharp ^(a)	.4	1.47	4	.132	.114	15.8
													8	.269	.273	-1.5
													12	.442	.440	.5

TABLE 4.1.3.3-B (Contd)

Ref.	Config.	A	λ_1	λ_0	η_B	Λ_{LE_1} (deg)	Λ_{LE_0} (deg)	$\frac{d}{b}$	$\frac{c}{c}$	LER	M	$R_{MAC} \times 10^{-6}$	α (deg)	C_L Calc	C_L Test	* Percent Error
30	WB	1.33	.302	.163	.403	82	60	.147	.03	Sharp ^(a)	.4	1.47	16	.611	.615	-.7
	WB	1.55	.301	0	.400	82	59	.144	.03	Sharp ^(a)	.7		20	.787	.790	-.4
	WB										.9		4	.145	.138	5.1
	WB										1		8	.293	.293	0
	WB										4		4	.152	.147	3.4
	WB										8		8	.317	.317	0
	WB										12		12	.428	.446	-4.0
	WB										16		16	.592	.628	-5.7
	WB										20		20	.764	.805	-5.1
	WB										4		4	.141	.145	-2.8
31	WBV	1.87	.488	0	.424	72.6	59	.131	.02-.03	Sharp	.13	17.1	4	.150	.152	-1.3
	WBV	1.46	.482	.189	.484	72.6	59	.149	.02-.03	Sharp			8	.340	.336	1.2
	WBV												12	.553	.556	-.5
	WBV												16	.769	.776	-.9
	WBV												20	.979	.986	-.7
	WBV												8	.335	.327	2.4
	WBV												12	.545	.546	-.2
	WBV												16	.757	.780	-2.9
	WBV												20	.965	1.006	-4.1
	WBV												8	.323	.308	4.9

TABLE 4.1 3.3-B (Contd)

Ref.	Config.	A	λ_i	λ_o	η_B	Λ_{LE_i} (deg)	Λ_{LE_o} (deg)	$\frac{d}{b}$	$\frac{t}{c}$	LER	M	$R_{MAC} \times 10^{-6}$	α (deg)	C_L Calc.	C_L Test	% Percent Error
31	WBV	1.73	.356	0	.414	77.4	59	.131	.02-.03	Sharp	.13	20.0	4	.143	.150	-4.7
	WBV	1.34	.356	.210	.473	77.4	59	.149	.02-.03	Sharp	.13	20.3	4	.130	.130	0
	WBV	1.87	.448	0	.332	77.2	59	.131	.02-.03	Sharp	.13	17.8	4	.146	.150	-2.7
	WBV	1.46	.448	.183	.379	77.2	59	.149	.02-.03	Sharp	.13	18.2	4	.144	.139	3.6
	WBVN	1.49	.483	.094	.180	84.75	62	.100	?	Sharp	?	?	4	.135	.150	-10.0
	WBVN	2.6	.200	0	.710	60	49.20	.090	.033	Round	.7	3.6	4	.214		
32	WBVN	2.6	.200	0	.709	60	49.20	.084	.035-.040	Round	.7	3.6	4	.229		
33	WBVN	2.6	.200	0	.709	60	49.20	.084	.035-.040	Round	.2	3.26	4	.242		
	WBVN	2.6	.200	0	.709	60	60	.084	.035-.040	Round	.2	3.26	4	.184		
	WBVN	2.6	.200	0	.709	60	60	.084	.035-.040	Round	.2	3.26	4	.350		
	WBVN	2.6	.200	0	.709	60	60	.084	.035-.040	Round	.2	3.26	4	.182	(b)	
	WBVN	3.0	.200	0	.654	60	42.08	.077	.035-.040	Round	.2	3.22	4	.184		
	WBVN	3.0	.200	0	.654	60	42.08	.077	.035-.040	Round	.2	3.22	4	.345		
	WBVN	3.0	.200	0	.654	60	42.08	.077	.035-.040	Round	.2	3.22	4	.523		
	WBVN	3.0	.200	0	.654	60	42.08	.077	.035-.040	Round	.2	3.22	4	.703		
	WBVN	3.0	.200	0	.654	60	42.08	.077	.035-.040	Round	.2	3.22	4	.879		
	WBVN	3.0	.200	0	.654	60	42.08	.077	.035-.040	Round	.2	3.22	4	.184		
	WBVN	3.0	.200	0	.654	60	42.08	.077	.035-.040	Round	.2	3.22	4	.349		
	WBVN	3.0	.200	0	.654	60	42.08	.077	.035-.040	Round	.2	3.22	4	.529		
	WBVN	3.0	.200	0	.654	60	42.08	.077	.035-.040	Round	.2	3.22	4	.712		
	WBVN	3.0	.200	0	.654	60	42.08	.077	.035-.040	Round	.2	3.22	4	.890		

(a) These models had theoretically round L.E.'s inboard but were analyzed as sharp because of small size of model and small t/c.

(b) This information is classified CONFIDENTIAL.

$$\text{Average Error} = \frac{\sum |e|}{n} = 4.6\%$$

TABLE 4.1.3.3-C
 SUBSONIC WING-LIFT VARIATION WITH ANGLE OF ATTACK
 CRANKED WINGS
 DATA SUMMARY

Ref.	Config.	A	λ_1	λ_o	η_B	Λ_{LE_1} (deg)	Λ_{LE_o} (deg)	$\frac{d}{b}$	$\frac{t}{c}$	LER	M	$R_f MAC \times 10^{-6}$	α (deg)	C_L Calc	C_L Test	* Percent Error
28	WBV	4.00	.580	.517	.600	49.2	6.6	.139	.06	Round	.80	2.5	8	0.553	0.500	10.6
											.85	2.66	12	0.726	0.675	7.6
											.90	2.81	16	0.910	0.826	10.3
											.90	2.81	20	1.081	0.925	16.9
											.90	2.81	8	0.558	0.530	5.3
											.90	2.81	12	0.734	0.690	6.4
											.90	2.81	16	0.924	0.865	6.8
											.90	2.81	20	1.099	0.995	10.5
											.90	2.81	8	0.603	0.530	13.8
											.90	2.81	12	0.794	0.730	8.8
34	WB	2.91	.333	.500	.500	87.01	81.7	.139	.04	Round	.60	2.20	8	0.372	0.370	0.5
											.80	2.94	12	0.544	0.575	- 5.4
											.80	2.94	8	0.428	0.390	9.7
											.80	2.94	12	0.631	0.586	7.9
											.90	3.30	8	0.477	0.405	17.8
											.90	3.30	12	0.701	0.610	14.9
36 ^(a)	WB	2.91	.641	.625	.600	53.13	32.16	.147	.06	Round	.60	1.50	8	0.444	0.480	- 7.5
											.80		12	0.616	0.688	-10.5
											.80		16	0.794	0.835	- 4.9
											.80		20	0.962	0.880	9.3
											.80		8	0.497	0.506	- 1.6
											.80		12	0.693	0.693	0
											.80		16	0.898	0.809	11.0
											.80		20	1.098	0.880	24.8
											.80		8	0.560	0.505	10.9
											.80		12	0.772	0.698	10.6
											.80		16	1.006	0.824	22.0
											.80		20	1.217	0.916	32.9
WB	2.91	.641	.625	.600	53.13	43.22	.147	.06	.03	Round	.60	1.5	8	0.435	0.500	-13.0
											.80		12	0.602	0.710	-15.2
											.80		16	0.774	0.840	- 7.9
											.80		20	0.937	0.900	4.1
											.80		8	0.452	0.615	-12.2
											.80		12	0.631	0.710	-11.1
											.80		16	0.818	0.825	- 0.8
											.80		20	0.991	0.860	15.2
											.80		8	0.564	0.540	4.4
											.80		12	0.776	0.715	8.5

TABLE 4.1.3.3-C (Contd)

Ref.	Config.	A	λ_i	λ_o	η_B	Λ_{LE_i} (deg)	Λ_{LE_o} (deg)	$\frac{d}{b}$	$\frac{t}{c}$	LER	M	R_L MAC $\times 10^{-6}$	α (deg)	C_L Calc.	C_L Test	ϵ Percent Error
37	W	5.20	.339	.268	.379	60.0	25.0	.147	0.45— 0.60	Round	.13	2.65	8	0.490	0.505	- 3.0
↓	↓	↓	↓	↓	↓	↓	↓	↓	↓	↓	↓	↓	12	0.647	0.695	- 6.9
38	WBV	8.47	.197	.386	.212	76.0	16.0	.062	—	Round	.20	3.6	8	0.472		
↓	↓	↓	↓	↓	↓	↓	↓	↓	↓	↓	↓	↓	12	0.694		
39	WB	6.18	.294	.463	.308	65.0	12.0	.066	0.06— 0.02	Round	.50	.73	8	0.512		
↓	↓	↓	↓	↓	↓	↓	↓	↓	↓	↓	↓	↓	12	0.664		
(a) Notched leading edge																
(b) This information is classified CONFIDENTIAL.																
$\text{Average Error} = \frac{\sum \epsilon }{n} = 10.5\%$																

TABLE 4.1.3.3-D
 SUBSONIC WING-LIFT VARIATION WITH ANGLE OF ATTACK
 CURVED (GOTHIC AND OGEET) WINGS
 DATA SUMMARY AND SUBSTANTIATION

Ref.	Config.	Planform	A	$\frac{b_w}{2L}$	p	$\frac{d}{b}$	$\frac{t}{c}$ (root)	M	$R_e \text{ MAC} \times 10^3$	α (deg)	C_L Calc.	C_L Test	% Percent Error
29	WB	Ogee	1.2	.300	.500	.133	.06	.4	1.7	4	.136	.132	3.0
								.7		8	.288	.285	1.1
								.8		12	.465	.465	0
								.8		4	.136	.132	3.0
								.8		8	.288	.297	-3.0
								.8		12	.466	.489	-4.7
								.8		4	.138	.139	-2.2
								.8		8	.288	.306	-5.6
40	WB	Ogee	2.00	.540	.540	.080	.03	.6	8.9	4	.183	.19	-3.7
								.7		8	.386	.385	.3
41	WB	Ogee	1.98	.450	.455	.127	.02	.7	0.58	4	.167	.19	-12.1
								.7		8	.352	.40	-12.0
9	W ₁	Gothic	.96	.250	.667	---	.01	.1	2.9	4	.125	.120	4.2
								.1		8	.263	.260	1.2
								.1		12	.426	.425	0
	W ₂	Gothic	1.00	.333	.667	---	.01	.1	2.9	4	.144	.140	2.9
								.1		8	.303	.310	-2.3
								.1		12	.490	.490	0
								.1		16	.698	.680	2.6
	W ₃		1.25	.417	.667	---				4	.161	.150	7.3
										8	.339	.326	4.3
										12	.549	.532	3.2
	W ₄		.94	.306	.651	---				4	.138	.140	-1.4
										8	.293	.290	1.0
										12	.470	.465	1.1
										16	.668	.659	1.4

TABLE 4.1.3.3-D (Contd)

Ref.	Config.	Planform	A	$\frac{b_w}{2L}$	p	$\frac{d}{b}$	$\frac{t}{c}$ (root)	M	R_L $\times 10^8$ MAC	α (deg)	C_L Calc.	C_L Test	* Percent Error
9	W ₅	Gothic	1.07	.333	.647	---	.01	.1	2.9	4	.144	.149	-3.4
	W ₁₁	Gothic	1.13	.333	.589	---	.01	.1	2.9	8	.303	.312	-2.9
	W ₁₂	Gothic	.76	.250	.658	---	.01	.1	2.9	12	.490	.500	-2.0
42	W	Ogee	.927	.209	.450	---		.18		4	.144	.150	-4.0
										8	.303	.320	-5.3
										12	.490	.509	-3.7
										16	.698	.705	-1.0
										20	.125	.119	5.0
										4	.265	.260	1.9
										8	.425	.423	.5
										12	.605	.608	.5
										16	.240	.230	4.3
										20	.388	.372	4.3
										4	.553	.525	5.3
										8	.722	.683	5.7
$\text{Average Error} = \frac{\sum e }{n} = 3.4\%$													

TABLE 4.1.3.3-E
SUPersonic WING-LIFT VARIATION WITH ANGLE OF ATTACK
SUBSONIC LEADING EDGE
DATA SUMMARY AND SUBSTANTIATION

Ref.	A	Λ_{LE} (deg)	λ	Airfoil Section	δ (deg)	M	β	α (deg)	C_L Calc.	C_L Test	% Percent Error
11	1.37	63	1.0	Biconvex (t/c = .06)	15	1.56	1.18	10	0.331	0.358	-7.5
								20	0.685	0.722	-5.1
								30	0.959	0.944	1.6
								40	1.091	1.005	8.5
12	2	63.4	C	Biconvex (t/c = .06)	12.6	1.97	1.70	10	0.344	0.335	2.7
								20	0.679	0.630	7.8
								30	0.912	0.858	6.3
								40	1.030	0.981	5.0
								50	1.030	0.958	7.6
16	1.73	66.6	0	65A003	16.8	2.41	2.19	5	0.123	0.132	-6.8
								10	0.270	0.268	0.7
								15	0.404	0.387	4.4
								20	0.520	0.498	4.4
18	0.375	84.6	0	Mod Bicon (t/c = .04)	35	1.96	1.69	10	0.162	0.16	1.2
								20	0.387	0.38	1.8
								30	0.694	0.58	2.4
								40	0.744	0.726	2.6
19	0.375	84.6	0	Mod Bicon (t/c = .04)	35	3.30	3.14	10	0.138	0.131	5.3
								20	0.311	0.30	3.6
								30	0.488	0.473	3.2
								40	0.641	0.62	3.4
19	1	76	0	Mod Bicon (t/c = .04)	16.6	1.96	1.69	10	0.275	0.264	4.2
								20	0.662	0.55	2.2
								30	0.769	0.779	-1.2
								40	0.874	0.892	-2.0
$\text{Average Error} = \frac{\sum e }{n} = 4.0\%$											

TABLE 4.1.3.3-F
SUPersonic WING-LIFT VARIATION WITH ANGLE OF ATTACK
WITH TRANSITION FROM ATTACHED TO DETACHED SHOCK
DATA SUMMARY AND SUBSTANTIATION

Ref.	A	Λ_{LE} (deg)	λ	Airfoil Section	δ (deg)	M	β	α (deg)	C_L Calc.	C_L Test	* Percent Error							
12	2	0	1.0	Biconvex (t/c = .06)	6	1.97	1.7	5	0.176	0.179	-1.6							
								10	0.356	0.364	-2.2							
								16.8*	0.636	0.622	2.2							
								25	0.883	0.861	2.6							
								35	1.024	1.023	0.1							
13	2.31	60	0	Mod. D.W. (t/c = .06)	24	6.9	6.82	3	0.031	0.0349	-11.2							
								6.4*	0.070	0.077	-9.1							
								12	0.143	0.147	-2.7							
								20	0.287	0.277	3.6							
								28	0.465	0.46	1.1							
15	4	45	0	Biconvex (t/c = .05)	8	2.46	2.24	3	0.093	0.0927	0.3							
								7*	0.218	0.218	0							
								12	0.378	0.367	3.0							
								18	0.573	0.542	5.7							
								25	0.724	0.688	5.2							
15	2	0	1.0	Biconvex (t/c = .05)	6	2.46	2.24	3	0.093	0.0927	0.3							
								7*	0.218	0.218	0							
								12	0.378	0.367	3.0							
								18	0.573	0.542	5.7							
								25	0.724	0.688	5.2							
15	2	0	1.0	Biconvex (t/c = .05)	6	2.46	2.24	3	0.093	0.0927	0.3							
								7*	0.218	0.218	0							
								12	0.378	0.367	3.0							
								18	0.573	0.542	5.7							
								25	0.724	0.688	5.2							
$\text{Average Error} = \frac{\sum e }{n} = 2.8\%$																		
^a Angle for incipient shock detachment																		

TABLE 4.1.3.3-G
SUPERSONIC WING-LIFT VARIATION WITH ANGLE OF ATTACK
DETACHED LEADING-EDGE SHOCK
DATA SUMMARY AND SUBSTANTIATION

Ref.	A	Λ_{LE} (deg)	λ	Airfoil Section	δ (deg)	M	β	α (deg)	C_L Calc.	C_L Test	* Percent Error
25	1.96	64	0	Mod. Flat Pl. (t/c = .02)	21	2.32	2.1	10	0.272	0.287	-5.2
↓	↓	↓	↓					20	0.574	0.552	3.6
↓	↓	↓	↓					30	0.838	0.810	3.4
25	4	45	0	Mod. Flat Pl. (t/c = 0.3)	20	2.32	2.1	10	0.298	0.320	-6.8
↓	↓	↓	↓					20	0.625	0.642	-2.6
↓	↓	↓	↓					30	0.905	0.936	-3.3
11	1.76	36	1.0	Biconvex (t/c = .11)	16	1.55	1.18	10	0.399	0.404	-1.2
↓	↓	↓	↓					20	0.765	0.810	-5.6
↓	↓	↓	↓					30	0.981	1.030	-4.8
12	4	45	0	Biconvex (t/c = .05)	8	1.97	1.70	5	0.202	0.20	1.0
↓	↓	↓	↓					15	0.602	0.56	7.6
↓	↓	↓	↓					25	0.895	0.835	7.2
↓	↓	↓	↓					35	1.024	1.024	0
13	1.62	68	0	Mod. D. W. (t/c = .08)	31	6.90	6.82	8	0.084	0.084	0
↓	↓	↓	↓					12	0.134	0.133	0.8
↓	↓	↓	↓					16	0.199	0.190	4.7
↓	↓	↓	↓					20	0.278	0.267	8.2
13	1.29	72.1	0	Mod. D. W. (t/c = .08)	36	6.90	6.82	8	0.077	0.071	8.4
↓	↓	↓	↓					12	0.124	0.117	6.0
↓	↓	↓	↓					16	0.180	0.174	3.4
↓	↓	↓	↓					20	0.244	0.243	0.4
↓	↓	↓	↓					24	0.309	0.32	-3.4
13	0.7	80	0	Mod. D. W. (t/c = .08)	52	6.90	6.82	8	0.065	0.068	12.0
↓	↓	↓	↓					12	0.110	0.102	7.8
↓	↓	↓	↓					16	0.164	0.158	3.8
↓	↓	↓	↓					20	0.226	0.220	2.7
↓	↓	↓	↓					24	0.292	0.288	1.4
↓	↓	↓	↓					28	0.381	0.359	6.1
16	2	63.4	0	Biconvex (t/c = .05)	12.6	2.48	2.24	10	0.278	0.276	0.7
↓	↓	↓	↓					20	0.519	0.517	0.4
↓	↓	↓	↓					30	0.701	0.726	-3.4
↓	↓	↓	↓					40	0.856	0.904	-5.3
16	3	53	0	65A003	11	2.41	2.19	5	0.150	0.154	-2.6
↓	↓	↓	↓					10	0.311	0.296	5.0
↓	↓	↓	↓					15	0.458	0.443	3.4
↓	↓	↓	↓					20	0.582	0.559	4.1
Average Error = $\frac{\sum e }{n} = 4.1\%$											

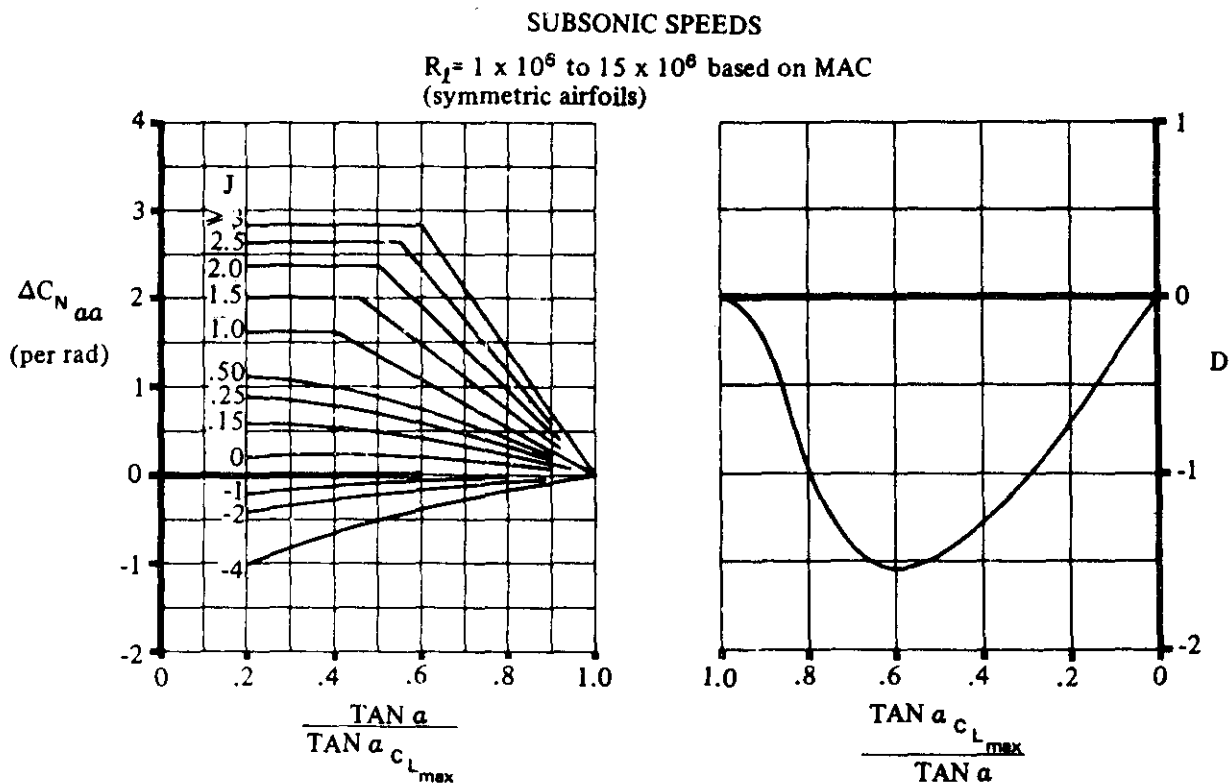


FIGURE 4.1.3.3-55a SUBSONIC LIFT VARIATION WITH ANGLE OF ATTACK

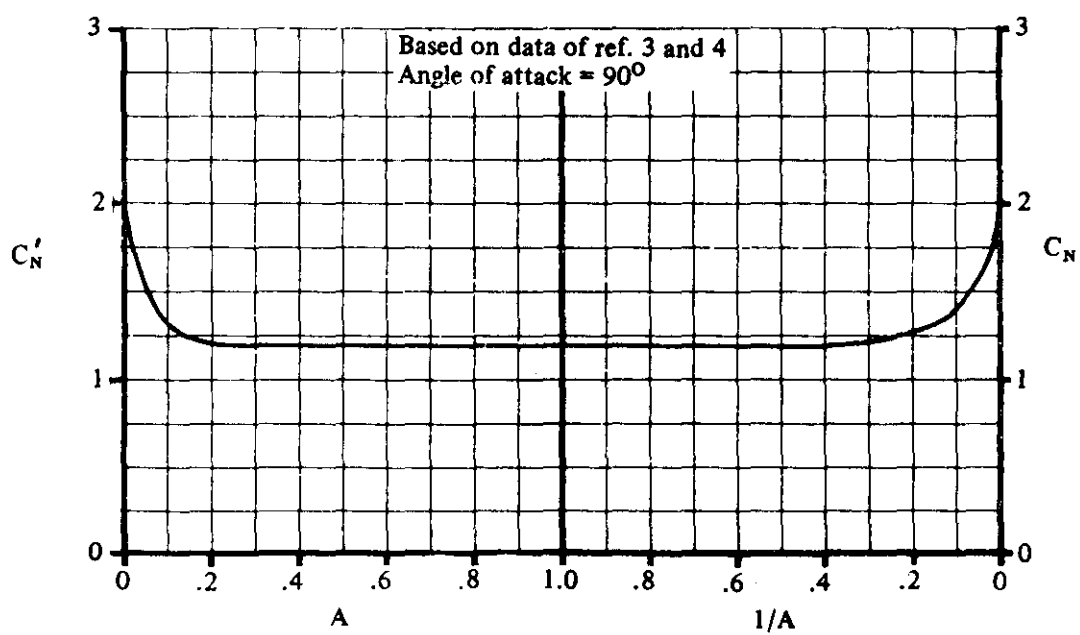


FIGURE 4.1.3.3-55b SUBSONIC LIFT VARIATION WITH WING ASPECT RATIO AT 90° ANGLE OF ATTACK

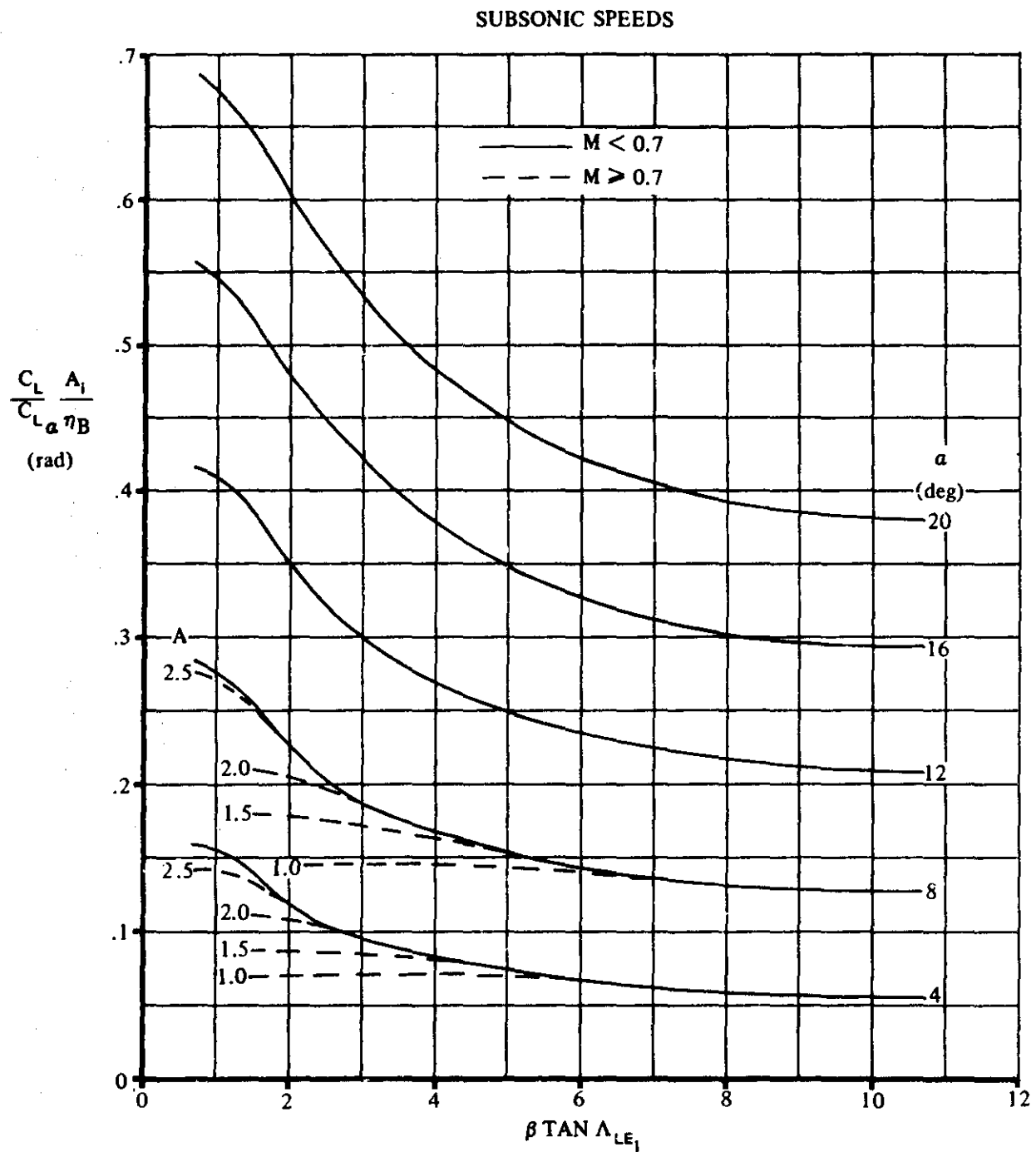


FIGURE 4.1.3.3-56 PREDICTION OF NONLINEAR LIFT OF DOUBLE-DELTA PLANFORMS AT SUBSONIC SPEEDS

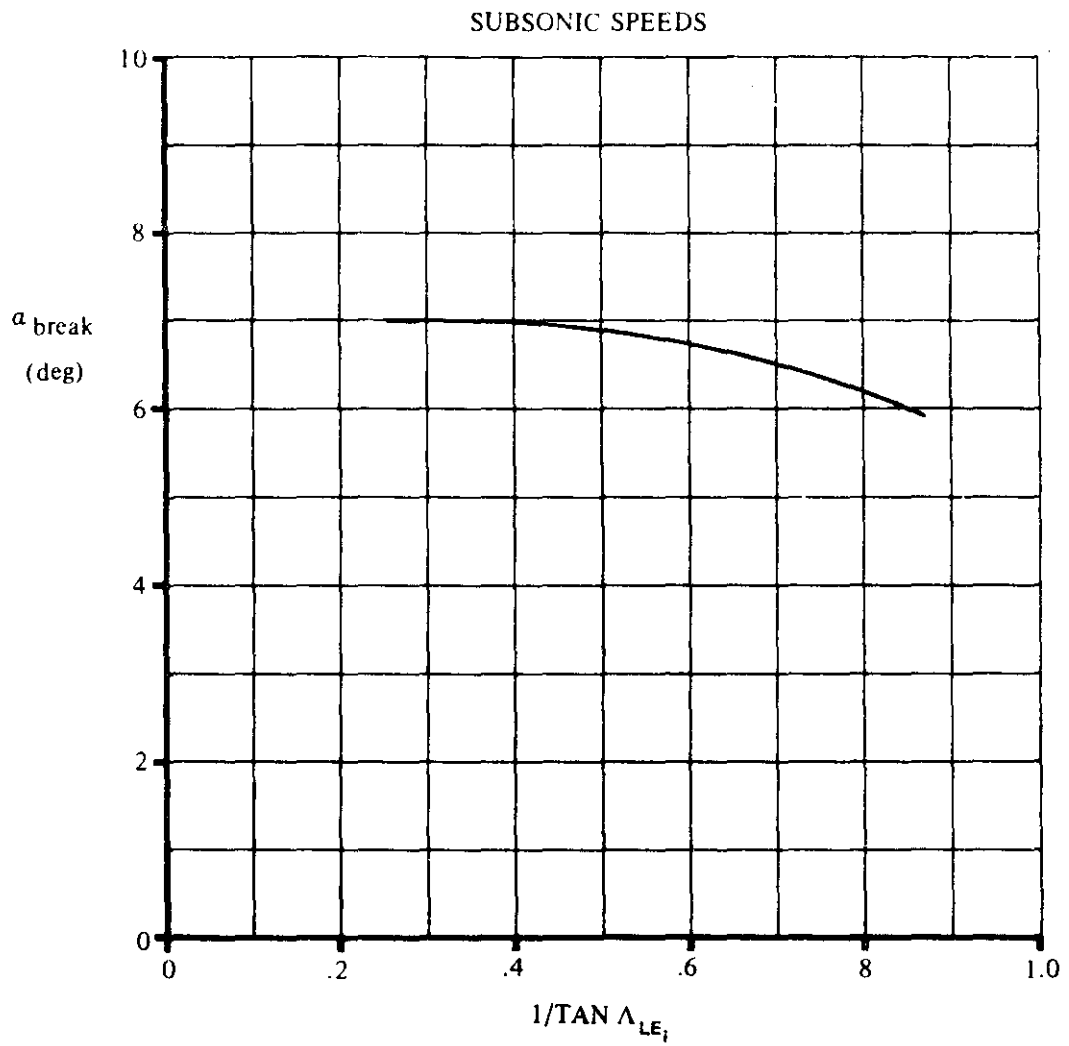


FIGURE 4.1.3.3-57 CORRELATION OF α_{break} FOR CRANKED PLANFORMS OF ASPECT RATIOS GREATER THAN 3 AND HAVING ROUND-NOSED AIRFOILS

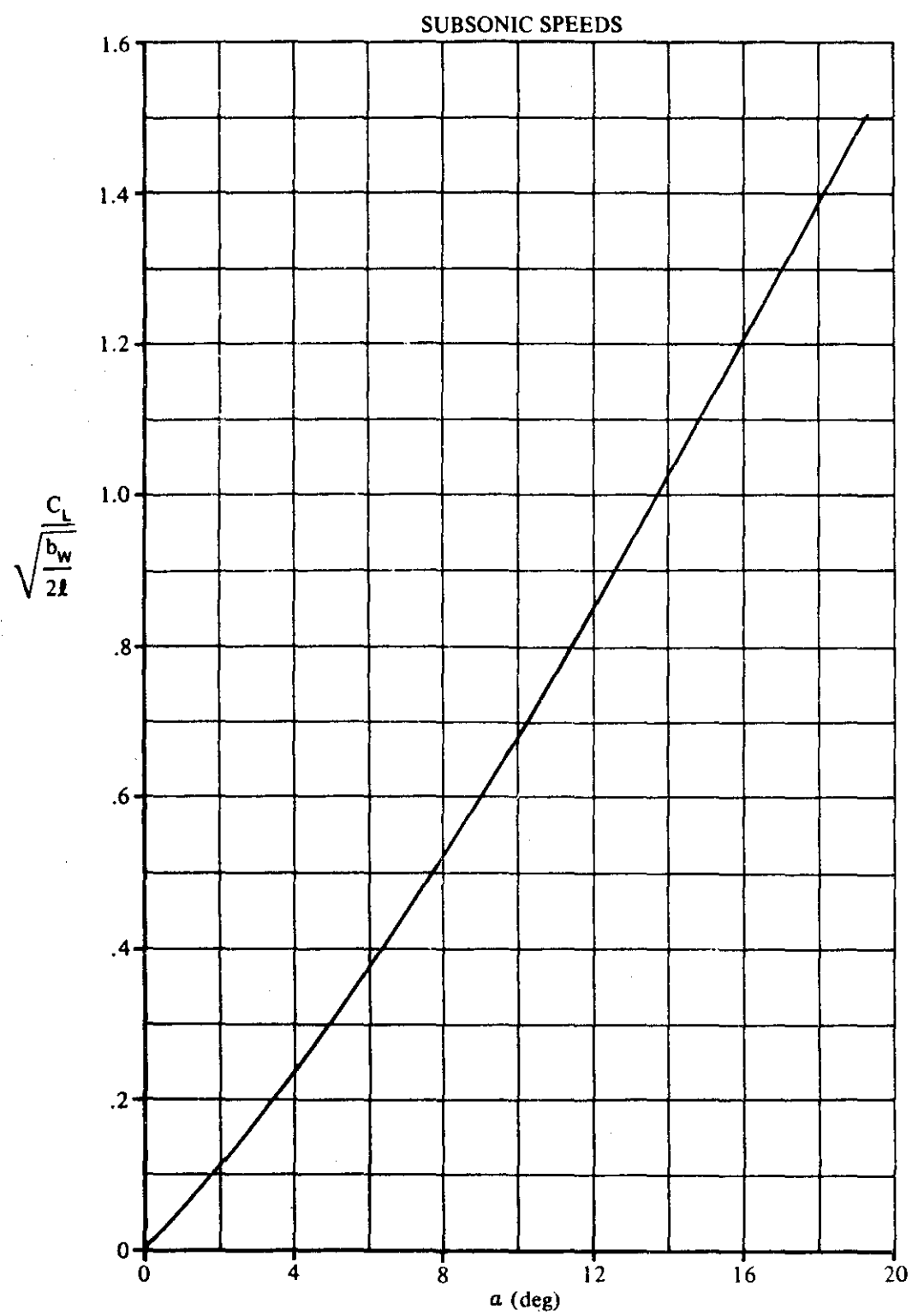


FIGURE 4.1.3.3-58 CORRELATION OF LIFT CURVES OF GOTHIC AND OGEE PLANFORMS

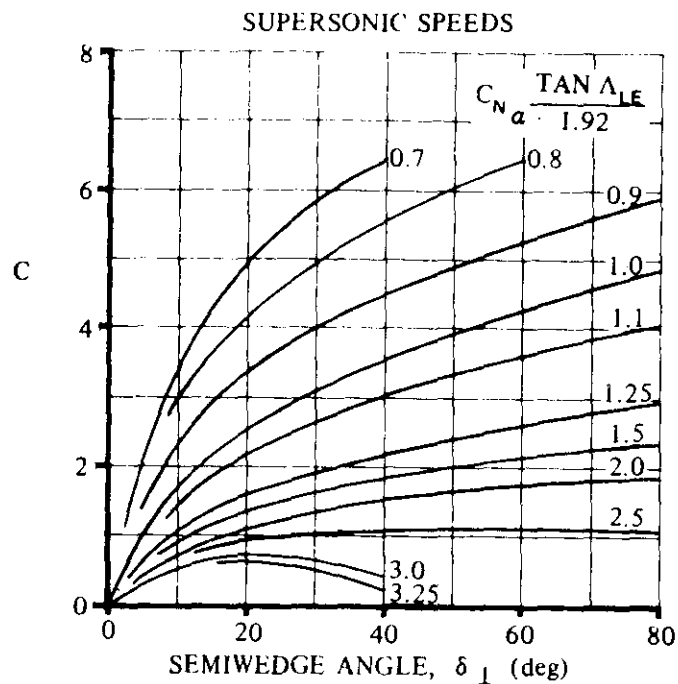


FIGURE 4.1.3.3-59a THICKNESS CORRECTION FACTOR FOR SUPersonic WING-LIFT VARIATION WITH ANGLE OF ATTACK

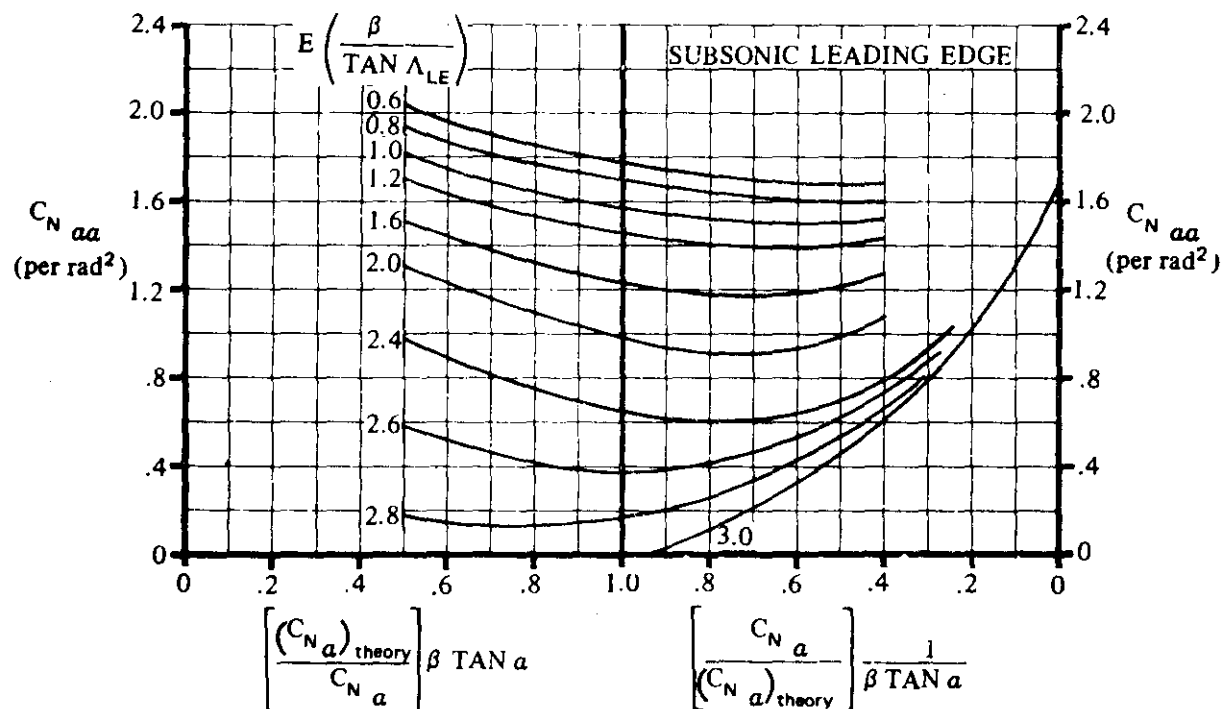


FIGURE 4.1.3.3-59b SUPersonic LIFT VARIATION WITH ANGLE OF ATTACK FOR WINGS WITH SUBSONIC LEADING EDGE

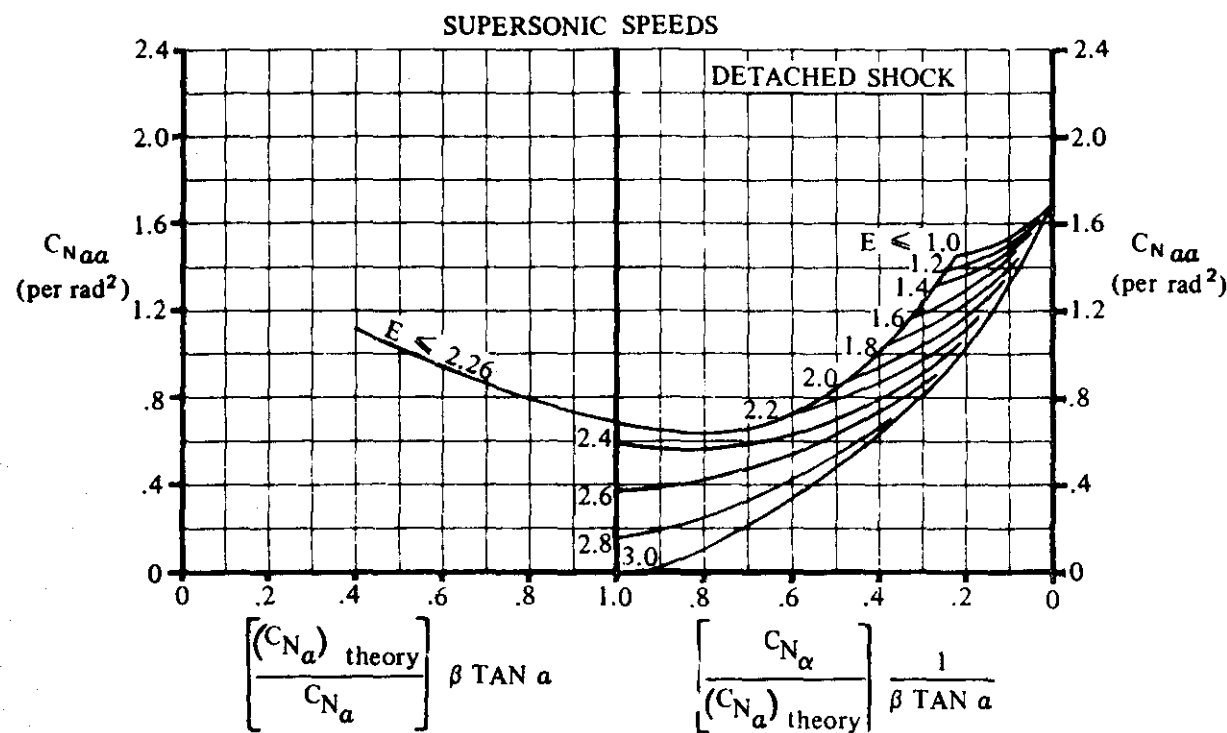


FIGURE 4.1.3.3-60a SUPersonic LIFT VARIATION WITH ANGLE OF ATTACK FOR WINGS WITH DETACHED SHOCK

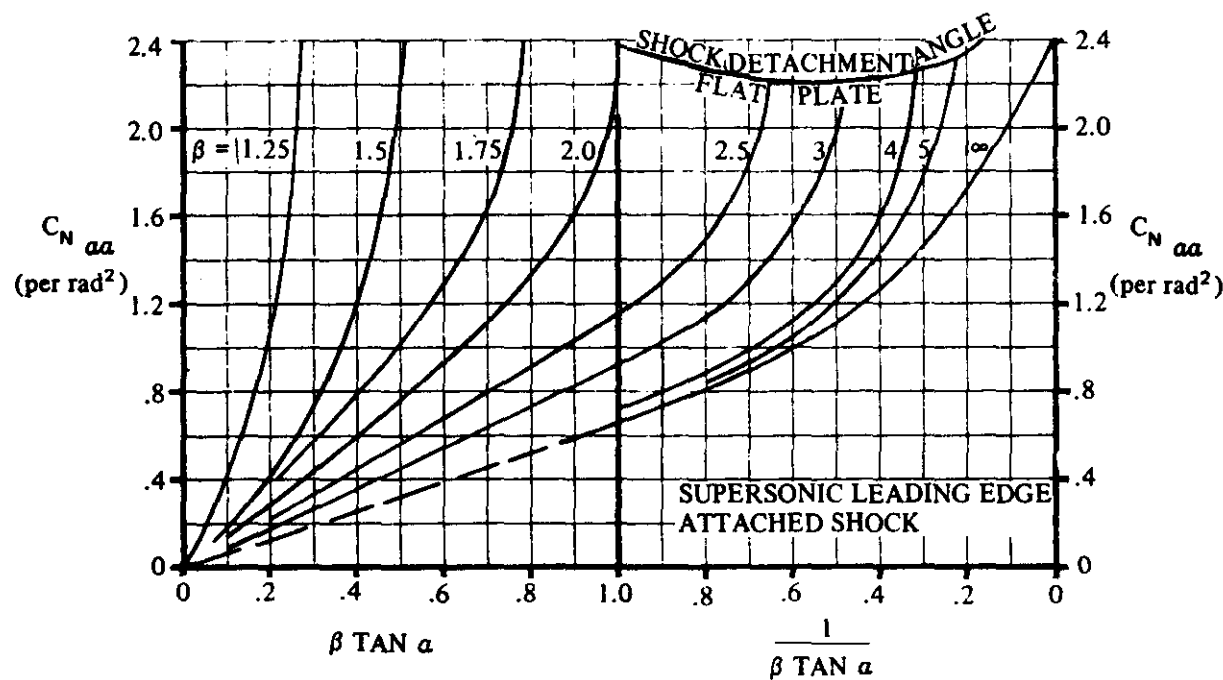


FIGURE 4.1.3.3-60b SUPersonic LIFT VARIATION WITH ANGLE OF ATTACK FOR WINGS WITH SUPersonic LEADING EDGE-ATTACHED SHOCK

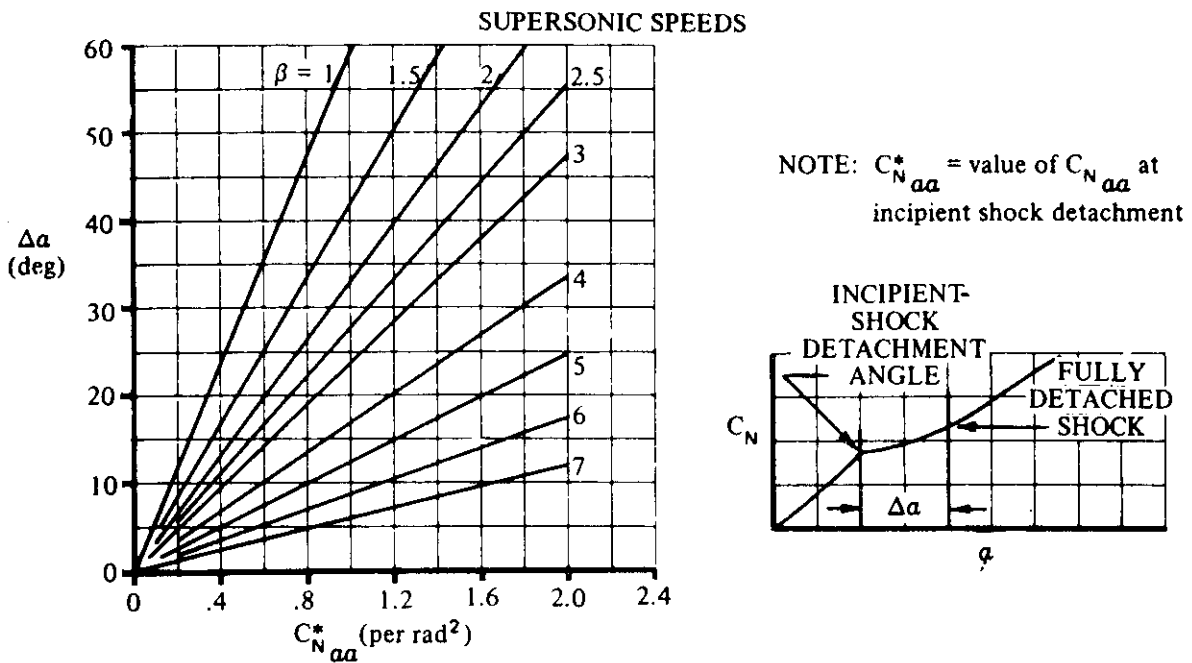


FIGURE 4.1.3.3-61a ANGLE-OF-ATTACK INCREMENT FROM INCIPENT-SHOCK DETACHMENT TO FULLY DETACHED SHOCK FOR SUPersonic WING-LIFT VARIATION WITH ANGLE OF ATTACK

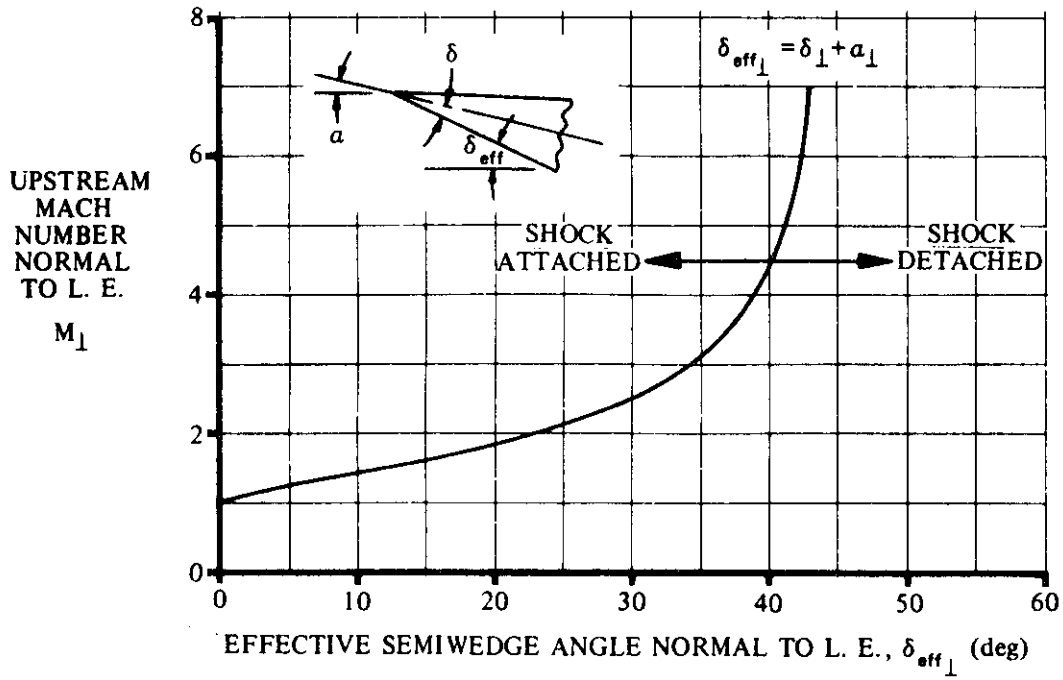


FIGURE 4.1.3.3-61b ANGLE FOR SHOCK DETACHMENT FOR WEDGE AIRFOILS

4.1.3.4 WING MAXIMUM LIFT

Methods are presented in this section for estimating the maximum lift of wings at subsonic, transonic, supersonic, and hypersonic speeds.

A. SUBSONIC

At subsonic speeds the wing maximum lift of high-aspect-ratio wings is directly related to the maximum lift of the wing airfoil section, with planform geometry of secondary importance. However, as the wing aspect ratio decreases, the wing planform shape becomes increasingly more significant. This is especially true for low-aspect-ratio delta-wing or non-straight-tapered planforms where leading-edge vortex effects are prevalent.

The complexity of modern wing designs (twisted wings with varying airfoil sections) precludes the application of empirical methods that yield consistently good results. Thus, the use of more exact theory is necessary for estimating maximum lift. Method 1 presented below requires the user to employ the most accurate wing spanwise-loading computer program available. In case no such program is available to the user, two additional empirical methods are presented. Method 2 is applicable to high-aspect-ratio configurations with constant-section untwisted wings. Method 3 is applicable to low-aspect-ratio configurations with constant-section untwisted wings.

Wing lift characteristics do not change discontinuously from one aspect-ratio regime to another. However, because of the different approaches used in Methods 2 and 3, values calculated by Method 2 will not necessarily match exactly the values of Method 3 for a border-line aspect-ratio configuration.

In general, however, the differences in values obtained by the two methods for the border-line aspect ratios should be small.

Flow Separation and Stalling Characteristics

For high-aspect-ratio wings, the three-dimensional maximum lift and stalling characteristics are, as a first approximation, determined by section properties (see Sections 4.1.1.3 and 4.1.1.4). There are, however, certain three-dimensional effects that may become important. These include the spanwise variations of induced camber and angle of attack, and the effect of spanwise pressure gradient on the boundary layer.

Because of these effects, the stall of three-dimensional wings, even untwisted wings of constant airfoil section, usually starts at some spanwise station and rapidly spreads with increasing angle of attack. Highly tapered wings tend to stall at the tips, while untapered wings tend to stall at the root.

On swept wings the induced effects combine to promote stall at the tip. The induced camber at the tip is negative and the induced angle of attack is high. The spanwise pressure gradient tends to draw the boundary layer from the wing root to the tip. All of these factors promote separation at the wing tip and suppress it at the root. It is therefore very difficult to prevent tip separation at high angles of attack on highly swept wings.

Regardless of where the separation first appears, it is the type of separation that determines the maximum lift. Trailing-edge separation, which is characteristic of thick wings, always results in a loss in maximum lift compared to the airfoil-section maximum lift. Leading-edge separation, where

the flow rolls up into a spanwise vortex, as on thin swept wings, results in an increase in normal force. The magnitude of the increase is related to the strength of the leading-edge vortex. These effects are illustrated by the variations of maximum lift with wing thickness at high sweep angles, as shown in Figure 4.1.3.4-21a. For more details regarding wing flow separation and stalling characteristics, the reader is referred to References 1 and 2.

Reynolds-Number Effects

The salient aspects of the Reynolds-number discussion presented in Reference 2 are presented below. From the available test data results, there appear to be essential differences between the Reynolds-number effects of thin airfoils ($t/c \approx 0.06$), of moderately thick airfoils ($t/c \approx 0.12$), and of thick airfoils ($t/c \approx 0.18$).

The maximum lift of thin airfoils is relatively constant up to a Reynolds number of 10×10^6 ; but when this Reynolds number is exceeded, the value of maximum lift begins to increase.

With moderately thick airfoils a very large increase of the maximum lift with increasing Reynolds number is found at low Reynolds numbers. However, at Reynolds numbers above 4 to 6×10^6 , the maximum lift tends to remain about constant.

The maximum lift of thick airfoils increases gradually up to high Reynolds numbers. At Reynolds numbers above 15×10^6 , the maximum lift tends to remain constant.

Mach-Number Effects

Mach-number effects on the maximum lift of unswept, thick wings are quite severe, starting as low as $M = 0.15$. This is to be expected from the analogy with section characteristics (see Section 4.1.1.4). For swept wings the losses due to Mach number are much less than they are for straight wings of a given thickness.

Mach-number effects are due in part to the larger pressure gradients associated with compressible flow. These larger pressure gradients can cause the boundary layer to separate at a lower lift value, thus resulting in a lower maximum lift with increasing Mach number. Large decreases in maximum lift can be related to the problem of shock-induced separation. For a complete discussion of the compressibility effects, the reader is referred to Reference 3.

Interference Effects

It must be recognized that the maximum lift of the wing alone, as given in this section, may be substantially altered by interference effects. The addition of fuselages, nacelles, pylons, and other protuberances can markedly change the aerodynamic characteristics of a given configuration near the stall. Interference effects of this type are discussed in Section 4.3.1.4.

DATCOM METHODS

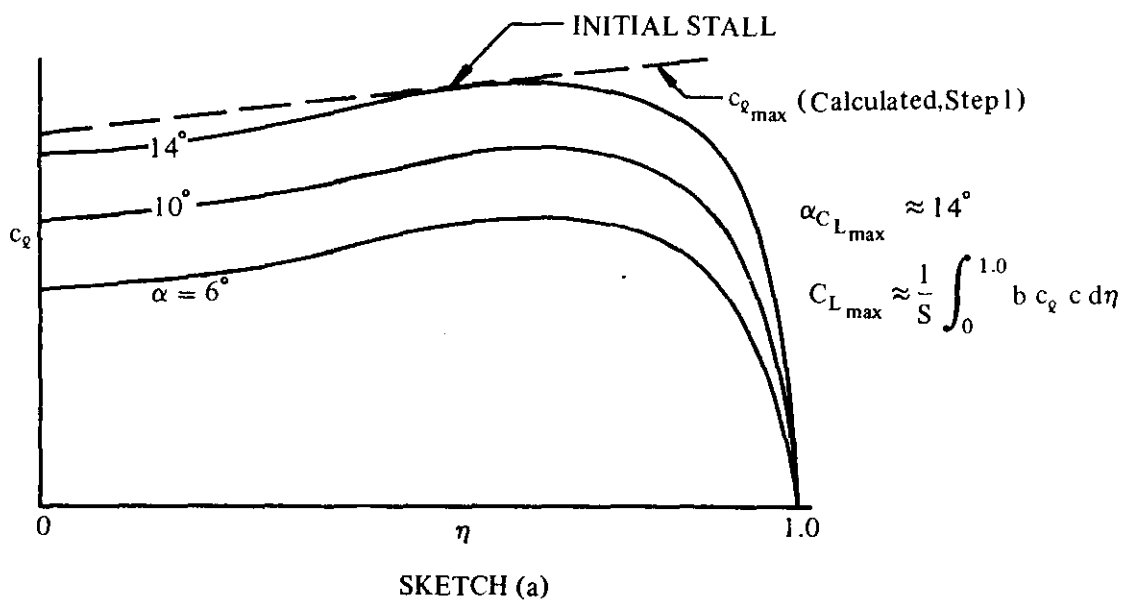
Method 1

The following method requires that the user have at his disposal an accurate wing spanwise-loading computer program, e.g., a lifting-surface theory computer program. If no such computer program is available, Methods 2 and 3 may be used to approximate the wing maximum lift.

Method 1 is limited to moderately swept configurations where leading-edge vortex effects are not significant. In addition, the spanwise location where stall is first detected should be limited to one local chord-length away from the wing root and tip sections.

Application of the method is as follows:

- Step 1. Determine the section $c_{\ell_{\max}}$ across the entire span of the wing, based on the appropriate Mach number and local Reynolds number, using Section 4.1.1.4. If section test data are available, they should be used whenever possible, and the appropriate corrections made for Mach number, Reynolds number, and surface roughness as given in Section 4.1.1.4.
- Step 2. Plot the section $c_{\ell_{\max}}$ from Step 1 as a function of spanwise station η (see Sketch (a)).



- Step 3. Apply the wing spanwise-loading method over a range of angle of attack until a value of the local wing loading coincides or exceeds the local wing $c_{\ell_{\max}}$ calculated from Step 1 (see Sketch (a)). The angle of attack at which the spanwise loading coincides with the calculated $c_{\ell_{\max}}$ value determines the angle of attack and spanwise position for initial stall. An approximate spanwise location where the stall will first occur can be calculated for an untwisted, tapered wing by

$$\eta_{\text{stall}} = 1 - \lambda \quad 4.1.3.4-a$$

where λ is the wing taper ratio.

- Step 4. Integrate the spanwise loading that coincides with the calculated $c_{\ell_{\max}}$ value to obtain the wing $C_{L_{\max}}$ value.

Although no substantiation of this method is presented, design experience has shown that the accuracy of this method is superior to that of both Methods 2 and 3.

Method 2

The following method is derived empirically, based on the experimental data of References 4 through 10. This method should therefore be restricted to those untwisted, constant-section, straight-tapered, high-aspect-ratio configurations that satisfy the following relationship:

$$A > \frac{4}{(C_1 + 1) \cos \Lambda_{LE}} \quad 4.1.3.4-b$$

where

A is the wing aspect ratio.

C_1 is given as a function of taper ratio in Figure 4.1.3.4-24b.

Λ_{LE} is the sweep of the wing leading edge.

Border-line configurations are those that satisfy the following relationship:

$$\frac{3}{(C_1 + 1) \cos \Lambda_{LE}} \leq A \leq \frac{4}{(C_1 + 1) \cos \Lambda_{LE}} \quad 4.1.3.4-c$$

For these aspect ratios either Method 2 or Method 3 may be used.

If neither Equation 4.1.3.4-b nor -c is satisfied, the low-aspect-ratio procedure presented in Method 3 may be used.

The subsonic maximum lift and angle of attack for maximum lift for those untwisted, constant-section, high-aspect-ratio configurations that satisfy Equation 4.1.3.4-b or -c are given as follows:

$$C_{L_{max}} = \left(\frac{C_{L_{max}}}{c_{\rho_{max}}} \right) c_{\rho_{max}} + \Delta C_{L_{max}} \quad 4.1.3.4-d$$

$$\alpha_{CL_{max}} = \frac{C_{L_{max}}}{C_{L_\alpha}} + \alpha_0 + \Delta \alpha_{CL_{max}} \quad 4.1.3.4-e$$

The first term on the right side of Equation 4.1.3.4-d is the maximum lift coefficient at $M = 0.2$, and the second term is the lift increment to be added for Mach numbers between 0.2 and 0.6.

$\frac{C_{L_{max}}}{c_{\rho_{max}}}$ is obtained from Figure 4.1.3.4-21a.

$c_{L_{max}}$ is the section maximum lift coefficient at $M = 0.2$ obtained from Tables 4.1.1-A, -B, or from Section 4.1.1.4.

$\Delta C_{L_{max}}$ is a Mach-number correction obtained from Figure 4.1.3.4-22.

C_{L_α} is the wing lift-curve slope (per degree) for the Mach number under consideration, obtained from test data or Section 4.1.3.2.

α_0 is the wing zero-lift angle for the appropriate Mach number, obtained from test data or Section 4.1.3.1.

$\Delta\alpha_{C_{L_{max}}}$ is obtained from Figure 4.1.3.4-21b. Note that this figure is valid for all subsonic Mach numbers up to 0.6.

The leading-edge parameter Δy , which does not explicitly appear in the equations, must be used in reading values from the charts. The value of Δy is for a streamwise airfoil section and is expressed in percent chord and obtained or approximated from Figure 2.2.1-8.

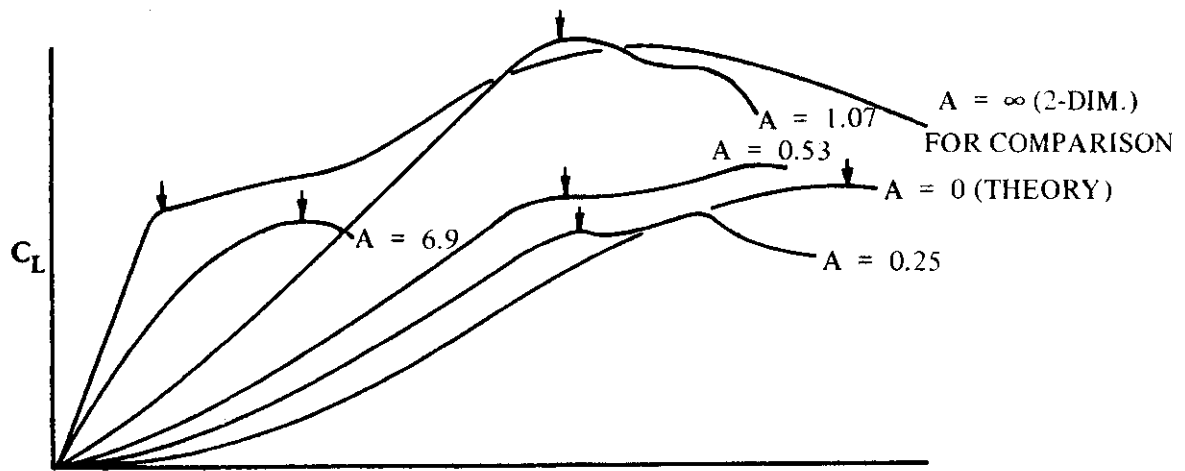
In calculating $\alpha_{C_{L_{max}}}$ the value of $C_{L_{max}}$ calculated from Equation 4.1.3.4-d is used as the numerator of the first term of Equation 4.1.3.4-e.

A comparison of test values of $C_{L_{max}}$ and $\alpha_{C_{L_{max}}}$ (based on the calculated $C_{L_{max}}$ value) with the corresponding values calculated by this method is shown in Table 4.1.3.4-A.

Method 3.

The following is an empirically derived method (Reference 11) that is applicable to untwisted, symmetrical-section, low-aspect-ratio wings.

Low-aspect-ratio wings at subsonic speeds exhibit extreme nonlinearities in the lift curve at high angles of attack, as shown in the accompanying sketch. Multiple lift peaks exist for many configurations. The charts of this section are for the first peak, as shown by the arrows in Sketch (b).



SKETCH (b)

For thin, low-aspect-ratio wings, Reynolds-number effects are small. Within the Reynolds-number and thickness limitations listed on Figures 4.1.3.4-23 through -25, Reynolds number is considered to have no effect.

This method is applicable to those low-aspect-ratio configurations (without considering Mach-number effects) that satisfy the following relationship:

$$A < \frac{3}{(C_1 + 1) \cos \Lambda_{LE}} \quad 4.1.3.4-f$$

where

A is the wing aspect ratio.

C_1 is given as a function of taper ratio in Figure 4.1.3.4-24b.

Λ_{LE} is the sweep of the wing leading edge.

Border-line configurations are those that satisfy the following relationship:

$$\frac{3}{(C_1 + 1) \cos \Lambda_{LE}} \leq A \leq \frac{4}{(C_1 + 1) \cos \Lambda_{LE}} \quad 4.1.3.4-c$$

For these aspect ratios either Method 2 or Method 3 may be used.

If neither Equation 4.1.3.4-f nor 4.1.3.4-c is satisfied, the high-aspect-ratio procedure presented in Method 2 may be used.

The subsonic maximum lift and angle of attack for maximum lift for those untwisted, symmetrical-section, low-aspect-ratio configurations that satisfy Equation 4.1.3.4-f or -c are given as follows:

$$C_{L_{max}} = (C_{L_{max}})_{base} + \Delta C_{L_{max}} \quad 4.1.3.4-g$$

$$\alpha_{C_{L_{max}}} = (\alpha_{C_{L_{max}}})_{base} + \Delta \alpha_{C_{L_{max}}} \quad 4.1.3.4-h$$

where

$(C_{L_{max}})_{base}$ is the base value of $C_{L_{max}}$ obtained from Figure 4.1.3.4-23a if the position of maximum airfoil-section thickness is forward of the 35-percent-chord point. If the maximum thickness is aft of this point, Figure 4.1.3.4-23b is used. For slab-sided wings the maximum-thickness point is considered to be the first chord-point at which the thickness reaches a maximum. The value of Δy , the leading-edge parameter used in reading these two charts, is obtained or approximated with the aid of Figure 2.2.1-8.

$\Delta C_{L_{max}}$ is the change in the base maximum-lift value. It is obtained from Figure 4.1.3.4-24a as a function of taper ratio, aspect ratio, leading-edge sweep, and Mach number.

$(\alpha C_{L_{max}})_{base}$ is the base value of $\alpha C_{L_{max}}$ obtained from Figure 4.1.3.4-25a. It is a function of aspect ratio, taper ratio, leading-edge sweep, and Mach number.

$\Delta \alpha_{C_{L_{max}}}$ is the change in the base value of angle of attack at maximum lift. It is obtained from Figure 4.1.3.4-25b as a function of taper ratio, aspect ratio, leading-edge sweep, and Mach number.

A comparison of test values of $C_{L_{max}}$ and $\alpha C_{L_{max}}$ with the corresponding values calculated by this method (where $\alpha C_{L_{max}}$ is based on the calculated $C_{L_{max}}$ value) is shown in Table 4.1.3.4-B.

Sample Problems

1. Method 2

Given: The following high-aspect-ratio configuration.

$$A = 5.0$$

$$\Lambda_{LE} = 46.6^\circ$$

$$\lambda = 0.565$$

$$R_2 = 2 \times 10^6$$

Airfoil: NACA 64A010 (free-stream direction)

$$C_{L_\alpha} = 0.061 \text{ per deg}$$

$$\alpha_0 = 0$$

$$M = 0.4$$

Compute:

Determine if the above configuration satisfies the high-aspect-ratio requirement for Method 2, as stipulated in Equation 4.1.3.4-b; i.e.,

$$A > \frac{4}{(C_1 + 1) \cos \Lambda_{LE}}$$

$$C_1 = 0.24 \quad (\text{Figure 4.1.3.4-24b})$$

$$\frac{4}{(C_1 + 1) \cos \Lambda_{LE}} = \frac{4}{(0.24 + 1.0) \cos 46.6^\circ} = \frac{4}{(1.24)(0.6871)} = 4.69$$

$$A = 5.0 > 4.69$$

The high-aspect-ratio requirement is satisfied; therefore, Method 2 is applicable to the above configuration.

Determine the maximum lift coefficient at $M = 0.40$

$$\Delta y = 2.12\% c \quad (\text{Figure 2.2.1-8})$$

$$c_{\ell_{\max}} = 1.23 \quad (\text{Table 4.1.1-B})$$

$$\frac{C_{L_{\max}}}{c_{\ell_{\max}}} = 0.83 \quad (\text{Figure 4.1.3.4-21a})$$

$$\Delta C_{L_{\max}} = -0.053 \quad (\text{Figure 4.1.3.4-22, interpolated})$$

$$\begin{aligned} C_{L_{\max}} &= \left(\frac{C_{L_{\max}}}{c_{\ell_{\max}}} \right) c_{\ell_{\max}} + \Delta C_{L_{\max}} \quad (\text{Equation 4.1.3.4-d}) \\ &= (0.83)(1.23) + (-0.053) \\ &= 1.02 - 0.053 \\ &= 0.97 \end{aligned}$$

Determine the angle of attack at the wing maximum lift

$$\Delta \alpha_{C_{L_{\max}}} = 6.7^\circ \quad (\text{Figure 4.1.3.4-21b})$$

$$\begin{aligned} \alpha_{C_{L_{\max}}} &= \frac{C_{L_{\max}}}{C_{L_{\alpha}}} + \alpha_0 + \Delta \alpha_{C_{L_{\max}}} \quad (\text{Equation 4.1.3.4-e}) \\ &= \frac{0.97}{0.061} + 0 + 6.7 \\ &= 15.9 + 6.7 \\ &= 22.6^\circ \end{aligned}$$

2. Method 3

Given: The following low-aspect-ratio configuration.

$$A = 1.0 \quad \Lambda_{LE} = 45^\circ \quad \lambda = 0.3$$

Airfoil: NACA 0005 (free-stream direction)

$$\text{Maximum thickness @ 30% chord} \quad M = 0.6$$

Compute:

Determine if the above configuration satisfies the low-aspect-ratio requirement for Method 3 as stipulated in Equation 4.1.3.4-f; i.e.,

$$A < \frac{3}{(C_L + 1) \cos \Lambda_{LE}}$$

$$C_1 = 0.5 \quad (\text{Figure 4.1.3.4-24b})$$

$$\frac{3}{(C_1 + 1) \cos \Lambda_{LE}} = \frac{3}{(0.5 + 1.0) \cos 45^\circ} = \frac{3}{(1.5)(0.7071)} = 2.83$$

$$A = 1 < 2.83$$

The low-aspect-ratio requirement is satisfied; therefore, Method 3 is applicable to the above configuration.

Determine the maximum-lift coefficient at $M = 0.6$

$$\Delta y = 1.37\% c \quad (\text{Figure 2.2.1-8})$$

$$\beta = \sqrt{1 - M^2} = \sqrt{1 - (0.6)^2} = 0.80$$

$$C_2 = 0.91 \quad (\text{Figure 4.1.3.4-24b})$$

$$(C_1 + 1) \frac{A}{\beta} \cos \Lambda_{LE} = (0.5 + 1.0) \frac{1}{0.80} \cos 45^\circ = 1.326$$

$$(C_{L_{max}})_{base} = 1.12 \quad (\text{Figure 4.1.3.4-23a})$$

$$(C_2 + 1) A \tan \Lambda_{LE} = (0.91 + 1.0)(1) \tan 45^\circ = 1.91$$

$$\Delta C_{L_{max}} = -0.08 \quad (\text{Figure 4.1.3.4-24a})$$

$$C_{L_{max}} = (C_{L_{max}})_{base} + \Delta C_{L_{max}} \quad (\text{Equation 4.1.3.4-g})$$

$$= 1.12 - 0.08$$

$$= 1.04$$

Determine the angle of attack at the wing maximum lift

$$(\alpha C_{L_{max}})_{base} = 30.8^\circ \quad (\text{Figure 4.1.3.4-25a})$$

$$A \cos \Lambda_{LE} [1 + (2\lambda)^2] = 1.0 \cos 45^\circ [1 + (0.6)^2] = 0.962$$

$$\Delta \alpha_{C_{L_{max}}} = 3.5^\circ \quad (\text{Figure 4.1.3.4-25b})$$

$$\alpha_{C_{L_{max}}} = (\alpha C_{L_{max}})_{base} + \Delta \alpha_{C_{L_{max}}} \quad (\text{Equation 4.1.3.4-h})$$

$$= 30.8 + 3.5$$

$$= 34.3^\circ$$

B. TRANSONIC

No method for high-aspect-ratio wings is presented herein in the transonic speed regime. However, for low-aspect-ratio wings an empirical method is presented.

For low-aspect-ratio wings, the maximum lift at transonic speeds was found to be basically a function of the same variables that were used in the subsonic speed regime (see References 12 through 15). Therefore, the design charts for the transonic speed regime are based on the subsonic design charts.

It should be noted that the transonic maximum-lift coefficient of thick wings may be limited by adverse pitching-moment variations and severe buffeting.

Both of these limitations are associated with extensive flow separation arising from compressibility, shock waves, and adverse pressure gradients.

DATCOM METHOD

The maximum lift and angle of attack at maximum lift for untwisted, symmetrical-section, low-aspect-ratio configurations are determined for Mach numbers between 0.6 and 1.2 by the following procedure:

- Step 1. Calculate the maximum lift and angle of attack at maximum lift for the wing under consideration at $M = 0.6$ by using Method 3 of Paragraph A of this section.
- Step 2. Determine the increments in maximum lift and angle of attack at maximum lift at the desired Mach number from Figures 4.1.3.4-26a through -26c. These increments are then added directly to the values obtained at $M = 0.6$ in Step 1; i.e.,

$$(C_{L_{\max}})_M = (C_{L_{\max}})_{M=0.6} + \Delta C_{L_{\max}} \quad 4.1.3.4-i$$

$$(\alpha_{C_{L_{\max}}})_M = (\alpha_{C_{L_{\max}}})_{M=0.6} + \Delta \alpha_{C_{L_{\max}}} \quad 4.1.3.4-j$$

A comparison of experimental data with results based on this method is presented in Table 4.1.3.4-C.

Sample Problem

Given: The same low-aspect-ratio configuration used in Sample Problem 2 of Paragraph A.

$$A = 1.0$$

$$\Lambda_{LE} = 45^\circ$$

$$\lambda = 0.3$$

Airfoil NACA 0005

$$\left. \begin{array}{l} C_{L_{\max}} = 1.04 \\ \alpha_{C_{L_{\max}}} = 34.3^{\circ} \\ C_2 = 0.91 \\ C_1 = 0.50 \end{array} \right\}$$

Sample Problem 2, Paragraph A

$$M = 1.0$$

Compute:

$$(C_2 + 1) A \tan \Lambda_{LE} = (0.91 + 1)(1.0)(1.0) = 1.91$$

$$C_3 = 1.0 \quad (\text{Figure 4.1.3.4-26b})$$

$$C_3 (C_1 + 1) A \cos \Lambda_{LE} = (1.0)(0.50 + 1)(1.0)(0.7071) = 1.06$$

$$\Delta C_{L_{\max}} = 0 \quad (\text{Figure 4.1.3.4-26a})$$

$$(C_1 + 1) A \cos \Lambda_{LE} = (0.50 + 1)(1.0)(0.7071) = 1.06$$

$$\Delta \alpha_{C_{L_{\max}}} = 0.5^{\circ} \quad (\text{Figure 4.1.3.4-26c})$$

Solution:

$$C_{L_{\max}} = (C_{L_{\max}})_{M=0.6} + \Delta C_{L_{\max}} \quad (\text{Equation 4.1.3.4-i})$$

$$= 1.04 + 0$$

$$= 1.04$$

$$\alpha_{C_{L_{\max}}} = (\alpha_{C_{L_{\max}}})_{M=0.6} + \Delta \alpha_{C_{L_{\max}}} \quad (\text{Equation 4.1.3.4-j})$$

$$= 34.3 + 0.5$$

$$= 34.8^{\circ}$$

C. SUPERSONIC

At supersonic speeds the lift is limited by geometric considerations rather than by flow separation. That is, maximum lift is reached when the component of the normal force in the lift direction ceases to increase with angle of attack.

The governing geometric parameters for the determination of maximum lift are those that influence the wing lift-curve slope; i.e., aspect ratio, sweep, taper ratio, and Mach number. It is therefore logical that a good correlating term might include the lift-curve slope. One such parameter that gives good results and is used here is $C_{N\alpha}/(4/\beta)$.

DATCOM METHOD

For the supersonic case the most accurate way of determining the wing maximum lift is by calculating the normal-force curve (using Sections 4.1.3.2 and 4.1.3.3) and converting it to a lift curve by means of the relationship $C_L = C'_N \cos \alpha$. However, design charts are presented herein for a more rapid procedure of estimating the wing maximum lift.

For Mach numbers greater than 1.4, the supersonic maximum lift and angle of attack at maximum lift may be approximated using Figures 4.1.3.4-27a and -27b. These figures are based on empirical data taken from References 16 through 26, and are presented as a function of $C_{N\alpha}$ and Mach number ($\beta = \sqrt{M^2 - 1}$). The lift-curve slope $C_{N\alpha}$ is obtained from test data or from Paragraph C of Section 4.1.3.2.

A comparison of experimental data with results based on this method is presented in Table 4.1.3.4-D.

Sample Problem

Given: The configuration of Reference 18.

$$A = 1.96$$

$$\Lambda_{LE} = 64^\circ$$

$$C_{N\alpha} = 1.72 \text{ per rad}$$

$$M = 2.32$$

Compute:

$$\beta = \sqrt{M^2 - 1}$$

$$= \sqrt{(2.32)^2 - 1}$$

$$= 2.093$$

$$\frac{1}{M} = \frac{1}{2.32} = 0.431$$

$$\frac{C_{N\alpha}}{4/\beta} = \frac{(1.72)(2.093)}{4} = 0.900 \text{ per rad}$$

Solution:

$$C_{L_{max}} = 1.02 \quad (\text{Figure 4.1.3.4-27a})$$

$$\alpha_{C_{L_{max}}} = 41.4^\circ \quad (\text{Figure 4.1.3.4-27b})$$

These compare with test values of $C_{L_{max}}$ of 0.98 and $\alpha_{C_{L_{max}}}$ of 43.8° from Reference 18.

D. HYPERSONIC

The supersonic method of Paragraph C above is used to estimate $C_{L_{max}}$ and $\alpha C_{L_{max}}$ at hypersonic speeds. The parameters that affect $C_{L_{max}}$ at the lower hypersonic Mach numbers are the same as those for the supersonic speeds, i.e., planform parameters. At high hypersonic speeds, $C_{L_{max}}$ is determined primarily by flow impact on the wing lower surface. Newtonian flow theory thus provides a reasonable approximation for $C_{L_{max}}$ values in this speed range. The high hypersonic limit ($1/M \rightarrow 0$) of Figures 4.1.3.4-27a and 4.1.3.4-27b is derived using the Newtonian equation

$$C_L = 2 \sin^2 \alpha \cos \alpha$$

4.1.3.4-k

REFERENCES

1. Harper, C. W., and Maki, R. L.: A Review of the Stall Characteristics of Swept Wings. NASA TN D-2373, 1964. (U)
2. van den Berg, B.: Reynolds Number and Mach Number Effects on the Maximum Lift and the Stalling Characteristics of Wings at Low Speeds. NLR TR 69025, 1969. (U)
3. Woottori, L. R.: The Effect of Compressibility on the Maximum Lift Coefficient of Airfoils at Subsonic Airspeeds. Jour. of Royal Aero. Soc., Vol. 71, July 1967. (U)
4. Turner, T. R.: Maximum Lift Investigation at Mach Numbers from 0.05 to 1.20 of a Wing with Leading Edge Swept Back 42°. NACA RM L9K03, 1950. (U)
5. Johnson, B. H., Jr., and Shibata, H. H.: Characteristics Throughout the Subsonic Speed Range of a Plane Wing and of a Cambered and Twisted Wing, Both Having 45° of Sweepback. NACA RM A51D27, 1951. (U)
6. Sutton, F. B., and Dickson, J. K.: A Comparison of the Longitudinal Aerodynamic Characteristics at Mach Numbers up to 0.94 of Sweptback Wings Having NACA 4-Digit or NACA 64A Thickness Distributions. NACA RM A54F18, 1954. (U)
7. Schneider, W. C.: A Comparison of the Spanwise Loading Calculated by Various Methods with Experimental Loadings Obtained on a 45° Sweptback Wing of Aspect Ratio 8.02 at a Reynolds Number of 4.0×10^6 . NACA TR 1208, 1954. (U)
8. Turner, T. R.: Effects of Sweep on the Maximum-Lift Characteristics of Four Aspect-Ratio-4 Wings at Transonic Speeds. NACA RM L50H11, 1950. (U)
9. Bollech, T. V., and Hadaway, W. M.: The Low-Speed Lift and Pitching-Moment Characteristics of a 45° Sweptback Wing of Aspect Ratio 8 With and Without High-Lift and Stall-Control Devices as Determined from Pressure Distributions at a Reynolds Number of 4.0×10^6 . NACA RM L52K26, 1953. (U)
10. Graham, R. R.: Low-Speed Characteristics of a 45° Sweptback Wing of Aspect Ratio 8 from Pressure Distributions and Force Tests at Reynolds Numbers from 1,500,000 to 4,800,000. NACA RM L51H13, 1951. (U)
11. White, C. O.: Maximum Lift Coefficients of Low Aspect Ratio Wings at Subsonic Speeds. Douglas Aircraft Company Report LB 30214, 1959. (U)
12. Nelson, W. H., and McDevitt, J. B.: The Transonic Characteristics of 22 Rectangular, Symmetrical Wing Models of Varying Aspect Ratio and Thickness. NACA TN 3501, 1955. (U)
13. Nelson, W. H., Allen, E. C., and Krumm, W. J.: The Transonic Characteristics of 36 Symmetrical Wings of Varying Taper, Aspect Ratio, and Thickness as Determined by the Transonic-Bump Technique. NACA TN 3529, 1955. (U)
14. Emerson, H. F.: Wind Tunnel Investigation of the Effects of Clipping the Tips of Triangular Wings of Different Thickness, Camber, and Aspect Ratio — Transonic Bump Method. NACA TN 3671, 1956. (U)
15. Few, A. G., Jr., and Fournier, P. G.: Effects of Sweep and Thickness on the Static Longitudinal Aerodynamic Characteristics of a Series of Thin, Low-Aspect-Ratio, Highly Tapered Wings at Transonic Speeds. Transonic Bump Method. NACA RM L54B25, 1954. (U)

4.1.3.4-13

16. Anon.: Proposal for a Study of Hypersonic Pressure Over Configurations Having Low Aspect Ratio Delta Wings. Douglas Aircraft Company Report SM 35518, 1958. (U)
17. Ames Research Staff: Equations, Tables, and Charts for Compressible Flow. NACA TR 1135, 1953. (U)
18. Gallagher, J. J., and Mueller, J. N.: An Investigation of the Maximum Lift of Wings at Supersonic Speeds. NACA TR 1227, 1955. (U)
19. Dugan, D. W.: Estimation of Static Longitudinal Stability of Aircraft Configurations at High Mach Numbers and at Angles of Attack Between 0° and $\pm 180^{\circ}$. NASA Memo 1-17-59A, 1959. (U)
20. Kaattari, G. E.: Pressure Distributions on Triangular and Rectangular Wings to High Angles of Attack – Mach Numbers 1.45 and 1.97. NACA RM A54D19, 1954. (U)
21. Kaattari, G. E.: Pressure Distributions on Triangular and Rectangular Wings to High Angles of Attack – Mach Numbers 2.46 and 3.36. NACA RM A54J12, 1955. (U)
22. Bertram, M. H., and McCauley, W. D.: An Investigation of the Aerodynamic Characteristics of Thin Delta Wings with a Symmetrical Double-Wedge Section at a Mach Number of 6.9. NACA RM L55B14, 1955. (U)
23. Pitts, W. C.: Force, Moment, and Pressure-Distribution Characteristics of Rectangular Wings at High Angles of Attack and Supersonic Speeds. NACA RM A55K09, 1956. (U)
24. Boatright, W. B.: Experimental Study and Analysis of Loading and Pressure Distributions on Delta Wings due to Thickness and to Angle of Attack at Supersonic Speeds. NACA RM L56I14, 1956. (U)
25. Smith, F. M.: Experimental and Theoretical Aerodynamic Characteristics of Two Low-Aspect-Ratio Delta Wings at Angles of Attack to 50° at a Mach Number of 4.07. NACA RM L57E02, 1957. (U)
26. Hill, W. A., Jr.: Experimental Lift of Low-Aspect-Ratio Triangular Wings at Large Angles of Attack and Supersonic Speeds. NACA RM A57I17, 1957. (U)
27. Cahill, J. F., and Gottlieb, S. M.: Low-Speed Aerodynamic Characteristics of a Series of Swept Wings Having NACA 65A006 Airfoil Sections (Revised). NACA RM L50F16, 1950. (U)
28. Rose, L. M.: Low-Speed Investigation of a Small Triangular Wing of Aspect Ratio 2.0. I – The Effect of Combination with a Body of Revolution and Height Above a Ground Plane. NACA RM A7K03, 1948. (U)
29. Graham, D.: Chordwise and Spanwise Loadings Measured at Low Speeds on a Large Triangular Wing Having an Aspect Ratio of 2 and a Thin, Subsonic-Type Airfoil Section. NACA RM A50A04a, 1950. (U)
30. Truckenbrodt, E., and Feindt, E. G.: Investigations on the Stalling Characteristics of Delta Wings in Incompressible Flow. AFOSR TN 57-538, 1957. (U)
31. Winter, H.: Flow Phenomena on Plates and Airfoils of Short Span. NACA TM 798, 1936. (U)
32. Tosti, L.P.: Low-Speed Static Stability and Damping-in-Roll Characteristics of Some Swept and Unswept Low-Aspect-Ratio Wings. NACA TN 1468, 1947. (U)
33. Bartlett, G. E., and Vidal, R. J.: Experimental Investigation of Influence of Edge Shape on the Aerodynamic Characteristics of Low Aspect Ratio Wings at Low Speeds. Jour. Aero. Sci., Vol. 22, No. 8, 1955. (U)
34. Anderson, A. E.: An Investigation at Low Speed of a Large-Scale Triangular Wing of Aspect Ratio Two. II – The Effect of Airfoil Section Modifications and the Determination of the Wake Downwash. NACA RM A7H28, 1947. (U)
35. Jacobs, E. N., and Rhode, R. V.: Airfoil Section Characteristics as Applied to the Prediction of Air Forces and Their Distribution on Wings. NACA TR 631, 1938. (U)

TABLE 4.1.3.4-A
HIGH-ASPECT-RATIO WINGS AT SUBSONIC SPEEDS
DATA SUMMARY AND SUBSTANTIATION

Ref.	t/c	A	ΔY (%C)	Δ_{LE} (deg)	M	$R \times 10^{-6}$	$C_{L\max}$ Calc.	$\alpha C_{L\max}$ Calc.	$C_{L\max}$ Test	$\alpha C_{L\max}$ Test	Percent Error, e	
											$C_{L\max}$	$\alpha C_{L\max}$
4	0.12	4.0	2.55	42	0.2	2.0	1.02	23.1	0.98	23	4.1	0.4
					0.4	3.0	0.93	21.0	0.92	22	1.1	-4.5
					0.6	4.0	0.88	19.6	0.85	20	3.5	-2.0
5	0.075	5.0	1.6	47	0.2	2.0	0.95	23.8	0.98	25	-3.1	-4.8
					0.4	2.0	0.91	22.0	0.95	24	-4.2	-5.0
					0.6	2.0	0.91	22.0	0.89	21	2.2	5.2
6	0.11	7.0	2.3	42	0.25	2.0	1.05	19.2	1.07	25.5	-1.9	-24.7
	0.10	6.0	2.1	47	0.25	2.0	1.04	21.6	1.06	24	-1.9	-10.0
	0.11	7.0	2.8	42	0.25	2.0	1.02	17.7	1.03	17.5	-1.0	1.1
	0.10	6.0	2.6	47	0.25	2.0	1.00	19.7	1.09	22	-8.3	-10.5
7	0.12	8.0	2.65	46	0.2	4.0	0.98	20.0	1.02	21	-3.9	-4.8
8	0.06	4.0	1.2	37	0.6	0.4	0.83	18.6	0.73	19	13.7	-2.1
					0.6	0.4	0.92	22.7	0.82	23	12.2	-1.3
					0.6	0.4	0.98	29.0	0.89	29	10.1	0
9	0.12	8.02	2.65	46.3	0.19	4.0	0.94	19.0	1.01	21	-6.9	-9.5
10	0.12	8.02	2.65	46.3	0.07	1.5	0.94	19.0	0.90	18	4.4	5.6
					0.11	2.2	0.94		0.97	20	-3.1	-5.0
					0.14	3.0	0.94		1.01	22	-6.9	-13.6
					0.19	4.0	0.94		1.01	21	-6.9	-9.5
					0.25	4.8	0.94		1.01	21	-6.9	-9.5
$\text{Average Error in } C_{L\max} = \frac{\sum e }{n} = 5.3\%$ $\text{Average Error in } \alpha C_{L\max} = \frac{\sum e }{n} = 6.5\%$												

TABLE 4.1.3.4-B
LOW-ASPECT-RATIO WINGS AT SUBSONIC SPEEDS
DATA SUMMARY AND SUBSTANTIATION

Ref.	Airfoil Section	%C @ (t/c) _{max}	Δγ (%c)	A	Α _{LE} (deg)	M	C _L _{max} Calc.	α _{C_L_{max}} Calc.	C _L _{max} Test	α _{C_L_{max}} Test	Percent Error, ε		
											C _L _{max}	α _{C_L_{max}}	
15	65A003	>35	0.60	4.0	45.0	0.6	0.83	20.2	0.87	21.0	-4.6	-3.8	
				4.0	51.3		0.89	21.7	0.94	22.0	-5.3	-1.4	
				4.0	36.8		0.78	19.9	0.83	20.0	-6.0	-0.5	
				4.0	26.6		0.72	20.4	0.79	24.0	-8.9	-15.0	
				4.0	14.0		0.70	22.1	0.70	20.0	0	10.5	
12	63A006	35	1.34	2.0	0	0.4	0.77	19.3	0.75	17.6	2.7	9.7	
	63A004	35	0.91	1.5	0	0.6	0.85	23.4	0.89	23.5	-4.5	-0.4	
	63A004	35	0.91	2.0	0	0.4	0.79	19.3	0.77	17.6	2.6	9.7	
13	63A004	35	0.91	2.0	18.5	0.6	0.74	22.5	0.79	19.4	-6.3	16.0	
27	65A006	>35	1.17	4.0	45.0	0.2	1.01	25.3	1.01	26.0	0	1.2	
	65A006	>35	1.17	4.0	48.6	0.2	1.08	25.9	1.09	25.0	-0.9	3.6	
28	DW*	<35	0.30	2.0	63.4	—	1.41	34.7	1.40	36.0	0.7	-3.6	
29	0005	<35	1.34	2.0	63.4	0.13	1.30	34.7	1.32	34.5	-1.5	0.6	
30	0005	<35	1.34	3.0	53.2	—	0.95	26.2	0.94	24.0	1.0	9.2	
31	FP*	<35	0.36	0.03	0	0.08	0.73	44.9	0.69	46.0	5.8	-2.4	
				0.53	0.134		0.92	44.7	0.83	48.5	10.8	-7.8	
				0.86	0.35		1.12	43.9	1.16	41.5	-3.4	5.8	
				1.03	0.50		1.16	43.0	1.26	41.5	-7.9	3.6	
				1.14	0.66		1.20	41.7	1.31	40.5	-8.4	3.0	
				1.46	1.00		1.16	37.2	1.29	39.0	-10.1	-4.6	
				1.62	1.25		1.05	31.0	1.16	30.5	-9.5	1.6	
				1.79	1.5		0.94	26.2	0.98	24.0	-4.1	9.2	
				2.06	2.0		0.80	20.2	0.87	21.0	-8.0	-3.8	
32	FP*	<35	0.49	0.5	82.9	—	0.88	35.2	0.86	34.0	2.3	3.5	
				0.77	1.0	76.0	—	1.15	35.0	1.12	31.0	2.7	12.9
				1.65	3.0	53.0	—	0.95	26.2	0.99	25.0	-4.0	4.8
33	DW*	<35	0.26	1.5	69.4	—	1.34	35.0	1.31	31.0	2.3	-12.9	
	DW*	<35	0.26	1.5	69.4	—	1.34	35.0	1.37	37.1	-2.2	-5.7	

TABLE 4.1.3.4-B (CONTD)
LOW-ASPECT-RATIO WINGS AT SUBSONIC SPEEDS
DATA SUMMARY AND SUBSTANTIATION

Ref.	Airfoil Section	%C @ $(t/c)_{max}$	Δy (%C)	A	Λ_{LE} (deg)	M	C_{Lmax} Calc.	αC_{Lmax} Calc.	C_{Lmax} Test	αC_{Lmax} Test	Percent Error, e	
											C_{Lmax}	αC_{Lmax}
34	DW*	<35	0.75	2.0	63.4	—	1.37	34.7	1.35	33.0	1.5	5.2
			0.75	↓	↓	↓	1.37	34.7	1.37	33.5	0	3.6
			0.9	↓	↓	↓	1.32	34.7	1.35	34.0	-2.2	2.1
14	63A004	35	0.9	4.0	45.0	0.6	0.82	20.5	0.81	21.0	1.2	-2.4
			2.5	58.0	58.0	1	1.02	27.6	1.02	26.0	0	6.2
			3.0	53.2	53.2	1	0.90	23.6	0.90	22.7	0	4.0
			1.33	45.0	45.0	1	1.01	29.6	0.98	24.5	3.1	20.8
			2.67	45.0	45.0	1	0.82	20.7	0.79	21.0	3.8	-1.4
			2.0	53.0	53.0	1	0.91	24.1	0.91	23.2	0	3.9
			1.67	58.0	58.0	1	1.04	27.7	1.06	27.5	-1.9	0.7
			1.62	53.0	53.0	1	0.98	26.4	0.95	23.5	3.2	12.3
			2.15	45.0	45.0	1	0.85	21.8	0.80	21.0	6.2	3.8
			↓	↓	↓	↓	↓	↓	↓	↓	↓	↓

*FP = Flat Plate, DW = Double Wedge

$$\text{Average Error in } C_{Lmax} = \frac{\sum |e|}{n} = 3.7\%$$

$$\text{Average Error in } \alpha C_{Lmax} = \frac{\sum |e|}{n} = 5.8\%$$

TABLE 4.1.3.4-C
LOW-ASPECT-RATIO WINGS AT TRANSONIC SPEEDS
DATA SUMMARY AND SUBSTANTIATION

Ref.	A	Λ_{LE} (deg)	ΔY	λ	M	$R \times 10^{-6}$	$C_{L_{max}}$ Calc.	$\alpha C_{L_{max}}$ Calc.	$C_{L_{max}}$ Test	$\alpha C_{L_{max}}$ Test	Percent Error, ϵ	
											$C_{L_{max}}$	$\alpha C_{L_{max}}$
12	1.5	0	0.91	1.0	0.6	1.7	0.85	23.4	0.89	23.5	-4.5	-0.4
					0.7	1.8	0.82	22.4	0.87	23	-5.7	-2.6
					0.8	1.9	0.80	22.1	0.87	23	-8.0	-3.9
					0.9	2.0	0.81	22.4	0.92	24	-12.0	-6.7
					1.0	2.1	0.97	24.1	1.02	-	-4.9	-
	2.0	0	1.34	1.0	0.6	1.7	0.73	19.0	0.72	18.5	1.4	2.7
15	4.0	26.5	0.49	0	0.6	0.75	0.85	18.5	0.83	19.0	2.4	-2.6
					0.8	0.85	0.86	17.5	0.89	21.0	-3.4	-16.7
					0.9	0.87	0.96	18.8	1.01	22.0	-5.0	-14.5
					1.0	0.88	1.25	19.9	1.32	24.0	-5.3	-17.1
					1.1	0.88	1.26	29.5	1.24	26.0	1.6	13.5
13	2.0	18.5	0.49	0.5	0.6	1.4 to 2	0.78	23.3	0.85	21.0	-8.2	11.0
					0.8		0.78	22.3	0.86	19.5	-9.3	14.4
					0.9		0.84	22.5	0.93	18.0	-9.7	25.0
					1.0		1.05	24.6	1.15	22.0	-8.7	11.8
14	3.27	45.0	0.91	0.1	0.6	1.87	0.81	20.5	0.80	20.0	1.2	2.5
					0.8	2.22	0.82	19.5	0.79	17.0	3.8	14.7
					0.9	2.35	0.89	20.5	0.86	23.0	3.5	-10.9
	2.67	45.0	0.91	0.2	0.6	1.92	0.82	20.7	0.79	21.0	3.8	-1.4
					0.8	2.28	0.83	19.7	0.78	21.0	6.4	-6.2
					0.9	2.41	0.89	20.2	0.83	22.0	7.2	-8.2
	2.15	45.0	0.91	0.3	0.6	1.98	0.85	21.8	0.80	21.0	6.3	3.8
					0.8	2.37	0.84	20.8	0.79	21.0	6.3	-1.0
	1.71	45.0	0.91	0.4	0.6	2.07	0.90	24.0	0.86	23.0	4.7	4.3
					0.8	2.46	0.86	23.0	0.84	22.0	2.4	4.5
					0.9	2.59	0.90	23.0	0.84	21.5	7.1	7.0
					1.0	2.69	1.08	24.8	1.00	22.0	8.0	12.7

TABLE 4.1.3.4-C (CONTD)
LOW-ASPECT-RATIO WINGS AT TRANSONIC SPEEDS
DATA SUMMARY AND SUBSTANTIATION

Ref.	A	Λ_{LE} (deg)	$\Delta\gamma$	λ	M	$R \times 10^{-6}$	$C_{L_{max}}$ Calc.	$\alpha C_{L_{max}}$ Calc.	$C_{L_{max}}$ Test	$\alpha C_{L_{max}}$ Test	Percent Error, e					
											$C_{L_{max}}$	$\alpha C_{L_{max}}$				
14	1.33	45.0	0.91	0.5	0.6	2.16	1.01	29.6	0.98	24.5	3.1	20.8				
					0.8	2.58	0.93	28.1	0.94	23.5	-1.1	19.6				
					0.9	2.72	0.92	28.1	0.93	23.5	-1.1	19.6				
					1.0	2.82	1.06	30.0	1.02	26.0	3.9	15.4				
	3.00	53.0	0.91	0	0.6	1.86	0.90	23.6	0.90	22.7	0	4.0				
					0.8	2.21	0.87	22.3	0.88	22.0	-1.1	1.4				
					0.9	2.32	0.90	22.4	0.90	23.0	0	-2.6				
	1.29	53.0	0.91	0.4	0.6	2.07	1.09	29.5	1.03	27.0	5.8	9.3				
					0.8	2.46	0.99	28.2	0.97	24.0	2.1	17.5				
					0.9	2.59	0.97	28.5	0.95	24.0	2.1	18.7				
					1.0	2.69	1.10	30.0	1.02	25.0	7.8	20.0				
	2.5	58.0	0.49	0	0.6	1.86	1.07	27.2	1.04	27.0	2.9	0.7				
					0.8	2.21	1.00	26.0	0.96	23.0	4.2	13.0				
					0.9	2.32	1.00	26.2	0.97	24.0	3.1	9.2				
	1.67	58.0	0.49	0.2	0.6	1.92	1.06	27.4	1.03	27.0	2.9	1.5				
					0.8	2.28	0.99	26.2	0.94	23.5	5.3	11.5				
					0.9	2.41	0.99	26.4	0.92	23.5	7.6	12.3				
$\text{Average Error in } C_{L_{max}} = \frac{\sum e }{n} = 4.7\%$																
$\text{Average Error in } \alpha C_{L_{max}} = \frac{\sum e }{n} = 9.3\%$																

TABLE 4.1.3.4-D
WINGS AT SUPERSONIC SPEEDS
DATA SUMMARY AND SUBSTANTIATION

Ref.	M	$R \times 10^{-6}$	A	Λ_{LE} (deg)	$C_{L_{max}}$ Calc.	$\alpha_{C_{L_{max}}}$ Calc.	$C_{L_{max}}$ Test	$\alpha_{C_{L_{max}}}$ Test	Percent Error, ϵ		
									$C_{L_{max}}$	$\alpha_{C_{L_{max}}}$	
18	1.9	0.3 to 0.7	1.76	36	1.04	42.3	1.01	42.4	3.0	-0.2	
	2.32		1.96	64	1.07	40.5	1.06	41.0	0.9	-1.2	
	2.43		1.96	64	1.03	41.0	0.98	43.8	5.1	-6.4	
	2.43		4.0	45	1.07	38.7	1.07	42.6	0	-9.2	
	2.43		2.0	0	1.02	42.0	0.97	40.8	5.2	2.9	
	2.43		1.96	64	1.13	39.5	1.06	41.1	6.6	-3.9	
	2.43		4.0	45	1.22	34.5	1.13	39.5	8.0	-12.7	
23	1.45	1.2 to 6.9	1.0	0	1.07	41.7	1.07	37.7	0	10.6	
	1.96		2.0	0	1.07	40.2	1.10	41.5	-2.7	-3.1	
	2.43		3.0	0	1.09	39.0	1.11	35.0	-1.8	-11.4	
	2.43		2.0	0	1.00	42.5	1.05	42.0	-4.8	1.2	
	2.43		3.0	0	1.01	41.5	1.07	38.0	-5.6	9.2	
	3.36		1.0	0	0.89	47.0	0.89	41.7	0	12.7	
	3.36		2.0	0	0.93	45.0	0.95	41.5	-2.1	8.4	
26	1.96	2.5 to 6.8	0.375	85'	0.772	50.8	0.786	51.0	-1.8	-0.4	
	2.42		0.667	80	0.86	48.7	0.836	49.0	2.9	-0.6	
	2.42		1.0	76	0.92	46.5	0.908	46.0	1.3	1.1	
	2.42		0.375	85	0.71	53.7	0.746	52.0	-4.8	3.3	
	2.42		0.667	80	0.814	50.8	0.802	52.0	1.5	-2.3	
	3.30		1.0	76	0.883	48.3	0.839	46.0	5.2	5.0	
	3.30		0.375	85	0.67	54.5	0.687	52.0	-2.5	4.8	
21	2.46	1.0 to 3.5	2.0*	0	0.99	42.5	1.00	40.0	-1.0	6.3	
	2.46		2.0	0	0.99	42.5	1.04	40.0	-4.8	6.3	
	2.46		2.0*	63	0.97	44.2	0.98	50.0	-1.0	-11.6	
	2.46		2.0	63	0.97	44.2	0.96	45.0	1.0	-1.8	
	2.46		4.0*	45	1.04	40.0	1.01	45.0	3.0	-11.1	
	3.36		3.4	2.0	63	0.91	45.7	0.84	45.0	8.3	1.6
	3.36		2.0	63	0.91	45.7	0.84	45.0	8.3	1.6	
20	1.45	1.0 to 3.5	4.0*	45	1.21	35.5	1.18	35.0	2.5	1.4	
	1.97		4.0*	45	1.11	38.0	1.09	43.0	1.8	-11.6	
	2.0*		63	1.02	42.7	1.01	45.0	1.0	-5.1		
	2.0*		0	1.07	40.0	1.07	45.0	0	-11.1		
	2		0	1.07	40.0	1.08	38.0	-0.9	5.3		

*with thickened wing root

$$\text{Average Error in } C_{L_{max}} = \frac{\sum |e|}{n} = 2.6\%$$

$$\text{Average Error in } \alpha_{C_{L_{max}}} = \frac{\sum |e|}{n} = 5.6\%$$

SUBSONIC SPEEDS

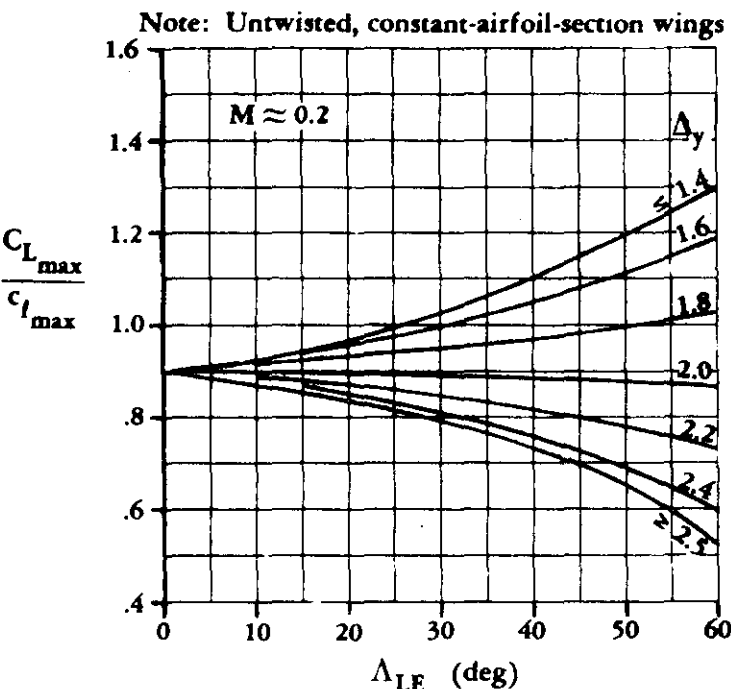


FIGURE 4.1.3.4-21a SUBSONIC MAXIMUM LIFT OF HIGH-ASPECT-RATIO WINGS

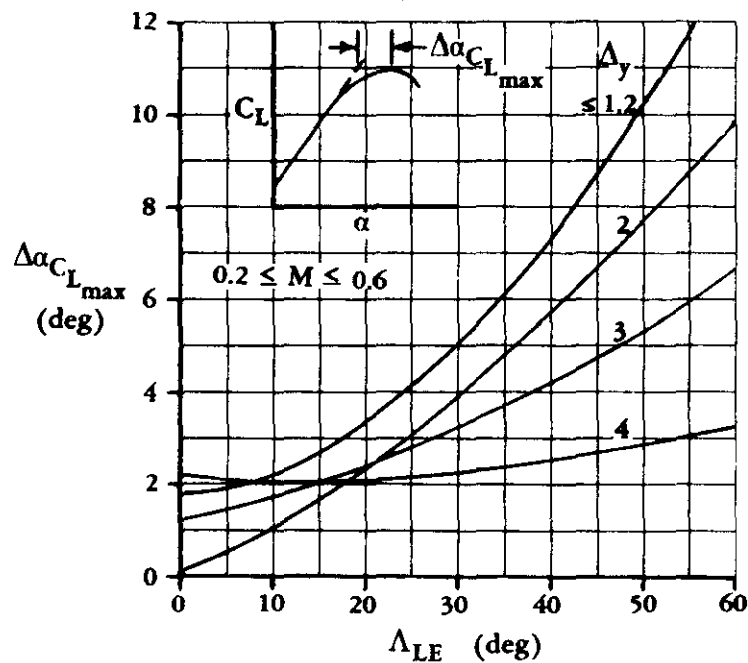


FIGURE 4.1.3.4-21b ANGLE-OF-ATTACK INCREMENT FOR SUBSONIC MAXIMUM LIFT OF HIGH-ASPECT-RATIO WINGS

SUBSONIC SPEEDS

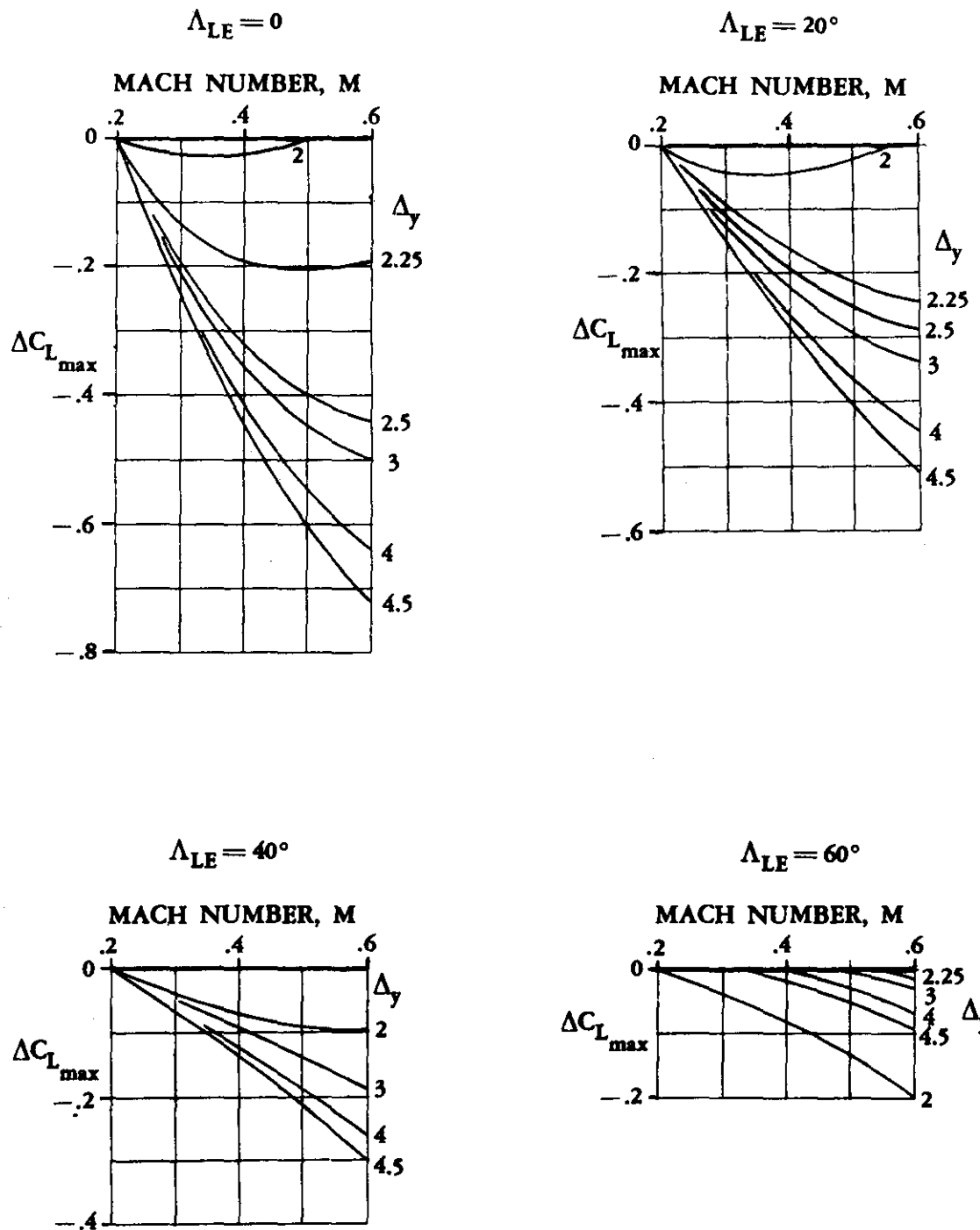


FIGURE 4.1.3.4-22 MACH-NUMBER CORRECTION FOR SUBSONIC MAXIMUM LIFT OF HIGH-ASPECT-RATIO WINGS

SUBSONIC SPEEDS

Notes: Symmetric airfoils
 $R = 1 \times 10^6$ to 10×10^6 based on MAC
 Δ_y for airfoil at MAC

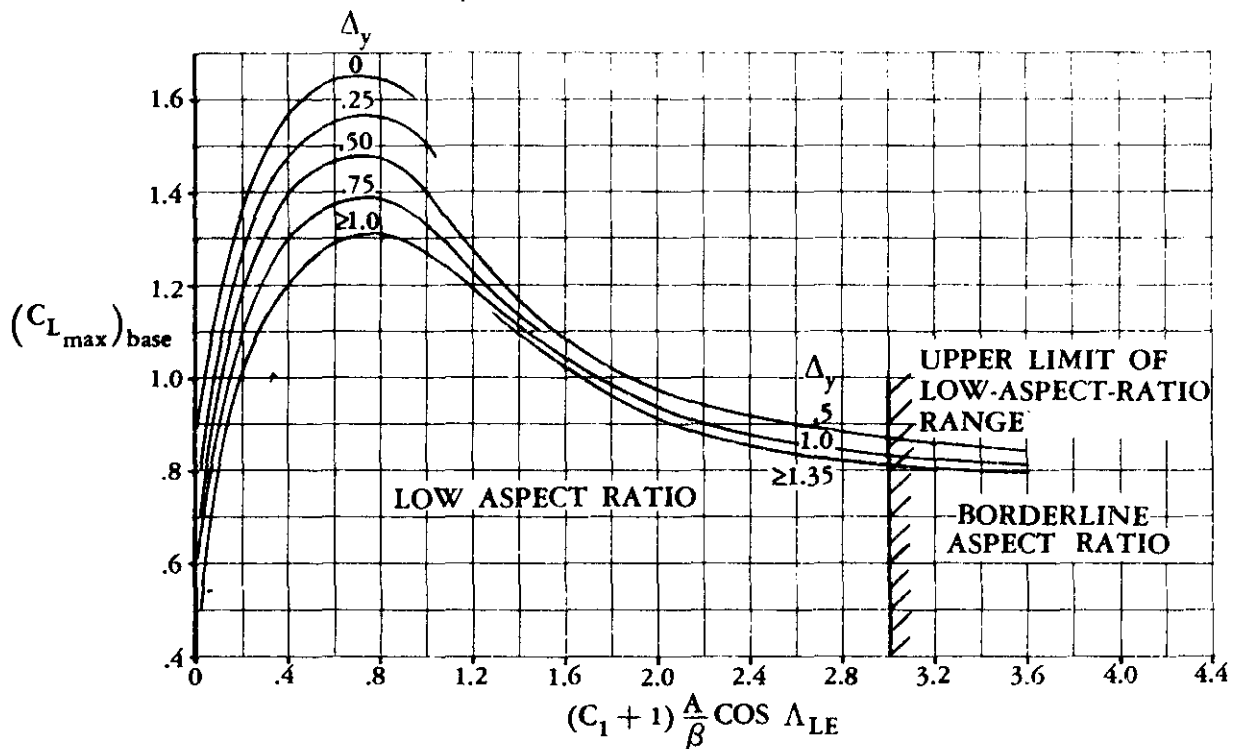


FIGURE 4.1.3.4-23a MAXIMUM LIFT OF WINGS WITH POSITION OF MAXIMUM THICKNESS AT OR FORWARD OF THE 35-PERCENT CHORD

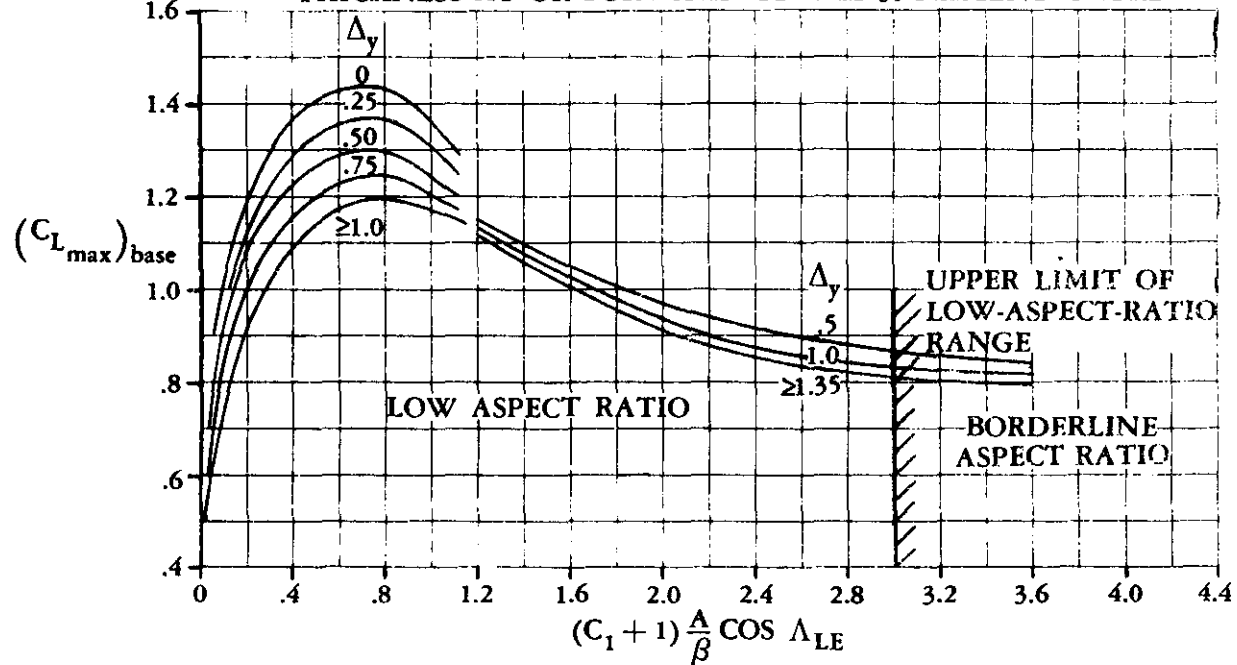


FIGURE 4.1.3.4-23b MAXIMUM LIFT OF WINGS WITH POSITION OF MAXIMUM THICKNESS BETWEEN 35- AND 50-PERCENT CHORD

SUBSONIC SPEEDS

Notes: Symmetric airfoils
 $R = 1 \times 10^6$ to 10×10^6 based on MAC
 Δy for airfoil at MAC

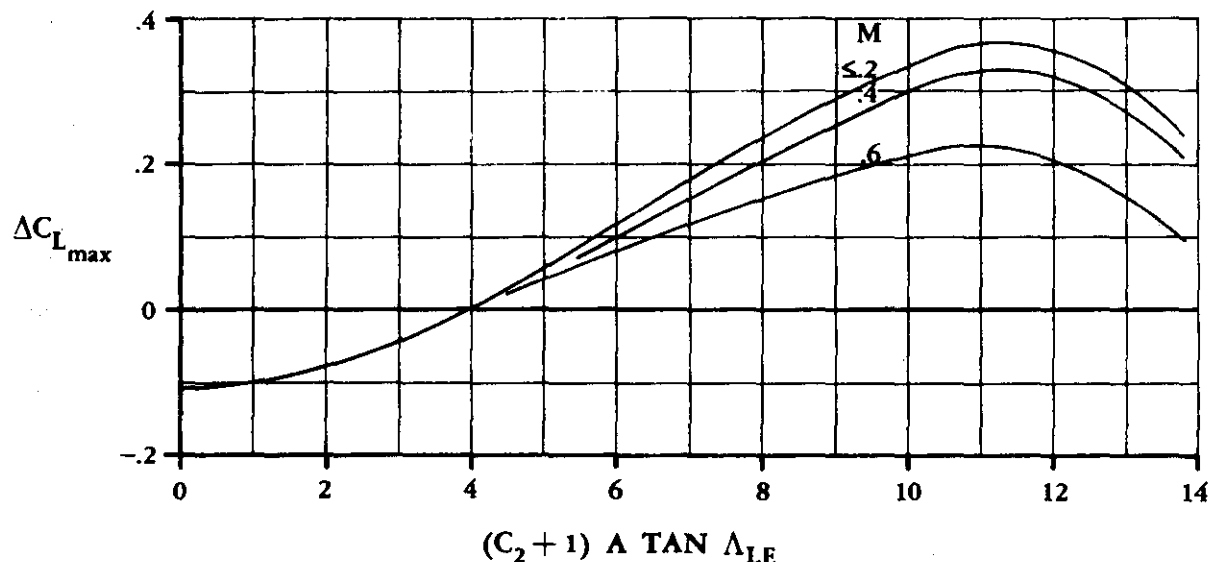


FIGURE 4.1.3.4-24a MAXIMUM-LIFT INCREMENT FOR LOW-ASPECT-RATIO WINGS

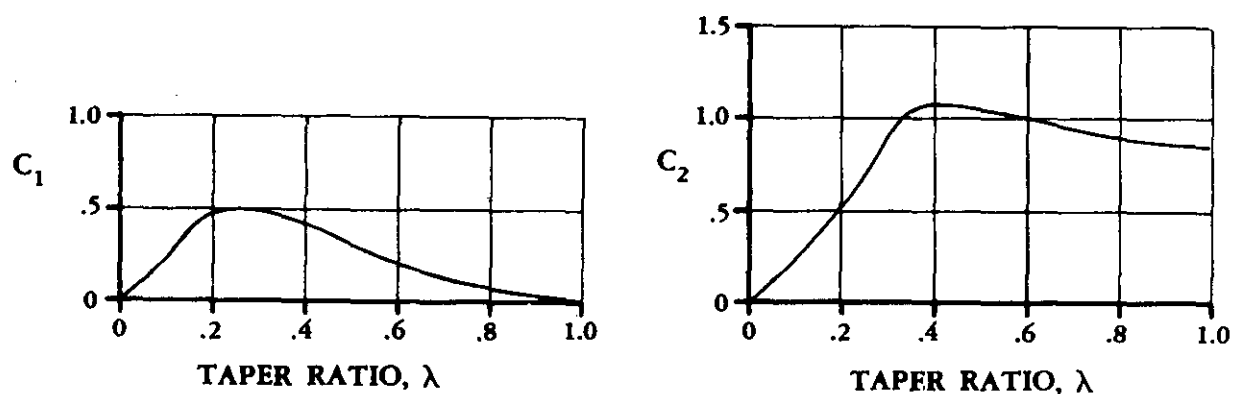


FIGURE 4.1.3.4-24b TAPER-RATIO CORRECTION FACTORS

SUBSONIC SPEEDS

Notes: Symmetric airfoils

$R = 1 \times 10^6$ to 10×10^6 based on MAC

Δy for airfoil at MAC

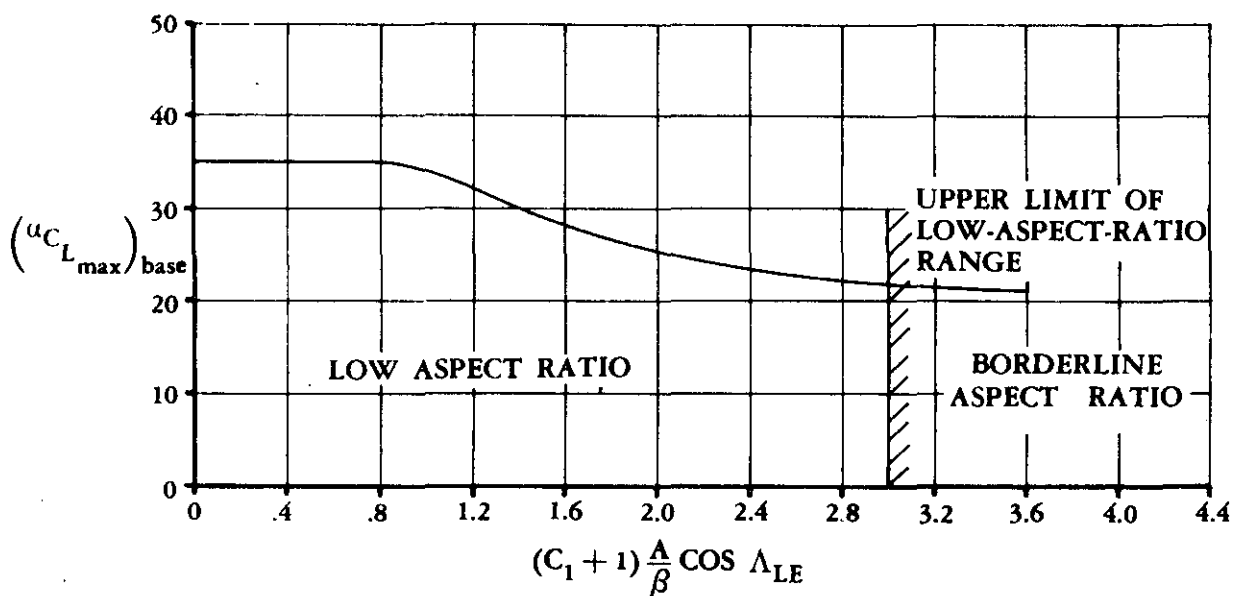


FIGURE 4.1.3.4-25a ANGLE OF ATTACK FOR SUBSONIC MAXIMUM LIFT OF LOW-ASPECT-RATIO WINGS

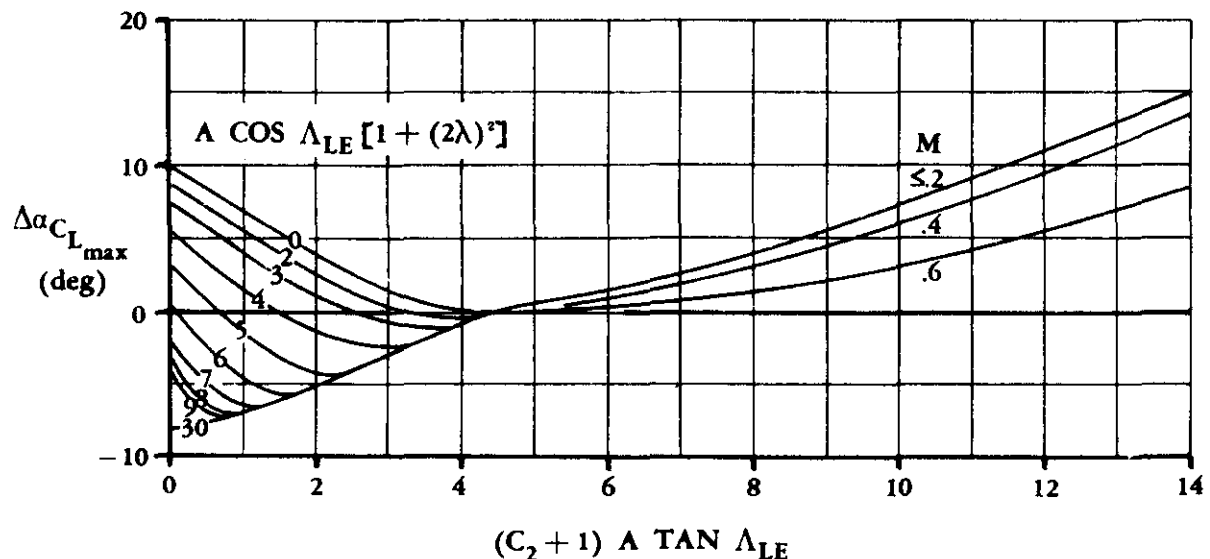


FIGURE 4.1.3.4-25b ANGLE-OF-ATTACK INCREMENT FOR SUBSONIC MAXIMUM LIFT OF LOW-ASPECT-RATIO WINGS

TRANSONIC SPEEDS
 Notes: Symmetric airfoils
 $R = 1 \times 10^6$ to 15×10^6 based on MAC

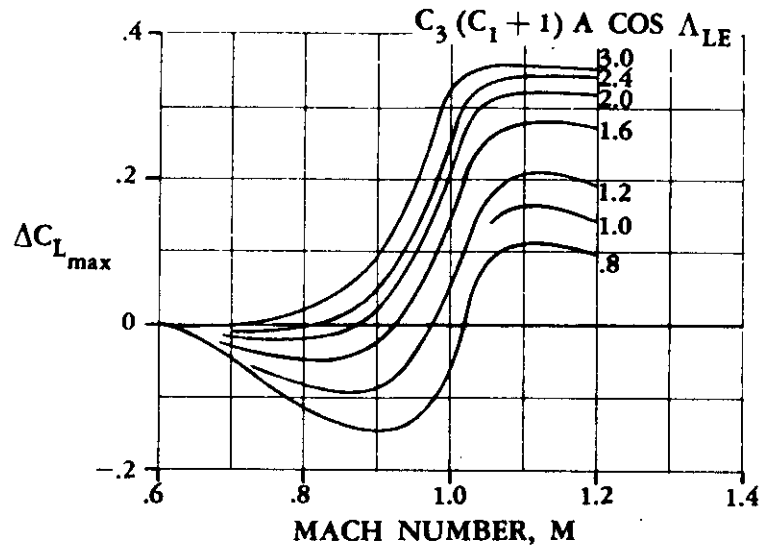


FIGURE 4.1.3.4-26a MAXIMUM LIFT OF LOW-ASPECT-RATIO WINGS

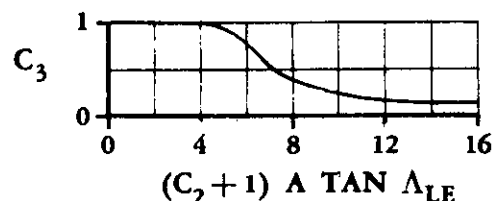


FIGURE 4.1.3.4-26b MAXIMUM-LIFT CORRECTION FACTOR

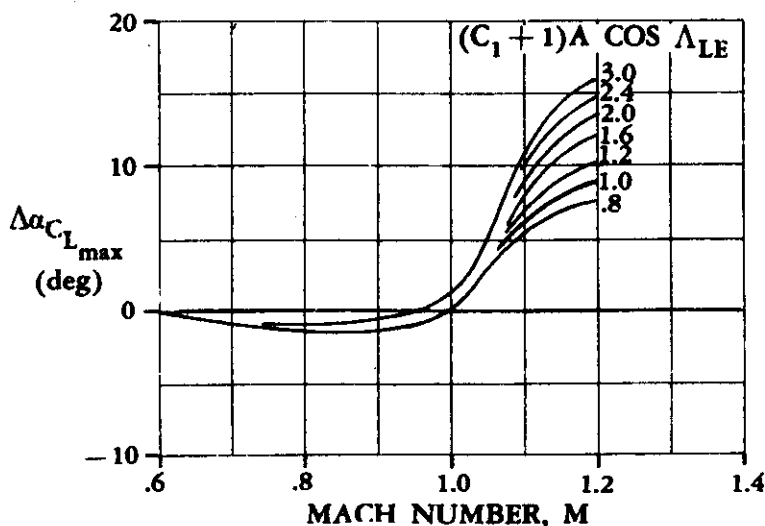


FIGURE 4.1.3.4-26c ANGLE-OF-ATTACK INCREMENT FOR LOW-ASPECT-RATIO WINGS

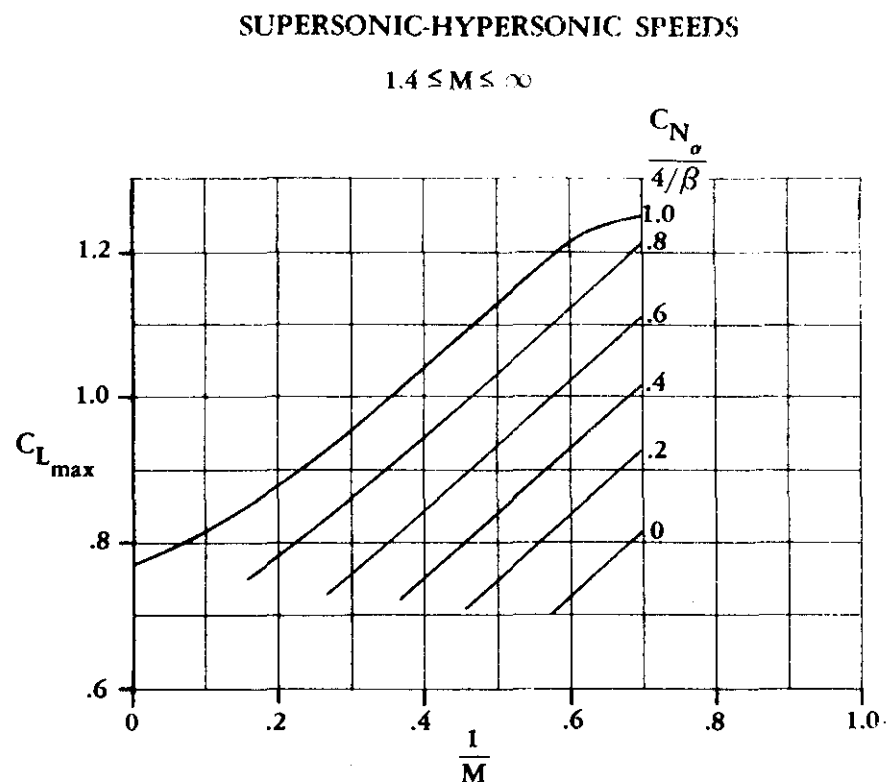


FIGURE 4.1.3.4-27a SUPersonic-HYPERSONIC WING MAXIMUM LIFT

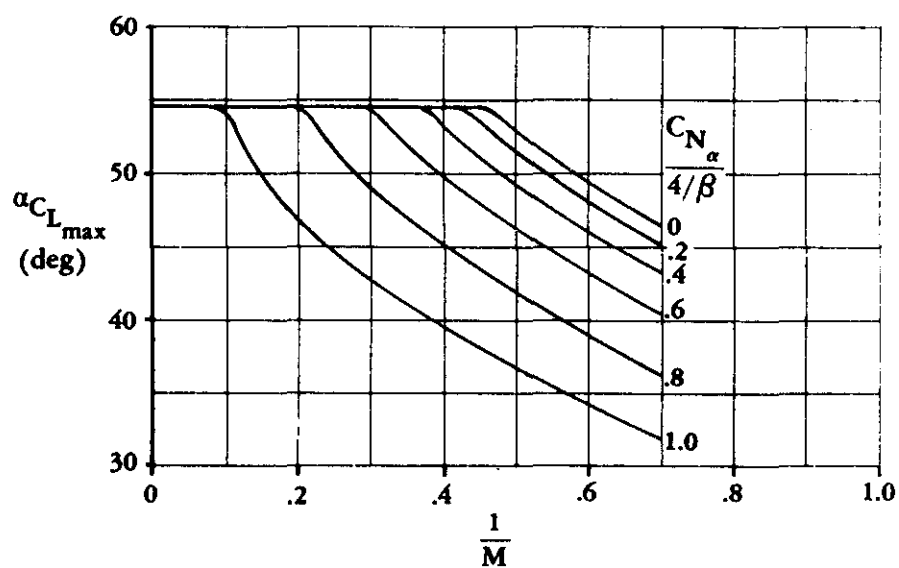


FIGURE 4.1.3.4-27b SUPersonic-HYPERSONIC WING ANGLE OF ATTACK FOR MAXIMUM LIFT

4.1.4 WING PITCHING MOMENT

The pitching-moment characteristics of aerodynamic surfaces are conventionally represented by specifying the wing aerodynamic-center location or the wing center of pressure.

The aerodynamic center is defined as that point on the wing plane of symmetry about which the pitching moment is invariant with lift, i.e., $\frac{dC_m}{dC_L} = 0$, for power-off flight of a rigid vehicle at a given Mach number.

The relationship between the wing aerodynamic center and the wing pitching-moment slope about any arbitrary point on the wing root chord is then given by the equation (neglecting wing drag):

$$\frac{dC_m}{dC_L} = \left(n - \frac{x_{ac}}{c_r} \right) \frac{c_r}{c} \quad 4.1.4-a$$

where

$\frac{x_{ac}}{c_r}$ is the chordwise distance from the wing apex to the aerodynamic center, measured in root chords, positive aft

n is the chordwise distance from the wing apex to the point about which the pitching moment is desired, measured in root chords, positive aft

$\frac{c_r}{c}$ is the ratio of the root chord to the pitching-moment reference chord, generally taken as the wing M.A.C.

$\frac{dC_m}{dC_L}$ is the slope of the wing pitching-moment coefficient about the point n with respect to the lift coefficient

The usefulness of the aerodynamic-center concept lies principally in the convenient way in which it presents pitching-moment information in the linear lift range. Within this range the forces on a wing are simply represented by a lift vector of varying magnitude acting through the aerodynamic center and a constant moment about the a.c. equivalent to the wing zero-lift moment.

The aerodynamic-center concept is often used beyond the linear lift range by specifying the locus of points at which $\frac{dC_m}{dC_L}$ is zero, as a function of lift (or angle of attack). The a.c. curve thus defined represents the successive points at which the surface has "neutral stability."

Center of pressure is defined as that point at which the wing total resultant force intersects the wing chord, i.e., it is the point on the wing chord at which $C_m = 0$.

If the wing center-of-pressure location is known, the wing pitching moment about any other point on the wing chord may be calculated, provided the direction of the resultant-force vector on the wing is also known. This fact, which is apparent from geometrical considerations, is reflected in the equations for determining the moment coefficient from the center of pressure. There are two cases, as follows:

A. Resultant-force vector perpendicular to the wing surface:

$$C_m = \left(n - \frac{x_{cp}}{c_r} \right) \frac{c_r}{c} C_N \quad 4.1.4-b$$

B. Resultant-force vector in the lift direction (perpendicular to the free stream):

$$C_m = \left(n - \frac{x_{cp}}{c_r} \right) \frac{c_r}{c} C_L \cos \alpha \quad 4.1.4-c$$

In the above equations $\frac{x_{cp}}{c_r}$ is the chordwise distance from the wing apex to the wing center of pressure, measured in

root chords, positive aft.

Since at low angles of attack the resultant-force vector on wings is essentially in the lift direction (see Section 4.1.3), equation 4.1.4-c is applicable. At high angles of attack, the resultant force is more nearly normal to the wing chord and thus equation 4.1.4-b is the more applicable. However, equation 4.1.4-b may also be used at low angles of attack. For the remainder of this Section, it is assumed that equation 4.1.4-b holds at all angles of attack, and that the C_N in this equation is equivalent to the C'_N as defined and discussed in Section 4.1.3.

In the linear lift range, the locations of the center of pressure and the aerodynamic center are the same for wings having symmetrical profiles but not the same for wings having cambered profiles.

Two sets of charts are presented in subsequent Sections. The charts for the linear lift range present the aerodynamic-center location of wings as a function of planform parameters. The charts for the nonlinear lift range give the wing center-of-pressure location also as a function of planform parameters. The two groups of charts taken together permit the calculation of the complete-pitching-moment curve from 0° to 90° angle of attack for symmetrical wings.

For cambered wings, no specific method is presented for calculating the pitching moments beyond the linear lift range. However, for angles of attack beyond the stall, it is not likely that there will be much difference between the pitching moments of symmetrical wings and those of cambered wings.

4.1.4.1 WING ZERO-LIFT PITCHING MOMENT

The methods presented in this section are restricted to subsonic speeds. In the transonic and supersonic speed regimes it is suggested that reference be made to experimental data.

A. SUBSONIC

Two methods are presented for estimating the wing zero-lift pitching moment. Method 1 is general and is applicable to the majority of moderately swept configurations. It is not advisable to use Method 1 for configurations having a quarter-chord-sweep angle greater than 45°. Method 2 is taken from Reference 1 and is applicable only at $M = 0.2$ for highly swept, constant-section, low-aspect-ratio, delta or clipped-delta configurations with large thickness ratios; i.e., $0.10 \leq t/c \leq 0.30$.

DATCOM METHODS

Method 1

The low-speed zero-lift pitching moment based on the product of the wing area and mean aerodynamic chord $S_w \bar{c}_w$, for untwisted, constant-section wings with elliptical loading may be approximated by

$$\left(C_{m0} \right)_{\theta=0} = \frac{A \cos^2 \Lambda_{c/4}}{A + 2 \cos \Lambda_{c/4}} c_{m0} \quad 4.1.4.1-a$$

where c_{m0} is the section pitching-moment coefficient at zero lift, obtained from Section 4.1.2.1. The airfoil section is defined parallel to the free stream.

For airfoil sections varying along the span

$$\left(C_{m0} \right)_{\theta=0} = \frac{A \cos^2 \Lambda_{c/4}}{A + 2 \cos \Lambda_{c/4}} \left(\frac{c_{m0_{root}} + c_{m0_{tip}}}{2} \right) \quad 4.1.4.1-b$$

where $c_{m0_{root}}$ and $c_{m0_{tip}}$ are the section pitching-moment coefficients at zero lift of the root and tip sections, respectively, both defined parallel to the free stream.

For wings with linear twist, lifting-line theory may be used as in Reference 2 to obtain C_{m0} by

$$C_{m0} = \left(C_{m0} \right)_{\theta=0} + \left(\frac{\Delta C_{m0}}{\theta} \right) \theta \quad 4.1.4.1-c$$

4.1.4.1-1

where

$$\left(C_{m0}\right)_{\theta=0}$$

is the zero-lift pitching-moment coefficient of an untwisted wing, obtained by using either Equation 4.1.4.1-a or Equation 4.1.4.1-b.

$$\frac{\Delta C_{m0}}{\theta}$$

is the change in wing zero-lift pitching-moment coefficient due to a unit change in linear wing twist. This parameter is obtained from Figure 4.1.4.1-5.

$$\theta$$

is the twist of the wing tip with respect to the root section, in degrees (negative for washout). A linear spanwise twist distribution is assumed (all constant-percent points of local chords lie in straight lines along the span).

The effect of Mach number on the wing zero-lift pitching-moment coefficient, up to the critical Mach number, is presented in Figure 4.1.4.1-6. This chart, based on test data, gives the ratio of wing or wing-body zero-lift pitching-moment coefficient in compressible flow to that in incompressible flow. When using this chart, no correction should be made to the section c_{m0} value. The use of this chart should give reasonable results up to $M = 0.8$. However, beyond this point the chart should be used with caution, since test data often show abrupt changes in zero-lift pitching moment at high transonic speeds.

The limited availability of test data, coupled with the fact that the wing zero-lift pitching-moment coefficient does not lend itself to accurate experimental measurement, precludes substantiation of this method.

Method 2

This semiempirical method is taken from Reference 1, ignoring the small wing-planform nose-radius effects. The semiempirical method was developed by using the test results of Reference 1, correlated with the theoretical predictions based on lifting-surface theory. Because of its semiempirical nature, the method should be restricted to $M = 0.2$ conditions for highly swept, constant-section, low-aspect-ratio, delta or clipped-delta configurations with the following geometric characteristics:

$$0.58 \leq A \leq 2.55$$

$$0 \leq \lambda \leq 0.3$$

$$63^\circ \leq \Lambda_{LE} \leq 80^\circ$$

$$0.10 \leq t/c \leq 0.30$$

$$\Lambda_{TE} = 0$$

For round-nosed-planform configurations the reader is referred to Reference 1, where three different planform nose-radius models were tested. No incremental nose planform effects are presented here because of their probable configuration dependence.

The wing zero-lift pitching-moment coefficient may be approximated by the following procedure:

Step 1. Determine the section zero-lift pitching-moment coefficient c_{m_0} for the particular airfoil under consideration. Lifting-surface theory was used in the method formulation of Reference 1 to estimate the section zero-lift pitching-moment coefficient. For this reason it is recommended that lifting-surface theory be used, if available, for the prediction of c_{m_0} .

If lifting-surface theory is not available, c_{m_0} may be estimated by using test data; e.g., those listed in Tables 4.1.1-A and -B.

- Step 2.** Determine a wing zero-lift pitching moment $(C_{m_0})_{\text{theory}}$ uncorrected for thickness effects from Figure 4.1.4.1-7 as a function of sweep, taper ratio, and section zero-lift pitching moment. (The value of Λ_c is defined as $\Lambda_c = 90^\circ - \Lambda_{LE}$.)
- Step 3.** Calculate the wing zero-lift pitching moment C_{m_0} , based on the wing area and wing root chord $S_w c_r$, using the following

$$C_{m_0} = \left[\frac{c_{m_0}}{(C_{m_0})_{\text{theory}}} \right] (C_{m_0})_{\text{theory}} \quad 4.1.4.1-d$$

where

$$\frac{c_{m_0}}{(C_{m_0})_{\text{theory}}}$$

is the ratio of zero-lift pitching moment corrected for thickness effects to the uncorrected zero-lift pitching moment. This ratio is obtained from Figure 4.1.4.1-8 as a function of thickness, planform geometry, and the uncorrected wing zero-lift pitching moment.

$$(C_{m_0})_{\text{theory}}$$

is the zero-lifting pitching-moment coefficient uncorrected for thickness effects obtained above in Step 2.

For the particular configurations to which this method is applicable, insufficient data are available to determine the usefulness of Figure 4.1.4.1-6 for estimating Mach number effects.

No substantiation of this method is possible because of the lack of wing-alone low-aspect-ratio test data having thickness ratios of $0.10 \leq t/c \leq 0.30$.

Sample Problems

1. Method 1

Given: The following straight-tapered wing of Reference 3.

$$A = 6.0 \quad \lambda = 0.5 \quad \Lambda_{c/4} = 9.67^\circ \quad \theta = 0 \quad \text{Low speed}$$

NACA 23012 airfoil (free-stream direction)

Compute:

$$c_{m0} = -0.014 \quad (\text{Table 4.1.1-A})$$

Solution:

$$\begin{aligned} (C_{m0})_{\theta=0} &= \frac{A \cos^2 \Lambda_{c/4}}{A + 2 \cos \Lambda_{c/4}} c_{m0} \quad (\text{Equation 4.1.4.1-a}) \\ &= \frac{6(0.9858)^2}{6 + 2(0.9858)} (-0.014) \\ &= -0.010 \end{aligned}$$

This compares with a test value of -0.012 from Reference 3.

2. Method 2

Given: The following constant-section, low-aspect-ratio, clipped-delta configuration.

$$A = 0.823 \quad \lambda = 0.18 \quad \Lambda_{LE} = 73.5^\circ$$

$$\text{NACA 2412 airfoil} \quad M = 0.2 \quad \Lambda_c = 16.5^\circ \quad (\text{complement of leading-edge sweep})$$

Compute:

$$c_{m0} = -0.047 \quad (\text{Table 4.1.1-A})$$

$$4 \tan \Lambda_c (1 + \pi \lambda^2 \tan \Lambda_c) = 4(0.2962) [1 + \pi(0.18)^2 (0.2962)] = 1.2205$$

$$(C_{m0})_{\text{theory}} = -0.010 \quad (\text{Figure 4.1.4.1-7})$$

$$\frac{C_{m0}}{(C_{m0})_{\text{theory}}} = 0.91 \quad (\text{Figure 4.1.4.1-8})$$

$$\begin{aligned} C_{m0} &= \left[\frac{C_{m0}}{(C_{m0})_{\text{theory}}} \right] (C_{m0})_{\text{theory}} \quad (\text{Equation 4.1.4.1-d}) \\ &= (0.91)(-0.010) \\ &= -0.0091 \end{aligned}$$

REFERENCES

1. Crosthwait, E. L., and Seath, D. D.: Subsonic Characteristics of Low Aspect Ratios. FDL-TDR-64-103, 1965. (U)
2. DeYoung, J., and Harper, C. W.: Theoretical Symmetric Span Loading at Subsonic Speeds for Wings Having Arbitrary Plan Form. NACA TR 921, 1948. (U)
3. Pearson, H. A., and Anderson, R. F.: Calculation of the Aerodynamic Characteristics of Tapered Wings with Partial-Span Flaps. NACA TR 665, 1939. (U)

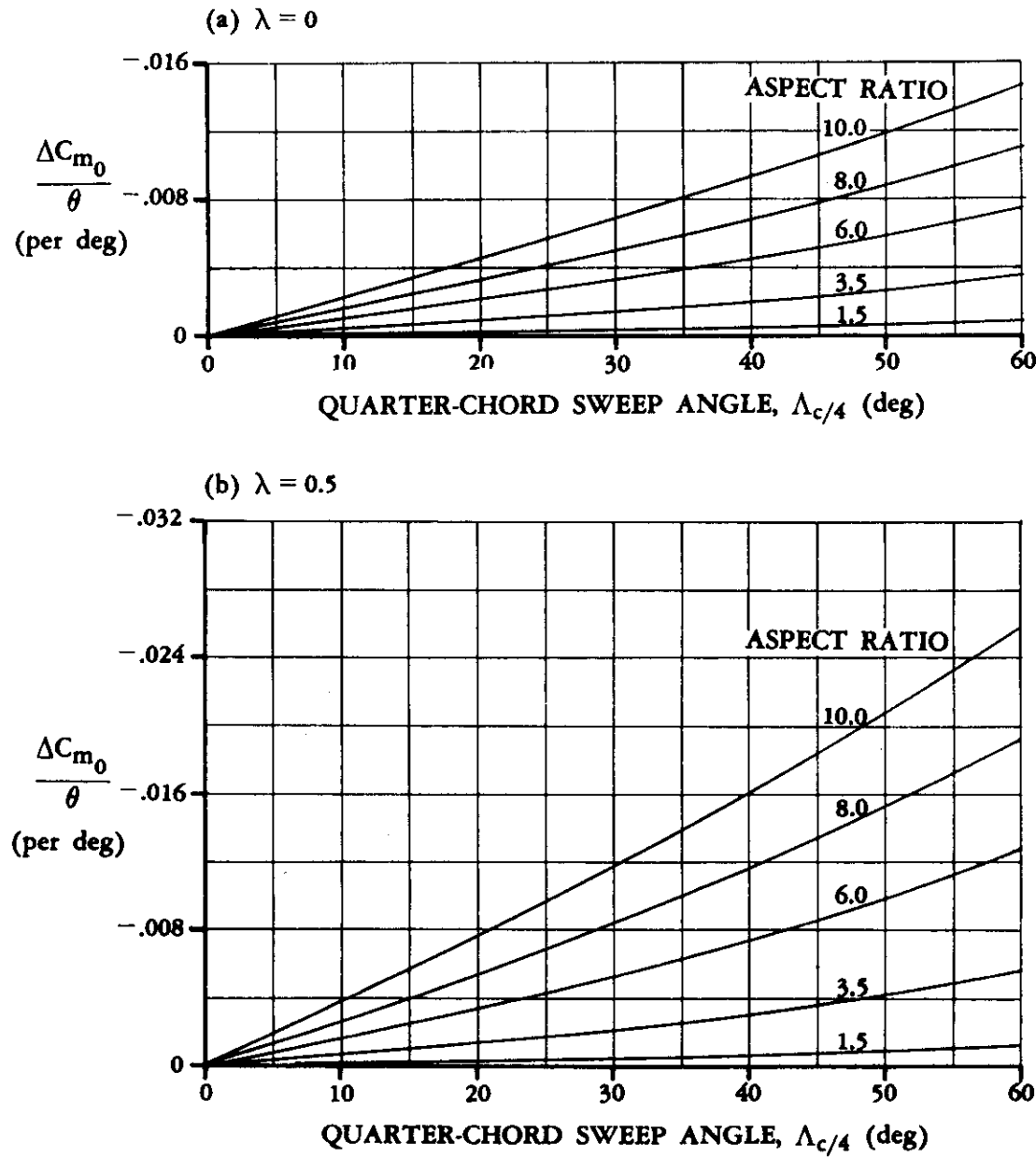


FIGURE 4.1.4.1-5 EFFECT OF LINEAR TWIST ON THE WING ZERO-LIFT PITCHING MOMENT

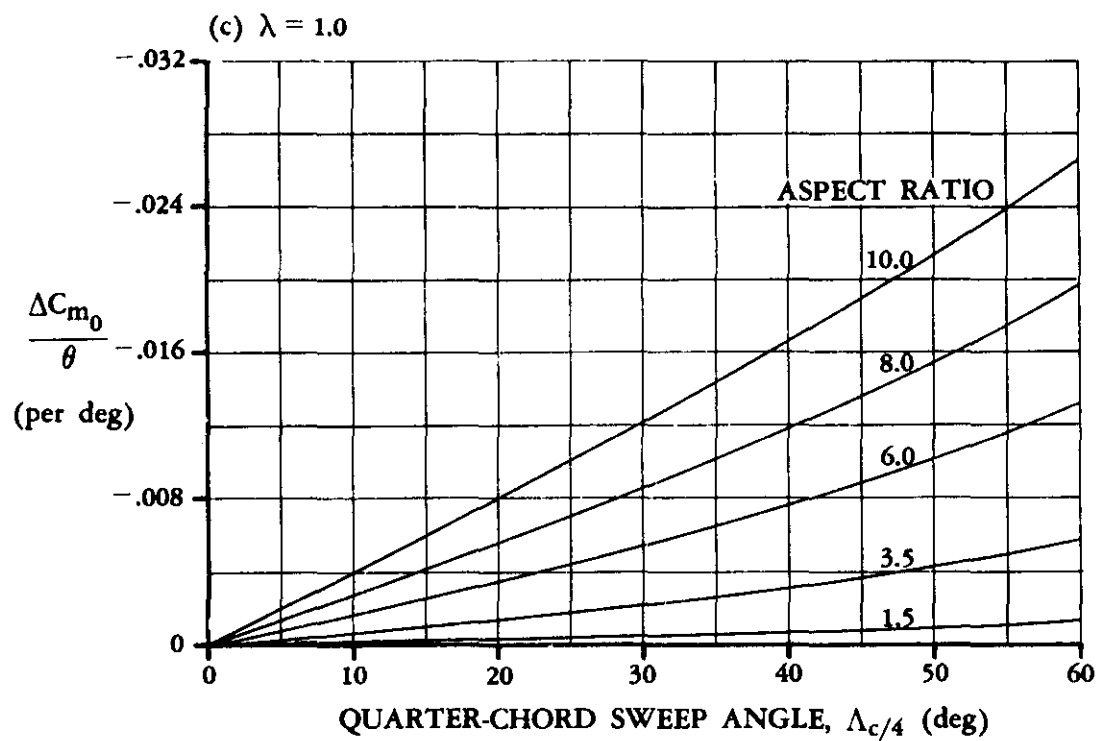


FIGURE 4.1.4.1-5 (CONTD)

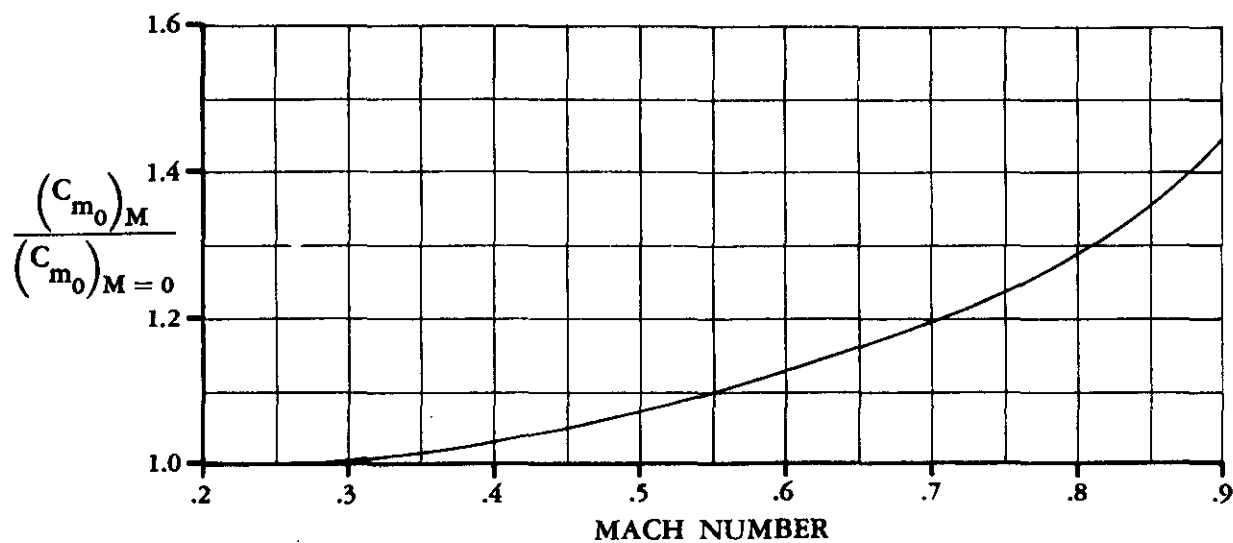


FIGURE 4.1.4.1-6 EFFECT OF COMPRESSIBILITY ON THE WING OR WING-BODY ZERO-LIFT PITCHING-MOMENT COEFFICIENT

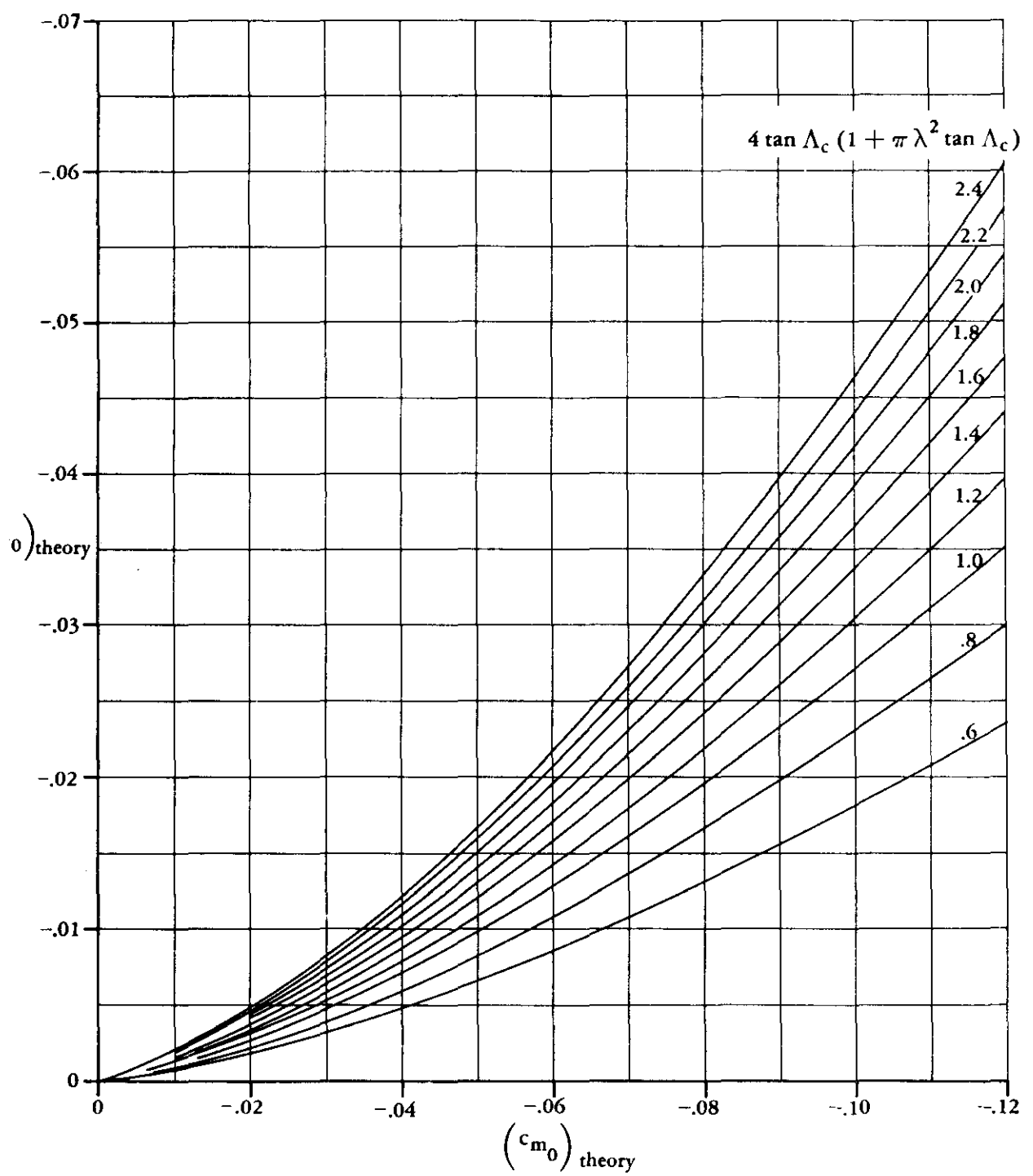


FIGURE 4.1.4.1-7 WING ZERO-LIFT PITCHING MOMENT

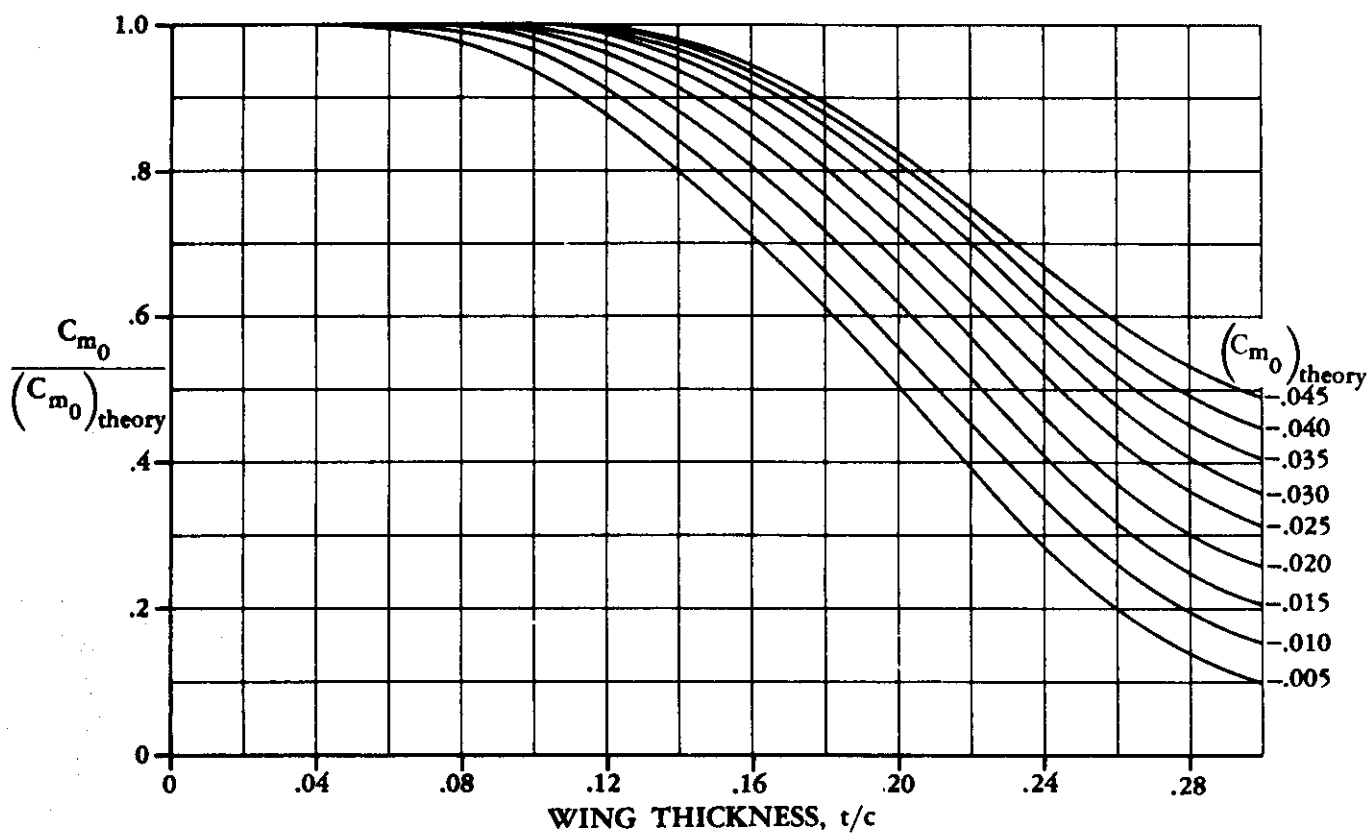


FIGURE 4.1.4.1-8 WING ZERO-LIFT PITCHING-MOMENT THICKNESS CORRECTION FACTOR

4.1.4.2 WING PITCHING-MOMENT-CURVE SLOPE

This section presents methods for calculating the pitching-moment characteristics of wings at low angles of attack at any speed.

The pitching-moment characteristics are generally presented in terms of the wing aerodynamic center. The aerodynamic center (Section 4.1.4) is that point about which the wing pitching moment is invariant with lift. Thus the pitching-moment slope based on the product of the wing area and the mean aerodynamic chord $S_w \bar{c}_w$ about any specified point on the wing chord line may be described by the following equation:

$$\frac{dC_m}{dC_L} = \left(n - \frac{x_{a.c.}}{c_r} \right) \frac{c_r}{\bar{c}} \quad 4.1.4.2-a$$

where

$\frac{x_{a.c.}}{c_r}$ is the distance from the wing apex to the aerodynamic center measured in root chords, positive aft.

n is the distance from the wing apex to the desired moment reference center measured in root chords, positive aft.

$\frac{c_r}{\bar{c}}$ is the ratio of the root chord to the mean aerodynamic chord.

A. SUBSONIC

At subsonic speeds methods are presented for predicting the aerodynamic center of the following two classes of wing planforms:

Straight-Tapered Wings (conventional, trapezoidal wings)

Non-Straight-Tapered Wings

Double-delta wings

Cranked wings

Curved (Gothic and ogee) wings

These three general categories of non-straight-tapered wings are illustrated in Sketch (a) of Section 4.1.3.2. Their wing-geometry parameters are presented in Section 2.2.2.

Two methods are presented for estimating the wing pitching-moment-curve slope for straight-tapered wings. Method 1 is general and is applicable to the majority of configurations. Method 2 is applicable only at $M = 0.2$ for highly swept, constant-section, low-aspect-ratio, delta or clipped-delta configurations with large thickness ratios; i.e., $0.10 \leq t/c \leq 0.30$.

All of the basic theories for calculating wing lift apply to wing pitching moments also. However, as is discussed in Section 4.1.3.2, there is no guarantee that a theory that gives accurate results for lift also gives accurate values for moments.

One theory that does give accurate results for both lift and moments of straight-tapered wings over the entire aspect-ratio range is the lifting-surface theory of Reference 1. Although the computation difficulties of this method are not as formidable as those of some other lifting-surface theories, solutions are nevertheless limited to certain specific planforms.

Most of the currently available methods that are applicable to a wide range of configurations are based largely on empirical data. A semiempirical method of this type is presented in Reference 2. The procedure of this reference uses certain simplified theories (see References 3 and 4) to define limiting locations for the aerodynamic-center positions as the wing aspect ratio approaches zero or infinity. For intermediate aspect ratios, some 150 experimental points from 40 different reports are used as a guide in fairing curves between the theoretically determined limits. In this way generalized charts are constructed for straight-tapered wings of arbitrary aspect ratio and taper ratio. Comparison between the aerodynamic-center locations given by the semiempirical method of Reference 2 and the available lifting-surface solutions of Reference 1 shows a high degree of correlation. The charts of Reference 2 also agree well with the other available semiempirical methods of less extensive scope, such as that of Reference 5.

In the Datcom the graphical aerodynamic-center information presented is basically that of Reference 2. However, the charts are presented in a slightly different form, and the effects of Mach number are added by means of the Prandtl-Glauert compressibility correction rule. The design charts for predicting the aerodynamic center are applicable only within the linear-lift range. Thus the charts apply to wings of very low aspect ratio at only very low angles of attack. These charts are directly applicable to straight-tapered wings. In treating non-straight-tapered wings, the wing is divided into two wing panels and the individual lift and aerodynamic center for each panel are used to establish the aerodynamic center for the composite wing.

Within the linear-lift range, profile parameters such as mean camber line, thickness, leading-edge shape, and others appear to have only minor influence on the aerodynamic-center location of either straight-tapered or non-straight-tapered wings.

Reynolds number, on the other hand, can have an appreciable effect. Reference 6 indicates that for a wing of aspect ratio 3 with a 3-percent biconvex section, the aerodynamic center can vary as much as 8 percent of the wing root chord between the Reynolds numbers 2.4×10^6 and 8×10^6 . Although this aerodynamic-center shift appears to be larger than usual, it does serve to indicate that wind-tunnel test conditions, such as tunnel turbulence level, model support system, and Reynolds number, can have an important bearing on the experimentally measured aerodynamic chord locations.

DATCOM METHODS

Straight-Tapered Wings

Method 1

Figures 4.1.4.2-26a through 4.1.4.2-26f present the a.c. location for straight-tapered wings at subsonic speeds. These charts give the a.c. location as a fraction of the wing root chord. The charts are based on planform characteristics only and thus are most applicable to low-aspect-ratio wings.

The characteristics of high-aspect-ratio wings are primarily determined by the wing two-dimensional section characteristics. For most airfoil sections the a.c. location is at or near the MAC quarter-chord point. However, if greater accuracy is desired, the a.c. location for the particular airfoil section under consideration may be determined from Section 4.1.2.2.

The applicability of the subsonic portions of Figures 4.1.4.2-26a through 4.1.4.2-26f is limited to $M \leq 0.6$. The form of presentation of the charts does not permit an indication of this limit in a manner that is applicable in all situations. Beyond $M = 0.6$ the a.c. location tends to become dependent on wing profile thickness and shape, as indicated in Paragraph B of this section.

However, for swept wings with $t/c \leq 0.04$ the thickness effects are much reduced, and Figures 4.1.4.2-26a through 4.1.4.2-26f may be applied to Mach numbers somewhat higher than $M = 0.6$.

Method 2

This semiempirical method is taken from Reference 7, ignoring the small wing-planform nose-radius effects. The semiempirical method was developed by using the test results of Reference 7, correlated with the theoretical predictions based on lifting-surface theory. Because of its semiempirical nature, the method should be restricted to $M = 0.2$ conditions for highly swept, constant-section, low-aspect-ratio, delta or clipped-delta configurations with the following geometric characteristics:

$$0.10 \leq t/c \leq 0.30$$

$$0.58 \leq A \leq 2.55$$

$$0 \leq \lambda \leq 0.3$$

$$63^\circ \leq \Lambda_{LE} \leq 80^\circ$$

$$\Lambda_{TE} = 0$$

The nonlinear region of the pitching-moment curve for configurations described above may be approximated by using Method 2 of Section 4.1.4.3.

For round-nosed-planform configurations the reader is referred to Reference 7, where three different planform nose-radius models were tested. No incremental nose planform effects are presented here because of their probable configuration dependence.

The wing pitching-moment-curve slope may be approximated by the following procedure:

Step 1. Calculate the aerodynamic-center location uncorrected for wing thickness effects by the following:

$$\frac{x_{a.c.}}{c_r} = \frac{\frac{2}{3}(1-\lambda) + \frac{1}{2} \left[1 - \frac{\lambda^2}{1+\lambda} \right] \pi \log_e \left(1 + \frac{A}{5} \right)}{1 + \pi \log_e \left(1 + \frac{A}{5} \right)} \quad 4.1.4.2-b$$

- Step 2. Determine the wing pitching-moment-curve slope uncorrected for wing thickness effects by using a modified form of Equation 4.1.4.2-a, i.e.,

$$\left(\frac{dC_m}{dC_L} \right)_{\text{theory}} = n - \frac{x_{a.c.}}{c_r}$$

where

n

is the distance from the wing apex to the desired moment reference center, measured in root chords, positive aft. If the semiempirical procedure presented in Method 2 of Section 4.1.4.3 is to be used to determine the nonlinear pitching-moment characteristics, the determination of the moment reference center n is not arbitrary. The moment reference center in this case should be taken at the root-chord midpoint, i.e., $n = 0.5$.

$\frac{x_{a.c.}}{c_r}$

is the distance from the wing apex to the aerodynamic center, measured in root chords, positive aft. This term is obtained from Step 1 above and is uncorrected for thickness effects.

- Step 3. Correct the pitching-moment-curve slope for thickness effects, based on the product of wing area and wing root chord $S_w c_r$, by

$$\frac{dC_m}{dC_L} = \left(\frac{dC_m}{dC_L} \right)_{\text{theory}} \left[\frac{dC_m/dC_L}{(dC_m/dC_L)_{\text{theory}}} \right] \quad 4.1.4.2-c$$

where

$$\left(\frac{dC_m}{dC_L} \right)_{\text{theory}}$$

is the wing pitching-moment-curve slope from Step 2, uncorrected for thickness effects.

$$\frac{dC_m/dC_L}{(dC_m/dC_L)_{\text{theory}}}$$

is the wing-thickness-correction factor for the wing pitching-moment-curve slope. This parameter is obtained from Figure 4.1.4.2-29 as a function of $(dC_m/dC_L)_{\text{theory}}$ and thickness.

No substantiation of this method is possible because of the lack of low-aspect-ratio test data having wing thickness ratios of $0.10 \leq t/c \leq 0.30$.

Non-Straight-Tapered Wings

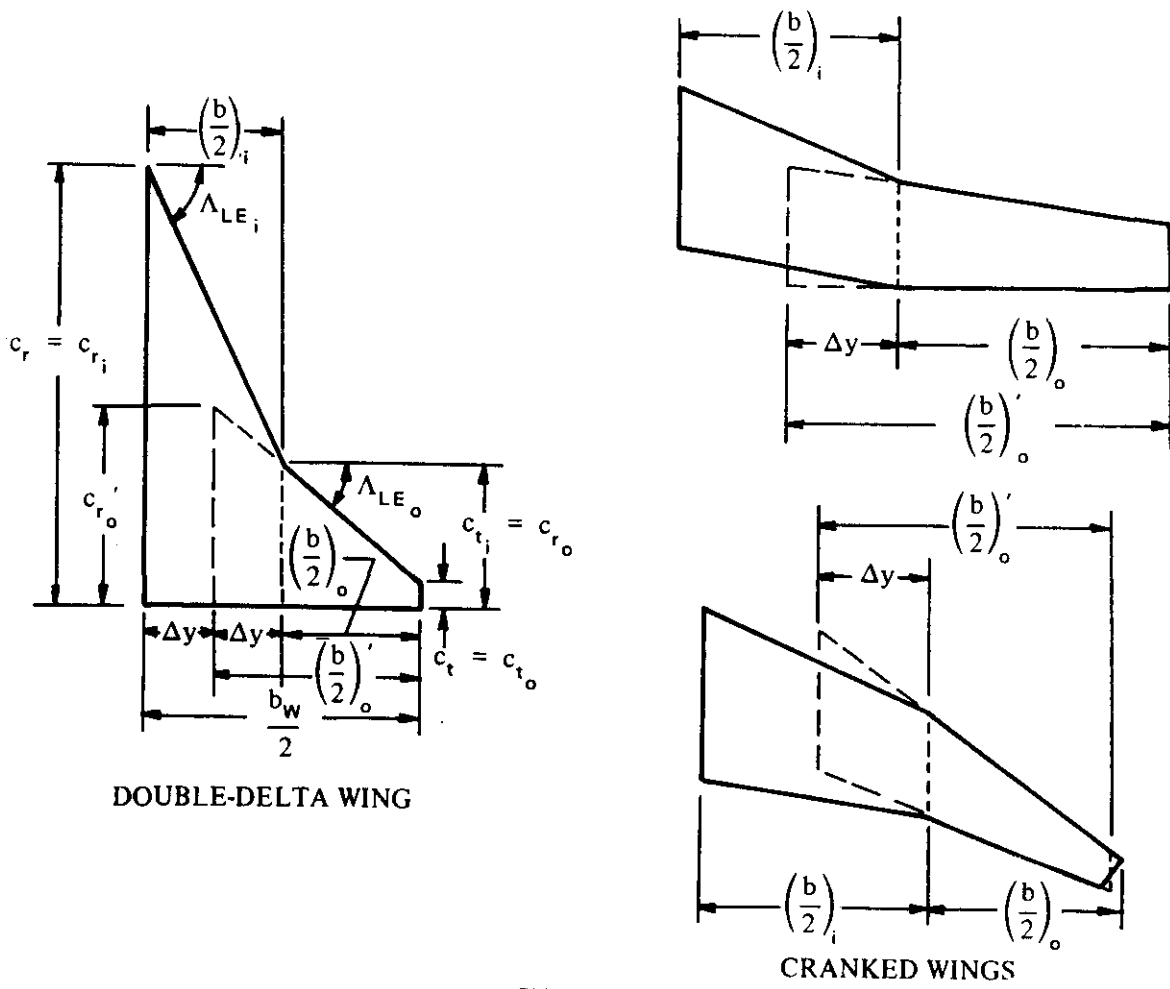
The method for predicting the a.c. location near zero lift of non-straight-tapered wings is taken from Reference 8. This method is used for all non-straight-tapered wings. The non-straight-tapered wing is divided into two panels with each panel having conventional, straight-tapered geometry. Then, for each of the constructed panels, the individual lift-curve slope and a.c. are estimated by

treating each constructed panel as a complete wing. The individual lift and a.c. location derived for each constructed panel are then mutually combined in accordance with an "inboard-outboard" weighted-area relationship to establish the predicted a.c. location for the basic non-straight-tapered wing. There is a difference between the construction geometry used to determine the inboard and outboard panels for the double-delta and cranked wings, and that for the curved wings. Application of the method requires that the wings be broken down as defined below.

Double-Delta and Cranked Wings (see Sketch (a))

Inboard Panel – the inboard leading and trailing edges extended to the center line. The tip-chord span station is fixed at the break formed by the discontinuity in the sweep of the leading edge of the composite wing. The constructed inboard panel is designated by subscript *i*.

Outboard Panel – the leading and trailing edges of the main outboard panel extended inboard to the midpoint between the center line and the break formed by the discontinuity in the sweep of the leading edge of the composite wing. The main outboard panel is designated by subscript *o* and the constructed outboard panel is designated by a prime and a subscript *o*.

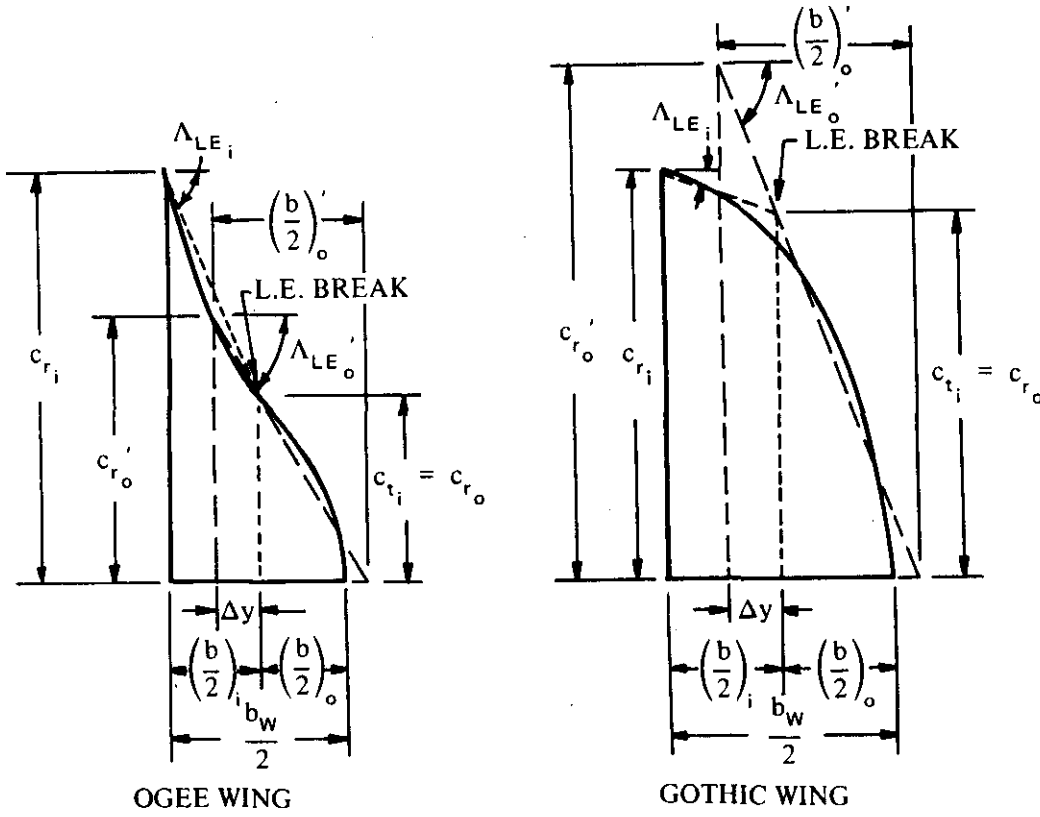


Many double-delta and cranked wings have non-straight trailing edges with the trailing-edge break occurring at a different span station from the leading-edge break. For such wings the irregular trailing-edge sweep angles of the divided panels are modified by using straight trailing-edge sweep angles for each panel, constructed so that the area moment about the respective wing-panel apex remains approximately the same.

Curved Wings (see Sketch (b))

The basic ogee and Gothic planforms must be modified to divide the wing into two panels having conventional, straight-tapered geometry. The modified inboard and outboard panels are designated in the same manner as noted in the double-delta- and cranked-wing breakdown. Both types of curved wings are divided by the following procedure:

1. The tip chord of the inboard panel is located at one-half of the curved wing semispan; i.e., $\left(\frac{b}{2}\right)_i = \left(\frac{b}{2}\right)_o = 0.50\left(\frac{b_w}{2}\right)$. This locates the span station of the leading-edge break, and tip-chord span station of the constructed inboard panel.
2. The root chord of the constructed outboard panel is located at one-fourth of the curved wing semispan; i.e., c_{r_o} span station is at $(0.25)\left(\frac{b_w}{2}\right)$.



SKETCH (b)

3. The semispan of the constructed outboard panel is 0.85 times the semispan of the basic curved wing; i.e., $\left(\frac{b}{2}\right)'_o = 0.85 \left(\frac{b_w}{2}\right)$. This locates the tip of the constructed outboard panel.
4. The tip chord of the constructed outboard panel is zero; i.e., $\lambda'_o = 0$.
5. The leading-edge sweep angles of the two panels are approximated by the use of straight-line segments as shown. Try to maintain an approximately constant area moment for the outboard panel about its apex.

The subsonic aerodynamic-center location of non-straight-tapered wings is obtained from the procedure outlined in the following steps:

- Step 1. Divide the non-straight-tapered wing into inboard and outboard panels as discussed above, and determine their pertinent geometric parameters.
- Step 2. Determine the lift-curve slope of the constructed inboard panel $(C_{L\alpha})_i$, from Figure 4.1.3.2-49, based on its respective area S_i .
- Step 3. Determine the a.c. location of the constructed inboard panel as a fraction of the root chord of the constructed inboard panel $\left(\frac{x_{a.c.}}{c_r}\right)_i$ from Figure 4.1.4.2-26. This a.c. location is aft of the apex of the constructed inboard panel.
- Step 4. Determine the lift-curve slope of the constructed outboard panel $(C_{L\alpha})'_o$, from Figure 4.1.3.2-49, based on its respective area S'_o .
- Step 5. Determine the a.c. location of the constructed outboard panel as a fraction of the root chord of the constructed outboard panel $\left(\frac{x_{a.c.}}{c_r}\right)'_o$ from Figure 4.1.4.2-26. This a.c. location is aft of the apex of the constructed outboard panel.
- Step 6. Convert the a.c. location determined in Step 5 to a fraction of the root chord of the constructed inboard panel and aft of the apex of the constructed inboard panel by

$$\left(\frac{x_{a.c.}}{c_r}\right)'_o = \left(\frac{x_{a.c.}}{c_r}\right)'_i \left(\frac{c'_{r_o}}{c'_{r_i}}\right) - \frac{\Delta y}{c'_{r_i}} \tan \Lambda_{LE_o} + \frac{b_i}{2c'_{r_i}} \tan \Lambda_{LE_i} \quad 4.1.4.2-d$$

- Step 7. Calculate the non-straight-tapered-wing aerodynamic center, measured in wing root chords aft of the wing apex, by

$$\frac{x_{a.c.}}{c_r} = \frac{(C_{L\alpha})_i S_i \left(\frac{x_{a.c.}}{c_r}\right)'_i + (C_{L\alpha})'_o S'_o \left(\frac{x_{a.c.}}{c_r}\right)'_o}{(C_{L\alpha})_i S_i + (C_{L\alpha})'_o S'_o} \quad 4.1.4.2-e$$

The limited availability of experimental data precludes the substantiation of this method for double-delta and cranked wings. No experimental wing-alone double-delta data are readily available for subsonic speeds. Test data for three wing-alone cranked-wing configurations are available. The results of the method applied to those configurations are compared with test results in the data summary presented as Table 4.1.4.2-A (taken from Reference 8).

On the other hand, for curved wings there are enough test data available for a limited substantiation of the method. A comparison of test data for four curved-wing configurations with $x_{a.c.}/c_r$ calculated by this method is presented as Table 4.1.4.2-B (taken from Reference 8). The table also includes two configurations which are wing-body combinations, but the bodies are very small and the wing planform projection effectively blankets nearly all of the body. All the wings investigated have straight trailing edges and one reflex curve in the leading edge. The ranges of Mach number and lift coefficient of the data are:

$$0.09 \leq M \leq 0.9$$

$$0 \leq C_L \leq 0.10$$

Sample Problems

1. Method 2

Given: The following straight-tapered, constant-section, low-aspect-ratio, clipped-delta configuration.

$$A = 0.823 \quad \lambda = 0.18 \quad \Lambda_{LE} = 73.5^\circ$$

$$\text{NACA 2412 airfoil} \quad M = 0.2$$

Compute:

$$\frac{x_{a.c.}}{c_r} = \frac{\frac{2}{3}(1-\lambda) + \frac{1}{2} \left[1 - \frac{\lambda^2}{1+\lambda} \right] \pi \log_e \left(1 + \frac{A}{5} \right)}{1 + \pi \log_e \left(1 + \frac{A}{5} \right)} \quad (\text{Equation 4.1.4.2-b})$$

$$= \frac{\frac{2}{3}(1-0.18) + \frac{1}{2} \left[1 - \frac{(0.18)^2}{1+0.18} \right] \pi \log_e \left(1 + \frac{0.823}{5} \right)}{1 + \pi \log_e \left(1 + \frac{0.823}{5} \right)}$$

$$= 0.527$$

$$\left(\frac{dC_m}{dC_L} \right)_{\text{theory}} = n - \frac{x_{a.c.}}{c_r} \quad (\text{Modified form of Equation 4.1.4.2-a})$$

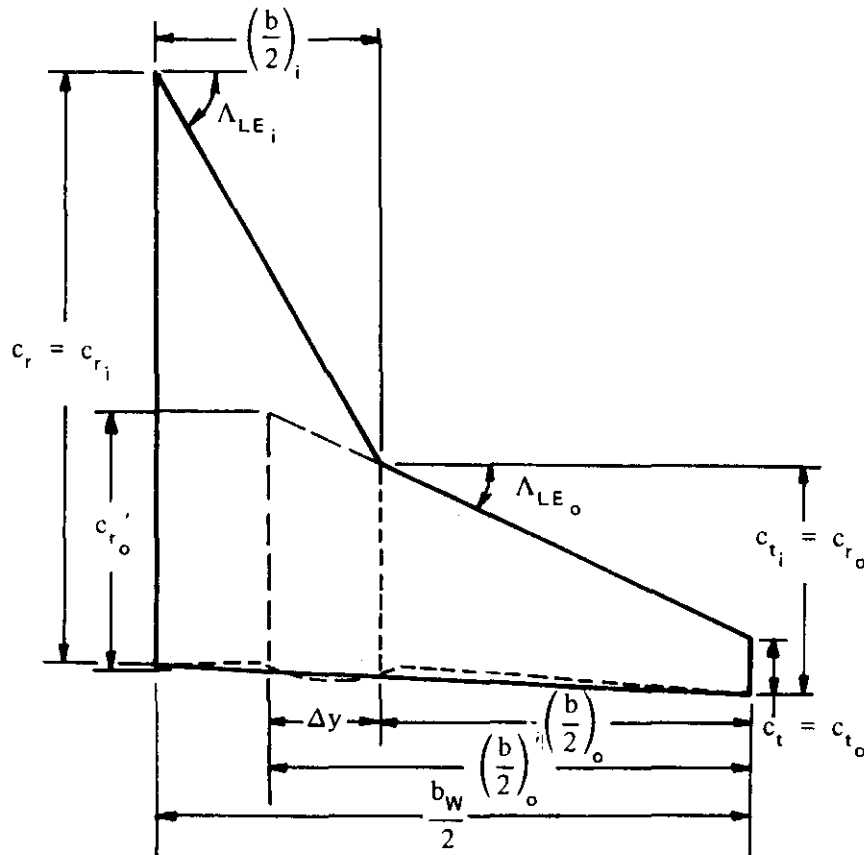
$$= 0.50 - 0.527 = -0.027$$

$$\frac{dC_m/dC_L}{(dC_m/dC_L)_{\text{theory}}} = 0.935 \quad (\text{Figure 4.1.4.2-29})$$

$$\begin{aligned} \frac{dC_m}{dC_L} &= \left(\frac{dC_m}{dC_L} \right)_{\text{theory}} \left[\frac{dC_m/dC_L}{(dC_m/dC_L)_{\text{theory}}} \right] \quad (\text{Equation 4.1.4.2-c}) \\ &= (-0.027)(0.935) \\ &= -0.0252 \quad (\text{based on } S_w c_r, \text{ about } \frac{c_r}{2}) \end{aligned}$$

2. Non-Straight-Tapered Wings

Given: The cranked wing of Reference 22.



Total-Wing Characteristics:

$$\begin{array}{llll} A_w = 5.194 & \lambda_w = 0.090 & \Lambda_{LE_i} = 60^\circ & \Lambda_{LE_o} = 25^\circ \\ \eta_B = 0.380 & c_{r_w} = 50.10 \text{ in.} & b_w/2 = 50.40 \text{ in.} & \end{array}$$

Constructed Inboard-Panel Characteristics:

$$A_i = 1.14 \quad \lambda_i = 0.339 \quad \Lambda_{LE_i} = 60^\circ \quad \Lambda_{TE_i} = 1.75^\circ$$

$$\left(\frac{b}{2}\right)_i = 19.15 \text{ in.} \quad S_i = 1285 \text{ sq in.} \quad (\Lambda_{c/2})_i = 40.9^\circ$$

$$c_{r_i} = 50.10 \text{ in.} \quad c_{t_i} = 16.98 \text{ in.}$$

Constructed Outboard-Panel Characteristics:

$$A'_o = 6.37 \quad \lambda'_o = 0.213 \quad \left(\frac{b}{2}\right)'_o = 40.83 \text{ in.} \quad S'_o = 1047 \text{ sq in.}$$

$$c_{r'_o} = 21.15 \text{ in.} \quad c_{t_o} = 4.50 \text{ in.} \quad \Lambda_{LE_o} = 25^\circ \quad \Lambda_{TE_o} = 1.75^\circ$$

$$(\Lambda_{c/2})_o = 14.7^\circ \quad \Delta y = 9.576 \text{ in.}$$

Additional Characteristics:

$$M = 0.13; \beta = 0.991 \quad \kappa = 1.0 \text{ (assumed)}$$

Compute:

$$\left(\frac{C_L a}{A}\right)_i \text{ (Section 4.1.3.2)}$$

$$\frac{A_i}{\kappa} \left[\beta^2 + \tan^2 (\Lambda_{c/2})_i \right]^{\frac{1}{2}} = \frac{1.14}{1.0} \left[(0.991)^2 + (0.8662)^2 \right]^{\frac{1}{2}} = 1.50$$

$$\left(\frac{C_L a}{A}\right)_i = 1.39 \text{ per rad} \quad (\text{Figure 4.1.3.2-49})$$

$$\left(\frac{C_L a}{A}\right)_i = \left(\frac{C_L a}{A}\right)_i A_i = 1.39 (1.14) = 1.58 \text{ per rad}$$

$$\left(\frac{x_{a.c.}}{c_r}\right)_i$$

$$(A \tan \Lambda_{LE})_i = (1.14)(1.7321) = 1.975; \frac{\beta}{\tan \Lambda_{LE_i}} = \frac{0.991}{1.7321} = 0.572$$

$$\left(\frac{x_{a.c.}}{c_r}\right)_i = 0.452 \quad (\text{Figures 4.1.4.2-26a through -26e, interpolated})$$

$$\left(\frac{C_L a}{A}\right)' \text{ (Section 4.1.3.2)}$$

$$\frac{\frac{A'}{\kappa}}{\kappa} \left[\beta^2 + \tan^2 (\Lambda_{c/2})_o \right]^{\frac{1}{2}} = \frac{6.37}{1.0} \left[(0.991)^2 + (0.2623)^2 \right]^{\frac{1}{2}} = 6.53$$

$$\left(\frac{C_L a}{A}\right)_o = 0.715 \text{ per rad (Figure 4.1.3.2-49)}$$

$$\left(\frac{C_L a}{A}\right)_o' = \left(\frac{C_L a}{A}\right)_o A'_o = (0.715)(6.37) = 4.55 \text{ per rad}$$

$$\left(\frac{x_{a.c.}}{c_r}\right)_o$$

$$\left(A \tan \Lambda_{LE}\right)_o' = (6.37)(0.4663) = 2.97; \frac{\tan \Lambda_{LE}_o}{\beta} = \frac{0.4663}{0.991} = 0.471$$

$$\left(\frac{x_{a.c.}}{c_r}\right)_o' = 0.543 \quad (\text{Figures 4.1.4.2-26a through -26e, interpolated})$$

$$\begin{aligned} \frac{(x_{a.c.})_o'}{c_{r_i}} &= \left(\frac{x_{a.c.}}{c_r}\right)_o' \left(\frac{c_{r_o'}}{c_{r_i}}\right) - \frac{\Lambda y}{c_{r_i}} \tan \Lambda_{LE}_o + \frac{b_i}{2c_{r_i}} \tan \Lambda_{LE}_i \quad (\text{Equation 4.1.4.2-d}) \\ &= (0.543) \left(\frac{21.15}{50.10}\right) - \frac{9.576}{50.10} (0.4663) + \frac{19.15}{50.10} (1.7321) \\ &= 0.802 \end{aligned}$$

Solution:

$$\begin{aligned} \frac{x_{a.c.}}{c_r} &= \frac{\left(C_L a\right)_i S_i \left(\frac{x_{a.c.}}{c_r}\right)_i + \left(C_L a\right)_o' S_o' \frac{\left(x_{a.c.}\right)_o'}{c_{r_i}}}{\left(C_L a\right)_i S_i + \left(C_L a\right)_o' S_o'} \quad (\text{Equation 4.1.4.2-e}) \\ &= \frac{1.58 (1285) (0.452) + 4.55 (1047) (0.802)}{1.58 (1285) + 4.55 (1047)} \\ &= 0.697 \end{aligned}$$

The calculated value compares with a test value of 0.688 from Reference 22.

B. TRANSONIC

Rather than producing linear results as in other speed regimes, application of small-perturbation theory to the transonic regime yields a nonlinear differential equation. This means that at transonic Mach numbers it is not possible to evaluate separately the effects of thickness, camber, and angle of attack, and then to add the individual solutions to obtain the total wing lift and pitching moment. The contributions of each of the above parameters are interrelated, and the wing must be treated as a unit. Theoretical solutions in the transonic speed range are available for only a few specific planforms. Most of the available information on the transonic characteristics of wings is in the form of wind-tunnel test data. As discussed in detail in Section 4.1.3.2, transonic test data are subject to wind-tunnel wall interference effects and must be used with caution.

The use of similarity parameters reduces to a minimum the number of charts required to present test data. Similarity parameters are derived from theoretical considerations and are subject to the limitations of the theory from which they are derived. Although the form of the parameters may be changed by rearranging the variables, the minimum number of parameters for a given theory does not change.

From the nonlinear equations describing transonic flow, it can be shown (Reference 9) that the minimum number of parameters necessary to present complete information in the transonic speed regime is one greater than the number of parameters necessary for the linear theories of both the subsonic and supersonic speed ranges. This means that the number of charts required to present information at transonic speeds is one order of magnitude larger than the number required for either of the other speed ranges.

Only a limited amount of work has been done in organizing transonic test data by means of similarity parameters. The most extensive effort along these lines is given in Reference 10. In this reference, test data from 50 rectangular wings of differing aspect ratio, airfoil thickness, and airfoil section are correlated by means of transonic similarity parameters, with a high degree of success.

For the Datcom, the charts of Reference 10 for rectangular, symmetrical wings at zero angle of attack are adopted directly. Charts for straight-tapered wings of other planform shapes are developed by applying transonic similarity parameters to the experimental data of References 11 through 15. The combined charts for all planforms are presented as Figures 4.1.4.2-30a through 4.1.4.2-30d.

These transonic charts are applicable only to uncambered straight-tapered wings with symmetric airfoil sections at low angles of attack. Wings with cambered airfoils, double-wedge airfoils, and airfoils with blunt trailing edges show different transonic moment and lift characteristics.

Wings with thickness ratios greater than about 7 percent are subject to shock-induced separation effects of significant magnitude. These effects are not accounted for by small-perturbation theory and thus cannot be handled by the similarity parameters of this section. Since there is great similarity between the effects of shock-induced separation on moment and on lift, the treatment of separation-induced moment characteristics in this section is based on the procedure of Section 4.1.3.2 for transonic lift.

DATCOM METHOD

The charts of the Datcom are presented in terms of the transonic similarity parameters of Reference 10. The similarity parameters used for velocity and aspect ratio, respectively, are

$$\bar{V} = \frac{\beta^2}{(t/c)^{2/3}} \quad \text{and} \quad \bar{A} = A(t/c)^{1/3}$$

The corresponding parameter for angle of attack is

$$\bar{\alpha} = \frac{\alpha}{(t/c)}$$

However, since all of the transonic charts of this section are for low angles of attack such that $\bar{\alpha} \approx 0$, this last parameter does not enter into the calculations.

Figures 4.1.4.2-30a through 4.1.4.2-30d give the a.c. location for symmetrical straight-tapered wings of arbitrary sweep angle, taper ratio, and thickness ratio. For rectangular wings a more thorough presentation of a.c. location as a function of the velocity parameter \bar{V} is given in Figure 4.1.4.2-30d.

The following steps outline the calculation procedure:

Step 1. Determine the aspect-ratio similarity parameter \bar{A} .

Step 2. For the appropriate values of λ , $A \tan \Lambda_{LE}$, and \bar{A} , read $\frac{x_{a.c.}}{c_r}$ from Figures 4.1.4.2-30a through 4.1.4.2-30d for values $\bar{V} = \frac{\beta^2}{(t/c)^{2/3}} = -2, -1, 0, +1$. (Cross plots must be made between taper ratios of 0.5 and 1.0.)

Step 3. Determine the Mach numbers corresponding to $\bar{V} = -2, -1, 0, +1$.

Step 4. Calculate $\frac{x_{a.c.}}{c_r}$ for $M = 0.6$ and $M = 1.4$ as outlined in the straight-tapered-wing methods of Paragraphs A and C, respectively, of this section.

Step 5. The complete transonic a.c.-location curve can now be constructed by fairing a curve through the points obtained by means of Steps 1 through 4.* (See Sketch (c))

Step 6. The slope of the pitching-moment curve can now be calculated from the equation

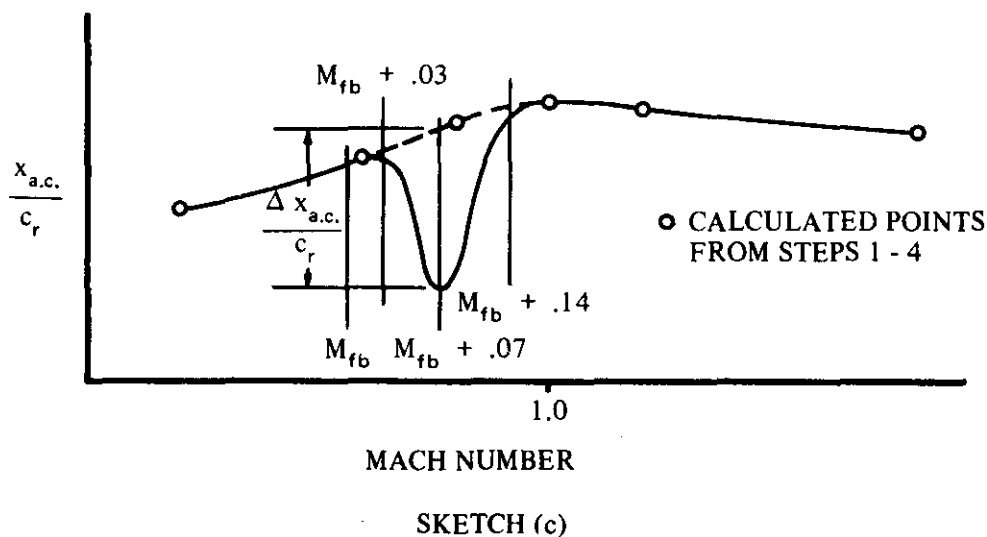
$$C_{m_\alpha} = \left(n - \frac{x_{a.c.}}{c_r} \right) \frac{c_r}{c} C_{L_\alpha} \quad 4.1.4.2-f$$

where C_{L_α} is the lift-curve slope at transonic speeds obtained from Paragraph B of Section 4.1.3.2.

*If the wing under consideration has a thickness ratio greater than 7 percent, the additional Step 7 is required.

Step 7. Determine the incremental a.c. location accounting for separation effects $\frac{\Delta x_{a.c.}}{c_r}$

from Figure 4.1.4.2-33. This increment is applied at the Mach number at which the transonic lift-curve slope reaches its minimum value ($M_{fb} + 0.07$). The force-break Mach number M_{fb} is obtained during the course of calculating the transonic $C_{L\alpha}$ values. Application of this a.c. increment and the required fairing technique are illustrated in Sketch (c).



The above sketch represents the a.c. location at zero angle of attack. As the angle of attack is increased, the bucket in the curve near Mach 1 disappears and the shape is more like the dashed portions of Sketch (c).

Sample Problem

Given: The following straight-tapered wing:

$$A = 4.0 \quad \lambda = 0.68 \quad \Lambda_{LE} = 46.32^\circ \quad \Lambda_{c/2} = 43.6^\circ$$

$$\text{NACA 63A012 airfoil} \quad c_r/c = 1.18 \quad n = 1.09$$

Compute:

$$\bar{A} = A \left(\frac{t}{c} \right)^{1/3} = (4.0)(0.493) = 1.972$$

$$A \tan \Lambda_{LE} = (4.0) (\tan 46.32^\circ) = 4.19$$

Determine $\frac{x_{a.c.}}{c_r}$ for $\bar{V} = -2, -1, 0, \text{ and } 1$, and the Mach numbers corresponding to \bar{V}

$$\bar{V} = \frac{\beta^2}{(t/c)^{2/3}} = \frac{\beta^2}{(0.2433)} ; \quad M = \sqrt{1 + 0.2433 \bar{V}}$$

\bar{V}	M	$\frac{x_{a.c.}}{c_r}$
	$\sqrt{1 + 0.2433 \bar{V}}$	Fig. 4.1.4.2-30
-2	.716	1.020
-1	.870	1.055
0	1.000	1.055
1	1.115	1.080

Determine $\frac{x_{a.c.}}{c_r}$ at $M = 0.6$ and 1.40

$$M = 0.6; \beta = 0.80; \frac{\beta}{\tan \Lambda_{LE}} = \frac{0.80}{\tan 46.32^\circ} = 0.764$$

$$\left(\frac{x_{a.c.}}{c_r} \right)_{M=0.6} = 1.05 \quad (\text{Figures 4.1.4.2-26d through -26f, interpolated})$$

$$M = 1.40; \beta = 0.98; \frac{\beta}{\tan \Lambda_{LE}} = \frac{0.98}{\tan 46.32^\circ} = 0.936$$

$$\left(\frac{x_{a.c.}}{c_r} \right)_{M=1.40} = 1.205 \quad (\text{Figures 4.1.4.2-26d through -26f, interpolated})$$

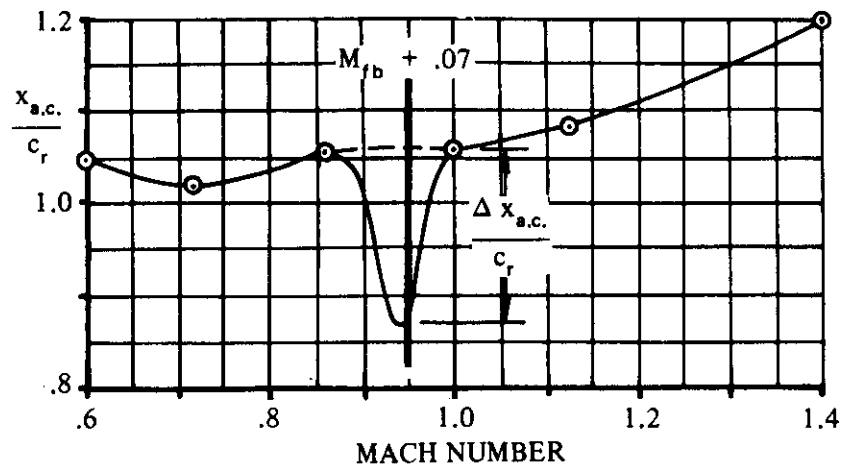
Since $(t/c) > 0.07$, step 7 of the Datcom method is required.

$$\left. \begin{aligned} (M_{fb})_{\Lambda=0} &= 0.82 \quad (\text{Figure 4.1.3.2-53a}) \\ (M_{fb})_{\Lambda} &= 0.88 \quad (\text{Figure 4.1.3.2-53b}) \end{aligned} \right\} \quad M_{fb} \text{ is obtained during the course of calculating } C_{L_a}. \text{ It is shown here, since the calculations for } C_{L_a} \text{ are not given.}$$

$$A \cos^2 \Lambda_{c/2} = (4.0) (\cos 43.6) = 2.10$$

$$\frac{\Delta x_{a.c.}}{c_r} = -0.19 \quad (\text{Figure 4.1.4.2-33}). \text{ This correction is applied at } M_{fb} + 0.07 = 0.95$$

Construct the transonic a.c. curve using Sketch (c) as a guide.



Determine $C_{m\alpha}$ from Paragraph B, Section 4.1.3.2 (see calculation table below).

Solution:

$$\begin{aligned}
 C_{m\alpha} &= \left(n - \frac{x_{a.c.}}{c_r} \right) \frac{c_r}{c} C_{L\alpha} \quad (\text{Equation 4.1.4.2-f}) \\
 &= \left(1.09 - \frac{x_{a.c.}}{c_r} \right) 1.18 C_{L\alpha}
 \end{aligned}$$

① M	② $\frac{x_{a.c.}}{c_r}$ (faired curve)	③ $n - \frac{x_{a.c.}}{c_r}$ $1.09 - ②$	④ $C_{L\alpha}$ (per deg) Sec. 4.1.3.2, Para. B	⑤ $C_{m\alpha}$ (per deg) Eq. 4.1.4.2-f $1.18 \cdot ③ \cdot ④$
0.70	1.020	.070	.043	.0036
0.87	1.055	.035	.045	.0019
0.95	0.865	.225	.047	.0125
1.00	1.055	.035	.024	.0010
1.10	1.075	.015	.040	.0007

C. SUPERSONIC

Methods are presented for determining the wing aerodynamic-center location of the following two classes of wing planforms:

Straight-Tapered Wings (conventional, trapezoidal wings)

Non-Straight-Tapered Wings

Double-delta wings

Cranked wings

Curved (Gothic and ogee) wings

These three general categories of non-straight-tapered wings are illustrated in Sketch (a) of Section 4.1.3.2. Their wing-geometry parameters are presented in Section 2.2.2.

As is the case at subsonic speeds, the supersonic design charts also present information that is basically that of Reference 2. The effects of Mach number have been added by means of the Prandtl-Glauert compressibility correction, and the resulting design charts are an extension of those used at subsonic speeds. The charts are directly applicable to straight-tapered wings. In treating non-straight-tapered wings, the wing is divided into two panels and the individual lift and aerodynamic-center location for each panel are used to establish the aerodynamic-center location for the composite wing.

The design charts are applicable only in the linear-lift range. Within this range the effects of camber, leading-edge radius, and trailing-edge angle are minor in regard to the aerodynamic-center characteristics.

Although wing profile thickness has little effect on the supersonic wing normal-force-curve slope at low angles of attack, provided the Mach lines do not lie near the wing leading edge (Sections 4.1.3.2 and 4.1.3.3), the situation regarding wing pitching moments is quite different. For unswept wings of high aspect ratio at supersonic speeds, the area influenced by the three-dimensional flow within the tip shock cones is relatively small compared to the large area between the tip shocks, where the flow is two-dimensional. Under these conditions the wing moment characteristics are closely related to the two-dimensional airfoil characteristics. In Section 4.1.2.2 it is shown that for airfoils the aerodynamic center is very much a function of thickness ratio. As a first approximation, the a.c. location for unswept wings at supersonic speeds may be taken as that of the corresponding two-dimensional section.

For swept wings the three-dimensional flow within the shock cones is much larger, and the wing cannot be treated as two-dimensional. Linear theory generally gives satisfactory results for these wings.

As the Mach lines approach the leading edges of wings at supersonic speeds, the lift may deviate considerably from linear-theory lift. These deviations (see Section 4.1.3.2, Paragraph C) are caused by the finite thickness of the wing leading edge, which forces the leading-edge shock to be located at a different position from that predicted by linear theory. For delta wings, at least, these effects on lift are not reflected in the pitching moments. This is perhaps due to the fact that linear theory predicts the same a.c. location for delta wings, whether the leading-edge shock is attached or

detached. For other wings, linear theory does predict minor changes in a.c. location when the leading-edge shock attaches. In general, however, it appears that the role of wing thickness in causing deviations from linear theory at the sonic-leading-edge condition is much less for moments than it is for lift.

DATCOM METHODS

Straight-Tapered Wings

The aerodynamic-center location of swept, straight-tapered wings at Mach numbers greater than 1.4 is obtained from Figures 4.1.4.2-26a through 4.1.4.2-26f. These charts give the a.c. location as a fraction of the wing root chord. For unswept wings, the method of Section 4.1.2.2 for two-dimensional sections in supersonic flow may be used.

Non-Straight-Tapered Wings

The method presented in Paragraph A for predicting the aerodynamic-center location of non-straight-tapered wings is also applicable at supersonic speeds. The normal-force-curve slopes of the constructed inboard and outboard panels are obtained from the straight-tapered-wing design charts of Paragraph C of Section 4.1.3.2 (Figures 4.1.3.2-56a through 4.1.3.2-56f). The a.c. locations of the constructed inboard and outboard panels, measured in root chords of the respective panels, are obtained from the supersonic portion of Figures 4.1.4.2-26a through 4.1.4.2-26f.

Equation 4.1.4.2-e expressed in terms of the normal-force-curve slope is

$$\frac{x_{a.c.}}{c_r} = \frac{\left(C_{N_\alpha}\right)_i S_i \left(\frac{x_{a.c.}}{c_r}\right)_i + \left(C_{N_\alpha}\right)'_o S'_o \left(\frac{x_{a.c.}}{c_r}\right)'_o}{\left(C_{N_\alpha}\right)_i S_i + \left(C_{N_\alpha}\right)'_o S'_o}$$

where $x_{a.c.}/c_r$ is the aerodynamic center of the non-straight-tapered wing, measured in wing root chords, aft of the wing apex.

The limited availability of experimental data precludes the substantiation of this method for double-delta and cranked wings. No experimental wing-alone cranked-wing data are readily available for supersonic speeds. Test data for one wing-alone double-delta configuration are available (Reference 31). This method predicts the a.c. location for this wing to within about one percent of the test value.

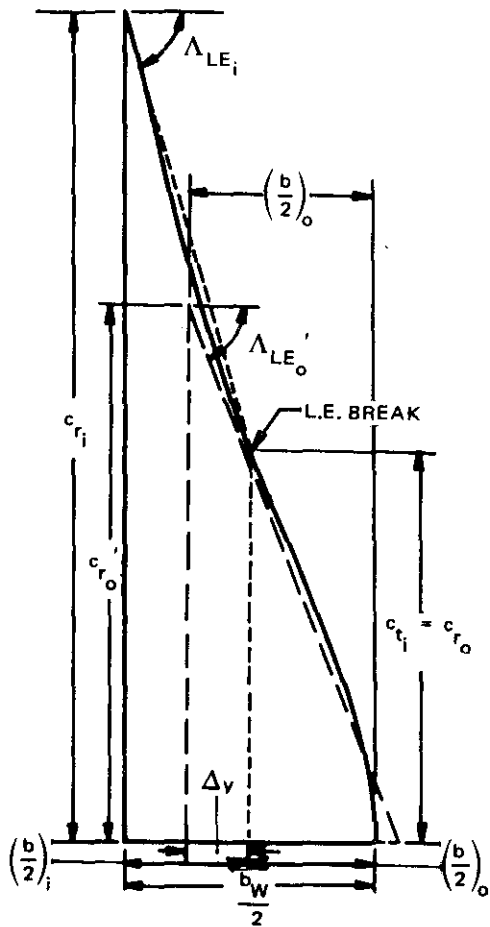
A comparison of test data for three curved-wing configurations with $x_{a.c.}/c_r$ calculated by this method is presented as Table 4.1.4.2-C (taken from Reference 8). One of the configurations is a wing-body combination, but the body is very small and the wing planform projection effectively blankets nearly all the body. All the wings investigated have straight trailing edges and one reflex curve in the leading edge. The Mach-number and lift-coefficient ranges of the data are:

$$1.02 \leq M \leq 2.60$$

$$0 \leq C_L \leq 0.10$$

Sample Problem

Given: The ogee wing-body configuration of Reference 29. Since the wing-planform projection blankets nearly all of the body, the combination is treated as a wing-alone configuration.



Total-Wing Characteristics:

$$A_w = 1.20 \quad \Lambda_{TE} = 0 \quad c_{r_w} = 20.0 \text{ in.}$$

$$\frac{b_w}{2} = 6.0 \text{ in.}$$

$t/c = 0.05$ (rhombic wing sections - free-stream direction)

Constructed Inboard-Panel Characteristics:

$$A_i = 0.407 \quad \lambda_i = 0.475 \quad \left(\frac{b}{2}\right)_i = 3.0 \text{ in.}$$

$$S_i = 88.5 \text{ sq in.} \quad c_{r_i} = 20.0 \text{ in.} \quad c_{t_i} = 9.50 \text{ in.}$$

$$\Lambda_{LE_i} = 74.6^\circ$$

Constructed Outboard-Panel Characteristics:

$$A'_o = 1.57 \quad \lambda'_o = 0 \quad \left(\frac{b}{2}\right)'_o = 5.10 \text{ in.}$$

$$S'_o = 66.3 \text{ sq in.} \quad c_{r'_o} = 13.0 \text{ in.} \quad \Lambda_{LE_o} = 68.6^\circ$$

$$\Delta y = 1.50 \text{ in.}$$

Additional Characteristics:

$$M = 1.82; \beta = 1.52$$

Compute:

$$(C_N a)_i \quad (\text{Section 4.1.3.2})$$

$$(A \tan \Lambda_{LE_i})_i = (0.407) (\tan 74.6^\circ) = 1.477$$

$$\frac{\beta}{\tan \Lambda_{LE_i}} = \frac{1.52}{\tan 74.6^\circ} = 0.419$$

$$\left[\tan \Lambda_{LE} (C_N a)_{\text{theory}} \right]_i = 2.67 \text{ per rad} \quad (\text{Figures 4.1.3.2-56c through -56e, interpolated})$$

$$\left[(C_N a)_{\text{theory}} \right]_i = \frac{2.67}{\tan 74.6^\circ} = 0.736 \text{ per rad}$$

$$\left[\frac{C_N a}{(C_N a)_{\text{theory}}} \right]_i$$

$$\delta_L = \frac{\text{semiwedge angle}}{\cos \Lambda_{LE}} = \frac{\frac{1}{2} \left(\frac{0.05}{0.5} \right)}{\cos 74.6^\circ} (57.3) = 10.8^\circ$$

$$\Delta y_L = 5.85 \tan \delta_L = 5.85 \tan 10.8^\circ = 1.116$$

$$\left[\frac{C_N a}{(C_N a)_{\text{theory}}} \right]_i = 1.0 \quad (\text{Figure 4.1.3.2-60})$$

$$(C_N a)_i = \left[\frac{C_N a}{(C_N a)_{\text{theory}}} \right]_i \left[(C_N a)_{\text{theory}} \right]_i = (1.0)(0.736) = 0.736 \text{ per rad}$$

$$\left(\frac{x_{a.c.}}{c_r} \right)_i$$

$$\left(\frac{x_{a.c.}}{c_r} \right)_i = 0.465 \quad (\text{Figures 4.1.4.2-26a through -26e, interpolated})$$

$$(C_N a)'_o \quad (\text{Section 4.1.3.2})$$

$$(A \tan \Lambda_{LE})'_o = 1.57 (\tan 68.6^\circ) = 4.01$$

$$\frac{\beta}{\tan \Lambda_{LE}_o} = \frac{1.52}{\tan 68.6^\circ} = 0.596$$

$$\left[\tan \Lambda_{LE} (C_N a)_{\text{theory}} \right]'_o = 4.92 \text{ per rad} \quad (\text{Figure 4.1.3.2-56a})$$

$$\left[(C_N a)_{\text{theory}} \right]'_o = \frac{4.92}{\tan 68.6^\circ} = 1.93 \text{ per rad}$$

$$\left[\frac{C_N a}{(C_N a)_{\text{theory}}} \right]'_o$$

$$\delta_L = \frac{\text{semiwedge angle}}{\cos \Lambda_{LE}} = \frac{\frac{1}{2} \left(\frac{0.05}{0.5} \right)}{\cos 68.6^\circ} (57.3) = 7.85^\circ$$

$$\Delta y_1 = 5.85 \tan \delta_1 = 5.85 \tan 7.85^\circ = 0.807$$

$$\left[\frac{C_{Na}}{(C_{Na})_{\text{theory}}} \right]' = 0.965 \quad (\text{Figure 4.1.3.2-60})$$

$$(C_{Na})'_o = \left[\frac{C_{Na}}{(C_{Na})_{\text{theory}}} \right]' \left[(C_{Na})_{\text{theory}} \right]'_o = 0.965 (1.93) = 1.86 \text{ per rad}$$

$$\left(\frac{x_{a.c.}}{c_r} \right)_o$$

$$\left(\frac{x_{a.c.}}{c_r} \right)_o = 0.670 \quad (\text{Figure 4.1.4.2-26a})$$

$$\frac{(x_{a.c.})'_o}{c_{r_i}} = \left(\frac{x_{a.c.}}{c_r} \right)'_o \left(\frac{c_{r_o}'}{c_{r_i}} \right) - \frac{\Delta y}{c_{r_i}} \tan \Lambda_{LE_o} + \frac{b_i}{2c_{r_i}} \tan \Lambda_{LF_i} \quad (\text{Equation 4.1.4.2-d})$$

$$\begin{aligned} &= (0.670) \frac{13.0}{20.0} - \frac{1.50}{20.0} (2.552) + \frac{3.0}{20.0} (3.630) \\ &= 0.789 \end{aligned}$$

Solution:

$$\begin{aligned} \frac{x_{a.c.}}{c_r} &= \frac{(C_{Na})_i S_i \left(\frac{x_{a.c.}}{c_r} \right)_i + (C_{Na})'_o S'_o \frac{(x_{a.c.})'_o}{c_{r_i}}}{(C_{Na})_i S_i + (C_{Na})'_o S'_o} \quad (\text{Equation 4.1.4.2-e}) \\ &= \frac{(0.736)(88.5)(0.465) + (1.86)(66.3)(0.789)}{(0.736)(88.5) + (1.86)(66.3)} \\ &= 0.677 \end{aligned}$$

The calculated value compares with a test value of 0.693 from Reference 29.

D. HYPERSONIC

The aerodynamic center of flat-plate straight-tapered wings approaches the area-centroid location as the Mach number becomes large. However, the interrelated effects of viscosity, heat transfer, and detached shock waves due to blunt leading edges cause deviations of the aerodynamic center from the theoretical values. The magnitude of these effects has not been thoroughly evaluated. The hypersonic method of this section is based on linear theory, which gives the location of the aerodynamic center at the area centroid for high Mach numbers.

DATCOM METHOD

The supersonic portions of Figures 4.1.4.2-26a through 4.1.4.2-26f give the a.c. location of straight-tapered wings at zero angle of attack. These charts are derived from linear theory in this region.

REFERENCES

1. Multhopp, H.: Methods for Calculating the Lift Distribution of Wings (Subsonic Lifting-Surface Theory). ARC R&M 2884, 1950. (U)
2. Holmboe, V.: Charts for the Position of the Aerodynamic Center at Low Speeds and Small Angles of Attack for a Large Family of Tapered Wings. SAAB TN 27 (Sweden), 1954. (U)
3. Jones, R.: Properties of Low-Aspect-Ratio Pointed Wings at Speeds Below and Above the Speed of Sound. NACA TR 835, 1946. (U)
4. De Young, J., and Harper, C.: Theoretical Symmetric Span Loading at Subsonic Speeds for Wings Having Arbitrary Plan Form. NACA TR 921, 1948. (U)
5. Anon: Royal Aeronautical Society Data Sheets – Aerodynamics. Vol. II, (Wings S.08.01.02), 1955. (U)
6. Hunton, L.: Effects of Fixing Transition on the Transonic Aerodynamic Characteristics of a Wing-Body Configuration at Reynolds Numbers from 2.4 to 12 Million. NACA TN 4279, 1958. (U)
7. Crosthwait, E. L., and Seeth, D. D.: Subsonic Characteristics of Low Aspect Ratios. FDL-TDR-64-103, 1965. (U)
8. Benepe, D. B., Kouri, B. G., Webb, J. B., et al: Aerodynamic Characteristics of Non-Straight-Taper Wings. AFFDL-TR-66-73, 1966. (U)
9. Warren, C.: Recent Advances in the Knowledge of Transonic Air Flow. Jour. Roy. Aero. Soc., Vol. 60, No. 544, April 1956. (U)
10. McDevitt, J.: A Correlation by Means of Transonic Similarity Rules of Experimentally Determined Characteristics of a Series of Symmetrical and Cambered Wings of Rectangular Plan Form. NACA TR 1253, 1955. (U)
11. Emerson, H.: Wind-Tunnel Investigation of the Effect of Clipping the Tips of Triangular Wings of Different Thickness, Camber and Aspect Ratio – Transonic Bump Method. NACA TN 3671, 1956. (U)
12. Few, A., Jr., and Fournier, P.: Effects of Sweep and Thickness on the Static Longitudinal Aerodynamic Characteristics of a Series of Thin, Low-Aspect Ratio, Highly Tapered Wings at Transonic Speeds. Transonic-Bump Method. NACA RM L54B25, 1954. (U)
13. Harris, W.: A Wind-Tunnel Investigation at High Subsonic and Low Supersonic Mach Numbers on a Series of Wings with Various Sweep-back, Taper, Aspect Ratio, and Thickness. AF TR 6669, 1952. (U)
14. Wiley, H. G.: Aerodynamic Characteristics Extended to High Angles of Attack at Transonic Speeds of a Small-Scale 0° Sweep Wing, 45° Sweptback Wing, and 60° Delta Wing. NACA RM L52I30, 1952. (U)
15. Turner, T. R.: Effects of Sweep on the Maximum-Lift Characteristics of Four Aspect-Ratio-4 Wings at Transonic Speeds. NACA RM L50H11, 1950. (U)
16. Puckett, A. E., and Stewart, H. J.: Aerodynamic Performance of Delta Wings at Supersonic Speeds. Jour. Aero. Sci., Vol. 14, No. 10, October 1947. (U)
17. White, C. O., and Gresham, J. W.: Simplified Design Charts for the Determination of the Approximate Aerodynamic Center Location of Low Aspect Ratio Wings at Small Angles of Attack. Douglas Aircraft Company Report LB 30153, 1959. (U)
18. Kaettari, G. E.: Pressure Distributions on Triangular and Rectangular Wings to High Angles of Attack – Mach Numbers 2.46 and 3.26. NACA RM A54J12, 1955. (U)
19. Letko, W.: Experimental Determination at Subsonic Speeds of the Oscillatory and Static Lateral Stability Derivatives of a Series of Delta Wings with Leading-Edge Sweep from 30° to 86.5°. NACA RM L57A30, 1957. (U)
20. Smith, F. M.: Experimental and Theoretical Aerodynamic Characteristics of Two Low-Aspect Ratio Delta Wings at Angles of Attack to 50° at a Mach Number of 4.07. NACA RM L57E02, 1957. (U)
21. Bateman, R. E., and Simms, J.: Aerodynamic Investigation of Wing Planforms at Transonic and Supersonic Speeds. Boeing Airplane Company Report D-12131, 1952. (C) Title Unclassified

22. Henderson, W. P. and Hammond, A. D.: Low-Speed Investigation of High-Lift and Lateral-Control Devices on a Semispan Variable-Sweep Wing Having an Outboard-Pivot Location. NASA TM X-542, 1961. (U)
23. Lange, R. H.: Maximum-Lift Characteristics of a Wing with Leading-Edge Sweepback Decreasing from 45° at the Root to 20° at the Tip at Reynolds Numbers from 2.4×10^6 to 6.0×10^6 . NACA RM L50A04a, 1950. (U)
24. Kruger, W.: Six-Component Measurements on a Cranked Swept-Back Wing. Great Britain Ministry of Supply Translation 816, 1947. (U)
25. Squire, L. C.: Further Experimental Investigations of the Characteristics of Cambered Gothic Wings at Mach Numbers From 0.60 to 2.0. ARC R&M 3310, 1963. (U)
26. Peckham, D. H. and Atkinson, S. A.: Preliminary Results of Low-Speed Wind-Tunnel Tests on a Gothic Wing of Aspect Ratio 1.0. ARC CP 508, 1960. (U)
27. Keating, R. F. A.: Low-Speed Wind-Tunnel Tests on Sharp-Edged Gothic Wings of Aspect-Ratio 3/4. ARC CP 576, 1961. (U)
28. Spencer, B., Jr., and Hammond, A. D.: Low-Speed Longitudinal Aerodynamic Characteristics Associated With a Series of Low-Aspect-Ratio Wings Having Variations in Leading-Edge Contour. NASA TN D-1374, 1962. (U)
29. Squire, L. C., and Capps, D. S.: An Experimental Investigation of the Characteristics of an Ogee Wing From M = 0.4 to M = 1.8. ARC CP 585, 1962. (U)
30. Taylor, C. R.: Measurements at Mach Numbers up to 2.8 of the Longitudinal Characteristics of One Plane and Three Cambered Slender 'Ogee' Wings. ARC R&M 3328, 1963. (U)
31. Durgin, F. A.: A Study of Twist and Camber on Wings in Supersonic Flow. FDL-TDR-64-109, 1964. (U)

TABLE 4.1.4.2-A
SUBSONIC AERODYNAMIC-CENTER LOCATION OF CRANKED WINGS
DATA SUMMARY

Ref.	Config.	A	λ	η_B	Λ_{LE_i} (deg)	Λ_{LE_0} (deg)	M	$\frac{x_{a.c.}}{c_r}$ Calc.	$\frac{x_{a.c.}}{c_r}$ Test	e Percent Error
22	W	5.19	.09	.380	60.0	25.0	0.13	.697	.688	1.3
		4.16	(a)	.430		45.0		.710	.708	0.3
		3.00		.508		60.0		.706	.738	-4.3
		1.89		.654		75.0		.619	.683	-9.4
23	W	4.18	.364	.300(b)	45.0	27.5(b)	0.13	.631	.630	0.2
24	W	5.02	.105	.296(b)	45.0	28.2(b)	0.13	.686	.638	7.5
(a) Raked wing tip										
(b) Multi-panel wing approximated by two panels.										
Average Error = $\frac{\sum e }{n} = 3.8\%$										

TABLE 4.1.4.2-B
SUBSONIC AERODYNAMIC-CENTER LOCATION OF CURVED WINGS
DATA SUMMARY AND SUBSTANTIATION

Ref.	Config.	Planform	A	$\frac{b_w}{2\lambda}$	Δ_{LE_i} (a) (deg)	Δ_{LE_o} (a) (deg)	M	$\frac{x_{a.c.}}{c_r}$ Calc.	$\frac{x_{a.c.}}{c_r}$ Test	e Percent Error
25	W	Gothic	.75	.250	66.0	78.0	.40	.508	.497	2.2
							.70	.511	.512	-0.2
							.80	.515	.516	-0.2
							.85	.516	.520	-0.8
							.90	.519	.520	-0.2
26	W	Gothic	1.00	.334	57.2	74.6	.13	.494	.491	0.6
27	W	Gothic	.75	.250	64.0	79.0	.09	.505	.511	-1.2
28	WB	Gothic	1.33	.400	64.6	69.0	.21	.549	.524	4.8
				.460	52.0	70.0		.478	.441	8.4
					46.5			.471	.448	5.1
				.500	18.0	72.0		.385	.386	-0.3
				.225	73.0	79.0		.566	.550	2.9
				.500	59.0	65.6		.561	.521	7.7
29	WB	Ogee	1.20	.300	74.6	68.6	.40	.635	.632	0.5
							.70	.641	.645	-0.6
							.80	.645	.650	-0.8
							.85	.648	.654	-0.9
							.90	.650	.659	-1.4
30	W	Ogee	.92	.208	80.5	73.3	.30	.696	.691	0.7
							.80	.704	.701	0.4
(a) Approximations used in a.c. prediction								Average Error = $\frac{\sum e }{n} = 2.0\%$		

TABLE 4.1.4.2-C
SUPERSONIC AERODYNAMIC-CENTER LOCATION OF CURVED PLANFORMS
DATA SUMMARY AND SUBSTANTIATION

Ref.	Config.	Planform	A	$\frac{b_w}{2\lambda}$	Λ_{LE_i} (a) (deg)	Λ_{LE_o}' (a) (deg)	M	$\frac{x_{a.c.}}{c_r}$ Calc.	$\frac{x_{a.c.}}{c_r}$ Test	e Percent Error						
25	W	Gothic	.75	.250	66.0	78.0	1.02	.542	.528	2.7						
							1.25	.549	.557	-1.4						
							1.30	.551	.557	-1.1						
							1.42	.553	.565	-2.1						
							1.61	.556	.580	-4.1						
							1.82	.557	.580	-4.0						
29	WB	Ogee	1.20	.300	74.6	68.6	1.25	.676	.693	-2.5						
							1.42	.674	.694	-2.9						
							1.61	.674	.693	-2.7						
							1.82	.677	.693	-2.3						
30	W	Ogee	.92	.208	80.5	73.3	1.40	.729	.745	-2.1						
							1.80	.723	.740	-2.3						
							2.20	.721	.735	-1.9						
							2.60	.720	.726	-0.8						
(a) Approximations used in a.c. prediction																
Average Error = $\frac{\sum e }{n} = 2.3\%$																

SUBSONIC AND SUPERSONIC SPEEDS

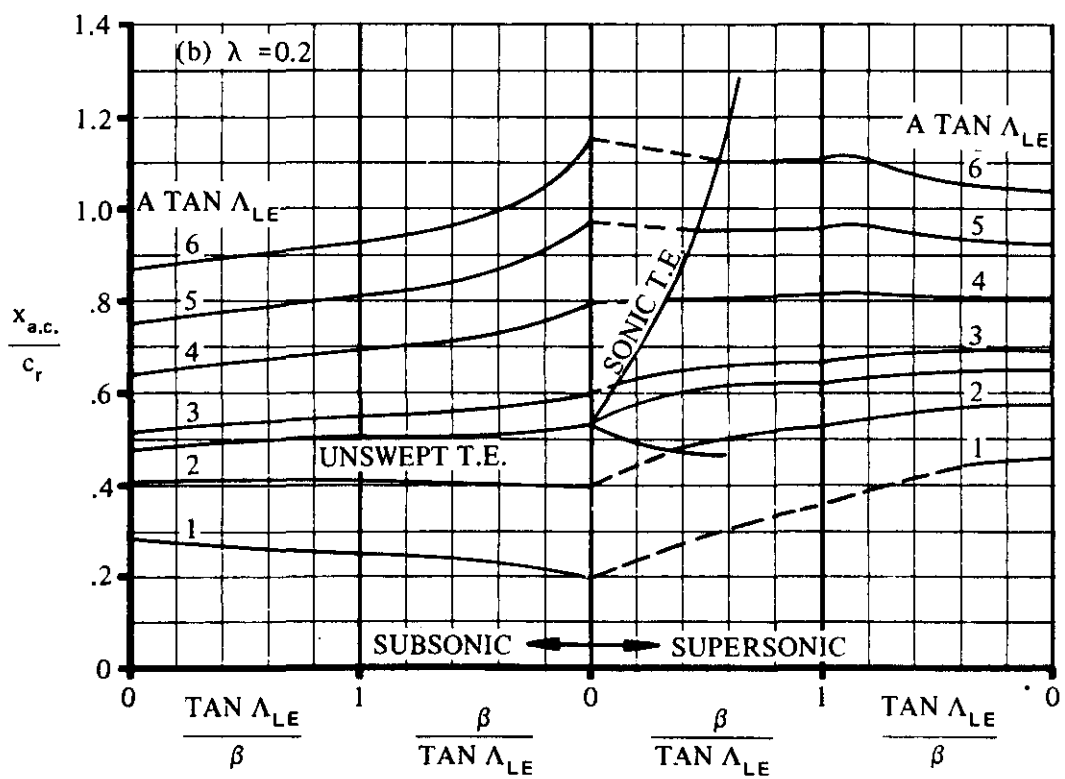
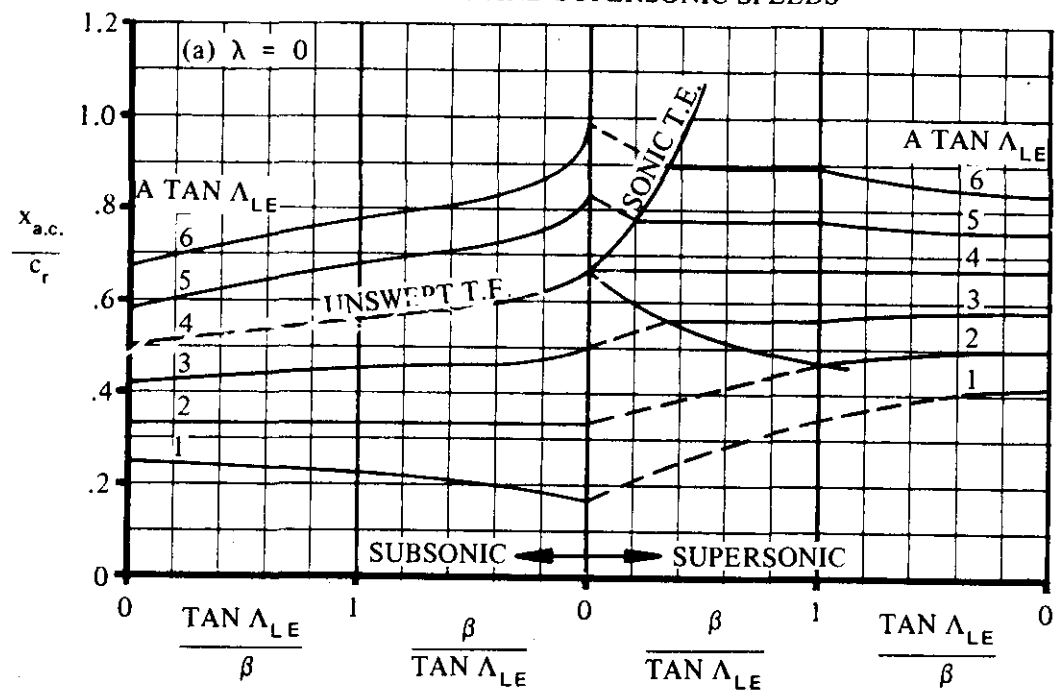


FIGURE 4.1.4.2-26 WING AERODYNAMIC-CENTER POSITION

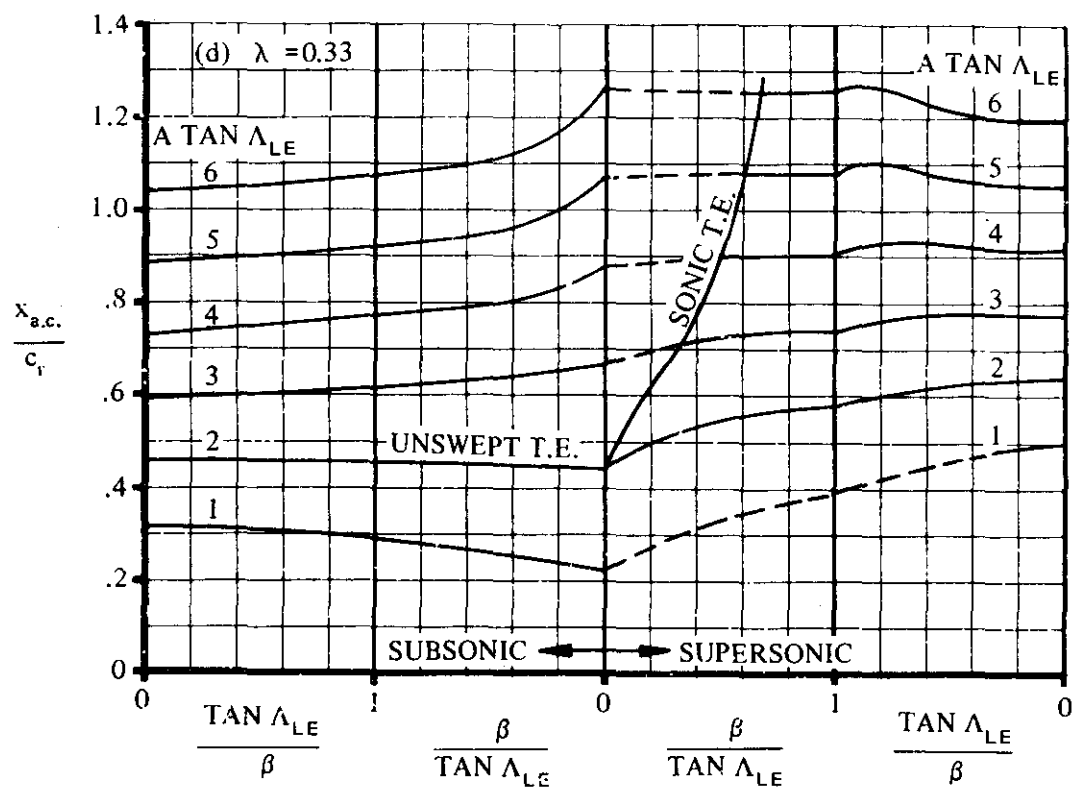
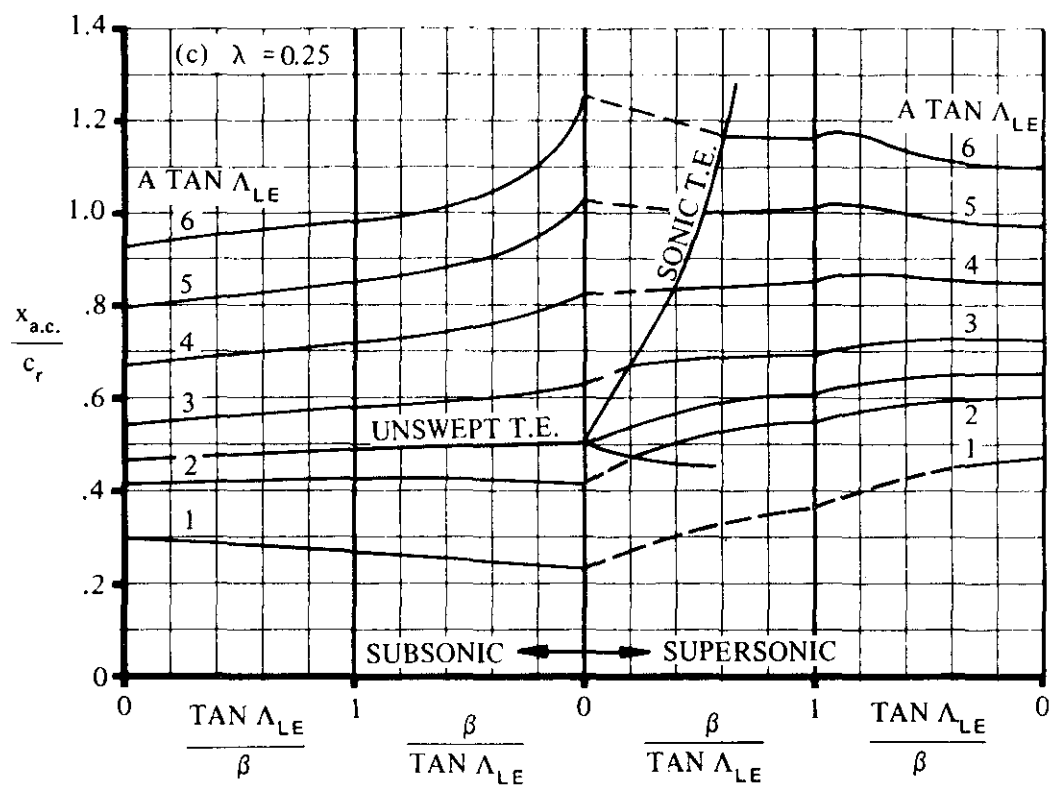


FIGURE 4.1.4.2-26(CONTD)

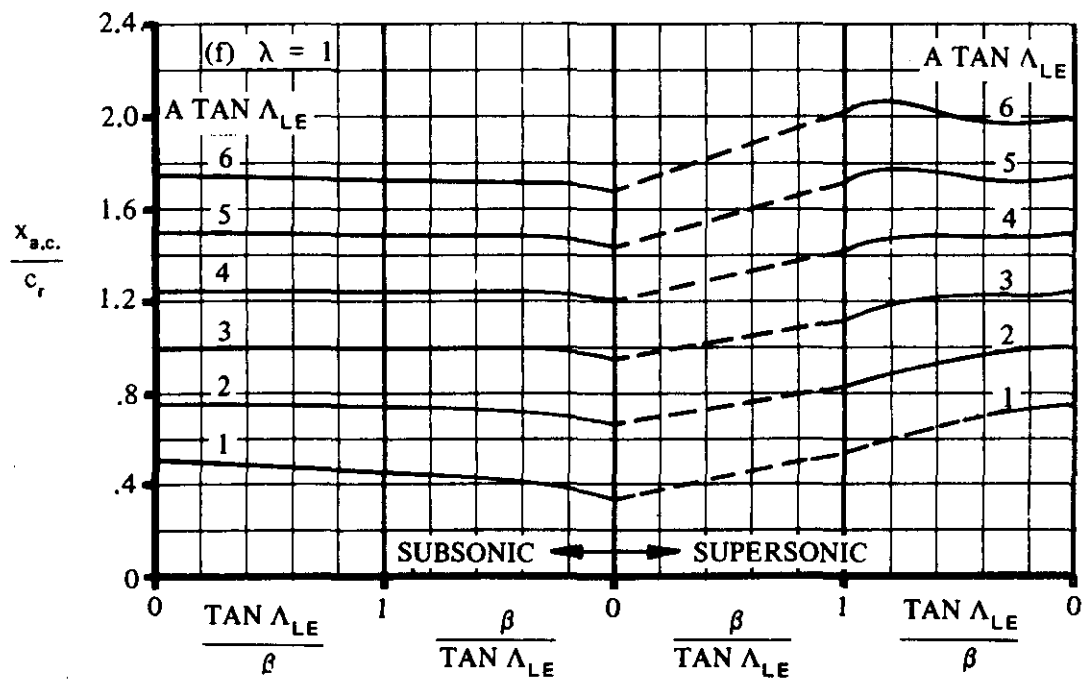
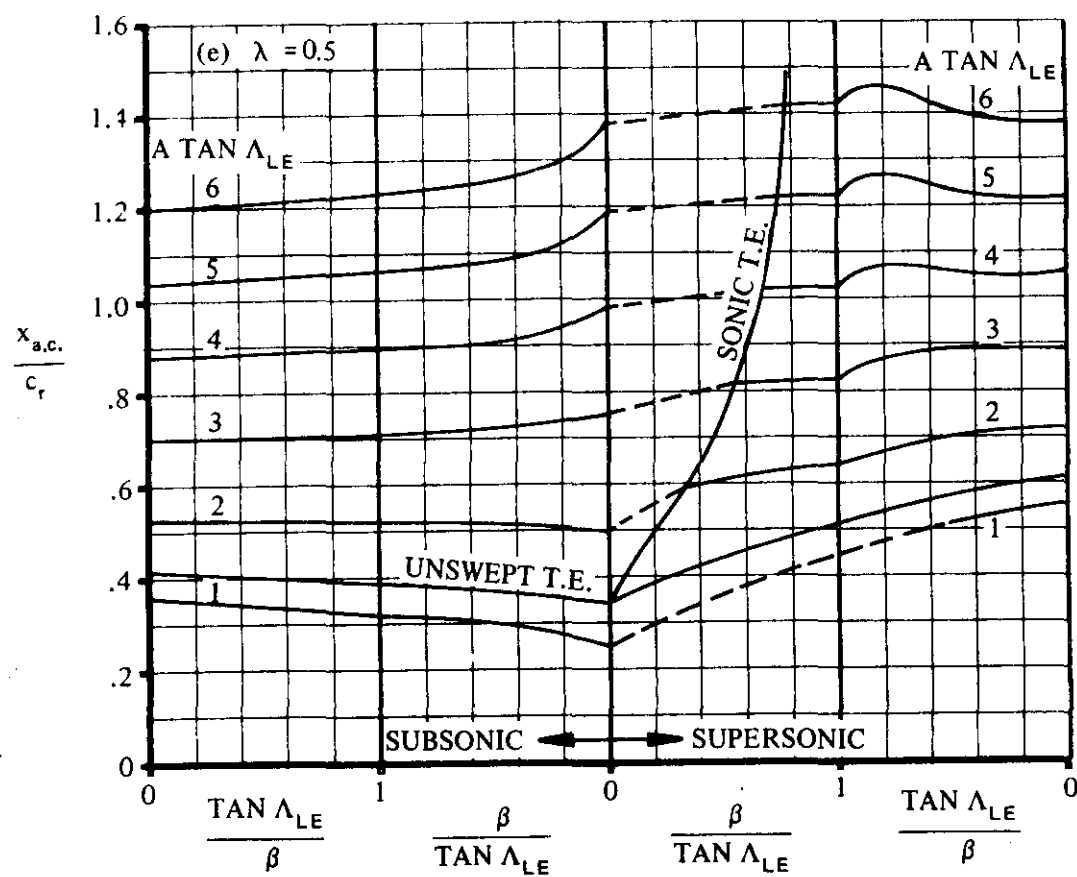


FIGURE 4.1.4.2-26 (CONTD)

SUBSONIC SPEEDS

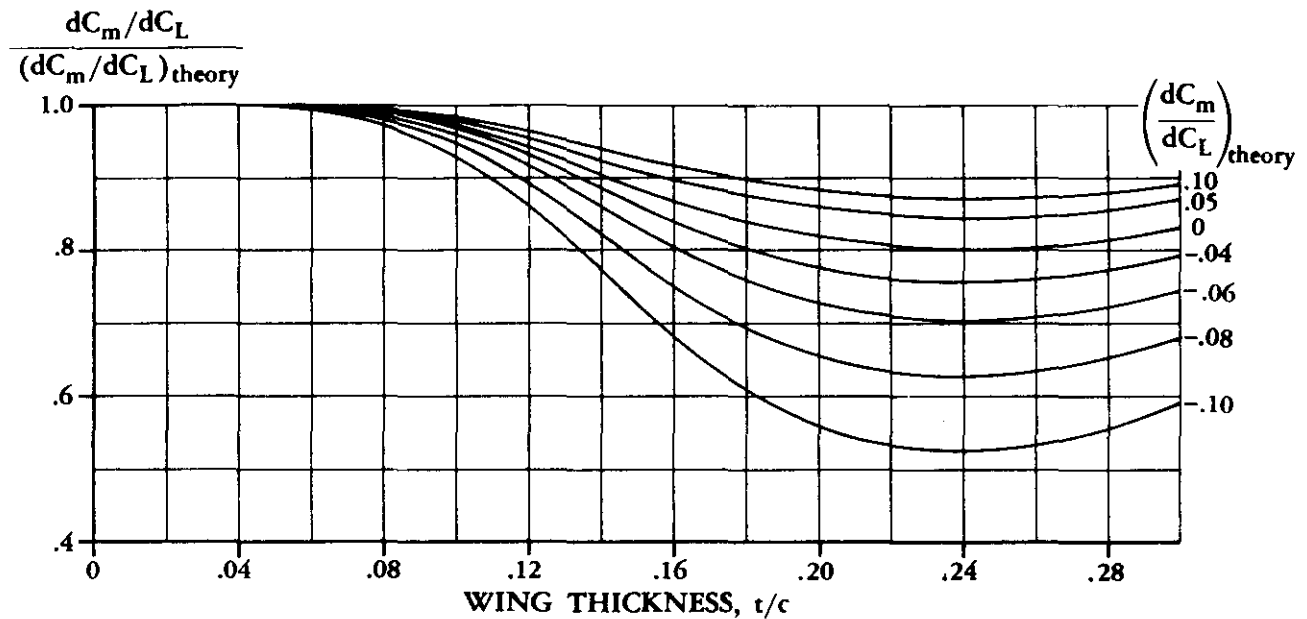


FIGURE 4.1.4.2-29 WING PITCHING-MOMENT-CURVE-SLOPE THICKNESS CORRECTION FACTOR

TRANSONIC SPEEDS

(a) $\lambda = 0$

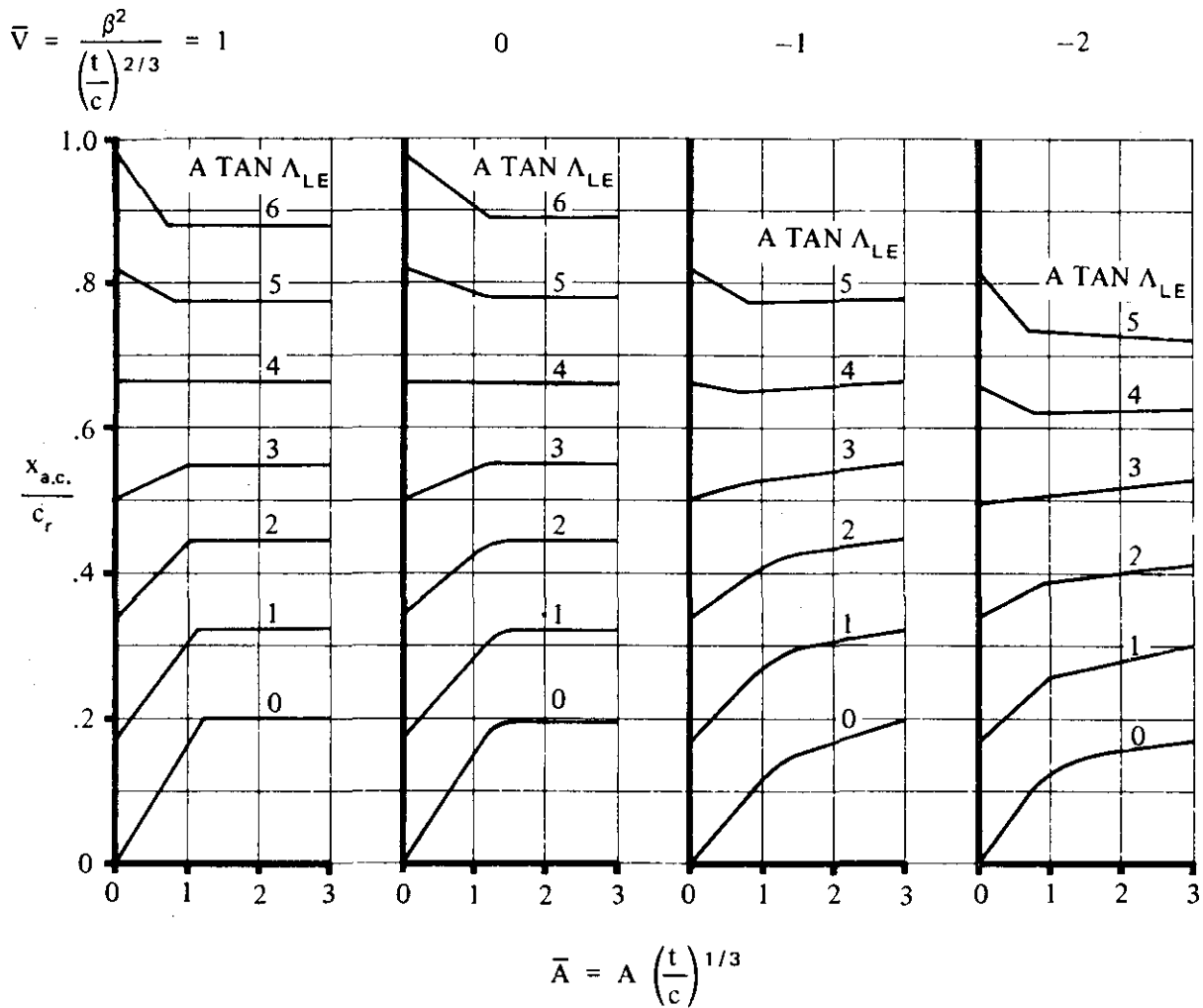


FIGURE 4.1.4.2-30 TRANSONIC WING AERODYNAMIC-CENTER LOCATION

TRANSONIC SPEEDS

(b) $\lambda = 0.2$

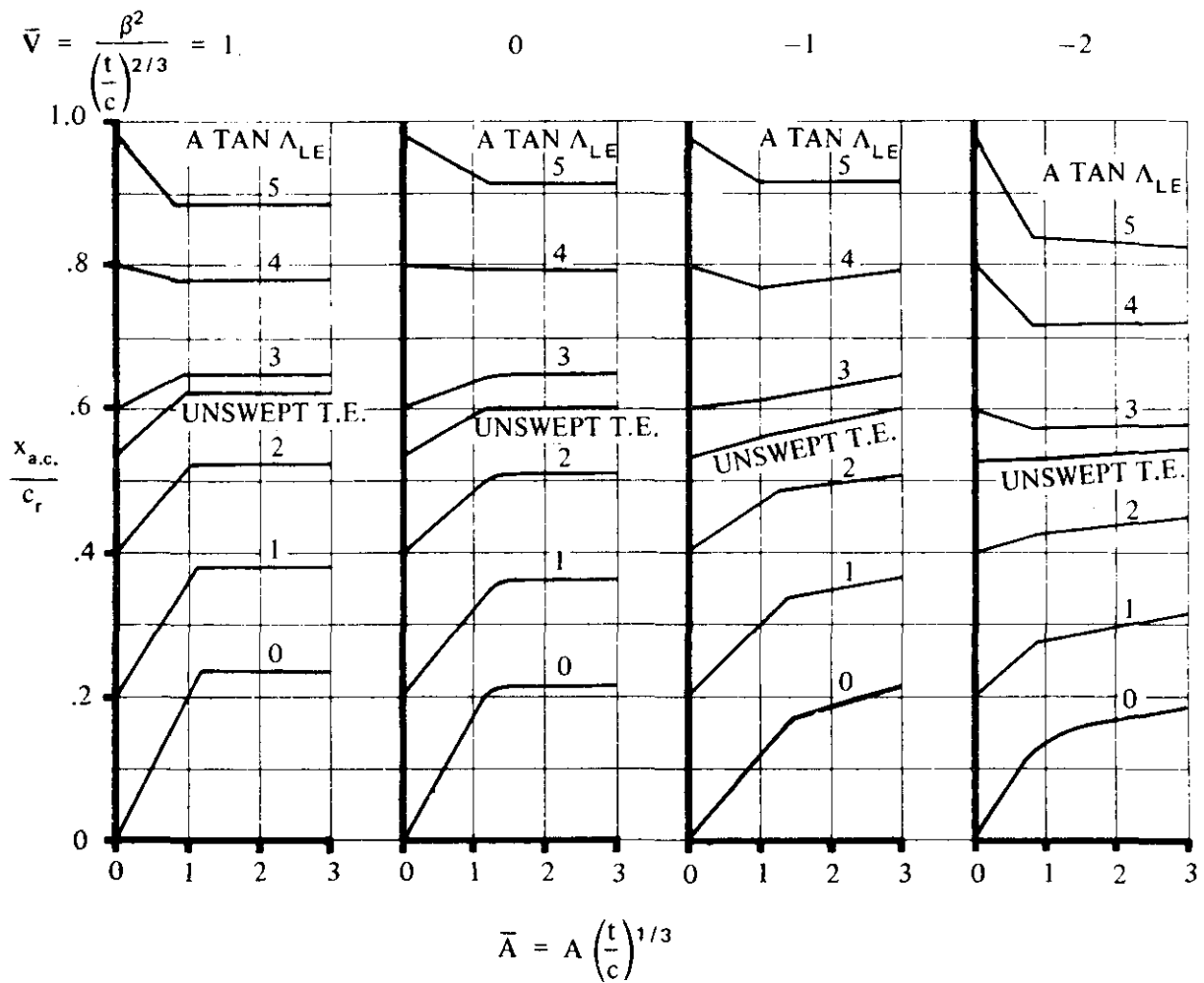


FIGURE 4.1.4.2-30 (CONTD)

TRANSONIC SPEEDS

(c) $\lambda = 0.5$

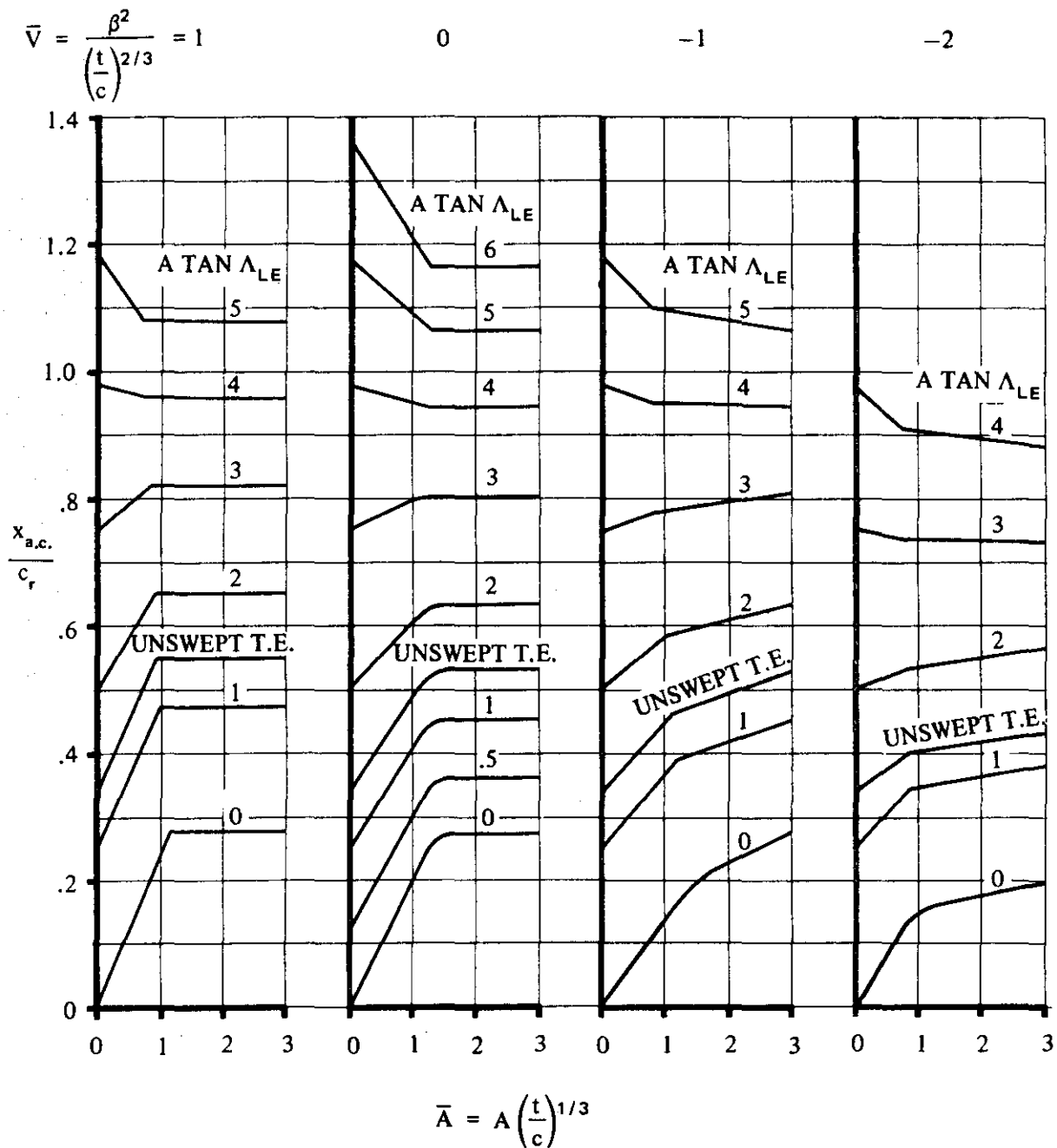


FIGURE 4.1.4.2-30 (CONTD)

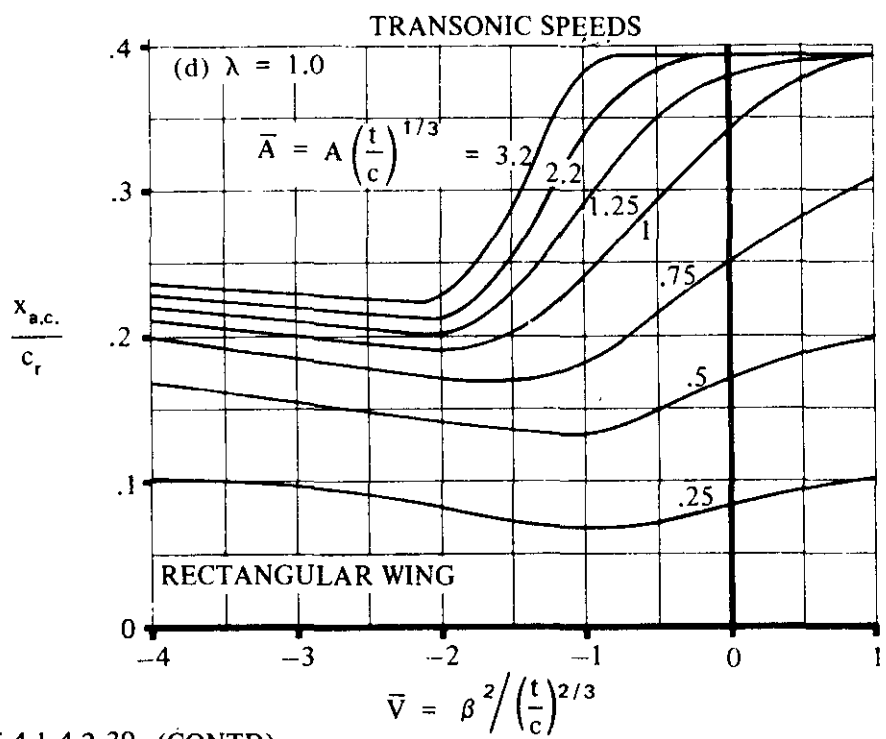


FIGURE 4.1.4.2-30 (CONTD)

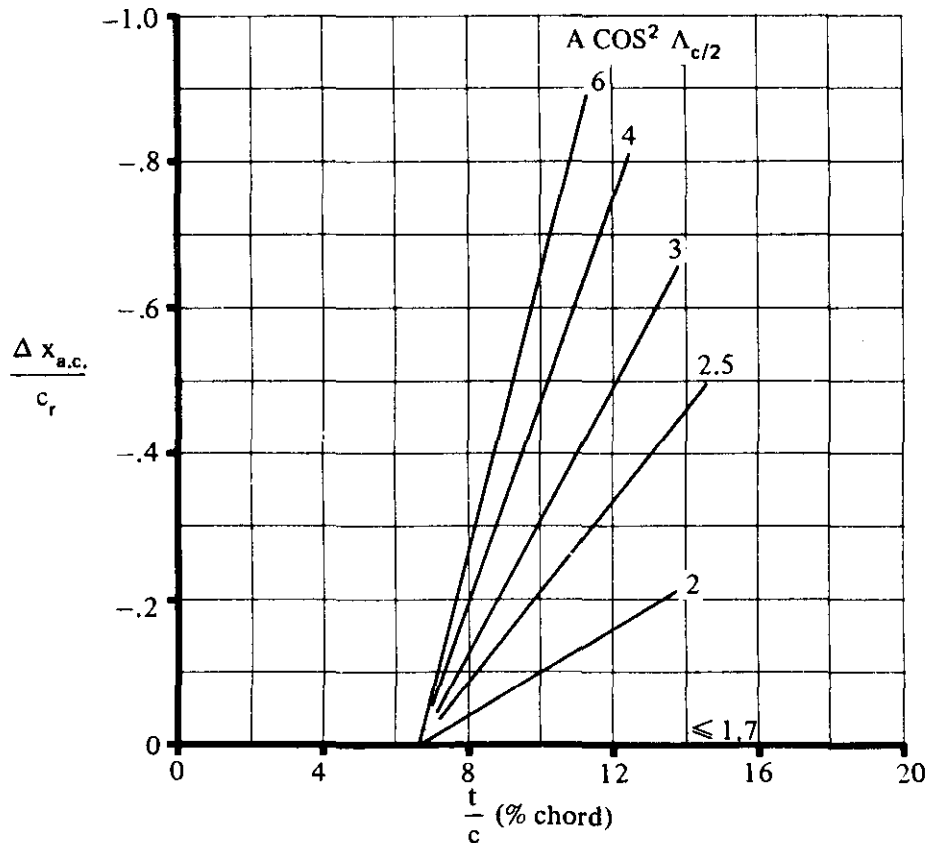


FIGURE 4.1.4.2-33 INCREMENTAL AERODYNAMIC-CENTER LOCATION ACCOUNTING FOR WING SEPARATION EFFECTS

4.1.4.3 WING PITCHING MOMENT IN THE NONLINEAR ANGLE-OF-ATTACK RANGE

Methods are presented herein for estimating the wing pitching-moment coefficient in the nonlinear angle-of-attack region. In the subsonic speed regime methods are presented for both straight-tapered and non-straight-tapered wings. No generalized methods are presented in the transonic or supersonic speed regimes. However, at supersonic speeds a discussion of pitching-moment characteristics is given for rectangular and triangular wings.

A. SUBSONIC

At subsonic speeds empirical methods are presented for predicting the pitching-moment characteristics of the following two classes of wing planforms:

Straight-Tapered Low-Aspect-Ratio Wings

Non-Straight-Tapered Wings (double-delta wings)

No method is presented for evaluating straight-tapered wings of high aspect ratios.* For high-aspect-ratio wings with low sweepback, the center-of-pressure location beyond the linear-lift range moves aft, tending toward the wing midchord at full stall. The magnitude and rate of this trend are variable, depending largely on the particular airfoil section. Insufficient data are available to predict, even from a qualitative standpoint, the pitching-moment characteristics of moderately swept high-aspect-ratio wings beyond the linear-lift range.

For thin, low-aspect-ratio wings there exist areas of flow separation, even at moderate angles of attack. Consequently, for these wings the pitching-moment curve has a tendency to become nonlinear at moderate angles of attack.

Two methods are presented for low-aspect-ratio straight-tapered wings. Method 1 is general and is applicable to most low-aspect-ratio planforms. Method 2 is more restrictive in that it is applicable only at $M = 0.2$ for highly swept, constant-section, low-aspect-ratio, delta or clipped-delta configurations with large thickness ratios; i.e., $0.10 \leq t/c \leq 0.30$. The unique feature of Method 2 is its consideration of the vortex-induced lift and its effect upon the pitching moment.

DATCOM METHODS

Straight-Tapered Wing

Method 1

The following empirical method is applicable to straight-tapered wings that satisfy the following relationship:

$$A \leq \frac{6}{(C_1 + 1) \cos \Lambda_{LE}}$$

*For the purposes of this section, high aspect-ratio wings are those for which $A > \frac{6}{(C_1 + 1) \cos \Lambda_{LE}}$, where C_1 is the empirical taper-ratio factor from Section 4.1.3.4.

where

A is the wing aspect ratio.

C_l is the empirical taper-ratio factor obtained from Figure 4.1.3.4-24b as a function of wing taper ratio.

Λ_{LE} is the sweepback angle of the wing leading edge.

The wing pitching-moment coefficient, based on the product of the wing area and wing MAC $S_w \bar{c}_w$, referred to the desired center-of-gravity location, is given by

$$C_m = \left(n - \frac{x_{c.p.}}{c_r} \right) \frac{c_r}{\bar{c}} C_N \quad 4.1.4.3-a$$

where

n is the chordwise distance in root chords from the wing apex to the desired center-of-gravity location, positive aft.

$\frac{c_r}{\bar{c}}$ is the ratio of the wing root chord to the wing mean aerodynamic chord.

C_N is the wing normal-force coefficient, based on the wing area. This parameter should be obtained from test data if available, or by using Equation 4.1.3-a, i.e.,

$$C_N = C_L \cos \alpha + C_D \sin \alpha$$

where

C_L is the wing lift coefficient from test data or from the methods of Sections 4.1.3.1, 4.1.3.2, and 4.1.3.3.

C_D is the wing drag coefficient from test data or from Sections 4.1.5.1 and 4.1.5.2.

α is the wing angle of attack.

It should be noted that in the absence of wing drag data, the normal force may be approximated (see Section 4.1.3.3) by

$$C_N = \frac{C_L}{\cos \alpha}$$

$\frac{x_{c.p.}}{c_r}$ is the wing center-of-pressure location, in wing root chords, measured positive aft from the wing apex. Because of the various relationships used to calculate $\frac{x_{c.p.}}{c_r}$ for angles of attack between 0 and 90°, the following step-by-step procedure is given to facilitate the calculation of $\frac{x_{c.p.}}{c_r}$ versus angle of attack.

- Step 1.** Calculate the center-of-pressure location at zero lift. The center-of-pressure location at zero lift may be approximated as the aerodynamic center of a wing with a symmetrical airfoil section, at zero angle of attack, which is given in Section 4.1.4.2 as a function of wing planform parameters.
- Step 2.** Calculate the center-of-pressure location at maximum lift by

$$\left(\frac{x_{c.p.}}{c_r} \right)_{C_L_{max}} = \left(\frac{x_{c.p.}}{c_r} \right)_1 + \Delta \left(\frac{x_{c.p.}}{c_r} \right)_2 \quad 4.1.4.3-b$$

where

$\left(\frac{x_{c.p.}}{c_r} \right)_1$ is obtained from Figure 4.1.4.3-21a as a function of Δy , the airfoil section leading-edge sharpness parameter. The value of Δy can be obtained from Figure 2.2.1-8.

$\Delta \left(\frac{x_{c.p.}}{c_r} \right)_2$ is obtained from Figures 4.1.4.3-21b and -22a as a function of wing taper ratio, aspect ratio, and leading-edge sweepback.

No specific Mach-number correction is included, because the experimental data show only small and inconsistent shifts up to $M \approx 0.6$.

Caution must be exercised when applying the method of this section to wings having large values of $(C_1 + 1) A \cos \Lambda_{LE}$. Configurations of this type show large forward shifts in center-of-pressure location with increasing lift coefficient. This forward shift is related to flow separation and local loss of lift aft of the area centroid. In situations where the forward shift in center of pressure takes place over a small range of lift coefficients, the phenomenon is known as pitch-up. Empirical charts have been developed to define approximate boundaries dividing configurations that show pitch-up from those that do not. One such chart is presented in Figure 4.1.4.3-25.

It is important to recognize that the pitch-up characteristics for any given wing can be strongly modified by wing twist and/or wing-leading-edge devices. An extensive summary of information on pitch-up control devices is given in Reference 1.

Because of their dependence on separation effects, pitch-up characteristics are also sensitive to Reynolds number. Lowering the Reynolds number aggravates pitch-up tendencies, and raising the Reynolds number suppresses them.

The charts for low-aspect-ratio wings apply to untwisted symmetrical-section wings at Reynolds numbers near 6×10^6 , based on the mean aerodynamic chord.

- Step 3.** Calculate the variation of center-of-pressure location between $\alpha = 0$ and
- $$\alpha = \tan^{-1} \left(\frac{\tan \alpha_{C_L_{max}}}{0.6} \right)$$

- a. Determine the stability index from Figure 4.1.4.3-22b as a function of the wing taper ratio, aspect ratio, and leading-edge sweepback.
- b. Determine the aspect-ratio index from Figure 4.1.4.3-24a as a function of wing taper ratio, aspect ratio, and leading-edge sweepback.
- c. Determine the values of $\Delta \left(\frac{x_{c.p.}}{c_r} \right)_3$ from Figure 4.1.4.3-23a or -23b as a function of the stability index and the ratio of $\frac{\tan \alpha}{\tan \alpha_{C_L \max}}$ or $\frac{\tan \alpha_{C_L \max}}{\tan \alpha}$, respectively. (The value of $\Delta \left(\frac{x_{c.p.}}{c_r} \right)_3$ at $\frac{\tan \alpha}{\tan \alpha_{C_L \max}} = 1$ is zero.)
- d. Determine the values of $\Delta \left(\frac{x_{c.p.}}{c_r} \right)_4$ from Figure 4.1.4.3-24b as a function of the aspect-ratio index and the ratio of $\frac{\tan \alpha}{\tan \alpha_{C_L \max}}$ or $\frac{\tan \alpha_{C_L \max}}{\tan \alpha}$. (The value of $\Delta \left(\frac{x_{c.p.}}{c_r} \right)_4$ at $\frac{\tan \alpha}{\tan \alpha_{C_L \max}} = 1$ is zero.)
- e. Determine the value of $\left(\frac{x_{c.p.}}{c_r} \right)_{ref}$ by

$$\left(\frac{x_{c.p.}}{c_r} \right)_{ref} = \frac{\left(\frac{x_{c.p.}}{c_r} \right)_{C_L \max}}{\sin \alpha_{C_L \max}} - \left(\frac{x_{c.p.}}{c_r} \right)_{C_L=0} \cot \alpha_{C_L \max} \quad 4.1.4.3-c$$

where

$$\left(\frac{x_{c.p.}}{c_r} \right)_{C_L \max} \quad \text{is obtained above in Step 2.}$$

$\alpha_{C_L \max}$ is the angle of attack at maximum lift obtained from Section 4.1.3.4.

$$\left(\frac{x_{c.p.}}{c_r} \right)_{C_L=0}$$

is the zero-lift center-of-pressure location from Step 1 above.

f. Using the above parameters determine the center-of-pressure location by

$$\frac{x_{c.p.}}{c_r} = \left(\frac{x_{c.p.}}{c_r} \right)_{C_L=0} \cos \alpha + \left[\left(\frac{x_{c.p.}}{c_r} \right)_{ref} + \Delta \left(\frac{x_{c.p.}}{c_r} \right)_3 + \Delta \left(\frac{x_{c.p.}}{c_r} \right)_4 \right] \sin \alpha \quad 4.1.4.3-d$$

Step 4. Calculate the center-of-pressure location at an angle of attack of 90° . This point is at the area centroid and is found by

$$\frac{x_{c.p.}}{c_r} = \frac{1}{3} \left(\lambda + \sigma + \frac{1 + \sigma\lambda}{1 + \lambda} \right) \quad 4.1.4.3-e$$

where

$$\sigma = \frac{1}{4} A (1 + \lambda) \tan \Lambda_{LE} \quad 4.1.4.3-f$$

where

A is the wing aspect ratio.

λ is the wing taper ratio.

Λ_{LE} is the sweepback angle of the wing leading edge.

Step 5. Calculate the center-of-pressure location between $\alpha = \tan^{-1} \left(\frac{\tan \alpha_{C_L \max}}{0.6} \right)$ and $\alpha = 90^\circ$ by assuming a linear variation of $\frac{x_{c.p.}}{c_r}$. (The center-of-pressure locations corresponding to $\alpha = \tan^{-1} \left(\frac{\tan \alpha_{C_L \max}}{0.6} \right)$ and $\alpha = 90^\circ$ are obtained from Steps 3 and 4, respectively.)

A comparison of test data with wing center-of-pressure locations computed by the use of the above procedure is shown in Table 4.1.4.3-A.

Method 2

This semiempirical method is taken from Reference 2, ignoring the small wing-planform nose-radius effects. The semiempirical method was developed by using the test results of Reference 2,

correlated with the theoretical predictions based on lifting-surface theory. Because of its semiempirical nature, the method should be restricted to $M = 0.2$ conditions for highly swept, constant-section, low-aspect-ratio, delta or clipped-delta configurations with the following geometric characteristics:

$$0.58 \leq A \leq 2.55$$

$$0 \leq \lambda \leq 0.3$$

$$63^\circ \leq \Lambda_{LE} \leq 80^\circ$$

$$0.10 \leq t/c \leq 0.30$$

$$\Lambda_{TE} = 0$$

For round-nosed-planform configurations the reader is referred to Reference 2, where three different planform-nose-radius models were tested. No incremental nose-planform effects are presented here because of their probable configuration dependence.

This method essentially accounts for the effect of leading-edge vortex-induced lift upon the pitching moment. For details regarding the leading-edge vortex-induced-lift increments, the reader is referred to Method 2 for straight-tapered planforms in Paragraph A of Section 4.1.3.2.

The nonlinear pitching-moment characteristics, taken about the midpoint of the wing root chord and based on the product of the wing area and root chord $S_w c_r$, for a given angle of attack, are estimated by

$$C_m = \left(\frac{dC_m}{dC_L} \right) C_{L_{basic}} + C_{m_0} + \Delta C_m \quad 4.1.4.3-g$$

where

$\frac{dC_m}{dC_L}$ is the pitching-moment-curve slope from Method 2 of Paragraph A of Section 4.1.4.2, taken about the root-chord midpoint.

$C_{L_{basic}}$ is the basic wing lift excluding any leading-edge vortex-induced effects, at the particular angle of attack. This value must come from constructing the lift curve using Section 4.1.3.1 for the determination of α_0 , and Method 2 of Paragraph A of Section 4.1.3.2 for the determination of $(C_{L_\alpha})_{basic}$.

C_{m_0} is the wing zero-lift pitching moment obtained from Method 2 of Paragraph A of Section 4.1.4.1.

ΔC_m is the pitching-moment increment about the root-chord midpoint due to the leading-edge vortex. This parameter is evaluated at the particular angle of attack using

$$\Delta C_m = \frac{-0.367 \Delta C_L}{(1 + \cos^2 \Lambda_{LE})(1 + \lambda^2) \cos(\alpha + \bar{\theta})}$$

4.1.4.3-h

where

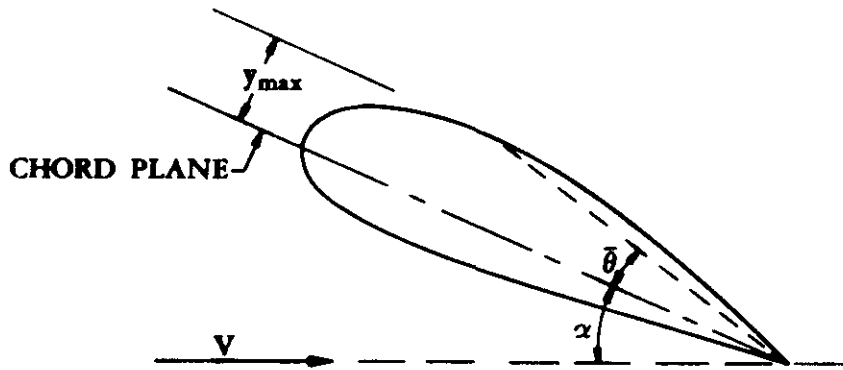
ΔC_L is the lift increment due to the leading-edge vortex at the particular angle of attack (see Sketch (b) in Section 4.1.3.2). This value is obtained using Method 2 of Section 4.1.3.2.

Λ_{LE} is the wing leading-edge sweep.

λ is the wing taper ratio.

α is the wing angle of attack.

$\bar{\theta}$ is the angle between the airfoil chord line and a line connecting the airfoil trailing edge to the airfoil maximum upper-surface ordinate (see Sketch (a)).



SKETCH (a)

No substantiation of this method is possible because of the lack of low-aspect-ratio test data having wing thickness ratios of $0.10 \leq t/c \leq 0.30$.

Non-Straight-Tapered Wings (Double Delta)

The empirical method (taken from Reference 3) presented herein is applicable only to double-delta wings. This method should be applied with caution because it is based on a limited amount of test data. The test data used in the formulation of the method were obtained for double-delta planforms having the following geometric limitations:

$$60^\circ \leq \Lambda_{LE_i} \leq 83^\circ$$

$$38^\circ \leq \Lambda_{LE_o} \leq 60^\circ$$

$$0.2 \leq \eta_B \leq 0.7$$

The majority of the test data used in the method formulation are wing-body test data, where the body effects have been ignored. The use of wing-body data can be justified because the data exhibit large values for the ratio of wing span to body diameter and because of the scarcity of wing-alone double-delta test data.

For a double-delta wing, the pitching-moment coefficient, based on the product of wing area and wing MAC, referred to the desired reference-center location, is given by

$$C_m = C_{m_0} + C_L \left(n - K_m \frac{x_{a.c.}}{c_r} \right) \frac{c_r}{\bar{c}} \quad 4.1.4.3-i$$

where

C_{m_0} is the zero-lift wing pitching-moment coefficient obtained from test data on a similar configuration or from Section 4.1.4.1.

C_L is the wing lift coefficient obtained from test data or from Sections 4.1.3.1, 4.1.3.2 and 4.1.3.3.

n is the chordwise distance in root chords from the wing apex to the desired reference-center location, positive aft.

K_m is the empirical nonlinear pitching-moment factor, obtained from Figures 4.1.4.3-26a through -26f as a function of angle of attack, Mach number, and wing leading-edge sweepback.

$\frac{x_{a.c.}}{c_r}$ is the distance from the wing apex to the aerodynamic center measured in root chords, positive aft. This parameter is obtained from test data or from the double-delta-wing method of Section 4.1.4.2.

$\frac{c_r}{\bar{c}}$ is the ratio of the root chord to the wing mean aerodynamic chord.

No substantiation table of this method is presented, because all available test data were used in the method formulation. However, a sample problem is presented to illustrate the method.

Sample Problems

1. Method 1

Given: Conventional, straight-tapered wing of Reference 4.

$A = 3.0$ $\lambda = 0.143$ NACA 65A003 airfoil

$\Lambda_{LE} = 51.3^\circ$ $M = 0.6$ $C_{L_{max}} = 0.94$ $\alpha_{C_{L_{max}}} = 22^\circ$

$\bar{c} = 0.240$ ft $c_r = 0.353$ ft $n = 0.572$

α (deg)	C_L	C_D
0	0	0.006
8	0.48	0.070
12	0.68	0.145
14	0.76	0.192
16	0.82	0.237
18	0.88	0.300
20	0.92	0.340
22	0.94	0.385
28	0.88	0.475

The variations of C_L and C_D with α , $C_{L_{max}}$, and $\alpha_{C_{L_{max}}}$ have been taken from the test data of Reference 2 to facilitate the calculations.

Compute:

$$\text{Determine if the straight-taper-wing method is applicable; i.e., if } A \leq \frac{6}{(C_1 + 1) \cos \Lambda_{LE}}.$$

$$C_1 = 0.36 \quad (\text{Figure 4.1.3.4-24b})$$

$$A \leq \frac{6}{(1.36)(0.6252)}$$

$$\leq 7.06$$

The aspect ratio of this configuration is 3.0; therefore, the method is applicable to this particular configuration.

Determine the normal-force coefficient using Equation 4.1.3-a, i.e.,

$$C_N = C_L \cos \alpha + C_D \sin \alpha$$

α	C_L	$\cos \alpha$	C_D	$\sin \alpha$	C_N
0	0	1.0	0.006	0	0
8	0.48	0.9903	0.070	0.1392	0.485
12	0.68	0.9781	0.145	0.2079	0.695
14	0.76	0.9703	0.192	0.2419	0.784
16	0.82	0.9613	0.237	0.2756	0.854
18	0.88	0.9511	0.300	0.3090	0.930
20	0.92	0.9397	0.340	0.3420	0.981
22	0.94	0.9272	0.385	0.3746	1.016
28	0.88	0.8829	0.475	0.4695	1.000

Determine the center-of-pressure location at zero lift

$$A \tan \Lambda_{LE} = (3.0)(1.2482) = 3.7446$$

$$\beta = \sqrt{1 - M^2}$$

$$= \sqrt{1 - 0.36}$$

$$= 0.80$$

$$\frac{\beta}{\tan \Lambda_{LE}} = \frac{0.80}{1.2482} = 0.641$$

$$\left(\frac{x_{a.c.}}{c_r} \right)_{C_L=0} = 0.635 \quad (\text{Figure 4.1.4.2-26, interpolated})$$

$$\left(\frac{x_{c.p.}}{c_r} \right)_{C_L=0} \cong 0.635$$

Determine the center-of-pressure location at maximum lift

$$\Delta y = 0.6 \quad (\text{Figure 2.2.1-8})$$

$$\left(\frac{x_{c.p.}}{c_r} \right)_1 = 0.55 \quad (\text{Figure 4.1.4.3-21a})$$

$$C_3 = 0.28 \quad (\text{Figure 4.1.4.3-21b})$$

$$(C_3 + 1) A \tan \Lambda_{LE} = (1.28)(3.0)(1.2482) = 4.78$$

$$\Delta \left(\frac{x_{c.p.}}{c_r} \right)_2 = 0.045 \quad (\text{Figure 4.1.4.3-22a})$$

$$\left(\frac{x_{c.p.}}{c_r} \right)_{C_{L_{max}}} = \left(\frac{x_{c.p.}}{c_r} \right)_1 + \Delta \left(\frac{x_{c.p.}}{c_r} \right)_2 \quad (\text{Equation 4.1.4.3-b})$$

$$= 0.55 + 0.045$$

$$= 0.595$$

Determine the variation of the center-of-pressure location between $\alpha = 0$ and

$$\alpha = \tan^{-1} \left(\frac{\tan \alpha_{C_L \max}}{0.6} \right)$$

$$\alpha = \tan^{-1} \left(\frac{\tan \alpha_{C_L \max}}{0.6} \right)$$

$$= \tan^{-1} \left(\frac{0.4040}{0.6} \right)$$

$$= 33.95^\circ$$

Stability Index = 1.2 (Figure 4.1.4.3-22b)

$$A \cos \Lambda_{LE} = (3.0)(0.6252) = 1.8756$$

Aspect-Ratio Index = 0.17 (Figure 4.1.4.3-24a)

α	$\frac{\tan \alpha}{\tan \alpha_{C_L \max}}$	$\Delta \left(\frac{x_{c.p.}}{c_r} \right)_3$ Fig. 4.1.4.3-23a	$\Delta \left(\frac{x_{c.p.}}{c_r} \right)_4$ Fig. 4.1.4.3-24b
8	0.348	-0.20	0.058
12	0.526	-0.12	-0.02
14	0.617	-0.07	-0.04
16	0.710	-0.03	-0.05
18	0.804	0.02	-0.06
20	0.901	0.01	-0.03
22	1.0	0	0
28	0.76*	-0.09**	0.15

$$\left(\frac{x_{c.p.}}{c_r} \right)_{ref} = \left(\frac{x_{c.p.}}{c_r} \right)_{C_L \max} - \left(\frac{x_{c.p.}}{c_r} \right)_{C_L=0} \cot \alpha_{C_L \max} \quad (\text{Equation 4.1.4.3-c})$$

$$= \frac{0.595}{0.3746} - 0.635 (2.475)$$

$$= 0.0168$$

*This value is the reciprocal, i.e., $\frac{\tan \alpha_{C_L \max}}{\tan \alpha} = 0.76$.

**From Figure 4.1.4.3-23b.

$$\frac{x_{c.p.}}{c_r} = \left(\frac{x_{c.p.}}{c_r} \right)_{C_L=0} \cos \alpha + \left[\left(\frac{x_{c.p.}}{c_r} \right)_{ref} + \Delta \left(\frac{x_{c.p.}}{c_r} \right)_3 + \Delta \left(\frac{x_{c.p.}}{c_r} \right)_4 \right] \sin \alpha$$

(Equation 4.1.4.3-d)

α	$\cos \alpha$	$\sin \alpha$	$\frac{x_{c.p.}}{c_r}$ (Eq. 4.1.4.3-d)
0	1.0	0	0.635
8	0.9903	0.1392	0.611
12	0.9781	0.2079	0.595
14	0.9703	0.2419	0.594
16	0.9613	0.2756	0.593
18	0.9511	0.3090	0.597
20	0.9397	0.3420	0.596
22	0.9272	0.3746	0.595
28	0.8829	0.4695	0.597

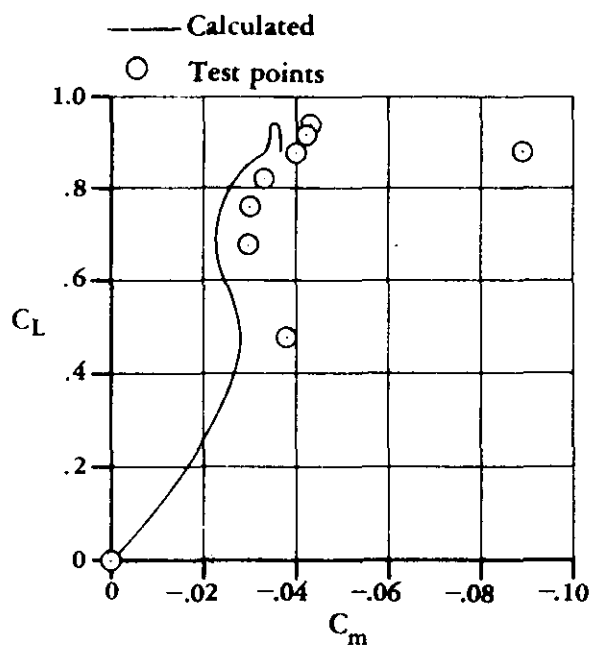
Solution:

$$C_m = \left(n - \frac{x_{c.p.}}{c_r} \right) \frac{c_r}{c} C_N \quad (\text{Equation 4.1.4.3-a})$$

$$= \left(0.572 - \frac{x_{c.p.}}{c_r} \right) \frac{0.353}{0.24} C_N$$

α (deg)	C_N	C_m
0	0	0
8	0.485	-0.0278
12	0.695	-0.0235
14	0.784	-0.0254
16	0.854	-0.0264
18	0.930	-0.0342
20	0.981	-0.0346
22	1.016	-0.0344
28	1.000	-0.0368

The calculated values are compared with test values from Reference 4 in Sketch (b).



SKETCH (b)

2. Method 2

Given: The following constant-section, low-aspect-ratio, clipped-delta configuration at $\alpha = 20^\circ$.

$$A = 0.823 \quad \lambda = 0.18 \quad \Delta_{LE} = 73.5^\circ \quad \text{NACA 2412 airfoil}$$

$$M = 0.2 \quad \theta = 0 \quad \bar{\theta} = 6.80^\circ$$

$$(C_{L\alpha})_{\text{basic}} = 0.0205 \text{ per deg}$$

$$C_{L\alpha_{II}} = 0.0272 \text{ per deg}$$

$$C_{L\alpha_{III}} = 0.0325 \text{ per deg}$$

$$C_{L_{II}} = 0.222$$

$$C_{L_{III}} = 0.467$$

$$C_{m_0} = -0.0091 \quad (\text{Sample Problem 2 Section 4.1.4.1})$$

$$\frac{dC_m}{dC_L} = -0.0252 \quad (\text{Sample Problem 1 Section 4.1.4.2})$$

{ Sample Problem 1 Method 2

Paragraph A Section 4.1.3.2)

Compute:

Determine α_0 using Section 4.1.3.1

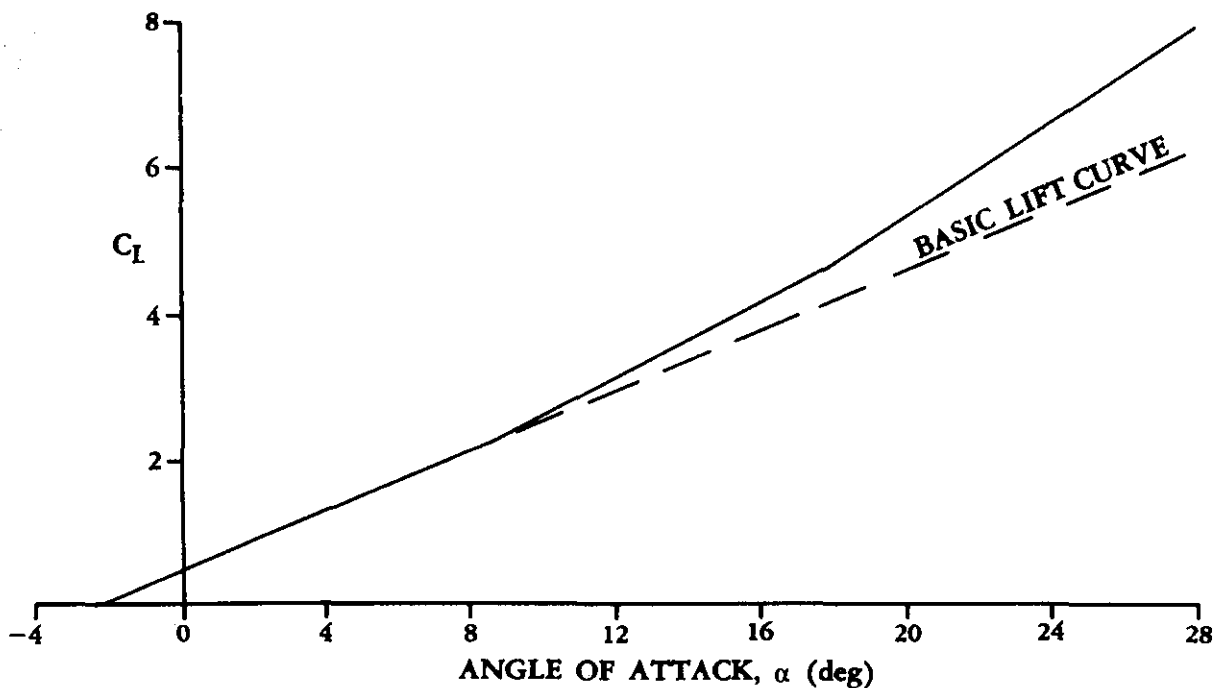
$$(\alpha_0)_{\theta=0} = \alpha_i - \frac{c_{q_i}}{c_{q_\alpha}} \quad (\text{Equation 4.1.3.1-a})$$

$$\left. \begin{array}{l} \alpha_i = 0.247 \\ c_{q_i} = 0.253 \end{array} \right\} \quad (\text{Table 4.1.1-D})$$

$$c_{q_\alpha} = 0.105 \text{ per deg} \quad (\text{Table 4.1.1-A})$$

$$\begin{aligned} (\alpha_0)_{\theta=0} &= 0.247 - \frac{0.253}{0.105} \\ &= -2.16^\circ \end{aligned}$$

Now the complete lift curve can be constructed.



From the constructed lift curve

$$\left. \begin{array}{l} \Delta C_L = 0.088 \\ C_{L_{\text{basic}}} = 0.449 \end{array} \right\} \quad \text{at } \alpha = 20^\circ$$

$$\Delta C_m = \frac{-0.367 \Delta C_L}{(1 + \cos^2 A_{LE})(1 + \lambda^2) \cos(\alpha + \theta)} \quad (\text{Equation 4.1.4.3-h})$$

$$= \frac{(-0.367)(0.088)}{(1 + 0.0806)(1 + 0.0324)(0.8926)}$$

$$= -0.0324$$

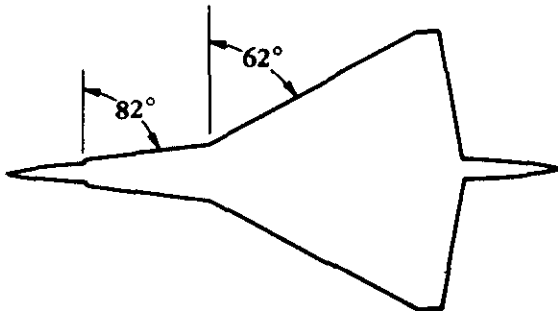
$$C_m = \left(\frac{dC_m}{dC_L} \right) C_{L_{\text{basic}}} + C_{m_0} + \Delta C_m \quad (\text{Equation 4.1.4.3-g})$$

$$= (-0.0243)(0.449) - 0.0091 - 0.0324$$

$$= -0.0524 \left(\text{based on } S_w c_r, \text{ about } \frac{c_r}{2} \right)$$

3. Double-Delta Wing

Given: The double-delta planform of Reference 5.



$$A = 1.66$$

$$\bar{c} = 21.68 \text{ ft}$$

$$S = 505.9 \text{ ft}^2$$

$$M = 0.15$$

$$(C_{m_0})_{WB} = 0.016$$

$$\frac{x_{a.c.}}{\bar{c}} = 1.125$$

$$n \left(\frac{c_r}{\bar{c}} \right) = 1.04$$

α (deg)	C_L
0	-0.06
4	0.10
8	0.29
12	0.51
16	0.74
20	0.96

Compute:

$$\beta = \sqrt{1 - M^2} = \sqrt{1 - 0.0225} = 0.989$$

$$\tan \Lambda_{LE_i} = \tan 82^\circ = 7.115$$

$$\frac{\beta}{\tan \Lambda_{LE_i}} = \frac{0.989}{7.115} = 0.139$$

Solution:

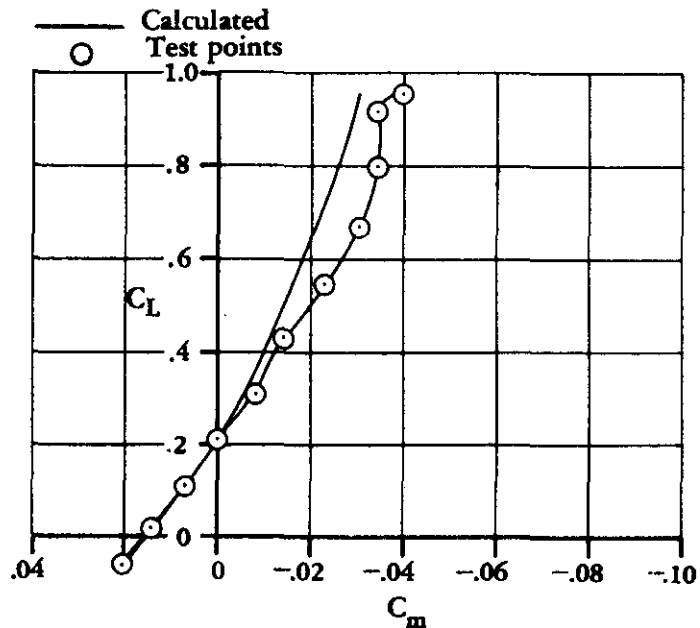
$$C_m = C_{m_0} + C_L \left(n - K_m \frac{x_{a.c.}}{c_r} \right) \frac{c_r}{\bar{c}}$$

$$= C_{m_0} + C_L \left(n \frac{c_r}{\bar{c}} - K_m \frac{x_{a.c.}}{\bar{c}} \right)$$

$$= 0.016 + C_L (1.04 - 1.125 K_m)$$

α (deg)	K_m (Figures 4.1.4.3-26a) through -26f)	C_m
0	1.0	0.021
4	0.995	0.008
8	0.985	-0.004
12	0.974	-0.013
16	0.971	-0.023
20	0.967	-0.030

The calculated values are compared with test values from Reference 5 in Sketch (c).



SKETCH (c)

B. TRANSONIC

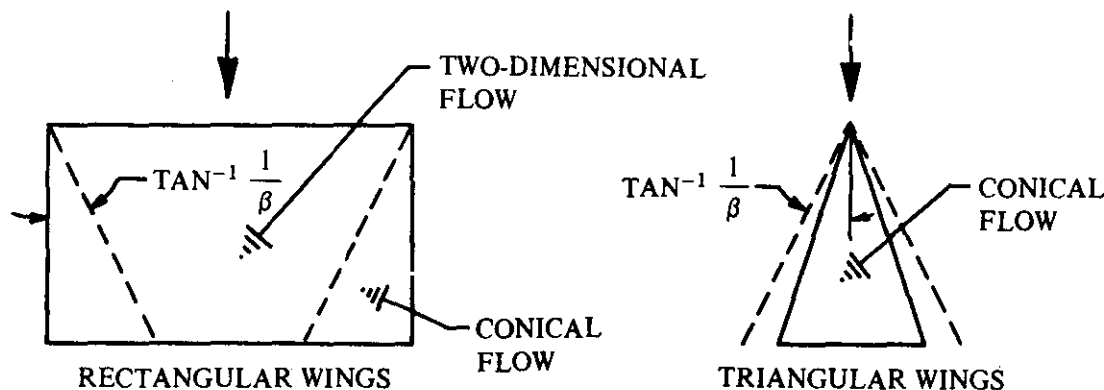
No generalized handbook method for estimating transonic values of the wing pitching-moment coefficient in the nonlinear angle-of-attack region is available in the literature. For double-delta planforms it is suggested that the method presented in Paragraph A of this section for double-delta planforms be applied with caution.

C. SUPERSONIC

No general method exists for predicting the supersonic pitching moments for wings at high angles of attack. For this reason no charts on this subject are presented in this section. However, a discussion of two particular types of configuration may provide some guides. The two configurations discussed are rectangular and triangular planforms.

Rectangular Wings

For rectangular wings in supersonic flow at low angles of attack there are two principal flow regimes — flow within the influence of the tip shock waves and flow at the center section. Flow within the influence of the tip shock waves is essentially conical in nature, and flow at the wing center section is two dimensional.



For the wing center section, then, two-dimensional pitching-moment characteristics apply. These are summarized in Section 4.1.2.2.

The effect of the tip influence on the three-dimensional wing is to force the center-of-pressure location forward.

The pitching-moment characteristics of rectangular wings in supersonic flow may be summarized as follows:

1. At low angles of attack the center-of-pressure location moves aft with increasing angle of attack, according to two-dimensional theory.
2. For situations where the tip influence is large compared to that of the two-dimensional region, the center-of-pressure location moves forward with increasing angle of attack. Trailing-edge separation on the wing center section also produces this effect.

3. For angles of attack beyond that at which the wing leading-edge shock detaches, the center-of-pressure location moves aft with increasing angle of attack. At an angle of attack of 90° the wing center-of-pressure location is at the area centroid.

These variations of the center-of-pressure location with angle of attack are illustrated experimentally in the data of Reference 13.

Triangular Wings

For triangular wings the flow is conical over the entire wing. Two conditions apply — subsonic leading edges and supersonic leading edges.

Triangular Wing with Subsonic Leading Edges

When the triangular wing has leading edges swept well within the Mach cone, slender-body theory applies. Slender-body theory makes no distinction between subsonic and supersonic speeds; therefore, the supersonic triangular-wing characteristics should be very similar to the subsonic triangular-wing characteristics. This is, in fact, the case and supersonic triangular wings with subsonic leading edges show a slight forward shift in center-of-pressure location with angle of attack that is remarkably similar to the subsonic shift. An illustration of this similarity is provided by a comparison of the supersonic data of Reference 14 with calculated subsonic characteristics of the same wing.

Triangular Wings with Supersonic Leading Edges

For triangular wings with supersonic leading edges, the center-of-pressure location changes very little with angle of attack. This is to be expected, since the aerodynamic-center location at zero angle of attack is at the area centroid, which is also the center-of-pressure location at an angle of attack of 90 degrees. Because shock waves separate from the leading edges of triangular wings at relatively low angles of attack (a result of sweep effects; see Section 4.1.3.3), the center of pressure will never be far from the area centroid. Reference 15 gives the center-of-pressure variation of a delta wing with supersonic leading edges.

REFERENCES

1. Furlong, G. C., and McHugh, J. G.: A Summary and Analysis of the Low-Speed Longitudinal Characteristics of Swept Wings at High Reynolds Numbers. NACA TR 1339, 1957. (U)
2. Crosthwait, E. L., and Seath, D. D.: Subsonic Characteristics of Low Aspect Ratios. FDL-TDR-64-103, 1965. (U)
3. Benepe, D. B., Kouri, B. G., Webb, J. B., et al: Aerodynamic Characteristics of Non-Straight-Taper Wings. AFFDL-TR-66-73, 1966. (U)
4. Faw, A. G., Jr., and Fournier, P. G.: Effects of Sweep and Thickness on the Static Longitudinal Aerodynamic Characteristics of a Series of Thin, Low-Aspect-Ratio, Highly Tapered Wings at Transonic Speeds. Transonic-Bump Method. NACA PM L54B25, 1954. (U)
5. Corsiglia, V. R., Koenig, D. G., and Morelli, J. P.: Large-Scale Tests of an Airplane Model with a Double-Delta Wing, Including Longitudinal and Lateral Characteristics and Ground Effects. NASA TN D-5102, 1969. (U)
6. McCormack, G. M., and Walling, W. C.: Aerodynamic Study of a Wing-Fuselage Combination Employing a Wing Swept Back 63° — Investigation of a Large-Scale Model at Low Speed. NACA RM A8D02, 1949. (U)
7. Nelson, W. H., Allen, E. C., and Krumm, W. J.: The Transonic Characteristics of 36 Symmetrical Wings of Varying Taper, Aspect Ratio, and Thickness as Determined by the Transonic-Bump Technique. NACA TN 3529, 1955. (U)

8. Nelson, W. H., and McDevitt, J. B.: The Transonic Characteristics of 22 Rectangular, Symmetrical Wing Models of Varying Aspect Ratio and Thickness. NACA TN 3501, 1955. (U)
9. Johnson, B. H., Jr., and Shibata, H. H.: Characteristics Throughout the Subsonic Speed Range of a Plane Wing and of a Cambered and Twisted Wing, Both Having 45° of Sweepback. NACA RM A51D27, 1951. (U)
10. Cahill, J. F., and Gottlieb, S. M.: Low-Speed Aerodynamic Characteristics of a Series of Swept Wings Having NACA 65A006 Airfoil Sections. (Revised) NACA RM L50F16, 1950. (U)
11. Michael, W. H., Jr.: Flow Studies in the Vicinity of a Modified Flat-Plate Rectangular Wing of Aspect Ratio 0.25. NACA TN 2790, 1952. (U)
12. Foster, G. V., and Griner, R. F.: Low-Speed Longitudinal Characteristics of a Circular-Arc 52° Sweptback Wing of Aspect Ratio 2.84 with and without Leading-Edge and Trailing-Edge Flaps at Reynolds Numbers from 1.6×10^6 to 9.7×10^6 . NACA RM L50F16a, 1950. (U)
13. Pitts, W. C.: Force, Moment, and Pressure-Distribution Characteristics of Rectangular Wings at High Angles of Attack and Supersonic Speeds. NACA RM A55K09, 1956. (U)
14. Hatch, J. E., Jr., and Hargrave, L. K.: Effects of Reynolds Number on the Aerodynamic Characteristics of a Delta Wing at Mach number of 2.41. NACA RM L51H06, 1951. (U)
15. Dunning, R. W., and Smith, F. M.: Aerodynamic Characteristics of Two Delta Wings and Two Trapezoidal Wings at Mach Number 4.04. NACA RM L53D30a, 1953. (U)
16. Shortal, J. A., and Maggin, B.: Effect of Sweepback and Aspect Ratio on Longitudinal Stability Characteristics of Wings at Low Speeds. NACA TN 1093, 1946. (U)

TABLE 4.14.3-A
SUBSONIC WING-CENTER-OF-PRESSURE POSITION OF STRAIGHT-TAPERED WINGS
DATA SUMMARY AND SUBSTANTIATION

Ref	A	Λ_{LE} (deg)	λ	Airfoil Section	ΔY	M	$R \times 10^{-6}$	$\frac{\tan \alpha}{\tan \alpha_{C_L \max}}$	α (deg)	$\left(\frac{x_{c.p.}}{c_r}\right)$ Calc	$\left(\frac{x_{c.p.}}{c_r}\right)$ Test	e Percent Error	
6	3.5	63	0.25	64A006	1.27	0.1	8.0		0	0	1.145	1.123	2.0
									0.2	7.6	1.231	1.181	4.2
									0.4	15.0	1.109	1.070	3.6
									0.6	21.9	1.024	0.994	3.0
									0.8	28.1	0.992	0.973	2.0
									1.0	33.8	0.989	0.983	0.6
7	3	9.5	0.6	63A004	0.87	0.6	1.4		0	0	0.265	0.295	-10.2
									0.2	2.85	0.264	0.253	4.3
									0.4	5.7	0.284	0.273	4.0
									0.6	8.5	0.307	0.293	4.8
									0.8	11.3	0.340	0.340	0
									1.0	14.0	0.365	0.386	-5.4
7	3	18.5	0.33	63A004	0.87	0.6	1.4		0	0	0.275	0.319	-13.8
									0.2	3.4	0.288	0.289	-0.3
									0.4	6.75	0.320	0.301	6.3
									0.6	10.1	0.341	0.344	-0.9
									0.8	13.4	0.363	0.373	-2.7
									1.0	16.5	0.375	0.388	-3.4
7	4	18.5	0.2	63A004	0.87	0.6	1.4		0	0	0.32	0.329	-2.7
									0.2	3.07	0.318	0.310	2.6
									0.4	6.1	0.335	0.328	2.1
									0.6	9.1	0.35	0.352	-0.6
									0.8	12.1	0.364	0.377	-3.4
									1.0	15.0	0.370	0.396	-6.6

TABLE 4.1.4.3-A (CONTD)

Ref	A	Λ_{LE} (deg)	λ	Airfoil Section	Δy	M	$R \times 10^{-6}$	$\frac{\tan \alpha}{\tan \alpha C_{L_{max}}}$	α (deg)	$\left(\frac{x_{c.p.}}{c_r}\right)_{Calc}$	$\left(\frac{x_{c.p.}}{c_r}\right)_{Test}$	e Percent Error
8	3	0	1.0	63A004	0.87	0.6	2.0	0	0	0.23	0.25	-8.0
									0.2	3.07	0.225	0
									0.4	6.1	0.243	3.4
									0.6	9.1	0.274	3.8
									0.8	12.1	0.317	5.0
									1.0	15.0	0.355	-5.3
8	6	0	1.0	63A006	1.34	0.6	—	0	0	0.25	0.25	0
									0.2	2.44	0.235	2.2
									0.4	4.9	0.230	-1.3
									0.6	7.3	0.250	3.3
									0.8	9.6	0.304	3.4
									1.0	12.0	0.345	0.3
9	5	46.5	0.565	64A010	2.1	0.1	2.0	0	0	0	1.16	2.2
									0.2	5.3	1.159	0.9
									0.4	10.6	1.13	0.1
									0.6	15.6	1.07	1.1
									0.8	20.5	1.036	0.6
									1.0	25.0	1.045	1.9
10	6	46.2	0.6	65A006	1.34	0.1	3.0	0	0	0	1.355	0.4
									0.2	7.06	1.338	-0.3
									0.4	13.9	1.178	-2.2
									0.6	20.4	1.118	-4.0
									0.8	25.4	1.162	-0.3
									1.0	31.8	1.18	1.7
11	0.25	0	1.0	Flat Plate $t/c = 0.02$	0.745	0.1	2.0	0	0	0	0.07	-30.0
									0.2	11.1	0.318	1.9
									0.4	21.4	0.357	-0.8
									0.6	30.4	0.368	2.2
									0.8	38.1	0.381	6.4
									1.0	44.4	0.378	6.2
12	2.84	52.0	0.616	Biconvex $t/c = 0.05$	0.6	0.12	5.9	0	0	0	0.856	0.7
									0.2	5.9	0.858	0.4
									0.4	11.6	0.877	-0.3
									0.6	17.1	0.837	-0.6
									0.8	22.3	0.823	0
									1.0	27.2	0.824	-2.9
4	4	51.3	0	65A003	0.6	0.6	0.75	0	0	0	0.70	1.2
									0.2	4.5	0.669	-1.6
									0.4	8.9	0.644	-0.9
									0.6	13.2	0.628	-1.3
									0.8	17.3	0.621	-1.9
									1.0	21.3	0.610	-3.2
4	3	51.3	0.143	65A003	0.6	0.6	0.78	0	0	0	0.635	2.4
									0.2	4.5	0.626	1.3
									0.4	8.9	0.606	-2.1
									0.6	13.3	0.595	1.7
									0.8	17.5	0.596	-0.2
									1.0	21.5	0.595	-0.8
$\text{Average Error} = \frac{\sum e }{n} = 2.9\%$												

SUBSONIC SPEEDS

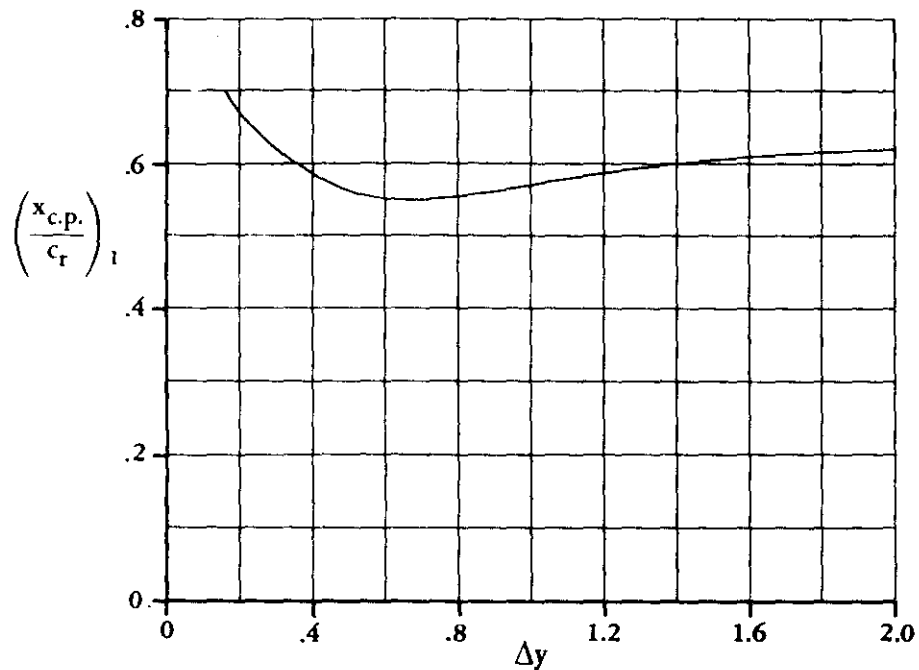


FIGURE 4.1.4.3-21a SUBSONIC CENTER-OF-PRESSURE LOCATION AT MAXIMUM LIFT — EFFECT OF LEADING-EDGE SHAPE

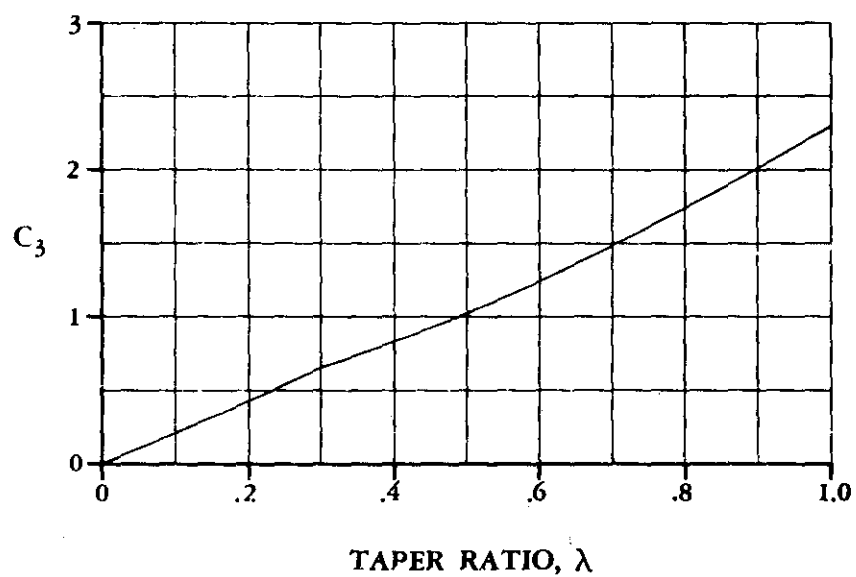


FIGURE 4.1.4.3-21b TAPER-RATIO CORRECTION FACTOR

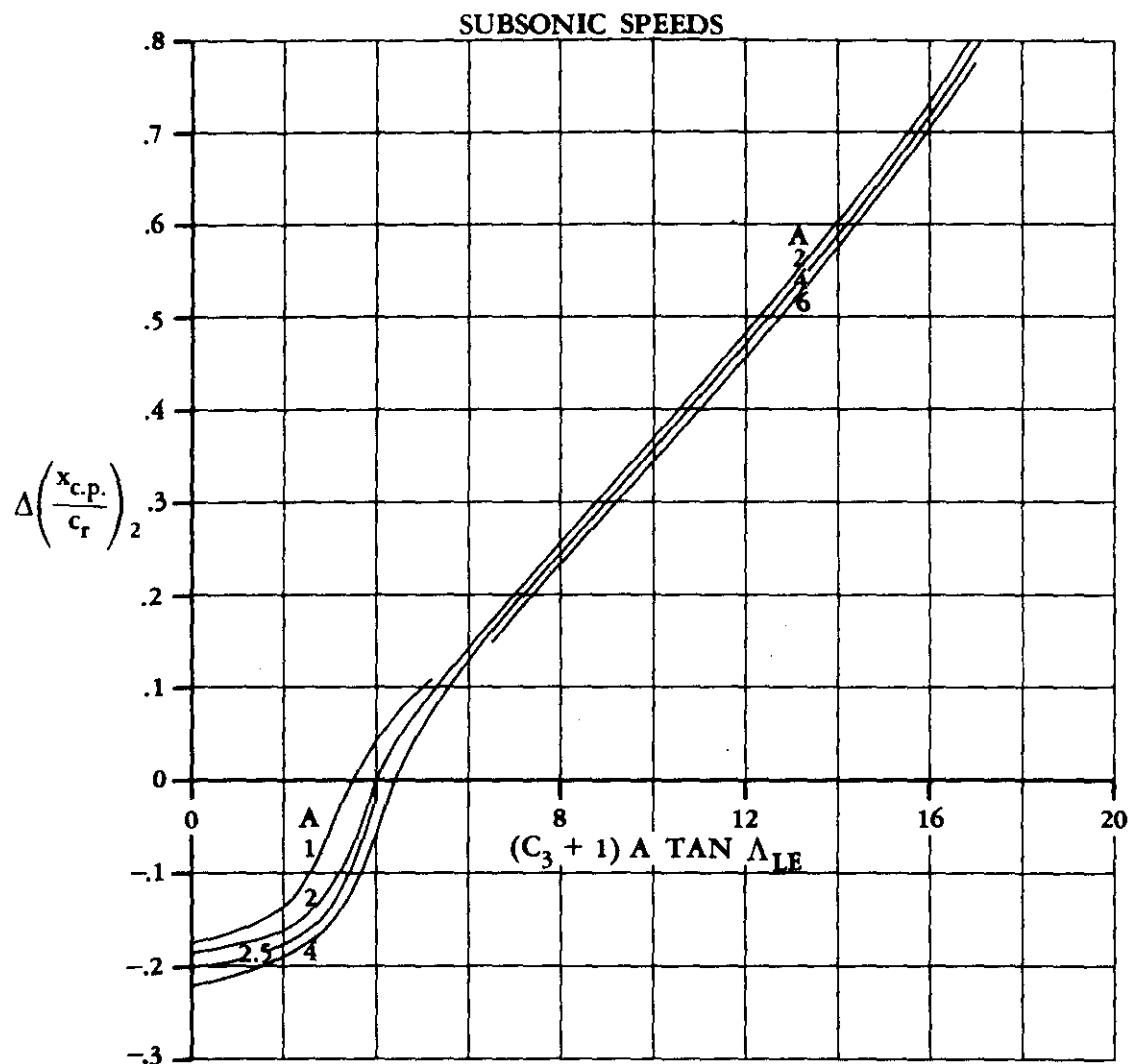


FIGURE 4.1.4.3-22a SUBSONIC CENTER-OF-PRESSURE INCREMENT AT MAXIMUM LIFT — PLANFORM EFFECT

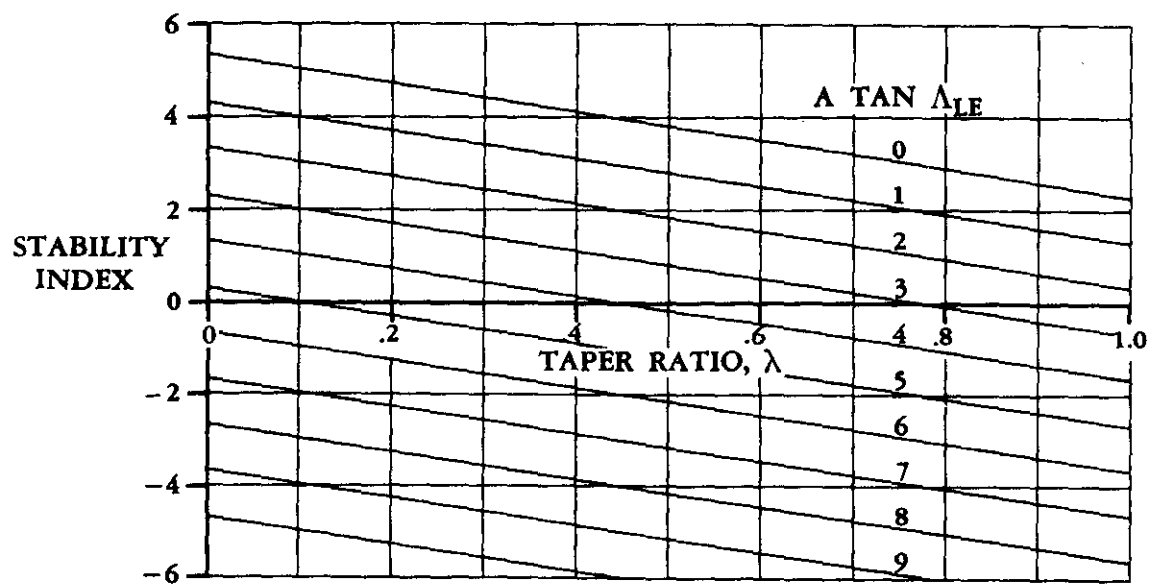


FIGURE 4.1.4.3-22b STABILITY INDEX

SUBSONIC SPEEDS

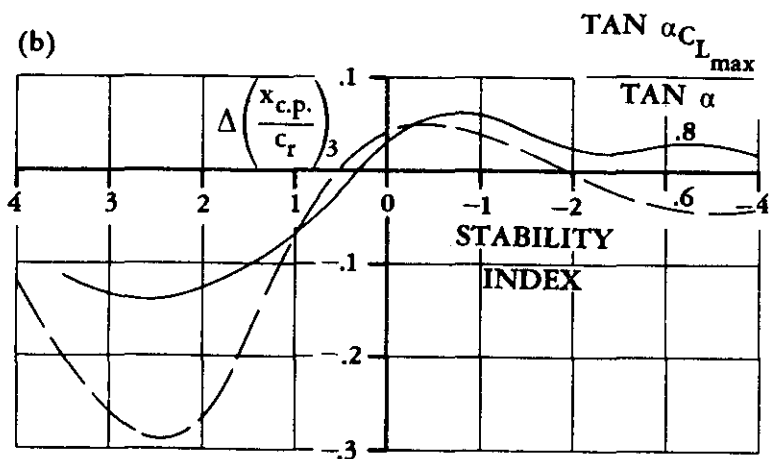
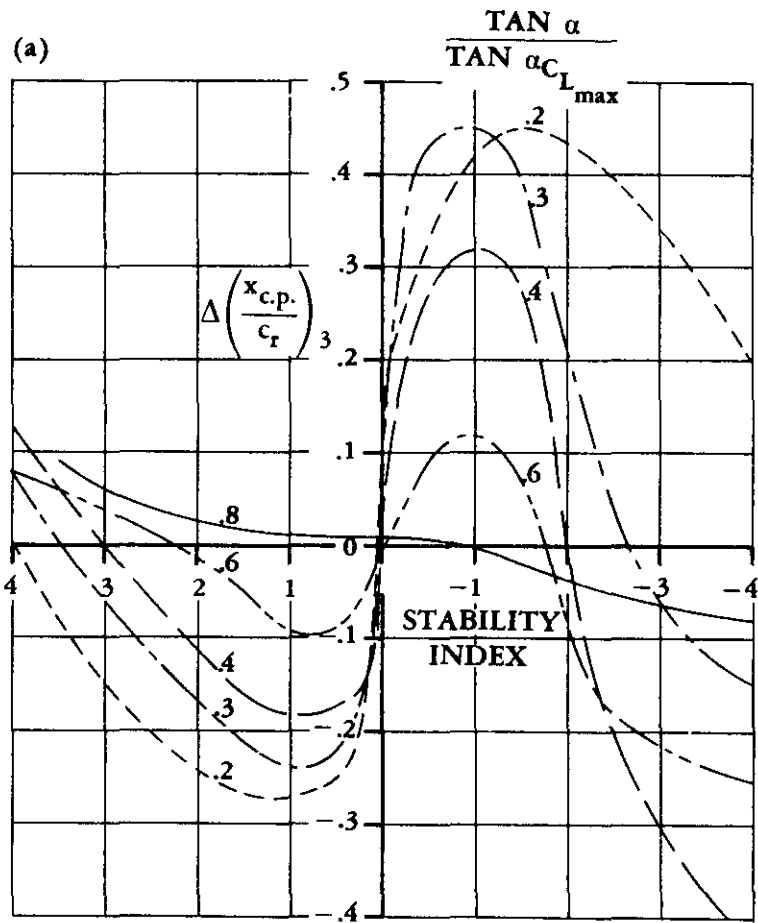


FIGURE 4.1.4.3-23 SUBSONIC WING CENTER-OF-PRESSURE INCREMENT — HIGH ANGLES OF ATTACK

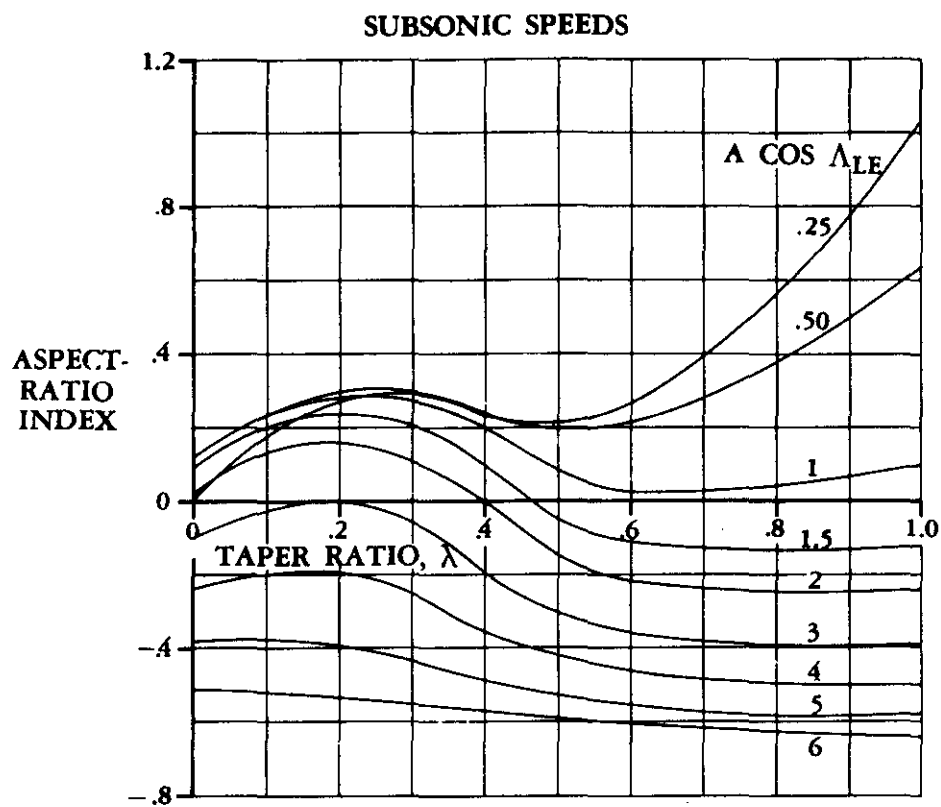


FIGURE 4.1.4.3-24a ASPECT-RATIO INDEX

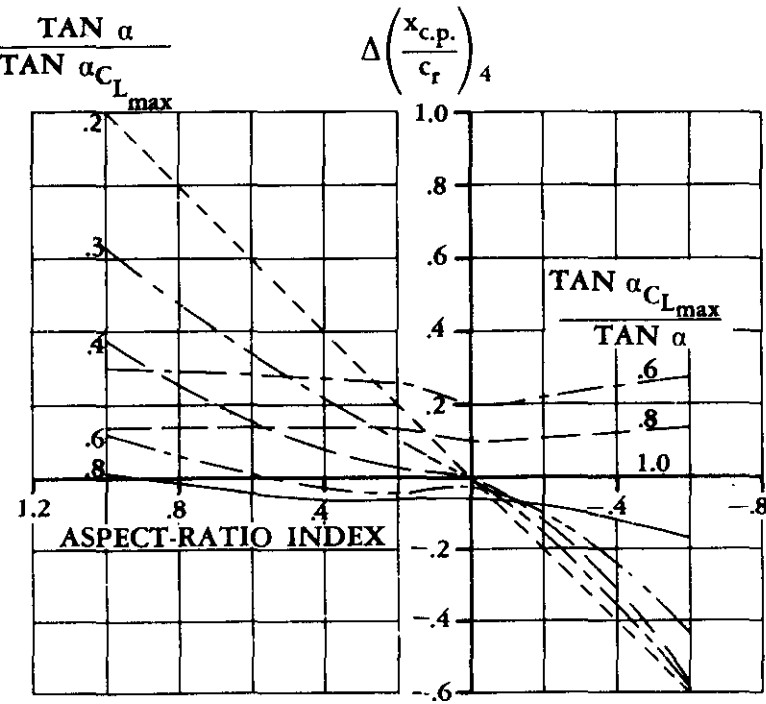


FIGURE 4.1.4.3-24b SUBSONIC WING CENTER-OF-PRESSURE INCREMENT — HIGH ANGLES OF ATTACK

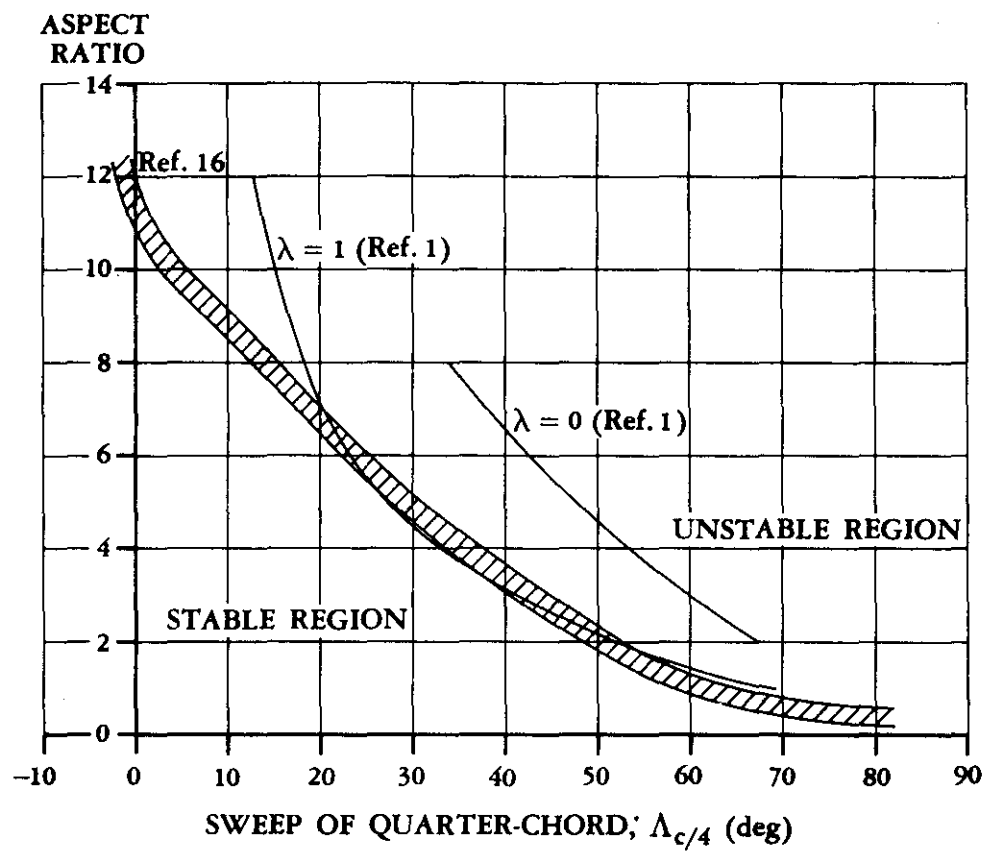


FIGURE 4.1.4.3-25 EMPIRICAL PITCH-UP BOUNDARY

SUBSONIC SPEEDS

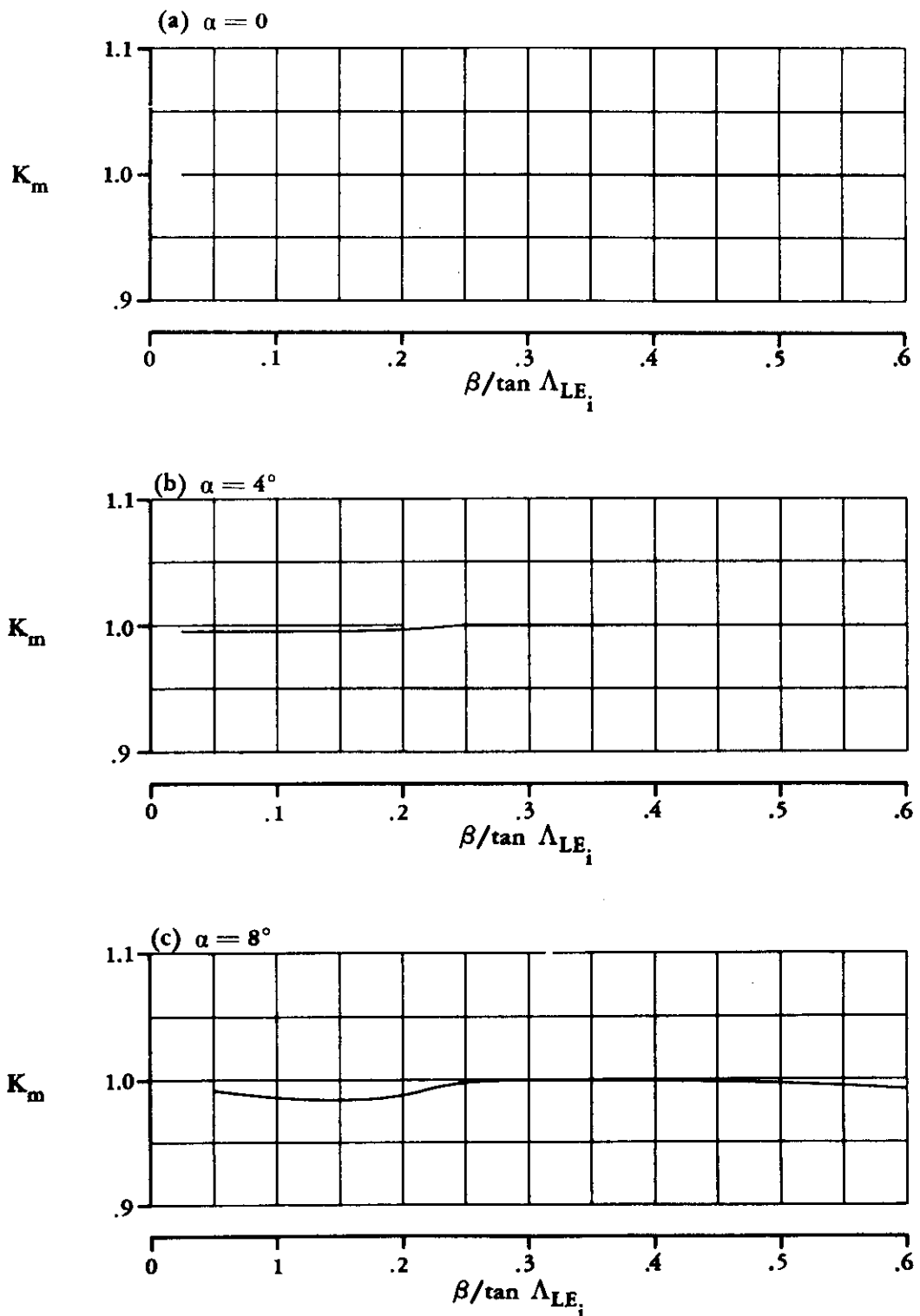


FIGURE 4.1.4.3-26 NONLINEAR PITCHING-MOMENT FACTOR FOR DOUBLE-DELTA WINGS

SUBSONIC SPEEDS

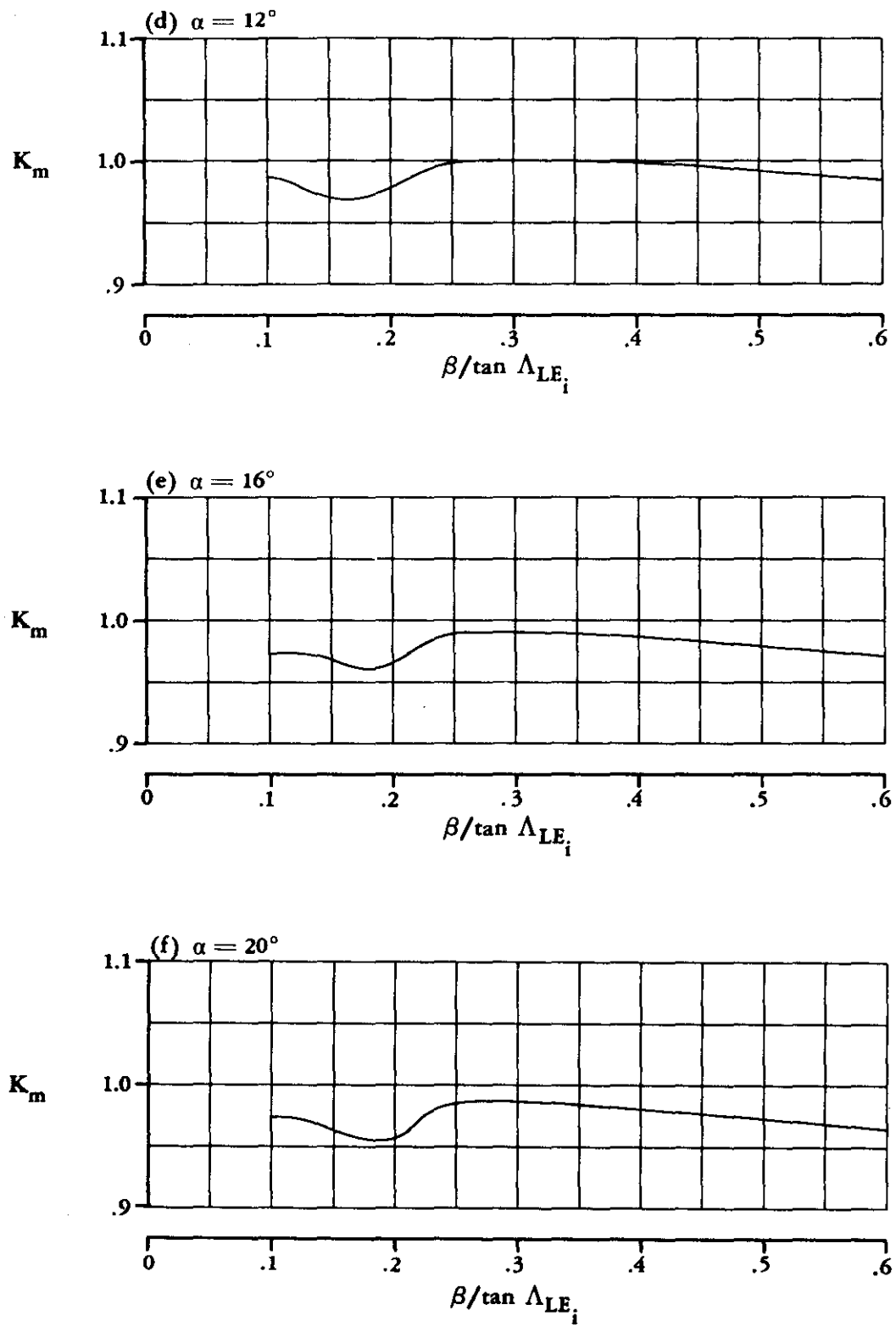


FIGURE 4.1.4.3-26 (CONTD)

4.1.5 WING DRAG

4.1.5.1 WING ZERO-LIFT DRAG

The total zero-lift drag or "profile" drag of a wing is usually considered to be composed of two parts, skin-friction drag and pressure drag. This division of drag is applicable in all speed regimes except the free-molecular-flow regime, where the normal concept of skin friction does not apply.

Skin Friction

Skin-friction drag is caused by shearing stresses within the thin layer of retarded air on the surface of the body known as the boundary layer. The boundary layer arises from the resistance of the viscous fluid to the motion of the body passing through it. Friction drag is extremely important, since it accounts for most of the drag at subsonic speeds and can be a major portion of the drag at high supersonic and hypersonic speeds.

The amount of viscous resistance depends greatly on whether the flow is laminar or turbulent, that is, whether the paths of the fluid particles remain in parallel layers or move in a chaotic or fluctuating fashion from layer to layer. The Reynolds number and the shape of the pressure distribution determine whether the flow over the wing is laminar or turbulent or a mixture of both. For practical considerations, transition from laminar to turbulent flow on a straight wing can be assumed to occur at a Reynolds number of approximately one million, based on distance from the leading edge. This usually corresponds to a position close to the leading edge. Transition will occur at an even lower Reynolds number on a swept wing. Accordingly, the methods presented for the subsonic, transonic, and supersonic regimes are for a fully turbulent boundary layer. In the hypersonic regime, however, the boundary layer is more likely to be laminar, because of the low Reynolds numbers associated with flight in the upper flight corridor.

Pressure Drag

At subsonic speeds pressure drag is usually small compared to skin-friction drag. It is caused by the displacement thickness of the boundary layer, which prevents full pressure recovery at the trailing edge. At transonic and supersonic speeds, pressure drag is identified with wave drag and is quite significant.

A. SUBSONIC

Methods for predicting subsonic zero-lift drag for wings are necessarily empirical and are commonly based on streamwise airfoil thickness ratio. The most frequently used method appears in chapter VI of reference 1 and in such standard references as reference 2. The Datcom method is essentially that of reference 1, but it has been refined by applying a lifting-surface correlation factor from reference 3 which accounts for the increased Reynolds-number length due to spanwise flow.

The Datcom method, taken from reference 3, is applicable to the following two classes of wing planforms:

Straight-Tapered Wings (conventional, trapezoidal planforms)

Non-Straight-Tapered Wings

Double-delta wings

Cranked wings

Curved (Gothic and ogee wings)

DATCOM METHOD

The subsonic wing zero-lift drag coefficient, based on the reference area S_{ref} , is given by

$$C_{D_0} = C_f \left[1 + L \left(\frac{t}{c} \right) + 100 \left(\frac{t}{c} \right)^4 \right] R_{L.S.} \frac{S_{wet}}{S_{ref}} \quad 4.1.5.1-a$$

where

C_f is the turbulent flat-plate skin-friction coefficient from figure 4.1.5.1-26 as a function of Mach number and the Reynolds number based on the reference length ℓ . Figure 4.1.5.1-27 is used in conjunction with figure 4.1.5.1-26 to determine C_f . Figure 4.1.5.1-27 presents the admissible roughness ℓ/k as a function of the Reynolds number based on the reference length.

- ℓ is the reference length in inches—for a wing (or wing panel in the case of composite wings) the length of the mean aerodynamic chord \bar{c} .
- k is the surface-roughness height in inches; it depends upon surface finish. Representative values for this parameter can be obtained from table 4.1.5.1-A.

The ratio ℓ/k is computed and figure 4.1.5.1-27 is used to obtain the cutoff Reynolds number. If the cutoff Reynolds number is greater than the computed Reynolds number for the specific configuration, the value of C_f is obtained from figure 4.1.5.1-26 at the computed Reynolds number. If the cutoff Reynolds number is less than the computed Reynolds number, the value of C_f is obtained from figure 4.1.5.1-26 at the cutoff Reynolds number.

$\frac{t}{c}$ is the average streamwise thickness ratio of the wing (or wing panel in the case of composite wings).

L is the airfoil thickness location parameter. $L = 1.2$ for $(t/c)_{max}$ located at $x_t \geq 0.30c$. $L = 2.0$ for $(t/c)_{max}$ located at $x_t < 0.30c$ (x_t is the chordwise position of maximum thickness).

S_{wet} is the wetted area of the wing (or wing panel in the case of composite wings).

S_{ref} is the reference area.

$R_{L.S.}$ is the lifting-surface correction factor obtained from figure 4.1.5.1-28b as a function of the Mach number and the cosine of the sweep angle of the airfoil maximum thickness line of the wing (or wing panel in the case of composite wings). The solid curves of figure 4.1.5.1-28b were developed in reference 4 from wing-alone test data for conventional trapezoidal planforms (including delta wings) having round-nosed airfoil sections. The dashed curves of figure 4.1.5.1-28b are from reference 3 and are arbitrary in the sense that no experimental data are available to justify their use.

Figure 4.1.5.1-28b is used in the following manner:

$R_{L.S.}$	Conventional trapezoidal planforms (including delta wings) Non-straight-tapered wings	Read value from solid curves. Read value from solid curves for outboard panels. Read value from dashed curves for inboard panels when $\cos\Lambda_{(t/c)_{max}} < 0.65$.
------------	---	--

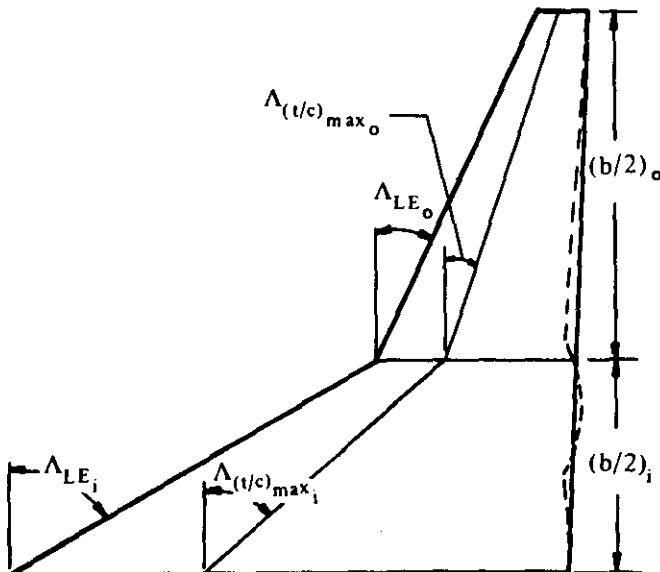
Non-straight-tapered-wing geometric parameters are presented in Section 2.2.2.

In treating non-straight-tapered planforms equation 4.1.5.1-a is applied to both the inboard and the outboard panels separately (based on a common reference area) and then summed. Curved planforms are approximated by combinations of trapezoidal panels, in which case two such panels are usually sufficient to give a satisfactory result.

For convenience, the bracketed term in equation 4.1.5.1-a is presented in figure 4.1.5.1-28a as a function of t/c and L . It should also be pointed out that the last term in equation 4.1.5.1-a represents the pressure drag of the wing.

Sample Problem

Given: The cranked wing of reference 23.



Inboard Panel:

NACA 63A004.5 airfoil (x_t @ 0.35c)

$$(t/c)_i = 0.045 \quad \left(\frac{b}{2}\right)_i = 1.594 \text{ ft}$$

$$\Lambda_{LE_i} = 60^\circ \quad \Lambda_{(t/c)_{max},i} = 48.4^\circ$$

$$\lambda_i = 0.339 \quad c_{r_i} = 4.175 \text{ ft}$$

$$A_i = 1.14 \quad S_i = 8.91 \text{ sq ft}$$

$$(S_{wet})_i = 17.82 \text{ sq ft}$$

$$\bar{c}_i = 3.02 \text{ ft}$$

Outboard Panel:

NACA 63A006 airfoil (x_t @ 0.35c) $\left(\frac{b}{2}\right)_o = 2.606 \text{ ft}$ $(t/c)_o = 0.06$

$$\Lambda_{LE_o} = 25^\circ \quad \Lambda_{(t/c)_{max},o} = 18.1^\circ \quad \lambda_o = 0.265 \quad c_{r_o} = 1.415 \text{ ft}$$

$$A_o = 5.824 \quad S_o = 4.665 \text{ sq ft} \quad (S_{wet})_o = 9.33 \text{ sq ft} \quad \bar{c}_o = 0.996 \text{ ft}$$

Additional Characteristics:

$$M = 0.13 \quad R_\ell = 0.90 \times 10^6 \text{ per ft} \quad \text{Smooth surface (assume } k = 0\text{)}$$

$$S_{ref} = S_w = 13.575 \text{ sq ft}$$

Compute:

Inboard Panel

$$R_\ell = (0.90 \times 10^6) (\bar{C}_i) = (0.90 \times 10^6) (3.02) = 2.718 \times 10^6$$

$$\frac{\ell}{k} = \infty; \text{ read } (C_f)_i \text{ at calculated } R_\ell$$

$$(C_f)_i = 0.00372 \text{ (figure 4.1.5.1-26)}$$

$$\left[1 + L \left(\frac{t}{c} \right) + 100 \left(\frac{t}{c} \right)^4 \right]_i = 1.053 \text{ (figure 4.1.5.1-28a, for } L = 1.2)$$

$$\cos \Lambda_{(t/c)_{max_i}} = \cos 48.4^\circ = 0.6639$$

$$(R_{L.S.})_i = 0.934 \text{ (figure 4.1.5.1-28b)}$$

$$\frac{(S_{wet})_i}{S_{ref}} = \frac{17.82}{13.575} = 1.313$$

Outboard Panel:

$$R_\ell = (0.90 \times 10^6) (\bar{C}_o) = (0.90 \times 10^6) (0.996) = 0.896 \times 10^6$$

$$\frac{\ell}{k} = \infty; \text{ read } (C_f)_o \text{ at calculated } R_\ell$$

$$(C_f)_o = 0.00451 \text{ (figure 4.1.5.1-26)}$$

$$\left[1 + L \left(\frac{t}{c} \right) + 100 \left(\frac{t}{c} \right)^4 \right]_o = 1.072 \text{ (figure 4.1.5.1-28a, for } L = 1.2)$$

$$\cos \Lambda_{(t/c)_{max_o}} = \cos 18.1^\circ = 0.9505$$

$$(R_{L.S.})_o = 1.067 \text{ (figure 4.1.5.1-28b)}$$

$$\frac{(S_{wet})_o}{S_{ref}} = \frac{9.33}{13.575} = 0.687$$

Solution:

$$C_{D_0} = (C_{D_0})_i + (C_{D_0})_o$$

$$(C_{D_0})_i = (C_f)_i \left[1 + L \left(\frac{t}{c} \right) + 100 \left(\frac{t}{c} \right)^4 \right]_i (R_{L.S.})_i \frac{(S_{wet})_i}{S_{ref}} \quad (\text{equation 4.1.5.1-a})$$

$$= (0.00372)(1.053)(0.934)(1.313) = 0.00480$$

$$(C_{D_0})_o = (C_f)_o \left[1 + L \left(\frac{t}{c} \right) + 100 \left(\frac{t}{c} \right)^4 \right]_o (R_{L.S.})_o \frac{(S_{wet})_o}{S_{ref}} \quad (\text{equation 4.1.5.1-a})$$

$$= (0.00451)(1.072)(1.067)(0.687) = 0.00354$$

$$C_{D_0} = (0.00480) + (0.00354) = 0.00834$$

This compares with a test value of 0.0086 from reference 23.

B. TRANSONIC

The transonic range varies greatly with airfoil shape and thickness, but for the purposes of consistency with the bulk of the Datcom it can be considered to begin at approximately $M = 0.6$ and to end at $M = 1.2$. The drag rise which marks the actual beginning of the transonic range occurs when the local Mach number on some part of the wing exceeds 1.0 and shock waves form on the surface.

Because of the mixed flows, drag in the transonic range does not lend itself either to simple theoretical or to experimental analysis. As in the subsonic regime, the total zero-lift drag can be separated into two parts—skin friction drag due to viscous forces and “wave” or pressure drag due to the viscous dissipation associated with the formation of shock waves on the wing.

In the lower transonic range the shock waves are essentially normal to the surface and serve to decelerate local supersonic flow back to subsonic values. In the upper transonic region there are two shocks, a bow shock ahead of the airfoil and a trailing-edge shock located near the trailing edge. When the bow shock attaches itself to a sharp-nosed airfoil, the entire flow field over the surface becomes supersonic, thus ending the transonic region. For round-nosed airfoils the end of this range is less clearly defined, but it occurs when the bow wave stands very close to the nose and supersonic flow predominates.

Skin Friction

Although it might be reasoned that skin friction should be increased for subsonic compressible flow (lower transonic range) because of the relatively higher local velocities, experimental results show little increase in drag due to viscosity. This is probably due to the compensating effects of Reynolds number and Mach number as well as unpredictable changes in the transition point throughout the Mach number range. Therefore, for the purpose of the Datcom the skin-friction drag will be assumed to be constant and equal to the subsonic value at $M = 0.6$ throughout the transonic range.

Wave Drag

For a given airfoil, it is possible to estimate the critical Mach number and subsequent drag rise accurately. However, the variables involved in a wing design that affect the manner in which the shock waves develop

on the surface, and hence the drag-rise characteristics, are many. They include not only sweep, aspect ratio, taper ratio, and thickness ratio, but also the variations between root and tip in thickness, position of maximum thickness, incidence, and leading-edge geometry. Also, wings designed to fly transsonically usually include some treatment, often made by contouring the fuselage, to minimize the "kink" effect at the root and tip. A wing can be designed to become critical from root to tip at the same time and have a flat drag curve with a delayed abrupt steep drag rise. Another wing can be designed which has an identical planform and the same average thickness ratio but has an entirely different shock development, producing a very gradual drag rise starting at a much lower Mach number.

For this reason, it is very difficult to correlate data in this region even on the basis of similarity parameters. The method presented here should be used only for first-order approximations on wings of relatively simple geometry. For cases where the design is aimed at optimizing transonic characteristics, detailed analysis of the isobar development on the wing must be made, in order to arrive at a reasonable drag estimate.

Since the transonic range begins when the first shocks form on the wing and ends when supersonic flow predominates, the amount of wave drag varies from zero at the lower speed to a peak value at the higher speeds within this range. From the standpoint of drag analysis, it is therefore convenient to relate this increase in drag to several parameters. These are discussed below.

The Mach Number for Drag Divergence

The free-stream Mach number at which sonic velocity is first attained on some portion of the wing is called the "theoretical critical Mach number." However, since experimental evidence indicates that there are no abrupt changes in force characteristics until the critical Mach number is exceeded by a substantial amount, it is usual to define the Mach number at which the drag starts to increase rapidly as the drag-divergence Mach number. It is further arbitrarily defined in the literature as the Mach number at which the numerical value of the slope of the curve of C_D vs M is 0.10.

$$M_D = M \left(\frac{\partial C_D}{\partial M} \right)_{C_L = \text{const}} = 0.10 \quad 4.1.5.1-b$$

The Maximum Wave-Drag Increment and the Mach Number at Which It Occurs

For two-dimensional airfoils, the peak wave drag occurs near $M = 1.0$. Linear theory predicts a pressure coefficient inversely proportional to $(1 - M^2)$ in high subsonic flow and $(M^2 - 1)$ in supersonic flow; thus indicating a maximum value near 1.0. In practice, however, the magnitude of this peak and the Mach number at which it occurs vary greatly with airfoil thickness, section shape, aspect ratio, and sweep; consequently, no reliable method has been devised to predict these values accurately.

The most useful tools available for correlating data in estimating wave drag in the transonic range are the von Kármán similarity laws (reference 5). These laws state that for two-dimensional flow, the flow pattern over two airfoils must be the same if the value of $(t/c)^{1/3} |1 - M^2|$ has the same value for each airfoil. Hence, if drag is known for one wing section as a function of Mach number, the corresponding quantity for similar sections can be computed by the simple relation $C_D \propto (t/c)^{5/3}$. Extensions of these laws have been made by Busemann and Spreiter to include three-dimensional effects (references 6 and 7).

The Datcom method is applicable only to conventional, trapezoidal planforms.

DATCOM METHOD

The zero-lift drag coefficient of conventional, trapezoidal planforms over the transonic speed regime is approximated by the following steps:

Step 1. Determine the skin-friction drag coefficient at $M = 0.60$ by

$$C_{D_f} = C_f \left[1 + L \left(\frac{t}{c} \right) \right] \frac{S_{wet}}{S_{ref}} \quad 4.1.5.1-c$$

where C_{D_f} is the skin-friction drag coefficient based on the reference area, and the remaining parameters are defined in the Datcom method of paragraph A. This value, calculated at $M = 0.6$, is assumed to be constant throughout the transonic region.

Step 2. Determine the wave-drag coefficient C_{D_w} at transonic Mach numbers for an unswept wing and construct the curve of C_{D_w} vs Mach number for the appropriate thickness and aspect ratio from figure 4.1.5.1-29. Values of $(t/c)^{1/3}$ and $(t/c)^{5/3}$ are given below to facilitate calculation:

t/c	$(t/c)^{1/3}$	$(t/c)^{5/3}$
0.12	0.493	0.0293
0.11	0.479	0.0254
0.10	0.464	0.0217
0.09	0.448	0.0181
0.08	0.431	0.0148
0.07	0.412	0.0118
0.06	0.392	0.0092
0.05	0.368	0.0068
0.04	0.342	0.00468
0.03	0.311	0.00292
0.02	0.271	0.00147

Step 3. From the curve of C_{D_w} vs M , read $C_{D_w \text{ peak}} \Delta_{c/4} = 0$, $M_{C_{D_w \text{ peak}}} \Delta_{c/4} = 0$, and $M_{D \Delta_{c/4} = 0}$. The Mach number for drag divergence $M_{D \Delta_{c/4} = 0}$ is obtained by a graphical interpretation of equation 4.1.5.1-b; i.e., $M_{D \Delta_{c/4} = 0}$ is read at the point of tangency to the C_{D_w} vs M curve of a line whose slope is $\partial C_D / \partial M = 0.10$.

Step 4. For a wing having sweep, convert values from the straight-wing curve as follows:

$$\frac{M_{D \Delta_{c/4} = 0}}{M_{D \Delta_{c/4} = n}} = \frac{M_{D \Delta_{c/4} = 0}}{(\cos n)^{1/2}} \quad 4.1.5.1-d$$

$$C_{D_w \text{ peak}} \Delta_{c/4} = n = C_{D_w \text{ peak}} \Delta_{c/4} = 0 \quad (\cos n)^{2.5} \quad 4.1.5.1-e$$

4.1.5.1-7

$$\frac{M_{C_D w \text{peak} \Lambda_{c/4}=0}}{M_{C_D w \text{peak} \Lambda_{c/4}=n}} = \frac{(cos n)^{1/2}}{(cos n)^{1/2}} \quad 4.1.5.1-f$$

Step 5. Construct the curve of C_{D_w} vs M for the swept wing by using the values determined in step 4 and the straight-wing curve of C_{D_w} vs M to aid in fairing.

Step 6. The zero-lift drag coefficient is obtained by adding the constant value of skin-friction drag coefficient determined in step 1 to the wave-drag over the transonic speed range determined in step 2 for unswept wings or in step 5 for swept wings.

$$C_{D_0} = C_{D_f} + C_{D_w} \quad 4.1.5.1-g$$

Sample Problem

Given: The zero-taper-ratio wing of reference 24.

$$A = 4.0 \quad \lambda = 0 \quad \Lambda_{c/4} = 14.5^\circ \quad S_{\text{wet}} = 1.390 \text{ sq ft}$$

NACA 63A006 airfoil ($x_t @ 0.35c$)

Additional characteristics:

$$R_g_{M=0.6} = 1.4 \times 10^6 \text{ (based on } \bar{c}) \quad S_{\text{ref}} = S_w = 0.695 \text{ sq ft}$$

Smooth surface (assume $k = 0$)

Compute:

Determine the skin-friction drag coefficient.

$$\frac{\ell}{k} = \infty; \text{ read } C_f \text{ at given } R_g \text{ at } M = 0.6.$$

$$C_f = 0.0042 \text{ (figure 4.1.5.1-26)}$$

$$C_{D_f} = C_f \left[1 + L \left(\frac{t}{c} \right) \right] \frac{S_{\text{wet}}}{S_{\text{ref}}} \quad (\text{equation 4.1.5.1-c})$$

$$= 0.0042 [1 + (1.2)(0.06)] \frac{1.390}{0.695}$$

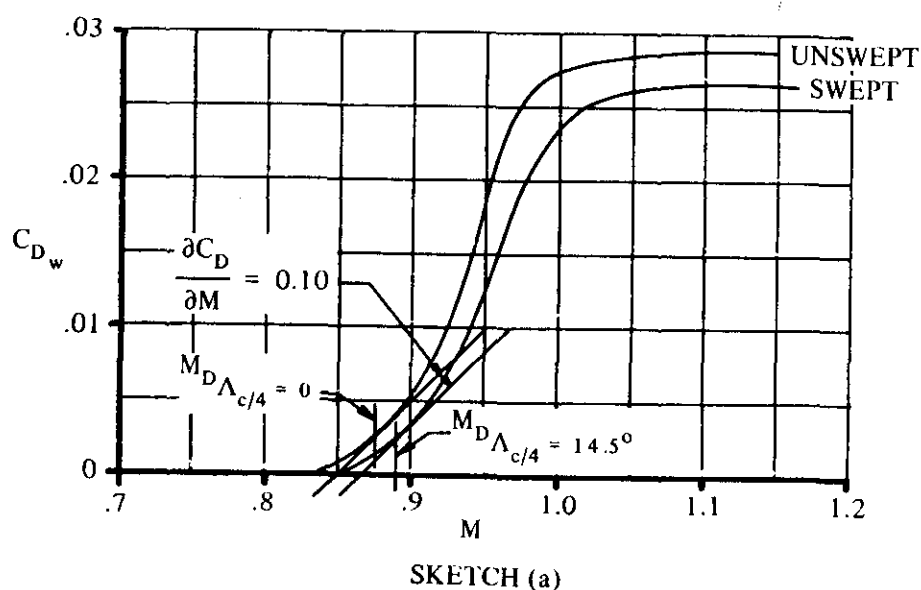
$$= 0.0090 \text{ (based on } S_w)$$

Determine and construct the variation of C_{D_w} with Mach number for an unswept wing.

$$A \left(\frac{t}{c} \right)^{1/3} = (4.0)(0.392) = 1.568$$

(1)	(2)	(3)	(4)
M	$\frac{\sqrt{ M^2 - 1 }}{(t/c)^{1/3}}$	$\frac{C_{D_w}}{(t/c)^{5/3}}$ fig. 4.1.5.1-29	C_{D_w} (3) (0.0092)
0.85	1.34	0.07	0.00064
0.90	1.11	0.58	0.0053
0.925	0.97	1.10	0.0101
0.95	0.80	1.95	0.0179
0.975	0.57	2.75	0.0253
1.00	0	3.02	0.0278
1.05	0.82	3.10	0.0285
1.10	1.17	3.12	0.0287
1.15	1.45	3.13	0.0288

Plot C_{D_w} vs M for the unswept wing (sketch (a)).



SKETCH (a)

Read the following values from the curve of C_{D_w} vs M for the unswept wing.

$$M_{D_{\Lambda_{c/4}=0}} = 0.875$$

$$C_{D_w \text{ peak}}_{\Lambda_{c/4}=0} = 0.029$$

$$M_{C_{D_w \text{ peak}}_{\Lambda_{c/4}=0}} = 1.10$$

Apply sweep corrections

$$M_{D_{\Lambda_{c/4}=14.5^\circ}} = \frac{M_{D_{\Lambda_{c/4}=0}}}{(\cos 14.5^\circ)^{1/2}} = \frac{0.875}{(0.9681)^{1/2}} = 0.889 \quad (\text{equation 4.1.5.1-d})$$

$$C_{D_w \text{ peak}}_{\Lambda_{c/4}=14.5^\circ} = C_{D_w \text{ peak}}_{\Lambda_{c/4}=0} (\cos 14.5^\circ)^{2.5} \quad (\text{equation 4.1.5.1-e})$$

$$\begin{aligned} &= (0.029) (0.9681)^{2.5} \\ &= 0.0267 \end{aligned}$$

$$M_{C_{D_w \text{ peak}}_{\Lambda_{c/4}=14.5^\circ}} = \frac{M_{C_{D_w \text{ peak}}_{\Lambda_{c/4}=0}}}{(\cos 14.5^\circ)^{1/2}} \quad (\text{equation 4.1.5.1-f})$$

$$\begin{aligned} &= \frac{1.10}{(0.9681)^{1/2}} \\ &= 1.12 \end{aligned}$$

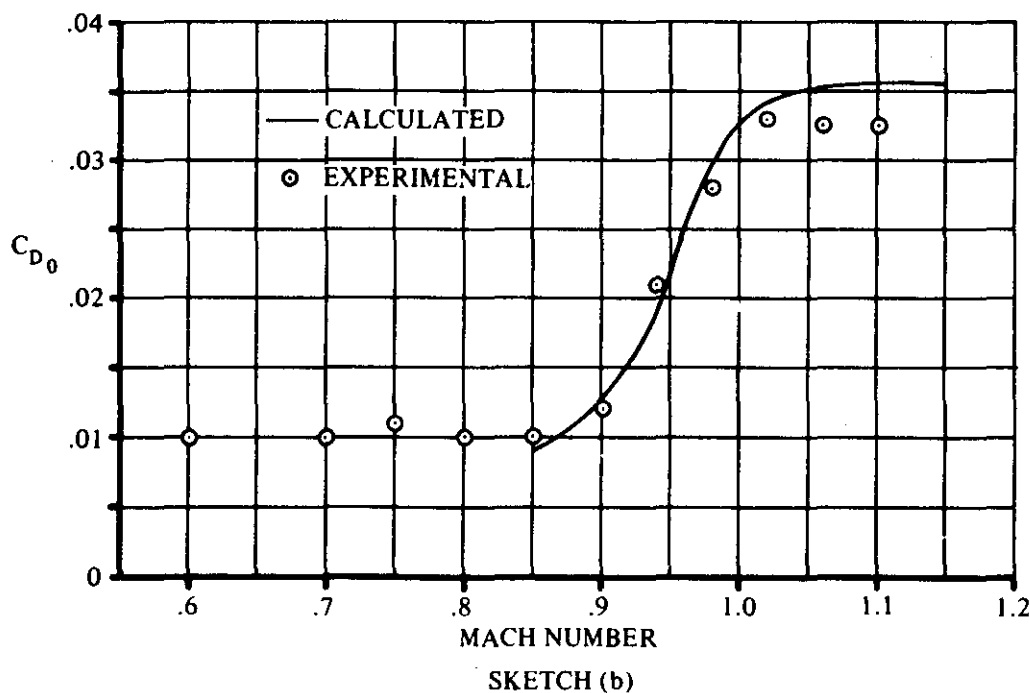
Construct the curve of C_{D_w} vs M for the swept wing using the straight-wing curve to aid in fairing.

Solution:

$$C_{D_0} = C_{D_f} + C_{D_w} \quad (\text{equation 4.1.5.1-g})$$

M	C_{D_f}	C_{D_w} sketch (a)	C_{D_0} $(2) + (3)$
0.85	0.0090	0	0.0090
0.90		0.0036	0.0125
0.925		0.0070	0.0160
0.950		0.0127	0.0217
0.975		0.0197	0.0287
1.000		0.0238	0.0328
1.050		0.0262	0.0352
1.100		0.0265	0.0355
1.150		0.0265	0.0355

The calculated results are compared with test values from reference 24 in sketch (b).



C. SUPERSONIC

Skin Friction

At supersonic speeds it can be shown theoretically that an increase in Mach number results in a decrease in the skin-friction coefficient at constant Reynolds number. This variation, when zero heat transfer is assumed, is due primarily to the variations in temperature and density. In actual cases, where the airplane is transmitting heat to the boundary layer, or where the aircraft is cooled to a point where heat from the boundary layer is transmitted to the skin, the reduction in skin-friction coefficient becomes a function of the heat-transfer condition. The full reduction in skin friction at supersonic Mach numbers is justified only when stabilized conditions and zero heat transfer are attained. Therefore, to obtain accurate supersonic skin-friction coefficients, it is necessary to know the heat-transfer conditions on various portions of a flight vehicle throughout its mission. Since this information can be obtained only by detailed analysis, some assumptions regarding the skin friction are usually made. For flights of long duration, equilibrium (zero heat transfer) is generally assumed. For transient flight, the skin-friction coefficient will vary between the incompressible value and that for zero heat transfer. Another important consideration for estimating the skin-friction drag at supersonic speeds is the Reynolds-number variation throughout the flight regime. The design chart used in the Datcom method presents the turbulent skin-friction coefficient on an insulated flat plate as a function of Mach number and Reynolds number.

Wave Drag

Numerous theories are available for calculating the wave drag of wing planforms at supersonic speeds. No attempt is made to discuss all of these theories and their limitations; however, table 4.1.5.1-B presents a summary of various planforms for which solutions exist. In general, the well-known linear supersonic theory has proved useful in indicating the trends of wing wave drag for the majority of conventional, tapered, trapezoidal planforms with subsonic leading edges (see reference 8).

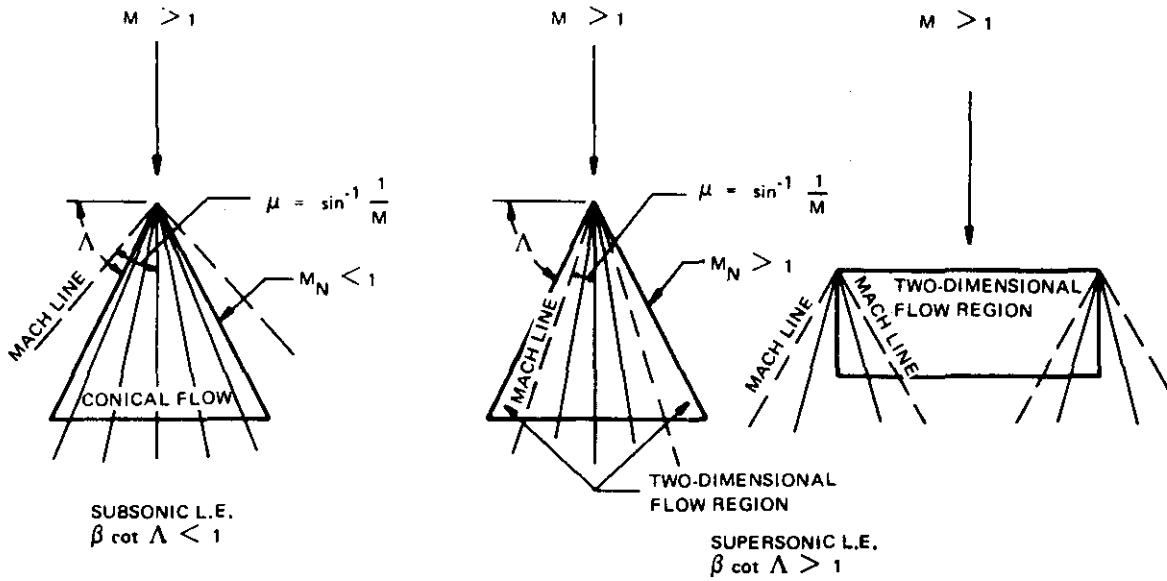
In discussing the flow regions over a wing, the following general classifications are convenient (see sketch (c)).

Subsonic Wing Leading Edge—If the leading edge of the wing is swept behind the Mach cone, the velocity component normal to the leading edge is subsonic and hence the leading edge is said to be subsonic.

Supersonic Wing Leading Edge—If the leading edge is forward of the Mach cone, the normal velocity component is supersonic and the wing is said to have a supersonic leading edge.

Similar terminology can be applied to the wing trailing edges. For either subsonic or supersonic leading edges the region inside the Mach cone is called the "conical flow" region. In this region the velocity components are constant along rays emanating from the apex and the flow is not influenced by the presence of the tip or trailing edge.

When the leading edge is supersonic, the region outside the Mach cone is called the "two-dimensional flow" region and the velocity distribution in this region is identical to that of an infinite wing having the same leading-edge sweep.



SKETCH (c)

It should be pointed out that due to the approximations of linear theory, kinks occur in the drag curves when lines across which the flow is turned become sonic, namely, leading and trailing edges and ridge lines of polygonal sections. These kinks do not occur in practice, since they correspond to flow conditions for which linear theory is no longer valid.

The Datcom method for estimating supersonic wave drag is taken from reference 3 and is based on the results that have been obtained from linear supersonic theory for the two-dimensional case.

The Datcom method is applicable to the following two classes of wing planforms:

Straight-Tapered Wings (conventional, trapezoidal planforms)

Non-Straight-Tapered Wings

Double-delta wings

Cranked wings

Curved (Gothic and ogee) wings

DATCOM METHOD

The wing zero-lift drag coefficient at supersonic speeds, based on the reference area S_{ref} , is given by

$$C_{D_0} = C_{D_f} + C_{D_w} \quad 4.1.5.1-h$$

where C_{D_f} and C_{D_w} are the supersonic skin-friction drag coefficient and the supersonic wave-drag coefficient, respectively, both based on a common reference area, and determined in the following manner:

Skin-Friction Drag Coefficient

The supersonic skin-friction drag coefficient is given by

$$C_{D_f} = C_f \frac{S_{wet}}{S_{ref}} \quad 4.1.5.1-i$$

for a conventional, trapezoidal planform, and

$$C_{D_f} = (C_f)_i \frac{(S_{wet})_i}{S_{ref}} + (C_f)_o \frac{(S_{wet})_o}{S_{ref}} \quad 4.1.5.1-j$$

for a non-straight-tapered planform.

where

C_f is the turbulent flat-plate skin-friction coefficient from figure 4.1.5.1-26 as a function of Mach number and the Reynolds number based on the reference length ℓ . The reference length ℓ is the mean aerodynamic chord of the wing (or wing panel in the case of composite wings). Figure 4.1.5.1-27 is used in conjunction with figure 4.1.5.1-26 to determine C_f . The procedure for determining C_f is fully explained in the Datcom method of paragraph A.

$\frac{S_{wet}}{S_{ref}}$ is the ratio of the wetted area of the wing (or wing panel in the case of composite wings) to the reference area.

The subscripts i and o refer to the inboard and outboard panels, respectively, of composite planforms.

Curved planforms are approximated by combinations of trapezoidal panels, in which case two such panels are usually sufficient to give a satisfactory result.

Non-straight-tapered wing geometric parameters are presented in Section 2.2.2.

Wave-Drag Coefficient

The form of the equation for the supersonic wave-drag coefficient is in accordance with the results that have been obtained from linear supersonic theory for the two-dimensional case. The effects of changes in wing planform and variable thickness ratio are accounted for by defining an effective thickness ratio and computing the wave-drag coefficient on a basic planform shape. A distinction is made between wings with sharp-nosed airfoil sections and wings with round-nosed airfoil sections.

Wings With Sharp-Nosed Airfoil Sections

For wings with sharp-nosed airfoil sections

$$C_{D_w} = \frac{K}{\beta} \left(\frac{t}{c} \right)_{eff}^2 \frac{S_{bw}}{S_{ref}} \quad 4.1.5.1-k$$

when the leading edge of the basic wing is supersonic ($\beta \cot \Lambda_{LE_{bw}} \geq 1$), and

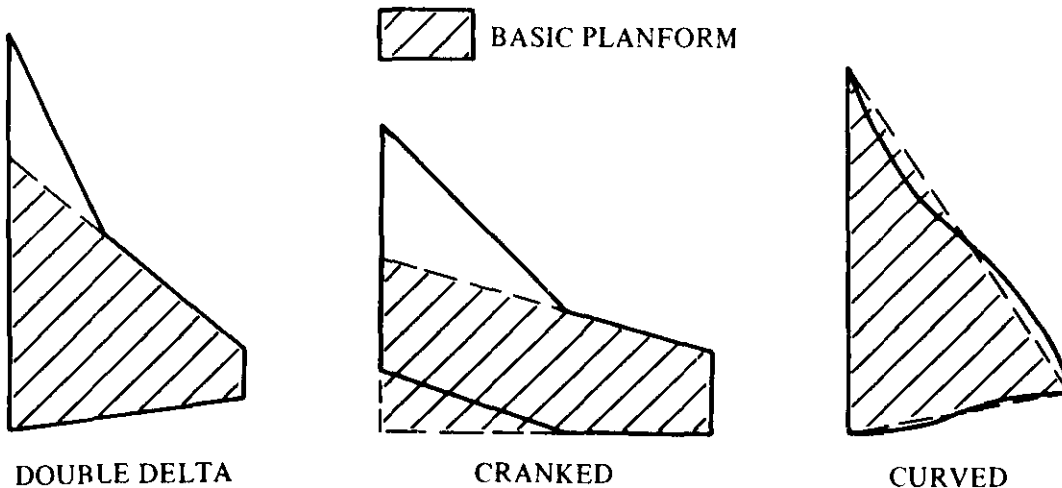
$$C_{D_w} = K \cot \Lambda_{LE_{bw}} \left(\frac{t}{c} \right)_{eff}^2 \frac{S_{bw}}{S_{ref}}$$

4.1.5.1-l

when the leading edge of the basic wing is subsonic ($\beta \cot \Lambda_{LE_{bw}} < 1$).

The subscript bw refers to the basic wing (straight leading and trailing edges), and

S_{bw} is the area of the basic wing – for conventional, trapezoidal planforms, the total wing area. The selection of the basic planform for non-straight-tapered wings is arbitrary, but should deviate as little as possible from the actual wing. Typical non-straight-tapered wings and the basic planforms used in wave-drag estimations are illustrated in sketch (d).



DEFINITION OF BASIC PLANFORMS OF NON-STRAIGHT-TAPERED WINGS FOR SUPERSONIC WAVE-DRAG ESTIMATION

SKETCH (d)

$\left(\frac{t}{c} \right)_{eff}$ is the effective thickness ratio (for a conventional, trapezoidal planform, use the average thickness ratio $(t/c)_{av}$). For a nonstraight-tapered planform the effective thickness ratio is defined in terms of the basic planform and is given by

$$\left(\frac{t}{c} \right)_{eff} = \left[\frac{\int_0^{b/2} \left(\frac{t}{c} \right)^2 c_{bw} dy}{\int_0^{b/2} c_{bw} dy} \right]^{1/2}$$

4.1.5.1-m

where c_{bw} is the chord of the basic wing. Note that in the numerator, the chord of the actual wing and the chord of the basic wing both appear. The denominator is one-half the planform area of the basic wing, so that

$$\left(\frac{t}{c} \right)_{eff} = \left[\frac{\int_0^{b/2} \left(\frac{t}{c} \right)^2 c_{bw} dy}{\left(\frac{S_{bw}}{2} \right)^{1/2}} \right]^{1/2}$$

4.1.5.1-m'

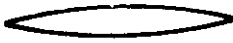
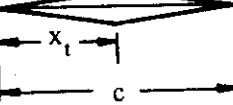
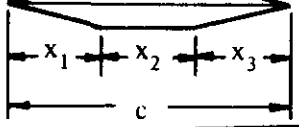
4.1.5.1-15

Numerical integration of the integrand in the numerator is illustrated in the sample problem.

$\Lambda_{LE_{bw}}$ is the leading-edge sweep of the basic wing.

K is a constant factor for a given sharp-nosed airfoil section. For basic wings with variable thickness ratios the K factor is based on the airfoil section at the average chord. K factors for sharp-nosed airfoils are presented in the following table:

SHARP-NOSED AIRFOILS

Basic Wing Airfoil Section	K	Section
Biconvex	$\frac{16}{3}$	
Double Wedge	$\frac{c/x_t}{1 - x_t/c}$	
Hexagonal	$\frac{c(c - x_2)}{x_1 x_3}$	

Wings With Round-Nosed Airfoil Sections

Wings with round-nosed airfoil sections exhibit a detached bow wave and a stagnation point, and the pressure-drag coefficient increases as a function of Mach number in a manner similar to the stagnation pressure. Consequently, a constant value of K cannot be used for basic wings with round-nosed airfoils.

The wave-drag coefficient of wings with round-nosed airfoil sections is approximated by adding the pressure drag of a blunt leading edge to the wave drag of the basic wing with an assumed sharp leading edge. By assuming a biconvex shape aft of the leading edge, the wave drag of a round-nosed leading-edge wing is given by

$$C_{D_w} = C_{D_{LE}} + \frac{16}{3\beta} \left(\frac{t}{c}\right)_{eff}^2 \frac{S_{bw}}{S_{ref}} \quad 4.1.5.1-n$$

when the leading edge of the basic wing is supersonic ($\beta \cot \Lambda_{LE_{bw}} \geq 1$), and

$$C_{D_w} = C_{D_{LE}} + \frac{16}{3} \cot \Lambda_{LE_{bw}} \left(\frac{t}{c}\right)_{eff}^2 \frac{S_{bw}}{S_{ref}} \quad 4.1.5.1-o$$

when the leading edge of the basic wing is subsonic ($\beta \cot \Lambda_{LE_{bw}} < 1$).

The second terms on the right-hand side of equations 4.1.5.1-n and 4.1.5.1-o are the wave-drag coefficients of the basic wing with sharp-nosed, biconvex airfoils at the appropriate leading-edge condition, and

$C_{D_{LE}}$ is the pressure-drag coefficient on a swept, cylindrical leading edge obtained as a function of the Mach number and the leading-edge sweep of the basic wing from figure 4.1.5.1-30a or figure 4.1.5.1-30b. The term $(2r_{LE_{bw}} b_{bw} / \cos \Lambda_{LE_{bw}})$ is the frontal area of the leading edge. For basic wings with variable thickness ratios the leading-edge radius $r_{LE_{bw}}$ is the radius of the section at the average chord.

The correlation of cylindrical leading-edge pressure-drag coefficients is derived in reference 19 and has been substantiated over the Mach number range from 0.5 to 8.0 and for sweep angles from 0 to 75° .

Sample Problem

Given: The double-delta wing designated 6-67-67, of reference 25.

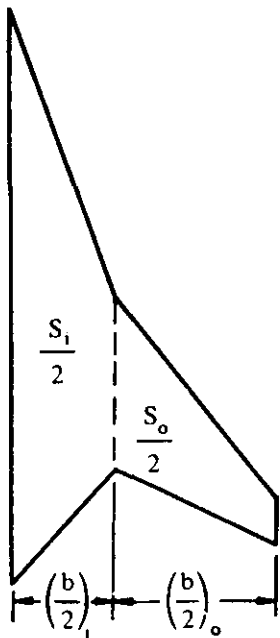
Actual Wing Characteristics:

$$A = 2.42 \quad \lambda = 0.086 \quad \Lambda_{LE_i} = 70.67^\circ \quad \Lambda_{LE_o} = 51.63^\circ$$

$$\Lambda_{TE_i} = -47.38^\circ \quad \Lambda_{TE_o} = 26.62^\circ \quad \frac{b}{2} = 12.0 \text{ in.} \quad \eta_B = 0.40$$

$$S_w = S_{ref} = 238 \text{ sq in.} \quad \frac{t}{c} \text{ varies, (see sketch (e))}$$

Inboard- and Outboard-Panel Characteristics (skin-friction drag calculations):



Inboard panel:

$$c_{r_i} = 26.58 \text{ in.} \quad \lambda_i = 0.293 \quad \bar{c}_i = 18.9 \text{ in.}$$

$$S_i = 165 \text{ sq in.} \quad (S_{wet})_i = 330 \text{ sq in.}$$

Outboard panel:

$$c_{r_o} = 7.77 \text{ in.} \quad \lambda_o = 0.2995 \quad \bar{c}_o = 5.54 \text{ in.}$$

$$S_o = 73 \text{ sq in.} \quad (S_{wet})_o = 146 \text{ sq in.}$$

Basic Wing Characteristics (wave-drag calculations):

$$\begin{array}{ll} c_{r_{bw}} = 11.43 \text{ in.} & \lambda_{bw} = 0.20 \\ \Lambda_{LE_{bw}} = 51.63^\circ & \Lambda_{TE_{bw}} = 26.62^\circ \\ \left(\frac{b}{2}\right)_{bw} = 12.0 \text{ in.} & S_{bw} = 146.6 \text{ sq in.} \end{array}$$

Airfoil Characteristics:

Hexagonal, sharp leading edge

$$\frac{x_1}{c} = \frac{x_2}{c} = \frac{x_3}{c} = \frac{1}{3} \quad (t/c)_{bw} = 0.06 \text{ (constant)}$$

Additional Characteristics:

$M = 2.01$; $\beta = 1.744$ Smooth surface (assume $k = 0$)

$$R_\ell = 3.35 \times 10^6 \text{ per ft}$$

Compute:

Skin-friction drag coefficient

Inboard panel

$$R_\ell = (3.35 \times 10^6)(\bar{C}_f) = (3.35 \times 10^6) \left(\frac{18.9}{12} \right) = 5.28 \times 10^6$$

$$\frac{\ell}{k} = \infty; \text{ read } (C_f)_i \text{ at calculated } R_\ell$$

$$(C_f)_i = 0.00255 \text{ (figure 4.1.5.1-26)}$$

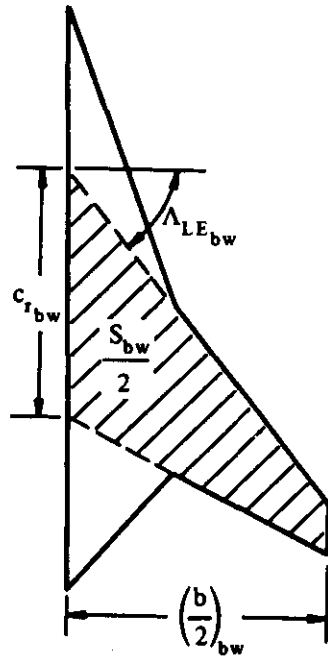
Outboard panel

$$R_\ell = (3.35 \times 10^6)(\bar{C}_f) = (3.35 \times 10^6) \left(\frac{5.54}{12} \right) = 1.55 \times 10^6$$

$$\frac{\ell}{k} = \infty; \text{ read } (C_f)_o \text{ at calculated } R_\ell$$

$$(C_f)_o = 0.00318 \text{ (figure 4.1.5.1-26)}$$

$$C_{D_f} = (C_f)_i \frac{(S_{wet})_i}{S_{ref}} + (C_f)_o \frac{(S_{wet})_o}{S_{ref}} \quad (\text{equation 4.1.5.1-j})$$



$$= (0.00255) \left(\frac{330}{238} \right) + (0.00318) \left(\frac{146}{238} \right)$$

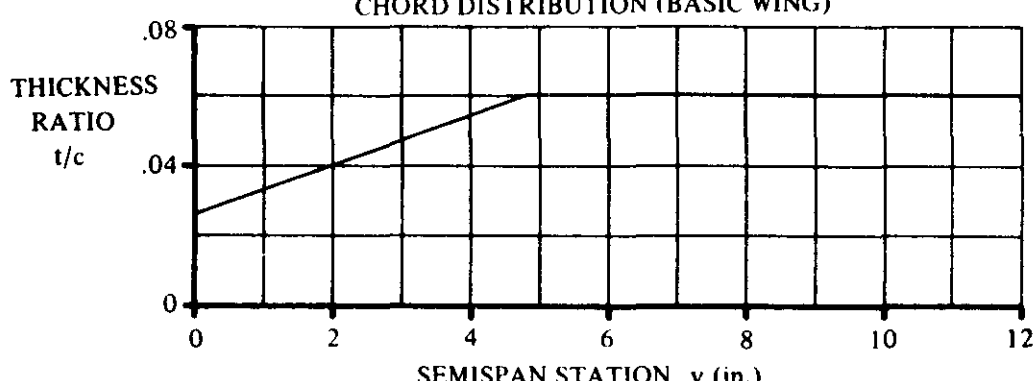
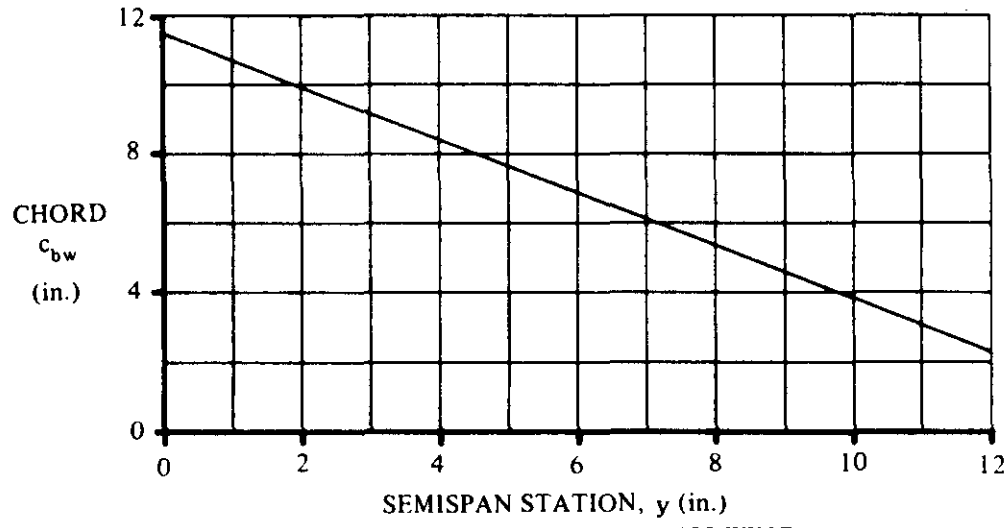
$$= 0.00548 \text{ (based on } S_{ref})$$

Wave-drag coefficient

$$K = \frac{c(c - x_2)}{x_1 x_3} = \frac{1 \left(1 - \frac{1}{3} \right)}{\left(\frac{1}{3} \right)^2} = 6.0$$

Determine $(t/c)_{eff}$

The thickness distribution of the actual wing and the chord distribution of the basic wing are shown in sketch (e).



SKETCH (e)

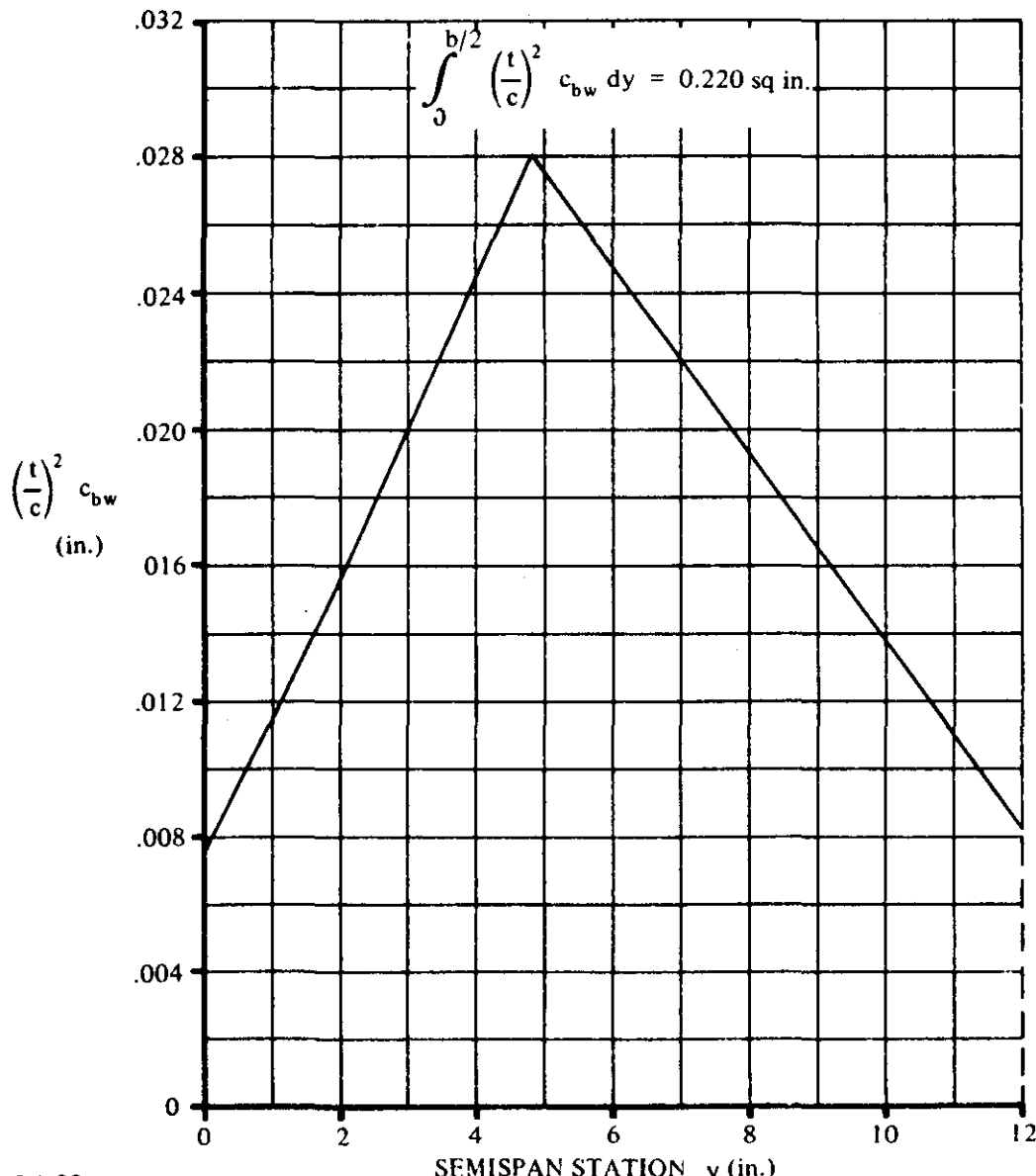
Sketch (f) shows $\left[(t/c)^2 c_{bw} \right]$ versus spanwise position.

Graphical integration of this curve gives $\int_0^{b/2} \left(\frac{t}{c} \right)^2 c_{bw} dy = 0.220 \text{ sq in.}$

$$\left(\frac{t}{c}\right)_{\text{eff}}^2 = \frac{\int_0^{b/2} \left(\frac{t}{c}\right)^2 c_{bw} dy}{\frac{1}{2} S_{bw}} \quad (\text{equation 4.1.5.I-m'})$$

$$= \frac{0.220}{\frac{1}{2} (146.6)} = 0.0030$$

$$\left(\frac{t}{c}\right)_{\text{eff}} = 0.0548$$



4.1.5.1-20

SKETCH (f)

$$\beta \cot \Lambda_{LE_{bw}} = (1.744) (\cot 51.63^\circ) = 1.381 \text{ (supersonic leading edge)}$$

$$C_{D_w} = \frac{K}{\beta} \left(\frac{t}{c}_{eff} \right)^2 \frac{S_{bw}}{S_{ref}} \quad (\text{equation 4.1.5.1-k})$$

$$= \left(\frac{6.0}{1.744} \right) (0.0548)^2 \left(\frac{146.6}{238} \right)$$

$$= 0.00636 \quad (\text{based on } S_{ref})$$

Solution:

$$C_{D_0} = C_{D_f} + C_{D_w} \quad (\text{equation 4.1.5.1-h})$$

$$= (0.00548) + (0.00636)$$

$$= 0.01184 \quad (\text{based on } S_{ref})$$

D. HYPERSONIC

The characteristics of hypersonic flow differ from those of supersonic flow in that

1. The shock waves in hypersonic flow lie close to the body causing a strong boundary-layer--shock-wave interaction which exerts an important influence on the flow field. The boundary layer in hypersonic flow may be 10 to 100 times thicker than at low speeds; consequently, a change in the effective body shape results, which in turn brings about a change in the shape of the nose shock wave.
2. High-temperature gas effects become evident at hypersonic speeds.
3. The flow becomes essentially nonlinear in nature.
4. Hypersonic similarity exists. It has been shown that at hypersonic Mach numbers the potential flow of similar airfoils is dynamically similar if the product $\beta(t/c)$ is a constant.

An approximate criterion for defining hypersonic flow is

$$\beta \frac{t}{c} \geq 0.5$$

Since, in hypersonic flow, β is very close to M , the relationship $M(t/c) = K_t$ is used as the hypersonic similarity parameter.

Because of the nonlinearity of hypersonic flow, approximate methods of estimating force characteristics are very desirable. Among the methods used, Newtonian and modified Newtonian theory have proved quite useful. Newtonian theory (reference 20) is based on the assumption that the shock coincides with the wing surfaces and that no friction exists between the wing and the shock layer. The fluid particles ahead of the wing are not disturbed until they encounter the wing surface, at which point the relative momentum normal to the surface is lost and the tangential flow has no further change in velocity. In this case, the air may be visualized as composed of discrete particles, which, after impact, travel parallel to the surface. When the particles reach the free-stream direction, they leave the surface, giving essentially zero pressure on the leeward side.

DATCOM METHOD

The drag at zero-lift is approximated by the drag of the forward-facing surface. Typical values of $C_{D_0}/2\tau^2$ for a wedge, as predicted by Newtonian theory, are presented in the following table from reference 20. (τ is one-half the thickness ratio of the forward-facing surface). It is to be noted that the drag can be reduced as much as one-half by optimization of the shape behind the initial wedge angle.

TYPICAL VALUES OF C_{D_0} FOR A WEDGE

Two-Dimensional
(Reference 20)

Shape	$\frac{1}{2\tau^2} C_{D_0}$	$\frac{C_{D_0}}{(C_{D_0})_{\text{abs. opt.}}}$
Wedge	1.000	2.000
0.864 Power	0.918	1.836
Proper Optimum	0.770	1.540
Absolute Optimum	0.500	1.000

Note that C_{D_0} is based on frontal area.

Detailed discussions of optimization methods are given in reference 20.

E. RAREFIED GAS

In the previous speed regimes it is assumed that the air behaves as a continuum. At very high altitudes, however, where very low densities are encountered, the actual molecular structure of the air becomes extremely important. Figure 4.1.5.1-32 presents a qualitative division of the various regimes of gas dynamics. It is to be noted that the region of rarefied gases is further divided into regions of varying amounts of rarefaction; i.e., "slip flow" or slightly rarefied, "transition" or moderately rarefied, and "free-molecule flow" or highly rarefied.

Slip Flow

The slip-flow region is of most interest to the aircraft and missile designer. In this region continuum theory becomes questionable, and satisfactory analytical results are uncommon, since the effects of slip flow are usually masked by large compressibility and viscous effects. Figure 4.1.5.1-33 (reference 21) presents test data points for skin friction in slip flow compared with incompressible theory for continuum flow (reference 22). It should be noted that in the subsonic case the test data are generally lower than the theoretical, while at supersonic speeds they are generally higher. This tends to confirm the theory that skin friction in the slip-flow regime is affected by two interrelated phenomena, the interaction of the thick boundary layer with the inviscid flow and the slip at the surface. The former is more important at the higher densities, gradually giving way to the latter for densities extending into the transition regime.

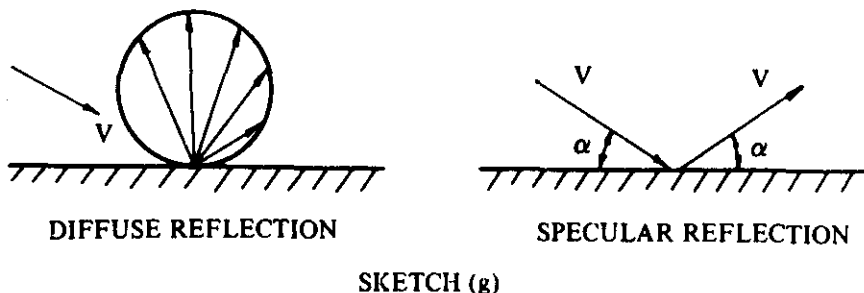
Transition Flow

Present knowledge about the transition regime is extremely limited and will not be covered here.

Free-Molecule Flow

In the free-molecule flow regime, the mean free path of the molecule is large compared to the characteristic dimension of an aerodynamic body in the flow, and the individual gas molecules striking the body do not interact with the surrounding molecules. For this reason the incident flow is assumed to be undisturbed by the presence of the body and no shock waves are expected to form. The boundary layer is very diffuse and has no effect on the flow incident on the body.

The problems associated with free-molecule flow are of particular interest to the satellite designer. In contrast to the other two regimes of rarefied-gas flow, the free-molecule regime can be treated analytically with less difficulty. The drag values of a flat plate with $\alpha = 0$ for diffuse and specular reflection are shown in figures 4.1.5.1-34a and 4.1.5.1-34b, respectively. Diffuse reflection is one in which the velocity of the reflected particles have a Maxwellian velocity distribution (see sketch (g)). Specular reflection is one in which the normal momentum is reversed at the surface and the tangential momentum remains constant.



REFERENCES

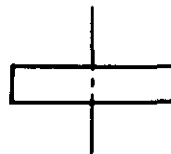
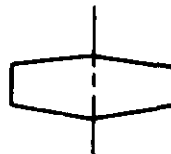
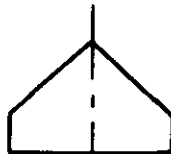
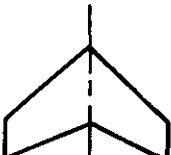
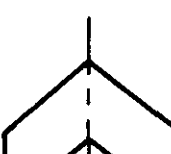
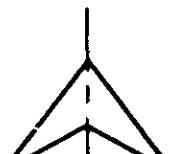
1. Hoerner, S.F.: Fluid-Dynamic Drag. Published by Author, 1958. (U)
2. Blakeslee, D.J., Johnson, R.P., and Skavdahl, H.: A General Representation of the Subsonic Lift-Drag Relation for an Arbitrary Airplane Configuration. Rand Report RM 1593, 1955. (U)
3. Benepe, D.B., Kouri, B.G., Webb, J.B., et al: Aerodynamic Characteristics of Non-Straight-Taper Wings. AFF DL-TR-66-73, 1966. (U)
4. Marquardt, R.F.: A General Method for Predicting Subsonic Minimum Drag of an Arbitrary Aircraft Configuration. General Dynamics, F/W MR-A-1261, 1961. (C) Title Unclassified
5. von Karman, T.: The Similarity Laws of Transonic Flow. J. Math. and Physics, Vol. XXVI, No. 3, Oct 1947. (U)
6. Busemann, A.: Application of Transonic Similarity. NACA TN 2687, 1952. (U)
7. Spreiter, J.R., and Alksne, A.: Theoretical Prediction of Pressure Distributions on Nonlifting Airfoils at High Subsonic Speeds. NACA TR 1217, 1955. (U)
8. Flecke, D.: Vergleich der theoretischen und experimentellen Widerstandsbeläge im Schall- und Überschallgebiet. Z. Flugwiss. 6, Heft 2, 1958. (U)
9. Bonney, E.A.: Aerodynamic Characteristics of Rectangular Wings at Supersonic Speeds. Jour. Aero. Sci., Vol. 14, No. 2, Feb. 1947. (U)
10. Puckett, A.E., and Stewart, H.J.: Aerodynamic Performance of Delta Wings at Supersonic Speeds. Jour. Aero. Sci., Vol. 14, No. 10, Oct. 1947. (U)

11. Beane, B.: The Characteristics of Supersonic Wings Having Biconvex Sections. Jour. Aero. Sci., Vol. 18, No. 1, Jan. 1951. (U)
12. Puckett, A.E.: Supersonic Wave Drag of Thin Airfoils. Jour. Aero. Sci., Vol. 13, No. 9, Sept. 1946. (U)
13. Margolis, K.: Supersonic Wave Drag of Sweptback Tapered Wings at Zero Lift. NACA TN 1448, 1947. (U)
14. Margolis, K.: Supersonic Wave Drag of Nonlifting Sweptback Tapered Wings With Mach Lines Behind the Line of Maximum Thickness. NACA TN 1672, 1948. (U)
15. Jones, R.T.: Thin Oblique Airfoils at Supersonic Speed. NACA TN 1107, 1946. (U)
16. Jones, R.T.: Properties of Low-Aspect-Ratio Pointed Wings at Speeds Below and Above the Speed of Sound. NACA TN 1032, 1946. (U)
17. Jones, R.T.: Wing Planforms for High Speed Flight. NACA TR 863, 1945. (U)
18. Bishop, R.A., and Cane, E.G.: Charts of the Theoretical Wave Drag of Wings at Zero-Lift. RAE TN 2421, 1956. (U)
19. Crosthwaite, E.L.: Drag of Two-Dimensional Cylindrical Leading Edges. General Dynamics, F/W Rpt. AIM No. 50, 1966. (U)
20. Hayes, W.D., and Probstein, R.F.: Hypersonic Flow Theory. Academic Press, New York, 1959. (U)
21. Emmons, H.W., ed.: Fundamentals of Gas Dynamics. Princeton University Press, Princeton, New Jersey, 1958. (U)
22. Janour, Z.: Resistance of a Plate in Parallel Flow at Low Reynolds Number. NACA TM 1316, 1951. (U)
23. Henderson, W.P., and Hammond, A.D.: Low-Speed Investigation of High-Lift and Lateral Control Devices on a Semispan Variable-Sweep Wing Having an Outboard Pivot Location. NASA TM X-542, 1961. (U)
24. Nelson, W.H., Allen, E.C., and Krumm, W.J.: The Transonic Characteristics of 36 Symmetrical Wings of Varying Taper, Aspect Ratio, and Thickness as Determined by the Transonic-Bump Technique. NACA RM A53I29, 1953. (U)
25. Cooper, M., and Sevier, J.R., Jr.: Effects of a Series of Inboard Plan-Form Modifications on the Longitudinal Characteristics of Two 47° Sweepback Wings of Aspect Ratio 3.5, Taper Ratio 0.2, and Different Thickness Distributions at Mach Numbers of 1.61 and 2.01. NACA RM L53E07a, 1953. (U)
26. Lin, C.C. (ed.): Turbulent Flows and Heat Transfer. Princeton University Press, Princeton, New Jersey, 1959. (U)
27. Skavdahl, H.: Pressure Drag at Zero Lift for Rounded Leading Edge Wings in the Presence of Bodies. Rand Report RM 1562, 1955 (C)
Title Unclassified
28. Blakeslee, D.J.: Pressure Drag at Zero Lift in Presence of Body for Wings With Sharp Leading Edges. Rand Report RM 1535, 1955. (C)
Title Unclassified

TABLE 4.1.5.1-A
REPRESENTATIVE VALUES OF SURFACE-ROUGHNESS HEIGHT

Type of Surface	Equivalent Sand Roughness k (inches)
Aerodynamically smooth	0
Polished metal or wood	$0.02 - 0.08 \times 10^{-3}$
Natural sheet metal	0.16×10^{-3}
Smooth matte paint, carefully applied	0.25×10^{-3}
Standard camouflage paint, average application	0.40×10^{-3}
Camouflage paint, mass-production spray	1.20×10^{-3}
Dip-galvanized metal surface	6×10^{-3}
Natural surface of cast iron	10×10^{-3}

TABLE 4.1.5.1-B
SUMMARY OF FINITE WING SOLUTIONS

PLANFORM	SECTION	WAVE-DRAG SOLUTION (ZERO LIFT)	
		Bonney	Ref. 9
		Bonney	Ref. 9
		Puckett & Stewart Beane	Ref. 10 Ref. 11
		Beane	Ref. 11
		Puckett Margolis	Ref. 12 Ref. 13, 14
		Beane	Ref. 11
		Puckett & Stewart Margolis Bishop & Cane	Ref. 10 Ref. 13, 14 Ref. 18
		Jones Beane Bishop & Cane	Ref. 15, 16, 17 Ref. 11 Ref. 18
		Bishop & Cane	Ref. 18
			
			
		Bishop & Cane	Ref. 18
			
			

4.1.5.1-26

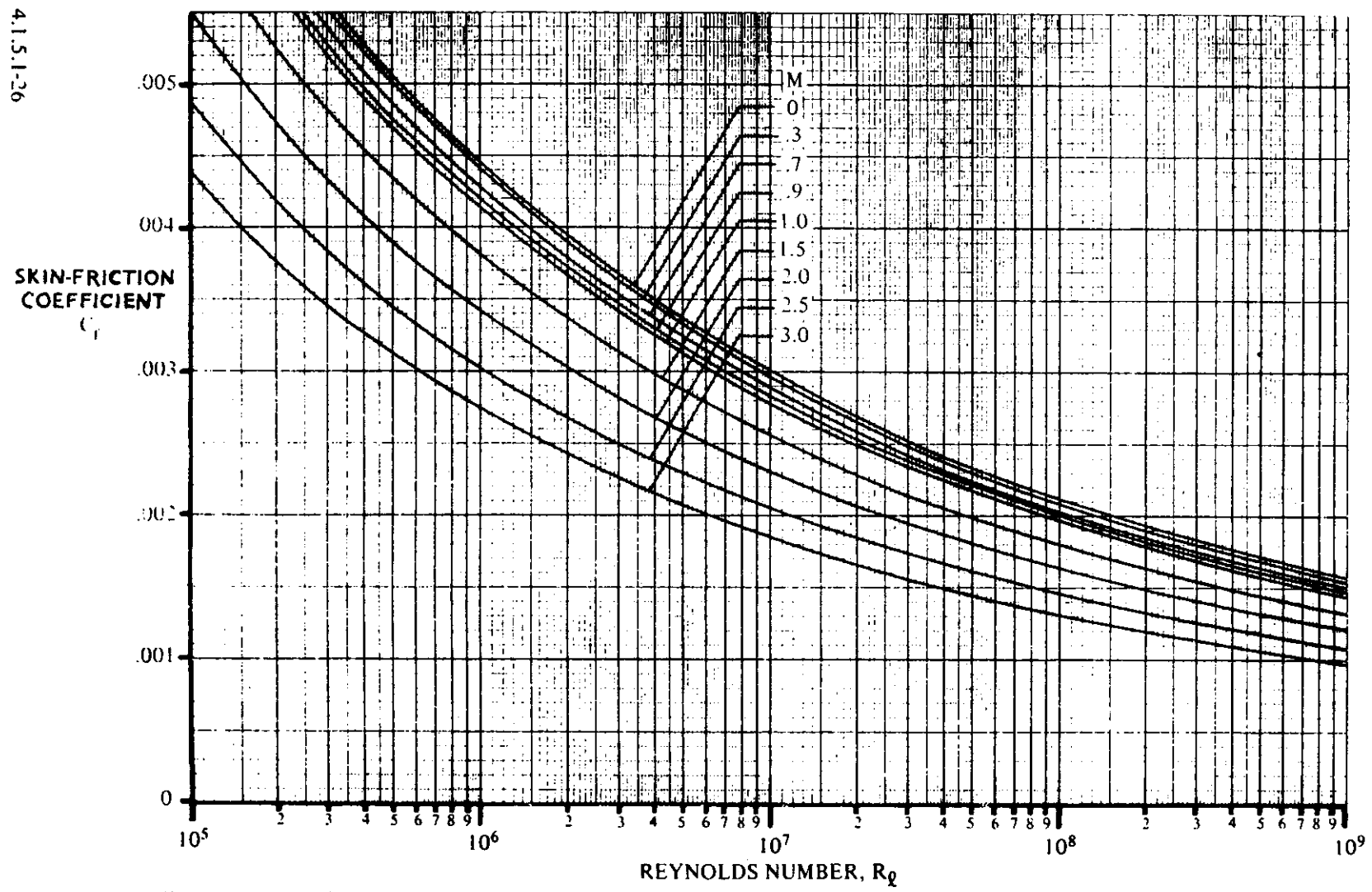


FIGURE 4.1.5.1-26 TURBULENT MEAN SKIN-FRICTION COEFFICIENT ON AN INSULATED FLAT PLATE

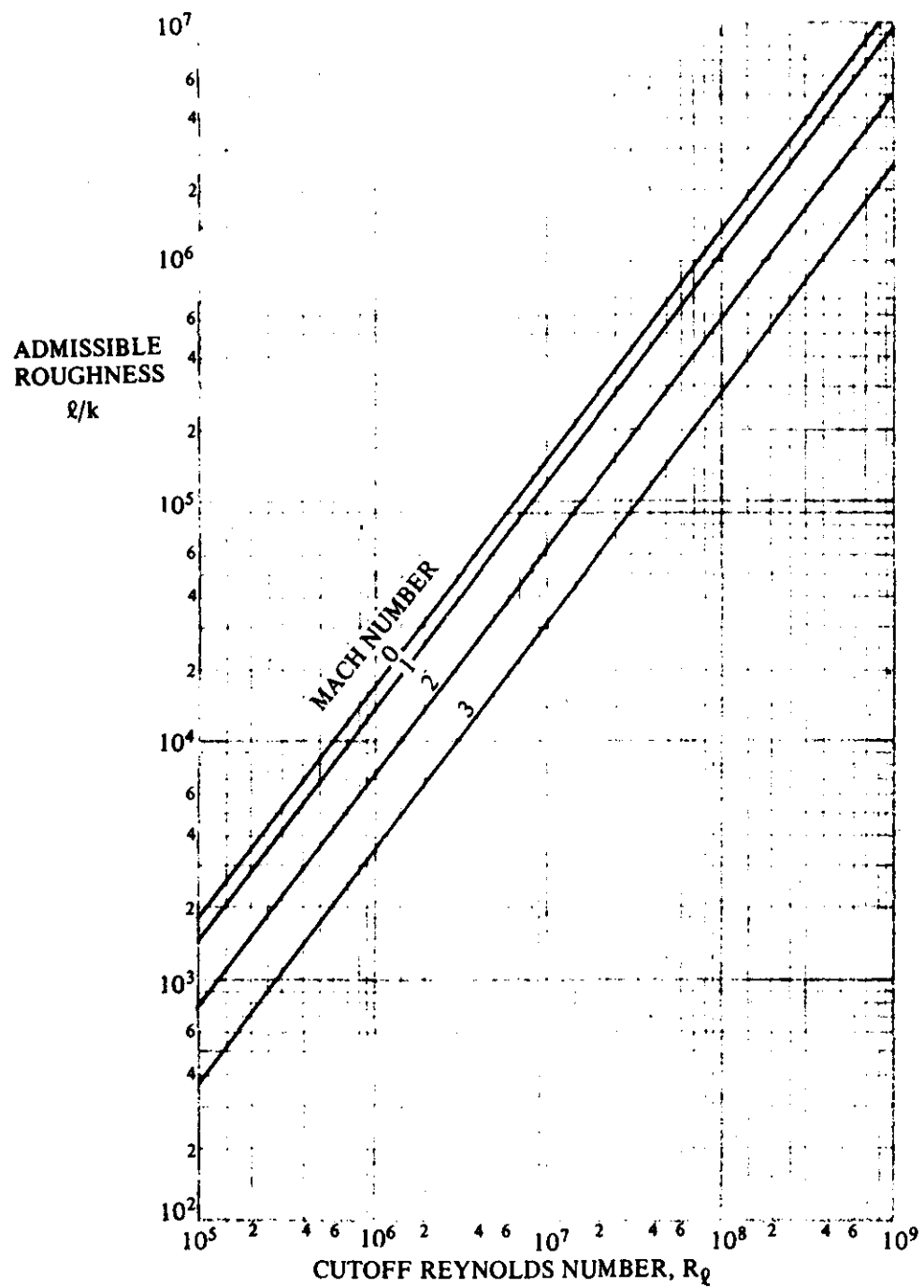


FIGURE 4.1.5.1-27 CUTOFF REYNOLDS NUMBER

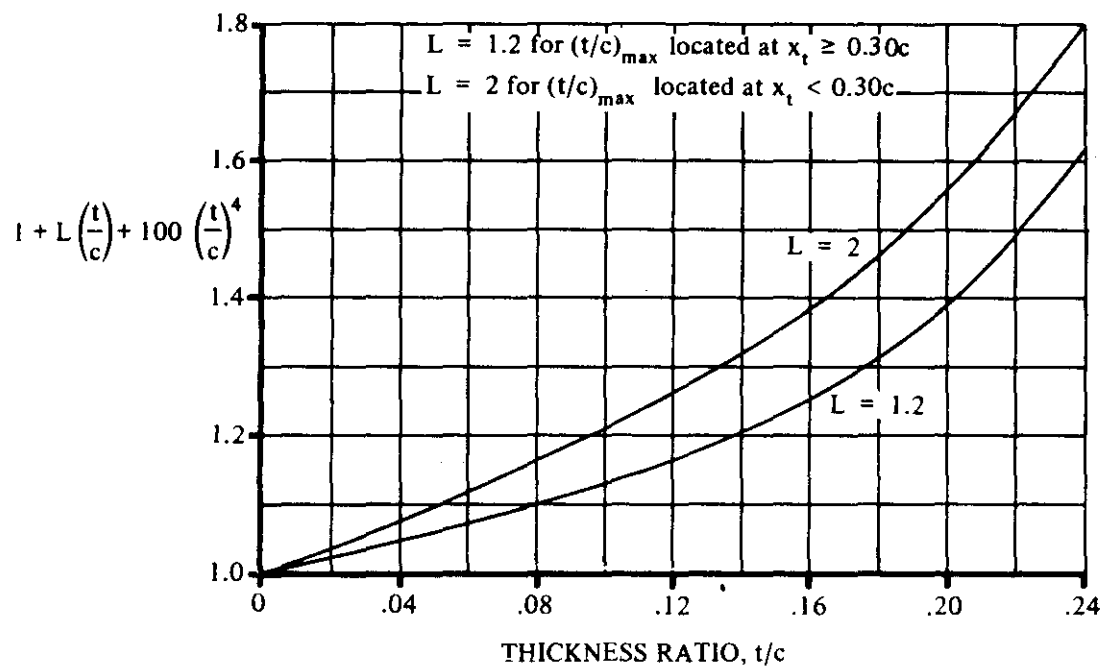


FIGURE 4.1.5.1-28a SUBSONIC WING MINIMUM-DRAG FACTOR

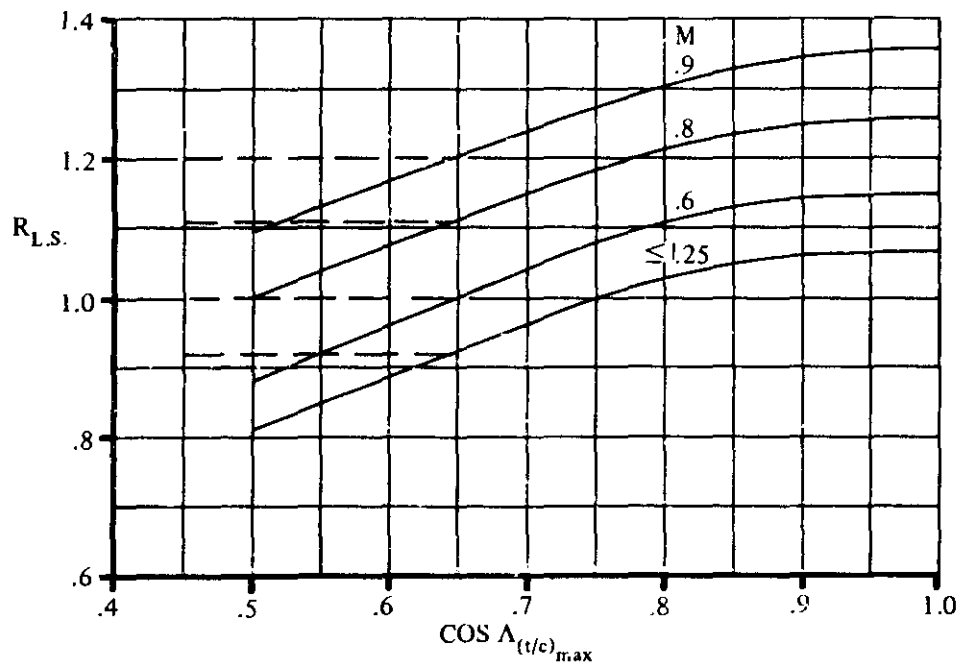


FIGURE 4.1.5.1-28b LIFTING-SURFACE CORRELATION FACTOR FOR SUBSONIC MINIMUM DRAG

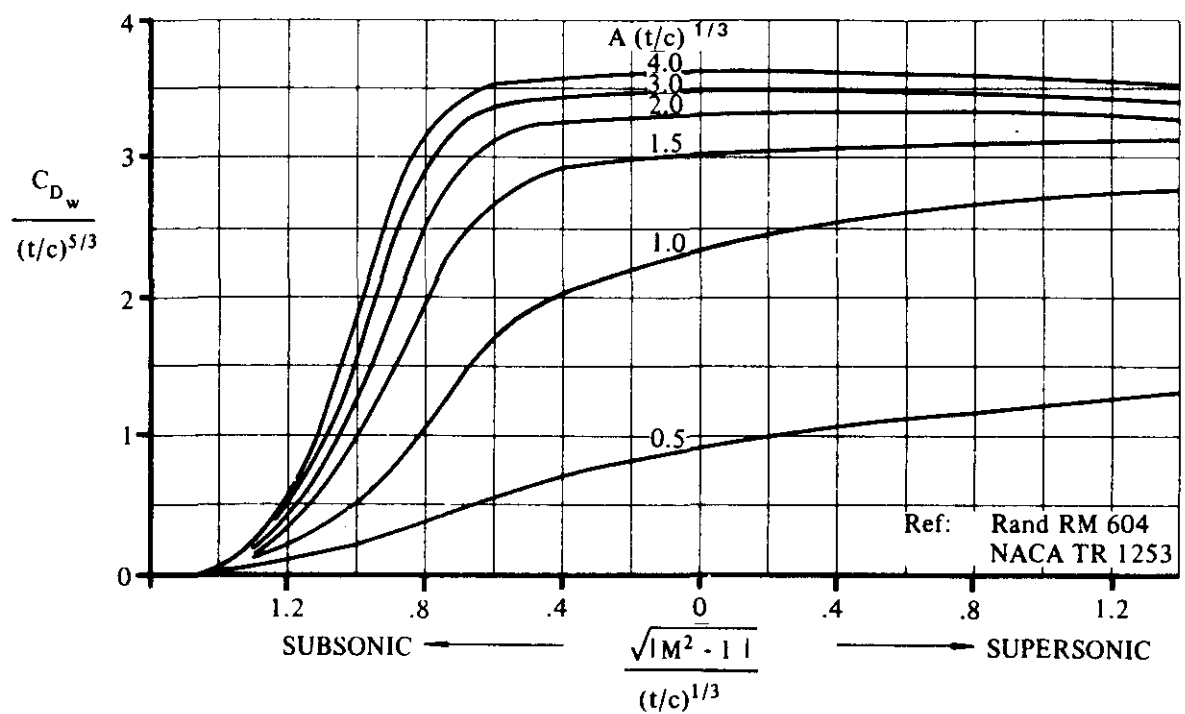


FIGURE 4.1.5.1-29 TRANSONIC ZERO-LIFT WING WAVE DRAG FOR UNSWEPT WINGS AND ROUND-NOSE AIRFOILS

$$C_{D_{LE}} \left[\frac{S_{ref}}{2r_{LE_{bw}} \left(\frac{b_{bw}}{\cos \Lambda_{LE_{bw}}} \right)} \right] = 1.28 \frac{M^3 \cos^6 \Lambda_{LE_{bw}}}{1 + M^3 \cos^3 \Lambda_{LE_{bw}}} \quad (\text{Ref. 19})$$

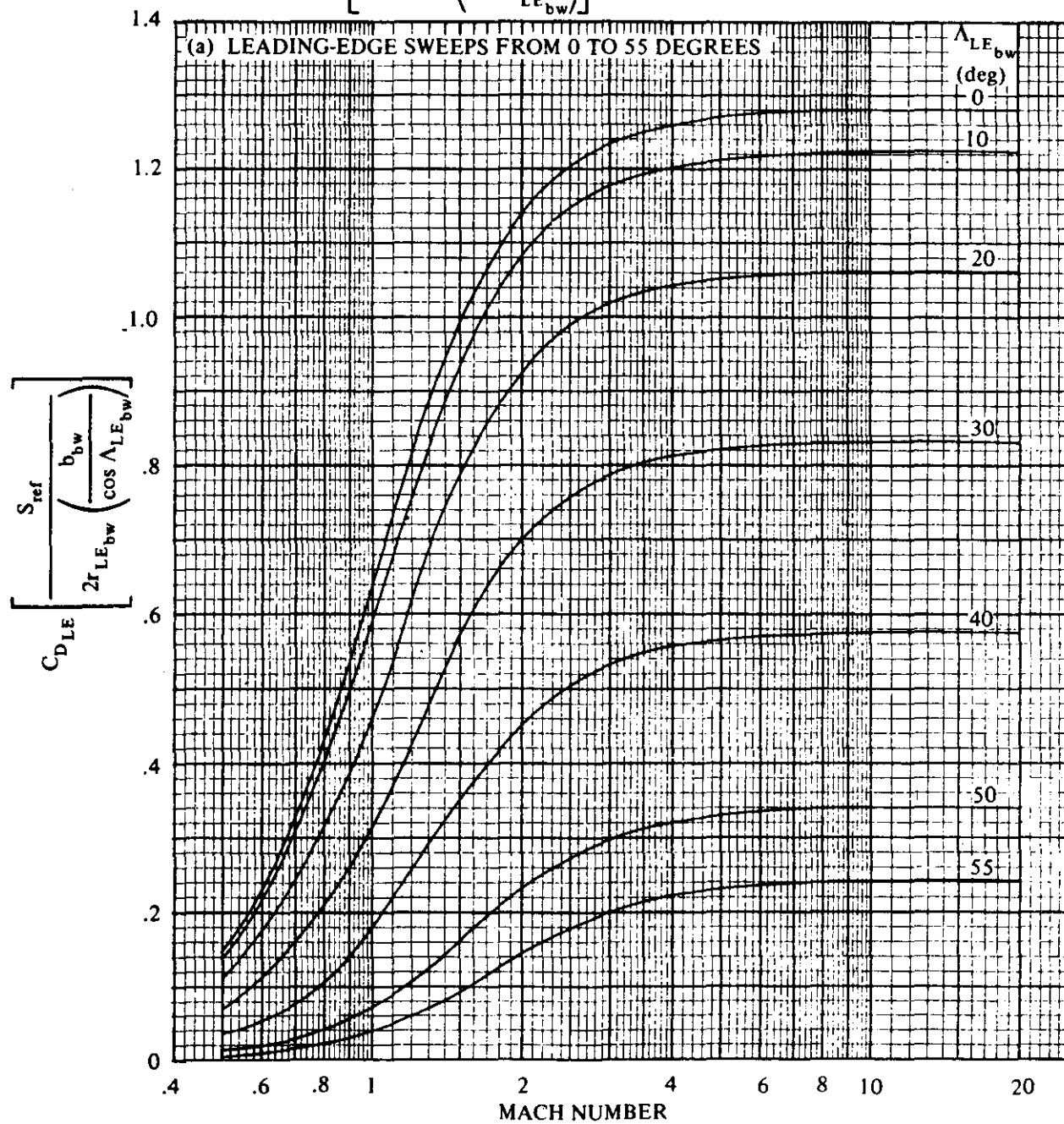


FIGURE 4.1.5.1-30 CORRELATION OF CYLINDRICAL LEADING-EDGE PRESSURE DRAG COEFFICIENTS

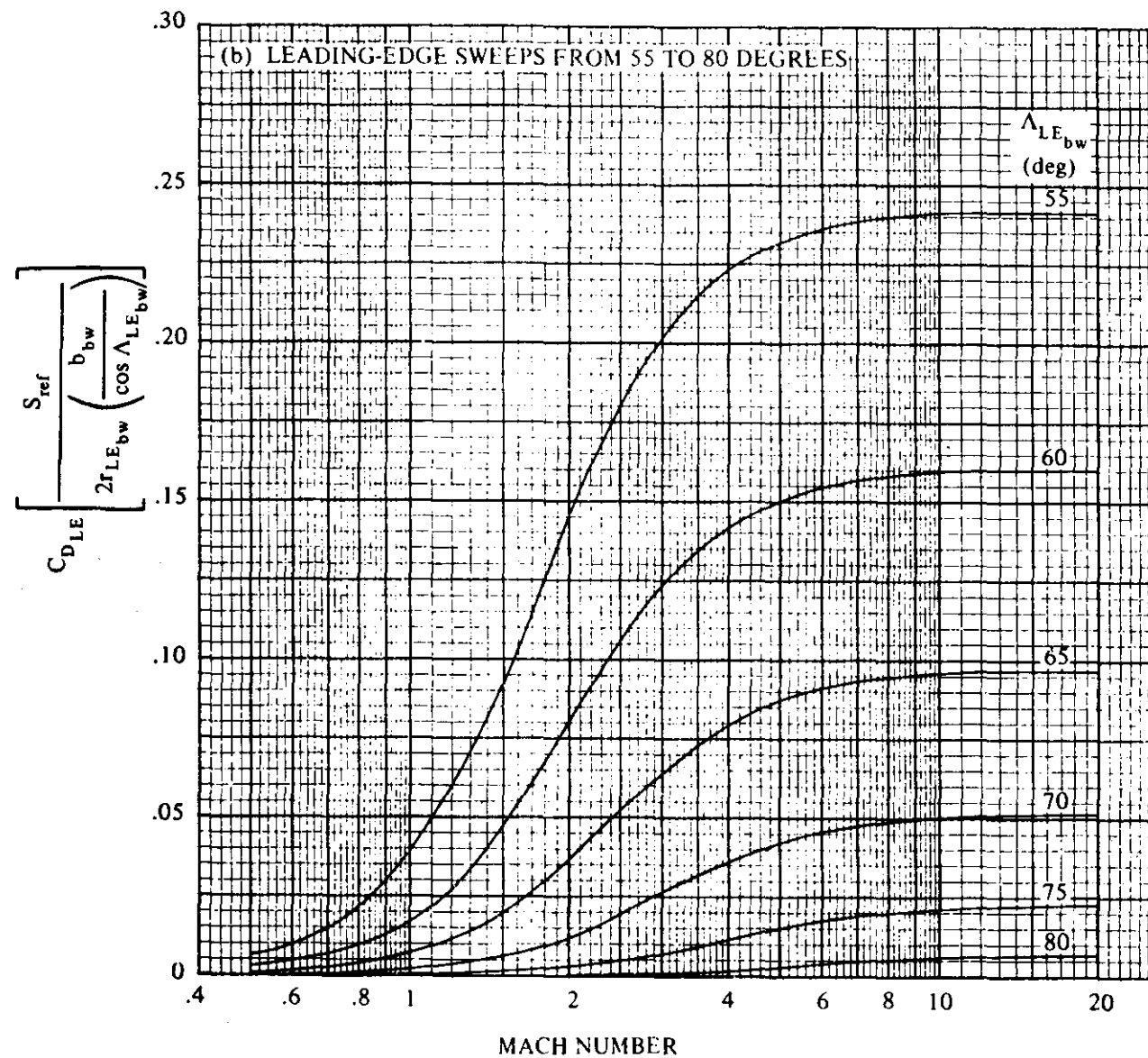


FIGURE 4.1.5.1-30 (CONTD)

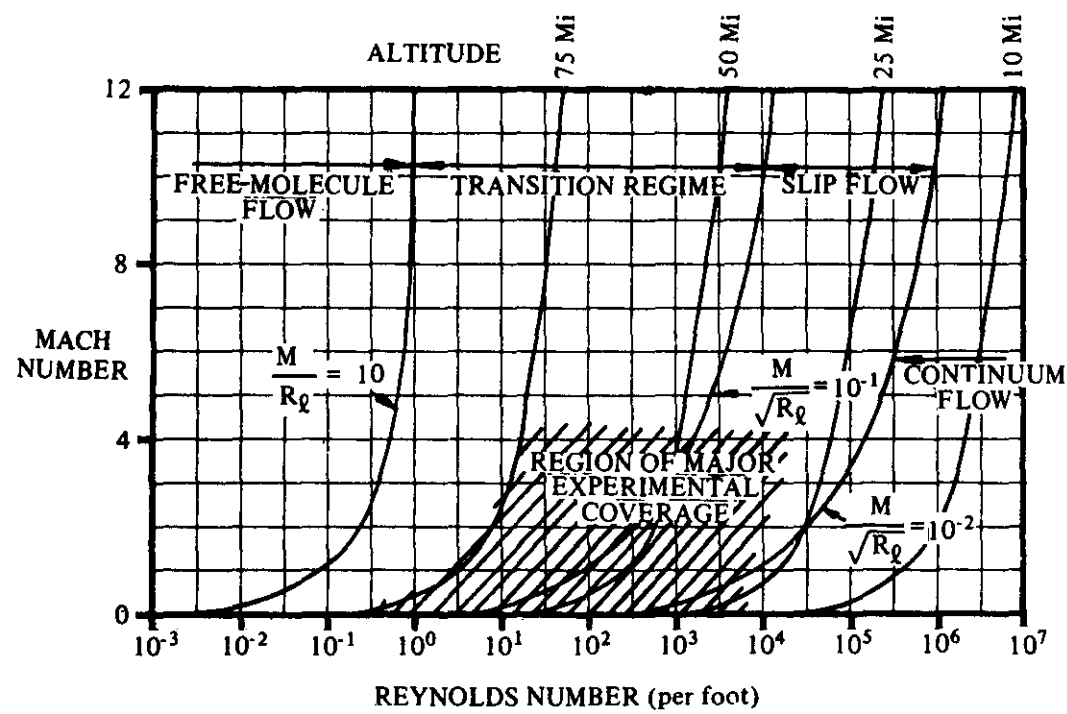


FIGURE 4.1.5.1-32 GENERALIZED RAREFIED GAS FLOW REGIMES

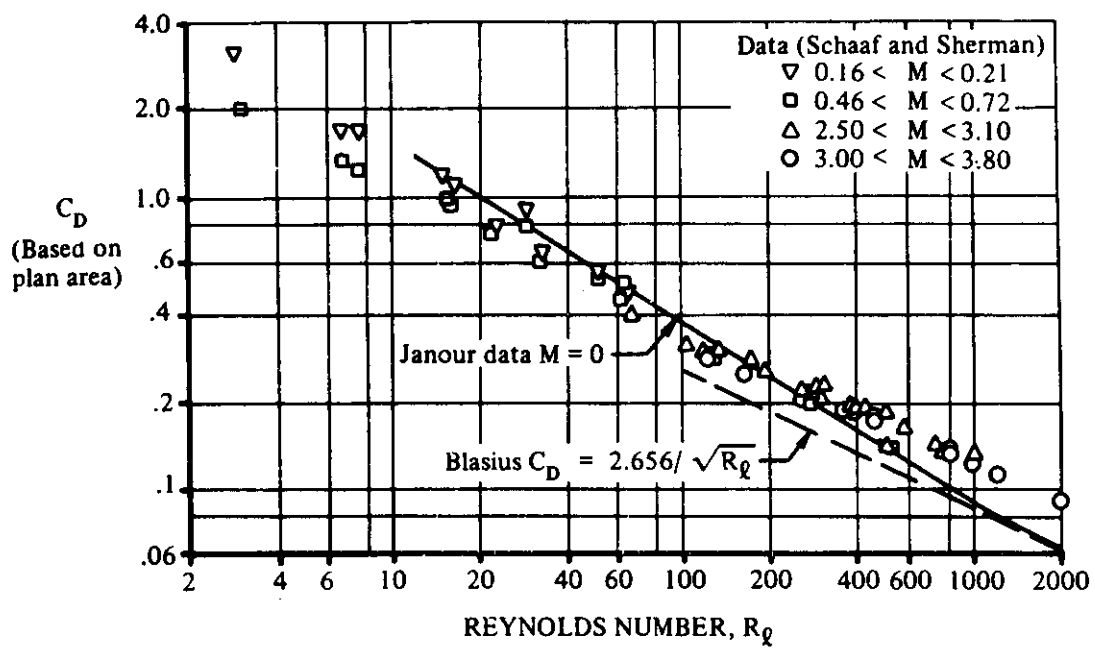


FIGURE 4.1.5.1-33 SKIN FRICTION IN SLIP FLOW

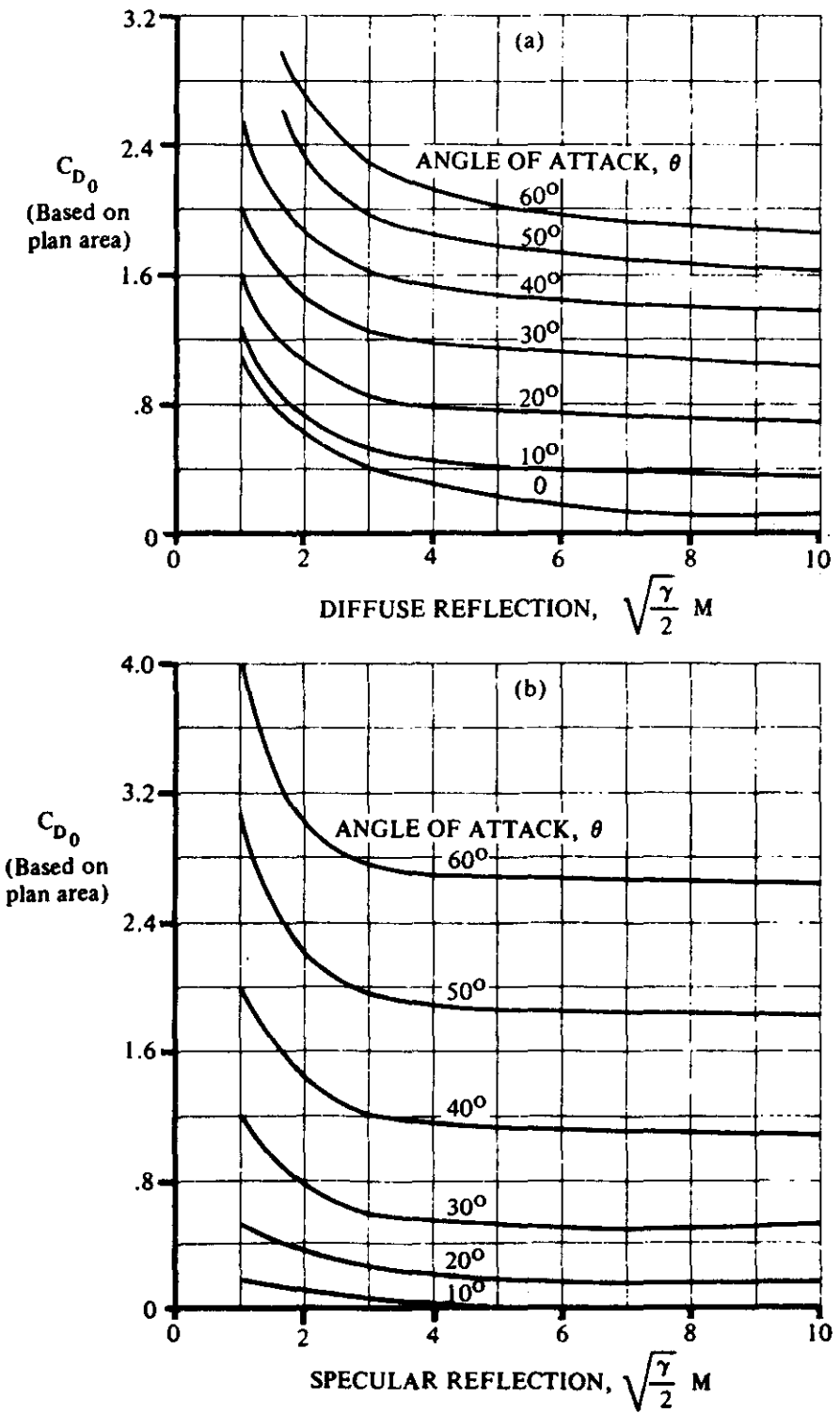


FIGURE 4.1.5.1-34 ZERO-LIFT FLAT-PLATE DRAG FOR FREE-MOLECULE FLOW

4.1.5.2 WING DRAG AT ANGLE OF ATTACK

The drag of a wing at angle of attack can be expressed in the form

$$C_D = C_{D_0} + C_{D_L}$$

where C_{D_0} is the zero-lift drag and the term C_{D_L} represents the drag due to lift. The zero-lift drag of a wing may be obtained by using the methods of Section 4.1.5.1. Methods are presented in this section for estimating the drag-due-to-lift term.

The drag due to lift of a wing increases approximately as the square of the lift coefficient or angle of attack and may be expressed in the form

$$C_{D_L} = \frac{K C_L^2}{\pi A} \quad 4.1.5.2-a$$

where K is the drag-due-to-lift factor.

Equation 4.1.5.2-a can further be written as the sum of two terms, the well-known induced drag (or trailing-vortex drag) C_{D_i} and the viscous drag due to lift C_{D_V} , so that

$$C_{D_L} = C_{D_i} + C_{D_V} \quad 4.1.5.2-b$$

These drag terms are discussed below.

Induced Drag

The induced drag depends on the wing spanwise loading distribution, since it results from the lift produced by the wing trailing-vortex system. The trailing-vortex system rotates the total wing-force vector rearward, giving the induced-drag component, which increases approximately as the square of the lift coefficient or angle of attack. Induced drag may be expressed as

$$C_{D_i} = \frac{C_L^2}{\pi A e^*} \quad 4.1.5.2-c$$

where e^* is the induced span-efficiency factor (or wing span-efficiency factor with $C_{D_V} = 0$).

The theoretical minimum induced drag attainable is obtained from a wing with elliptic span loading, in which case an induced span-efficiency factor of 1.0 represents the theoretically ideal wing.

Viscous Drag Due to Lift

The viscous drag due to lift results from the change in boundary-layer development with lift over the wing. The upper-surface boundary layer increases in thickness as the angle of attack increases, which results in an increase in wing profile drag (skin-friction + pressure drag).

With the induced drag expressed by equation 4.1.5.2-c, the total drag due to lift is given by

$$C_{D_L} = \frac{C_L^2}{\pi A e^*} + C_{D_v} \quad 4.1.5.2-d$$

Since the viscous drag due to lift also varies directly with C_L^2 , the total drag due to lift is often expressed as

$$C_{D_L} = \frac{C_L^2}{\pi A} \quad 4.1.5.2-e$$

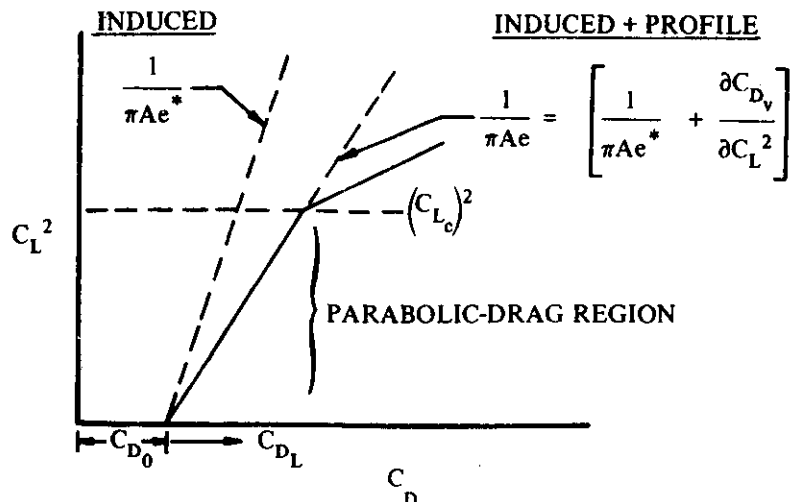
which is of the form of equation 4.1.5.2-a with the drag-due-to-lift factor K expressed as $1/e$, where e is the span-efficiency factor, including the effect of viscosity. Therefore, the span-efficiency factor may be expressed in the familiar form

$$e = \frac{1}{\frac{\partial C_{D_L}}{\pi A \frac{\partial C_L^2}{\partial C_L^2}}} \quad 4.1.5.2-f$$

or, in the more basic form

$$e = \frac{1}{\pi A \left[\frac{1}{\pi A e^*} + \frac{\partial C_{D_v}}{\partial C_L^2} \right]} \quad 4.1.5.2-g$$

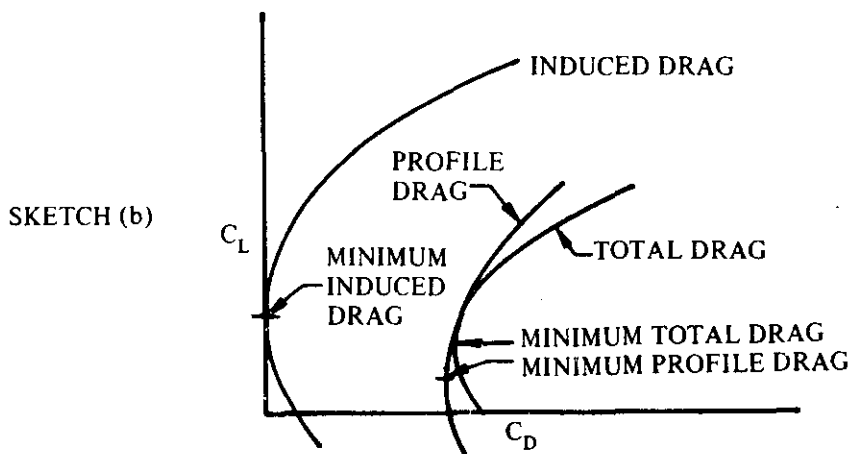
The drag-due-to-lift factor is constant over a lift-coefficient range from zero to a certain value of C_L , termed the "critical" lift coefficient C_{L_c} . Over this range, referred to as the parabolic-drag region, the variation of drag with C_L^2 is linear (see sketch (a)).



SKETCH (a)

Above C_{L_c} the polar breaks away from a simple parabolic representation because of separation effects, which cause the drag to increase significantly and the drag polar to deviate considerably from the parabolic-drag variation. High sweepback and sharp leading edges promote leading-edge separation at relatively low lift coefficients, resulting in low values of the "critical" lift coefficient.

Cambered and/or twisted wings have a somewhat more complicated drag characteristic. Neither the minimum profile drag nor the minimum induced drag necessarily occurs at zero lift. Sketch (b) illustrates these drag components for a typical cambered and twisted wing. Furthermore, the span-efficiency factor, at any given lift coefficient, varies within wide limits for these wings.



In supersonic flow the wing drag-due-to-lift breakdown is similar to that described above. In addition to the induced drag resulting from the trailing-vortex system (sweptback at the Mach angle), there exists shock-wave drag due to lift resulting from the viscous dissipation associated with the shock waves.

A. SUBSONIC

Many attempts have been made to develop empirical methods for predicting the subsonic span-efficiency factor over the parabolic-drag region. Three recent attempts are reported in references 1, 2, and 3. Frost and Rutherford (reference 1) have used a measure of leading-edge suction as a function of the leading-edge-radius Reynolds number to correlate ϵ based on equation 4.1.5.2-e. This correlation has been further refined in reference 2 to account for planform geometry. In reference 3, Gardner and Weir take a more basic approach to the problem by correlating the viscous drag due to lift as a function of streamwise-thickness ratio and the loss in lift-curve slope due to viscosity. The empirical results of reference 3 are used as the basis of the method presented in reference 4 for estimating the viscous drag due to lift.

At subsonic speeds methods are presented for determining the drag due to lift of the following two classes of wing planforms:

Straight-Tapered Wings (conventional, trapezoidal wings)

Non-Straight-Tapered Wings

- Double-delta wings
- Cranked wings
- Curved (Gothic and ogee) wings

These general categories of non-straight-tapered wings are illustrated in sketch (a) of Section 4.1.3.2. Their wing-geometry parameters are presented in Section 2.2.2.

DATCOM METHODS

Straight-Tapered Wings

This method is based on the empirical correlation of the span-efficiency factor as a function of leading-edge suction as presented in reference 1. This correlation is further refined in reference 2 to account for planform geometry. The effect of linear wing twist on the subsonic inviscid induced drag of swept wings is accounted for by the methods of reference 5.

The subsonic drag due to lift of twisted, sweptback wings of straight-tapered planform for lift coefficients up to the "critical" lift coefficient is given by

$$C_{D_L} = \frac{C_L^2}{\pi A e} + C_L \theta c_{L\alpha} v + (\theta c_{L\alpha})^2 w \quad 4.1.5.2-h$$

where

C_L is the wing lift coefficient.

$c_{L\alpha}$ is the airfoil section lift-curve slope (2π per radian is sufficiently accurate for this method.)

θ is the wing twist, positive for washin (a linear twist distribution is assumed).

v is the induced-drag factor due to linear twist obtained from figures 4.1.5.2-42a through 4.1.5.2-42i.

w is the zero-lift drag factor due to linear twist obtained from figures 4.1.5.2-48a through 4.1.5.2-48i.

e is the span-efficiency factor determined by

$$e = \frac{1.1 (C_{L\alpha}/A)}{R(C_{L\alpha}/A) + (1 - R)\pi} \quad 4.1.5.2-i$$

where

$C_{L\alpha}$ is the wing lift-curve slope obtained by the method presented for straight-tapered wings in paragraph A of Section 4.1.3.2.

R is the leading-edge-suction parameter defined as the ratio of leading-edge suction actually attained to that theoretically possible. This parameter is presented in figure 4.1.5.2-53 as a function of leading-edge-radius Reynolds number, Mach number, aspect ratio, and sweepback. The leading-edge-radius Reynolds number $R_{\rho_{LER}}$ is based on the leading-edge radius of the airfoil at the wing mean aero-dynamic chord.

For values of the parameter $R_{\rho_{LER}} \cot \Lambda_{LE} \sqrt{1 - M^2 \cos^2 \Lambda_{LE}} > 1.3 \times 10^5$, R is read from figure 4.1.5.2-53b.

For wings with sharp leading edges $R_{\lambda_{LER}} = 0$ and $R = 0$. For such configurations the method results in the approximation $C_{D_L}/C_L^2 = 1/(1.1 C_{L\alpha})$.

A comparison of test data with results calculated by this method is presented as table 4.1.5.2-A. Most of the configurations listed in the table are wing-body combinations with small values of the ratio of body diameter to wing span. For these configurations, the predictions were made using the total wing planform geometry and neglecting body effects. The ranges of planform and flow parameters of the test data are:

$$\begin{aligned} 2 &\leq A \leq 10.7 \\ 0 &\leq \lambda \leq 0.713 \\ 19.1^\circ &\leq \Lambda_{LE} \leq 63.4^\circ \\ 0.72 \times 10^6 &\leq R_{\lambda_{MAC}} \leq 16.6 \times 10^6 \\ 0.13 &\leq M \leq 0.81 \end{aligned}$$

Since the effect of camber is not accounted for in the method, no cambered wing data are included in table 4.1.5.2-A.

The limited amount of data available precludes substantiation of the effect of linear wing twist as given in reference 5. The design charts for the induced-drag factor due to linear twist and the zero-lift drag factor due to linear twist have resulted from the use of 59 Weissinger span stations to compute these quantities by means of an automatic digital computer program. In addition, the effect of compressibility on these parameters has been accounted for by applying the Prandtl-Glauert transformation.

Application of the method to an untwisted, sweptback wing is illustrated by sample problem 1 on page 4.1.5.2-9.

Non-Straight-Tapered Wings

Semiempirical methods, taken from reference 2, are presented for estimating the subsonic induced drag of non-straight-tapered wings. The methods presented for double-delta and curved planforms are applicable only to wings with sharp leading edges. In the development of these methods the effect of leading-edge suction was neglected, and the expression used as a basis for the correlation of induced drag was written solely in terms of the normal-force coefficient.

The method presented for cranked planforms is applicable only to wings with round leading edges. All the cranked wings analyzed in reference 2 had round leading edges; therefore, the development of the prediction technique was based on properly accounting for the leading-edge suction force. The resulting method is an extension of the straight-tapered-wing method presented above. It was assumed that given an accurate estimate of the leading-edge-suction parameter on both the inboard and outboard panels of a cranked wing, an effective leading-edge-suction parameter can be estimated by a span-weighted average.

The method presented for cranked wings is applicable in the higher lift-coefficient range where the drag polar deviates from a parabolic variation, as well as in the lower lift-coefficient range. The method presented for sharp-edged double-delta and curved planforms is valid only for the higher lift coefficients. In each case an empirical correlation has been derived that accounts for the effects of flow separation at the higher values of lift coefficient.

Double-Delta Wings

The subsonic induced drag of double-delta wings with sharp leading edges is given by

$$C_{D_L} = 0.95 C_L \tan \alpha$$

4.1.5.2-j

where

C_L is the wing lift coefficient at angle of attack obtained by the method presented for double-delta wings in paragraph A of Section 4.1.3.3.

The constant in equation 4.1.5.2-j is the drag-due-to-lift factor. This factor has been determined during the course of the work reported in reference 2 by plotting test values of $C_{D_L}/(C_L \tan \alpha)$ versus α .

This correlation showed that at $\alpha > 8^\circ$, the ratio of $C_{D_L}/(C_L \tan \alpha)$ approaches 0.95. However, below $\alpha = 8^\circ$ there was considerable scatter in the data. This is attributed to the inability to determine C_{D_L} accurately from the test data at the lower angles of attack. The method should not be expected to give satisfactory results below $\alpha = 8^\circ$.

A sample problem illustrating the use of this method is presented on page 4.1.5.2-10.

A comparison of test data with results calculated by this method is presented as table 4.1.5.2-B (taken from reference 2). The test results have been compiled entirely from reference 15 and were the only available low-speed data for sharp-edged double-delta wings. Although all the configurations listed in the table are wing-body combinations, all predictions were made by using the total wing planform geometry and neglecting body effects. Note that at $\alpha = 4^\circ$ the method does not adequately predict C_{D_L} for sharp-edged double-delta wings.

Since all the test data of table 4.1.5.2-B were included in the drag-due-to-lift-factor correlation, application of the method to configurations with geometric parameters falling outside those of table 4.1.5.2-B should be approached with caution. The ranges of planform parameters used in the correlation are:

$$\begin{aligned} 1.34 &< A < 1.87 \\ 72.6^\circ &< \Lambda_{LE_i} < 77.4^\circ \\ \Lambda_{LE_o} &= 59^\circ \\ 0.332 &< \eta_B < 0.628 \end{aligned}$$

Although the data in table 4.1.5.2-B are for $M = 0.13$, the method should be applicable at higher subsonic Mach numbers, provided an accurate estimation of the C_L versus α variation can be made.

The effects of wing twist and/or camber are not accounted for in the method.

For double-delta wings with round leading edges, it is suggested that the subsonic drag due to lift be approximated by using the method for cranked wings.

Cranked Wings

The subsonic drag due to lift of cranked wings with round leading edges is given by

$$C_{D_L} = \frac{C_L^2}{\pi A e} + \Delta C_{D_L}$$

4.1.5.2-k

where

C_L is the wing lift coefficient.

ΔC_{D_L} is that portion of the drag due to lift resulting from a breakdown in the leading-edge suction at lift coefficients above the parabolic-drag-polar region. An empirical correlation of ΔC_{D_L} as a function of lift coefficient and aspect ratio is presented as figure 4.1.5.2-54.

e is the span-efficiency factor over the parabolic-drag region, given by

$$e = \frac{C_{L\alpha}/A}{R' (C_{L\alpha}/A) + (1 - R') \pi} \quad 4.1.5.2-1$$

where

$C_{L\alpha}$ is the wing lift-curve slope obtained by the method presented for cranked wings in paragraph A of Section 4.1.3.2.

R' is the effective leading-edge-suction parameter given by

$$R' = R_i(\eta_B) + R_o(1 - \eta_B) \quad 4.1.5.2-m$$

where

R_i is the leading-edge suction parameter of the inboard panel, obtained from figure 4.1.5.2-53, but with the parameter $A\lambda/\cos \Lambda_{LE} = 0$.

R_o is the leading-edge-suction parameter of the outboard panel, obtained from figure 4.1.5.2-53 by assuming the outboard panels to be an isolated wing.

The leading-edge-radius Reynolds numbers required to read R_i and R_o from figure 4.1.5.2-53 are based on the leading-edge radius of the mean aerodynamic chord of the inboard and outboard panels, respectively. For values of the parameter $R_{\rho_{LER}} \cot \Lambda_{LE} \sqrt{1 - M^2 \cos^2 \Lambda_{LE}} > 1.3 \times 10^5$, R_i and/or R_o are read from figure 4.1.5.2-53b.

A sample problem illustrating the use of this method is presented on page 4.1.5.2-11.

A comparison of test data with results calculated by this method is presented as tables 4.1.5.2-C and 4.1.5.2-D (both taken from reference 2). Table 4.1.5.2-C compares the parabolic drag-due-to-lift factor $C_{D_L}/C_L^2 = 1/(\pi Ae)$ with test data. Table 4.1.5.2-D compares the drag due to lift over the nonparabolic region of the drag polar with test data. In table 4.1.5.2-D only the calculated results for references 16 and 18 are based on the predicted value of the parabolic drag-due-to-lift factor. The remainder of the data used the test value of C_{D_L}/C_L^2 combined with ΔC_{D_L} from figure 4.1.5.2-54.

Where test data were available for wing-body configurations, the portion of the inboard panel submerged in the body was accounted for in calculating the parabolic drag due to lift. This was accomplished by defining the effective leading-edge-suction parameter by

$$R' = R_i \left(\eta_B - \frac{d}{b} \right) + R_o (1 - \eta_B) \quad 4.1.5.2-m'$$

and basing the leading-edge-radius Reynolds number used to obtain R_i on the leading-edge radius of the mean aerodynamic chord of the exposed inboard panel.

The effect of Reynolds number on the accuracy of predicting ΔC_{D_L} cannot be assessed quantitatively, since all the data used in the empirical correlation were for low Reynolds numbers except those from reference 22. Although a comparison of the data of reference 22 with the low Reynolds-number data shows no effect of Reynolds number, it must be expected that Reynolds number will affect ΔC_{D_L} .

The effect of wing twist is not accounted for in the method. The test data include cambered-wing data, and camber seems to have no effect on ΔC_{D_L} ; however, there are not enough data to allow a quantitative evaluation of camber effects.

Finally, it should be pointed out that all the test data of table 4.1.5.2-D were used to derive the ΔC_{D_L} correlation. Therefore, no independent evaluation of the accuracy of the method in the nonparabolic region has been accomplished. In view of this, figure 4.1.5.2-54 should be used with caution outside the range of planform parameters used in the correlation (see figure 4.1.5.2-54).

Curved Wings

The correlation of $C_{D_L}/(C_L \tan \alpha)$, of reference 2, for determining the drag-due-to-lift factor of double-delta wings with sharp leading edges also included data on both Gothic and ogee wings at Mach numbers from 0.1 to 0.7. Therefore, the prediction method is essentially the same as that for double-delta wings.

As previously noted, the correlation for the drag-due-to-lift factor showed considerable scatter in the data below $\alpha = 8^\circ$. Although the data scatter for the curved planforms was not as widely dispersed as that for the double-delta planforms, the method should not be expected to give satisfactory results below $\alpha = 8^\circ$.

The subsonic drag due to lift of curved wings with sharp leading edges is given by equation 4.1.5.2-j; i.e.,

$$C_{D_L} = 0.95 C_L \tan \alpha$$

where C_L is the wing lift coefficient at angle of attack obtained by the method presented for curved wings in paragraph A of Section 4.1.3.3.

A sample problem illustrating the use of this method is presented on page 4.1.5.2-13.

A comparison of test data with results calculated by this method is presented as table 4.1.5.2-E (taken from reference 2). The test data are for two thin Gothic and two thin ogee wings. It is noted that the calculated results below $\alpha = 8^\circ$ compare more favorably with the test data than those for double-delta wings at low angles of attack. However, since no consistent trend is indicated by the comparison at the lower angles of attack, there is no basis for lowering the angle-of-attack limit below 8° .

Since all the data are for low Reynolds numbers, the effect of Reynolds number cannot be assessed. However, it is expected that Reynolds number will affect the results even at low lift coefficients, since leading-edge separation is almost immediate for the sharp-nosed airfoils.

Since all the test data of table 4.1.5.2-E were included in the drag-due-to-lift-factor correlation, application of the method to configurations with geometric parameters falling outside those of table 4.1.5.2-E should be approached with caution. The ranges of planform parameters used in the correlation are:

$$0.75 \leq A \leq 1.98$$

$$0.455 \leq p \leq 0.667$$

$$0.250 \leq \frac{b_w}{2\ell} \leq 0.450$$

The method is limited to thin wings ($t/c < 0.06$). Tests on one 12-percent thick Gothic wing showed less drag due to lift than did the tests on the thin wings. This is attributed to the development of significant suction forces on the forward-facing slopes of the thick wing. The correlation of $C_{DL}/(C_L \tan \alpha)$ for the 12-percent-thick wing resulted in a constant drag-due-to-lift factor of 0.87.

The effects of wing twist and/or camber are not accounted for in the method.

Sample Problems

1. Conventional, Straight-Tapered Wing

Given: The sweptback wing of reference 14.

Wing Characteristics:

$$A = 5.14 \quad \lambda = 0.713 \quad \Lambda_{LE} = 36.2^\circ \quad \Lambda_{c/2} = 33.7^\circ \quad \bar{c} = 1.166 \text{ ft}$$

$$\text{NACA } 65_1 A012 \text{ airfoil} \quad LER = 0.00922c \quad \text{No twist}$$

Additional Characteristics:

$$M = 0.75; \beta = 0.661 \quad R_{\varrho_{MAC}} = 2 \times 10^6 \quad R_{\varrho_{LER}} = 18.4 \times 10^3$$

$$\kappa = 1.0 \text{ (assumed)}$$

Compute:

Leading-edge-suction parameter

$$R_{\varrho_{LER}} \cot \Lambda_{LE} \sqrt{1 - M^2 \cos^2 \Lambda_{LE}} = (18.4 \times 10^3) (1.3663) \sqrt{1 - (0.75)^2 (0.8070)^2} = 20.0 \times 10^3$$

$$\frac{A\lambda}{\cos \Lambda_{LE}} = \frac{(5.14)(0.713)}{(0.8070)} = 4.54$$

$$R = 0.803 \text{ (figure 4.1.5.2-53)}$$

$$\frac{A}{\kappa} \sqrt{\beta^2 + \tan^2 \Lambda_{c/2}} = \frac{5.14}{1} \sqrt{(0.661)^2 + (0.6675)^2} = 4.83$$

$$\frac{C_{L\alpha}}{A} = 0.870 \text{ (figure 4.1.3.2-49)}$$

Span-efficiency factor

$$e = \frac{1.1 \left(C_{L\alpha} / A \right)}{R \left(C_{L\alpha} / A \right) + (1 - R) \pi} \quad (\text{equation 4.1.5.2-j})$$

$$= \frac{(1.1)(0.870)}{(0.803)(0.870) + (1 - 0.803)\pi} = 0.726$$

Solution:

$$C_{D_L} = \frac{C_L^2}{\pi Ae} \quad (\text{equation 4.1.5.2-h})$$

$$\frac{C_{D_L}}{C_L^2} = \frac{1}{\pi Ae} = \frac{1}{\pi (5.14)(0.726)} = 0.085$$

This compares with a test value of 0.090 from reference 14.

2. Double-Delta Wing

Given: A double-delta planform of reference 15.

Wing Characteristics:

$A_w = 1.73$	$A_i = 0.409$	$S_w = 560.0 \text{ sq ft}$	$S_i = 407.0 \text{ sq ft}$
$S_o = 153.0 \text{ sq ft}$	$\Lambda_{LE_i} = 77.4^\circ$	$\Lambda_{LE_o} = 59^\circ$	$\Lambda_{TE} = -10^\circ$
$\eta_B = 0.414$			

Additional Characteristics:

$$M = 0.13$$

Compute:

Variation of C_L with α (Section 4.1.3.3)

The predicted values of C_L versus α for this configuration are listed in table 4.1.3.3-B
(This configuration is shown under "reference 31" of the table)

Solution:

$$C_{D_L} = 0.95 C_L \tan \alpha \quad (\text{equation 4.1.5.2-j})$$

α (deg)	C_L table 4.1.3.3-B	$\tan \alpha$	C_{D_L} eq. 4.1.5.2-j
4	0.143	0.0699	0.00950
8	0.302	0.1405	0.04031
12	0.491	0.2126	0.09917
16	0.685	0.2867	0.1866
20	0.974	0.3640	0.3368

The calculated results are compared with test values in table 4.1.5.2-B.

3. Cranked Wing

Given: The cranked wing-body configuration of reference 16. This is the configuration of the cranked-wing sample problem of paragraph A of Section 4.1.3.2.

Wing Characteristics:

$$\begin{array}{llll} A_w = 4.0 & A_o = 2.37 & \Lambda_{LE_i} = 48.6^\circ & \Lambda_{LE_o} = 7.7^\circ \\ \lambda_o = 0.517 & \eta_B = 0.60 & \text{NACA 65A006 airfoil} & LER = 0.00229c \\ \bar{c}_i = 0.933 \text{ ft} & \bar{c}_o = 0.525 \text{ ft} & & \end{array}$$

Additional Characteristics:

$$M = 0.80 \quad R_\ell = 3.645 \times 10^6 \text{ per ft} \quad \frac{d}{b} = 0.139$$

Compute:

Leading-edge-suction parameters, R_i and R_o

Inboard panel:

$$\begin{aligned} (R_{\ell,LER})_i &= (3.645 \times 10^6) (0.00229 \bar{c}_i) = (3.645 \times 10^6) (0.00229) (0.933) = 7.79 \times 10^3 \\ (R_{\ell,LER} \cot \Lambda_{LE} \sqrt{1 - M^2 \cos^2 \Lambda_{LE}})_i &= (7.79 \times 10^3) (0.8816) \sqrt{1 - (0.8)^2 (0.6613)^2} \\ &= 5.83 \times 10^3 \end{aligned}$$

$$R_i = 0.470 \quad (\text{figure 4.1.5.2-53, with } \left(A \lambda / \cos \Lambda_{LE} \right)_i = 0. \text{ See definition of } R_i, \text{ page 4.1.5.2-7})$$

Outboard panel:

$$\left(R_{\ell_{LER}} \right)_o = (3.645 \times 10^6) (0.00229 \bar{c}_o) = (3.645 \times 10^6) (0.00229) (0.525) = 4.38 \times 10^3$$

$$\begin{aligned} \left(R_{\ell_{LER}} \cot \Lambda_{LE} \sqrt{1 - M^2 \cos^2 \Lambda_{LE}} \right)_o &= (4.38 \times 10^3) (7.396) \sqrt{1 - (0.8)^2 (0.9910)^2} \\ &= 1.973 \times 10^4 \end{aligned}$$

$$\left(\frac{A\lambda}{\cos \Lambda_{LE}} \right)_o = \frac{(2.37)(0.517)}{0.9910} = 1.236$$

$$R_o = 0.766 \text{ (figure 4.1.5.2-53)}$$

Effective leading-edge-suction factor

$$R' = R_i \left(\eta_B - \frac{d}{b} \right) + R_o (1 - \eta_B) \quad (\text{equation 4.1.5.2-m'})$$

$$= (0.470)(0.60 - 0.139) + (0.766)(1 - 0.60)$$

$$= 0.523$$

$$C_{L\alpha}/A = 1.081 \text{ per rad (sample problem, paragraph A, Section 4.1.3.2)}$$

Span-efficiency factor over parabolic-drag region

$$e = \frac{C_{L\alpha}/A}{R' (C_{L\alpha}/A) + (1 - R') \pi} \quad (\text{equation 4.1.5.2-l})$$

$$= \frac{1.081}{(0.523)(1.081) + (1 - 0.523)\pi}$$

$$= 0.524$$

$$\frac{C_{D_L}}{C_L^2} = \frac{1}{\pi Ae} = \frac{1}{\pi (4.0)(0.524)} = 0.152$$

Solution:

$$C_{D_L} = \frac{C_L^2}{\pi Ae} + \Delta C_{D_L} \quad (\text{equation 4.1.5.2-k})$$

$$= \frac{C_{D_L}}{C_L^2} C_L^2 + \Delta C_{D_L}$$

C_L	C_L/A $(1)/4$	ΔC_{D_L} fig 4.1.5.2-54	$\frac{C_{D_L}}{C_L^2}$	$\frac{C_{D_L}}{C_L} C_L^2$ $(4)(1)^2$	C_{D_L} eq 4.1.5.2-k $(5) + (3)$
0	0	---	0.152	0	0
0.1	0.025	---		0.0015	0.0015
0.2	0.050	---		0.0061	0.0061
0.3	0.075	---		0.0137	0.0137
0.4	0.100	0.0080		0.0243	0.0323
0.5	0.125	0.0240		0.0380	0.0620
0.6	0.150	0.0510		0.0547	0.1067
0.7	0.175	0.0840		0.0745	0.1585
0.8	0.200	0.1245		0.0973	0.2218

The test values for this configuration are presented in tables 4.1.5.2-C and 4.1.5.2-D for the cranked wing mounted on a circular-ogive body. The calculated results presented in tables 4.1.5.2-C and 4.1.5.2-D take into account the portion of the inboard panel submerged in the body by applying the corrections noted on page 4.1.5.2-7. The leading-edge-radius Reynolds number used to obtain R_e is based on the leading-edge radius of the mean aerodynamic chord of the exposed inboard panel, and the effective leading-edge-suction parameter is determined by using equation 4.1.5.2-m'.

4. Curved Wing

Given: The ogee wing of reference 23. This is the same configuration as the curved-wing sample problem of paragraph A of Section 4.1.3.3.

Wing Characteristics:

$$A = 1.20$$

$$b = 12.0 \text{ in.}$$

$$\ell = 20.0 \text{ in.}$$

Additional Characteristics:

$$M = 0.4$$

Compute:

Variation of C_L with α (Section 4.1.3.3)

The predicted values of C_L versus α are obtained from the curved-wing sample problem of paragraph A of Section 4.1.3.3.

Solution:

$$C_{D_L} = 0.95 C_L \tan \alpha \text{ (equation 4.1.5.2-j)}$$

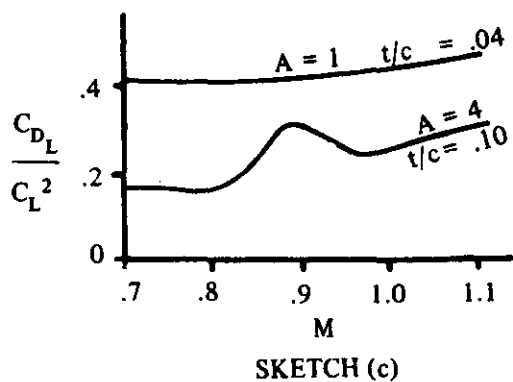
α (deg)	C_L Sec. 4.1.3.3	$\tan \alpha$	C_{D_L} eq. 4.1.5.2-j
4	0.136	0.0699	0.0090
8	0.288	0.1405	0.0384
12	0.465	0.2126	0.0939

The calculated results are compared with test values in table 4.1.5.2-E.

B. TRANSONIC

Test data on straight-tapered wings show that the variation of the drag-due-to-lift parameter C_{D_L}/C_L^2 with

Mach number at transonic speeds is somewhat analogous to that of the lift-curve slope. That is, for thick and/or high-aspect-ratio wings this parameter experiences significant deviations with Mach number, while for thin and/or low-aspect-ratio wings this parameter varies uniformly with Mach number (see sketch (c)).



SKETCH (c)

Transonic data on non-straight-tapered wings are too few to allow quantitative analysis of the variation of drag due to lift with Mach number.

The only available approach to the estimation of transonic drag due to lift of conventional, trapezoidal wings appears to be through the use of transonic similarity parameters. This is a particularly useful approach where the quantity of data available for correlation is limited. The method presented, therefore, uses transonic similarity parameters. It should be pointed out, however, that the bulk of existing data at transonic speeds is derived from "bump tests," which are frequently questioned because of the spanwise Mach number gradients.

DATCOM METHOD

The transonic drag due to lift of conventional, trapezoidal planforms of symmetrical section may be approximated by using figures 4.1.5.2-55a through 4.1.5.2-55c for given values of the transonic similarity parameters, $A \tan \Lambda_{LE}$ and $\frac{M^2 - 1}{(t/c)^{2/3}}$

Sample Problem

Given: The following straight-tapered wing from reference 26.

$$A = 4.0$$

$$\lambda = 0$$

$$\Lambda_{LE} = 45^\circ$$

NACA 63A004 airfoil

Compute:

$$(t/c)^{1/3} = 0.342; \quad (t/c)^{2/3} = 0.116; \quad A(t/c)^{1/3} = 1.368$$

$$A \tan \Lambda_{LE} = 4.0$$

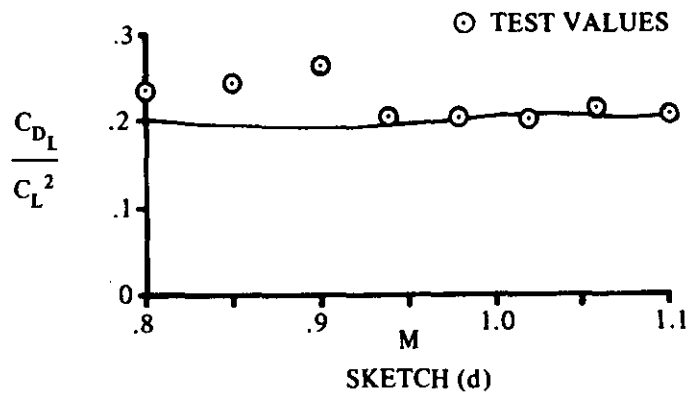
$$\frac{M^2 - 1}{(t/c)^{2/3}} \quad (\text{see calculation table below})$$

$$\left(\frac{t}{c}\right)^{-1/3} \left(\frac{C_{D_L}}{C_L^2}\right) \quad (\text{figures 4.1.5.2-55a and -55b extrapolated, see calculation table below})$$

Solution:

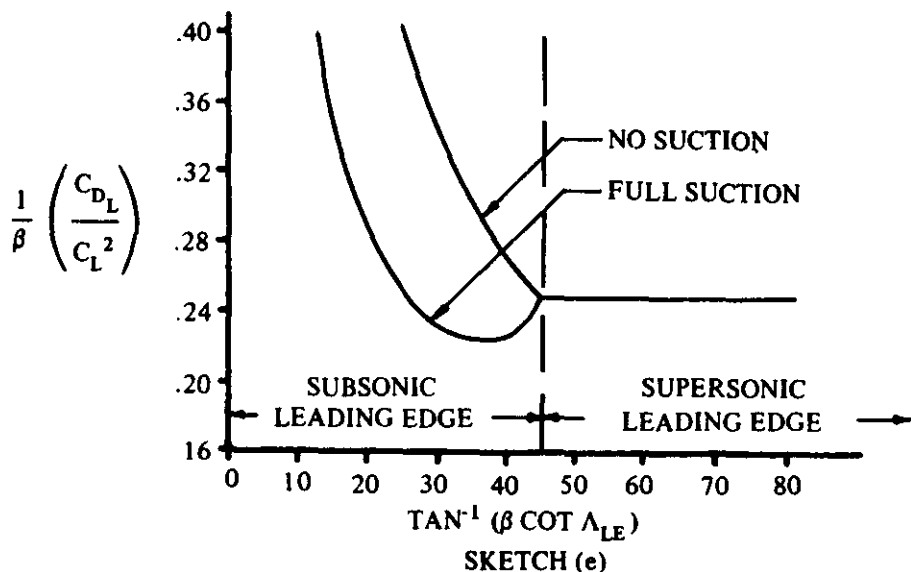
①	②	③	④
M	$\frac{M^2 - 1}{(t/c)^{2/3}}$	$\left(\frac{t}{c}\right)^{-1/3} \frac{C_{D_L}}{C_L^2}$ fig. 4.1.5.2-55	C_{D_L}/C_L^2 $(3) (t/c)^{1/3}$
0.8	-3.10	0.59	0.202
0.9	-1.64	0.57	0.195
0.94	-1.00	0.57	0.195
0.98	-0.34	0.58	0.198
1.00	0	0.60	0.205
1.05	0.88	0.60	0.205
1.10	1.81	0.59	0.202

The calculated values of C_{D_L}/C_L^2 are compared with test values from reference 26 in sketch (d).

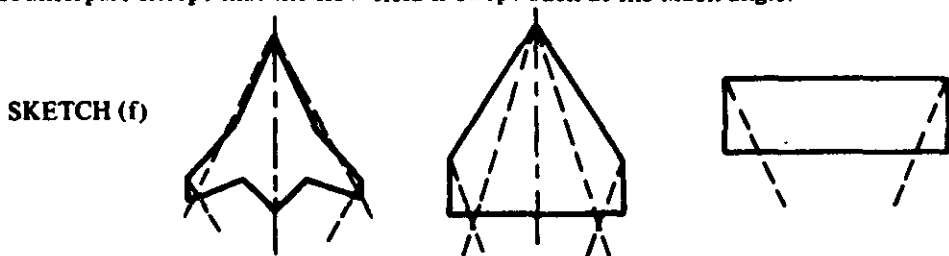


C. SUPERSONIC

At supersonic speeds, wings are generally classified according to whether the Mach number component perpendicular to the leading edge is subsonic or supersonic. A typical presentation of supersonic drag due to lift is shown in sketch (e). For supersonic-leading-edge wings, certain regions of the wing will be in two-dimensional flow where the spanwise pressure loading on the surface is constant.



Other portions of the wing are influenced by tip effects and by the wing apex. Three cases are shown in sketch (f). The two-dimensional region has wave drag due to lift, which can be calculated by simple linear theory or by shock-expansion theory. But because the span loading is constant, this region does not produce any vortex drag. The three-dimensional region has shock-wave drag due to lift, but not as much as that of the two-dimensional region. The three-dimensional region also has a drag-due-to-lift contribution associated with the vortex that is shed because of the varying span loading. This phenomenon is exactly like its subsonic counterpart except that the flow field is swept back at the Mach angle.



In general, the drag due to lift of a wing quickly approaches the two-dimensional value as the leading edge progresses from the sonic into the supersonic region. The two-dimensional value from linear theory is

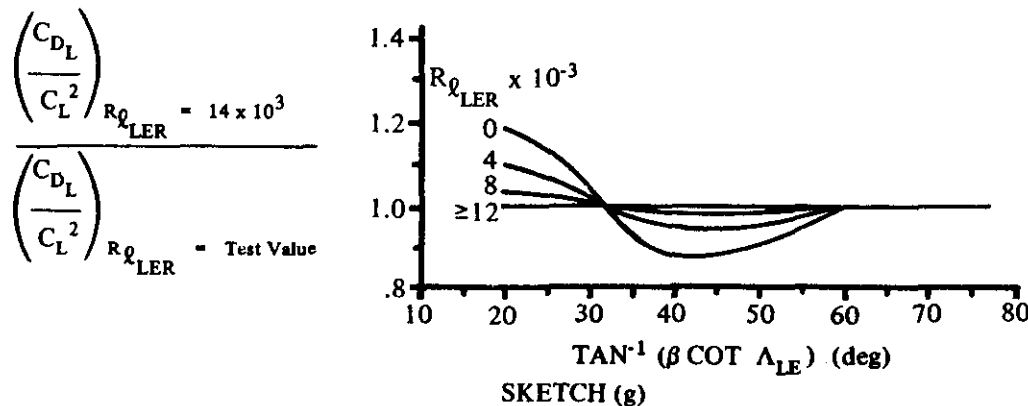
$$C_{D_L} = \frac{\beta C_L^2}{4}$$

For subsonic leading edges, no part of the wing is in two-dimensional flow and the span pressure loading, in general, varies continuously across the span. Wave drag due to lift and vortex drag exist as for the supersonic leading-edge case. However, an additional phenomenon occurs. The subsonic Mach number component perpendicular to the leading edge allows leading-edge-suction pressures to develop similar to those that occur on wings in subsonic flow. These suction pressures can cause significant reductions in drag, which, to date, cannot be predicted for a given wing. The amount of suction depends upon the leading-edge shape and the wing-camber shape and distribution. Several authors have, however, calculated the maximum amount of suction attainable for several types of wings (e.g., references 6 and 7). Camber can also produce a significant drag-due-to-lift reduction that is not affected by leading-edge suction. Sketch (e) above shows typical drag reduction due to suction for a cambered delta wing.

Test results for subsonic leading-edge wings generally fall between the limits of wings with no leading-edge suction and wings with full leading-edge suction. For a given test on a cambered wing, however, it is impossible to determine what fraction of the drag reduction is attributable to camber, since camber and leading-edge-suction effects are very similar in nature.

For conditions where the leading edge is slightly supersonic, the theoretical results for cambered wings are less than the two-dimensional value because the forward inclination of the integrated force vector due to the pressures on the cambered portion of the wing persists into the supersonic leading-edge region. In practice, uncambered wings of finite thickness exhibit the same trend, because the leading-edge shock is detached and causes the leading edge to operate at a lower effective Mach number; that is, the airfoil operates at a subsonic leading-edge condition where leading-edge suction can reduce the drag even though the theoretical leading-edge condition is supersonic.

The Reynolds number based on leading-edge radius can also significantly affect the drag due to lift. At low Reynolds number, local leading-edge flow separation can occur with a loss in leading-edge suction. Low Reynolds number also affects the boundary-layer transition point on the wing. In general, increasing Reynolds number causes an increase in friction drag at low angles of attack (forward-moving transition point) and no change in friction drag at high angles of attack (transition point is already forward). Sketch (g) shows the effect of leading-edge-radius Reynolds number based on test data (reference 8). The ordinate of this sketch is the ratio of the induced-drag parameter C_{D_L}/C_L^2 at a Reynolds number of 14×10^3 based on leading-edge radius to the value of the parameter at a given value of leading-edge Reynolds number.



Methods are presented for determining the wing drag due to lift over the parabolic-drag region for the following two classes of wing planforms:

Straight-Tapered Wings (conventional, trapezoidal wings)

Non-Straight-Tapered Wings

Double-delta wings

Cranked wings

Curved (Gothic and ogee) wings

These three general categories of non-straight-tapered wings are illustrated in sketch (a) of Section 4.1.3.2. Their wing-geometry parameters are presented in Section 2.2.2.

The methods presented are based on the conclusions of an analysis of the experimental results of the drag due to lift of slender uncambered wings at supersonic speeds reported in reference 9. It was shown therein that the drag-due-to-lift factor at supersonic speeds collapses into a fairly well-defined single curve when plotted as a function of the wing planform shape and slenderness parameters.

The supersonic design chart presented for non-straight-tapered wings is taken from reference 2, and the parameters used to collapse the data are modifications of those presented in reference 9. The correlation makes no distinction between round and sharp leading edges nor between cambered and uncambered wings.

The parameters used to collapse the data for non-straight-tapered wings in reference 2 have also been applied to uncambered straight-tapered wings. The resulting correlation showed a distinction between straight-tapered wings with round leading edges and those with sharp leading edges.

DATCOM METHODS

Straight-Tapered Wings

The supersonic drag due to lift over the parabolic-drag region for straight-tapered wings is obtained using the procedure outlined in the following steps:

Step 1. Using the given wing geometry, calculate the aspect ratio, the planform shape parameter p , and the wing slenderness parameter $\frac{b_w}{2\ell}$. (See Section 2.2.2 for wing-geometry parameters).

Step 2. At the desired value of $\frac{\beta b_w}{2\ell}$ obtain $\pi A \frac{C_{D_L}}{C_L^2} \frac{p}{1+p}$ from the proper design curve of figure 4.1.5.2-58.

Step 3. Calculate the drag due to lift by

$$\frac{C_{D_L}}{C_L^2} = \left[\pi A \frac{C_{D_L}}{C_L^2} \frac{p}{1+p} \right] \left(\frac{1}{\pi A} \right) \left(\frac{1+p}{p} \right) \quad 4.1.5.2-n$$

A comparison of test data with results calculated by this method is presented as table 4.1.5.2-F. With one exception, all the configurations listed in the table are wing-body combinations with small ratios of body diameter to wing span. The calculations for these configurations were made by using the theoretical planform extended to the body center line and neglecting body effects. The test configurations are about equally divided between wings with sharp leading edges and those with round leading edges. None of the wings are cambered. The ranges of the planform parameters covered for each leading-edge shape are

Round Leading Edge	Sharp Leading Edge
$1.313 \leq A \leq 4.0$	$1.5 \leq A \leq 3.5$
$35^\circ \leq \Lambda_{LE} \leq 73^\circ$	$0 \leq \Lambda_{LE} \leq 71^\circ$
$0 \leq \lambda \leq 0.5$	$0 \leq \lambda \leq 1.0$
$0.237 \leq p \leq 0.502$	$0.333 \leq p \leq 0.995$
$0.271 \leq \frac{b_w}{2\ell} \leq 1.00$	$0.333 \leq \frac{b_w}{2\ell} \leq 1.070$

The sample problem presented on page 4.1.5.2-20 for a double-delta wing illustrates the application of the straight-tapered-wing method.

Non-Straight-Tapered Wings

The supersonic drag due to lift over the parabolic-drag region for non-straight-tapered wings is obtained by following the procedure outlined above for straight-tapered wings. The value of the parameter

$$\pi A \frac{C_{D_L}}{C_L^2} \frac{p}{1+p} \text{ at the desired value of } \frac{\beta b_w}{2\ell} \text{ is obtained from figure 4.1.5.2-59. This correlation}$$

makes no distinction between wing planforms, between round and sharp leading edges, nor between cambered and uncambered wings.

A comparison of test data with results calculated by this method is presented in table 4.1.5.2-G for double-delta and cranked wings, and in table 4.1.5.2-H (taken from reference 2) for curved wings.

All the configurations listed in table 4.1.5.2-G are wing-body combinations with small ratios of body diameter to wing span. The calculations for these configurations were made by using the theoretical planform extended to the body center line and neglecting body effects. The table includes double-delta wings with both round and sharp leading edges and cranked wings with round leading edges. Some of the wings with round leading edges are cambered. The ranges of the planform parameters of the test data are:

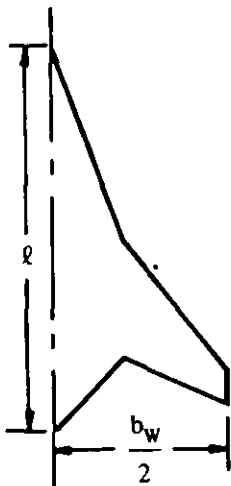
Double-Delta Wings	Cranked Wings
$1.74 \leq A \leq 3.15$	$2.91 \leq A \leq 4.0$
$0.292 \leq p \leq 0.500$	$0.491 \leq p \leq 0.666$
$0.353 \leq \frac{b_w}{2\ell} \leq 0.787$	$0.710 \leq \frac{b_w}{2\ell} \leq 1.333$

The results presented in table 4.1.5.2-H for curved wings with sharp leading edges agree quite well with test data. This is probably due to the fact that the curved planforms have a more limited range of geometric parameters than the double-delta and cranked wings. The ranges of planform parameters of the test data are:

$$\begin{aligned} 0.75 &\leq A \leq 1.39 \\ 0.384 &\leq p \leq 0.667 \\ 0.208 &\leq \frac{b_w}{2\ell} \leq 0.389 \end{aligned}$$

Sample Problem

Given: The double-delta wing of reference 30 designated X-67-67.



Wing Characteristics:

$$A = 2.42$$

$$S_w = 1.651 \text{ sq ft}$$

$$b_w = 2.0 \text{ ft}$$

$$l = 2.22 \text{ ft}$$

Additional Characteristics:

$$M = 2.01; \quad \beta = 1.742$$

Compute:

$$\frac{b_w}{2l} = \frac{2.0}{(2)(2.22)} = 0.450$$

$$\frac{\beta b_w}{2l} = (1.742)(0.450) = 0.784$$

$$p = \frac{S_w}{b_w l} = \frac{1.651}{(2.0)(2.22)} = 0.372$$

$$\frac{1+p}{p} = \frac{1+0.372}{0.372} = 3.688$$

$$\frac{C_{D_L}}{\pi A} \frac{p}{C_L^2} = 0.961 \quad (\text{figure 4.1.5.2-59})$$

Solution:

$$\frac{C_{D_L}}{C_L^2} = \left[\frac{C_{D_L}}{\pi A} \frac{p}{C_L^2} \right] \left(\frac{1}{\pi A} \right) \left(\frac{1+p}{p} \right) \quad (\text{equation 4.1.5.2-n})$$

$$= (0.961) \left(\frac{1}{2.42\pi} \right) (3.688) = 0.466$$

This compares with a test value of 0.479 from reference 30.

REFERENCES

1. Frost, R.C., and Rutherford, R.: Subsonic Wing Span Efficiency. AIAA Journal, Vol. 1, No. 4, April 1963. (U)
2. Benepe, D.B., Kouri, B.G., Webb, J.B., et al: Aerodynamic Characteristics of Non-Straight-Taper Wings. AFFDL-TR-66-73, 1966. (U)
3. Gardner, D., and Weir, J.: The Drag Due to Lift of Plane Wings at Subsonic Speeds. RAS Journal, Vol. 70, May 1968. (U)
4. Anon: Royal Aeronautical Society, Engineering Sciences Data (Aeronautical Series). Vol. 2, Item 66032, 1966. (U)
5. Lundry, J.: Charts for Obtaining Subsonic Inviscid Induced Drag of Twisted Swept Wings. Douglas Aircraft Company, Report LB-31689, 1964. (U)
6. Puckett, A.E., and Stewart, H.J.: Aerodynamic Performance of Delta Wings at Supersonic Speeds. Jour. Aero. Sci., Vol. 14, No. 10, Oct. 1947. (U)
7. von Kármán, T.: Supersonic Aerodynamics—Principles and Applications. Jour. Aero. Sci., Vol. 14, No. 7, July 1947. (U)
8. Blakeslee, D.J.: Correlation of Wing-Body Drag-Due-to-Lift at Supersonic Speeds for Use in Airplane Design Studies. Rand Report RM 2014, 1957. (C) Title Unclassified
9. Courtney, A.L.: A Collection of Data on the Lift-Dependent Drag of Uncambered Slender Wings at Supersonic Speeds. ARC CP 757, 1964. (U)
10. Hall, C.F.: Lift, Drag, and Pitching Moment of Low-Aspect-Ratio Wings at Subsonic and Supersonic Speeds. NACA RM A53A30, 1953. (U)
11. Graham, R.R.: Low-Speed Characteristics of a 45° Sweptback Wing of Aspect Ratio 8 From Pressure Distributions and Force Tests at Reynolds Numbers from 1,500,000 to 4,800,000. NACA RM L51H13, 1951. (U)
12. Woithart, W.D., and Thomas, D.F., Jr.: Static Longitudinal and Lateral Stability Characteristics at Low Speed of 60° Sweptback-Midwing Models Having Wings with an Aspect Ratio of 2, 4, or 6. NACA TN 4397, 1958. (U)
13. Kuhn, R.E., and Wiggins, J.W.: Wind-Tunnel Investigation of the Aerodynamic Characteristics in Pitch of Wing-Fuselage Combinations at High Subsonic Speeds—Aspect Ratio Series. NACA RM L52A29, 1952. (U)
14. Tinling, B.E., and Kolk, W.R.: The Effects of Mach Number and Reynolds Number on the Aerodynamic Characteristics of Several 12-Percent-Thick Wings Having 35° of Sweepback and Various Amounts of Camber. NACA RM A50K27, 1951. (U)
15. Anon: Large-Scale Double-Delta Wing-Body Planform Investigation at Low Speed. Unpublished Data. (U)
16. Goodson, K.W., and Becht, R.E.: Wind-Tunnel Investigation at High Subsonic Speeds of the Stability Characteristics of a Complete Model Having Sweepback-, M-, W-, and Cranked-Wing Planforms and Several Horizontal-Tail Locations. NACA RM L54C29, 1954. (U)
17. Grant, F.C., and Sevier, J.R., Jr.: Transonic and Supersonic Wind-Tunnel Tests of Wing-Body Combinations Designed for High Efficiency at a Mach Number of 1.41. NASA TN D-435, 1960. (U)
18. Henderson, W.P., and Hammond, A.D.: Low-Speed Investigation of High-Lift and Lateral Control Devices on a Semispan Variable-Sweep Wing Having an Outboard Pivot Location. NASA TM X-542, 1961. (U)
19. Lockwood, V.E., McKinney, L.W., and Lamar, J.E.: Low-Speed Aerodynamic Characteristics of a Supersonic Transport Model With a High Aspect Ratio Variable Sweep Warped Wing. NASA TM X-979, 1964. (C) Title Unclassified
20. Jernell, L.S.: The Effects of Conical Camber on the Longitudinal Aerodynamic Characteristics of a Variable-Sweep Wing-Fuselage Configuration at Mach Numbers from 0.60 to 3.50. NASA TM X-804, 1963. (C) Title Unclassified
21. Anon: System 125A, Convair Model 25, Summary Data Report, Subsonic Tests of a Preliminary 1/27-Scale Force Model (CVAL 201). Convair, General Dynamics, F/W, Report FZT-25-004, 1956. (C) Title Unclassified
22. Trescot, C.D., and Spencer, B., Jr.: Effect of Reynolds Number on the Low-Speed Longitudinal Aerodynamic Characteristics of Two Variable-Wing-Sweep Airplane Configurations. NASA TM X-434, 1961. (C) Title Unclassified
23. Squire, L.C., and Capps, D.S.: An Experimental Investigation of the Characteristics of an Ogee Wing from $M = 0.4$ to $M = 1.8$. ARC CP 585, 1962. (U)

24. Hicks, R.M., and Hopkins, E.J.: Effects of Spanwise Variation of Leading-Edge Sweep on the Lift, Drag, and Pitching Moment of a Wing-Body Combination at Mach Numbers from 0.7 to 2.94. NASA TN D-2236, 1964. (U)
25. Peckham, D.H.: Low-Speed Wind-Tunnel Tests on a Series of Uncambered Slender Pointed Wings with Sharp Edges. RAE Aero 2613, 1958. (U)
26. Emerson, H.F.: Wind-Tunnel Investigation of the Effect of Clipping the Tips of Triangular Wings of Different Thickness, Camber, and Aspect Ratio—Transonic Bump Method. NACA TN 3671, 1956. (U)
27. Feryn, M.O., and Campbell, J.F.: Effects of Wing Dihedral and Planform on Stability Characteristics of a Research Model at Mach Numbers from 1.80 to 4.63. NASA TN D-2914, 1965. (U)
28. Boyd, J.W., Migotsky, E., and Wetzel, B.E.: A Study of Conical Camber for Triangular and Sweptback Wings. NACA RM A55G19, 1955. (U)
29. Palazzo, E.B., and Spearman, M.L.: Static Longitudinal and Lateral Stability and Control Characteristics of a Model of a 35° Swept-Wing Airplane at a Mach Number of 1.41. NACA RM L54G08, 1955. (U)
30. Cooper, M., and Sevier, J.R., Jr.: Effects of a Series of Inboard Plan-Form Modifications on the Longitudinal Characteristics of Two 47° Sweptback Wings of Aspect Ratio 3.5, Taper Ratio 0.2, and Different Thickness Distributions at Mach Numbers of 1.61 and 2.01. NACA RM L53E07a, 1953. (U)
31. Sevier, J.R., Jr.: Effect of a Series of Inboard Plan-Form Modifications on the Longitudinal Characteristics of Two Unswept Wings of Aspect Ratio 3.5, Taper Ratio 0.2, and Different Thickness Distributions at Mach Numbers of 1.61 and 2.01. NACA RM L53K11, 1954. (U)
32. Robins, A.W., Harris, R.V., Jr., and Jackson, C.M., Jr.: Characteristics at Mach Number of 2.03 of a Series of Wings Having Various Spanwise Distributions of Thickness Ratio and Chord. NASA TN D-631, 1960. (U)
33. Wetzel, B.E.: Effect of Taper Ratio on Lift, Drag, and Pitching-Moment Characteristics of Thin Wings of Aspect Ratio 3 with 53.1° Sweepback of Leading Edge at Subsonic and Supersonic Speeds. NACA RM A54J20, 1955. (U)
34. Sevier, J.R., Jr.: Investigation of the Effects of Body Indentation and of Wing-Plan-Form Modification on the Longitudinal Characteristics of a 60° Swept-Wing-Body Combination at Mach Numbers of 1.41, 1.61, and 2.01. NACA RM L55E17, 1955. (U)
35. Holdaway, G.H., and Mellenthin, J.A.: Evaluation of Blended Wing-Body Combinations with Curved Plan Forms at Mach Numbers up to 3.60. NASA TM X-379, 1960. (U)
36. Wakefield, R.M.: Effects of Wing-Crank, Leading-Edge Chord Extensions, and Horizontal-Tail Height on the Longitudinal Stability of Swept-Wing Models at Mach Numbers from 0.6 to 1.4. NASA TM X-92, 1969. (U)
37. Bielat, R.P., Harrison, D.E., and Coppolino, D.A.: An Investigation at Transonic Speeds of the Effects of Thickness Ratio and of Thickened Root Sections on the Aerodynamic Characteristics of Wings With 47° Sweepback, Aspect Ratio 3.5, and Taper Ratio 0.2 in the Slotted Test Section of the Langley 8-Foot High-Speed Tunnel. NACA RM L51I04a, 1951. (U)
38. Spearman, M.L., and Foster, G.V.: Stability and Control Characteristics at a Mach Number of 2.01 of a Variable-Wing-Sweep Configuration With Outboard Wing Panels Swept Back 75°. NASA TM X-32, 1959. (U)
39. Foster, G.V.: Stability and Control Characteristics at Mach Numbers of 2.50, 3.00, and 3.71 of Variable-Wing-Sweep Configuration With Outboard Wing Panels Swept Back 75°. NASA TM X-267, 1960. (U)
40. Sevier, J.R., Jr.: Aerodynamic Characteristics at Mach Numbers of 1.41 and 2.01 of a Series of Cranked Wings Ranging in Aspect Ratio from 4.00 to 1.74 in Combination With a Body. NASA TM X-172, 1960. (U)
41. Kuhns, R.M.: HSWT-083-0 Analysis Report, Supersonic Transport Lifting Fuselage Investigation. Convair, General Dynamics, San Diego, Report AD-SST-012, 1961. (U)
42. Pierce, S.R.: System 125A, Convair Model 25 Summary Data Report, Wind-Tunnel Tests of a 1/125 Scale Model. (JPL Test 20-202). Convair, General Dynamics, F/W, Report FZT-26-006, 1956. (U)
43. Taylor, C.R.: Measurements, at Mach Numbers up to 2.8, of the Longitudinal Characteristics of One Plane and Three Cambered Slender 'Ogee' Wings. ARC R&M 3328, 1963. (U)

TABLE 4.1.5.2-A
SUBSONIC DRAG DUE TO LIFT OF STRAIGHT-TAPERED WINGS
DATA SUMMARY AND SUBSTANTIATION
NO TWIST

Ref.	Config.	A	λ	Λ_{LE} (deg)	NACA Airfoil	R_0 $_{MAC} \times 10^{-6}$	R_0 $_{LER} \times 10^{-3}$	M	$\frac{C_{D_L}}{C_L^2}$ Calc.	$\frac{C_{D_L}}{C_L^2}$ Test	e Percent Error
10	WB	3.0	0	53.1	0003-63	3.1 ↓ 5.9 10.6 1.9 4.8 4.9 9.3 16.6 3.0 6.0 7.6 2.7 ↓ 5.01 9.1 1.7 1.7 2.9 ↓ 4.2 1.5	3.1 ↓ 5.9 10.6 1.9 4.8 4.9 ↓ 9.3 16.6 3.0 6.0 7.6 1.215 ↓ 2.25 4.095 0.765 1.305 ↓ 1.89 4.12	0.25 0.60 0.25 0.25 0.61 0.61 0.25 0.60 0.25 0.25 0.61 0.81 0.61 0.61 0.25 0.60 0.25 0.81 0.61 0.81 0.81 0.61 0.81 0.40 0.60 0.80	0.251 0.242 0.215 0.185 0.269 0.218 0.336 0.331 0.291 0.255 0.366 0.353 0.330 0.301 0.245 0.227 0.214 0.183 0.226 0.180 0.226 0.216 0.195 0.210 0.208 0.194 0.360 0.341 0.334	0.296 0.250 0.251 0.217 0.270 0.250 0.367 0.373 0.290 0.270 0.345 0.325 0.325 0.325 0.245 0.240 0.226 0.180 0.226 0.216 0.195 0.210 0.210 0.190 0.190 0.350 0.330 0.315	-15.2 - 3.2 -14.3 -14.7 - 0.4 -12.8 - 8.4 -11.5 0.3 - 5.6 6.1 8.6 1.5 - 7.4 0 - 5.4 - 5.3 - 1.7 4.6 5.1 7.1 7.9 - 1.0 2.1 2.9 2.7 6.0
		2.0	0	63.4	0003-63						
		4.0	0	45.0	biconvex t/c = 0.03						
		2.0	0	63.4	0006-63						

TABLE 4.1.5.2-A (CONTD)

Ref.	Config.	A	λ	Λ_{LE} (deg)	NACA Airfoil	R_0 $_{MAC} \times 10^{-6}$	R_0 $_{LER} \times 10^{-3}$	M	$\frac{C_{DL}}{C_L^2}$ Calc.	$\frac{C_{DL}}{C_L^2}$ Test	% Percent Error
10	WB	2.0	0	63.4	0006-63	3.0	8.25	0.24	0.300	0.320	- 6.3
						5.0	13.75	0.40	0.310	0.290	6.9
						8.0	22.0	0.60	0.294	0.310	- 5.2
						3.0	8.25	0.80	0.288	0.310	- 7.1
						7.5	20.6	0.25	0.267	0.262	1.9
					0008-63	3.0	21.15	0.61	0.240	0.220	9.1
						5.0	35.25	0.79	0.236	0.254	- 7.1
						8.0	56.4	0.24	0.242	0.240	0.8
						15.0	106.75	0.40	0.240	0.240	0
					biconvex $t/c = 0.03$	1.9	0.855	0.60	0.238	0.250	- 4.8
		2.0	0.333	45.0		4.8	2.16	0.80	0.235	0.260	- 9.6
						2.4	0	0.25	0.218	0.205	6.3
		3.06	0.388	19.1	biconvex $t/c = 0.03$	4.6		0.61	0.202	0.195	3.6
						8.3		0.71	0.188	0.195	- 3.6
								0.81	0.345	0.325	6.2
								0.71	0.338	0.300	12.6
								0.81	0.328	0.302	8.6
								0.71	0.304	0.290	4.8
								0.81	0.300	0.291	3.1
								0.25	0.264	0.255	3.5
								0.60	0.244	0.230	6.1
								0.25	0.264	0.240	10.0
								0.25	0.264	0.240	10.0

TABLE 4.1.5.2-A (CONT'D)

Ref.	Config.	A	λ	Λ_{LE} (deg)	NACA Aerofoil	$R_0 \times 10^{-6}$	$R_0 \times 10^{-3}$	M	$\frac{C_{DL}}{C_L^2}$ Calc.	$\frac{C_{DL}}{C_L^2}$ Test	* Percent Error
10	WB	3.08	0.388	19.1	biconvex $t/c = 0.03$	1.4	0	0.61	0.243	0.240	1.3
						2.4		0.71	0.235	0.235	0
						3.8		0.81	0.226	0.220	2.7
								0.61	0.243	0.245	- 0.8
								0.71	0.235	0.230	2.2
								0.76	0.227	0.230	- 1.3
								0.81	0.226	0.205	10.2
								0.61	0.243	0.230	5.7
								0.71	0.235	0.220	6.8
								0.81	0.226	0.210	7.6
11	W	8.02	0.450	46.3	63A012	3.0	32.1	0.14	0.065	0.068	- 4.4
12	WB	2	0.600	61.7	65A008	1.02	4.16	0.13	0.373	0.340	9.7
		4		60.8		0.72	2.94	0.13	0.308	0.300	2.7
13	WB	2	0.600	48.4	65A006	3.33	7.63	0.40	0.251	0.240	4.6
						3.94	9.02	0.50	0.240	0.240	0
						4.53	10.4	0.60	0.232	0.240	- 3.3
						5.05	11.6	0.70	0.226	0.240	- 5.8
						5.46	12.5	0.80	0.222	0.240	- 7.5
		4	0.600	46.7		2.05	4.69	0.40	0.188	0.173	8.7
						2.42	5.54	0.50	0.172	0.164	4.9
						2.78	6.37	0.60	0.164	0.150	9.3
						3.10	7.10	0.70	0.158	0.155	1.9
						3.35	7.67	0.80	0.153	0.145	5.5
		6	0.600	46.2		1.57	3.60	0.40	0.167	0.160	4.4
						1.86	4.26	0.50	0.156	0.140	11.4
						2.14	4.90	0.60	0.149	0.140	6.4
						2.39	5.47	0.70	0.141	0.135	4.4
						2.59	5.93	0.80	0.135	0.130	3.8

TABLE 4.1.5.2-A (CONTD)

Ref.	Config.	A	λ	Λ_{LE} (deg)	NACA Airfoil	$R_0 \lambda_{MAC} \times 10^6$	$R_0 \lambda_{LER} \times 10^{-3}$	M	$\frac{C_{D_L}}{C_L^2}$ Calc.	$\frac{C_{D_L}}{C_L^2}$ Test	e Percent Error
14	W	5.14	0.713	36.2	65 ₁ A012	2.0	18.4	0.25	0.086	0.087	- 1.1
								0.40	0.087	0.090	- 3.3
								0.60	0.086	0.093	- 7.5
								0.70	0.085	0.094	- 9.6
								0.75	0.085	0.090	- 5.6
								0.80	0.085	0.094	- 9.6
								0.25	0.057	0.054	5.6
								0.40	0.057	0.056	1.8
								0.60	0.056	0.061	- 8.2
								0.80	0.055	0.061	- 9.8
$\text{Average Error} = -\frac{\sum e_i }{n} = 5.8\%$											

TABLE 4.1.5.2-B
SUBSONIC DRAG DUE TO LIFT OF SHARP-LEADING-EDGED
DOUBLE-DELTA WINGS

DATA SUMMARY AND SUBSTANTIATION

Ref.	Config.	A	λ_i	λ_o	η_B	Λ_{LE_i} (deg)	Λ_{LE_o} (deg)	$\frac{d}{b}$	$\frac{t}{c}$	M	$R_d \times 10^6$ (based on \bar{c})	α (deg)	C_L Calc.	C_{D_L} Calc.	C_{D_L} Test	e Percent Error
15	WBV	1.87	0.488	0	0.424	72.6	59.0	0.131	0.02-0.03	0.13	17.1	4	0.150	0.0100	0.0040	150.0
	WBV	1.46	0.482	0.189	0.484	72.6	59.0	0.149	0.02-0.03	0.13		8	0.340	0.0450	0.0410	10.7
	WBV	1.73	0.346	0	0.551	73.0	59.0	0.131	0.02-0.03	0.13		12	0.553	0.1117	0.1170	- 4.5
	WBV	1.34	0.346	0.240	0.628	73.0	59.0	0.149	0.02-0.03	0.13		16	0.769	0.2095	0.2240	- 6.5
	WBV	1.73	0.346	0	0.551	73.0	59.0	0.131	0.02-0.03	0.13		20	0.979	0.3385	0.3520	- 3.8
	WBV	1.46	0.482	0.189	0.484	72.6	59.0	0.149	0.02-0.03	0.13	17.3	4	0.148	0.0098	0.0080	22.6
	WBV	1.73	0.346	0	0.551	73.0	59.0	0.131	0.02-0.03	0.13	19.3	8	0.335	0.0447	0.0430	4.0
	WBV	1.34	0.346	0.240	0.628	73.0	59.0	0.149	0.02-0.03	0.13	19.5	12	0.545	0.1101	0.1120	- 1.7
	WBV	1.73	0.346	0	0.551	73.0	59.0	0.131	0.02-0.03	0.13	19.5	16	0.757	0.2062	0.2180	- 5.4
	WBV	1.34	0.346	0.240	0.628	73.0	59.0	0.149	0.02-0.03	0.13	19.5	20	0.965	0.3337	0.3520	- 5.2

TABLE 4.1.5.2-B (CONT'D)

Ref.	Config.	A	λ_i	λ_o	η_B	Λ_{LE_i} (deg)	Λ_{LE_o} (deg)	$\frac{d}{b}$	$\frac{t}{c}$	M	$R\varrho \times 10^{-6}$ (based on c)	α (deg)	C_L Calc.	C_{DL} Calc.	C_{DL} Test	% Percent Error
15	WBV	1.73	0.356	0	0.414	77.4	59.0	0.131	0.02-0.03	0.13	20.0	4	0.143	0.0095	0.0085	11.8
												8	0.302	0.0403	0.0420	- 4.0
												12	0.491	0.0992	0.1090	- 9.0
												16	0.685	0.1866	0.2110	- 11.6
												20	0.974	0.3368	0.3410	- 1.2
	WBV	1.34	0.356	0.210	0.473	77.4	59.0	0.149	0.02-0.03	0.13	20.3	4	0.130	0.0086	0.0060	43.4
												8	0.298	0.0398	0.0390	2.1
												12	0.484	0.0978	0.1080	- 9.4
												16	0.676	0.1841	0.2050	- 10.2
												20	0.960	0.3320	0.3350	- 0.9
	WBV	1.87	0.448	0	0.332	77.2	59.0	0.131	0.02-0.03	0.13	17.8	4	0.146	0.0097	0.0075	29.4
												8	0.335	0.0447	0.0430	4.0
												12	0.524	0.1058	0.1120	- 5.5
												16	0.759	0.2068	0.2130	- 2.9
												20	0.971	0.3358	0.3360	- 0.1
	WBV	1.46	0.448	0.183	0.379	77.2	59.0	0.149	0.02-0.03	0.13	18.2	4	0.144	0.0096	0.0060	60.0
												8	0.330	0.0441	0.0400	10.3
												12	0.538	0.1087	0.1070	1.6
												16	0.749	0.2040	0.2110	- 3.3
												20	0.958	0.3313	0.3370	- 1.7

TABLE 4.1.5.2-C
SUBSONIC PARABOLIC DRAG DUE TO LIFT OF
ROUND-LEADING-EDGED CRANKED WINGS

DATA SUMMARY

Ref.	Config.	A	λ_i	λ_o	η_B	Λ_{LE_i} (deg)	Λ_{LE_o} (deg)	$\frac{d}{b}$	$\frac{t}{c}$	$(LER)_i$ (% \bar{c}_i)	$(LER)_o$ (% \bar{c}_o)	M	$R\ell \times 10^{-6}$ (based on \bar{c})	C_{D_L}/C_L^2 Calc.	C_{D_L}/C_L^2 Test	ϵ Percent Error
16	WB	4.0	0.580	0.517	0.600	48.6	7.7	0.139	0.06	0.229	0.229	0.80	3.65	0.152	0.154	-1.3
17	WB	2.91	0.333	0.500	0.500	67.0	61.7	0.139	0.04-0.03	0.089	0.067	0.60	3.5	0.320	0.336	-4.8
18	W	5.2	0.339	0.268	0.379	60.0	25.0	---	0.045-0.06	0.149	0.265	0.13	2.65	0.186	0.203	-8.4
$\text{Average Error} = \frac{\sum e }{n} = 4.8\%$																

TABLE 4.1.5.2-D
SUBSONIC DRAG DUE TO LIFT BEYOND DRAG POLAR
BREAK FOR ROUND-LEADING-EDGED CRANKED WINGS
DATA SUMMARY AND SUBSTANTIATION

Ref.	Config.	A	λ_i	λ_o	η_B	Λ_{LE_i} (deg)	Λ_{LE_o} (deg)	$\frac{d}{b}$	$\frac{t}{c}$	M	$R_d \times 10^{-6}$ (based on c)	C_L	C_{D_L} Calc.	C_{D_L} Test	e Percent Error
16	WB	4.0	0.580	0.517	0.600	48.6	7.7	0.138	0.06	0.80	3.645	0.4	0.0323	0.0300	7.7
												0.5	0.0620	0.0620	0
												0.6	0.1057	0.1060	-0.3
												0.7	0.1585	0.1610	-1.6
												0.8	0.2218	0.2250	-1.4
												0.9	0.2727	0.2619	4.1
18	W	E.2	0.339	0.268	0.379	60.0	25.0	---	0.045-0.06	0.13	2.65	0.4	0.0328	0.0321	2.2
												0.5	0.0645	0.0614	5.0
												0.6	0.1010	0.1015	-0.5
												0.7	0.1480	0.1427	3.7
												0.8	0.2040	0.1968	3.7
												0.9	0.2727	0.2619	4.1
19	WBV	8.47	0.197	0.386	0.212	76.0	16.0	0.062	---	0.20	3.6	0.678	0.0365	(a)	
												0.762	0.0830		
												0.847	0.1720		
20	WE	6.18	0.294	0.463	0.308	65.0	12.0	0.066	0.06-0.02	0.50	0.73	0.618	0.0420		
												0.680	0.0700		
												0.742	0.1120		

TABLE 4.1.5.2-D (CONT'D)

Ref.	Config.	A	λ_i	λ_o	η_B	Λ_{LE_i} (deg)	Λ_{LE_o} (deg)	$\frac{d}{b}$	$\frac{t}{c}$	M	$R_d \times 10^{-6}$ (based on c)	C_L	$C_{D,L}$ Calc.	$C_{D,L}$ Test	% Percent Error
20	WB	4.43	0.389	0.464	0.405	65.0	45.0	0.080	0.06-0.02	0.50	0.65	0.354	0.0175		
												0.443	0.0365		
												0.532	0.0640		
												0.620	0.1010		
												0.709	0.1470		
												0.797	0.1965		
21	WBVN	3.0	0.200	0	0.654	60.0	42.1	0.077	0.035-0.040	0.20	3.22	0.420	0.0275		
												0.480	0.0420		
												0.540	0.0620		
												0.600	0.0886		
												0.660	0.1160		
												0.720	0.1470		
	WBVN	4.0	0.200	0.138	0.550	60.0	18.1	0.065	0.035-0.040	0.20	3.07	0.320	0.0135		
												0.400	0.0280		
												0.480	0.0500		
												0.560	0.0811		
												0.640	0.1195		
												0.720	0.1640		
22	WBV	5.95	0.440	0	0.345	60.0	25.0	0.121	0.045	0.36	10.24	0.595	0.0320		
												0.655	0.0500		
												0.714	0.0790		
(a) This information is classified CONFIDENTIAL															
Average Error = $\frac{\sum e }{n} = 4.1\%$															

TABLE 4.1.5.2-E
SUBSONIC DRAG DUE TO LIFT OF SHARP-
LEADING-EDGED CURVED WINGS
DATA SUMMARY AND SUBSTANTIATION

Ref.	Config.	Planform	A	p	$\frac{b_w}{2L}$	$\frac{d}{b}$	$\frac{t}{c}$ (root)	M	$R\chi \times 10^{-6}$ (based on c)	α (deg)	C_L Calc.	C_{D_L} Calc.	C_{D_L} Test	% Percent Error
23	WB	Ogee	1.20	0.500	0.300	0.133	0.05	0.40	1.7	4	0.136	0.0090	0.0080	12.5
										8	0.288	0.0384	0.0360	6.7
										12	0.465	0.0939	0.0980	- 4.2
24	WB	Ogee	1.98	0.455	0.450	0.127	0.02	0.70	0.58	4	0.167	0.0111	0.0110	0.9
										8	0.352	0.0470	0.0485	- 3.1
25	W	Gothic	0.75	0.667	0.250	---	0.01	0.10	2.9	6.1	0.165	0.0168	0.0136	23.5
										10.1	0.303	0.0613	0.0476	7.8
										14.1	0.465	0.1110	0.1091	1.7
	W	Gothic	1.25	0.667	0.417	---	0.01	0.10	2.9	18.1	0.645	0.2003	0.2016	- 0.6
										10.15	0.389	0.0661	0.0610	8.4
										14.15	0.599	0.1435	0.1420	1.1

(a) Flat-plate models with beveled leading edges; α and C_L are adjusted to account for camber.

Average Error = $\frac{\sum |e|}{n} = 6.6\%$

TABLE 4.1.5.2-F
SUPersonic DRAG DUE TO LIFT OF STRAIGHT-
TAPERED WINGS

DATA SUMMARY AND SUBSTANTIATION

Ref.	Config.	A	λ	p	$\frac{b_w}{2\ell}$	LER	M	$\frac{\pi A}{C_L^2}$ Calc.	$\frac{\pi A}{C_L^2}$ Test	% Percent Error
27	WB	1.313	0.150	0.412	0.271	Round	1.80	2.04	2.00	2.0
							2.16	2.38	2.36	0.8
							2.50	2.71	2.54	6.7
							2.86	3.05	3.34	- 8.7
							3.95	4.09	4.02	1.7
							4.63	4.69	4.70	- 0.2
28	WB	2.0	0	0.500	0.500	Round	1.30	1.81	2.01	-10.0
							1.70	2.57	2.67	- 3.7
							1.90	2.92	2.95	- 1.0
							1.20	2.02	1.65	22.4
							1.30	2.37	2.05	15.6
							1.50	2.98	2.55	16.9
29	WB	4.0	0.500	0.320	0.643	Round	1.41	3.34	2.94	13.6
							1.90	4.06	3.79	7.1
							1.70	3.54	3.16	12.0
							1.61	3.39	3.39	0
							2.01	4.54	4.73	4.0
							3.15	3.14	2.99	5.0
30	W	3.5	0.200	0.393	0.688	Sharp	1.61	2.89	2.84	1.8
							2.01	3.86	4.09	- 5.6
							2.86	0.120	0.441	0.630
							1.61	2.89	2.84	1.8
							3.15	0.150	0.437	0.688
							2.01	3.14	2.99	5.0
31	WB	3.50	0.200	0.600	1.050	Sharp	1.61	3.75	3.67	2.2
							2.01	5.09	5.12	- 0.6
							3.15	0.150	0.500	0.787
							1.61	3.23	3.34	- 3.3
							2.01	4.36	4.64	- 6.0
							2.03	3.33	2.75	21.1
32	W	2.5	0.200	0.363	0.441	Sharp	2.31	2.29	0.9	
							1.5	0.546	0.409	

TABLE 4.1.5.2-F (CONTD)

Ref.	Config.	A	λ	p	$\frac{b_w}{2\ell}$	LER	M	$\frac{C_{DL}}{\pi A \frac{C_L^2}{2}}$ Calc.	$\frac{C_{DL}}{\pi A \frac{C_L^2}{2}}$ Test	% Percent Error
33	WB	3.0	0	0.502	0.750	Round	1.20	2.01	2.46	-18.0
		3.0	0.200	0.430	0.643		1.30	2.37	2.86	-17.1
		3.0	0.400	0.389	0.585		1.50	3.00	3.39	-11.6
		3.0	0.678	0.980	1.045		1.70	3.55	3.96	-10.4
		3.08	0.388	0.694	1.07	Sharp	1.20	4.07	4.05	0.5
24	WB	2.174	0	0.500	0.544	Sharp	1.40	1.87	2.39	-21.8
		2.174	0.678	0.980	1.045		1.98	3.06	3.21	-5.0
		2.174	0.388	0.694	1.07		2.94	4.76	4.61	3.3
10	WB	4.0	0	0.500	1.00	Round	1.20	2.50	2.50	0
		4.0	0.678	0.980	1.045		1.30	2.98	2.80	6.8
		4.0	0.388	0.694	1.07		1.40	3.41	3.30	3.3
		4.0	0.678	0.980	1.045		1.63	3.93	3.72	5.6
		4.0	0.388	0.694	1.07	Sharp	1.60	4.19	4.01	4.5
		4.0	0.678	0.980	1.045		1.70	4.57	4.30	6.3
		4.08	0.388	0.694	1.07		1.20	1.95	1.97	-1.0
		4.08	0.678	0.980	1.07		1.50	3.13	3.25	-3.7

TABLE 4.1.5.2-F (CONTD)

Ref.	Config.	A	λ	p	$\frac{b_w}{2\ell}$	LER	M	$\frac{C_{D_L}}{\pi A \frac{C_L^2}{2}}$ Calc.	$\frac{C_{D_L}}{\pi A \frac{C_L^2}{2}}$ Test	e Percent Error
10	WB	2.0	1.00	0.995	1.00	Sharp	1.20	1.51	1.57	- 3.8
							1.30	1.87	1.93	- 4.7
							1.40	2.13	2.10	1.4
							1.50	2.41	2.15	12.1
							1.60	2.67	2.32	15.1
							1.70	2.88	2.44	18.0
10	WB	2.0	0.333	0.665	0.672	Sharp	1.20	1.43	1.60	-10.6
							1.30	1.63	1.68	- 3.0
							1.40	1.88	1.78	5.6
							1.50	2.11	2.05	2.9
							1.60	2.33	2.17	7.4
							1.70	2.53	2.46	2.8
34	WB	4.0	0.333	0.237	0.475	Round	1.41	3.38	3.14	7.6
							1.61	4.02	3.90	3.1
							2.01	5.17	4.90	5.5
							1.55	2.05	1.95	5.1
							1.80	2.52	2.44	3.3
							1.95	2.78	2.66	4.5
35	WB	2.0	0	0.500	0.500	Sharp	2.10	3.03	3.05	- 0.7
							2.35	3.45	3.52	- 2.0
							2.50	3.70	3.93	- 5.9
							3.00	4.49	4.66	- 3.6
							3.50	5.29	5.45	- 2.9
							2.50	3.41	3.30	3.3
							3.00	4.12	4.37	- 5.7
							3.50	4.81	5.03	- 4.4

TABLE 4.1.5.2-F (CONT'D)

Ref.	Config.	A	λ	ρ	$\frac{b_w}{2\ell}$	LER	M	$\frac{\pi A}{C_L^2} \frac{C_{D_L}}{\text{Calc.}}$	$\frac{\pi A}{C_L^2} \frac{C_{D_L}}{\text{Test}}$	% Percent Error				
36	WB	3.0	0.400	0.389	0.584	Round	1.00	1.93	1.93	0				
							1.10	1.93	1.98	- 2.5				
							1.20	2.08	2.12	- 1.9				
							1.30	2.36	2.40	- 1.7				
							1.40	2.66	2.60	1.9				
		3.0	0.400	0.482	0.723		1.00	1.67	1.72	- 2.9				
							1.10	1.71	1.85	- 7.6				
							1.20	2.01	2.11	- 4.7				
							1.30	2.37	2.36	0.4				
							1.40	2.70	2.64	2.3				
37	WB	3.50	0.200	0.393	0.688	Round	1.00	1.91	1.86	2.7				
							1.06	1.91	1.92	- 0.6				
							1.10	1.96	1.94	1.0				
$\text{Average Error} = \frac{\sum e_i }{n} = 6.4\%$ <table style="margin-left: auto; margin-right: auto;"> <tr> <td style="width: 45%;">Round Leading Edge</td> <td style="width: 5%;">6.8%</td> </tr> <tr> <td>Sharp Leading Edge</td> <td>6.8%</td> </tr> </table>											Round Leading Edge	6.8%	Sharp Leading Edge	6.8%
Round Leading Edge	6.8%													
Sharp Leading Edge	6.8%													

TABLE 4.1.5.2-G
SUPERSONIC DRAG DUE TO LIFT OF DOUBLE-DELTA
AND CRANKED WINGS
DATA SUMMARY AND SUBSTANTIATION

Ref.	Config.	Planform	A	ρ	$\frac{b_w}{2L}$	LER	M	$\frac{C_{D_L}}{\pi A \frac{C_L^2}{2}}$ Calc.	$\frac{C_{D_L}}{\pi A \frac{C_L^2}{2}}$ Test	% Percent Error
30	WB	Double Delta	3.15	0.359	0.565	Sharp	1.61	3.37	3.32	1.5
			2.86	0.395	0.565			3.14		
			2.62	0.400	0.525			2.94		
			2.86	0.335	0.479			3.12		
			2.62	0.365	0.479			2.93		
			2.42	0.372	0.450			2.77		
			2.86	0.335	0.479		2.01	4.04	4.31	-6.3
			2.42	0.372	0.450		↓	3.54	3.64	-2.7
31	WB	Double Delta	2.62	0.400	0.525	Sharp	1.61	2.94	3.58	-17.9
			2.42	0.372	0.450			2.77		
			3.15	0.500	0.787		2.01	4.88	4.95	-1.4
			2.86	0.440	0.630		↓	4.30	4.81	-10.6
			2.62	0.400	0.525		↓	3.88	4.68	-17.5
			2.86	0.440	0.630		↓	4.30	4.57	-5.9
			2.62	0.400	0.525		↓	3.86	4.52	-14.6
			2.42	0.372	0.450		↓	3.54	4.46	-20.6
38	WB	Double Delta	1.86	0.412	0.384	Round	2.01	2.90	2.66	9.0
39	WB	Double Delta	1.86	0.412	0.384	Round	2.50	3.67	2.90	26.6
34	WB	Double Delta	2.91	0.292	0.425	Round	3.00	4.47	3.28	36.3
							3.71	6.57	3.97	40.3
34	WB	Double Delta	2.91	0.292	0.425	Round	1.41	2.77	2.65	4.6
							1.61	3.19	3.08	3.6
34	WB	Double Delta	2.91	0.292	0.425	Round	2.01	4.07	3.89	4.6

TABLE 4.1.5.2-G (CONT'D)

Ref.	Config.	Planform	A	p	$\frac{b_w}{2L}$	LER	M	$\frac{C_{D_L}}{\pi A \frac{C_L^2}{2}}$ Calc.	$\frac{C_{D_L}}{\pi A \frac{C_L^2}{2}}$ Test	% Percent Error
40	WB	Double Delta	2.67	0.429	0.571	Round	1.41	2.50	2.89	-13.5
			2.29	0.389	0.444		2.01	3.98	4.19	-5.0
			2.35	0.486	0.571		1.41	2.29	2.70	-15.2
			1.96	0.456	0.444		2.01	3.39	3.83	-11.5
			2.29	0.389	0.444		1.41	2.29	2.54	-9.8
			2.00	0.364	0.364		2.01	3.65	3.69	-1.1
			2.50	0.467	0.571		1.41	2.04	2.20	-7.3
			2.06	0.433	0.444		2.01	3.04	3.26	-6.7
			1.74	0.418	0.364		2.01	3.39	3.86	-12.2
			2.39	0.295	0.363	I-Round o-Sharp	1.20	2.26	2.67	-18.7
41	WB	Double Delta	2.39	0.295	0.363		2.00	3.46	3.59	-15.0
			2.00	0.364	0.364		1.41	2.39	2.87	-16.7
42	WBVN	Double Deltas	2.60	0.484	0.600	Round	2.01	3.81	3.93	-3.1
			2.16	0.431	0.444		1.41	2.12	2.50	-15.2
			2.56	0.520	0.520		2.01	3.15	3.48	-9.5
			3.07	0.615	0.615		1.41	1.97	2.19	-10.0

TABLE 4.1.5.2-G (CONT'D)

Ref.	Config.	Planform	A	ρ	$\frac{b_w}{2\bar{x}}$	LER	M	$\frac{C_{D_L}}{\pi A \frac{C_L^2}{2}}$ Calc.	$\frac{C_{D_L}}{\pi A \frac{C_L^2}{2}}$ Test	% Percent Error
40	WB	Cranked	4.0	0.866	1.333	Round	1.41	3.96	3.33	18.9
			3.2	0.500	0.800		1.41	2.92	3.10	-5.8
			2.97	0.540	0.800		2.01	4.94	4.54	8.8
			3.20	0.500	0.800		1.41	2.77	2.99	-7.4
			2.91	0.491	0.710		2.01	4.69	4.26	10.1
36	WB	Cranked	2.91	0.491	0.710	Round	1.00	1.52	2.01	-24.3
			1	1	1		1.10	1.69	2.01	-15.9
			1	1	1		1.20	2.01	2.29	-12.2
			1	1	1		1.30	2.34	2.56	-8.6
			1	1	1		1.40	2.65	2.74	-3.3
$\text{Average Error} = \frac{\sum e }{n} = 10.7\%$ <p>Double Delta 10.5% Cranked 11.5%</p>										

TABLE 4.1.5.2-H
SUPERSONIC DRAG DUE TO LIFT OF CURVED PLANFORMS
DATA SUMMARY AND SUBSTANTIATION
SHARP LEADING EDGES

Ref.	Config.	Planform	A	ρ	$\frac{b_w}{2L}$	M	$\frac{C_{D_L}}{\pi A \frac{C_L}{2}}$ Calc.	$\frac{C_{D_L}}{\pi A \frac{C_L}{2}}$ Test	% Percent Error
9	W	Ogee	1.27	0.384	0.244	1.81	2.12	1.90	11.6
						1.91	2.18	2.01	8.5
						2.27	2.47	2.38	3.8
						2.65	2.83	2.77	2.2
						2.95	3.07	3.07	0
	W	Ogee	1.27	0.409	0.259	1.65	1.95	1.90	2.6
						1.84	2.10	2.05	2.4
						2.18	2.38	2.37	0.4
						2.53	2.71	2.71	0
						2.83	2.97	3.05	- 2.6
	W	Ogee	1.20	0.500	0.300	1.00	1.50	1.45	3.4
						1.30	1.56	1.64	- 4.9
						1.60	1.77	1.70	4.1
						1.79	1.94	2.00	- 3.0
						2.00	1.91	1.82	4.9
	W	Gothic	1.39	0.560	0.389	1.54	1.74	1.82	- 4.4
						1.63	1.92	1.90	1.1
						1.84	2.19	2.07	5.8
						2.06	2.44	2.31	5.6
						2.28	2.70	2.61	3.4
						2.53	3.02	2.93	3.1
						2.61	3.14	3.07	2.3

TABLE 4.1.5.2-H (CONTD)

Ref.	Config.	Planform	A	P	$\frac{b_w}{2L}$	M	$\frac{C_{DL}}{\pi A \frac{C_L^2}{2}}$ Calc.	$\frac{C_{DL}}{\pi A \frac{C_L^2}{2}}$ Test	% Percent Error
9	W	Gothic	1.09	0.611	0.333	1.55	1.60	1.56	2.6
						1.80	1.82	1.75	4.0
						2.06	2.07	1.94	6.7
						2.31	2.30	2.14	7.5
						2.60	2.57	2.34	9.8
						2.84	2.81	2.55	10.2
9	W	Gothic	1.00	0.667	0.333	1.56	1.53	1.44	6.3
						1.71	1.65	1.56	5.8
						1.97	1.86	1.81	2.8
						1.00	1.25	1.23	1.6
						1.42	1.30	1.27	2.4
						1.60	1.38	1.32	4.5
43	W	Ogee	0.924	0.450	0.208	1.82	1.46	1.36	7.4
						1.94	1.65	1.52	2.0
						1.40	1.63	1.53	6.5
						1.60	1.69	1.68	0.6
						1.80	1.77	1.80	- 1.7
						2.00	1.87	1.91	- 2.1
						2.20	1.98	2.06	- 3.4
						2.40	2.11	2.18	- 3.2
						2.60	2.23	2.35	- 5.1
						$\text{Average Error} = \frac{\sum e }{n} = 4.1\%$			

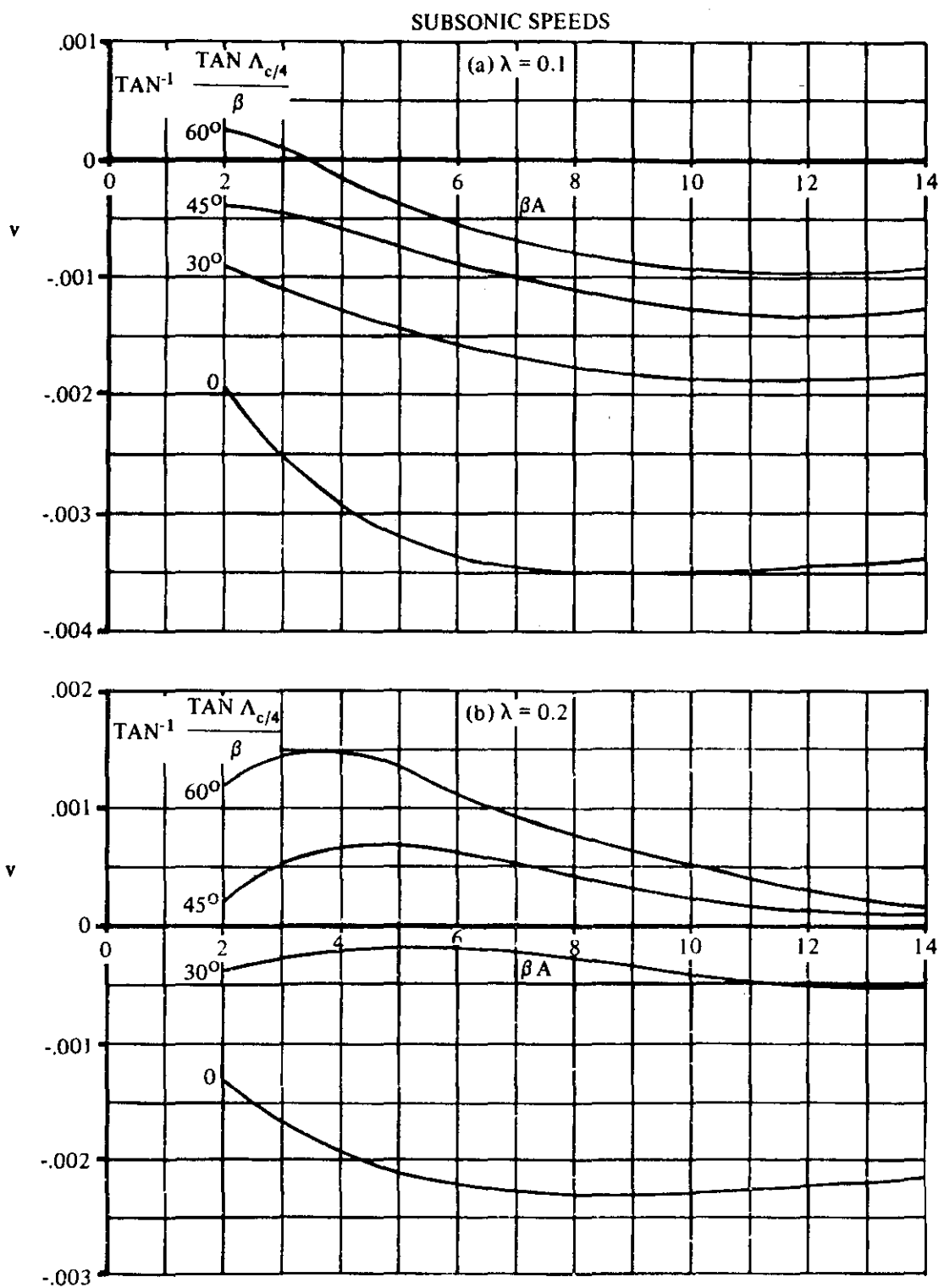


FIGURE 4.1.5.2-42 LIFT-DEPENDENT DRAG FACTOR DUE TO LINEAR TWIST
WEISSINGER METHOD

SUBSONIC SPEEDS

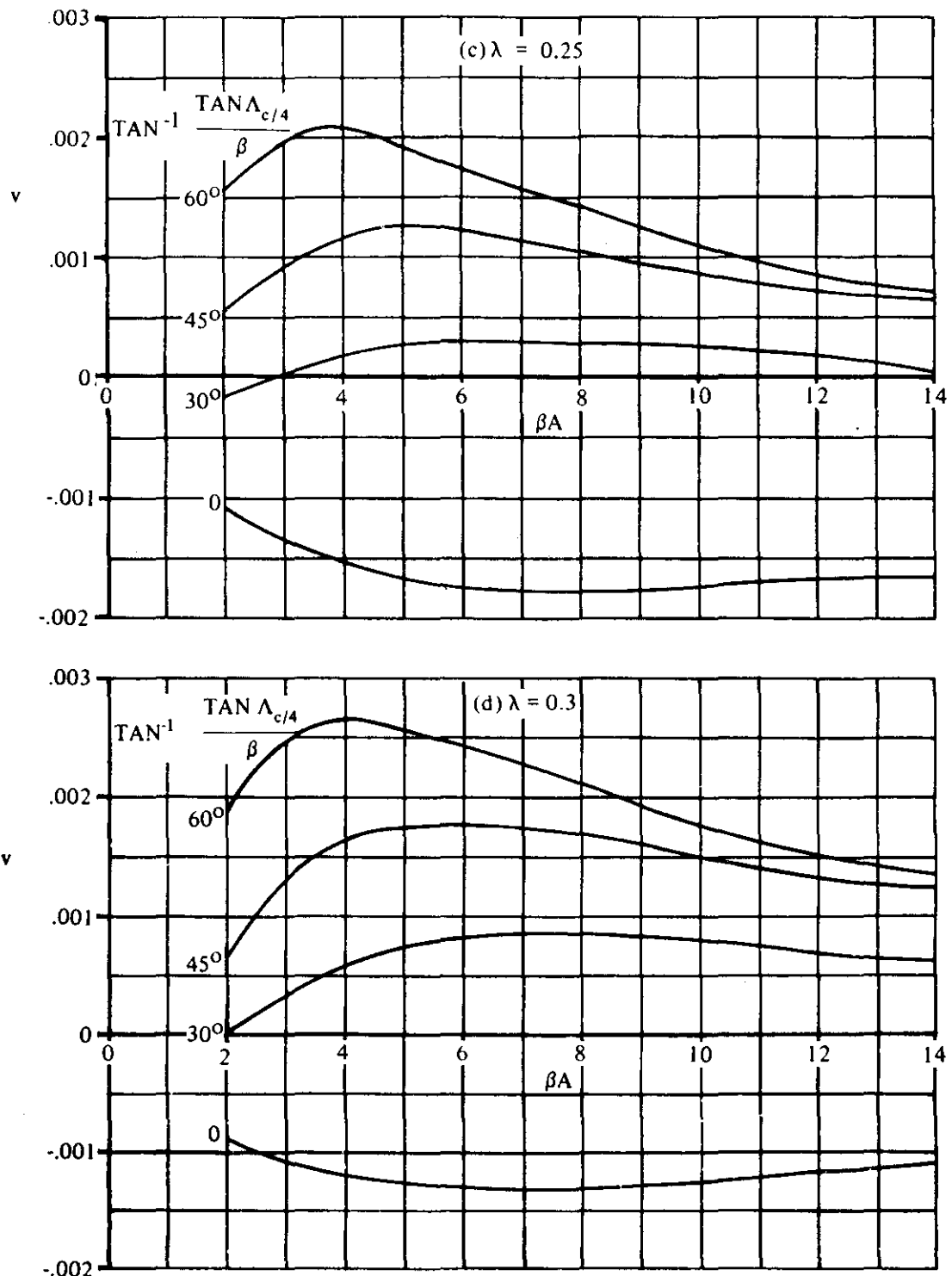


FIGURE 4.1.5.2-42 (CONTD)

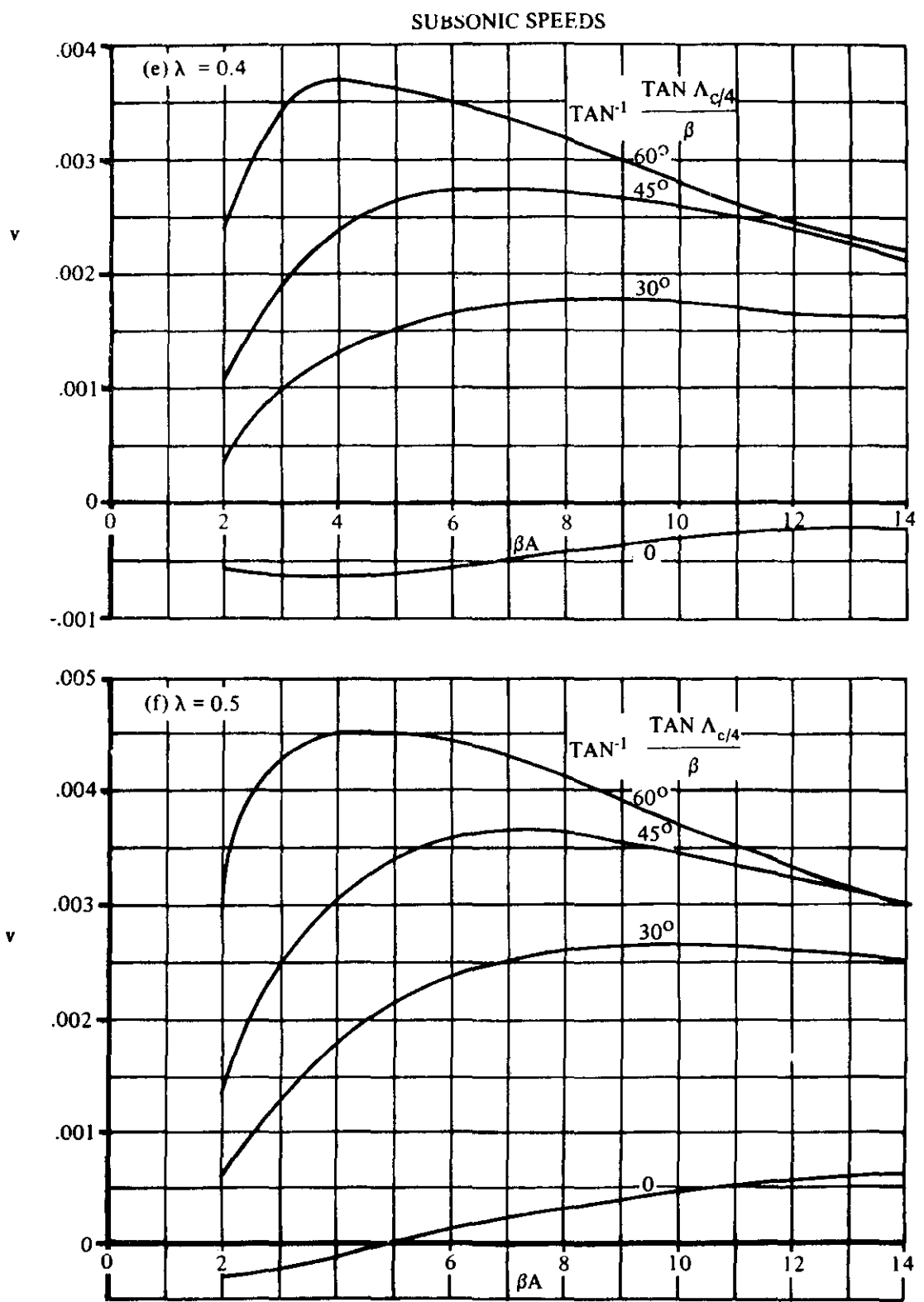


FIGURE 4.1.5.2-42 (CONTD)

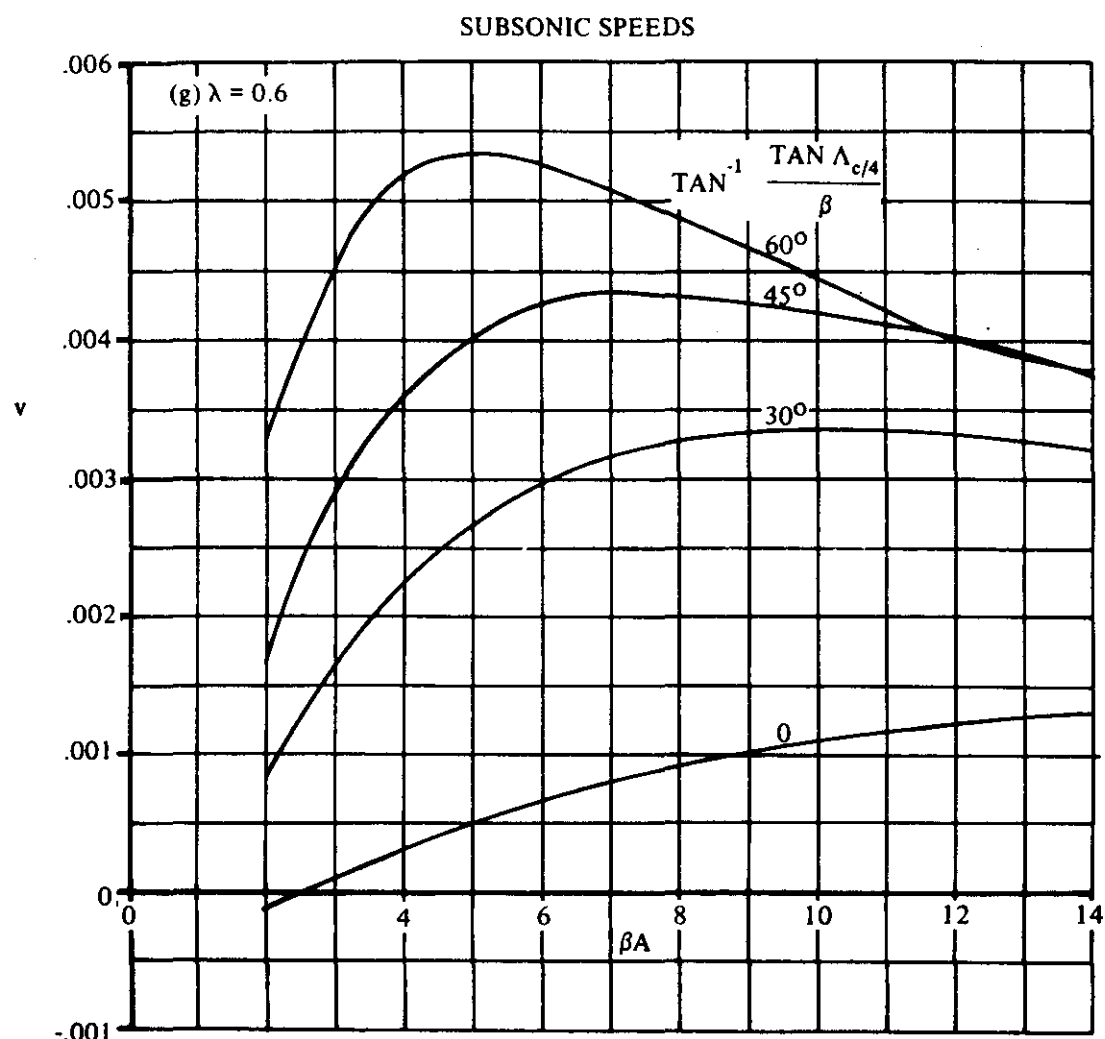


FIGURE 4.1.5.2-42 (CONTD)

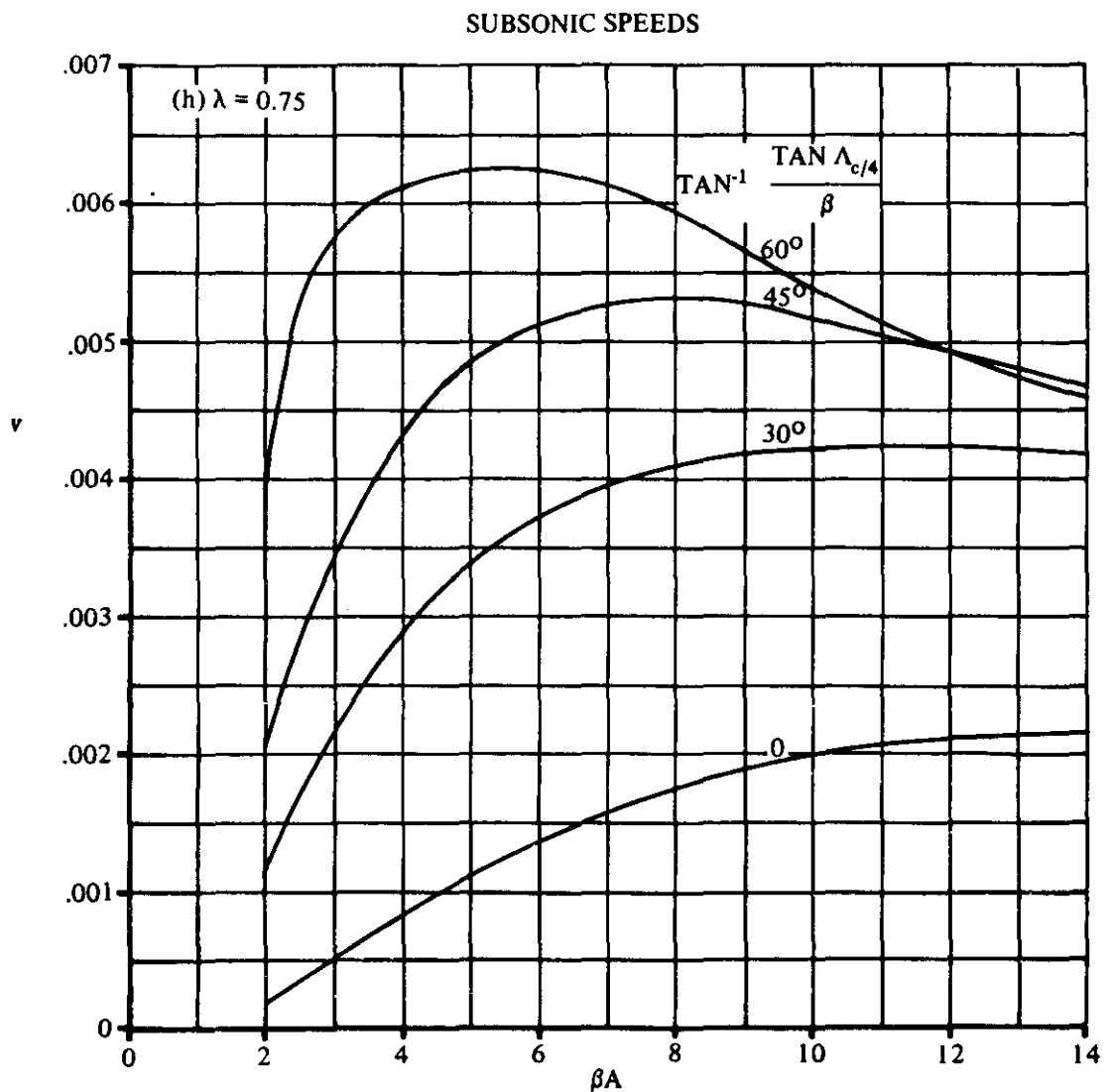


FIGURE 4.1.5.2-42 (CONTD)

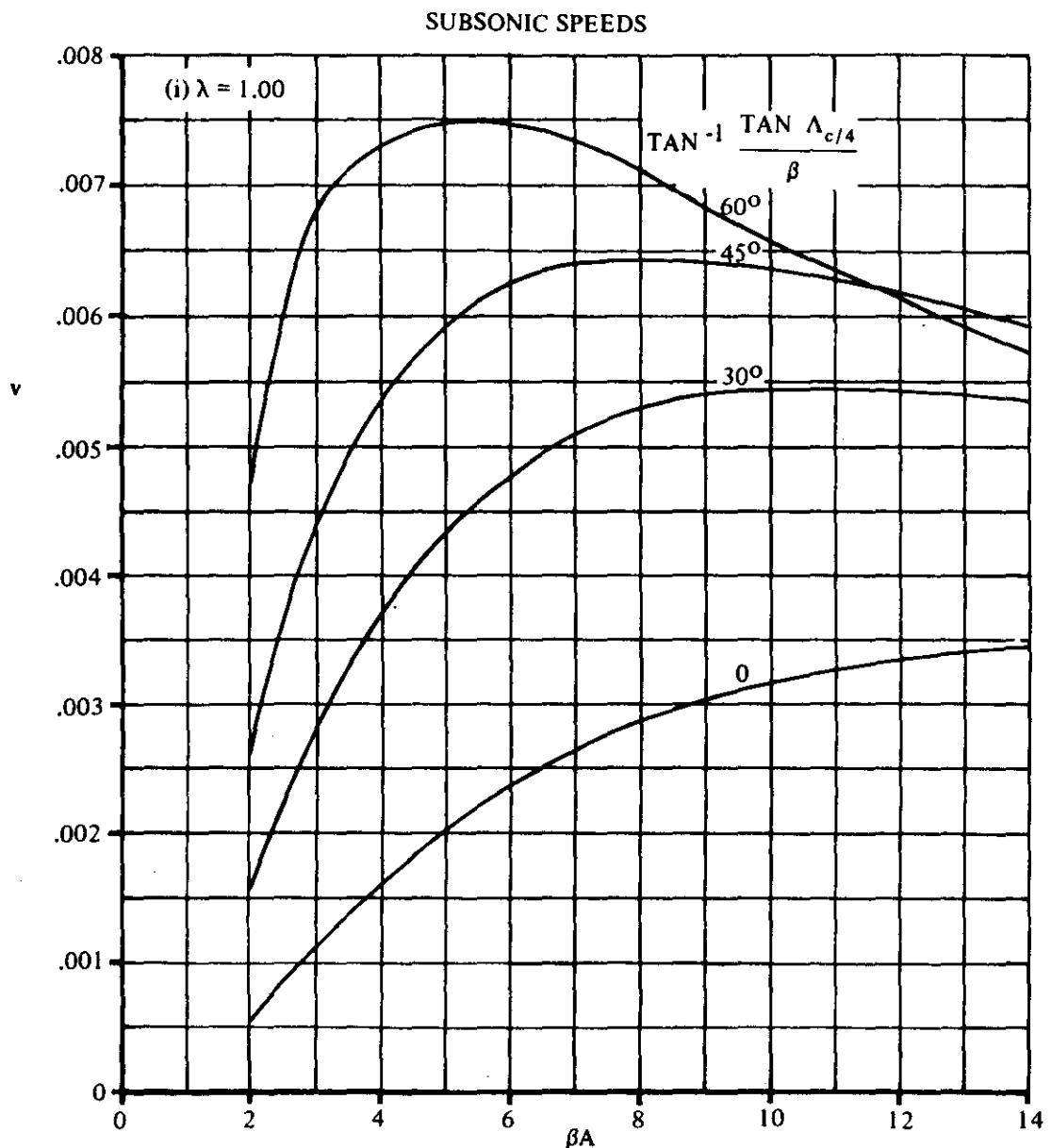


FIGURE 4.1.5.2-42 (CONTD)

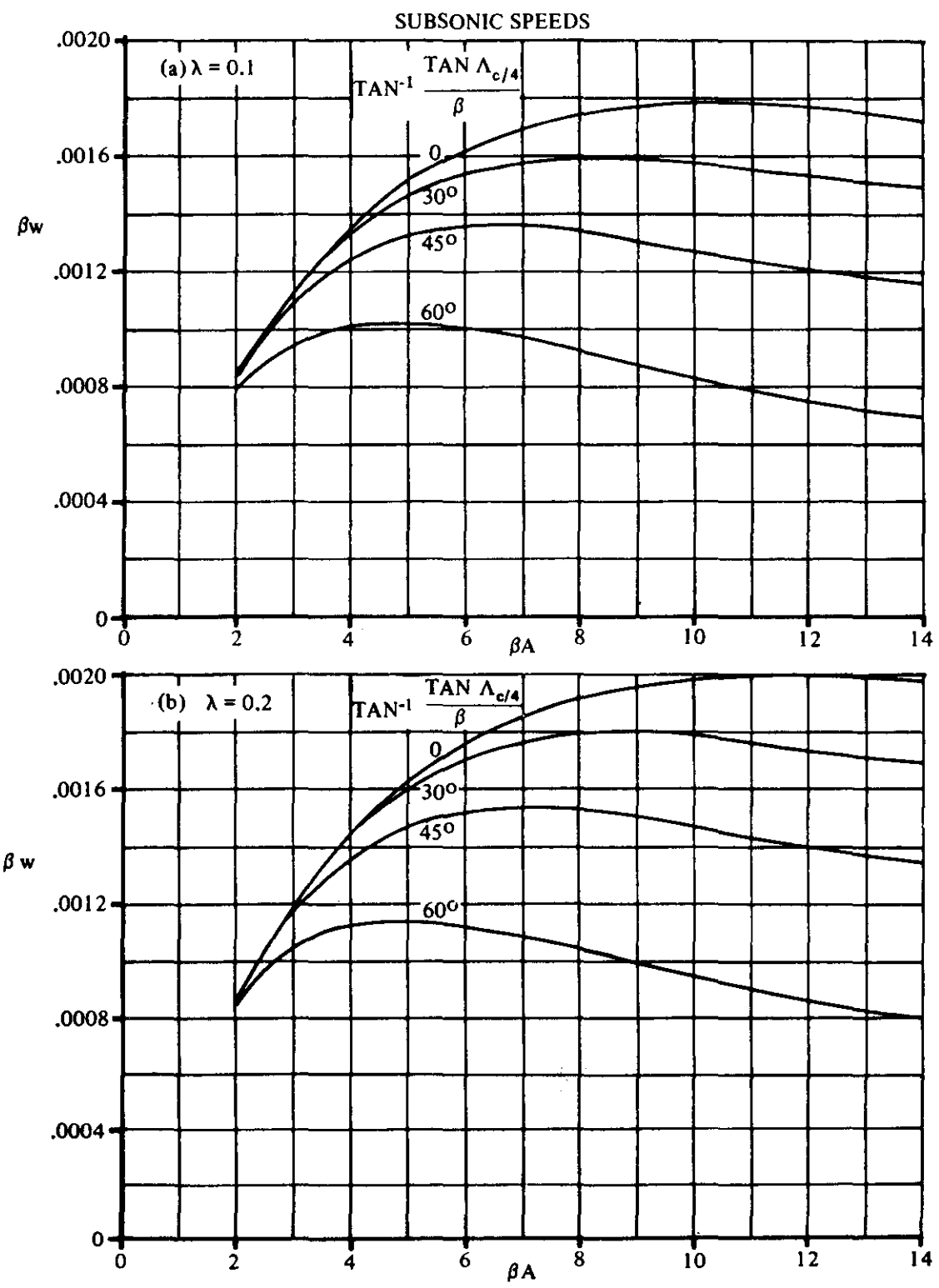


FIGURE 4.1.5.2-48 ZERO-LIFT DRAG FACTOR DUE TO LINEAR TWIST
WEISSINGER METHOD

4.1.5.2-48

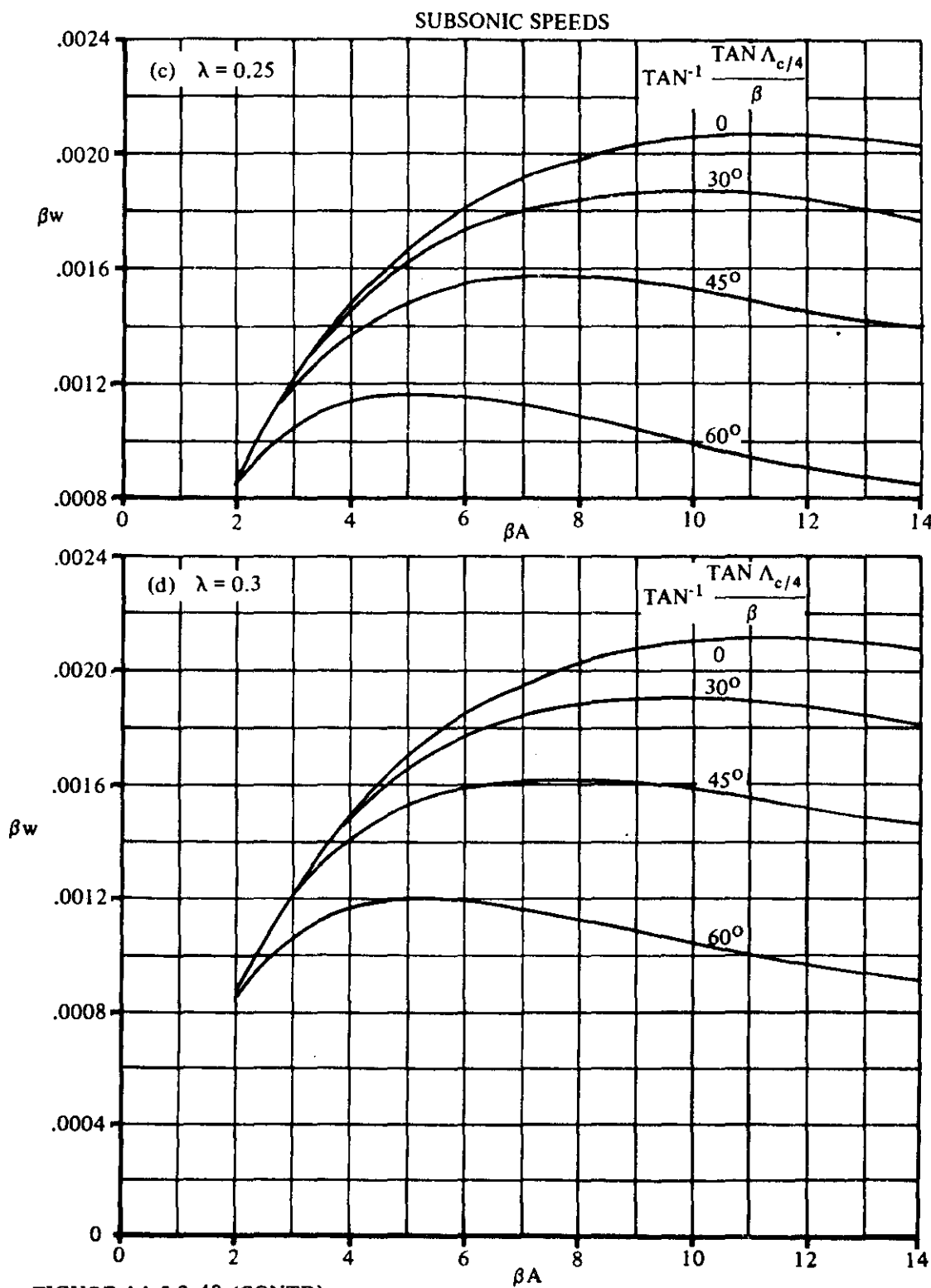


FIGURE 4.1.5.2-48 (CONTD)

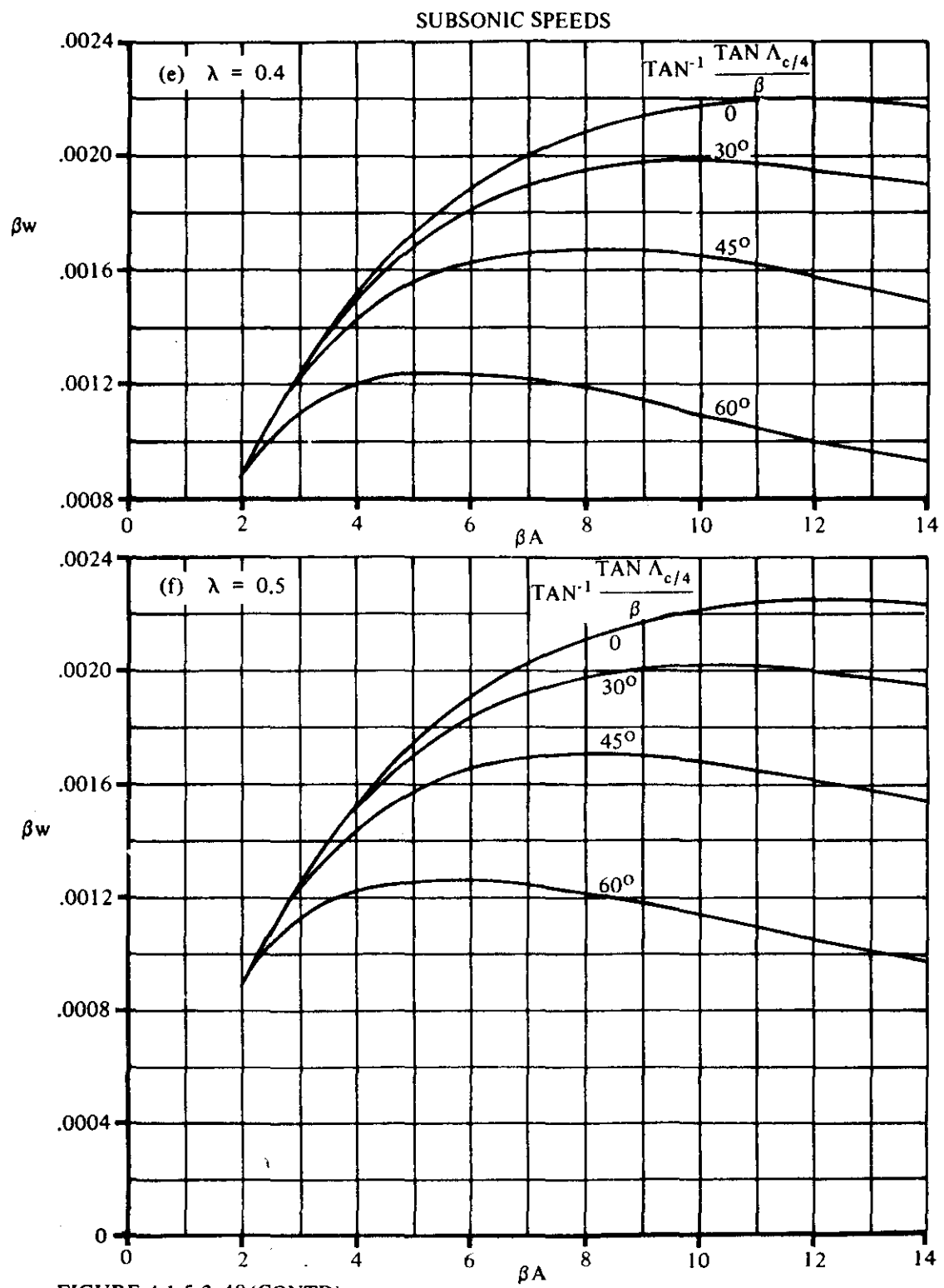


FIGURE 4.1.5.2-48 (CONT'D)

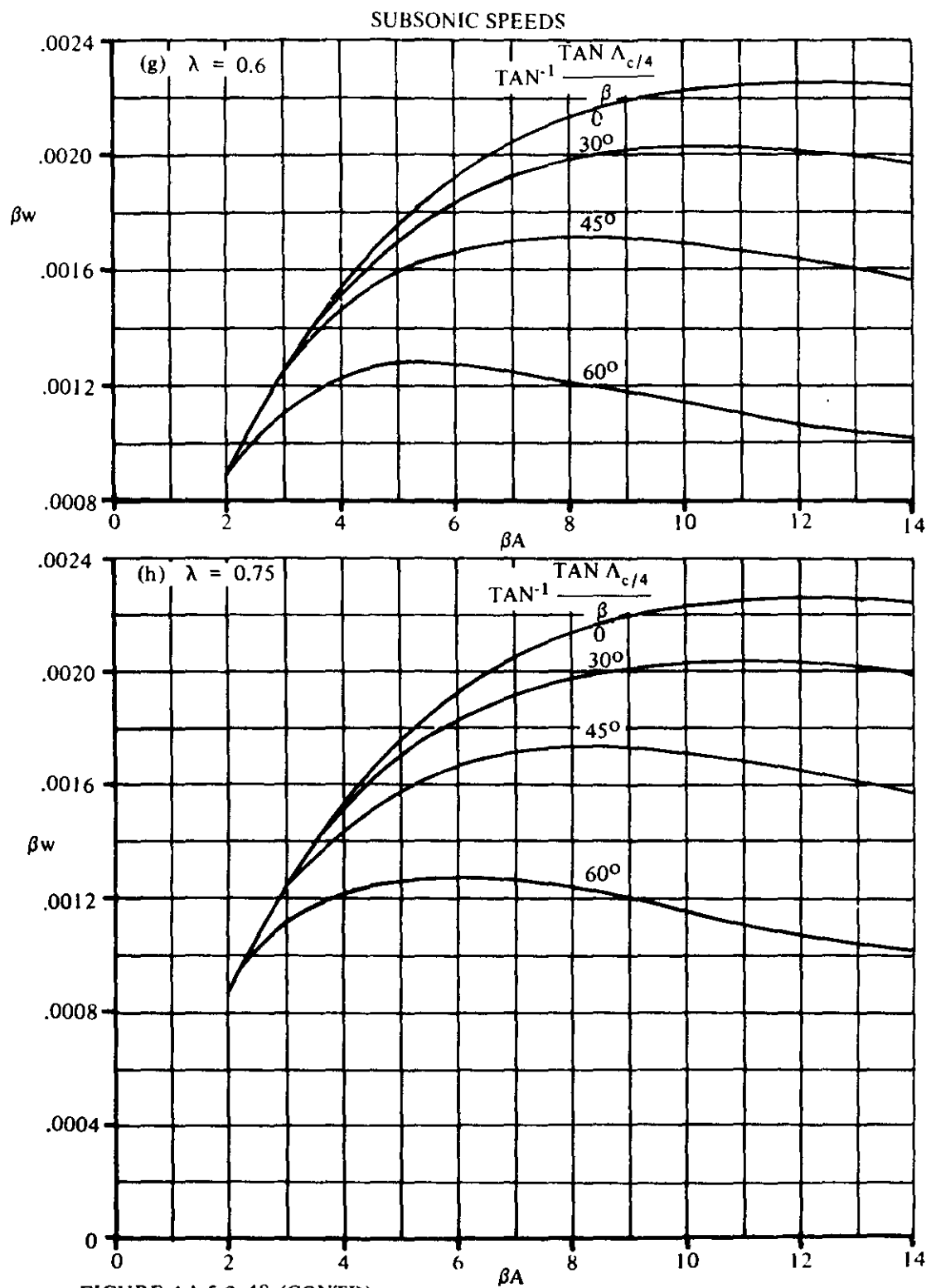


FIGURE 4.1.5.2-48 (CONT'D)

SUBSONIC SPEEDS

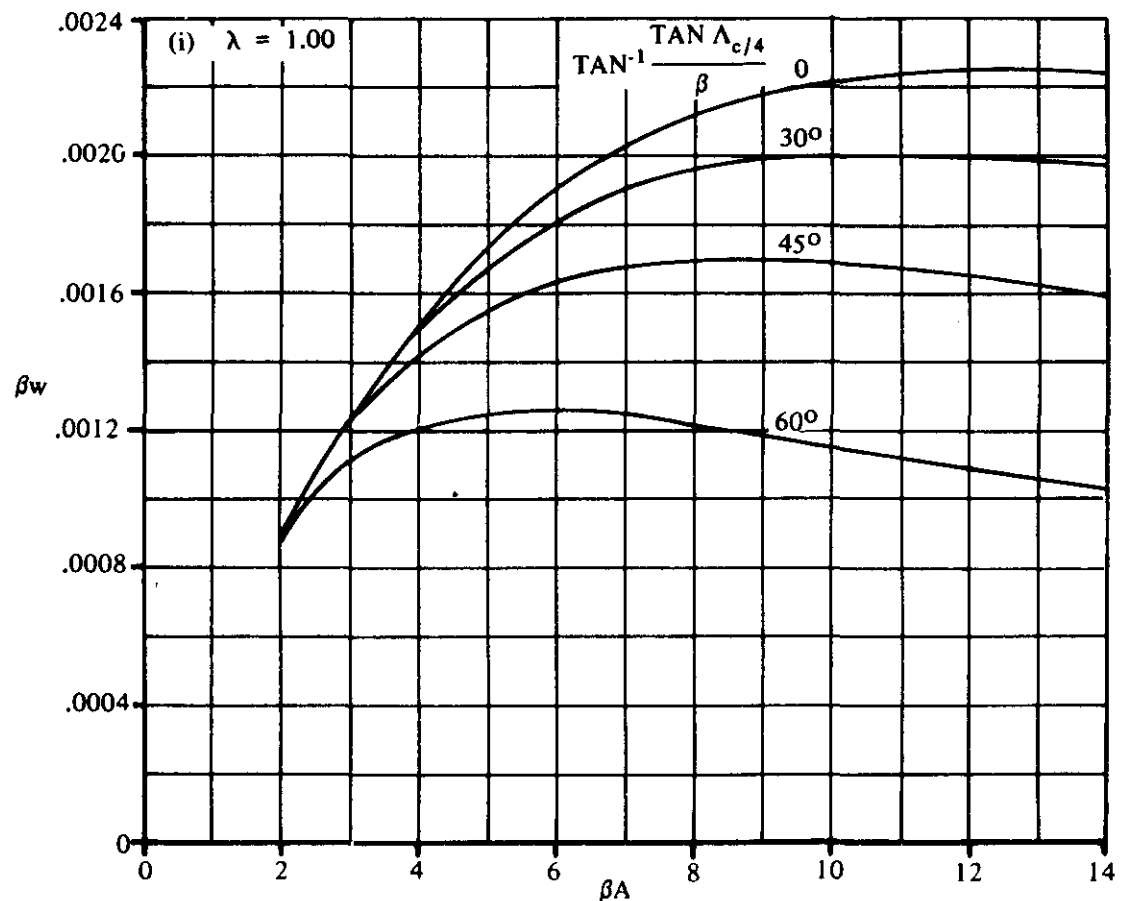


FIGURE 4.1.5.2-48 (CONTD)

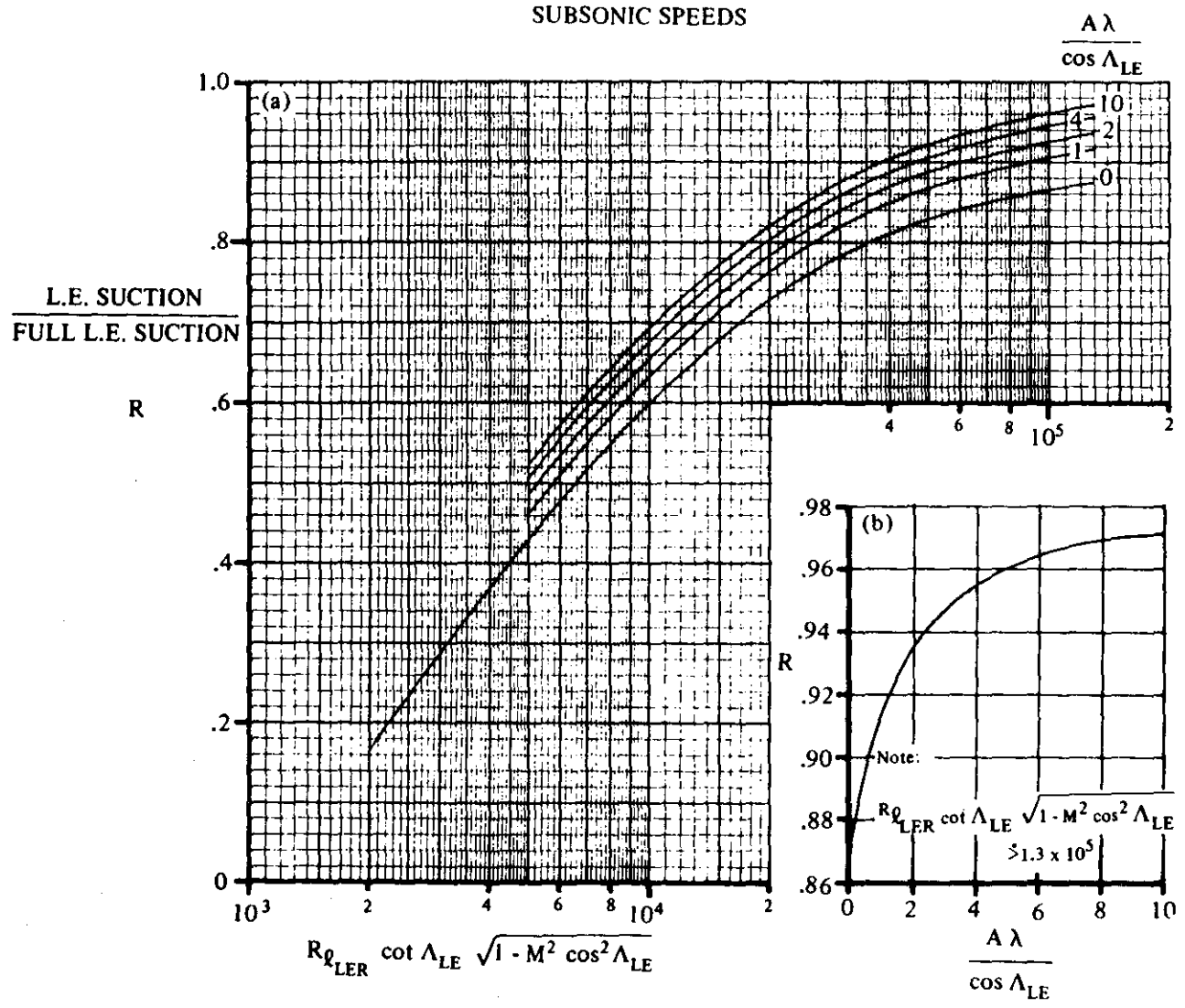


FIGURE 4.1.5.2-53 LEADING-EDGE SUCTION PARAMETER AT SUBSONIC SPEEDS. $M \leq 0.8$

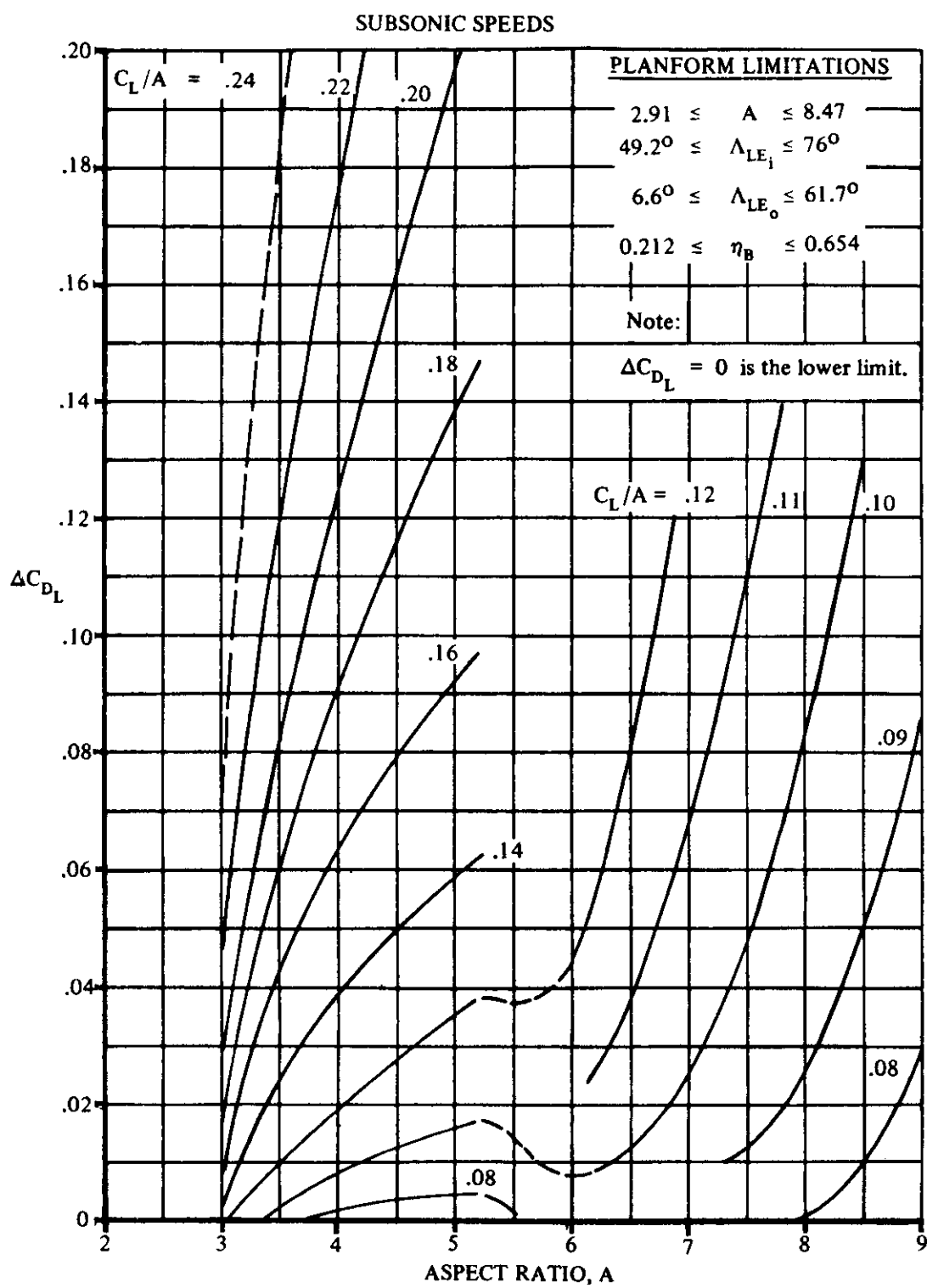


FIGURE 4.1.5.2-54 INDUCED DRAG INCREMENT ABOVE POLAR BREAK FOR CRANKED WINGS HAVING ROUND-NOSED AIRFOILS